Research Programme of the Research Fund for Coal and Steel

Steel RTD

Project carried out with a financial grant of the

Research Programme of the Research Fund for Coal and Steel

Robustness of car parks against localised fire

Grant Agreement Number RFSR-CT-2008-00036

Deliverable II: Experimental tests and development of sophisticated behavioural models

March 2012

Authors: Cécile Haremza (FCTUCOIMBRA)

Aldina Santiago (FCTUCOIMBRA)

Luís Simões da Silva (FCTUCOIMBRA)

Ludivine Comeliau (ULGG)

Long Van Hoang (ULGG)

Jean-François Demonceau (ULGG)

Jean-Pierre Jaspart (ULGG)

Cheng Fang (ICST)

Bassam Izzuddin (ICST)

Ahmed Elghazouli (ICST)

David Nethercot (ICST)

Renata Obiala (ARCELORPROFIL)

Table of contents

I. Introduction

The objectives of Work Package 2 (WP2) are to acquire the required knowledge on: A) the behavioural response of the individual frame structural elements directly affected by the localised fire, and B) the resultant reduction of carrying capacity of: i) the heated column in compression and bending; ii) the heated beam subject to bending and axial force (membrane effects); and iii) the heated beam-to-column joints subject to bending and axial force (membrane effects). To reach this goal, experimental, numerical and analytical developments were carried out, with the aim, at the end, to derive behavioural models for elements at two different levels: a "sophisticated level" (FEM models) and a "simplified" level (models for designers).

As an outcome of WP2, the present deliverable (DII) is about the experimental tests, and the development of sophisticated behavioural models, which are of particular importance as they are the only ones able to follow as closer as possible the reality. Experimental tests and sophisticated models can be considered as references in research, they are of full confidence for parametrical studies, and the models can be used as a direct design tool for complex structures, for which the use by the designer of simplified behavioural models would be questionable.

Seven experimental tests were performed within the present project, with the main objective to observe the combined bending moment and axial loads in the heated composite steel-concrete joint after the loss of the column due to a localised fire. The behavioural responses of columns, beams and joints were studied at a sophisticated level, and this document describes in detail the following: i) a column benchmark example about a steel sub-frame subject to a natural fire, and a simple behaviour study of a column under elevated temperatures for the columns study; ii) a composite beam benchmark about composite beams loaded at ambient temperature and under fire; iii) a component model in predicting the response of joints under elevated temperature conditions (joint benchmark), and a sophisticated thermal model to study the evolution of the temperature distribution within a composite beam-to-column joint subjected to the standard fire curve.

The initial WP2 period was extended during the project, because of delays with the experimental tests (as explained and justified in the 6-month reports). Nevertheless, during the new period (from 01/01/2009 to 30/06/2011), the WP2 objectives were fully contemplated.

The contractors involved in this WP2 were FCTUCOIMBRA, ULGG, ICST and ARECELORPROFIL.

II. Experimental tests results

Seven experimental tests of composite beam-to-column joints subject to axial and bending loadings under elevated temperatures were performed. The tested composite frame was subjected to mechanical (bending and axial forces) and thermal loadings (constant temperature equal to 20ºC, 500ºC or 700ºC; or linear increase up to 800ºC); the effect of the axial restraint to the beam was simulated. The two dimension sub-frame was extracted from an actual composite open car park building, keeping the real cross-section dimensions of the beams (IPE 550, S355) and the columns (HEB 300, S460), and using bolts M30, cl 10.9 in the composite connection. The final deformation of the sub-frame of test 6 is showed in Figure 1. The steel tests specimens were fabricated in the shop of ARECELORPROFIL in Luxembourg.

Figure 1. Final deformation of the tested structure (test 6)

A document dedicated to the experimental tests was prepared (Haremza et al., 2012a - see Annex A): the testing arrangement, the thermal and mechanical loadings, the beam axial restraints to the beams

and the instrumentation of the sub-frames are described; the tensile coupon tests results are presented, and the seven sub-frame tests results are discussed in detail (for each test, global behaviour of the joint is described, and additional detailed results are provided for each loading step); finally, the comparison between the seven experimental tests is performed, and the effects of the temperature or the axial restraint to the beam are highlighted.

III. Behavioural response of the columns

The behaviour of columns under elevated temperatures was studied within two sophisticated studies: a benchmark example about a steel sub-frame subject to a natural fire, and a simple behaviour study of a column under elevated temperatures for the columns study.

III.1. Column benchmark

The column benchmark example was about a natural fire test on a fully loaded, two dimensional, unprotected steel framework carried out in a purpose-built compartment in Cardington (Franssen et al., 1995). The main objective of this work was to validate the utilisation of the finite element programs that were used during the present project for FEM simulations of steel structures subjected to fire. Three FE programs were used: i) the specialized homemade finite element software dedicated to the analyses of structures subjected to fire, SAFIR (Franssen, 2005), used by the University of Liege (ULGG), ii) the commercially available program Abaqus (2007) used by the University of Coimbra (FCTUCOIMBRA) and iii) the homemade finite element program ADAPTIC (Izzuddin, 1991), used by the Imperial College of London (ICST).

A document dedicated to the column benchmark was prepared (Haremza et al., 2010 - see Annex B) and presents the detailed comparisons between the three finite element programs results. The influence of the model definition, axial restraint to beam, frame continuity, thermal expansion and non-uniform temperature were analysed by the three programs, and were discussed. First, a thermal analysis was performed with SAFIR and Abaqus (ADAPTIC only deals with structural analysis) to obtain temperature distributions in the beam and the column. The results obtained by SAFIR and Abaqus showed a very good correlation. Then, for the structural analysis, results of the three programs for the reference frame and for each study case were compared; Figure 2 shows a) the beam vertical displacement and b) the axial force in the beam. Good correlations between the three FE programs Abaqus, SAFIR and ADAPTIC were shown, and they were validated for analysis of steel structures subjected to fire.

a)

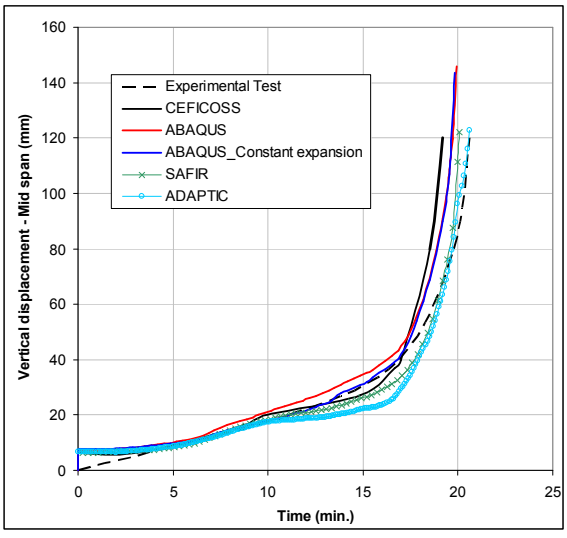

b)

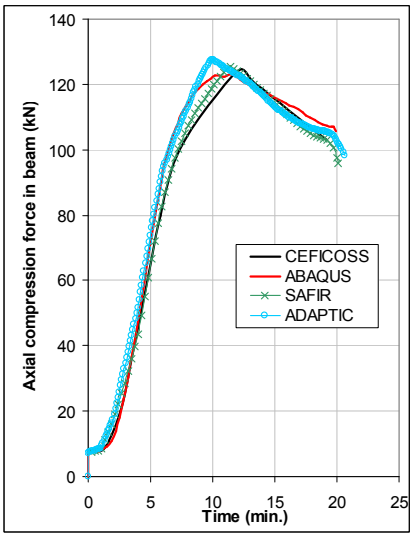

Figure 2. a) Vertical displacement of the beam; b) Calculated axial force in the beam

III.2. Behaviour study of a steel column subject to a localised fire

The purpose of this study was to show that the column completely loses any resistance once the localised fire develops around it, so that for the ROBUSTFIRE project studies, the column loss could be

assumed by the total removal of the column. The studied steel column is 3 m height, HEB 300 steel cross-section, class S460.

A document dedicated to the behaviour study of the column subject to elevated temperatures was prepared (Haremza et al., 2012b - see Annex C). Two alternative studies were developed: i) the column behaviour was analysed under constant temperatures, using the Eurocode 3 parts 1.1 and 1.2, and a numerical model; and ii) the column behaviour was analysed under localised fire, using the method described in Franssen (2000). It was shown that around 600ºC, the column is not able anymore to support the column axial force design value for the fire situation $N_{Ed,fi,20ºC}$ (2713 kN), and no residual resistance was observed.

IV. Behavioural response of the beams

A composite beam benchmark example was performed, in which composite beams were studied based on the paper published by Huang *et al.*, 1999. The latter selected two test programmes (one for ambient condition and one for fire condition) and compared these test results with the simulation results obtained from their in-house software VULCAN (Bailey, 1995). At ambient temperature, two simply-supported composite beam tests (Tests A3 and A5) conducted by Chapman and Balakrishnan (1964) were considered. For the elevated temperature conditions, two fire tests (Tests 15 and 16) on simply-supported composite beams conducted by Wainman and Kirby (1988) were referred to. Within this project, the structural behaviour of the tests was simulated using the commercially available program Abaqus (2007) and the homemade FE program ADAPTIC (Izzuddin, 1991). A document dedicated to the behaviour study of the composite beams at ambient and elevated temperature was prepared (Fang et al., 2010 - see Annex D): the corresponding response predicted by ADAPTIC, Abaqus, VULCAN and the test results were detailed and good correlation was observed (Figure 3 shows the comparison of temperature-deflection response for Tests 15 and 16), but small discrepancies existed between the numerical results and the test results, particularly for Test 16 at elevated temperature. These differences were due to the difficulties in building a perfect simple support condition in the furnace at elevated temperatures (Huang *et al.*, 1999). Additionally, three concrete-steel interactions were considered, namely, zero interaction, partial interaction and full interaction, respectively.

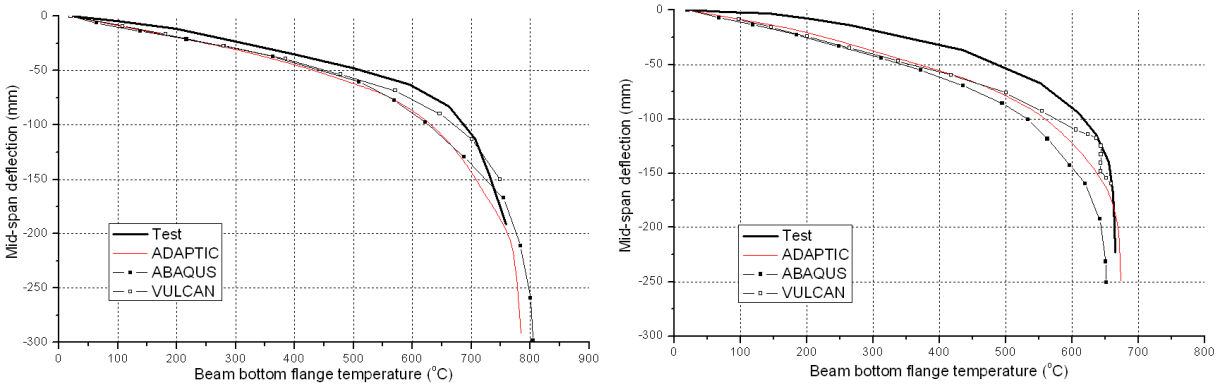

a) b)

Figure 3. a) Comparison of temperature-deflection response for Test 15; b) Comparison of deflection-temperature response for Test 16

Further to the benchmark study, composite beams with additional axial restraints were considered. For A3 and A5 (ambient cases), five levels of axial stiffness were assumed, namely, axially rigid, EA/L, 0.5EA/L, 0.2EA/L, and simply-supported, respectively, where EA/L is the axial stiffness of the bare steel beam (221.8kN/mm). With respect to Test 15 and Test 16 (elevated temperature cases), the restraining conditions of axially rigid, 0.2EA/L and simply-supported were assumed, where in these two tests EA/L was 254kN/mm. Good comparisons were achieved between the results obtained from ADPATIC and Abaqus.

V. Behavioural response of the joints

Two sophisticated models of joints were developed with the WP2: a component model (the 'joint benchmark'), developed to predict the response of joints under elevated temperature conditions, and a

thermal finite element model of a composite beam-to-column joint submitted to the standard temperature-time curve (ISO 834).

V.1. Joint benchmark

A component model in predicting the response of joints under elevated temperature conditions was proposed; this model was established in ADAPTIC (Izzuddin, 1991) employing spring and rigid link elements (the spring assembly for half of the joint model is illustrated in Figure 4). A document was prepared (Fang et al., 2011 - see Annex E) with the aim at validating the reliability of the proposed component model in predicting the response of joints under elevated temperature conditions: the modelling assumptions, the joint fire test and the component joint modelling are described in details. Failure of the joint in the component-based model is associated with tensile failure of the lowest bolt-row, where the elongation exceeds the allowed value of 25mm which is determined as one of the joint failure criteria for this study (see Annex E). Results from the ROBUSTFIRE joint tests were used for comparison, and good correlations were observed for test 2, but for tests 3 and 6 the initial stiffness is overestimated. The bending capacities were well predicted for all the three tests.

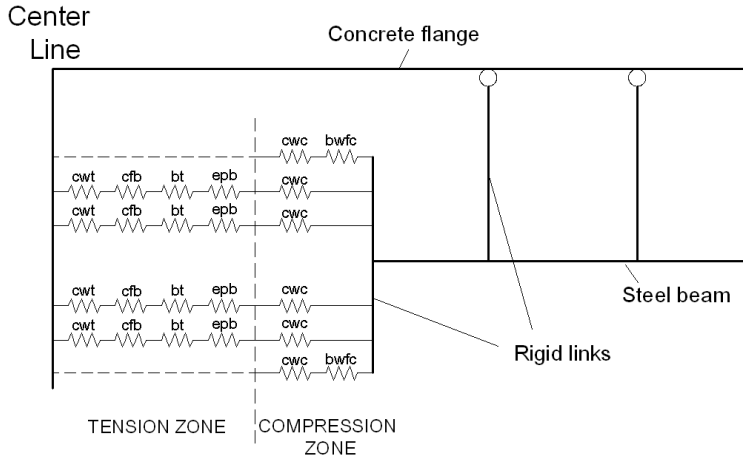

Figure 4. Frame model with joint components

V.2. Joint thermal finite element model

A thermal finite element model of a composite beam-to-column joint subject to the standard temperature-time curve (ISO 834) was developed. The studied joint links two IPE550 beams to a HEB300 column, and is the same as the one designed for the reference car park structure, investigated in the present project (the resistance of the joint is studied in Deliverable III (Haremza et al., 2012c), section II). A 12cm thick solid concrete slab is considered here instead of a composite slab. The temperature analysis was performed with the finite element software SAFIR (Franssen, 2005 and 2008), and Figure 5 shows the joint model.

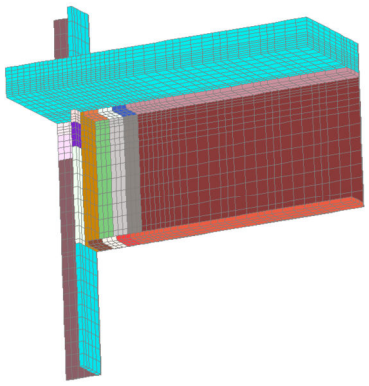

Figure 5. Joint model

A document dedicated to the joint thermal finite element model was prepared (Comeliau et al., 2012 - see Annex F) and the numerical model and the temperature distribution are described in details. Such simulations could be carried out for other limit conditions corresponding to particular fire scenarios or

for other joint configurations. The temperature of the different joint components at any moment during the fire can be deduced from these analyses, which is necessary to evaluate the joint resistance. Indeed, the material resistances decrease with the increase in temperature.

VI. Concluding remarks

Within this work package 2, behavioural models for beams, columns and joints were derived at two different levels: the FEM models (sophisticated level) and the designer's models (simplified level).

Seven experimental tests were performed on a composite steel-concrete beam-to-column frame under mechanical (bending and axial forces) and thermal loadings (constant temperature equal to 20ºC, 500ºC or 700ºC). The tests results were analysed in detail, and they allowed the calibration of the sophisticated joint benchmark (component model in predicting the response of joints under elevated temperature conditions), as well as the simplified joint model (analytical method predicting the resistance of steel or composite joints submitted to both an axial force and a bending moment at elevated temperature - see Deliverable III (Haremza et al., 2012c), section II). Additionally to the joint benchmark, a sophisticated thermal model studied the evolution of the temperature distribution within a composite beam-to-column joint subjected to the standard fire curve.

The behavioural response of the heated beams and columns was studied: i) the column benchmark was performed by three FE programs SAFIR, ADAPTIC and Abaqus, and results were compared to experimental results described in Franssen et al. (1995); ii) a simple study of the columns subject to localised fire was detailed, and it was shown that the column loss can be assumed by the total removal of the column; and finally, iii) the composite beam benchmark was developed using ADAPTIC (Izzuddin, 1991) and Abaqus (2007), and models were calibrated against experimental results from Huang et al. (1999). Good consistency of the results obtained from the three software's SAFIR, ADAPTIC and Abaqus was showed. Moreover, the influence of various parameters on the response of the elements (acting forces, axial restraint to beam, distribution of temperatures, level of temperatures, …) was investigated in these models, and the so-validated tools for the investigation of the structural components are used in WP3 when investigation the sub-structures and the structures at the simplified and sophisticated levels (see Deliverables IV and V, in Fang et al., 2012a and 2012b).

VII. References

Abaqus (2007) Theory Manual & Users Manuals, Version 6.7, Hibbitt, Karlsson and Sorensen, Inc. USA.

Bailey CG. (1995). "Simulation of the structural behaviour of steel-framed buildings in fire", PhD thesis, The University of Sheffield, UK.

Chapman J.C., Balakrishnan S. (1964). "Experiments on composite beams", The Structural Engineering, 42(11), 369–83.

EN 1993-1-1:2005 – "Eurocode 3: Design of steel structures – Part 1-1: General rules and rules for buildings", European committee for standardization, May 2005.

EN 1993-1-2:2005. "Eurocode 3: Design of steel structures – Part 1-2: General rules – Structural fire design". European committee for standardization, April 2005.

Fang C., Izzuddin B. A., Elghazouli A. Y., Nethercot D. A., Haremza C., Santiago A., Simões da Silva L. (2010). "ROBUSTFIRE report - Benchmark Study of Composite Beams", Internal Report, Imperial College London.

Fang C., Izzuddin B. A., Elghazouli A. Y., Nethercot D. A. (2011). "ROBUSTFIRE report – Component modelling of sagging composite joints under fire", Internal Report, Imperial College London.

Fang et al. (2012a). "Deliverable IV: Development of FEM model for car parks under localised fire", Robustness of car parks against localised fire, Grant Agreement Number RFSR-CT-2008-00036.

Fang et al. (2012b). "Deliverable V: Practical behavioural models for car park structures towards design practice", Robustness of car parks against localised fire, Grant Agreement Number RFSR-CT-2008-00036.

Franssen J.-M. (2000). “Failure temperature of a system comprising a restrained column submitted to fire”, Fire Safety Journal, 34, p191-207.

Franssen J.-M. (2005). “SAFIR – A Thermal/Structural Program Modelling Structures under Fire”, Engineering Journal, A.I.S.C., 42(3), 143-158. 2005.

Franssen J.-M. (2008). “User’s manual for SAFIR 2007a – A computer program for analysis of structures subjected to fire”, University of Liège, Belgium, January 2008.

Franssen J.-M., Cooke G.M.E., Latham D.J. (1995). “Numerical Simulation of a Full Scale Fire Test on a Loaded Steel Framework”. Journal of Constructional Steel Research, 35, 377-408, 1995.

Franssen J.-M., Kodur V.K.R., and Mason J. (2000). “User Manual for SAFIR 2001, A computer program for analysis of structures submitted to the fire”, University of Liège, Belgium.

Haremza C., Santiago A., Simões da Silva L., Fang C., Izzuddin B. A., Elghazouli A. Y., Nethercot D. A., Ly H., Jaspart J.-P., Demonceau J.-F., Franssen J.-M., Hanus F. (2010). “ROBUSTFIRE Project – Document 4 – Benchmark example 1: Column_v3(2)”, Internal Report, University of Coimbra.

Haremza C., Santiago A., Simões da Silva L. (2012a). “ROBUSTFIRE Project – Document 6 – Experimental tests_v2(1)”, Internal Report, University of Coimbra.

Haremza C., Santiago A., Simões da Silva L. (2012b). “ROBUSTFIRE Project – Document 7 – Behaviour study of columns subject to fire”, Internal Report, University of Coimbra.

Haremza et al. (2012c). “Deliverable III: Development of simplified behavioural models”, Robustness of car parks against localised fire, Grant Agreement Number RFSR-CT-2008-00036.

Huang Z., Burgess I.W., Plank R.J. (1999). “The influence of shear connectors on the behaviour of composite steel-framed buildings in fire”, Journal of Constructional Steel Research, 51, 219-237.

Izzuddin B.A. (1991). “Nonlinear Dynamic Analysis of Framed Structures”, PhD Thesis, Department of Civil Engineering, Imperial College, University of London, London, UK.

Wainman D.E., Kirby B.R. (1988). “Compendium of UK standard fire test data, unprotected structural steel – 1”, Ref. No. RS/RSC/S10328/1/87/B. Rotherham (UK): Swinden Laboratories, British Steel Corporation.

ANNEX A – Experimental tests

Departamento de Engenharia Civil
Faculdade de Ciências e Tecnologia da Universidade de Coimbra

ROBUSTFIRE Project

Document 6: Experimental tests_v2(1)

Cécile Haremza
Aldina Santiago
Luís Simões da Silva

January 2012

TABLE OF CONTENTS

I Introduction

I.1 Composite steel-concrete open car park building

During the European project ROBUSTFIRE, a standard open car park structure (Figure 1) was specially designed for the project (Gens, 2010). This building was chosen to be the most general possible in order to obtain, at the end of the project, general rules on the design of such structures that ensure sufficient robustness under fire conditions The selected structure is a braced open car park structure with eight floors of 3 m height, composite slabs, composite beams and steel columns. The steel beam sections are made with IPE, grade S355, and steel column sections are made with HEB profiles, grade S460.

The experimental testing procedure performed within the ROBUSTFIRE project was based on the experimental test performed at the University of Liege in 2007 by Demonceau (Demonceau, 2008), and outlined in the following section (§I.2).

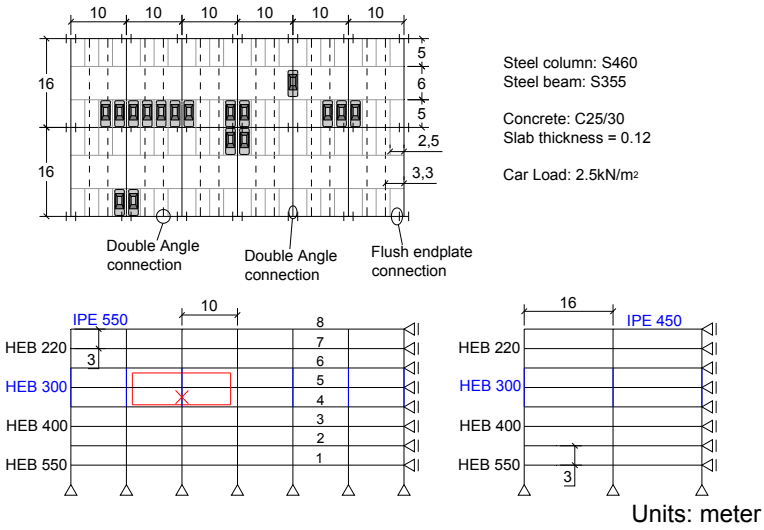

Figure 1: Steel composite open car park building

I.2 Outline of the test realised by Demonceau

The aim of the Demonceau test was to study the behaviour of a composite structure subject to the loss of a column at ambient temperature (Demonceau, 2008). The tested sub-structure was extracted from an actual composite building composed of three main frames spaced of 3 m, and three storeys (Figure 2). The bottom storey was isolated from the internal frame, and the sub-structure width was reduced according to the laboratory facilities.

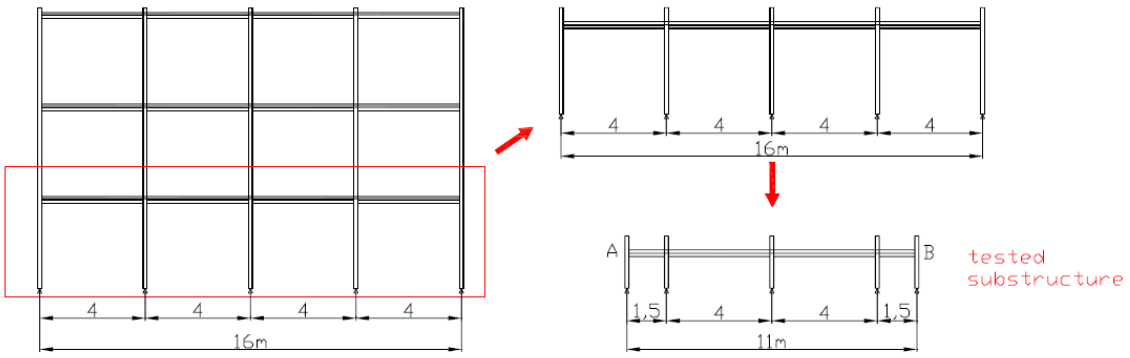

Figure 2: From the actual frame to the tested sub-structure (Demonceau, 2008)

The sub-structure test configuration is shown in Figure 3. Steel columns were HEA 160, grade S355. Steel beams were IPE 140, grade S355, and 12 cm of a reinforced concrete slab (C25/30) was fully connected to the steel beam. Flush end-plate connections were used for all the beam-to-column connections. The behaviour of the composite internal joint (Beam B – Column C) was studied when the sub-frame was subjected to the loss of the column.

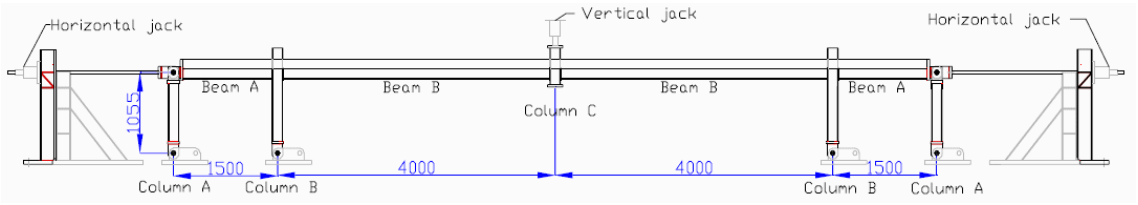

Figure 3: Sub-structure configuration tested at the University of Liege (Demonceau, 2008)

The lateral restraints coming from the undamaged structure and influencing the catenary action were computed through an elastic linear analysis. They were placed at each side of the test in order to induce a symmetric response (Figure 4), and were simulated by two horizontal jacks, able to apply a maximum load of 160 kN (Figure 3). The restraint was assumed to be elastic during the entire test.

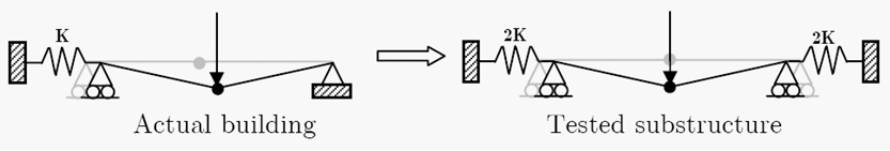

Figure 4: Symmetric response of the tested sub-structure (Demonceau, 2008)

The column in the centre was simulated at the beginning of the test by two locked jacks (Figure 5a). During the test, the load path was the following: A) Application of a uniformly distributed load on the beams (with steel plates and concrete blocks) equal to 6kN/m, the maximum load safely applicable in the laboratory. The purpose was to simulate the reaction of the concrete slab on the main frame in the actual building; B) Progressive removal of the column by unlocking the jacks (all the actions were applied statically to observe the physic phenomena linked to the loss of a column in a frame and to be able to measure

all the displacements, rotations, loads and strains). The free deflection of the system was observed; C) Application of a vertical load with two jacks on the column to increase the deformation (Figure 5b)).

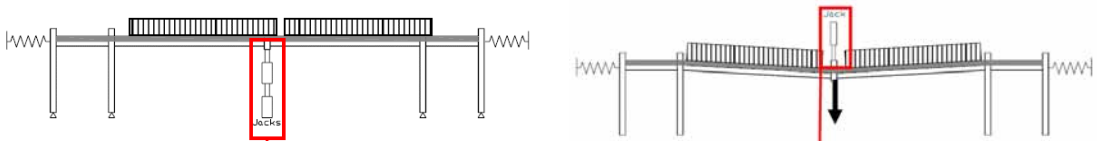

a) b)

Figure 5: a) Column at the middle simulated by two locked jacks; b) Application of a vertical load with two vertical jacks (Demonceau, 2008)

The maximum vertical load applied by the vertical jack was 120-130 kN, with a corresponding maximum deflection at the middle of around 750 mm.

I.3 Objectives of the tests performed at Coimbra

The main objective of the experimental tests was to observe the combined bending moment and axial loads in the heated joint when catenary action develops in the frame after the loss of the column. The effect of the localised fire (that led to the column loss) was simulated by the application of elevated temperatures in the composite joint zone. According to previous experimental works performed in real composite steel-concrete open car park buildings subjected to fire, a majority of the temperatures measured in the beam bottom flanges were lower than 500ºC; however temperatures of 700ºC were observed in recent tests performed in France (Jaspart et al., 2008), probably due to the manufacture evolution of cars, with more combustible plastic materials as well as higher petrol tank capacity. Seven beam-to-column sub-frames were tested in Coimbra: one reference test at ambient temperature; five tests at 500ºC or 700ºC; and a demonstration test, for which the sub-frame was subjected to an increase of the temperature up to the failure of the column. The effect of the axial restraint to beam coming from the unaffected part of the building was also studied: two tests without axial restraints to the beam; two tests with total axial restraint to the beam; and three tests with realistic axial restraint to the beam. Table 1 presents the objectives of each test.

Table 1: Objectives of the seven experimental tests of sub-frames subject to the loss of a column

Test	Objectives
T1	Derivation of the joint M-N curve at ambient temperature – Realistic axial restraint to the beam. *Due to testing problems, this test was performed without any axial beam restraint (see §II.7.2.3), and only the joint properties at ambient temperatures were derived.*
T2	Derivation of the joint properties at 500ºC – No axial restraint to the beam
T3	Derivation of the joint properties at 700ºC – No axial restraint to the beam
T4	Derivation of the joint M-N curve at 500ºC – Total axial restraint to the beam
T5	Derivation of the joint M-N curve at 700ºC – Total axial restraint to the beam
T6	Derivation of the joint M-N curve at 700ºC – Realistic axial restraint to the beam
T7	Demonstration of the real joint behaviour of a sub-frame subjected to the loss of a column due to a localised fire – Realistic axial restraint to the beam

II Experimental tests

II.1 Extracted sub-frame tested at Coimbra University

The two dimensions sub-frame was selected from the fifth floor of the typical composite steel-concrete car park building (see Figure 1). Because of the restrictions from the laboratory dimensions, the beam length was reduced from 10 m in the real building to 3 m in the sub-frame to be tested. Figure 6 presents the seven beam-to-column sub-frames tested in Coimbra, including the corresponding studied axial restraint to the beam.

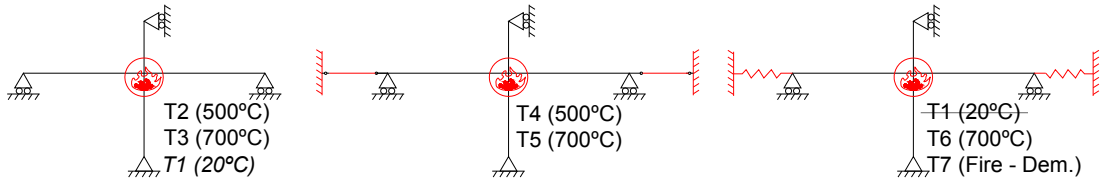

Figure 6: Seven experimental tests

II.2 Testing arrangement

Each sub-frame was defined by two unprotected composite beams with IPE 550 steel cross-sections, grade S355, and one unprotected HEB 300 cross-section steel column, grade S460 (Figure 7). A reaction frame perpendicular to the plane of the sub-frame supported the hydraulic jack at the column top, which was linked by a pin to the top of the column. The column base was hinged and fixed to a reinforced concrete footing. The two vertical supports of the beams ends were columns HEB 220 cross-sections, each being laterally restrained by four diagonals HEB 140 cross-sections. These members were all bolted at the base on two steel footings. The two steel footings and the concrete footing corrected the irregularities of the floor and were secured in vertical position by Dywidag bars passing through the laboratory strong floor. The three footings were also connected horizontally using steel profiles. When the axial restraint to the beam was simulated, the beam restraints were connected to the two strong walls via horizontal HEB 300 cross-section beams, reinforced by bracing diagonals (linked to the strong wall by Dywidag bars passing through the 5 m wall). The column was restrained: i) at the top of the joint (lateral restraint in Figure 8), and ii) at the bottom column (column restraint in Figure 7). This restraints system allowed vertical displacements of the column, and prevented any horizontal displacement or rotation in the plane or out of the plane of the sub-frame.

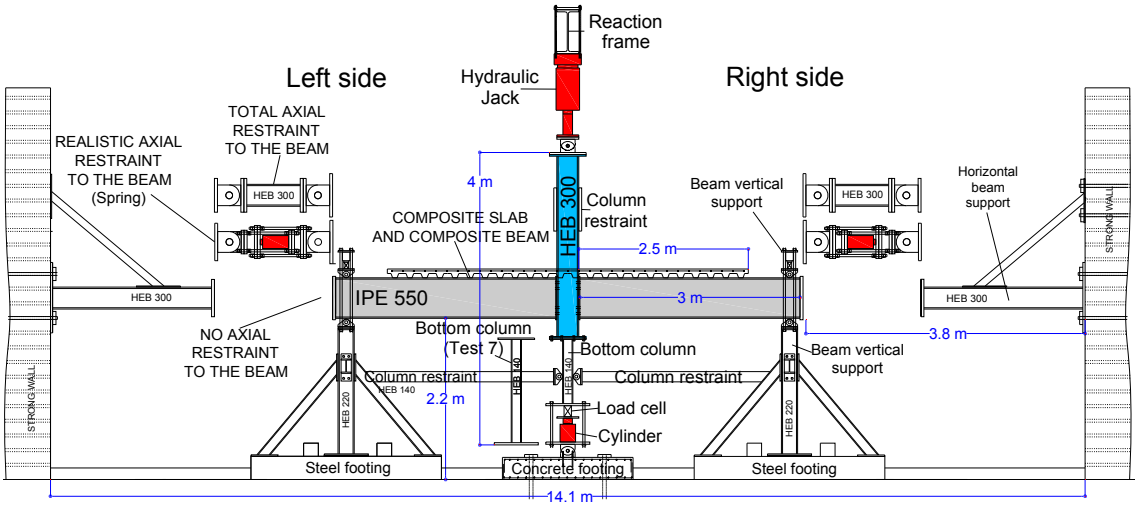

Figure 7: General layout, longitudinal view

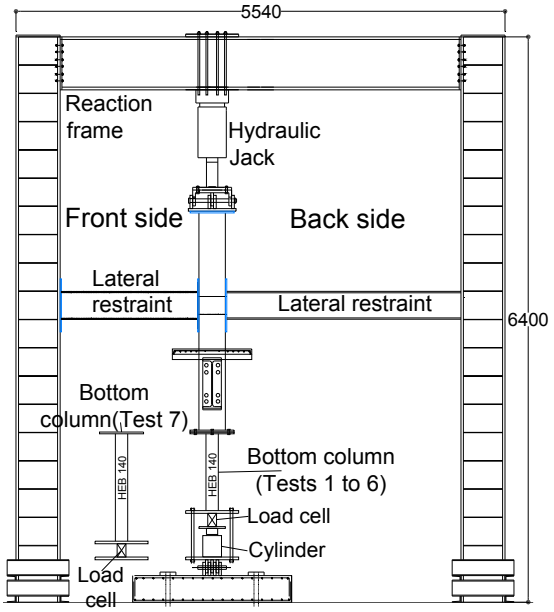

Figure 8: General layout, lateral view

II.3 Joint configuration

Figure 9 shows the composite joint, which is representative of usual joint typologies used in open composite steel-concrete car park structures. Bolts M30, cl. 10.9, and a steel end-plate of 15 mm thick, S355, were used. In order to ensure the composite behaviour of the beam-to-column joint, ten steel rebars of diameter 12 mm were placed in the composite slab (five at each side of the column). The composite joint was designed by the coordinator of the ROBUSTFIRE project, the University of Liège (Demonceau, 2009).

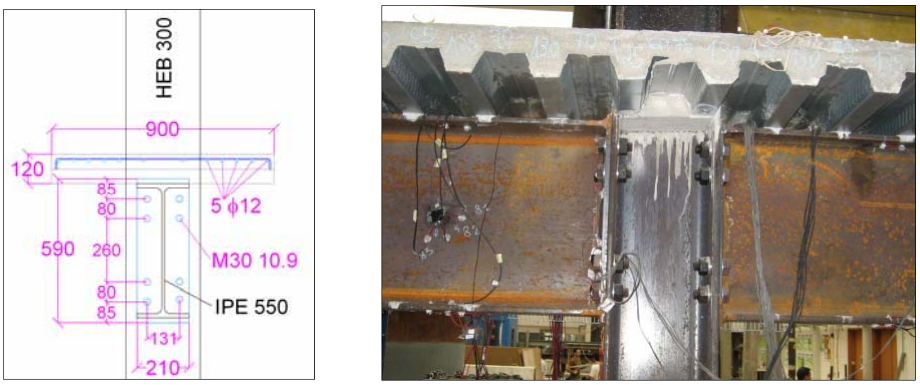

Figure 9: Tested joint

II.4 Composite slab reinforcement and studs

The composite slab was of steel deck and light-weight in-situ concrete composite floor, and had 900 mm width, 1 mm thick steel sheeting and reinforced concrete C25/30. Note that the studied joint was a main joint (main beam linked to the flanges of the column). In practice, the ribs of the steel sheeting should be installed parallel to the beam span. But in the laboratory, the ribs were positioned perpendicularly to the beam in order to facilitate the concreting. Nevertheless, difficulties were experienced during concreting and the average total slab thickness was 130 mm instead of the 120 mm defined by Gens (2010) and shown in Figure 10.

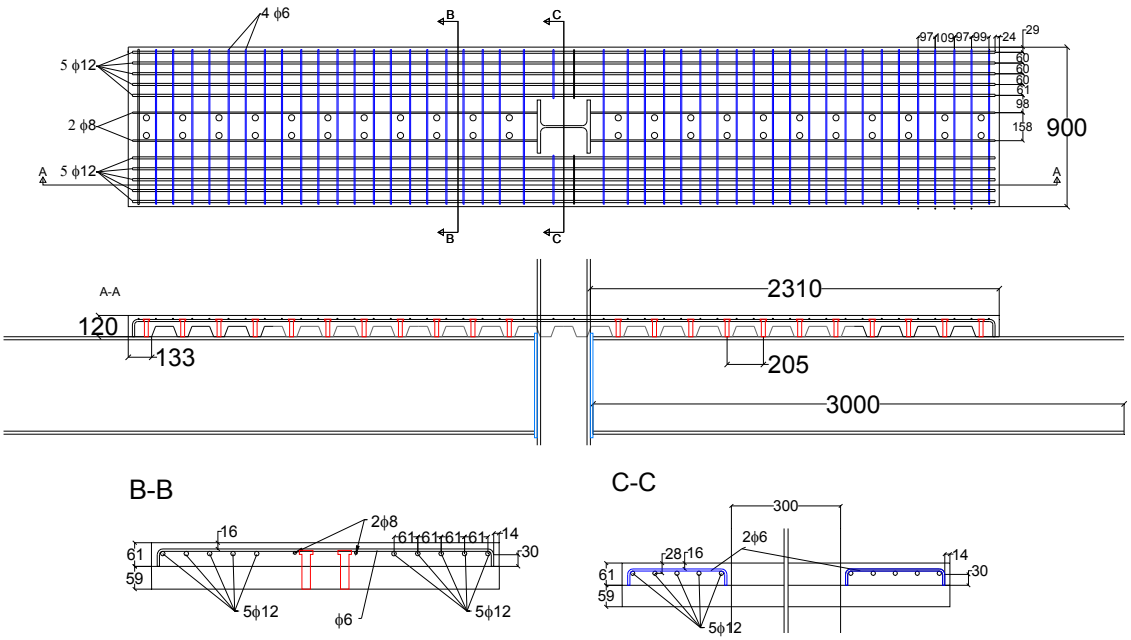

Figure 10: Composite slab and steel rebars

In practice, the ten 12 mm rebars should only be added to the mesh of the slab in the joint zone. In the laboratory, these rebars also worked as longitudinal rebars along the entire slab, and constructional longitudinal (8 mm diameter) and transversal rebars (6 mm diameter) were added notably to respect the maximum spacing defined by Eurocode 4 part 1.1 (EN 1994-1-1:2004). The steel beam was fully connected to the composite slab by 22 shear studs

(diameter = 19 mm; height = 100 mm). The beam was not composite all along its length (Figure 7); in order to apply the initial hogging bending moment in the sub-frame, a steel beam was considered to apply the restraints to the vertical displacements of the beams ends (see §II.6.1.2). This structural consideration was accepted because the reduced slab length was sufficient for the anchorage of the steel rebars included in the behaviour of the composite joint.

II.5 Description of the loading sequence

II.5.1 Tests 1 to 6

Each test, from test 1 to test 6, was divided into 3 main steps (see Figure 11): step 1 - application of an initial hogging bending moment in the joint; step 2 - heating of the joint zone up to 500ºC or 700ºC (except for test 1 at 20ºC); and step 3 - simulation of the loss of the column and increase of the sagging bending moment up to the failure of the joint.

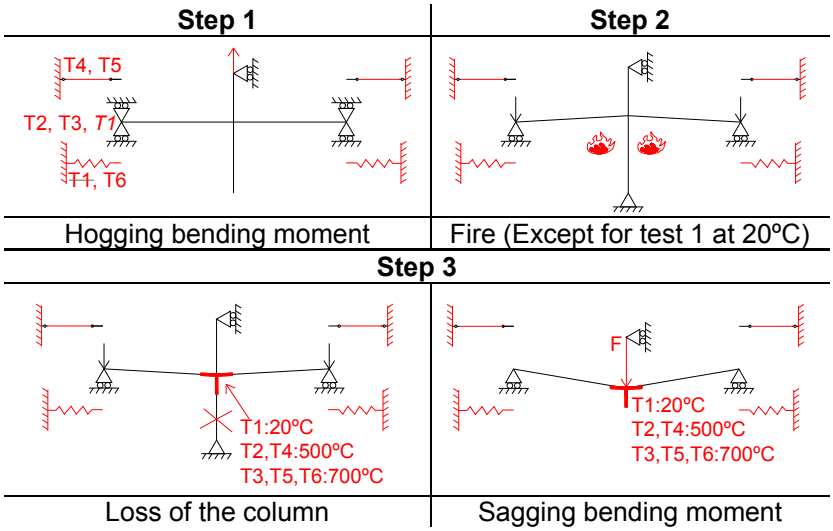

Figure 11: Outline of the tests 1 to 6

Step 1 simulated the internal loads in the connection as in the real car park structure; a hogging bending moment equal to -450 kNm was applied in the joint for the test 1 at ambient temperature; this value was calculated in a simple 2D model in Abaqus (2007), considering the loads at the service limit state (SLS) defined during the design of the car park building (Gens, 2010). According to Eurocode 1 part 1.2, effects of actions under fire may be deduced from those determined in normal temperature design, by calculating the reduction factor η_{fi}, resulting in a target hogging bending moment of -236 kNm for tests 2 to 7:

$$\eta_{fi} = \frac{G_k + 0.5Q_{k.1}}{1.35G_k + 1.5Q_{k.1}} = 52{,}53\%$$

where $G_k = 26.4\ kN/m$ and $Q_{k.1} = 26.7\ kN/m$.

The load to be applied by the jack was deducted from the bending moment calculation of an equivalent cantilever beam subjected to a single load at its end: M = F x L.

During step 2, temperatures increased with a linear rate, up to reach 500ºC in tests 2 and 4, and 700ºC in tests 3, 5 and 6, in beam bottom flange (see

§II.6.2.1). Finally, temperatures were kept constant during the entire step 3, for which the progressive loss of the column was simulated (by removing the cylinder from the column base, see II.6.1). Then, the vertical load at the column top was increased in the downward direction in order to increase the sagging bending moment in the joint and to reach the joint failure. During the increase of the sagging bending moment, the column was assumed to be completely failed.

II.5.2 Test 7

The loading sequence and the loads values were chosen in order to reach: i) the buckling of the bottom column due to the increase of temperatures (Figure 7, steel profile HEB 140, S355); ii) the progressive collapse of the sub-frame after the loss of the column. As shown in the Figure 12, the following load path was planned: step 1 - application of an initial hogging bending moment in the joint (-236 kNm, see §II.5.1); step 2 - application of a constant load (+250 kN) at the column top; step 3 - heating of the joint zone and the bottom column respectively up to 400ºC and 800ºC; step 4 - heating of the joint zone up to the failure of the sub-frame.

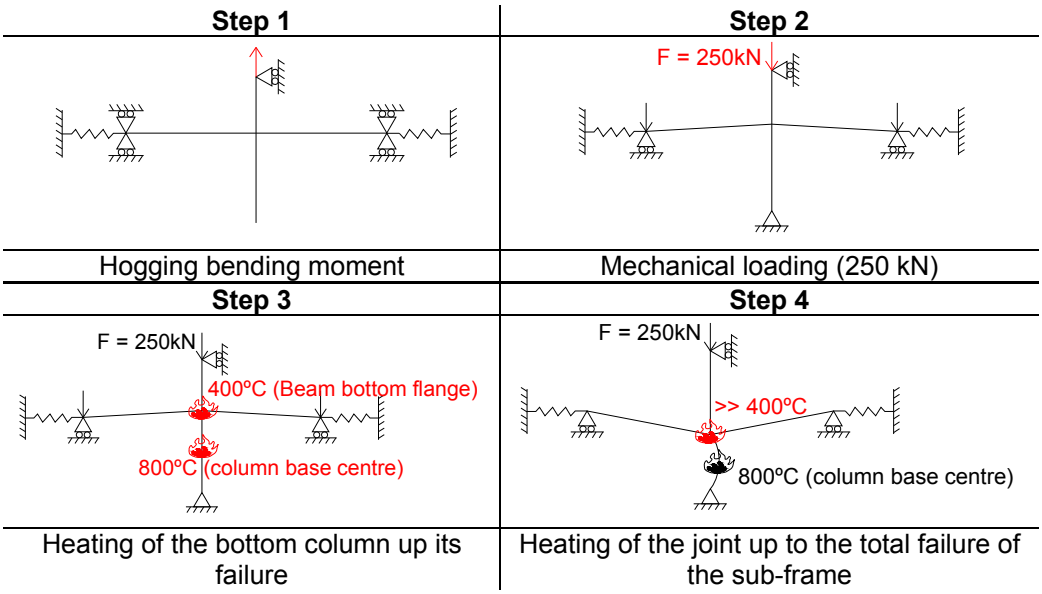

Figure 12: Outline of the test 7

The mechanical loading of the sub-frame in steps 1 and 2 was applied at the column top by the hydraulic jack, and was kept constant during the entire test. The realistic value of the compression load in the column as in the real car park building should be 2713 kN (according to a 2D numerical model performed in Abaqus (2007), in fire situation). However, the jack capacity was limited to 1000 kN, and the steel section of the lower part of the column was reduced from HEB 300 to HEB 140 for the experimental test. The load to be applied should be sufficient to reach the buckling of the bottom column under high temperatures: the critical temperature of the steel profile HEB 140 (1.3 m long and steel S355) was calculated equal to 696ºC under 250 kN of compression load.

In step 3, the temperature was increased up to: i) 800ºC in the bottom column in order to reach the critical temperature of the steel profile and the complete loss of the column; ii) 400ºC in the joint (measured in the beam bottom flanges). The

joint temperature was limited in order to avoid the joint failure once the column fails, it was based on the previous tests results. Finally, in step 4, after the column loss, the joint temperature was increased up to the failure of the sub-frame. The load at the column top (250 kN) and the temperature in the bottom column (800ºC) were kept constant.

II.6 Loading definition

II.6.1 Mechanical loading

II.6.1.1 The hydraulic jack at the column top

The mechanical loading at the column top was applied by the Servosis hydraulic jack (Figure 13), which has a capacity $F_{max.}$ = 1000 kN and a maximum stroke $\Delta_{max.}$ = 280 mm.

Figure 13: Hydraulic jack at the column top

The hydraulic jack was controlled in term of load during the application of the hogging bending moment (step 1) and the increase of temperatures (velocity of 0.08 Tm/s). In tests 2 to 6, in step 2 (heating), the jack applied a constant load equal to 0.1 Tf at the top of the column, in order to let the column free to expand under elevated temperatures (this load should not influence the behaviour of the structure). Under sagging bending moment (step 3), the jack was in displacement control (according to the test, the velocity was equal to 0.01 mm/sec, 0.02 mm/sec or 0.03 mm/sec. The hydraulic jack stroke (Δ_{max} = 280 mm) was increased in tests 1, 3, 5, 6 and 7 under the sagging bending moment. The load applied by the hydraulic jack had to be removed from the sub-frame, and the following phases were performed:

1. Except for the test 7, some steel bars were put at the column base in order to fix the vertical position of the sub-frame (Figure 14a). It was not possible to do the same for the test 7, and two steel profiles were put at each side of the slab and were linked to the ground by dywidag bars in order to fix the vertical position of the sub-frame (Figure 14c);

2. The column was gradually unloaded (and the vertical displacement of the sub-frame remained constant);
3. Some steel plates were inserted between the jack pin and the column top (Figure 14c);
4. The sub-frame was progressively reloaded.

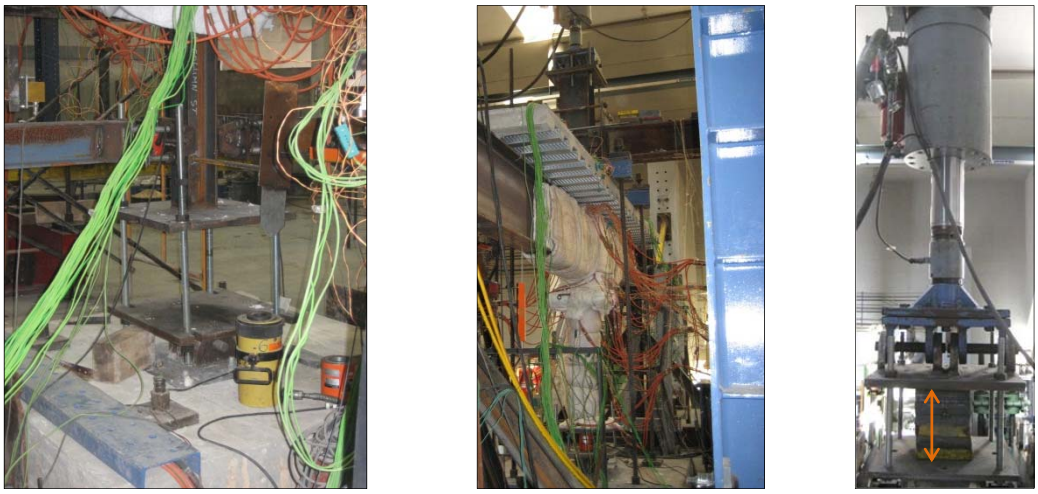

a) b) c)

Figure 14: Increase of the hydraulic jack stroke

In order to define the required capacities of the load cells, displacement transducers and hydraulic jack, preliminary numerical simulations were performed and estimated the global behaviour of the sub-frames to be tested in the laboratory. The non-linear finite element package Abaqus (2007) was used to perform the structural model. Beam and shell elements were used to model beam/column, and concrete slab respectively (Figure 15). A static general analysis was performed with thermal and mechanical loadings. No initial imperfections were applied, but geometrical and material non linearities were taken into account. Materials temperature dependent properties were defined according to Eurocode 3 part 1.2 and Eurocode 2 part 1.2. The thermal expansion coefficient was defined constant equal to 1.4 x 10^{-5} /ºC and 1.8 x 10^{-5} /ºC for steel and concrete respectively.

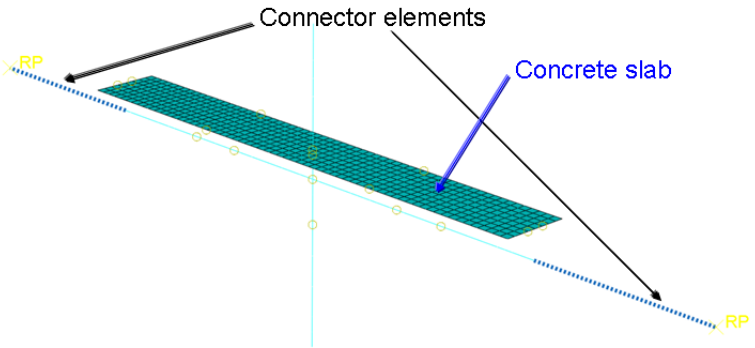

Figure 15: Simplified model of the sub-structure to be tested

II.6.1.2 The beams vertical displacements restraints

Figure 16 shows the beam support, which restrained any vertical displacements of the beam end, in order to apply the hogging bending moment at the joint during steps 1 and 2. A load cell and a cylinder were located on the beam top flange in order to measure the reaction loads and to apply the initial pre-loading (see §II.6.1.3). This system of support allowed the free horizontal displacement of the beams thanks to two pins.

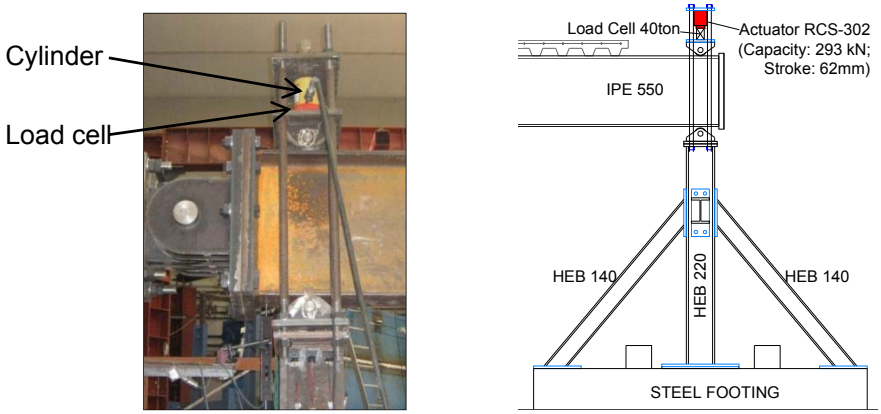

Figure 16: Beam support (vertical displacement restrained using steel bars)

II.6.1.3 The application of the joint hogging bending moment

The initial hogging bending moment was introduced to the sub-frame using the hydraulic jack at the top of the column (Figure 17): i) any vertical displacement of the beams ends was restrained at the supports (see Figure 16), and a pre-load was applied, using the cylinders, in order to keep constant the beam position (the column was free at the base); ii) the hydraulic jack increased the vertical load at the column top and pulled the column upwards; iii) the support at the column base was put in contact; iv) the load at the column top was decreased and transferred to the column base support.

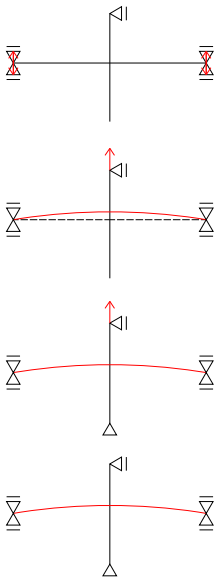

Pre-loading at the beams supports (using the cylinders)

Loading at the column top (hydraulic jack): a tensile load was applied by the jack.

Application of the column base support (cylinder)

Decrease of the tensile load at the jack and transfer of the load to the column base support

Figure 17: Initial hogging moment in the joint

II.6.1.4 Progressive loss of the column in tests 1 to 6

Figure 18 shows the hydraulic cylinder located at the column base (except for the last test 7), which simulated the loss of the column. This cylinder kept a constant vertical displacement of the column during the application of the initial loads and the increase of temperatures, and was finally taken out by decreasing the oil pressure in order to simulate the column loss. During the heating phase (step 2) of tests 2 to 6, the axial load in the column was varying because of the thermal expansion of the column, and the oil pressure in the cylinder was adapted to keep the constant vertical position. Once the axial load decreased due to loss of resistance, the four vertical bars (Figure 18) prevented, as far as possible, the vertical displacements in the upwards direction.

The smaller steel profile HEB 140 cross-section was used at the bottom column in order to facilitate the concreting: the composite sub-frame could be located at the floor level, as shown in Figure 19.

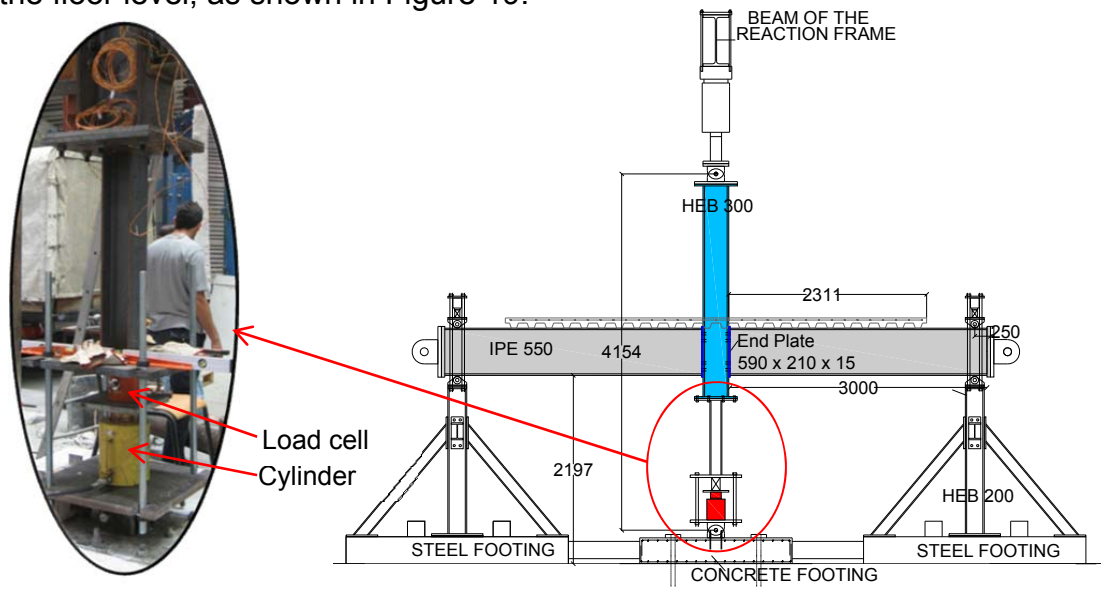

Figure 18: Loss of the column

Figure 19: Specimens after the concreting of the composite slabs, at the floor level

II.6.2 Thermal loading

II.6.2.1 Tests 2 to 6

Steel temperatures were increased using Flexible Ceramic Pad (FCP) heating elements. The heated zone consisted of a length around 0.6 m of beam at each side of the joint, of the bolts and of 1 m of column (Figure 20).

Figure 20: Heated connection zone using Ceramic Pad Heating elements

The FCP heating elements were positioned in alternation on the beam web and the column web, with one element on one side, the next one on the other side, etc… (Figure 21). The elements were connected to the 6 channels of the 70 kVA transformer (Figure 23a, b). One FCP element has a power of 2.7 kW, and four FCP elements can be connected to each channel, with maximum 24 resistances can be connected to the transformer. The control of temperatures was automatic thanks to the programmer, which is connected to the transformer: the heating rate and the target temperature were defined (Figure 23c). Six thermocouples (one at each channel) were connected to the programmer and controlled the evolution of the temperatures in six points of the sub-frame. They were located in the beams bottom flanges, at 25 cm from the connection. Rock-wool was used for thermally insulating the heating elements, as shown in Figure 22.

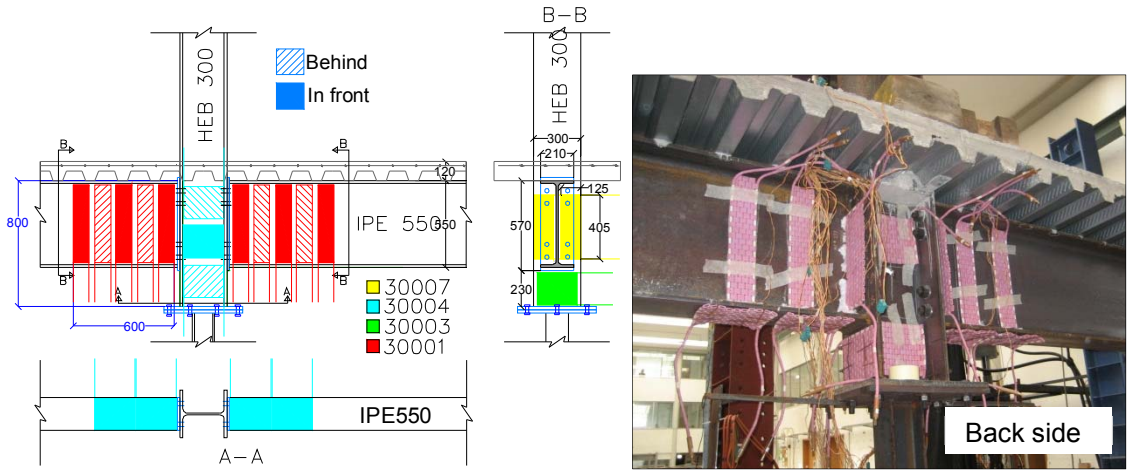

Figure 21: Position of the 23 ceramic pad heating elements

Figure 22: Thermal insulation of the ceramic pad heating elements (rock-wool of density 128kg/m^3)

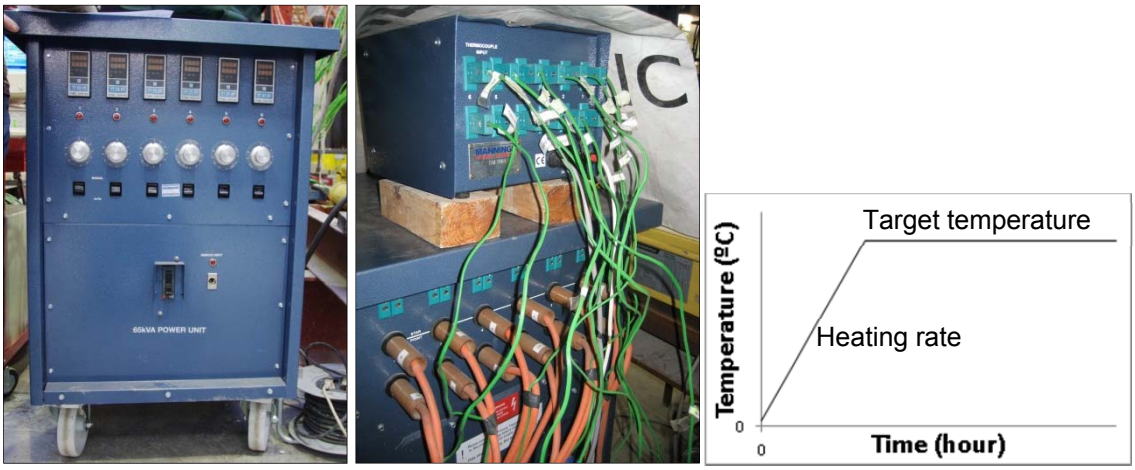

a) b) c)

Figure 23: a) 70 kVA transformer; b) cable connections (from the FCP elements to the transformer and from the thermocouples to the programmer)

A slow heating rate (around 300ºC/hour) was used for tests 2 to 6; this heating rate is far from the ISO 834 nominal curve but allowed a better control of the sub-frame behaviour. When the temperature reached 500ºC or 700ºC in the beam bottom flanges, the increase of the temperature was stopped and temperatures remained constant until the end of the test.

II.6.2.2 Test 7

In the demonstration test, the lower part of the column was also heated, as shown in Figure 24.

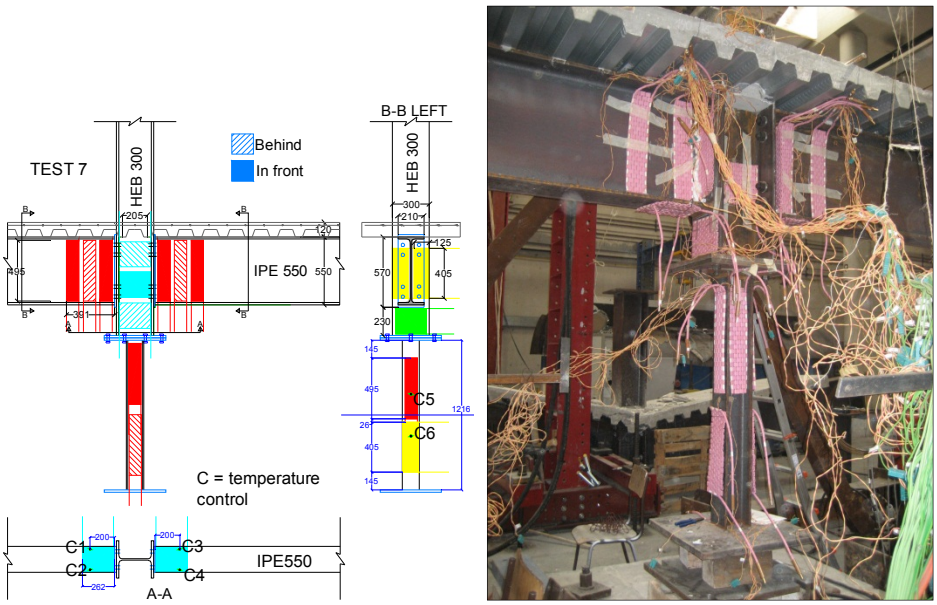

Figure 24: Heated zones

The evolution of the temperature for the joint zone (4 channels of the transformer) was automatically controlled by the programmer (step 3 - first increase up to 400ºC with a slow heating rate equal to 200ºC/hour, then step 4 - increase up to 800ºC with a heating rate equal to 300ºC/hour). The heating of the bottom column was not controlled by the programmer (manual mode) and the bottom column was heated at around 260ºC/hour, up to 800ºC. Six thermocouples controlled the evolution of the temperatures. Four were located in the beams bottom flanges, at 20 cm from the connection (C1 to C4 in Figure 24), and two at the bottom column, on the flange near the column lower part center (C5 and C6 in Figure 24). All the electrical elements were protected by rock-wool, as shown in Figure 25.

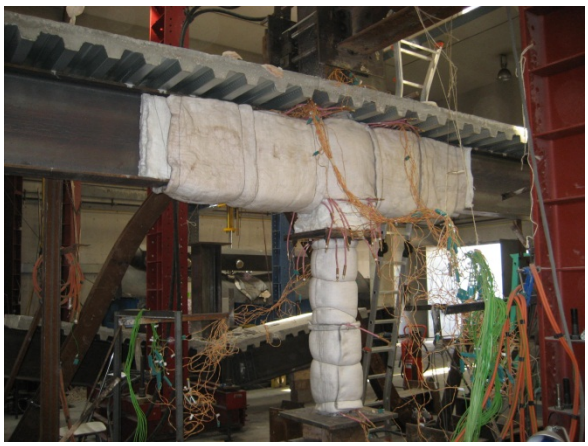

Figure 25: Thermal insulation of the ceramic pad heating elements (rock-wool of density 128kg/m^3)

II.7 Beam axial restraints

The effect of the axial restraint to the beam coming from the unaffected part of the building was studied, and three different restraints stiffness's were considered: tests 2 and 3 - no axial restraint to the beam; tests 4 and 5 - total axial restraint to the beam; and tests 1, 6 and 7 - realistic axial restraint to the beam. When no restraint was applied, the beams were free to displace and were not linked to the strong walls.

II.7.1 Total restraint

The beam was totally restrained in the axial direction by a steel profile HEB 300 that linked the end of the tested beams to strong walls. Each restraint was pinned and allowed the rotation. The axial force was deduced from the strains measured by five strain gauges: two on the top flange, two on the bottom flange and one on the web; in order to know the reaction force direction, the restraint rotation was deducted from the vertical displacements measured by displacements transducers (D023 and D024 in Figure 26).

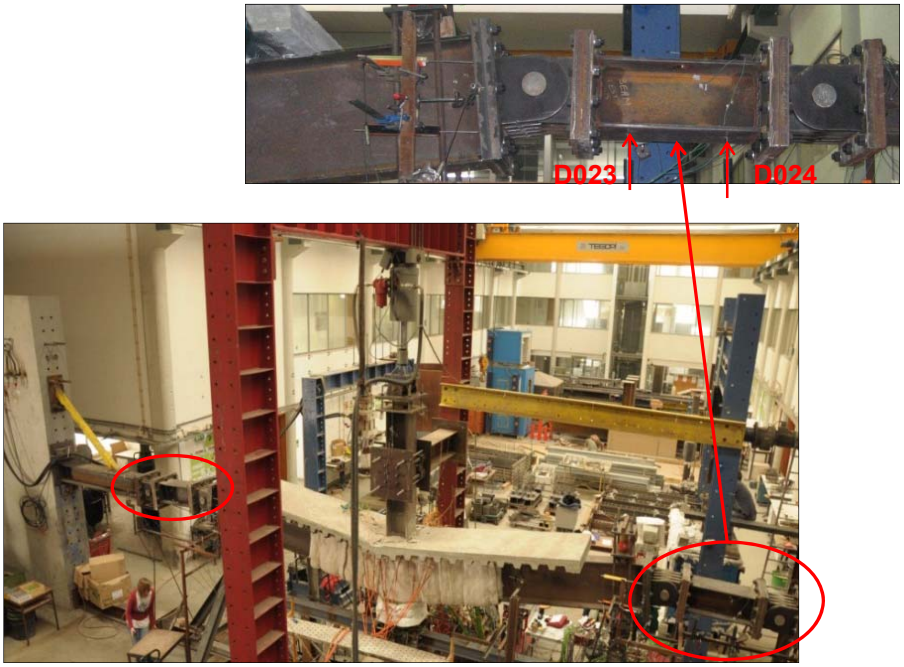

Figure 26: Total axial restraint to the beam

II.7.2 Spring restraint

II.7.2.1 The spring restraint in the real car park building

The realistic axial restraint to the beam provided by the part of the building not directly affected by the localised fire and the loss of the column was initially estimated by a simple elastic analysis performed in Abaqus (2007): five column loss locations at the fifth floor were simulated; Figure 27 presents the configuration of the loss of the middle column. A horizontal unitary load was applied at the beam-to-column connection level at the end of the sub-frame subjected to the loss of the column, and the displacement was measured. Table 2 presents the computed lateral restraint K of the equivalent single spring for

each loss of the column configuration. The smaller computed lateral restraint K of the equivalent single spring was 64.4 kN/mm. During the tests, two springs were applied at each beam ends to have symmetric deformations. The stiffness of each spring was equal to two times the stiffness of the equivalent single spring calculated in Abaqus: 2K (128.8 kN/mm).

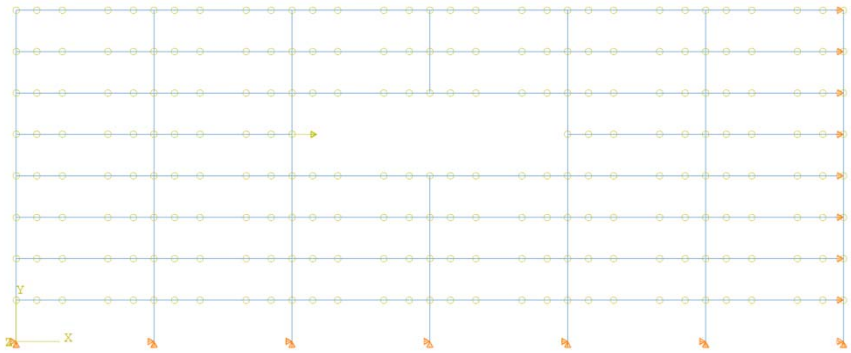

Figure 27: Lateral restraints to beam – configuration 3

Table 2: Calculated lateral stiffness

Sub-frame	Stiffness of the equivalent single spring - K	Stiffness of each spring of the test - 2K
1	91.158 kN/mm	182.315 kN/mm
2	78.431 kN/mm	156.862 kN/mm
3	64.392 kN/mm	128.783 kN/mm
4	78.431 kN/mm	156.862 kN/mm
5	91.158 kN/mm	182.315 kN/mm

II.7.2.2 The spring restraint in the laboratory

In the laboratory, the spring restraints were simulated using hydraulic cylinders. The two restraints were working separately using two separated hydraulic circuits, composed by a cylinder to apply the load at the sub-frame and a hydraulic pump to adapt the oil pressure in the cylinder. The cylinder had the ability to work in tension (max. load of 435 kN) or in compression (max. load of 933 kN). The hydraulic pump had a maximum capacity of 500 bars, which limited the load that could be applied by the system to 654 kN in compression and 304 kN in tension. Figure 28 shows the spring restraint made with the double acting long stroke cylinder and a system of transversal bars and steel plates (in order to invert the cylinder from compression to tension).

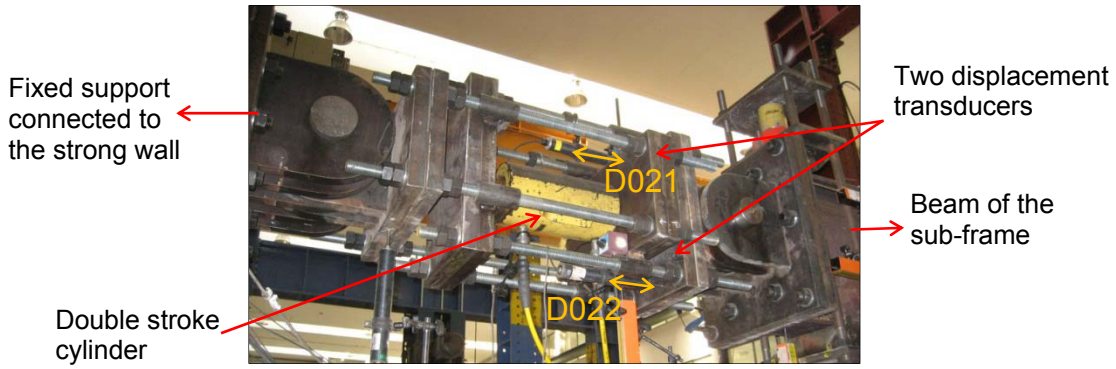

Figure 28: Spring restraint (left)

Even the smaller value of the spring stiffness calculated in the real building (129 kN/mm) would lead to a very low displacement (2.6 mm) under the maximum load able to be applied by the hydraulic circuit (654 kN). So the spring stiffness considered for the tests was reduced to 50 kN/mm. Displacements were measured in the spring direction by two displacement transducers for each restraint (D021 and D022 in Figure 28). The considered displacement (at the gravity centre of the steel beam section) was the average between the two measured values. Taking into account this value, the pressure in the cylinder (measured by pressure transducers) was manually modified in order to adjust the spring stiffness. The following expression gives the spring axial load:

$$F[N] = A[cm^2] \times p[bars] \times 9.81[N/(bars \times cm^2)]$$

Where *A* is the cylinder effective area (133 cm^2 in compression and 62 cm^2 in traction) and *p* is the measured pressure in the cylinder.

II.7.2.3 Special note about the spring restraint behaviour during the tests

Three tests should have been performed with spring axial restraint to beam: test 1 at ambient temperature, test 6 at elevated temperature (700ºC) and finally the demonstration test 7. In order to simplify the test 1 (20ºC), it was assumed that the spring restraints should only apply the tensile loads once the column loss happened and the catenary action developed. This assumption was based on the fact that the test was performed at ambient temperature without any thermal expansion of the beams, and no compression loads should be developed at the beams ends. An initial tensile load was applied in the springs in order to allow the beginning of the control. However, after the column loss (step 3), the beams ends were moving outwards instead of moving inside like it was planned, and the spring restraints should had worked in compression, but this was not possible because it was not planned. This was only after the failure of two bolts that one beam end begun to apply tensile forces at the restraint. In conclusion, the reference test could be considered as performed without any restraint to the beam. The spring was linked to the beam at the gravity centre (GC) of the steel beam section (IPE 550) but not at the GC of the CO section: so when the beam rotated, the measured displacements at the GC of the steel beam end showed an outward movement (Figure 29). Tests 6 and 7 were performed with the spring restraints working in compression for the most part of the test.

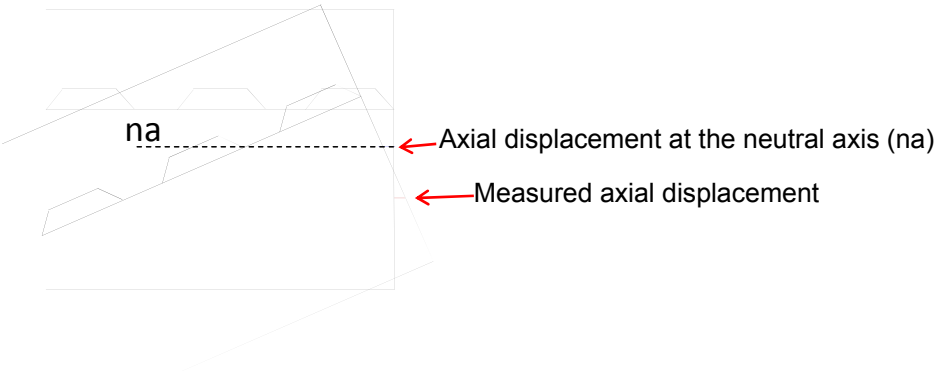

Figure 29: Rotation of the beam end and displacement outwards of the geometrical centre of the steel beam section

II.8 Instrumentation of test specimens

II.8.1 Load cells

Figure 30 presents the measured reaction loads for each test. Load cells F1 and F2 were placed at the top of each beam because they were considered to apply the initial hogging bending moments (see §II.6.1.2). The load cell F3 was located at the bottom of the column (see Figure 18 in §II.6.1.4); the load cell F-HJ was included in the hydraulic jack at the column top and measured the applied load; load cells F4 and F5 were added to the lateral restraint of the bottom column (see §II.2). The reaction loads from the axial restraints to beams were measured by: i) pressure transducers in case of the spring restraints; ii) strain gauges in case of the total restraints (for which the stresses and then the axial loads can be deducted).

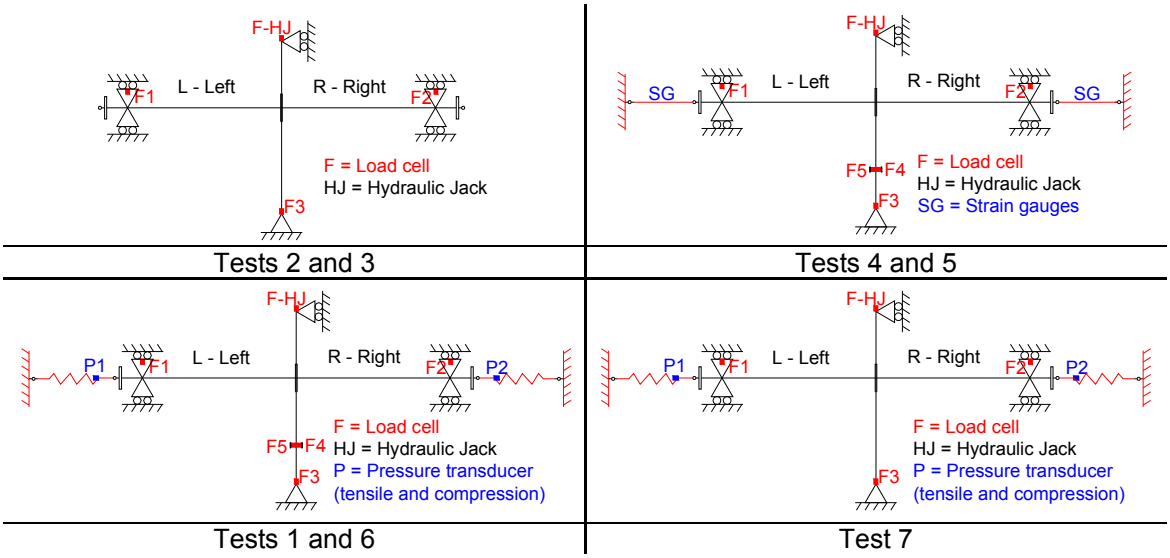

Figure 30: Load cells, pressure transducers and strain gauges to measure the reaction loads

II.8.2 Displacement transducers

Around 30 displacement transducers were used in order to measure the displacements and deformations of the specimen (Figure 31) and to check the residual displacements of the auxiliary structures, such as footings, frames,

etc… Displacement transducers of 200 mm, 100 mm and 50 mm, and wire transducers of maximum deflection 1000 mm were used.

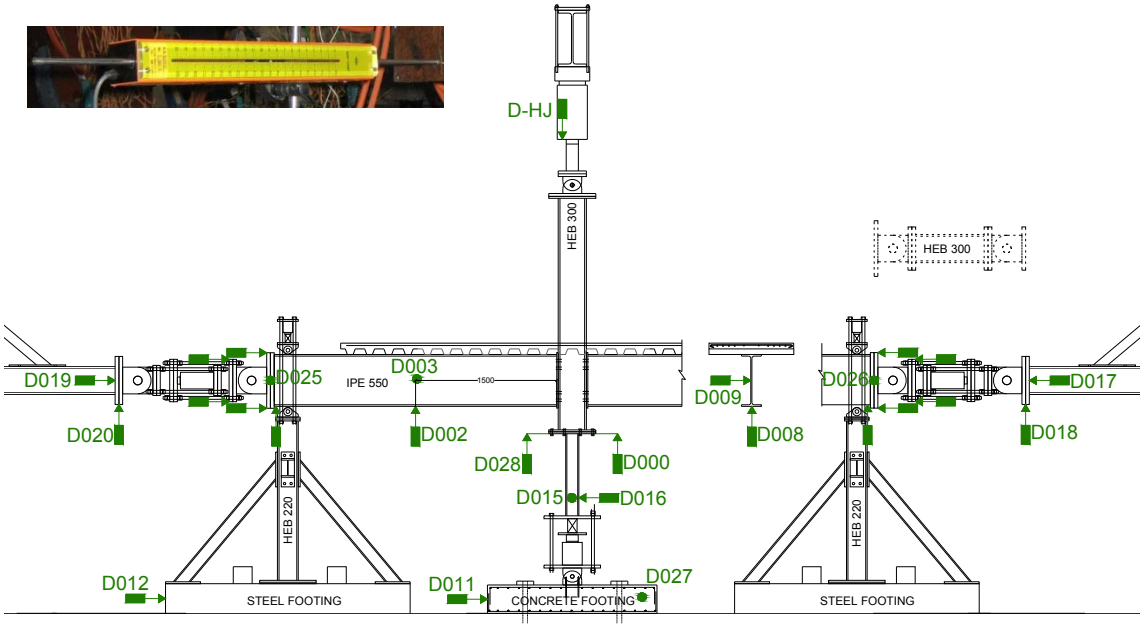

Figure 31: Displacement transducers

II.8.3 Thermocouples

Around 90 (or 70 for tests 4, 5 and 6) thermocouples of K type with two 0.7 mm wires measured the temperature in the elements: end-plates, bolts, beams, column, and composite slab. The thermocouples of the beams were applied as shown in Figure 32 at 250 mm, 500 mm and 1000 mm from the end-plate. In test 7, as the heated zone of the beam was reduced, and the bottom column was heated, the arrangement of thermocouples was slightly different. Figure 33 shows, as an example, the thermocouples located on the steel members of the test 5. Some thermocouples were also located in the composite slab as described in Figure 34.

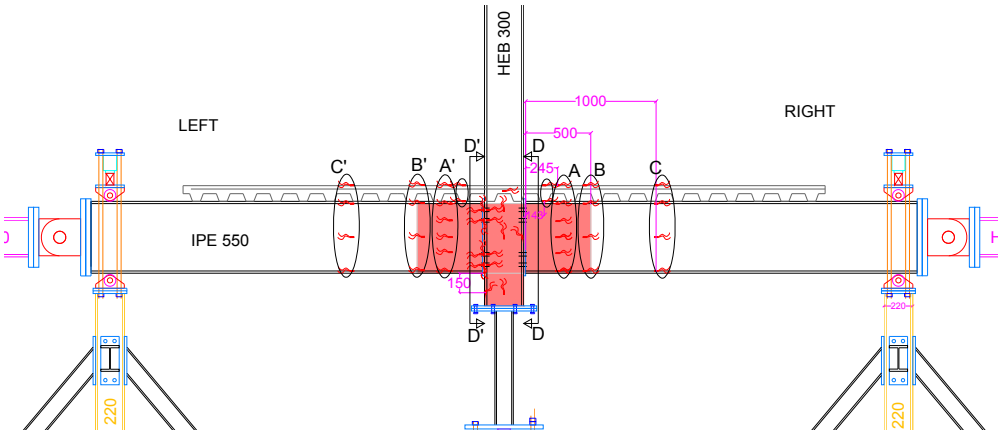

Figure 32: Instrumentation (thermocouples) of the heated zone for tests 2, 3, 4, 5 and 6

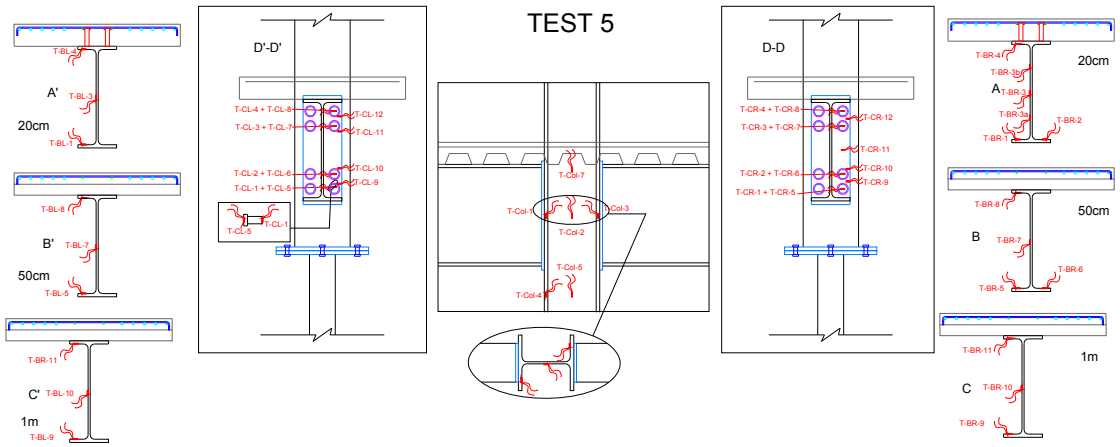

Figure 33: Thermocouples at the steel beams, column and joint of the test 5

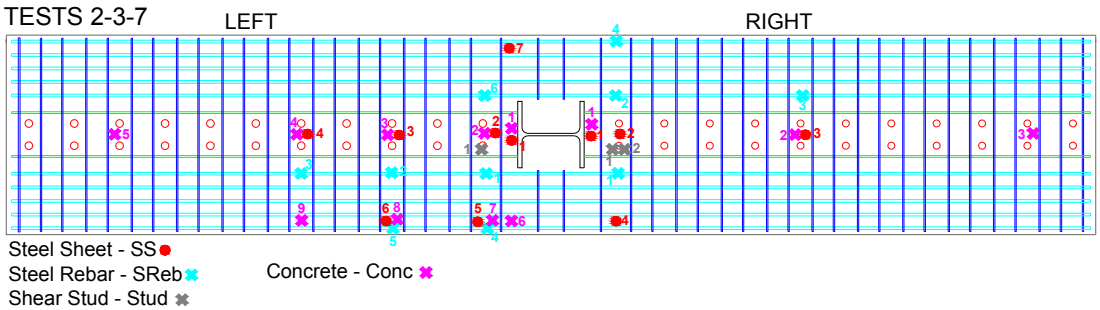

Figure 34: Thermocouples in the composite slab

II.8.4 Strain gauges

Around 50 strain gauges were stocked on the beam axial restraints on flanges and web of the HEB 300 profiles to measure the strains and to derive the stresses and the axial load from the total beam restraint (Figure 35). For the reference test 1 at ambient temperature, strain gauges were located into bolts, at 50 cm from each beam end, on the column web and on the steel rebars in the composite slab (Figure 36).

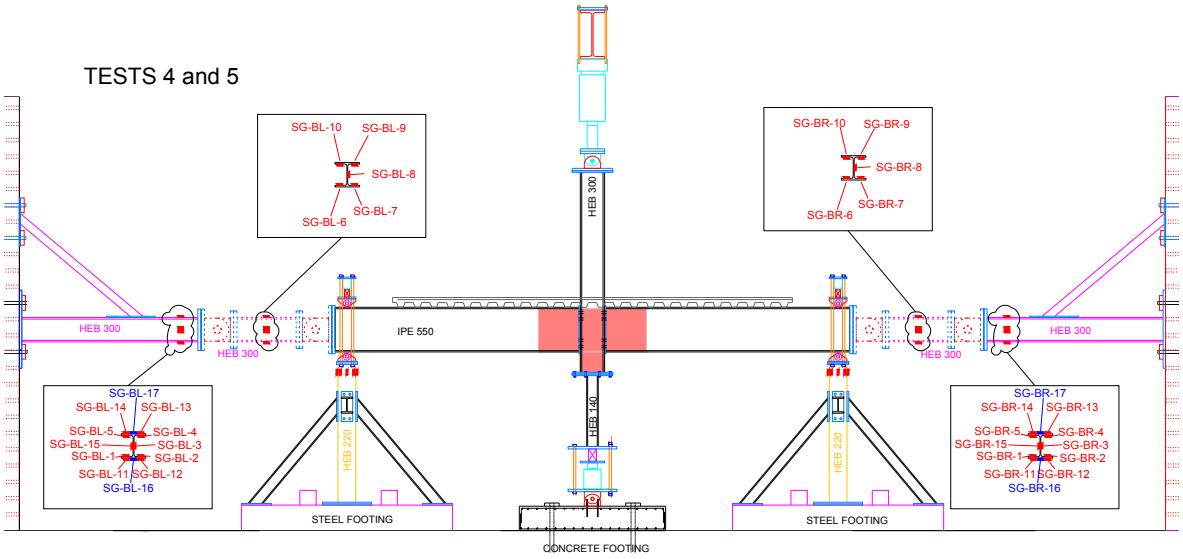

Figure 35: Strain gauges at the beam axial restraints (tests 4 and 5)

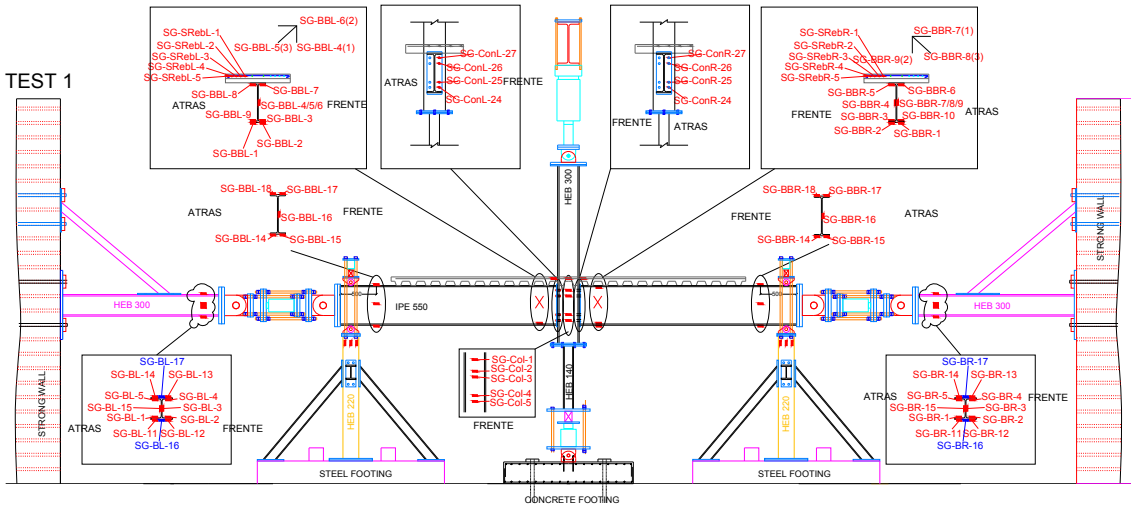

Figure 36: Strain gauges used for the test 1 at ambient temperature

II.9 Control tests

Control tests were performed in order to determine material properties of the steel joint components and concrete slab for the calibration of the numerical and analytical models against the test results.

II.9.1 Mechanical properties of steel from beams, columns and end-plates

Mechanical properties of the steel from the beam, the column and the end-plate were defined by 38 tensile coupon tests. From the steel profiles, the coupons were extracted from the webs and flanges, and three tensile tests were performed for each, at 20ºC, 500ºC and 700ºC. In the case of the steel end-plate, only two coupons were performed and tested at ambient temperature. Steady-state tests were considered, for which the coupon was heated up to a specific temperature and then tested in tension (constant displacement speed).

Figure 37 shows the testing furnace and some steel coupons before and after the tests at 20ºC and 700ºC.

Figure 37: Testing furnace and steel coupons before or after the tests

II.9.1.1 Steel S355 from beam IPE 550

Figure 38 and Figure 39 show the stress-strain curves from the tensile tests performed at 20ºC, 500ºC and 700ºC, respectively for steel coupons extracted from the web and the flange of the IPE 550 steel beam (S355). Table 3 presents the yield strength *Re* (MPa), the tensile strength *Rm* (MPa) and the elongation after fracture *A* (%) for each test, defined according to NP EN 10002-1: 1996 and NP EN 10002-5: 1991.

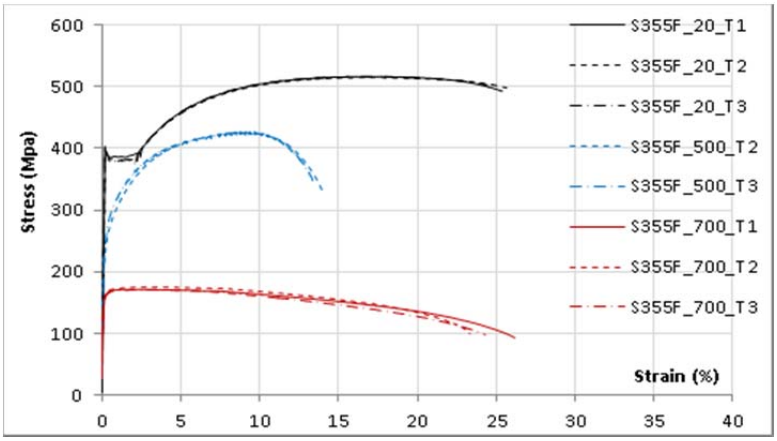

Figure 38: Stress-strain curves at 20ºC, 500ºC and 700ºC for steel S355 - IPE 550 (flange)

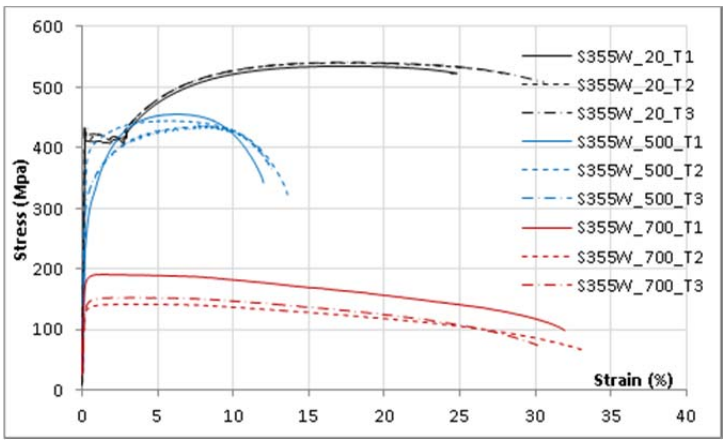

Figure 39: Stress-strain curves at 20ºC, 500ºC and 700ºC for steel S355 - IPE 550 (web)

Table 3: Tensile tests results – Beam IPE 550 (S355)

Reference	Temp. (ºC)	Yield strength Re (MPa)	Tensile strength Rm (MPa)	Elongation after fracture A (%)
S355W*_20_T1	20	425	535	30
S355W_20_T2	20	435	540	31.9
S355W_20_T3	20	437	541	31.4
S355F*_20_T1	20	403	517	32
S355F_20_T2	20	387	516	33
S355F_20_T3	20	397	517	32.4
S355W_500_T1	500	357	447	23.7
S355W_500_T2	500	412	440	22.5
S355W_500_T3	500	363	433	30.1
S355F_500_T1	500	437	445	31.6
S355F_500_T2	500	318	429	31.6
S355F_500_T3	500	334	432	27.7
S355W_700_T1	700	140	142	65.9
S355W_700_T2	700	190	190	68.6
S355W_700_T3	700	151	153	59.5
S355F_700_T1	700	170	171	52.5
S355F_700_T2	700	173	175	44.1
S355F_700_T3	700	164	166	49.9

* W = Web; F = Flange

II.9.1.2 Steel S355 from end-plate 15 mm thick

In Figure 40 are depicted the stress-strain curves from the two tensile tests performed at ambient temperature of the S355 steel end-plate. Table 4 presents the yield strength *Re* (MPa), the tensile strength *Rm* (MPa) and the elongation after fracture *A* (%) for each test, defined according to NP EN 10002-1: 1996.

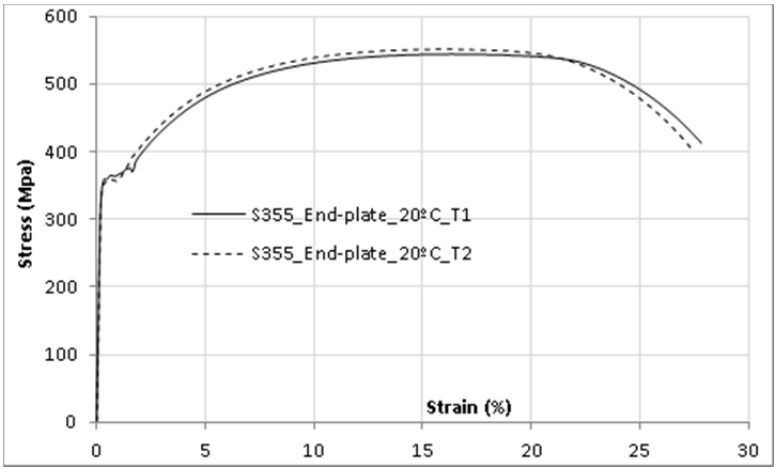

Figure 40: Stress-strain curves at 20ºC for steel S355 – End-plate 15 mm thick

Table 4: Tensile tests results – End-plate 15 mm thick (S355)

Reference	Temp. (ºC)	Yield strength Re (MPa)	Tensile strength Rm (MPa)	Elongation after fracture A (%)
S355E_20_T1	20	359	544	32.7
S355E_20_T2	20	356	551	32.7

* E = End-plate

II.9.1.3 Steel S460 from column HEB 300

Figure 41 and Figure 42 show the stress-strain curves from the tensile tests performed at 20ºC, 500ºC and 700ºC, respectively for steel coupons extracted from the web and the flange of the HEB 300 steel column (S460). Table 5 presents the yield strength *Re* (MPa), the tensile strength *Rm* (MPa) and the elongation after fracture *A* (%) for each test, defined according to NP EN 10002-1: 1996 and NP EN 10002-5: 1991.

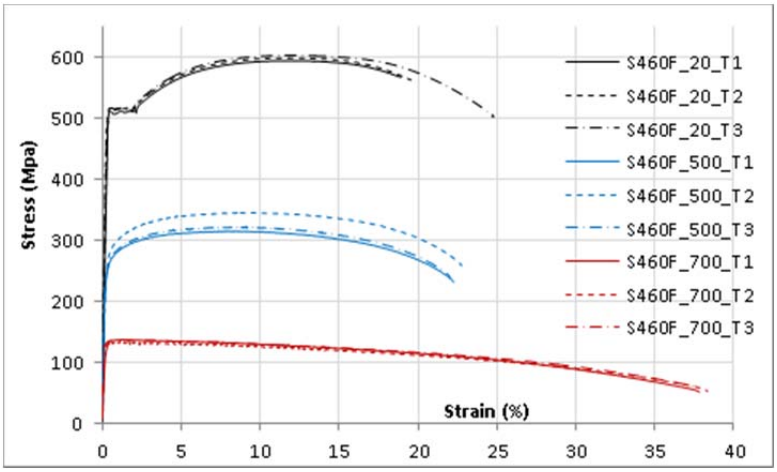

Figure 41: Stress-strain curves at 20ºC, 500ºC and 700ºC for steel S460 - HEB 300 (flange)

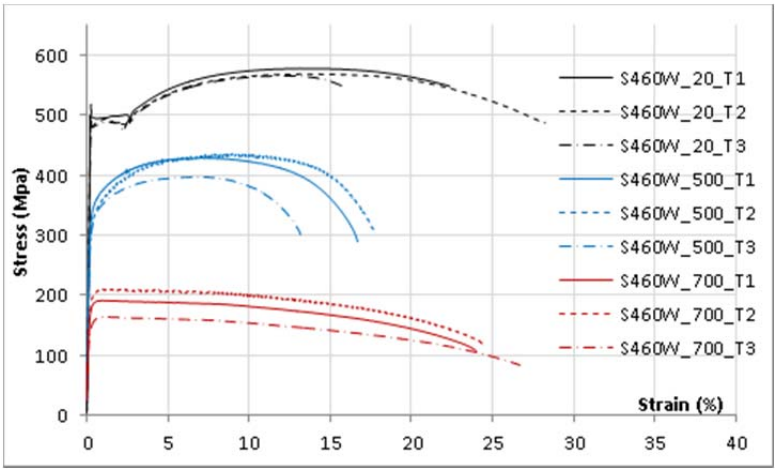

Figure 42: Stress-strain curves at 20ºC, 500ºC and 700ºC for steel S460 - HEB 300 (web)

Table 5: Tensile tests results – Column HEB 300 (S460)

Reference	Temp. (ºC)	Yield strength Re (MPa)	Tensile strength Rm (MPa)	Elongation after fracture A (%)
S460W*_20_T1	20	500	579	25.6
S460W_20_T2	20	520	569	26.4
S460W_20_T3	20	491	566	24.8
S460F*_20_T1	20	513	595	26.5
S460F_20_T2	20	517	599	26.8
S460F_20_T3	20	517	603	28.3
S460W_500_T1	500	382	430	31.3
S460W_500_T2	500	368	436	26.8
S460W_500_T3	500	356	397	28.5
S460F_500_T1	500	284	315	27.2
S460F_500_T2	500	307	345	21.2
S460F_500_T3	500	284	315	21.2
S460W_700_T1	700	186	190	48.3
S460W_700_T2	700	209	211	52.3
S460W_700_T3	700	163	164	53.7
S460F_700_T1	700	137	137	42.8
S460F_700_T2	700	132	134	40.7
S460F_700_T3	700	136	137	41.1

* W = Web; F = Flange

II.9.2 Mechanical properties of M30 grade 10.9 bolts

Mechanical properties of the bolts M30 10.9 were defined by 15 tensile coupon tests (Figure 43). Three tensile tests were performed at ambient temperature, and two tests were performed at each temperature equal to 200ºC, 400ºC, 500ºC, 600ºC, 700ºC and 800ºC. Steady-state tests were performed. Table 6 presents the yield strength $R_{p0.2\%}$ (MPa), the tensile strength R_m (MPa) and the elongation after fracture A (%) for each test, defined according to NP EN 10002-1: 1996 and NP EN 10002-5: 1991.

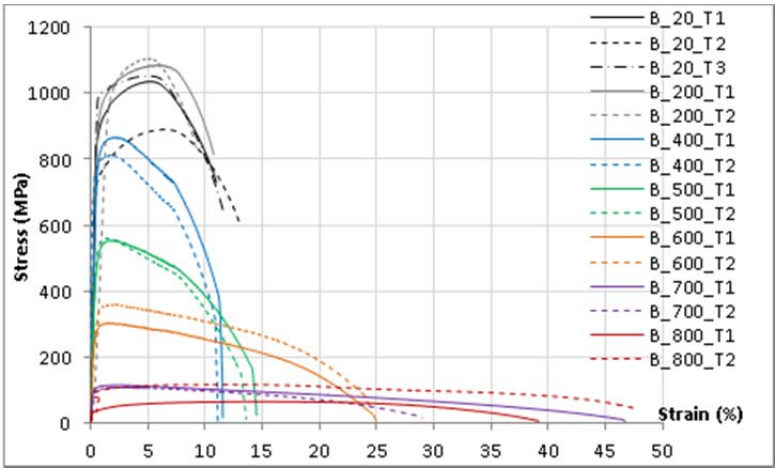

Figure 43: Stress-strain curves of bolts M30 10.9 at 20ºC, 200ºC, 400ºC, 500ºC, 600ºC, 700ºC and 800ºC

Table 6: Tensile tests results – Bolts M30 10.9

Reference	Temp. (ºC)	Yield strength Rp0.2% (Mpa)	Tensile strength Rm (MPa)	Elongation after fracture A (%)
B_20_T1	20	870	1035	15.1
B_20_T2	20	733	733	18
B_20_T3	20	995	1052	15.5
B_200_T1	200	935	1086	14.2
B_200_T2	200	973	1107	14.8
B_400_T1	400	804	868	17.9
B_400_T2	400	761	813	16.7
B_500_T1	500	497	554	23.2
B_500_T2	500	520	561	22.7
B_600_T1	600	279	305	42
B_600_T2	600	317	360	41.7
B_700_T1	700	102	115	68
B_700_T2	700	95	108	54
B_800_T1	800	33	65	80.4
B_800_T2	800	86	117	73.4

* B = Bolt

II.9.3 Compression test of the slab concrete

Compression tests on 24 concrete blocks were performed. Three tests were performed after 7 days, 14 days, 28 days (Figure 44) and then the day each test. The concrete properties C25/30 at 28 days were confirmed according to NP EN 206-1 2007: i) the average of each three tests cube strength ($f_{ck,cube}$ = 35 MPa) was higher than the C25/30 characteristic cube strength plus 1 (31 MPa) and was smaller than the C30/37 characteristic cube strength plus one (38 MPa); ii) each individual value was higher than the C25/30 characteristic cube strength minus 4 (26 MPa).

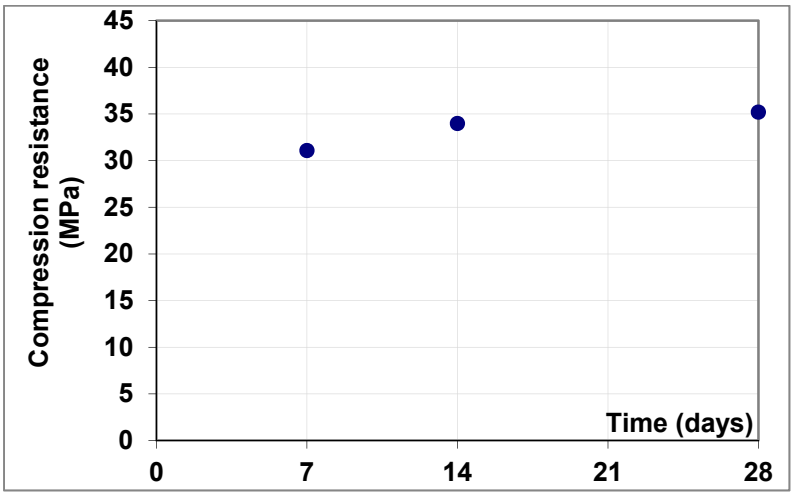

Figure 44: Evolution of the concrete resistance in compression

III Experimental results

In this section, the global joint behaviour and the detailed results are given for each experimental test. But first, section III.1 describes how the rotations, the

reaction loads and the bending moments were deducted from the measured values of displacements and loads.

III.1 Rotations, loads and bending moments definitions

III.1.1 Rotations

III.1.1.1 Rotations at the joint and column rotation

As shown in Figure 45, the rotation was estimated using the vertical displacements measured at the beams mid-spans (D002 and D008) and at the column (D000 and D028). The joint rotation could not be exactly measured near the connection because of the elevated temperatures at the joint zone.

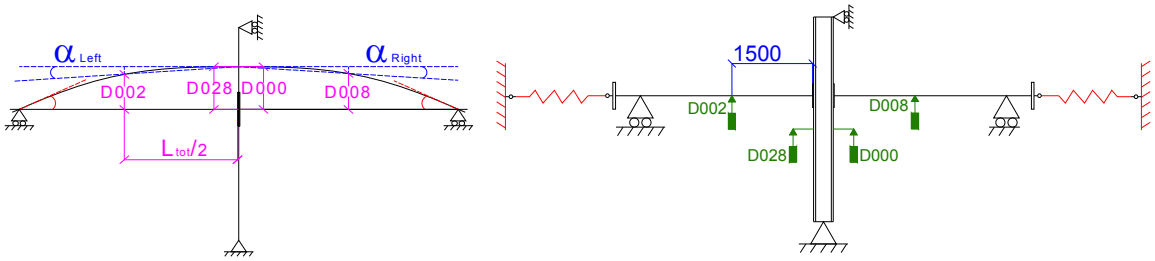

Figure 45: Estimated rotation of the joint using the measured displacements

The following expressions were used to estimate the rotation (calculated at the front of the connection steel end-plate), taken into account the eventual column rotation. A slight difference was made in the calculation between tests 1 and 2 and the others, because the displacement D028 was not measured in tests 2 and 3:

Tests 2, 3:

$$\alpha_{connection,L} = atan\left(\frac{D000-D002}{1500mm+D_{beam,h,L}}\right) \times 1000 - \alpha_{column} \text{ [mrad]} \qquad > 0 \text{ for } M^{+}$$

$$\alpha_{connection,R} = atan\left(\frac{D000-D030}{1500mm+D_{beam,h,R}}\right) \times 1000 + \alpha_{column} \text{ [mrad]} \qquad > 0 \text{ for } M^{+}$$

Tests 1, 4, 5, 6, 7:

$$\alpha_{connection,L} = atan\left(\frac{(D028+D000/2)-D002}{1500mm+D_{beam,h,L}}\right) \times 1000 - \alpha_{column} \text{ [mrad]} \qquad > 0 \text{ for } M^{+}$$

$$\alpha_{connection,R} = atan\left(\frac{(D028+D000/2)-D030}{1500mm+D_{beam,h,R}}\right) \times 1000 + \alpha_{column} \text{ [mrad]} \qquad > 0 \text{ for } M^{+}$$

Where $D_{beam,h,R\ or\ L}$ is the horizontal displacement estimated at the end of the steel beam axis according to the measured displacements:

Tests 2, 3:

$$D_{beam,h,L} = \frac{D005+D006}{2} \quad \text{and} \quad D_{beam,h,R} = \frac{D007+D010}{2} \quad \text{(see Figure 46)}$$

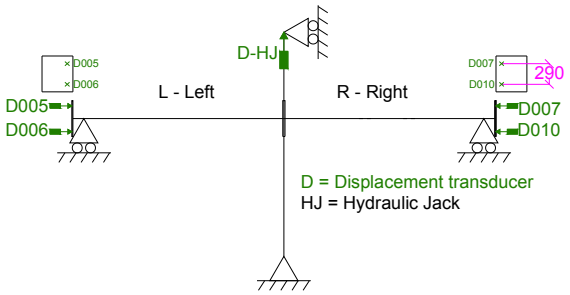

Figure 46: Position of the displacement transducers D005, D006, D007 and D010 at the beam ends – tests 2, 3

Tests 1, 4, 5, 6, 7:

$D_{beam,h,L} = \frac{D005+D006}{2}$ and $D_{beam,h,R} = \frac{D001+D007}{2}$ (see Figure 47 and Figure 48)

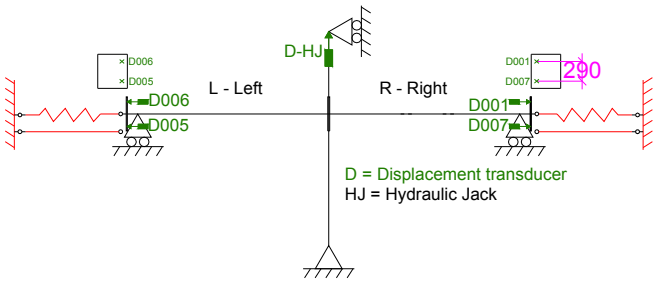

Figure 47: Position of the displacement transducers D001, D005, D006 and D007 at the beam ends – tests 1, 5, 6, 7

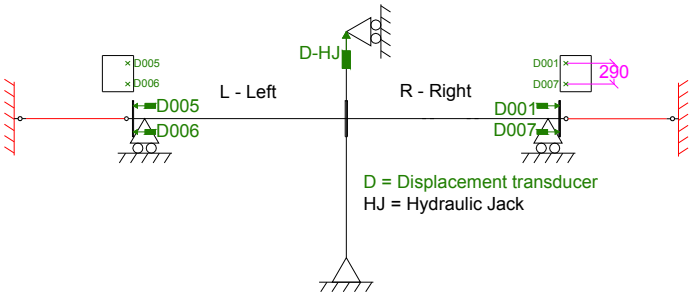

Figure 48: Position of the displacement transducers D001, D005, D006 and D007 at the beam ends – test 4

For tests 1 to 6, the column rotation α_{column} was calculated according to:

$\alpha_{column} = atan\left(\frac{D016}{h_x - D_{HJ}}\right) \times 1000$ [mrad] (rotation > 0 in the clockwise)

Where D016 (mm) and D_{HJ} (mm) are the displacements measured by the displacement transducers at the bottom of the column and by the hydraulic jack, and h_x (mm) is the distance between the transducer D016 and the pin at the column top (Figure 49). This distance varies for some tests (see Table 7) because of the increase of the jack length capacity, with steel plates collocated between the column pin and the hydraulic jack (§II.6.1.1).

Table 7: Distance h_x between the transducer D016 and the column top for each test

Test	h_x (mm)
T1	*From 0 to 3h37min:* 2964; *From 3h37min to the end*: 3099
T2	*Not used*
T3	*From 0 to 4h50min*: 3250; *From 4h50min to the end*: 3350
T4	2951 mm
T5	*From 0 to 5h04min:* 1964; *From 5h04min to the end:* 3084
T6	*From 0 to 4h55min:* 2710; *From 4h55min to 7h39min:* 2847; *From 7h39min to the end:* 2981
T7	*Not used*

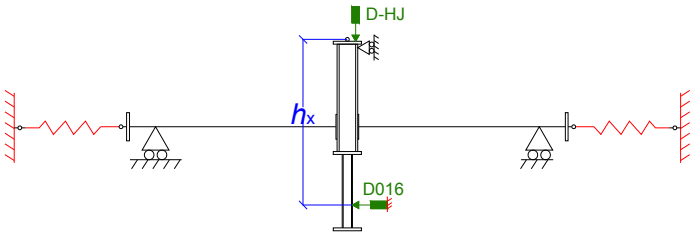

Figure 49: Measured displacements for the calculation of the column rotation

For test 7, the column rotation was estimated by:

$\alpha_{column} = \frac{D000-D028}{1500mm}$ [mrad] (rotation > 0 in the clockwise)

III.1.1.2Rotations at the beams ends

The rotations of the end-plates at the beams ends were calculated to be used in the projection of the restraint forces (tests 1, 4, 5, 6, 7) according to the beam axis (§III.1.2). The measured horizontal displacements shown in Figure 46, Figure 47 and Figure 48 were used:

Tests 1, 5, 6, 7:

$\alpha_{beam,L} = atan\left(\frac{D006-D005}{290mm}\right) \times 1000$ [mrad]

$\alpha_{beam,R} = atan\left(\frac{D007-D001}{290mm}\right) \times 1000$ [mrad]

Test 4:

$\alpha_{beam,L} = atan\left(\frac{D005-D006}{290mm}\right) \times 1000$ [mrad]

$\alpha_{beam,R} = atan\left(\frac{D007-D001}{290mm}\right) \times 1000$ [mrad]

III.1.1.3Rotations of the axial restraints to beams

The rotations of the beam axial restraints are shown in Figure 50 (spring restraints) and Figure 51 (total restraints). Rotations were calculated using the vertical measured displacements:

Tests 4 and 5 (total restraints):

$$\alpha_{restr,L} = atan\left(\frac{D022-D021}{429\,mm}\right) \times 1000 \text{ [mrad]} \qquad > 0$$

$$\alpha_{restr,R} = atan\left(\frac{D023-D024}{429\,mm}\right) \times 1000 \text{ [mrad]} \qquad > 0$$

Tests 1, 6, 7 (spring restraints):

$$\alpha_{restr,L} = atan\left(\frac{D029-D031}{650\,mm}\right) \times 1000 \text{ [mrad]} \qquad > 0$$

$$\alpha_{restr,R} = atan\left(\frac{D030-D010}{680\,mm}\right) \times 1000 \text{ [mrad]} \qquad > 0$$

Figure 50: Springs rotations, evaluated by the measured vertical displacements D031 and D029 on the left, and D030 and D010 on the right – Tests 1, 6, 7

Figure 51: Restraint rotations, evaluated by the measured vertical displacements D021 and D022 on the left, and D023 and D024 on the right – Tests 4 and 5

III.1.2 Loads

III.1.2.1 Reaction loads at the beams supports

The reaction loads F_L and F_R at the beams supports left and right respectively were calculated based on i) the load measured by the load cell F1 or F2 (§II.8.1); ii) the load applied by the hydraulic jack; and iii) the load cell F3 at the base of the column. In tests 1 to 6, during step 1 (hogging bending moment) and step 2 (temperatures), the two load cells F1 and F2 situated at the top of the beams measured the reaction loads at the two beam supports. The self-weight (SW) of the sub-frame was not measured by the load cells and had to be added to the reaction loads calculations:

$$F_{L,Steps\ 1-2} = F_{1,initial} + F_1 + \frac{SW}{2}$$

$$F_{R,Steps\ 1-2} = F_{2,initial} + F_2 + \frac{SW}{2}$$

Where $F_{1,initial}$ and $F_{2,initial}$ are the initial loads measured during the pre-tension of the steel bars at the beam supports, before the beginning of the test. After the column loss and during the increase of the sagging bending moment (step 3), the beam supports were unloaded in tests 1, 3, 5, 6 and 7, and the load cells F1 and F2 stopped to measure. The total load in the column (sum of the loads measured by the hydraulic jack F_{HJ} and by the load cell F3) was used to estimate the reaction loads in the beam supports, assuming a symmetrical behaviour between left and right. For tests 2 and 4, the supports were not

unloaded, which increased the support rigidity (see §III.3 and III.5). The reaction load at the beam supports was equal to the total load in the column, reduced by the two reaction loads F1 and F2:

$$F_{L,Step\ 3} = \frac{F_{HJ}+F_3-F_1-F_2}{2} \quad \text{and} \quad F_{R,Step\ 3} = \frac{F_{HJ}+F_3-F_1-F_2}{2}$$

where F_3 is null after the loss of the column.

In test 7, the reaction loads F_L and F_R at the beams supports left and right were calculated as:

$$F_{L,test7} = \frac{F_{HJ}+F_3}{2} \quad \text{and} \quad F_{R,test7} = \frac{F_{HJ}+F_3}{2}$$

Note that in tests 1, 4, 5, 6 and 7, the vertical components of the axial restraint loads were included in the equilibriums (see §III.1.2.2).

III.1.2.2Reaction loads from the axial restraints to beams

The restraint loads can be projected according to the horizontal and vertical axis, as shown in Figure 52, with:

$F_{restr,vertical} = F_{restr} \times \sin(\alpha_{restr})$ and $F_{restr,horiz} = F_{restr} \times \cos(\alpha_{restr})$.

Figure 52: Projection of the spring forces according to the vertical and horizontal axis

The beam axial force used for the M-N behaviour of the joint is considered to be the load measured at the end of the beams, and the projection of the restraint load in the beam direction is given by (Figure 53):

$$F_{restr,axial,L\ or\ R} = F_{restr,L\ or\ R} \times \cos(\alpha_{beam,\ L\ or\ R} + \alpha_{restr,L\ or\ R})$$

where $F_{restr,L\ or\ R}$ is the load applied by the restraints, $\alpha_{beam,\ L\ or\ R}$ is the beam rotation at the end, and $\alpha_{restr,L\ or\ R}$ is the restraint rotation, and were defined previously.

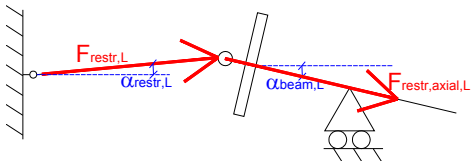

Figure 53: Projection of the restraint loads according to the beam axis

III.1.3 Bending moments

The bending moment at the joint was calculated based on the reaction loads: i) at the beams supports; ii) at the beams ends, from the axial restraints for tests 1, 4, 5, 6 and 7:

$$M_{Left} = F_{L,steps1-2\ or\ step\ 3} \times L_L + F_{restr,v,L} \times L_{restr,L} + F_{restr,h,L} \times z_L$$

$$M_{Right} = F_{R,steps1-2\ or\ step\ 3} \times L_R + F_{restr,v,R} \times L_{restr,R} + F_{restr,h,R} \times z_R$$

Where $F_{L,steps1-2\ or\ step\ 3}$ and $F_{R,steps1-2\ or\ step\ 3}$ are the reaction loads at the beam supports defined previously, L_L and L_R are the distances between each beam support and half of the column flange thickness:

$$L_{L,R} = L_{beam} + t_{pl} + \frac{t_{fl,HEB300}}{2} - x_{le,L,R}$$

Where L_{beam} is the total length of the steel beam profile (3000 mm), t_{pl} is the end-plate thickness (15 mm), $t_{fl,HEB300}$ is the column flange thickness (19 mm), and x_{leR} and x_{leL} are the measured distances of the part of the steel profile out of the beam support (Figure 54), given in Table 8.

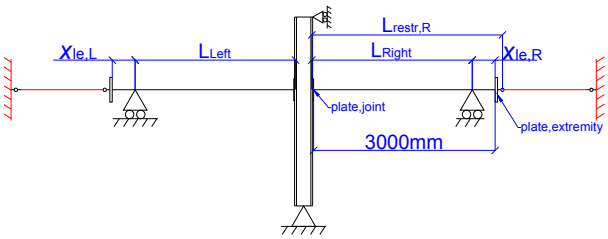

Figure 54: Horizontal distances considered in the bending moment calculation

Table 8: Dimension values for each test

Test	L_L (mm)	L_R (mm)	dx_L (mm)	dx_R (mm)	dv,in_L (mm)	dv,in_R (mm)
T1	2815	2819	160	156	290	290
T2	*No*	*No*	*No*	*No*	*No*	*No*
T3	*No*	*No*	*No*	*No*	*No*	*No*
T4	2813	2813	172	167	280	285
T5	2815	2819	160	156	290	290
T6	2827	2823	153	157	285	285
T7	2815	2813	160	152	290	300

$F_{restr,v,L}$ and $F_{restr,v,R}$ are the vertical projections of the load in each restraint, and $F_{restr,h,L}$ and $F_{restr,h,R}$ are the horizontal ones (in case of a spring restraint, the load can be noted $F_{sp,h\ or\ v}$). L_{restr} is the distance between half of the column flange thickness and the application point of the restraint force (Figure 54):

$$L_{restr,L} = \mathrm{L_L} + \mathrm{dx_L} + \mathrm{dv_L}$$

$$L_{restr,R} = \mathrm{L_R} + \mathrm{dx_R} + \mathrm{dv_R}$$

Where $\mathrm{dx_L}$ and $\mathrm{dx_R}$ are the constant distances between each beam support and the displacement transducers D013 on the left side and D014 on the right side (Figure 55 and Table 8), and *dv* is the variable distance between the displacement transducer D013 or D014 and the application point of the spring force on each side:

$$dv_L = dv_{in,L} + D_{beam,h,L} \quad \text{and} \quad dv_R = dv_{in,R} + D_{beam,h,R}$$

where $\mathrm{dv_{in,L,R}}$ are the initial distances values, measured in the laboratory (Table 8), and $D_{beam,h,LandR}$ was defined previously.

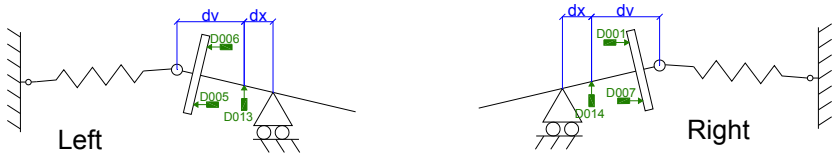

Figure 55: Definition of the horizontal distances from the beam support to the application point of the spring force

z_L and z_R are the vertical distances between the application point of the spring force and the joint (Figure 56):

$$z_L = D028 - x_L \qquad \text{and} \qquad z_R = D000 - x_R$$

where D028 and D000 are the vertical displacements measured at the joint, and x_L and x_R are:

$$x_L = \frac{dx_L + dv_L}{dx_L} \times D013 \qquad \text{and} \qquad x_R = \frac{dx_R + dv_R}{dx_R} \times D014$$

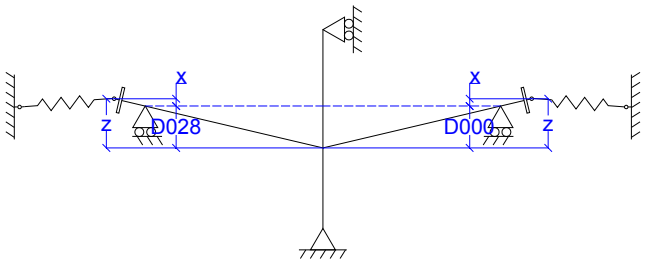

Figure 56: Vertical distance between the application point of the spring force and the joint

III.2 Results of test 1 (reference test at ambient temperature)

The global behaviour of the joint during the test is described in the following section, then the step by step behaviour is detailed, for each loading step, and finally, additional data a presented.

III.2.1 Joint behaviour (entire test)

The evolution of the total vertical reaction load (F_L+F_R) *versus* the vertical displacement of the joint, and the bending moment versus the rotation are depicted in Figure 57 and Figure 58. Step 1 corresponds to the hogging bending moment; step 3 corresponds to the sagging bending moment, and a transition phase is defined between hogging and sagging bending moments (see §III.2.2).

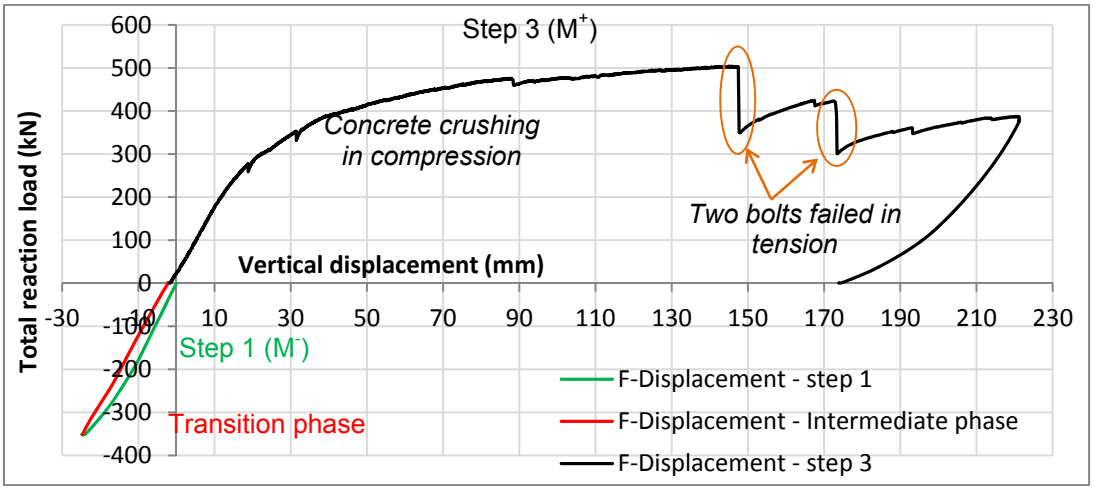

Figure 57: Vertical reaction load (FL+FR) s vertical displacements of the column

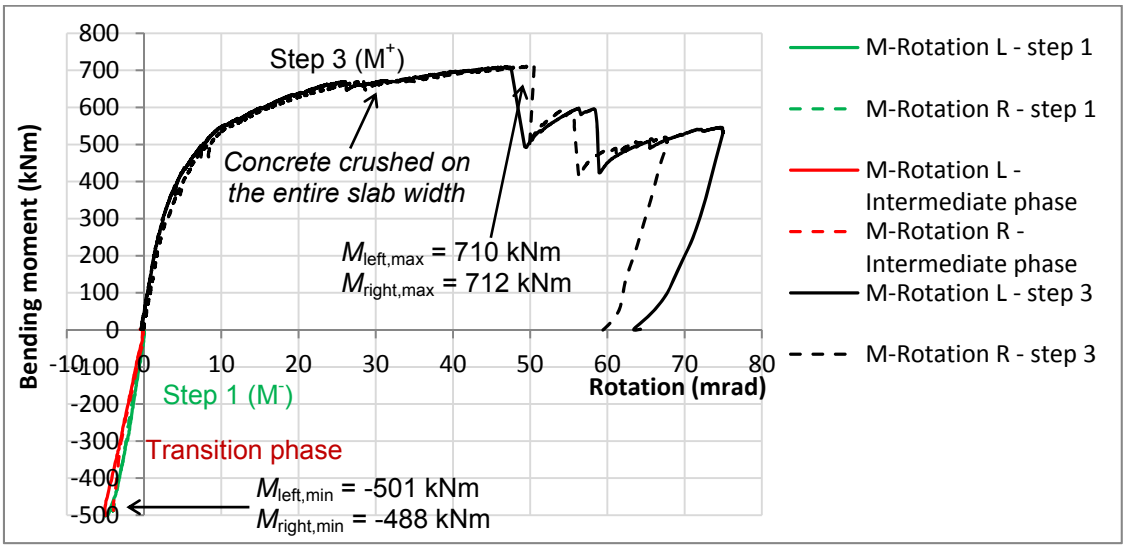

Figure 58: Bending moment vs rotation at the joint

Concrete crushing in compression was the first failure observed, but this failure was really progressive and cannot be identified on the force-displacement / moment-rotation curves. Around 30 mrad of rotation, it could be observed that the concrete from the composite slab was crushed on the entire slab width. One first bolt suddenly failed after 148 mm of joint vertical displacement and the applied load reduced from 503 kN to 351 kN. The corresponding bending moment was reduced from 707 kNm to 494 kNm, and the rotation increased from 47.5 mrad to 49 mrad on the left side because of the sudden slight rotation of the column once the bolt failed (despite the horizontal restraints at the bottom column shown in Figure 59). The deformation of the left side of the joint and the one of the right side began to differ, notably because of the slight column rotation. A second bolt failed under a load equal to 393 kN, with a vertical displacement equal to 173 mm (that corresponded to 600 kNm of bending moment and 59 mrad of rotation on the left side).

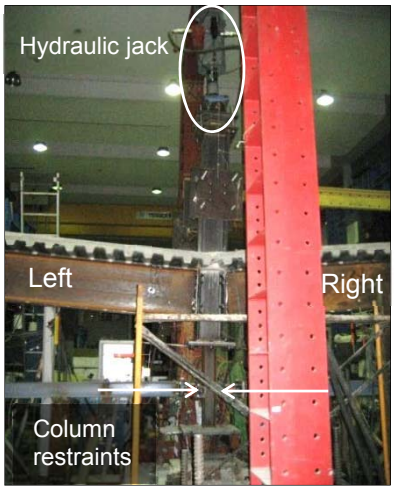

Figure 59: Final deformation of the sub-frame: view from the back side

Figure 60 presents the final deformations of the joint at the end of the test, after the failure of the two bolts. The failed bolts were identified: i) in the bottom bolt rows - because of higher tensile forces under sagging bending moment, and ii) in the left connection due to a slight asymmetric joint deformation. Due to high stresses/deformations, a crack at the base of the steel end-plate, just above the weld, was observed at the end of the test. Moreover, a new localised deformation mode was observed at the steel end-plate centre. This end-plate deformation should happened because of the joint configuration: i) 4 bolt rows and quite a high space between the rows 2 and 3 (260 mm), ii) the end-plate (15 mm) was thinner than the column flange (19 mm), and iii) an initial deformation noticed just after the bolts pre-loading (0.6 mm was measured for the reference test). Moreover, it seems that the beam web was pulling the end-plate (due to the effect of the deformation under sagging bending moment), and the deformation of the end-plate was amplified where the end-plate was not linked by bolts to the column flange: in the bottom part and in the centre of the end-plate.

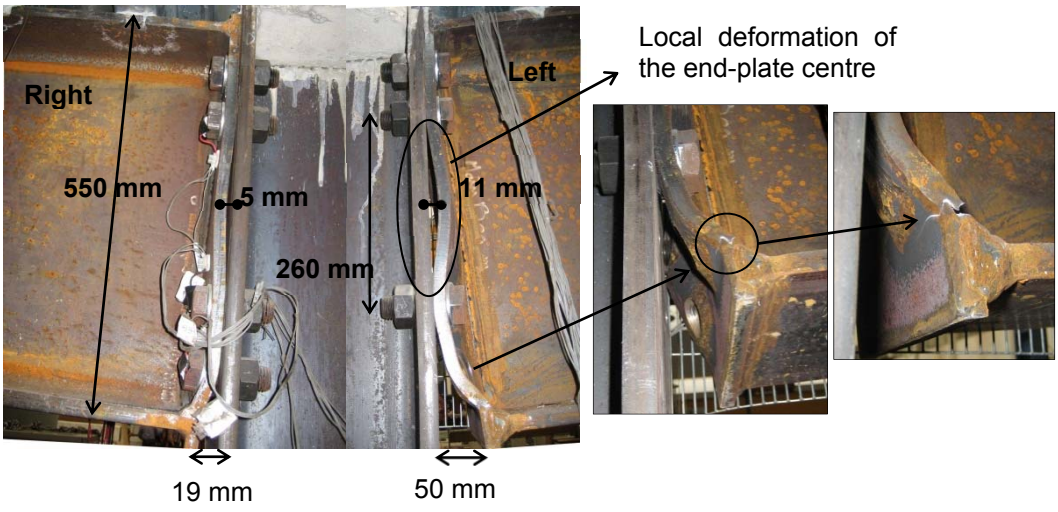

Figure 60: Deformations of the joint (view from the back side)

Finally, the test was stopped at 75 mrad and 68 mrad of connection left and right rotations. The deformation of the sub-frame at the end of the test is shown in Figure 59, and Figure 61 shows the rotations at the joint left and right sides *versus* time, as well as the column rotation. The difference between the rotations right and left comes from the slight column rotation on the right side (-6 mrad) once the bolts failed.

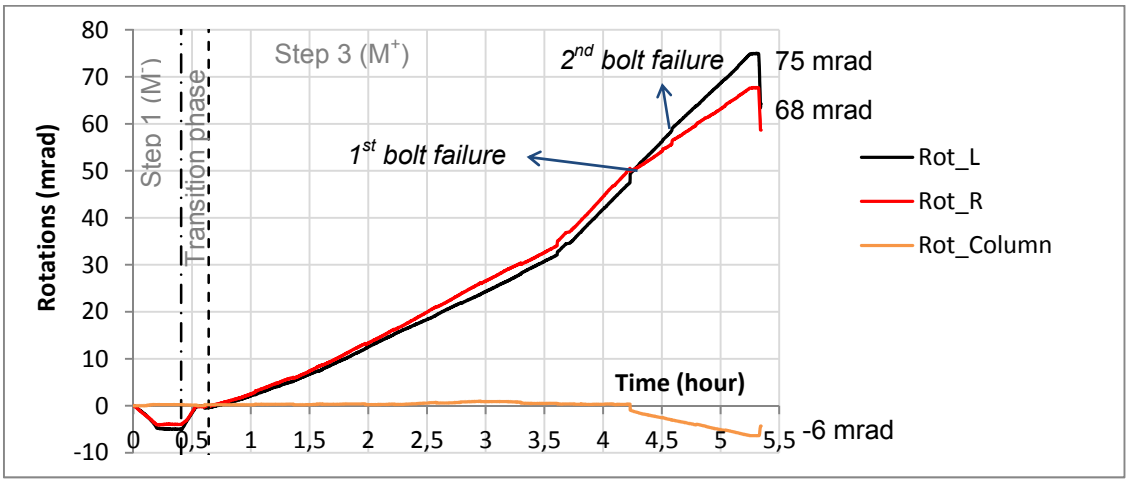

Figure 61: Rotations at the connections (L-Left and R-Right); and column rotation

Projections of the spring's forces along the beam axis are depicted in Figure 62. The springs restraints were only applied during step 3: i) first, an initial load of around 38 kN was applied in order to facilitate the beginning; ii) after, the beam ends were moving outwards instead of moving inside and springs should had worked in compression, but they could not as explained in §II.7.2; iii) finally, two bolts failed on the joint left side: this end-plate deformed more and the left beam end suffered less displacements than the right beam end, so the springs were activated in tension on the right side for the last 30 minutes of the test. This test is considered performed without axial restraints to the beams.

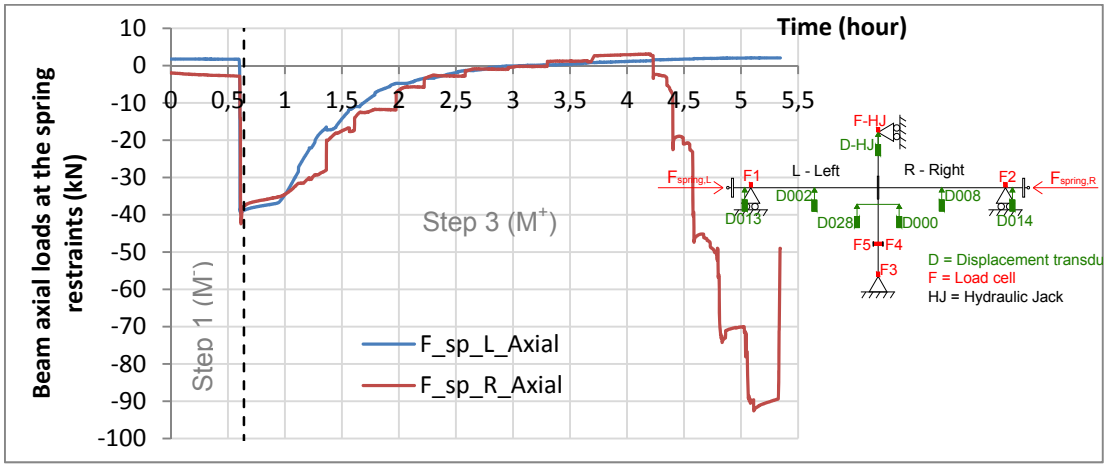

Figure 62: Projections of the spring forces along the beam axis direction – T1

III.2.2 Step by step behaviour: step 1 - Initial hogging bending moment

The initial hogging bending moment was introduced to the sub-frame using the hydraulic jack at the column top, as shown in Figure 63. In this test, the column base support was not put after the application of the hogging bending moment because no temperatures (step 2) were applied and the column was assumed to fail at ambient temperature. The transition phase between the hogging and sagging bending moments (steps 1 and 3) was made by: i) decreasing the load at the jack up to zero; ii) removing the pre-loads at the supports (F1 = F2 = 0, see §II.6.1.2); and iii) an initial load into the springs restraints was introduced at the beginning of the step 3 (around 38 kN) in order to have a better initial control of the oil pressure in the cylinders.

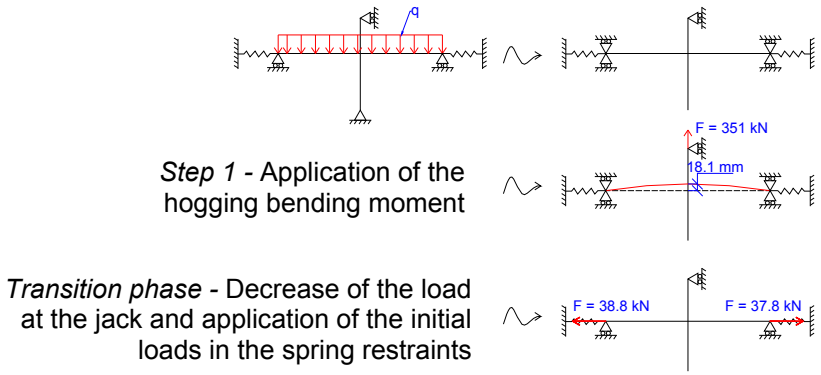

Figure 63: Application of the hogging moment in the joint

Figure 64 presents the evolution of the vertical displacements measured near the beam-to-column joint. Table 9 presents the values of displacements and reaction loads at the end of the step 1.

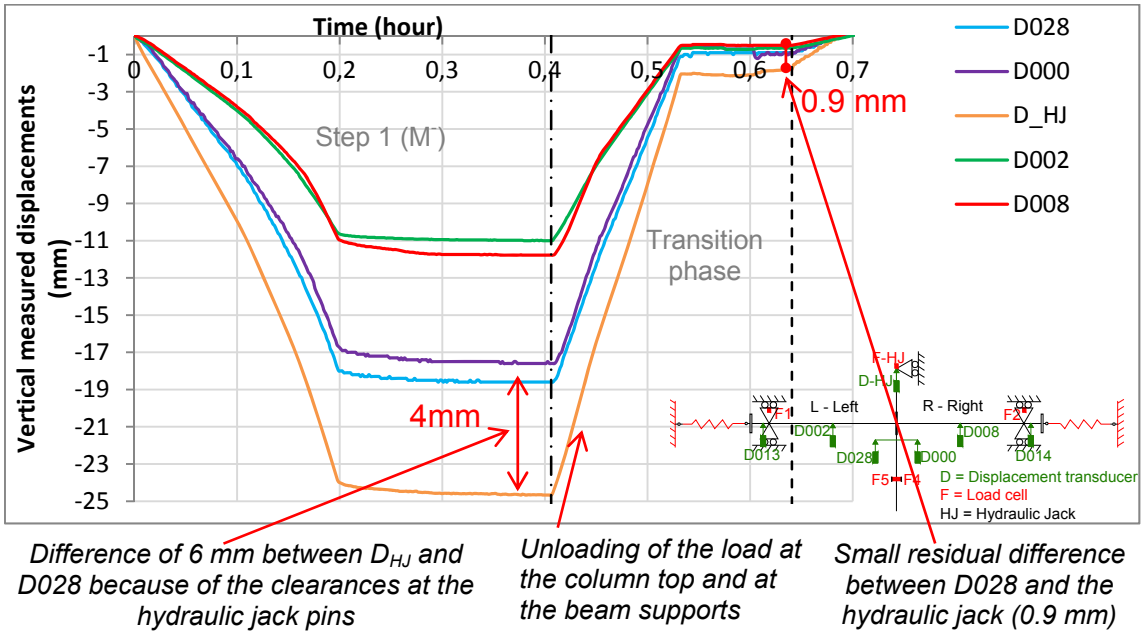

Figure 64: Vertical displacements near the beam-to-column joint in step 1 (hogging bending moment)

Figure 65 presents the comparison between the loads measured at the column top (F_{HJ}) and the sum of the reaction loads measured at the beam supports (F1+F2). Before loading the joint, the end of each beam was vertically restrained and an initial load was measured by the load cells F1 and F2, respectively equal to -121.9 kN and -124.8 kN, at which the self-weight of the sub-frame was added (see §II.6.1). The total initial load was equal to -280.2 kN. At the end of the step 1, the hogging bending moment applied to the connection was equal to around -485 kNm on the right side and -499 kNm on the left side.

Table 9: Displacements and loads (step1)

	Step 1 (25 min)	
Step 1 - Initial hogging bending moment	Load (kN)	Displ. (mm)
Column base (F3 and D000)	0	-18.1*
Beam mid-span Left (D002)	----	-11
Beam mid-span Right (D008)	----	-11.8
Beam support Left (F_{Left})	-177.8	----
Beam support Right (F_{Right})	-172.7	----
Spring left ($F_{sp,L}$)	0	----
Spring right ($F_{sp,R}$)	0	----
Hydraulic Jack (F_{HJ} and D_{HJ})	-351.2	-24.7
Hogging bending moments at the joint	M_{left} = -499 kNm M_{right} = -485 kNm	

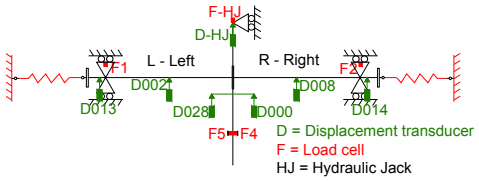

* Average value between by the wire transducers D000 and D028

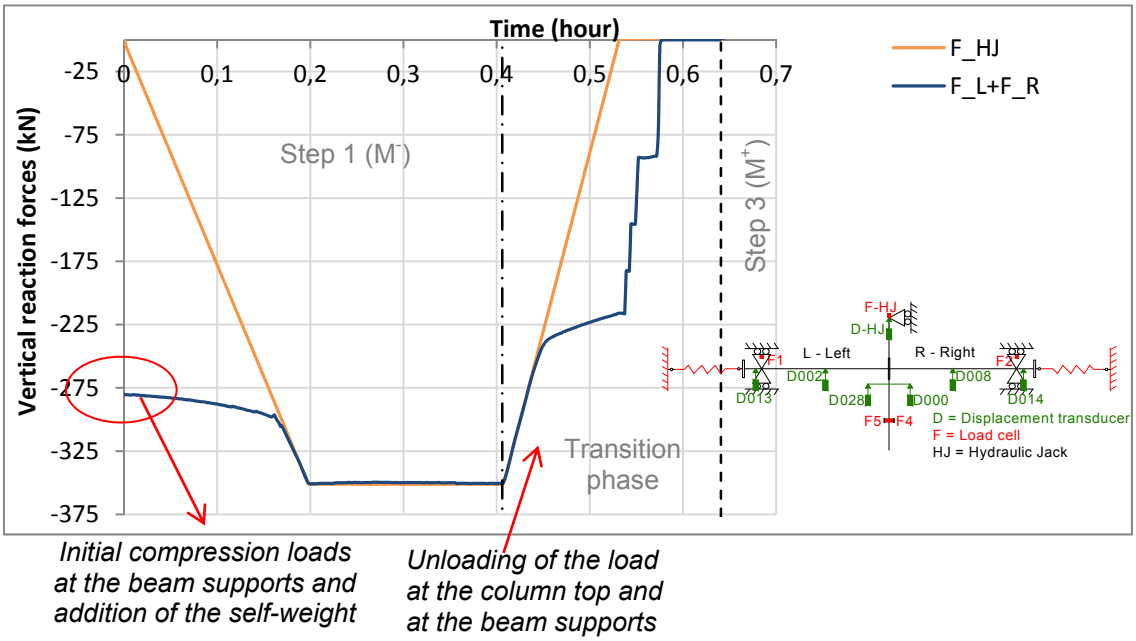

Figure 65: Load applied by the hydraulic jack compared to the sum of the reaction loads at the supports

III.2.3 Step by step behaviour: step 3 - Loss of the column and sagging bending moment

Figure 66 shows the evolution of the vertical loads measured by the hydraulic jack F_{HJ} at the column top; by the load cells F_1+F_2 at the top of the beam supports; and the vertical components of the spring forces. The test was

stopped two times at the beginning because of the spring restraints being working in compression (see §II.7.2.3). The concrete crushing is really progressive, without any sudden failure. It was observed that the concrete crushed against the column flanges around 2h03min (2.05h), and the entire slab width failed around 3h18min (3.3h). Even though, the load at the column top, F_{HJ}, continued to increase. The increase of the jack stroke (of 135 mm) was performed after the concrete failure, around 3h36min (3.61h). Each failure of bolt (Figure 67a) was really sudden, with a loud noise. The first bolt failed at 4h14min (4.23h): the vertical load at the jack reduced from 502 kN to 350 kN (Figure 66). The second bolt failure occurred at 4h35min (4.59h), and the load suddenly reduced from 393 kN to 300 kN. At the end of the test, the concrete crushing at the end of the left slab was observed (Figure 67b). This failure happened under sagging bending moment, and should be due to the concrete compression struts created on the last row of the shear studs because the slab was stopped before the end of the beam. Perhaps this failure corresponded to the sound heard around 3h09min (3.15h), which seemed to come from the concrete slab. The crack in the steel end-plate was not registered on this curve and should happen only after the bolts failures, once deformations of the end-plate increased.

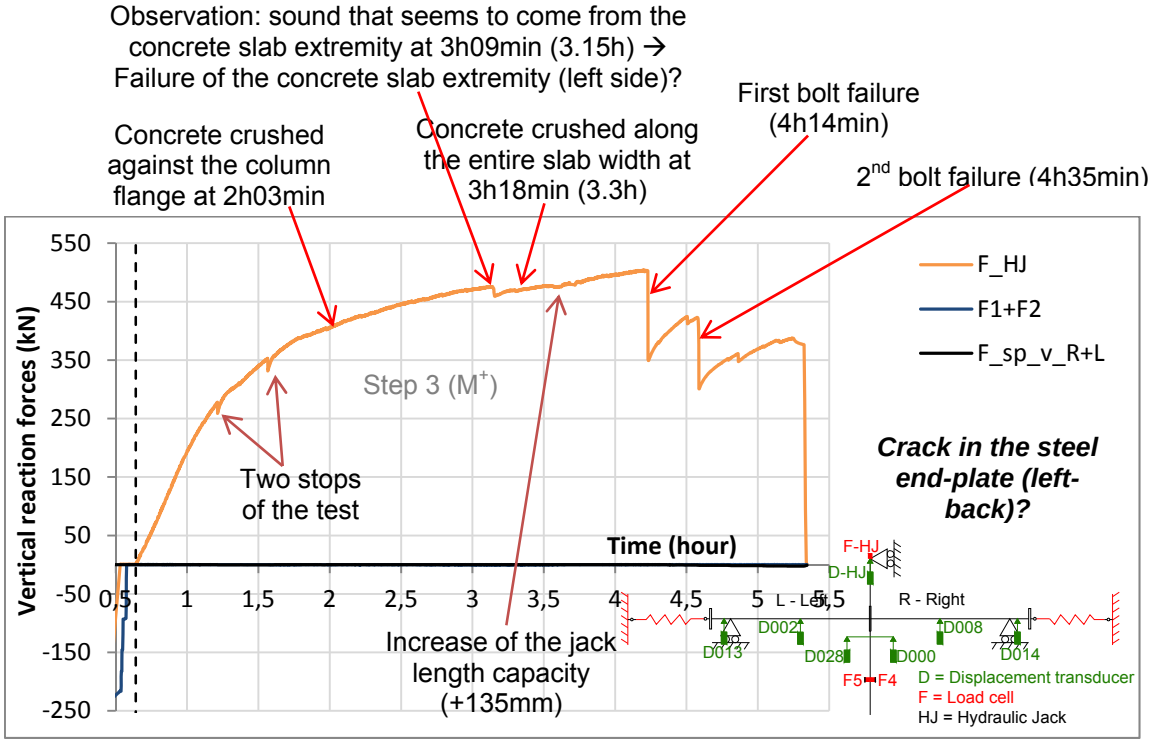

Figure 66: Evolution of the vertical loads during the step 3 (increase of sagging bending moment)

a) 

b) 

Figure 67: a) the two bolts failed; b) Concrete crushed at the end of the composite slab (left side)

The evolution of the composite joint deformation is shown in Figure 68. The rotation of the column increases in the opposite direction of the connection side where bolts from the bottom row failed: the column rotation suddenly increased on the right direction (Figure 69).

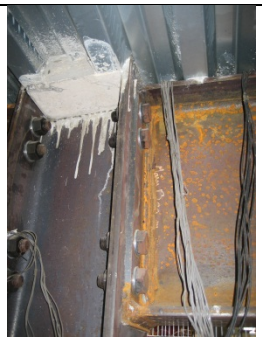
11min – Back/Left side


2h25min – Back/Left side

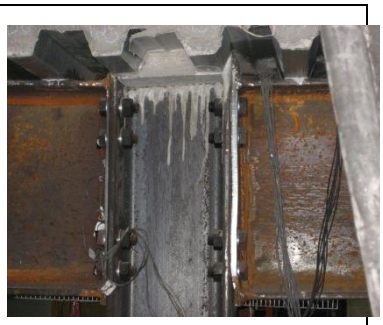
2h33min – Back side


3h18min – Back side


3h18min – Back side


3h54min – Front side


4h41min – Back side


End of the test – Back/left side

Figure 68: Evolution of the joint failure

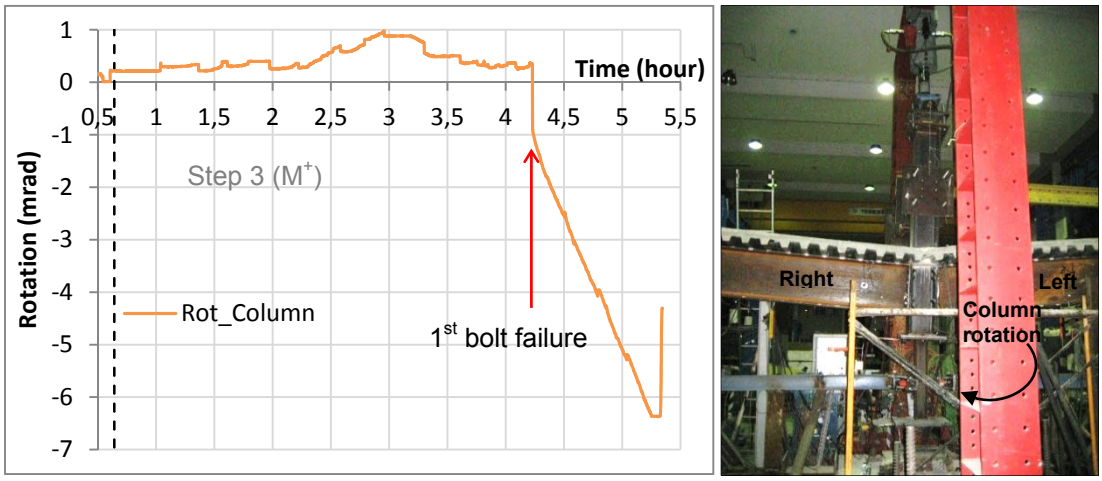

a) b)

Figure 69: Column rotation a) *vs* time (step 3); b) at the end of the test (view from the back)

Finally, the test was stopped after 5h21min. Figure 70 shows the evolution of the vertical displacements measured by the hydraulic jack D_{HJ}, by the wire transducers D000 and D028, and by the displacement transducers at mid-span of the beams (D008 and D002). The control of the hydraulic jack at the column top was made in term of displacement, and around 3h36min (3.6 h), the velocity was changed from 0.01 mm/sec to 0.02 mm/sec. The decrease at the end of the test corresponds to the unloading of the load at the column top. The rotation of the column is also showed by the change of rate for the measured dispalcements D000 and D028 from 4h14min.

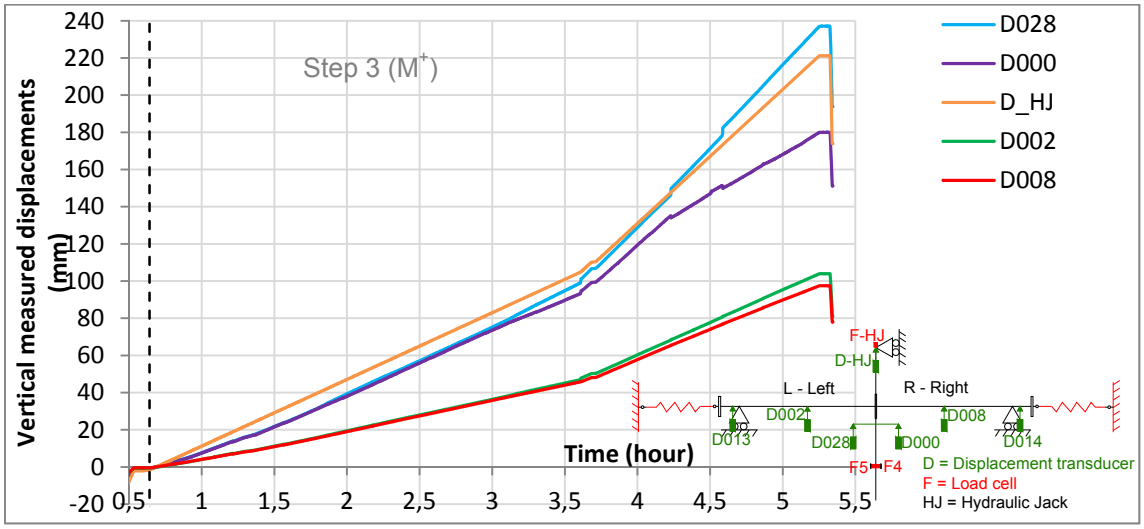

Figure 70: Vertical displacements near the beam-to-column joint during the entire test

Figure 71 shows the evolution of the total reaction loads during the entire test: i) the measured loads at the beam supports, F1+F2 (in step 3, the load cells F1 and F2 did not measure anymore the real reaction loads because of the unloading of the support system (see § II.6.1)); ii) the hydraulic jack load F_{HJ}; and iii) the reaction loads from the spring restraints. Just after the first bolt failure (on the left side), the column slightly rotated in the right direction, and the beam right end began to displace in the inside direction: the spring restraint

(right side) began to work in tension (maximum load at the end of the test: 91 kN).

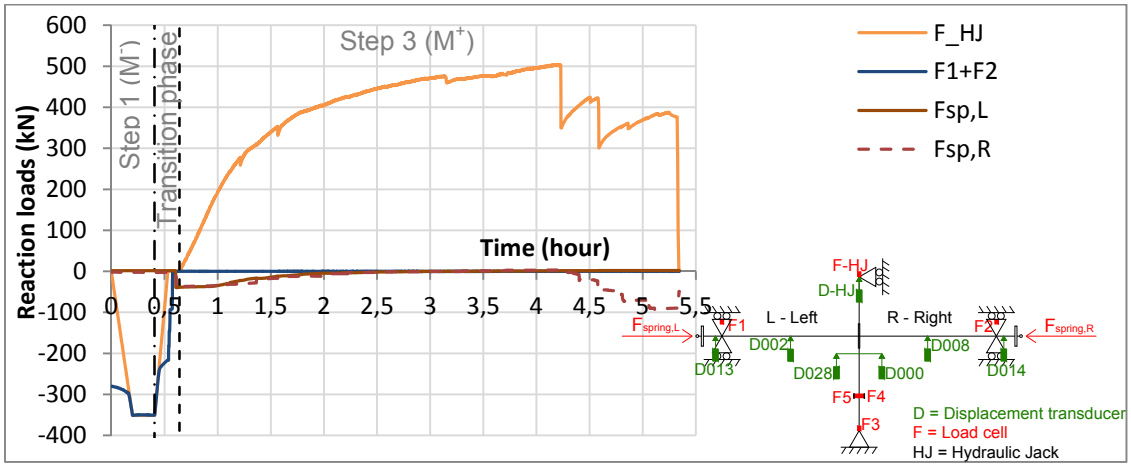

Figure 71: Evolution of the loads during the entire test

Figure 72 shows the evolution of the bending moment at the joint left and right sides *versus* time.

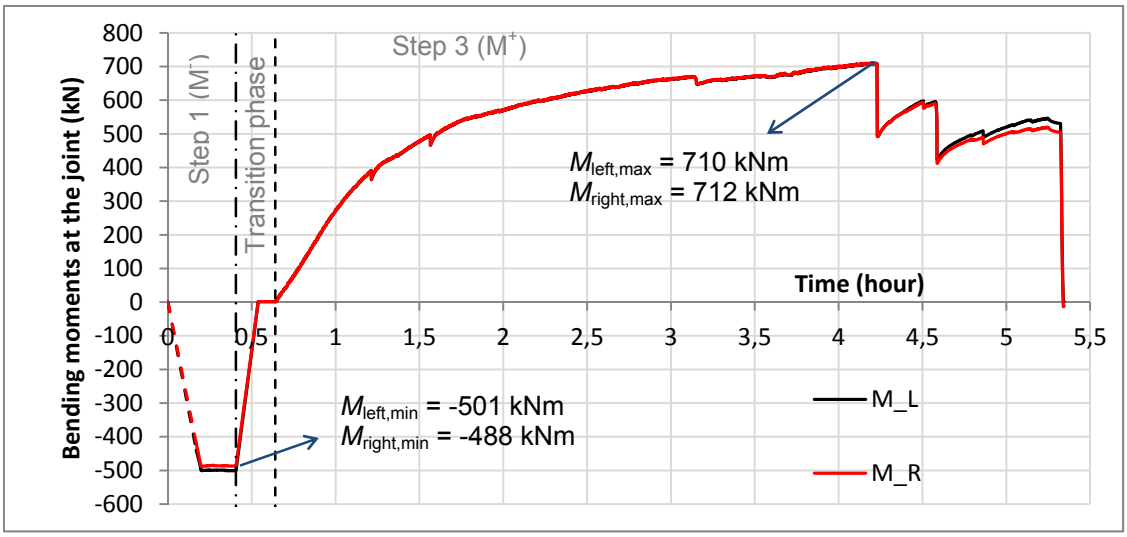

Figure 72: Bending moments at the connections left and right

III.2.4 Additional data

III.2.4.1 Strain gauges results

The results of the strain gauges presented in this section were not used during the joint behaviour study, but they could be used in future works, as the calibration of finite element models against the tests. Figure 73 and the equation hereafter present the loads in bolts versus time:

$$F = \varepsilon \times E \times A_s$$

where ε is the measured strain, E is the elastic Modulus equal to 205 869 mm^2 (estimation from the tensile coupon tests results in §0), and A_s = 561 mm^2 is the bolt section. The first bolt to fail was instrumented (with a strain gauge inside), but it did not measured well; the second bolt failed was not instrumented. The

bolt with the higher load in the chart corresponds to the bolt on the connection right, row 4. The elastic limit corresponds to 523 kN (black horizontal line), and the measured loads upper this value cannot be taken into account. Moreover, the strain gauges limitation in bolts corresponds to 0.5% (or 577.5 kN – blue horizontal line).

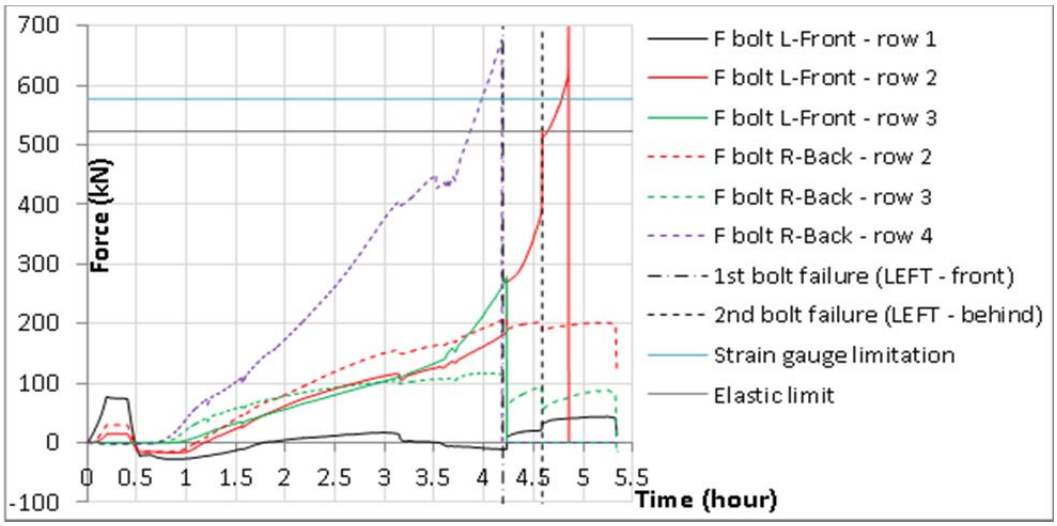

Figure 73: Loads into bolts calculated from the measured strain

Figure 74 shows the measured strains in 5 points on the column web, corresponding to the level of each bolt and of the steel rebars. The hogging bending moment was applied at 18min (0.3h – red curve), and the compression was well developed on the web bottom part, whereas tensile loads were more or less equals at the level of the two bolts from rows 1 and 2. However, under sagging bending moment (from 1h to 5h), a smaller tensile strain was measured at the level of bolt from row 4.

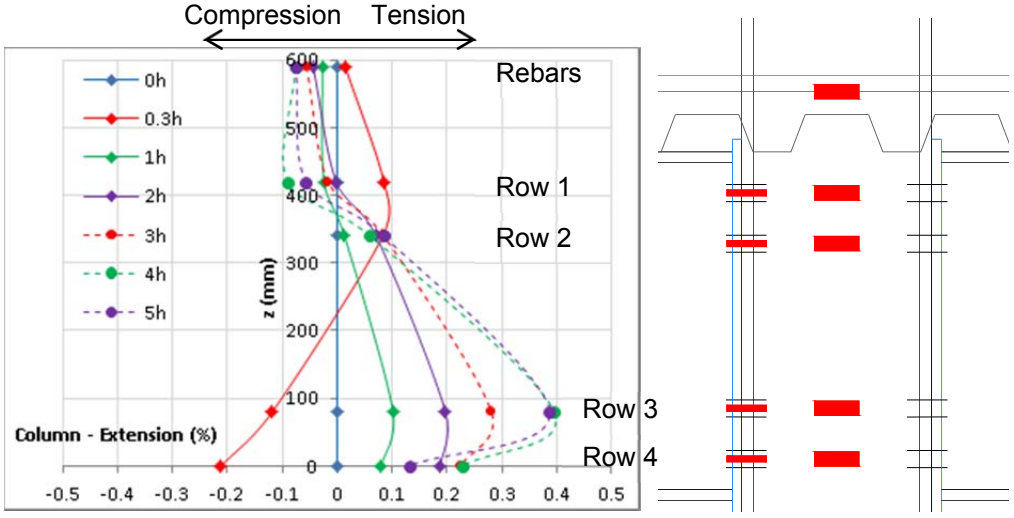

Figure 74: Measured strains on the column web

Figure 75 and Figure 76 show the strain measured at 500 mm from the end-plate on the web and on the bottom and top flanges of the steel beam. The sagging bending moment cannot be estimated based on the strains because the concrete component in compression was not measured.

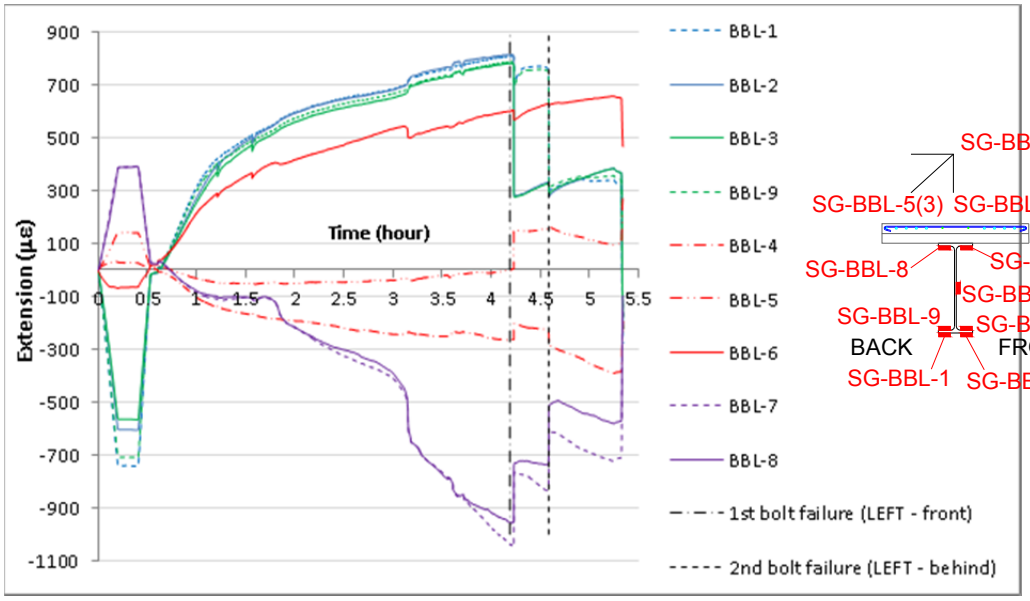

Figure 75: 500 mm from the connection left

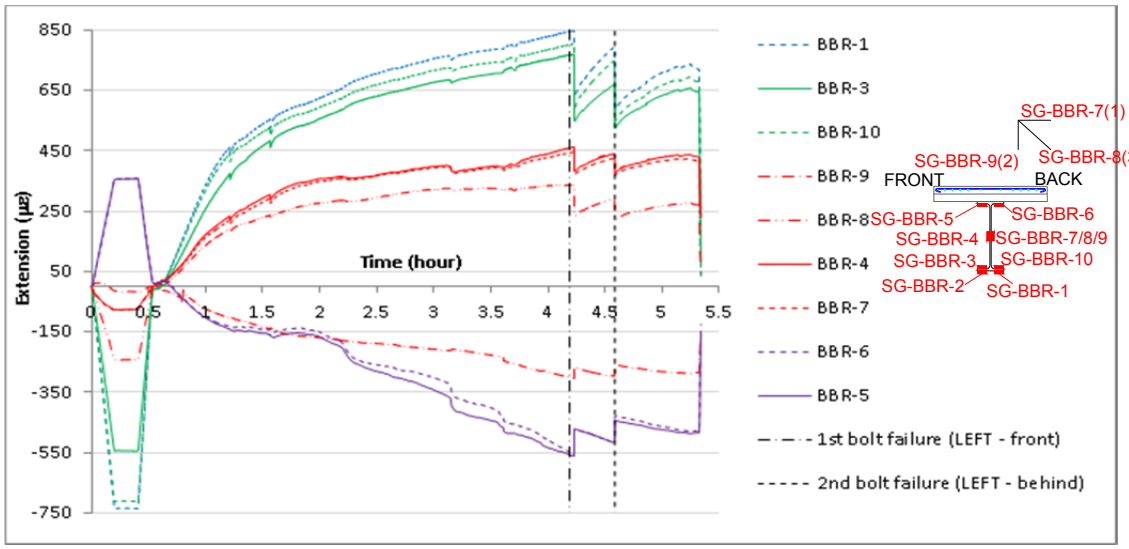

Figure 76: 500 mm from the connection right

Figure 77 and Figure 78 show the strain measured into the steel beam at 2500 mm from the end-plate (beams ends), on the web and on the bottom and top flanges.

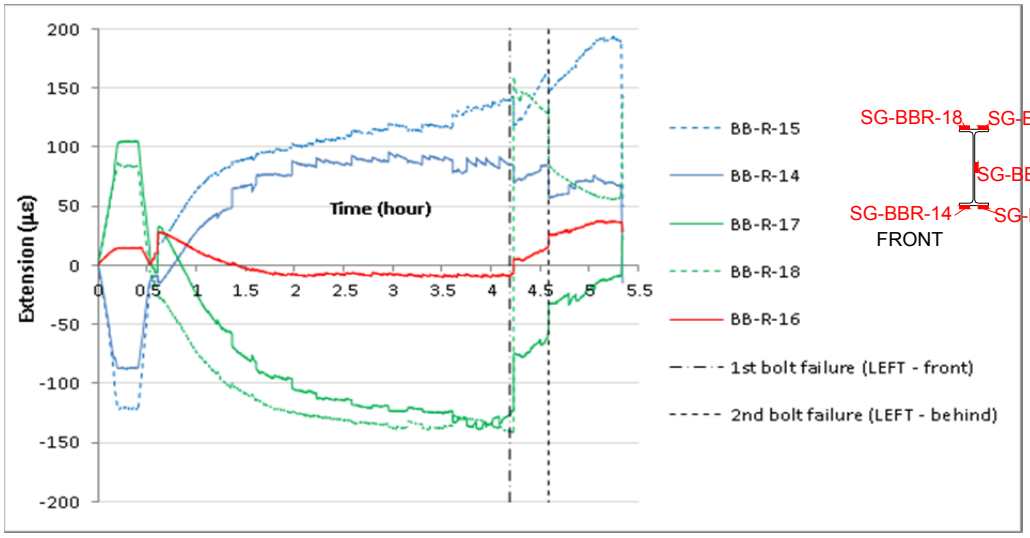

Figure 77: 2500 mm from the connection right

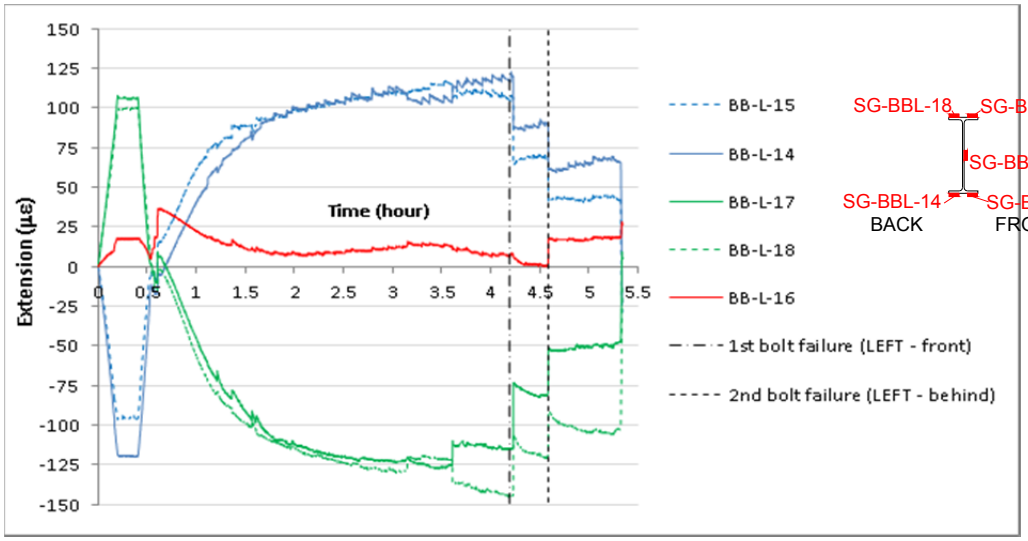

Figure 78: 2500 mm from the connection left

III.2.4.2Additional displacements measured during the test

The rotations of the springs are shown in Figure 79.

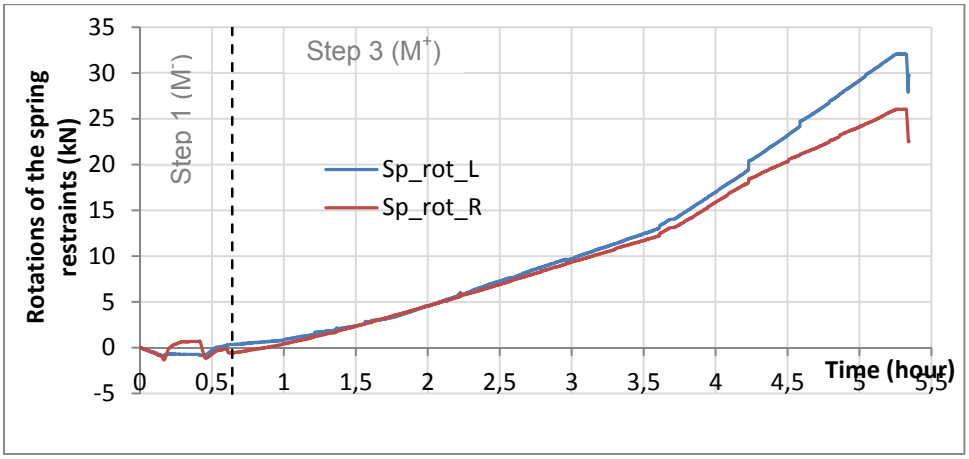

Figure 79: Spring rotations (L = left; R = right)

Figure 80 and Figure 81 show the evolution of, respectively, the bending moment at the joint and the total reaction load, versus the beam axial load (measured at the spring restraint and projected in the beam direction, $F_{sp,ax}$).

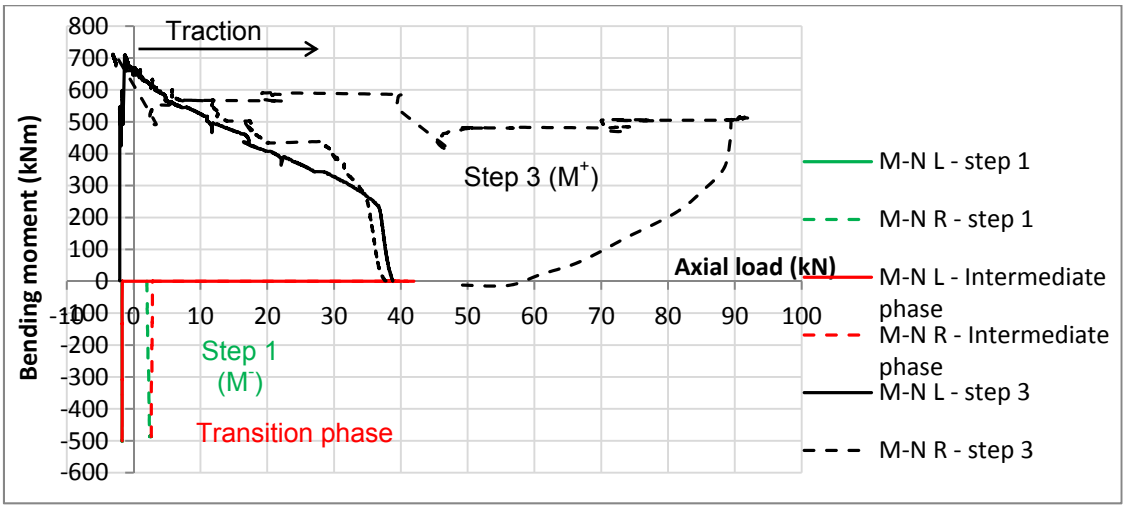

Figure 80: Joint bending moment vs axial forces at the joint ($F_{sp,ax}$)

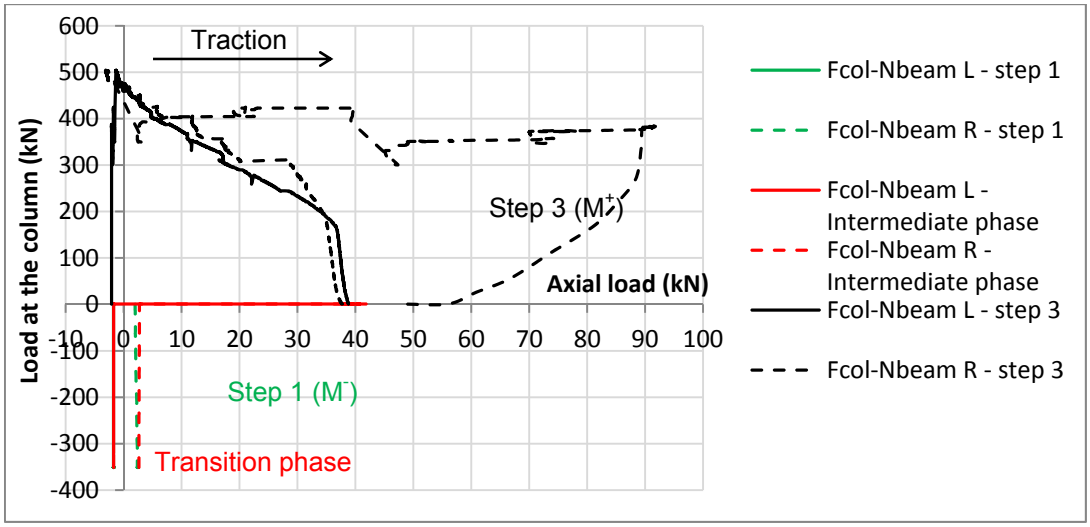

Figure 81: Vertical force at the column F_{HJ} vs vertical displ. measured at the column top (D_{HJ})

Figure 82 presents the evolution of the total vertical reaction load (F_L+F_R) versus the joint rotation.

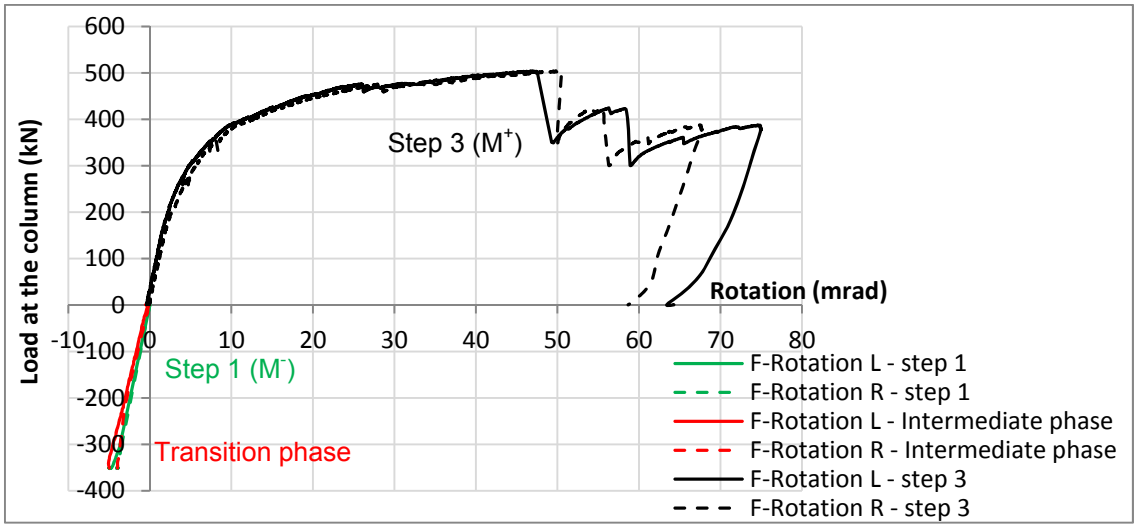

Figure 82: Vertical load at the column F_{HJ} vs rotation at the connection

The horizontal displacements measured at the beam ends are shown in Figure 83. The estimated horizontal displacements at the neutral axis of the steel beams $D_{beam,h,L \text{ and } R}$ (see §III.1.1.1) are represented by the black curves, and it can be observed that the left beam displaced in the outward direction, whereas the right side began to displace in the inward direction, then after the bolt failure, it displaced in the inward one.

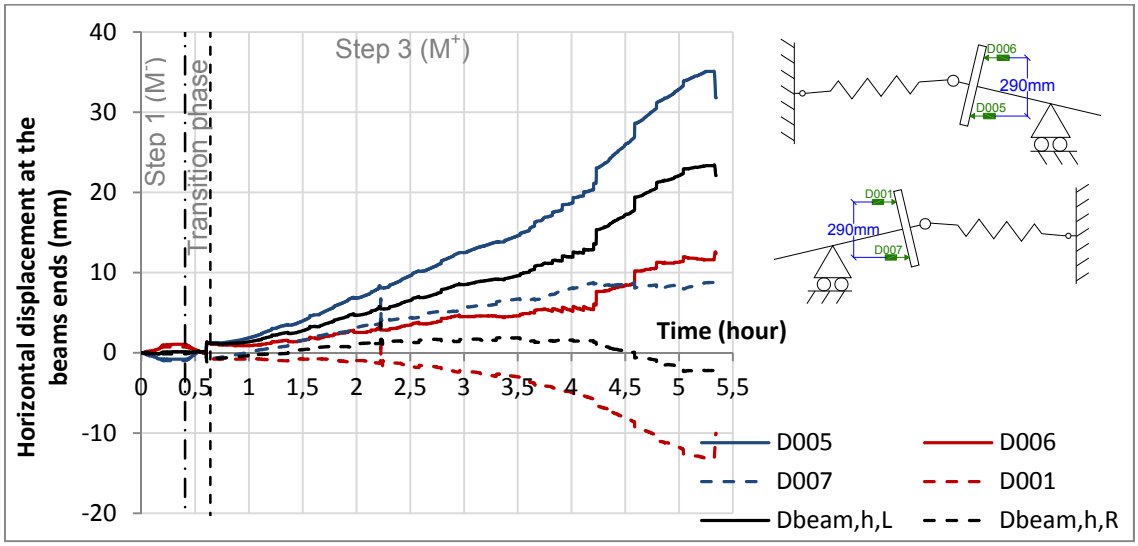

Figure 83: Horizontal displacements at the end of the left beam

Figure 84 presents the displacements of the beams out of the plan, measured by the two displacement transducers D025 and D026 at the beam ends, and by the two transducers D003 and D009 on the beam webs, initially situated at 1500 mm from the end-plate. The largest out of the plane displacement was measured at the bottom column (D015 = 23.5 mm).

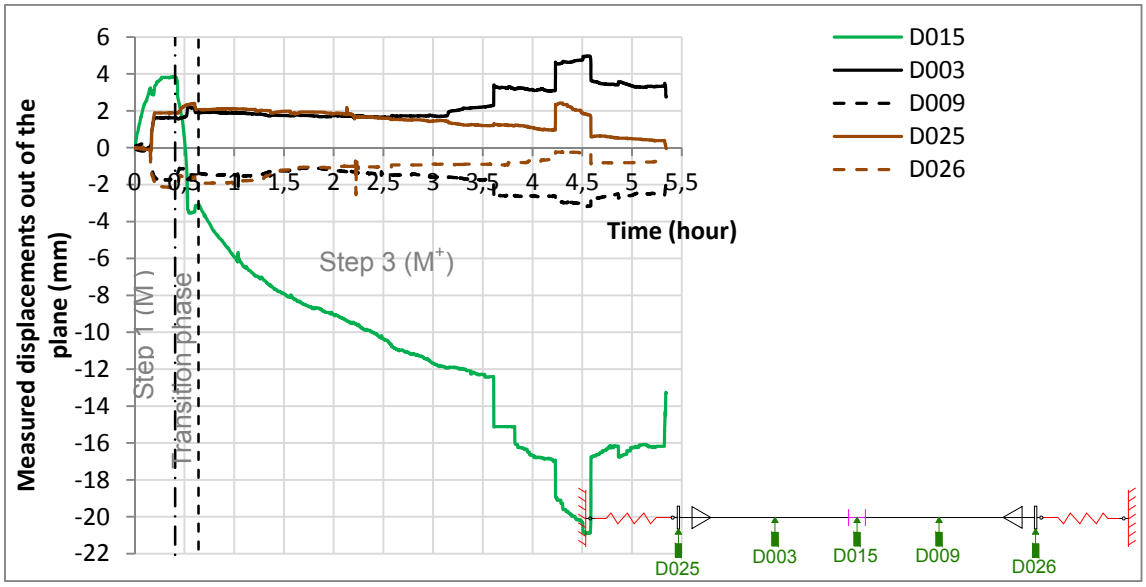

Figure 84: Evolution of the displacements measured out of the plan

III.3 Results of test 2

The global behaviour of the joint during the test is described in the following section, then the step by step behaviour is detailed, for each loading step, and finally, additional data a presented.

III.3.1 Joint behaviour (entire test)

III.3.1.1 Temperature results

Figure 85 presents the temperatures evolution during the entire test 2 in the right and left beams (at 200 mm from the connection), in the column centre, in the bottom bolt row, and in the concrete. Around 40 min., during step 2, the temperature increase rate was modified from the maximum rate to 300ºC/hour, which created a peak in temperatures curves. Finally, 500ºC was reached in the beam bottom flanges, whereas the temperature increased faster in the web because of the reduced thickness. Temperatures in beams top flanges were much lower because they were only heated by heat transfer from web, which was reduced by the composite slab protection. During step 3, the temperature was well kept constant in the beam bottom flanges. Concrete temperatures did not rise above 200ºC, and the temperature increase due to conduction in the column above the composite slab was very limited (maximum 114ºC was measured in the column flange at 100 mm from the concrete slab). At the end of the test, maxima temperatures measured in the joint were: 407ºC in bolts heads (row 4), 397ºC in end-plates, 469ºC in the column web and 398ºC in column flanges. The temperatures of the right beam (web and top flange) needed to be increased more than on the left beam to maintain the 500ºC in the beam bottom flange, perhaps due to differences in the thermal insulation. The evolutions of all measured temperatures are detailed in §III.3.3.

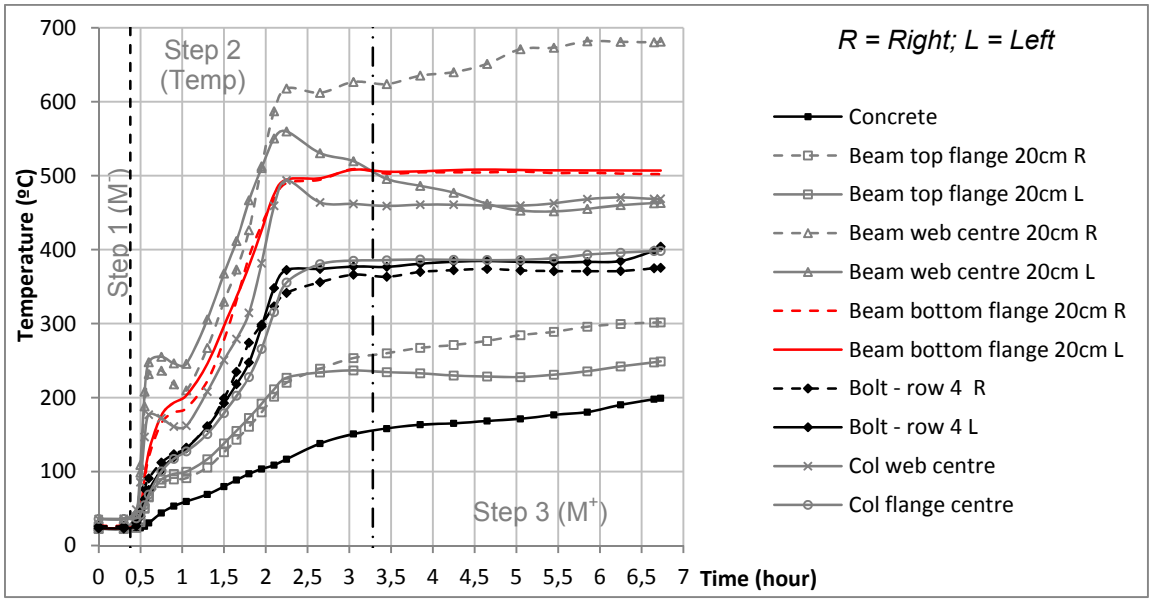

Figure 85: Evolution of the temperatures during test 2

III.3.1.2 Bending moments variation and failure modes

The evolution of the total reaction load *versus* the vertical displacement of the joint, and the bending moment *versus* the rotation are depicted in Figure 86 and Figure 87. The hogging bending moment was initially reached during step 1 (around -200 kNm), followed by a variation of this moment during the increase of temperatures in step 2. At the beginning of step 2, reaction loads increased due to the thermal expansion of the structure. After a while, these reaction loads decreased because of the steel properties degradation due to high temperatures (Figure 86). In step 3, the loss of the column was really progressive as the hydraulic jack at the column top imposed a constant displacement rate, and the vertical load at the column top increased up to the failure of the joint under sagging bending moment. Concrete crushing in compression was the first failure observed, but this failure was really progressive and cannot be seen on the load-displacement or moment-rotation curves (Figure 87). The sagging bending moment reached a maximum value of 565 kNm (500ºC). One first bolt suddenly failed after 74 mrad of connection rotation and the sagging bending moment reduced from 528 kNm to 348 kNm. Then a second bolt failed and the bending moment decreased at 200 kNm. Finally, the test was stopped at 85 mrad of connection rotation; a third bolt suddenly failed after the end of the test.

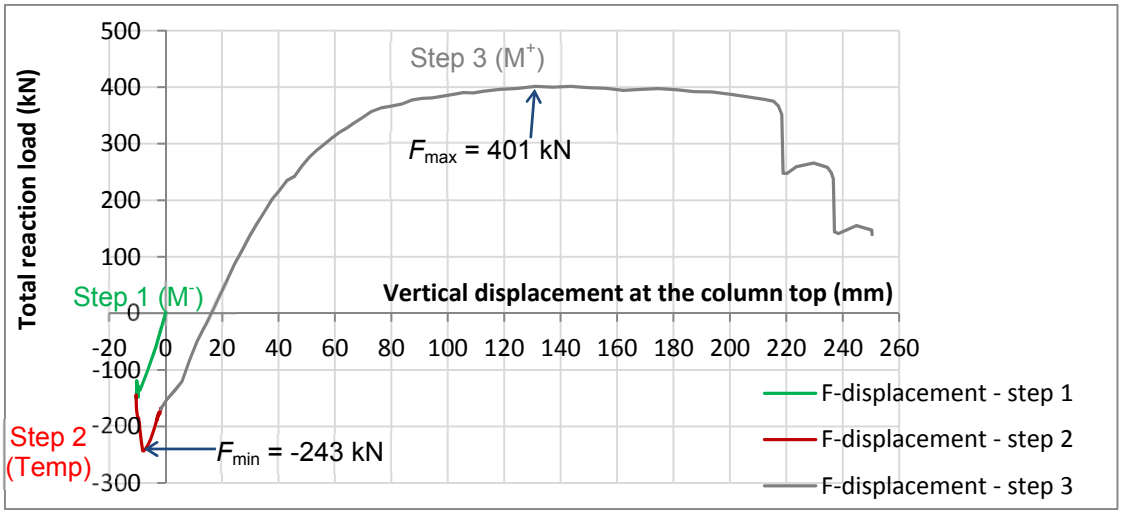

Figure 86: Total reaction load (F_L+F_R) vs vertical displ. measured at the column top (D_{HJ})

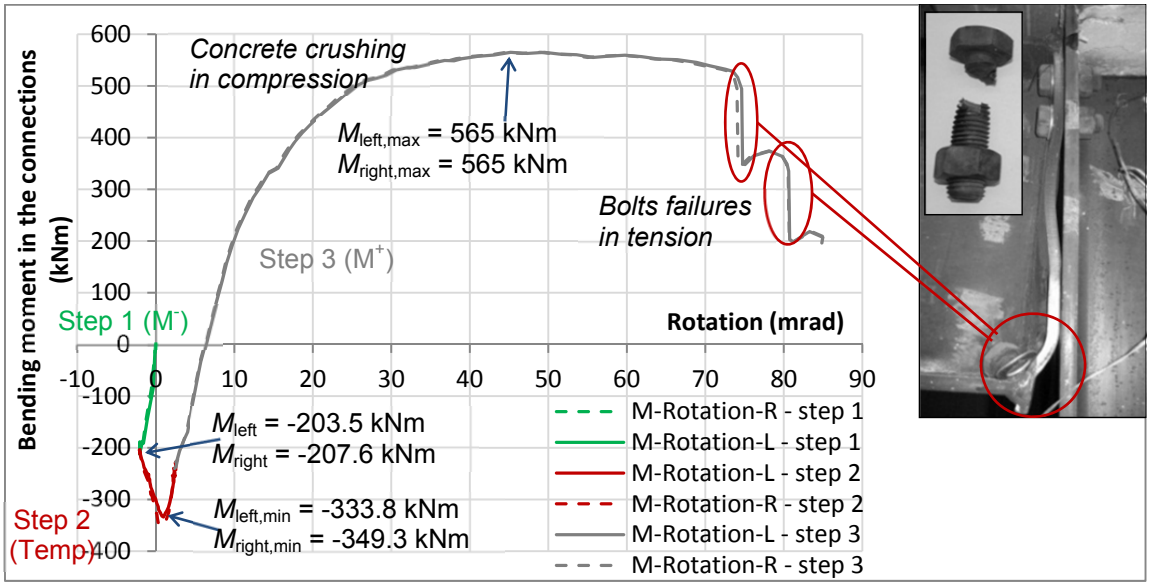

Figure 87: Bending moment at the joint vs rotation of the connections

Figure 88 shows the deformation of the joint at the end of the test: the test was stopped at 250 mm of vertical displacement, and 85 mrad of connection rotation. No difference of rotation between left and right sides could be highlighted because the column rotation was not measured in the test; however, it seemed that the column remained in the vertical position. The failed bolts were localised: i) in the bottom bolt rows - because of higher tensile loads under sagging bending moment, ii) in the left connection due to a slight asymmetric joint deformation. The steel end-plates mainly deformed in the bottom and centre parts and showed a high ductility; the left end-plate slightly deformed on the top, under hogging bending moment. The crushed concrete slab is shown in Figure 89, and the final sub-frame deformation is shown in Figure 90.

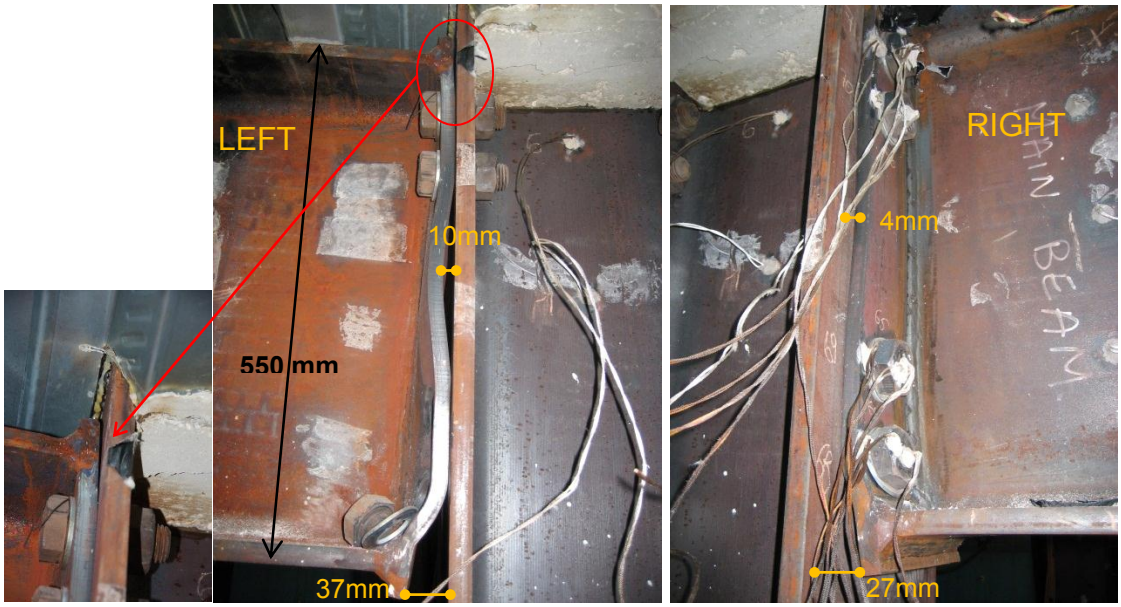

Figure 88: Joint deformation – front view

Figure 89: Crushed concrete slab at the end of the test

Figure 90: Final deformation of the sub-frame at the end of the test

III.3.2 Step by step behaviour: step 1 - Initial hogging bending moment

The initial hogging bending moment was introduced in two phases: i) phase 1: the hydraulic jack at the top of the column increased the load; ii) phase 2: the column base support (cylinder) was positioned (Figure 91).

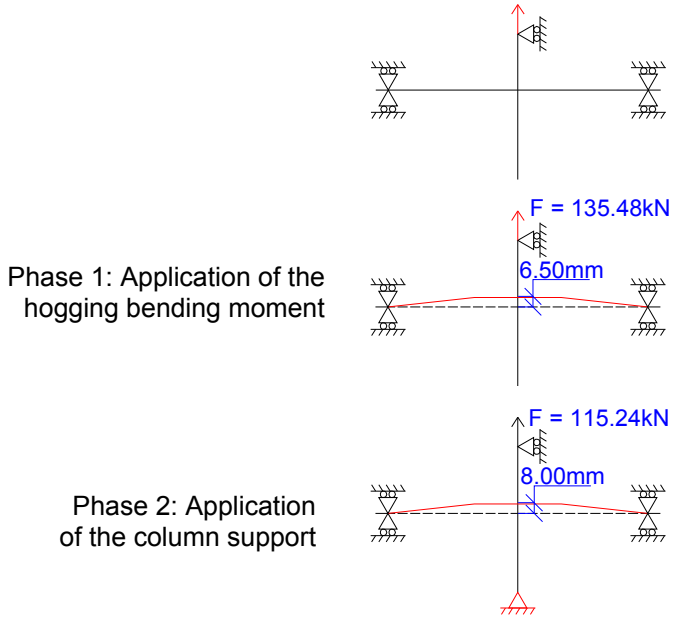

Figure 91: Initial hogging moment in the connection

Figure 92 shows the displacements and loads measured by the displacement transducers (in green) and the load cells (in red).

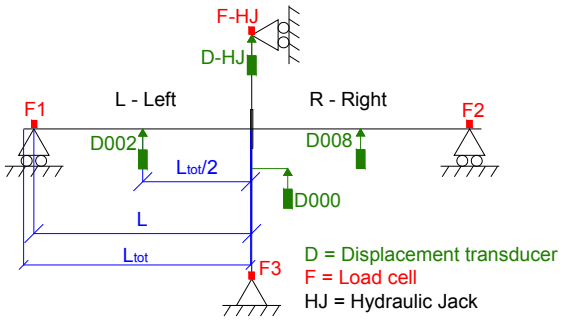

Figure 92: Main displacements and loads measured during the test

During the phase 1, the load and displacement of the jack were increased up to reach the loads at the beam supports that would create the hogging bending moment $M_{fi,d}$=236.4kNm.

Figure 93 presents the evolution of the vertical displacements measured near the beam-to-column joint. The displacement transducer located at mid-span of the left beam (D002) was trapped at the beginning of the test and the displacement evolution *versus* time was estimated by the dashed green curve.

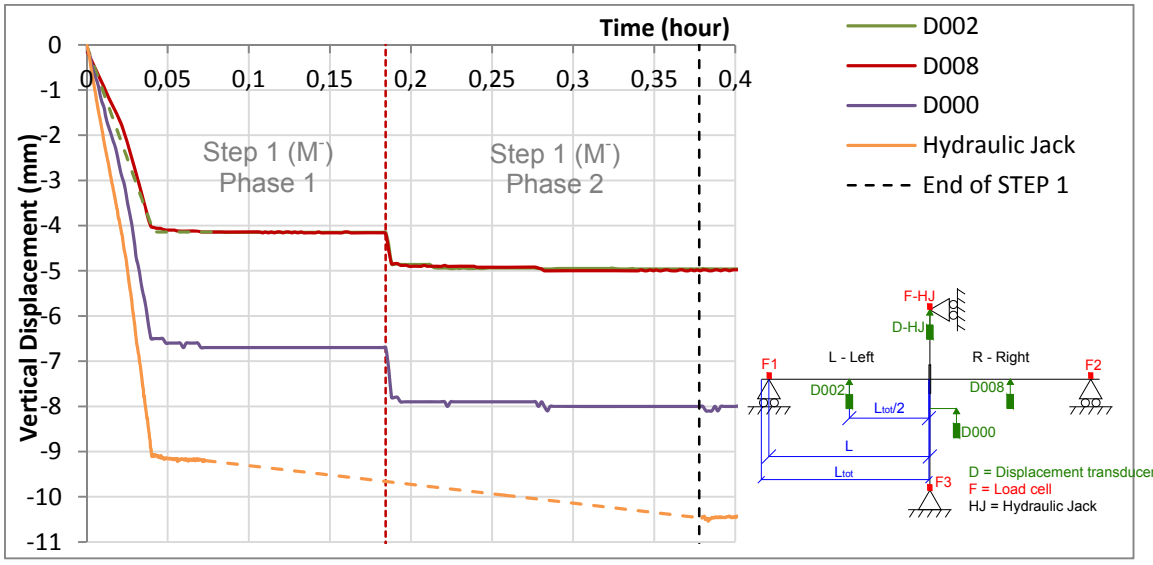

Figure 93: Vertical displacements near the beam-to-column joint during the application of the initial loads (hogging bending moment)

The hydraulic jack was stopped after 5 min and the evolution of the load and the displacement at the column top was not visible anymore, but was estimated by the dashed orange curve. During the phase 2, the cylinder at the column base increased the load (in order to enter in contact with the column), and slightly modified the displacement of the column joint (increase of the hogging bending moment) as well as the reaction load at the column top (see Table 9). The variation of displacement during the phase 2 at the hydraulic jack was registered and observed at the beginning of the step 2 (application of temperatures), when it was connected again. However, the apparent load was initialized (equal 0), so the real decrease of the load in the hydraulic jack was not known, but was estimated according to the static equilibrium of the reaction loads: $F_1+F_2 = F_{HJ} + F_3$, including the slight difference ΔF observed between the hydraulic jack value and the load cells values at the end of the phase 1. Table 10 presents the values of displacements and reaction loads during the step1, at the end of each phase, 1 and 2.

Table 10: Displacements and loads measured just after the application of the hogging bending moment and the column base support

	Phase 1 - Hogging bending moment (2min)		Phase 2 - Column support (23min)	
STEP 1 - Initial loads	Load (kN)	Displ. (mm)	Load (kN)	Displ. (mm)
Column base (F3 and D000)	0.00	-6.50*	+30.92	-8.00*
Beam mid-span (LEFT – D002)	----	-4.14	----	-4.96
Beam mid-span (RIGHT – D008)	----	-4.02	----	-4.98
Beam support (LEFT – F1)	-66.71	----	-72.30	----
Beam support (RIGHT – F2)	-68.86	----	-73.77	----
Hydraulic Jack (F-HJ and D-HJ)	-135.48	-9.07	*-115.24***	-10.50
Hogging bending moment at the connection	M_{left} = -187.74 kNm M_{right} = -193.82 kNm		M_{left} = -203.48 kNm M_{right} = -207.62 kNm	

* Measured by the wire displacement transducer at the bottom column D000

** Estimated value (not measured: the jack measures were stopped after 5 min)

Figure 94 presents the comparison between the sum of the loads measured at the column (FHJ+F3) and the sum of the reaction loads measured at the beam supports. Before loading the joint (phase 1), the end of each beam was restrained and an initial load was measured by the load cells F1 and F2, respectively equal to -51,1kN and -50,8kN, which gives the total initial load equal to -101.9kN.

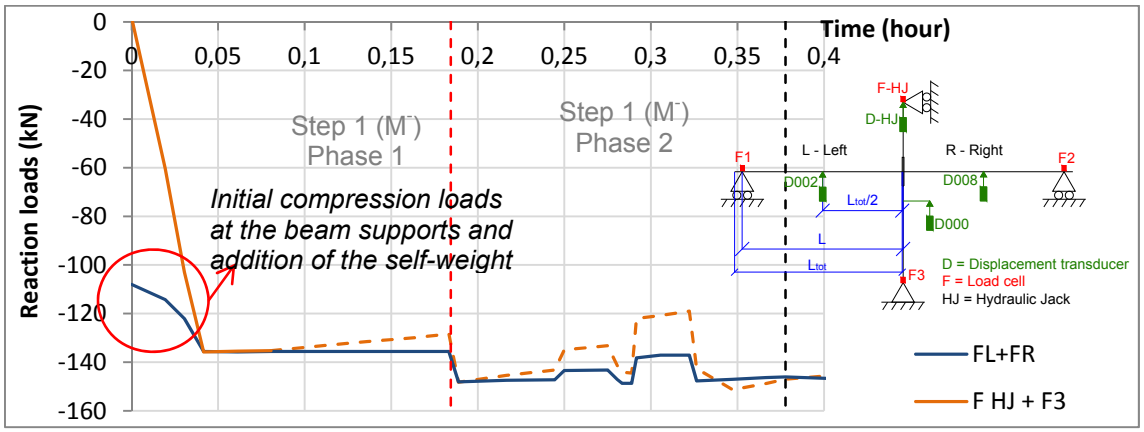

Figure 94: Load applied by the hydraulic jack compared to the sum of the reaction loads at the supports

III.3.3 Step by step behaviour: step 2 - Temperatures (500ºC)

The second loading step consisted to increase slowly the temperature of the heated zone until 500ºC in the beam bottom flanges (at a distance 20 cm from the joint). The thermal expansion of the beams was completely free.

III.3.3.1 Evolution of the temperatures

Figure 95, Figure 96 and Figure 97 show the evolution of the temperatures in the beam at respectively 20 cm, 50 cm and 1 m from the end-plate. During the step 3, the temperature was well kept constant in the beam bottom flanges, but was increased on the right and decreased on the left beams webs. Indeed, the thermocouples connected to the controller only controlled the temperature in the bottom flanges, and the temperature in the web depended of the intensity with which the electrical power was sent to the FCP elements; as the web was thinner than the flanges, the temperature did not evolve in the same way.

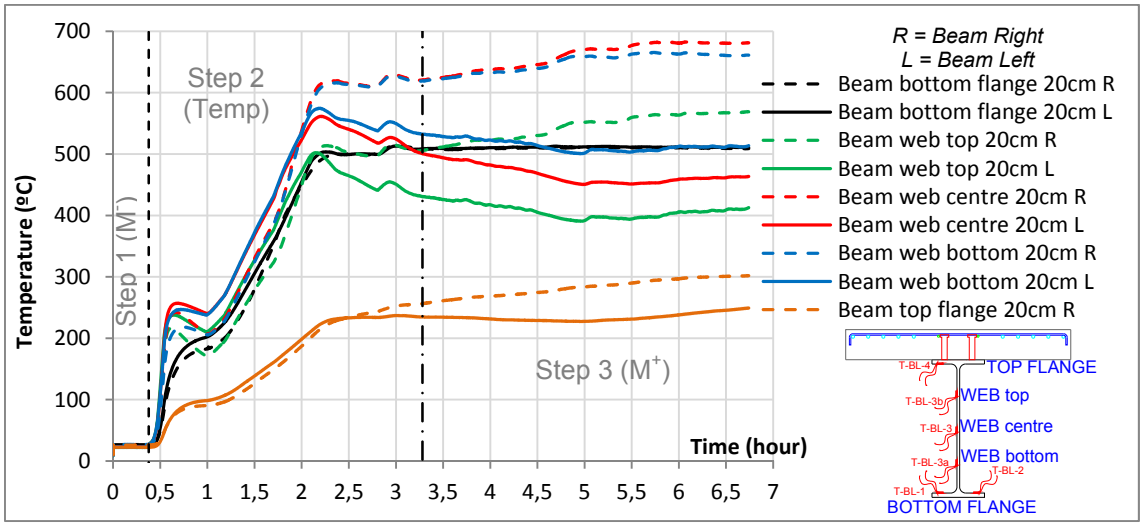

Figure 95: Evolution of the temperatures (T) in the beams at 20 cm from the connection during the test 2 (R = right; L = left)

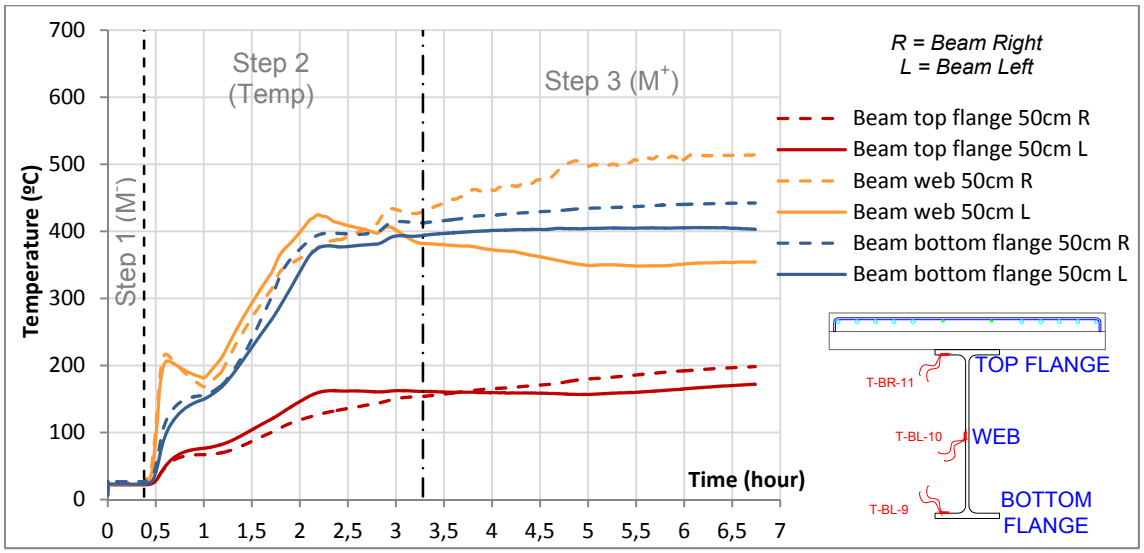

Figure 96: Evolution of the temperatures (T) in the beams at 50 cm from the connection during the test 2 (R = right; L = left)

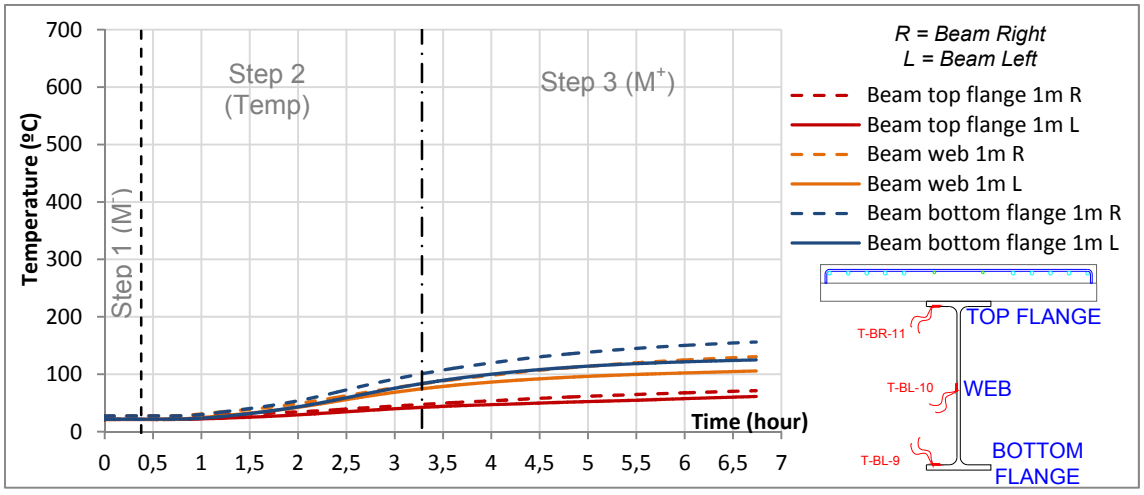

Figure 97: Evolution of the temperatures (T) in the beams at 1 m from the connection during the test 2 (R = right; L = left)

Figure 98 shows the evolution of the temperatures of bolt heads at each side of the joint. Table 11 shows that temperatures measured at the head of the bolt, inside the bolt (around 3 cm from the head) and at the end-plate surface were much closed, at three different moments of the test: at the end of the increase of the temperatures during the step 2, at the end of the step 2, and at the end of the test. The differences (diff.) between the connections left and right are showed. The evolution of temperatures in the column is presented in Figure 99.

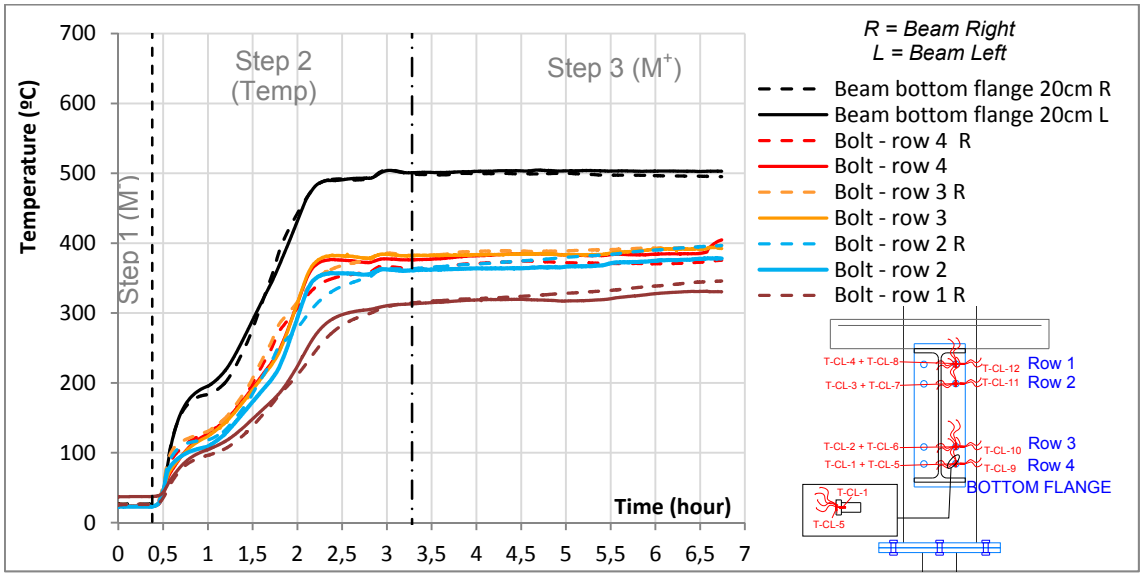

Figure 98: Evolution of the temperatures (T) in the bolts heads during test 2 (R = right; L = left)

Table 11: Main temperatures measured along the test at the connection zones

	TEMPERATURES								
	Stop of the increase (2h12min)			End of step 2 (3h17min)			End of the test (6h44min)		
	Left	Right	Diff. (%)	Left	Right	Diff. (%)	Left	Right	Diff. (%)
Bolt head row 1	268.2	245.3	8.5	313.1	314.4	-0.4	330.4	345.8	-4.7
Bolt head row 2	349.4	311.1	11.0	361.3	363.2	-0.5	378.1	396.6	-4.9
Bolt head row 3	372.7	347.6	6.7	382.2	382.5	-0.1	392.5	396.7	-1.1
Bolt head row 4	368.3	336.7	8.6	376.3	363.2	3.5	404	375.5	7.1
Bolt In row 1	278.5	240.9	13.5	315.5	310.9	1.5	333.5	344.7	-3.4
Bolt In row 2	365.5	315.7	13.6	373.2	363.2	2.7	385.3	396.0	-2.8
Bolt In row 3	384.6	365.1	5.1	387.4	384.9	0.6	395.0	396.0	-0.3
Bolt In row 4	440.6	357.1	19.0	393.1	348.3	11.4	406.4	352.1	13.4
End-Plate row 1	271.4	251.9	7.2	316.8	320.3	-1.1	335.9	349.0	-3.9
End-Plate row 2	353.7	298.6	15.6	376.0	357.3	5.0	395.3	387.3	2.0
End-Plate row 3	358.9	341.8	4.8	383.6	379.5	1.1	397.3	395.5	0.5
End-Plate row 4	351.2	330.2	6.0	375.4	361.5	3.7	394.1	374.0	5.1

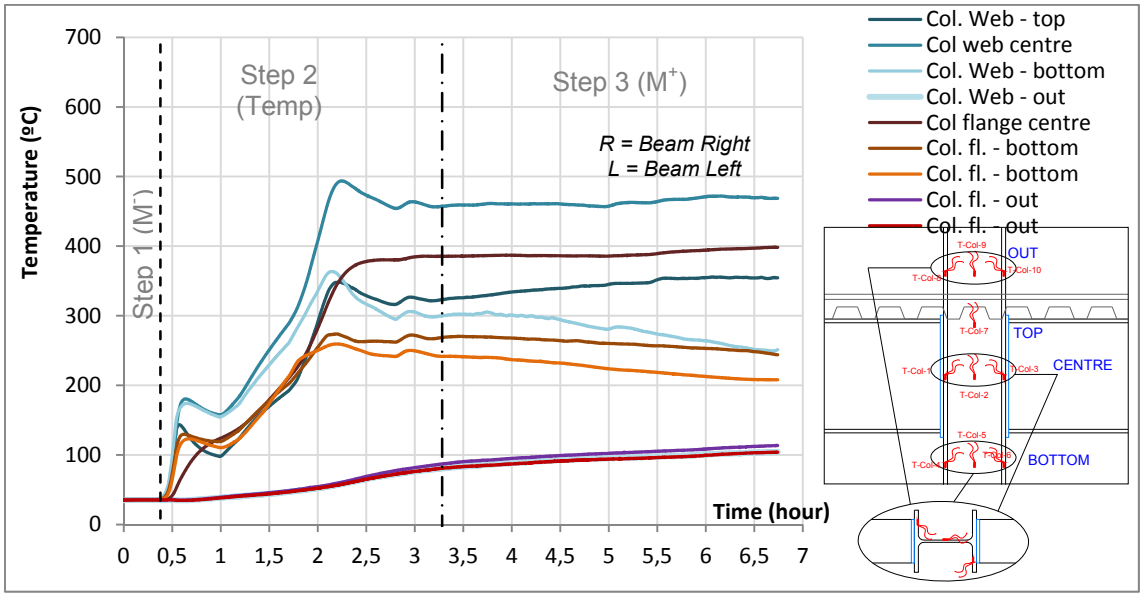

Figure 99: Evolution of the temperature during test 2 in the column

The maxima temperatures registered into the composite slab at the end of the test were equal to 200ºC in the concrete, 278ºC in the steel sheet, 96ºC in the steel rebar and 196ºC in the head of the shear stud connector. It was also observed that the increase of temperature due to conduction in the column above the composite slab was very limited, with a maximum measured temperature equal to 114ºC in the column flange at the end of the test. Table 12 details the main temperatures measured in beams and column.

Table 12: Main Temperatures measured along the test in beams and column

	TEMPERATURES								
	Stop of the increase (2h12min)			End of step 2 (3h17min)			End of the test (6h44min)		
	Left (ºC)	Right (ºC)	Diff. (%)	Left (ºC)	Right (ºC)	Diff. (%)	Left (ºC)	Right (ºC)	Diff. (%)
Top flange 20cm	223.1	215.1	3.6	234.5	256.3	-9.3	234.5	301.9	-28.7
Web 20cm *	545.0	577.9	-6.0	487.7	582.0	-19.3	462.7	637.2	-37.7
Bottom Flange 20cm **	491.8	485.4	1.3	504.7	503.2	0.3	507.0	502.1	1.0
Top flange 50cm	160	127.2	20.5	161.3	154.1	4.5	172.1	198.3	-15.2
Web 50cm	424.6	377.5	11.1	382.0	429.5	-12.4	354.3	514.1	-45.1
Bottom Flange 50cm ***	375.0	389.5	-3.9	394.6	407.8	-3.3	403.8	438.0	-8.5
Top flange 1m	31.3	36.1	-15.3	42.3	47.4	-12.1	61.2	71.2	-16.3
Web 1m	47.5	54.1	-13.9	74.6	83.3	-11.7	105.7	130.4	-23.4
Bottom Flange 1m	49.1	60.9	-24.0	83.7	100.8	-20.4	124.9	156.0	-24.9
Column web centre	490.8		---	457.1		---	468.7		---
Column flange centre	345.6		---	385.4		---	398.3		---

* Average of the three temperatures measured in the web (574.1; 561.3; 499.7 after 2h12min)
** Average of the two temperatures measured in the flange (481.8 and 501.8 after 2h12min)
*** Average of the two temperatures measured in the flange (375.9 and 374.1 after 2h12min)

III.3.3.2Evolution of the displacements and loads

Figure 100 shows the variation of the vertical displacements of the joint (D000), of the beams mid-span (D002 and D008) and of the column top (Hydraulic Jack). The displacement D000 was measured using a wire transducer at the bottom column, and decreased much faster than the other displacements, from -8 mm at the beginning of the step to +4.6 mm at the end of the step 2 (see Table 13). The variation of displacement was around 6 mm for each transducer D002 and D008, 9 mm at the hydraulic jack and 13 mm at the wire transducer. The cylinder at the column base began to lose oil and let the sub-frame to slowly drop.

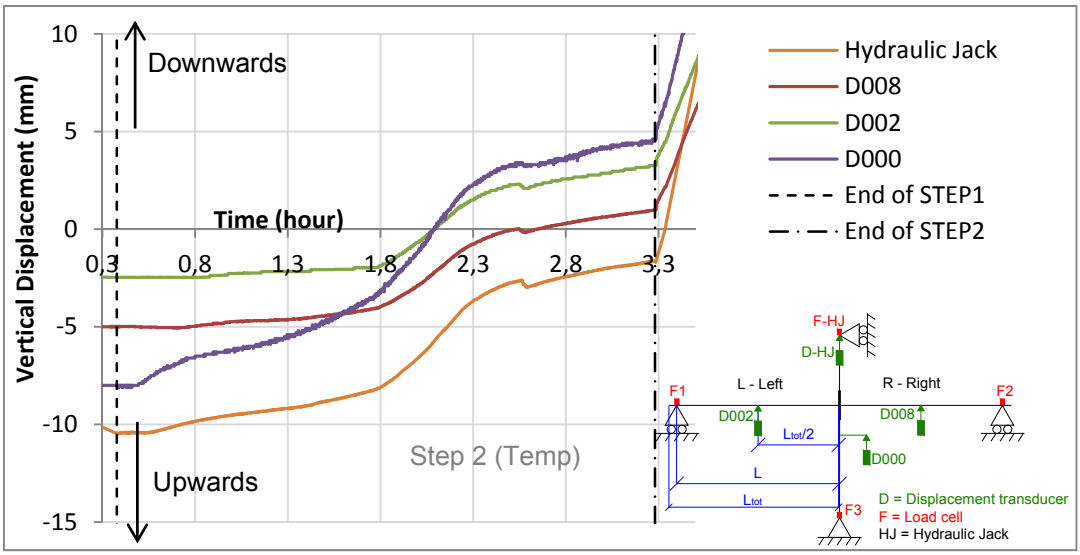

Figure 100: Vertical displacements near the beam-to-column joint during the increase of temperatures

Table 13: Main reaction loads and displacements during the step 2

	STEP 2 - Temperatures	Begin of step 2 (23min)	Max. Load (1h50min)	Stop of the increase (2h12min)	End of step 2 (3h17min)
TEMP (ºC)	Beam bottom flange LEFT - 20cm	23.5	407.3	491.8	504.65
	Beam bottom flange RIGHT - 20cm	26.85	418.7	485.4	503.2
Load (kN)	Beam support LEFT (FL)	-72.30	-118.60	-104.47	-80.83
	Beam support RIGHT (FR)	-73.77	-124.09	-110.56	-85.25
	Total reaction Load (FL+FR)	-146.07	-242.69	-215.03	-166.08
	Column base (F3)	-30.20	-128.02	-98.88	-51.70
	Column top (F-HJ)	-115.24	-115.27	-114.88	-117.72
	Total reaction column	-147.02	-243.29	-213.76	-169.42
Displ. (mm)	Beam mid-span LEFT (D002)	-4.96	-4.07	-1.69	0.77
	Beam mid-span RIGHT (D008)	-4.98	-3.70	-1.44	0.98
	Column base (D000)	-8.00	-2.60	1.20	4.60
	Column Top (D-HJ)	-10.50	-7.73	-4.63	-1.68

Figure 101 compares the evolution of the reaction loads in the two beam supports (F_L+F_R) to the reaction loads in the entire column (F_{HJ}+F_3), and Figure

102 presents the temperatures evolution in the beams during the step 2. At the beginning of the temperatures increase, the joint zone tended to expand and reaction loads increased. The maximum load measured in the column was 243.29 kN, and happened around 400ºC in the bottom flange. The temperatures increase stopped around 2h12min (2.2h), and the displacements continued to go downwards (Figure 100) due to the cylinder at the column base that was losing oil.

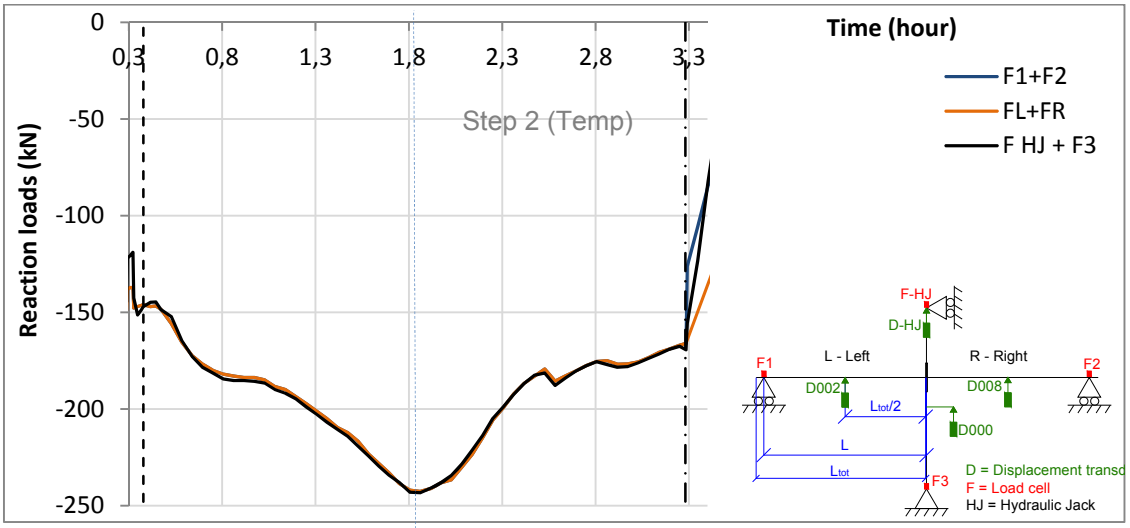

Figure 101: Comparison of the total load into the column (F_{HJ}+F_3) with the total reaction load at the two supports of the beam (F_L+F_R)

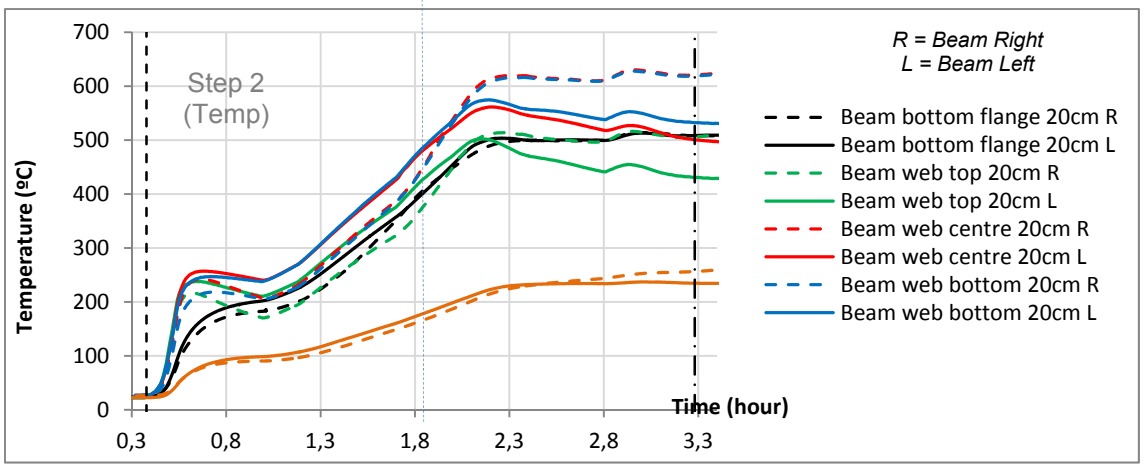

Figure 102: Evolution of the temperatures in the beams (20 cm from the end-plates)

The hogging bending moment increased during the heated phase, up to minima values of -333.8 kNm on the left and -349.3 kNm on the right connections (Figure 103).

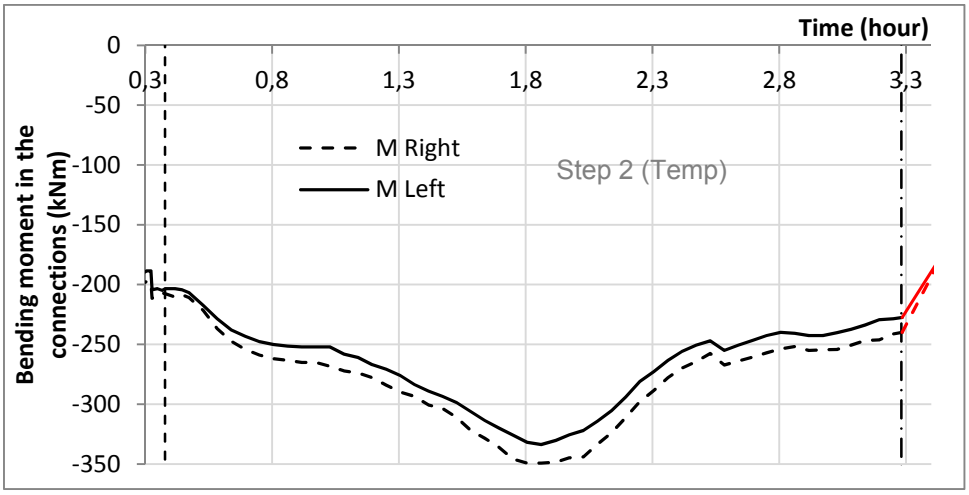

Figure 103: Evolution of the bending moment in the connections left and right

III.3.4 Step by step behaviour: step 3 - Loss of the column and sagging bending moment

In this step, the hydraulic jack at the column top was in displacement control: velocity of 0.01mm/s, and target displacement of +250 mm (downward). When the cylinder at the column base was removed (to simulate the column loss), the hydraulic jack at the column top limited the displacements to 0.01 mm by second, and the loss of the column was really progressive. The evolution of the total reaction loads is shown in Figure 104. Note that the structural system at the beams supports (see Figure 16 in section II.6.1.2) was not unloaded after the loss of the column: the beams supports continued to apply vertical loads, measured by F_1 and F_2.

The first failure that happened was the concrete crushing, but this failure was really progressive and it is not visible on the chart; the curve seems to continue without sudden failures. The separation between the concrete and the steel sheeting, and the crushing of the concrete at the connection zone was visible around 5h33min (5.56hour). The first bolt suddenly failed after 6h25min (6.41hour), and the total load (F_L+F_R) reduced from 380 kN to 247 kN. Then the load increased up to 381kN after 6h30min (6.5hour) before the second bolt failure around 6h34min (6.57hour). These two bolts were localised in the bottom row (row 4) of the connection left (see Figure 88). Finally the hydraulic jack reached its maximum stroke (280 mm), and the test was stopped. The hydraulic jack was stopped and the load was decreased in other to disconnect the jack. During this decrease of the load, the joint displaced upwards; then the third bolt (row 3 of the connection left) suddenly failed, which is not visible in the following charts.

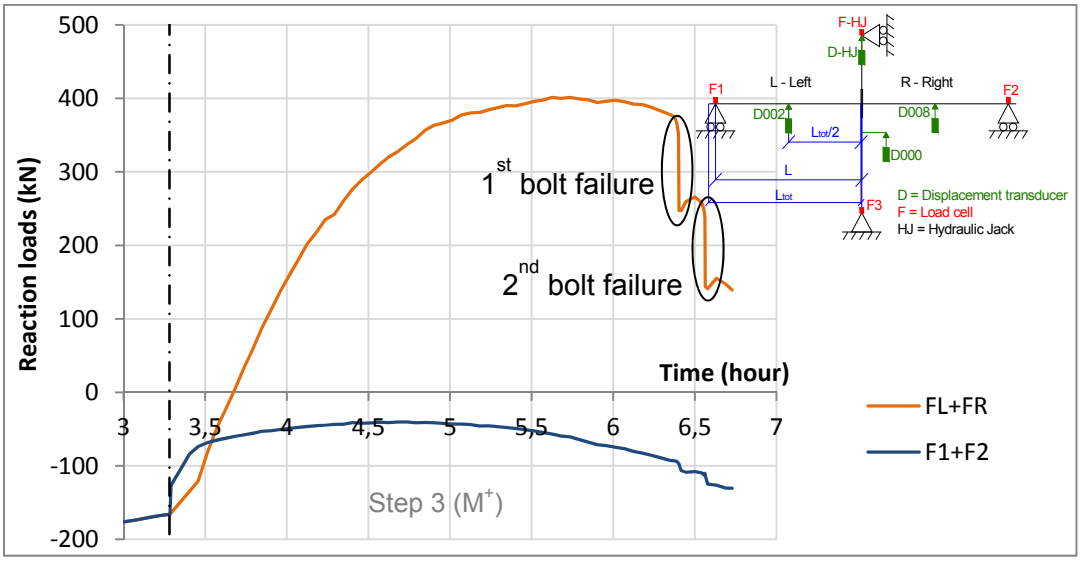

Figure 104: Evolution of the loads during the step 3 (sagging bending moment)

Figure 105 shows the evolution of the vertical displacements measured by the hydraulic jack at the column top, by the wire transducer D000 at the joint, and by the displacement transducers at mid-span of the beams D002 and D008, during the step 3. The final vertical displacement measured at the column top was equal to 250 mm (the wire transducer registered a displacement 4% lower at the end of the test, probably due to the slight displacement of the reaction frame at the hydraulic jack base, or to imperfections in the vertical position of the wire transducer). Table 14 presents the load and displacement values measured during step 3, at the beginning, at the maximum total reaction load and just before each bolt failures.

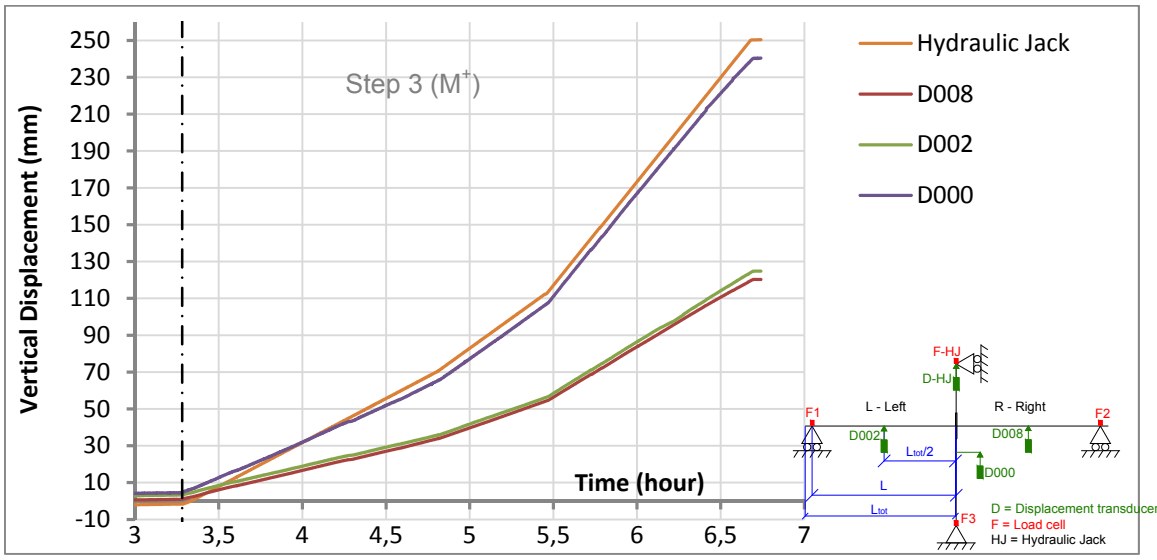

Figure 105: Vertical displacements near the beam-to-column joint during the entire test

Table 14: Main reaction loads and displacements during the step 3

	step 3 – Loss of the column	Begin of step 3 (3h17min)	Max. Load (5h37min)	First bolt failure (6h25min)	Second bolt failure (6h34min)
TEMP (ºC)	Beam bottom flange LEFT – 20 cm	504.7	506.8	504.7	504.7
	Beam bottom flange RIGHT – 20 cm	503.2	418.7	418.7	418.7
Load (kN)	Beam support LEFT (F1)	-80.83	-27.83	-44.61	-51.38
	Beam support RIGHT (F2)	-85.25	-28.81	-52.55	-61.58
	Column base (F3)	-51.70	0.00	0.00	0.00
	Column top (F-HJ)	-117.7	+458.13	+344.82	+257.02
	FL+FR	**-166.08**	**+401.48**	**+247.66**	**+144.07**
Displ. (mm)	Beam mid-span LEFT (D002)	+0.77	+62.96	+105.97	+115.11
	Beam mid-span RIGHT (D008)	+0.98	+63.18	+105.62	+113.86
	Column base (D000)	+4.60	+125.10	+210.9	+227.6
	Column Top (D-HJ)	-1.68	+131.06	+218.82	+237.06

Figure 106 shows the evolution of the reaction loads during the entire test. Some loads were still measured by F1 and F2 during step 3 whereas they should have been unloaded (see §III.1.2.1), and the load applied at the column top was reduced by the two loads F_1 and F_2 measured at the beam supports: $F_{HJ}+F_3+F_1+F_2$, with F_1 and $F_2 < 0$.

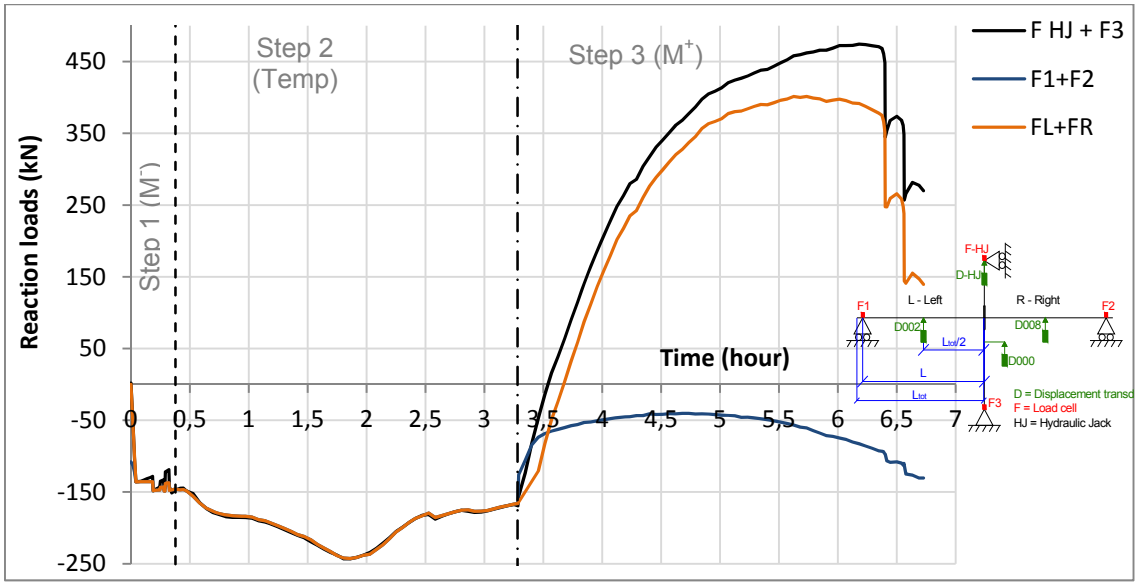

Figure 106: Evolution of the loads during the entire test

Figure 107 shows the evolution of the vertical displacements during the entire test. The rotation of the connections is shown in Figure 108, and the last values corresponded to 85 mrad. Figure 109 shows the evolution of the bending moment at the joint left and right sides versus time. Finally, Figure 86 shows the total reaction load (F_L+F_R) versus the rotation.

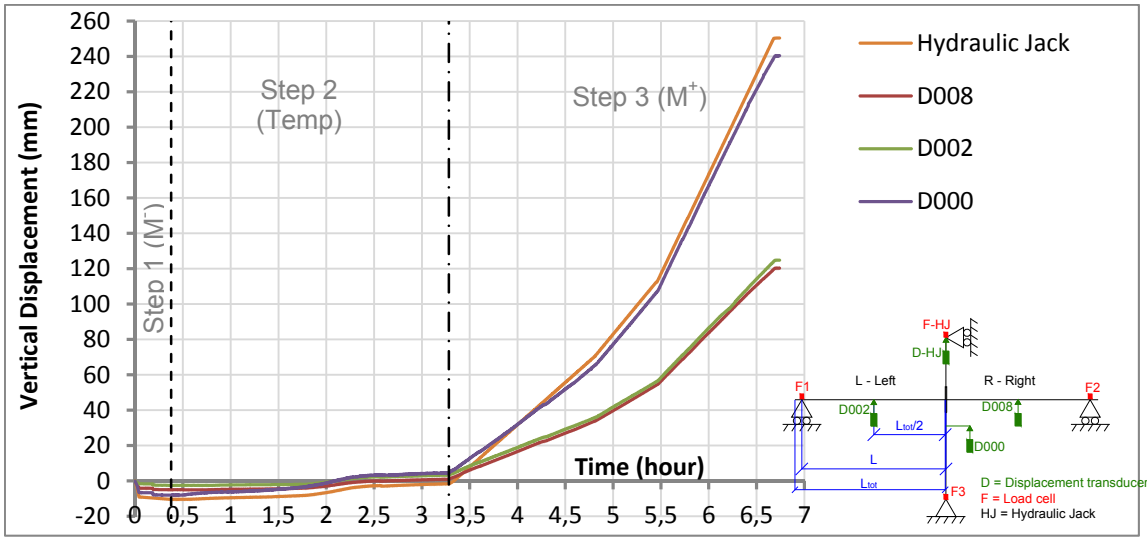

Figure 107: Vertical displacements near the beam-to-column joint during the entire test

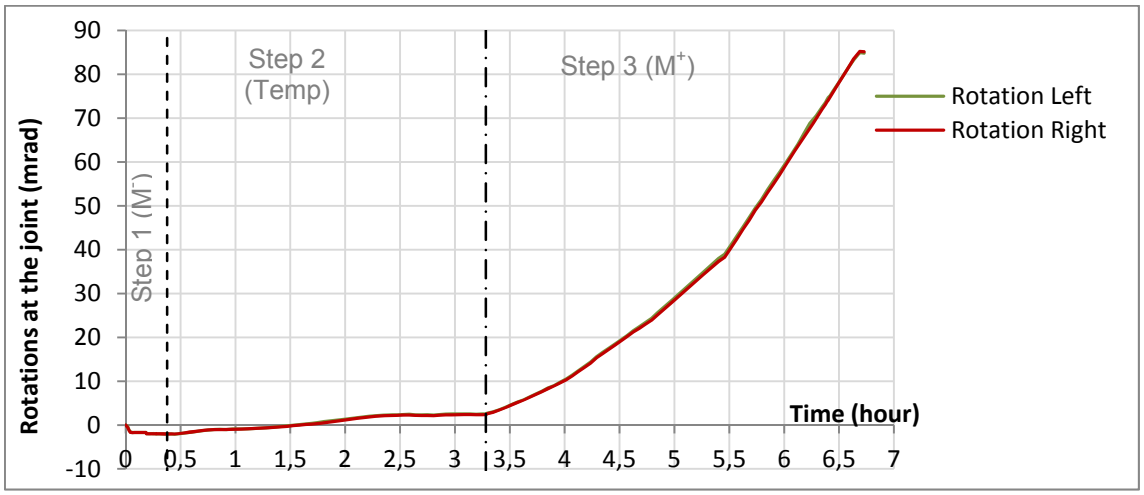

Figure 108: Rotations at the connections

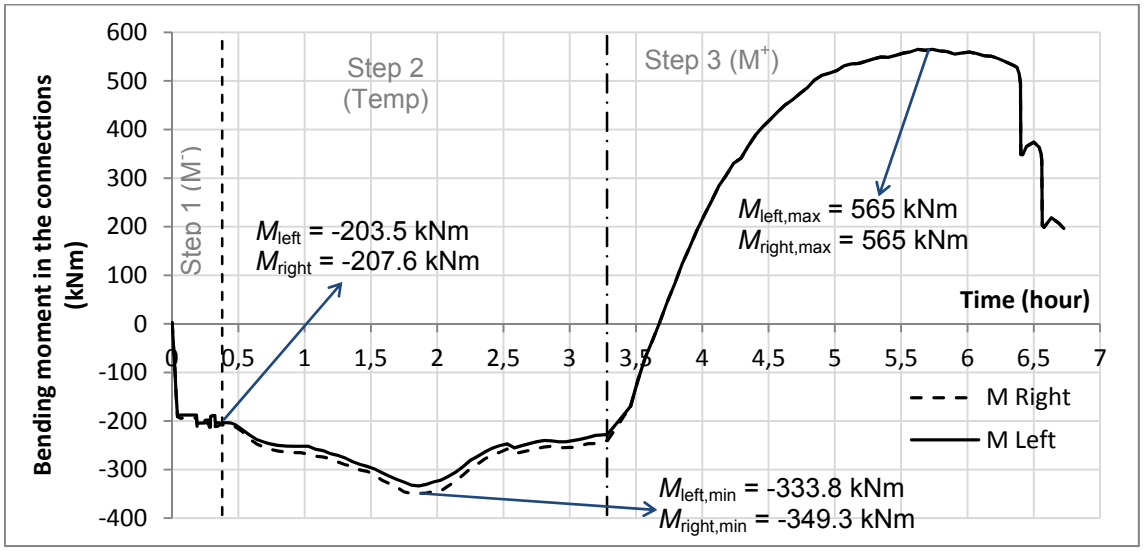

Figure 109: Bending moments at the joint vs time

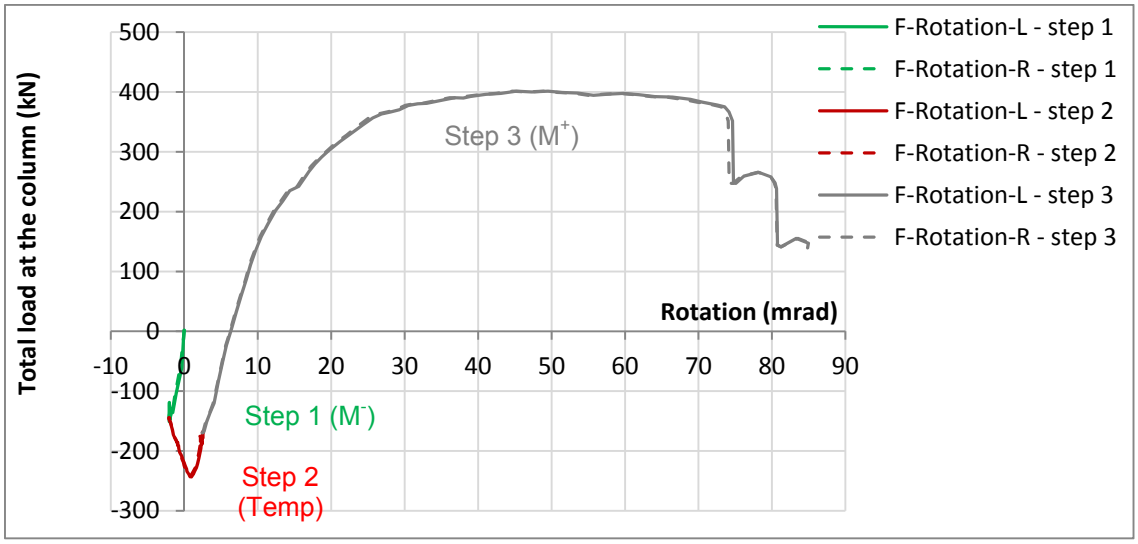

Figure 110: Total reaction load vs rotation at the connections

III.3.5 Additional data

The horizontal displacements measured at the beam ends are showed in Figure 111. The estimated horizontal displacements at the neutral axis of the steel beams $D_{beam,h,L \text{ and } R}$ (see §III.1.1.1) are represented by the red curves; they displace in the outward direction during the entire test.

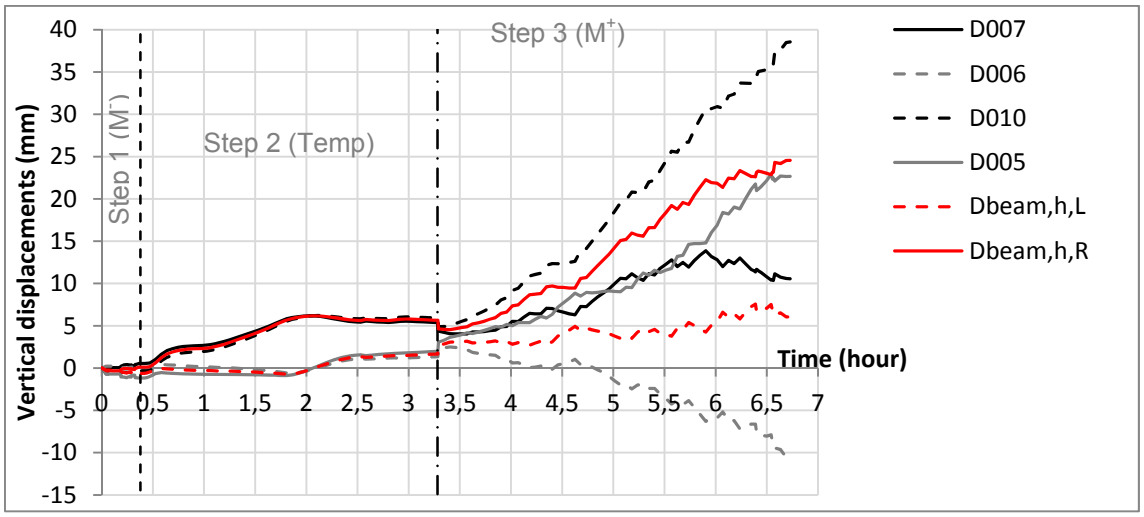

Figure 111: Horizontal displacements at the end of the beams

Figure 112 presents the displacements of the beams out of the plan, measured by the two displacement transducers D003 and D009 on the beams webs, (initially situated at 1500 mm from the end-plate); these displacements are really small.

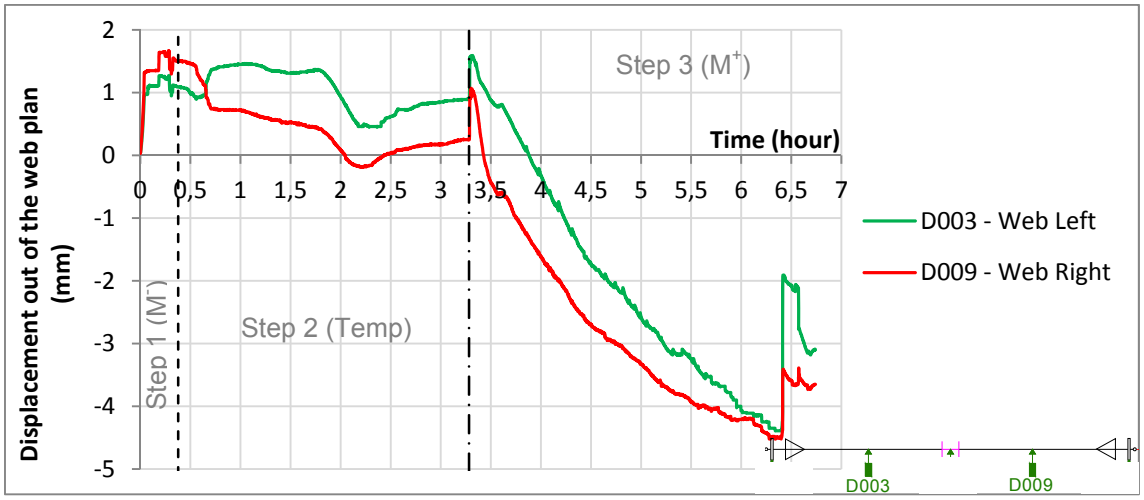

Figure 112: Evolution of the displacements measured out of the plan

III.4 Results of test 3

The global behaviour of the joint during the test is described in the following section, then the step by step behaviour is detailed, for each loading step.

III.4.1 Joint behaviour (entire test)

III.4.1.1 Temperature results

Figure 113 presents the temperatures evolution during the entire test 3 in the right and left beams (at 200 mm from the connection), in the column centre and in the bottom bolt row on the right and left connection. The temperature increase rate was 400ºC/hour. At the end of the step 2, temperatures in the beam bottom flanges of the right and left beams were different: 741ºC on the left and 612ºC on the right. This difference happened because of a problem with the FCP elements connections and was corrected around 4h20min. Temperatures in beams top flanges were much lower because they were only heated by heat transfer from web, which was reduced by the composite slab protection. During step 3, once the bottom flanges temperatures were uniform, the temperature of 700ºC was well kept constant up to the end of the test. The maximum concrete temperature measured in the slab was 216ºC, and the temperature increase due to conduction in the column above the composite slab was very limited, with maximum 118ºC measured in the column flange at 100 mm from the concrete slab. At the end of the test, maxima temperatures measured at the joint were: 505ºC in bolt heads, 529ºC in beams end-plates, 568ºC in column web and 483ºC in column flanges. The evolutions of all measured temperatures are detailed in §III.4.3.

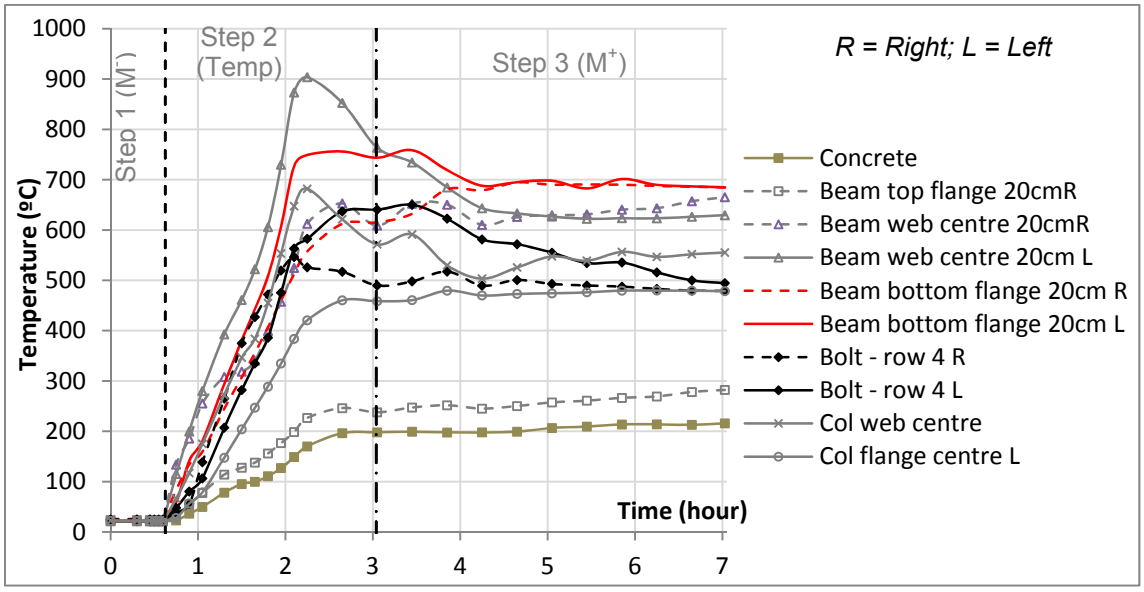

Figure 113: Evolution of the temperatures during test 3

III.4.1.2 Bending moments variation and failure modes

The evolution of the total vertical reaction load (F_{Left} + F_{right}) *versus* the vertical displacement of the joint is shown in Figure 114, and the evolution of the bending moment *versus* the joint rotation is shown in Figure 115. The hogging bending moment was initially reached during step 1 (around -400 kNm). At the beginning of step 2, reaction loads increased due to the thermal expansion of the structure. After a while, these reaction loads decreased because of the steel properties degradation due to high temperatures. However, the bottom part of the column web locally deformed under compression (Figure 116) from the hogging bending moment. During step 2, a sudden decrease of the loads happened due to the unloading of the beam supports F1 and F2 (see step by step behavior, §III.4.3). In step 3, the loss of the column was really progressive as the hydraulic jack at the column top imposed a constant displacement rate, and finally the vertical load at the column top increased up to the failure of the joint under sagging bending moment. In order to a better characterization of the elastic stiffness of the joint, an “unloading-reloading” was performed at the beginning of step 3 (before the concrete crushing in compression). Concrete crushing in compression was the first failure observed, but this failure was really progressive and cannot be seen on the moment-rotation curves. The sagging bending moment reached a maximum value of 359 kNm. No failure of the bolts was observed during the test; however one bolt failed in tension in the bottom bolt row of the left side during the cooling phase (see Figure 118). The test was stopped at 311 mm of vertical displacement because of the uncontrolled increase of the column rotation, and the stroke of the hydraulic jack was increased after 100 mm of vertical displacement.

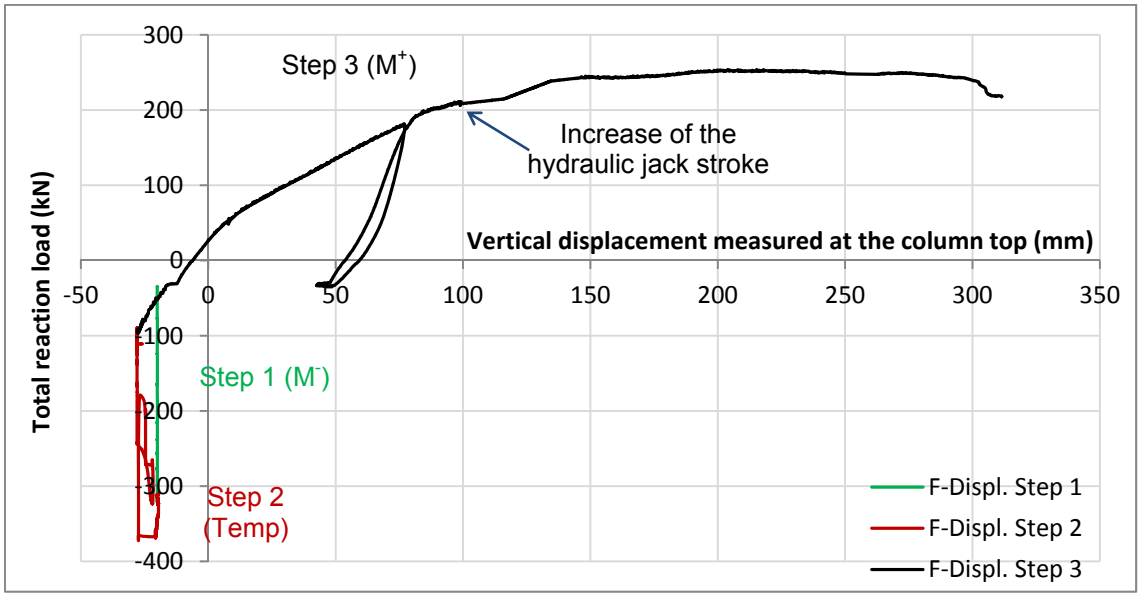

Figure 114: Total reaction load vs vertical displacement measured at the column top (DHJ)

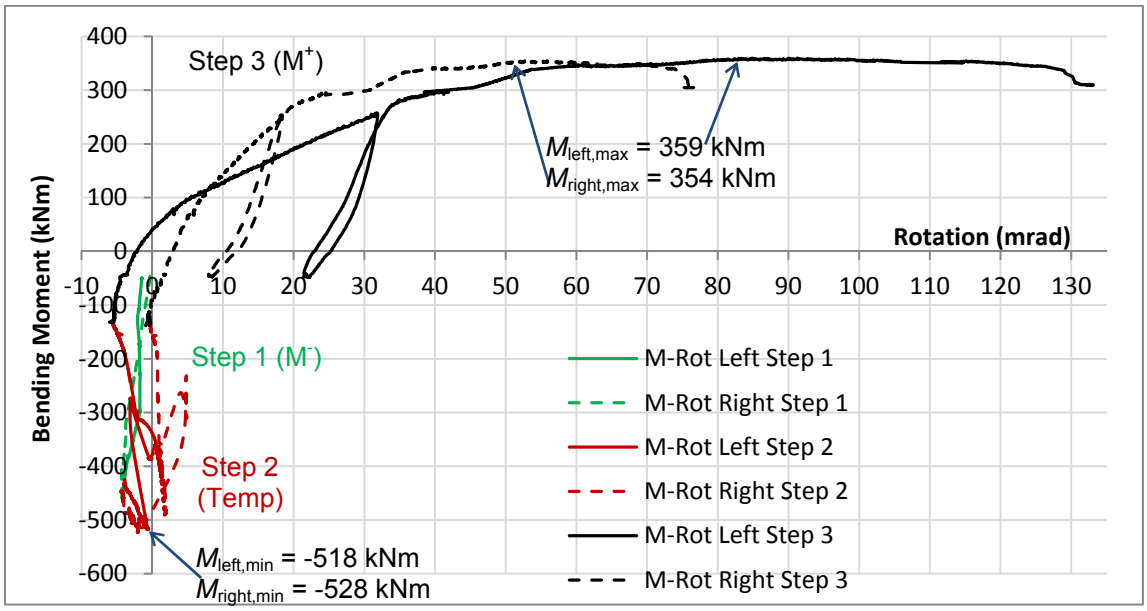

Figure 115: Bending moment at the joint vs rotation at the connections

Figure 116: Local buckling of the column web on the bottom part (level of the bolt rows 3 and 4) under hogging bending moment

Figure 117 shows the rotations at the joint left and right sides versus time, as well as the column rotation. The difference between the rotations right and left

happened because the column rotated up to around 32 mrad in the opposite direction of clockwise and created an asymmetric joint deformation (the lateral restraints of the column at the base were not yet built (see Figure 7 in §II.2)). Finally, the test was stopped at 132 mrad and 75 mrad of connection left and right rotations.

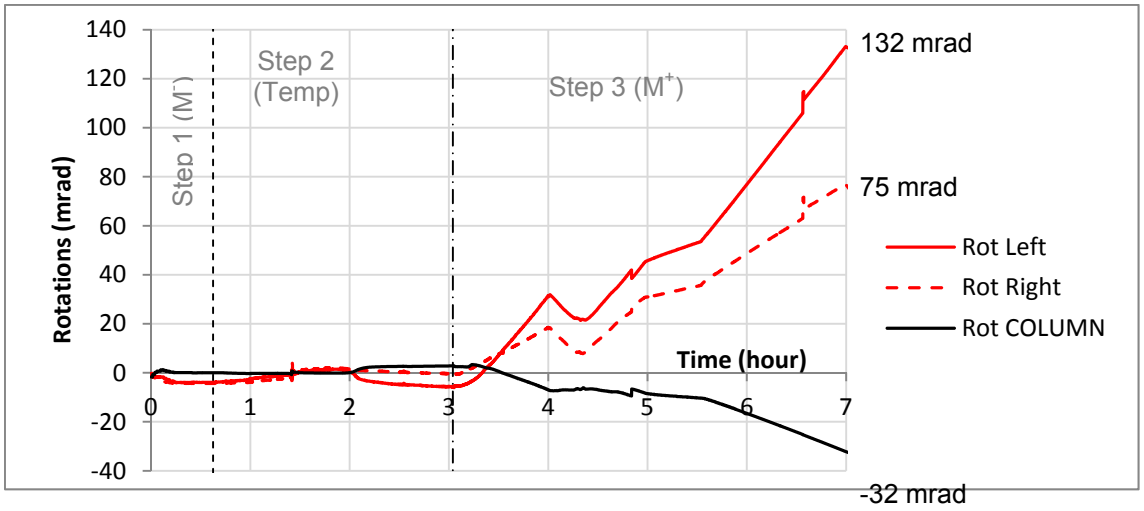

Figure 117: Rotations at the connections and column rotation

The steel end-plates deformed in the bottom and centre parts and showed a high ductility (Figure 118).

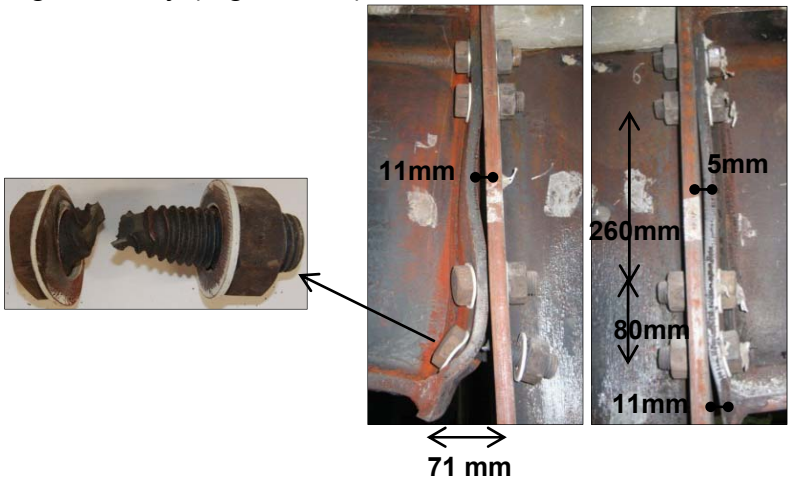

Figure 118: Deformation of the joint at the end of the test

Figure 119 shows the final deformation of the sub-frame the day after the test. It can be observed in Figure 120 that the bottom flange of the left beam slightly deformed, and the deformation was located at the boundary between the heated zone and the unheated part of the beam. The total rotation of the joint included this small rotation of the beam, and the real left connection rotation should be slightly smaller than calculated.

Figure 119: Final deformation of the sub-frame under sagging bending moment (back view)

Figure 120: Deformation of the beam bottom flange (left side) – Front view

III.4.2 Step by step behaviour: step 1 - Initial hogging bending moment

In this test, another way to apply the initial hogging bending moment was used and is shown in Figure 121. An initial space between each beam and its support was created, and the two cylinders located at the end of each beam were used to increase the loads and close the spaces. However, it was really difficult to obtain a perfect symmetry and to create exactly the same small space equal to 8 mm (necessary space to reach the target bending moment) at each side, because of eccentricities and slight differences of self-weight between the two beams. In order to obtain similar bending moments on the left and on the right, the right support was elevated in order to have similar spaces, and bending moments. However, this modification initiated the column rotation, later, under sagging bending moment (step 3).

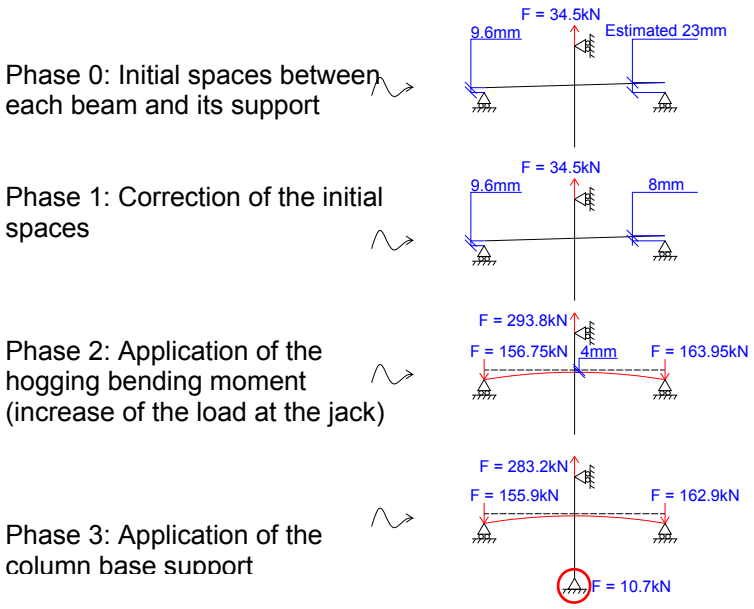

Figure 121: Initial hogging moment in the connection

Figure 122 shows the displacements and loads measured by the displacement transducers (in green) and the load cells (in red).

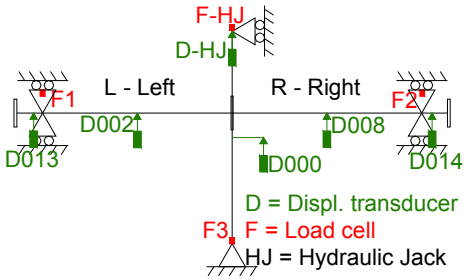

Figure 122: Main displacements and loads measured during the test 3

Figure 123 presents the evolution of the vertical displacements measured during step 1. The initial values correspond to the position of the sub-frame at the beginning of the test, relative to the beam supports. Figure 124 shows the measured reaction loads, and the initial loads corresponded to the self-weight of the sub-frame. The two loads F_1 and F_2 applied by the cylinders at the beams ends were increased progressively, which created the different levels in the charts. Figure 125 shows the concrete cracks developed under hogging bending moment.

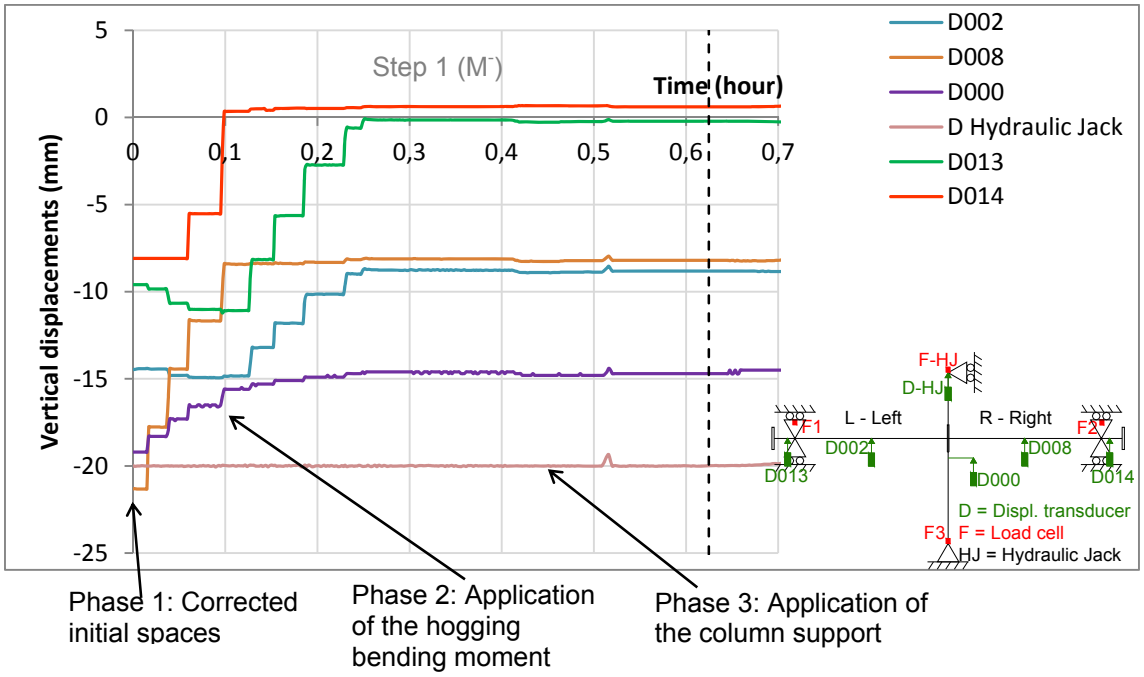

Figure 123: Vertical displacements near the beam-to-column joint

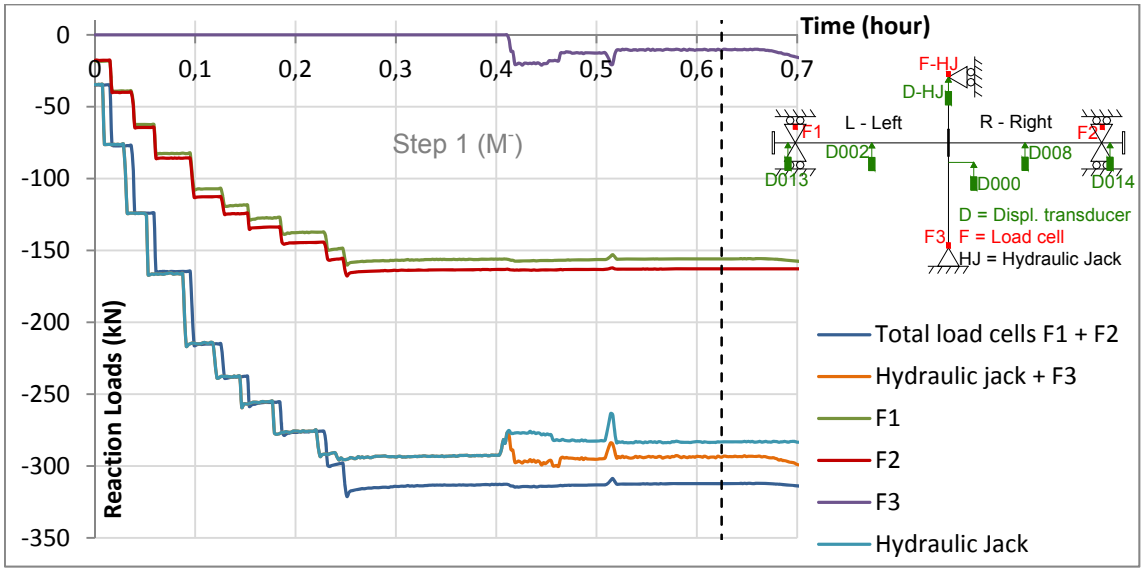

Figure 124: Measured reaction loads during the step 1

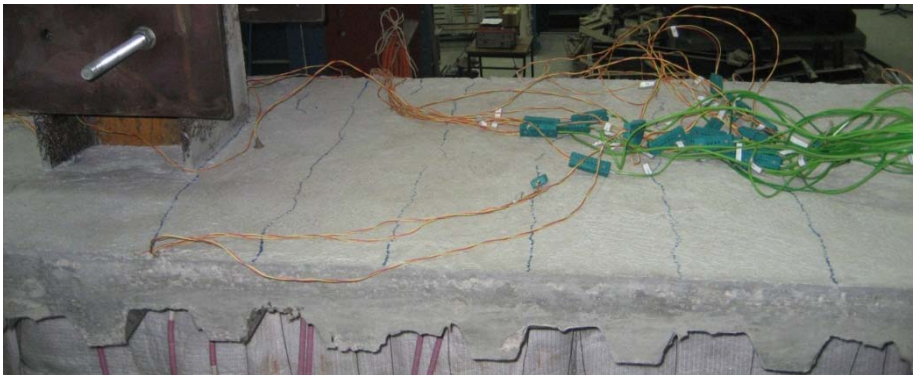

Figure 125: Initial concrete cracks under the initial hogging bending moment (step 1)

III.4.3 Step by step behaviour: step 2 - Temperatures (700ºC)

III.4.3.1 Evolution of the temperatures

Figure 126, Figure 127 and Figure 128 show the evolution of the temperatures in the beam at respectively 20 cm, 50 cm and 1 m from the end-plate of the beam. Temperatures in the beam bottom flange right was lower than 700ºC at the beginning of the step 3, but the difference was rapidly corrected.

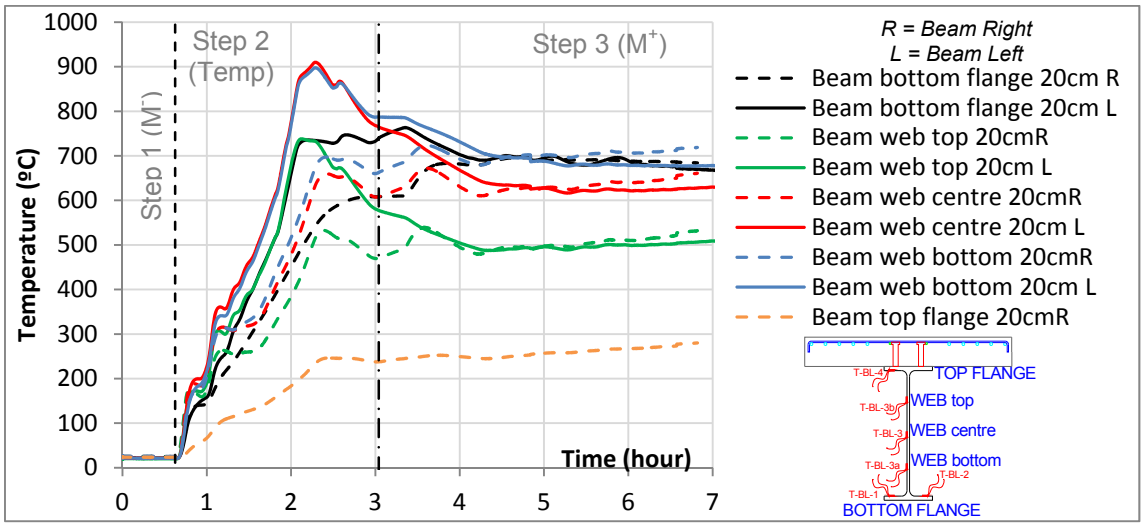

Figure 126: Evolution of the temperatures (T) in the beams at 200 mm from the connection

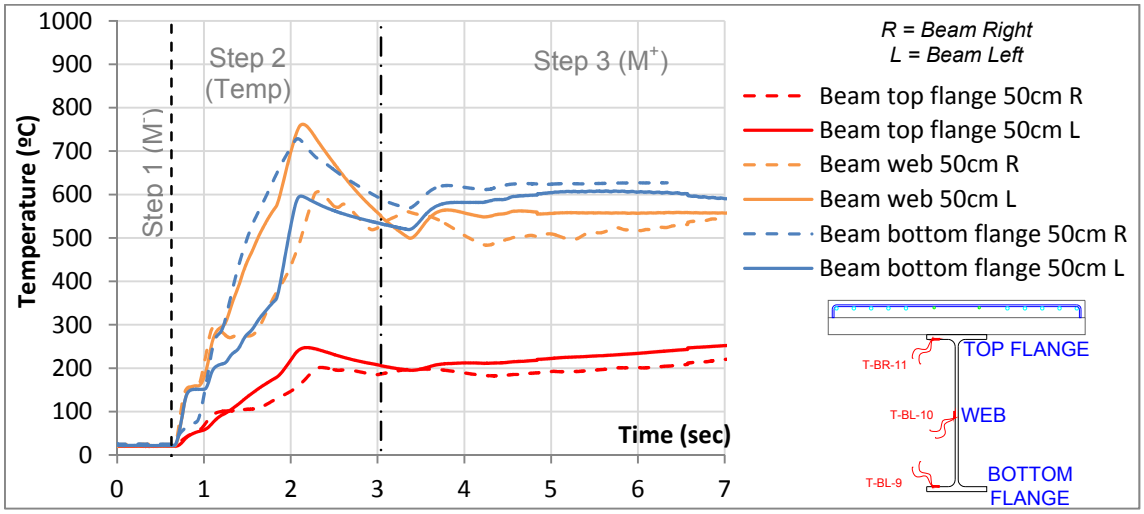

Figure 127: Evolution of the temperatures (T) in the beams at 500 mm from the connection

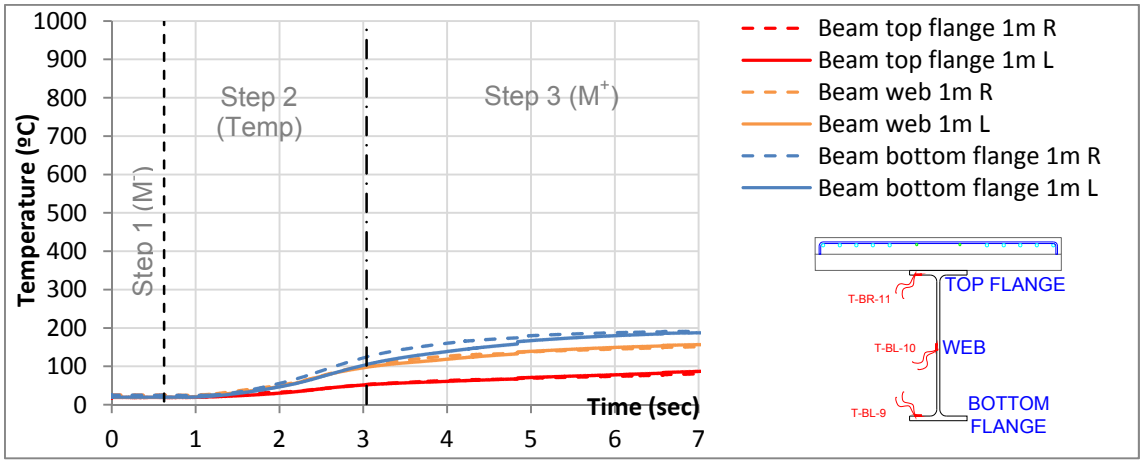

Figure 128: Evolution of the temperatures (T) in the beams at 1 m from the connection

Figure 129, Figure 130 and Figure 131 show the evolution of the temperatures at the head and at the shank of the bolts at each side of the joint, and at the end-plate surfaces. For each row, the three measured temperatures (bolt head, bolt shank and end-plate) were quite closed.

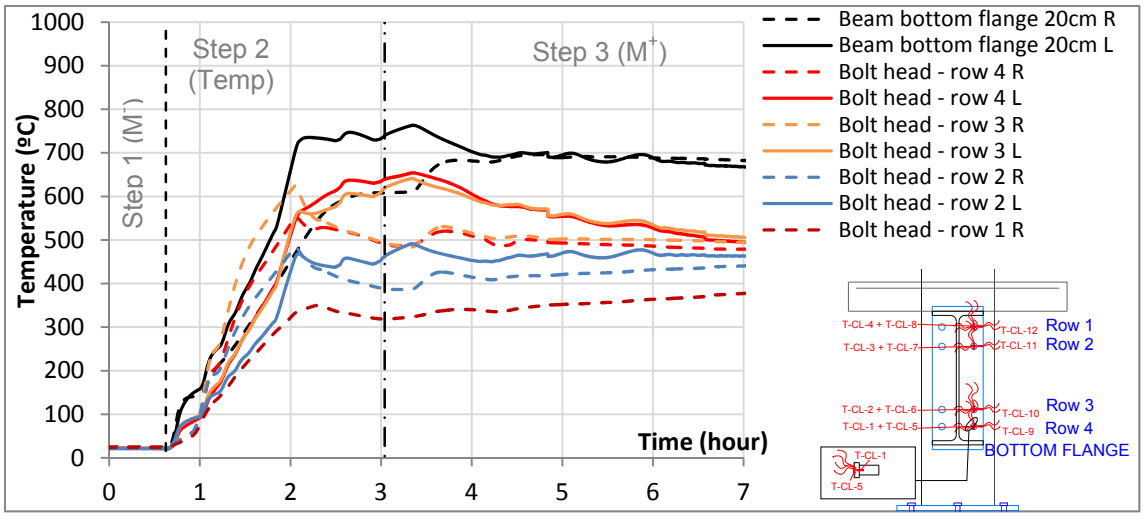

Figure 129: Evolution of the temperatures (T) in the head of the bolts

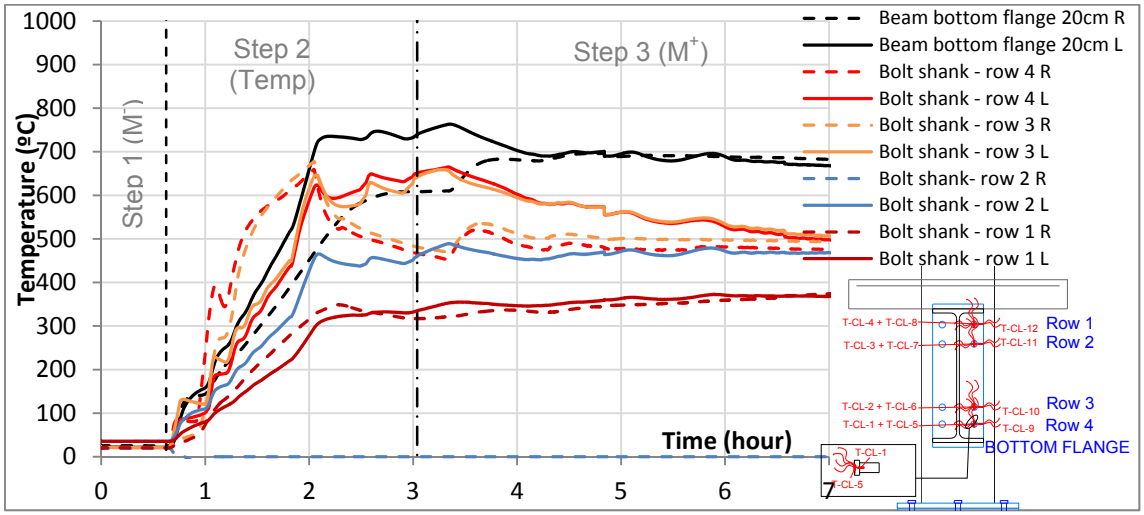

Figure 130: Evolution of the temperatures (T) in the bolts shanks

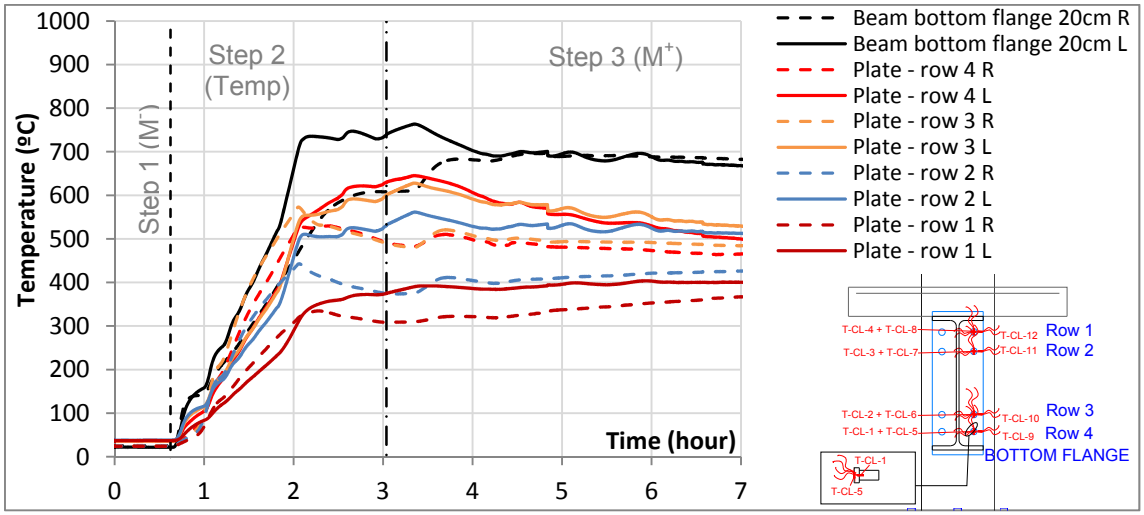

Figure 131: Evolution of the temperatures (T) in the end-plates

The evolution of temperatures in the column is presented in Figure 132. Temperatures varied between 300ºC at the top web and 600ºC at the center web during the step 3.

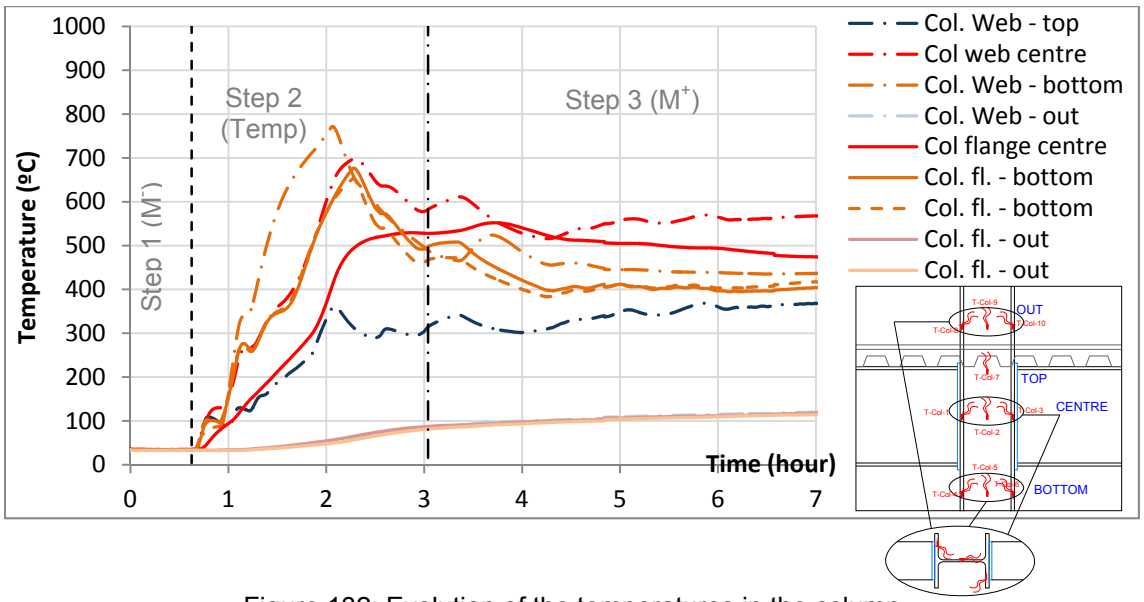

Figure 132: Evolution of the temperatures in the column

The maxima temperatures measured in the composite slab (16 cm from the column flange) were: 216ºC in the concrete, 272ºC in the steel sheet, 95ºC in the steel rebar and 200ºC in the head of the shear connector.

Table 15 presents the values of temperatures measured at the minimum hogging bending moment, at the decrease of the loads (1h48min – see following §III.4.3.2) at the end of step 2 and at the end of the test; differences (diff.) between connections left and right are showed.

Table 15: Temperatures details

	Min. Hogging bending moment			Localised max load			End of the step 2			End of the Test		
	1h24min (1.4h)			1h48min (1.8h)			3h02min (3.04h)			7h01min (7.03h)		
	Left	Right	Diff. (%)	Left	Right	Diff. (%)	Left	Right	Diff (%)	Left	Right	Diff. (%)
Top fl. 20 cm	---	121.0	---	---	156.3	---	---	237.8	---	---	282.3	---
Web top 20 cm	357.0	257.0	28.0	512.1	321.0	37.3	577.2	471.1	18.4	508.6	537.0	-5.6
Web centre 20 cm	419.5	313.7	25.2	606.6	400.1	34.0	764.3	608.4	20.4	629.4	665.3	-5.7
Web bott. 20 cm	406.4	318.5	21.6	599.5	431.0	28.1	787.1	663.0	15.8	677.6	722.2	-6.6
Bottom fl. 20 cm*	336.2	268.5	20.2	510.0	396.1	22.3	741.5	611.7	17.5	676.2	683.4	-1.1
Top flange 50 cm	117.6	103.8	11.7	174.8	125.7	28.1	205.8	186.8	9.2	252.2	220.5	12.6
Web centre 50 cm	389.9	276.8	29.0	563.7	361.9	35.8	549.2	532.6	3.0	557.4	545.6	2.1
Bott. fl. 50 cm*	248.1	413.6	-66.7	356.5	603.7	-69.3	534.8	580.9	-8.6	592.9	615.7	-3.9
Top flange 1 m	22.3	26.5	-18.8	27.1	30.9	-14.0	52.0	52.8	-1.5	86.9	80.6	7.2
Web centre 1 m	29.1	33.0	-13.4	40.5	44.4	-9.6	97.9	102.6	-4.8	156.6	151.2	3.4
Bott. fl. 1 m	26.8	29.5	-10.1	38.9	45.4	-16.7	105.1	124.8	-18.7	187.4	191.4	-2.1
Col. web centre	326.3		---	468.6		---	583.0		---	567.8		---
Col. fl. centre	187.7		---	292.9		---	499.5		---	482.6		---
Bolt head r-1	---	189.2	---	---	281.6	---	---	319.1	---	---	377.8	---
Bolt head r-2	203.8	294	-44.3	308.3	416.5	-35.1	463.3	388.1	16.2	462.7	440.4	4.8
Bolt head r-3	243.7	404.8	-66.1	380.7	561.8	-47.6	619.4	492.7	20.5	505.4	494.8	2.1
Bolt head r-4	242	327.3	-35.2	386.6	472.5	-22.2	639.9	490.2	23.4	494.4	479	3.1
Bolt In r-1	151.6	184.8	-21.9	218.3	275.5	-26.2	335.1	317.1	5.4	367.7	374	-1.7
Bolt In r-2	218.6	---	---	316.9	---	---	461.2	---	---	467.7	---	---
Bolt In r-3	313.3	484.1	-54.5	446.7	626.6	-40.3	643	480.9	25.2	505.5	493.9	2.3
Bolt In r-4	283.9	524.2	-84.6	432.2	607.8	-40.6	651.4	466.4	28.4	496.5	476.4	4.0
End-plate r-1	155.9	181	-16.1	229.5	271	-18.1	375.2	308.6	17.8	400.3	367.1	8.3
End-plate r-2	229.8	270.5	-17.7	338.1	387.1	-14.5	532.2	374.4	29.7	512.1	426.2	16.8
End-plate r-3	248.2	336.6	-35.6	372.8	495.3	-32.9	601.3	489.3	18.6	528.6	484.4	8.4
End-plate r-4	245	288.2	-17.6	378.2	437.6	-15.7	630.4	491	22.1	498.8	465.5	6.7

III.4.3.2Evolution of the displacements and loads

At the end of the step 1, the hydraulic jack was not unloaded, and continued to apply a vertical load in the upwards direction: the column was in suspension at the top instead of being supported at the base. It was not observed during the test because the apparent load was initialized (equal 0), and it was asked to the jack to maintain the load constant during the step 2 (force control). In reality, it was asked to the jack to maintain the tensile force at the top of the column equal to 283 kN (Figure 133). During the heating, the structure began to expand and to be supported by the cylinder at the column base, releasing loads at the

top of the column (at the jack). In order to keep constant the load in the jack, the stroke had to displace in the upward direction (Figure 134).

Thew deformation under hogging bending moment was increasing too much and the loads were slightly decreased at: i) the beams supports around 1h24min. However, instead of a slight reduction, the hydraulic pump removed too much oil pressure in the two small cylinders at the beams supports, which is showed by the sudden decrease of the loads (A in Figure 133); then a certain level of oil pressure was increased again; ii) the jack (decrease of 50kN) (B). The sub-frame reached its maximum resistance capacity at 1h48min (C); after this point, all the loads began to decrease because of the material capacities decreasing (maximum temperature equal to 606ºC in the left beam web, and 506ºC and 396ºC in beams bottom flanges left and right). Finally, at 2h05min (D), the hydraulic jack reached its displacement capacity (jack completely closed – see Figure 134) and the loads decreased. Table 16 presents all the values of temperatures, loads and displacements (step 2) for each point from A to D.

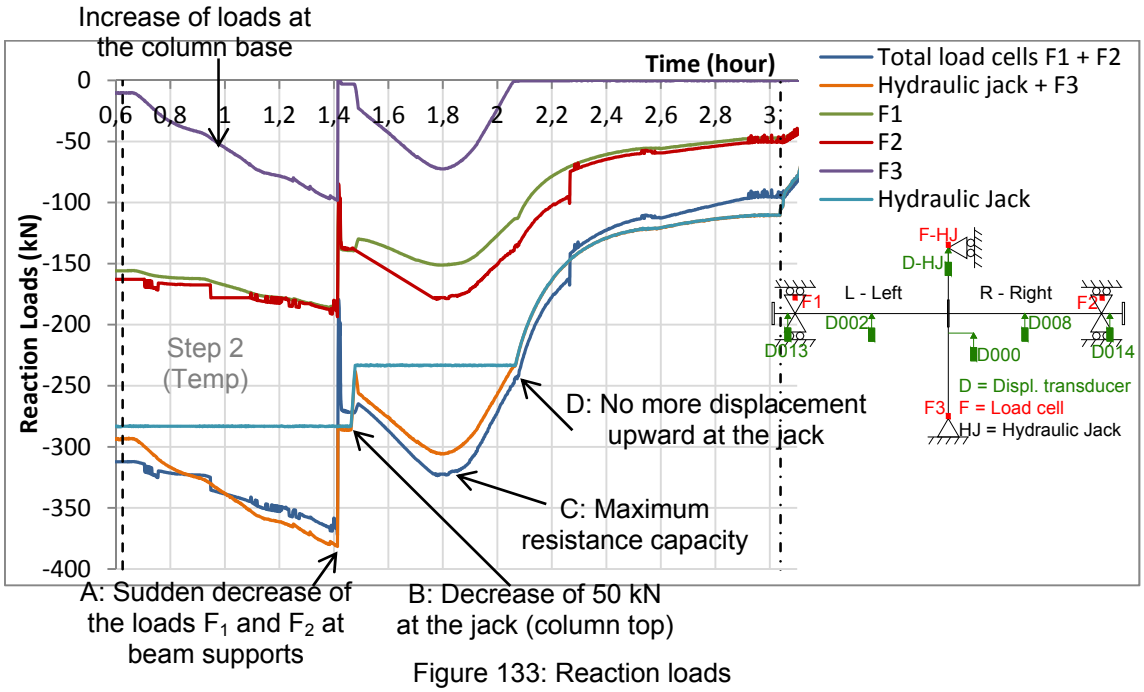

Figure 133: Reaction loads

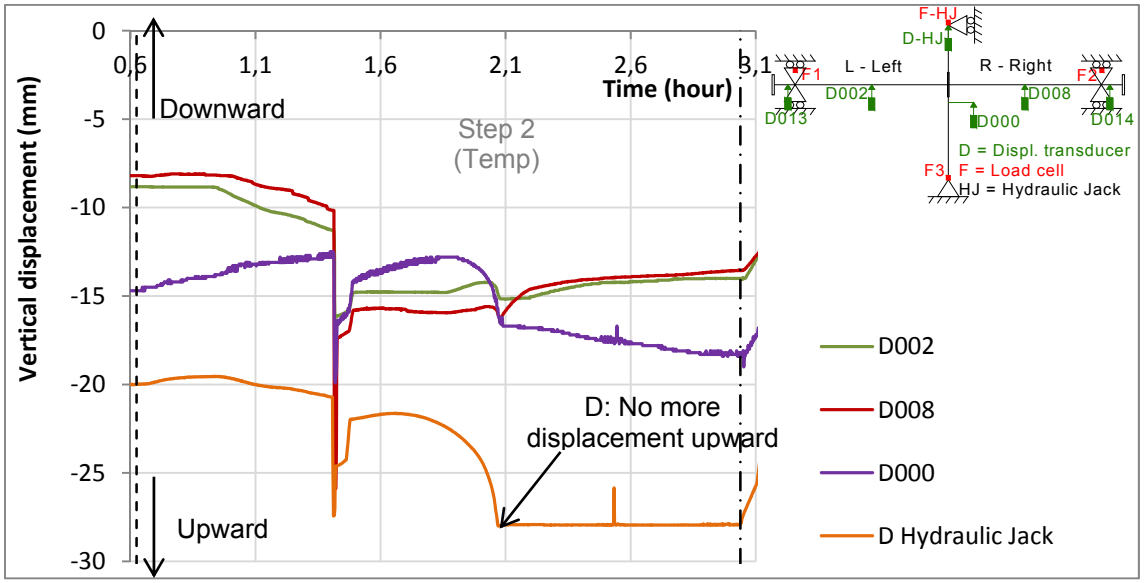

Figure 134: Vertical displacements near the beam-to-column joint during the increase of temperatures

Table 16: Main reaction loads and displacements during the step 2

STEP 2 - Temperatures		Begin of the step 2	A: Hogging bending moment too high	B: Modif. of the load at the jack	C: Local Max load	D: Min displ. at the jack	End of the step2
Time		37min (0.62h)	1h24min (1.4h)	1h28min (1.47h)	1h48min (1.8h)	2h05min (2.1h)	3h02min (3.04h)
TEMP (ºC)	Beam bottom flange LEFT - 20cm	21.75	336.2	371.75	510	709	741.45
	Beam bottom flange RIGHT - 20cm	25.25	268.45	291	396.1	485.9	611.7
Load (kN)	Beam support LEFT (F1)	-138.6	-168.5	-122	-133.9	-96.4	-30.1
	Beam support RIGHT (F2)	-145.6	-162.7	-120.9	-160.7	-122	-33.2
	Total reaction Load (F1+F2)	-284.2	-331.2	-242.9	-294.6	-218.4	-63.3
	Col. base (F3)	-10.7	-96.5	-3	-72.4	-0.7	-0.3
	Col. top (F-HJ)	-283.2	-283.1	-251.8	-233.3	-233.2	-105.2
	Total reaction col. (F-HJ+F3)	-293.9	-379.6	-254.8	-305.7	-233.9	-105.5
Displ. (mm)	Beam mid-span LEFT (D002)	-8.82	-11.26	-15.82	-14.78	-14.5	-14
	Beam mid-span RIGHT (D008)	-8.2	-10.14	-17	-15.92	-15.74	-13.54
	Col. base (D000)	-14.7	-12.6	-15.9	-13.1	-15.3	-18.3
	Col. top (D-HJ)	-19.99	-20.71	-22.8	-22.01	-27.19	-27.89

Figure 135 presents the evolution of the bending moments during the increase of temperatures.

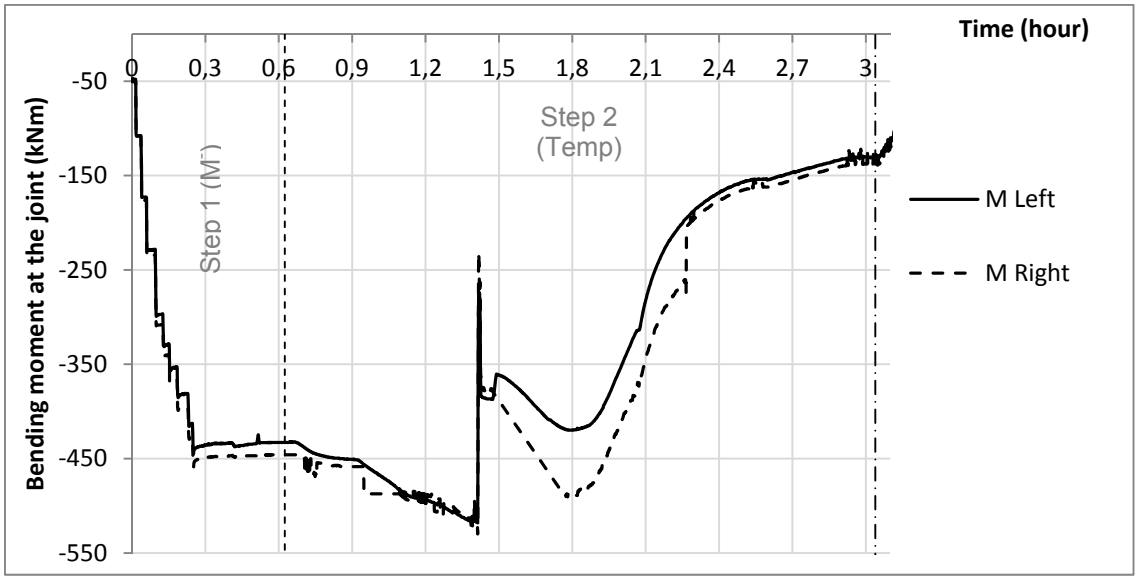

Figure 135: Evolution of the bending moment in the connections during the steps 1 and 2

III.4.4 Step by step behaviour: step 3 - Loss of the column and sagging bending moment

Figure 136 shows the evolution of the vertical displacements measured by the hydraulic jack at the column top, by the wire transducer D000 at the joint, and by the displacement transducers at mid-span of the beams D002 and D008, during the step 3. The hydraulic jack measured a final vertical displacement equal to 311 mm (the wire transducer registered a displacement 8% lower at the end of the test, probably due to the slight displacement of the reaction frame at the hydraulic jack base, or to imperfections in the vertical position of the wire transducer). whereas the wire transducer registered a displacement equal to 287 mm. The horizontal displacement measured at the column base (D016) and used for the rotation calculation is also presented.

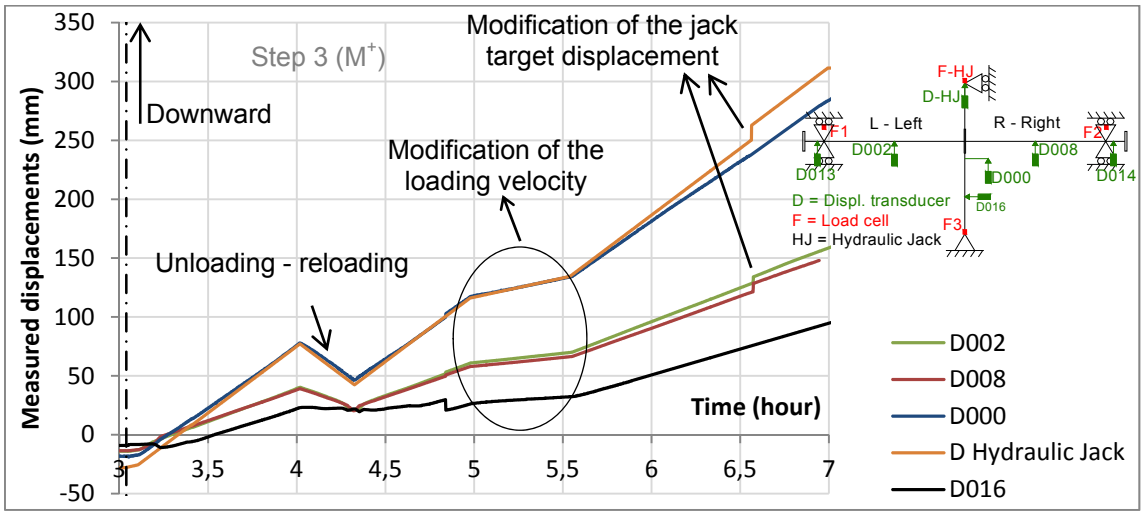

Figure 136: Vertical displacements near the beam-to-column joint during the entire test

The evolution of the loads measured by the load cells during the loss of the column and the increase of the vertical load is shown in Figure 137. The first failure that happened was the concrete crushing, but this failure was really

progressive. The maximum load reached by the jack was 253 kN. No bolts failed during the test. Figure 138 shows the evolution of the bending moment at the joint left and right sides versus time. Figure 139 and Figure 140 present the evolution of respectively the reaction load *versus* the rotation, and the bending moment *versus* the vertical displacement of the joint.

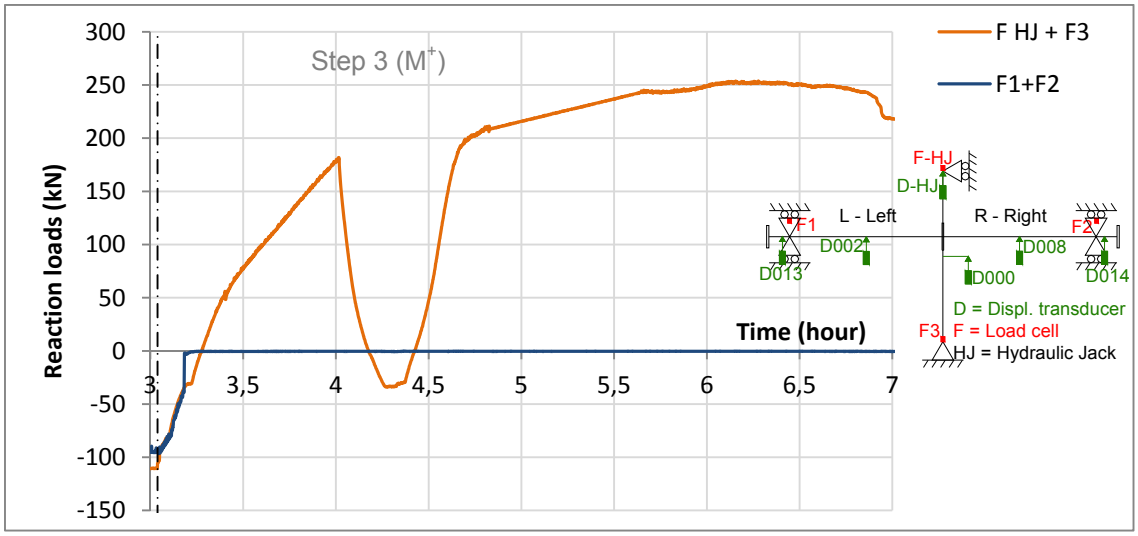

Figure 137: Evolution of the loads during the step 3 (sagging bending moment)

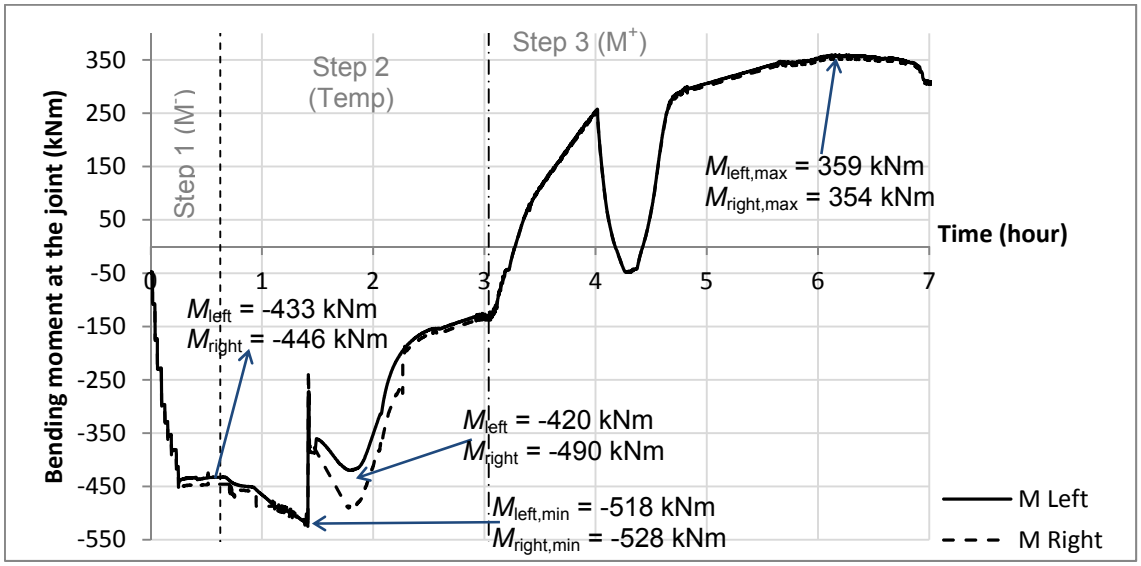

Figure 138: Bending moments (M) at the connections left and right

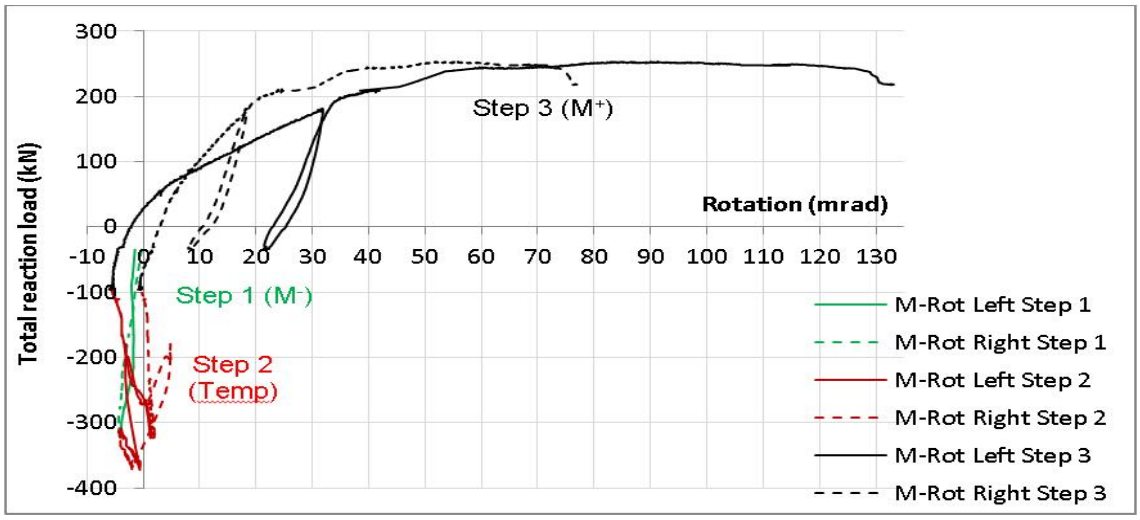

Figure 139: Total reaction load vs rotation at the connections

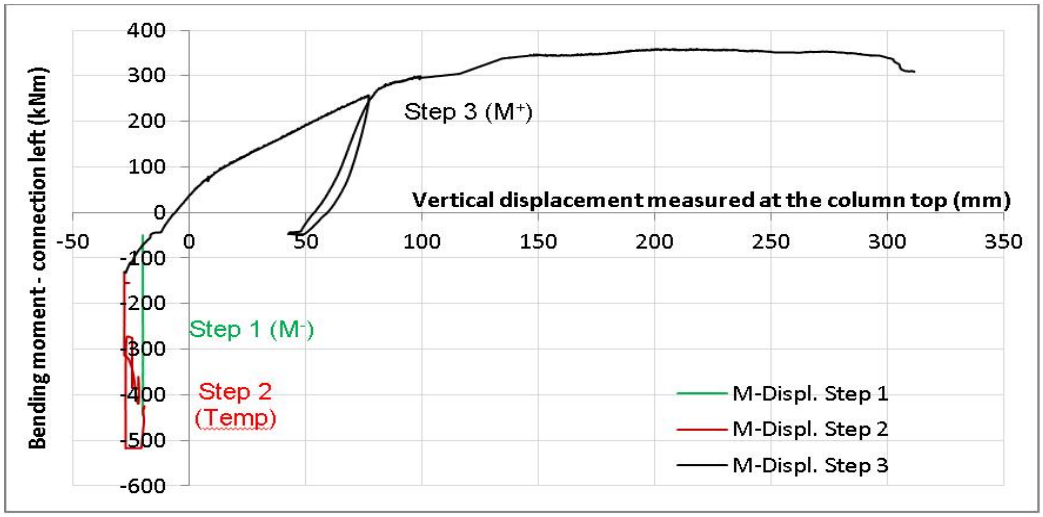

Figure 140: Bending moment in the left connection vs vertical displacement measured at the column top by the hydraulic jack

The horizontal displacements measured at the beam ends are showed in Figure 141 The estimated horizontal displacements at the neutral axis of the steel beams $D_{beam,h,L \text{ and } R}$ (see §III.1.1.1) are represented by the black curves; during step 3, because of the column rotation, the left and right beams ends displaced respectively in the outwards and inwards directions.

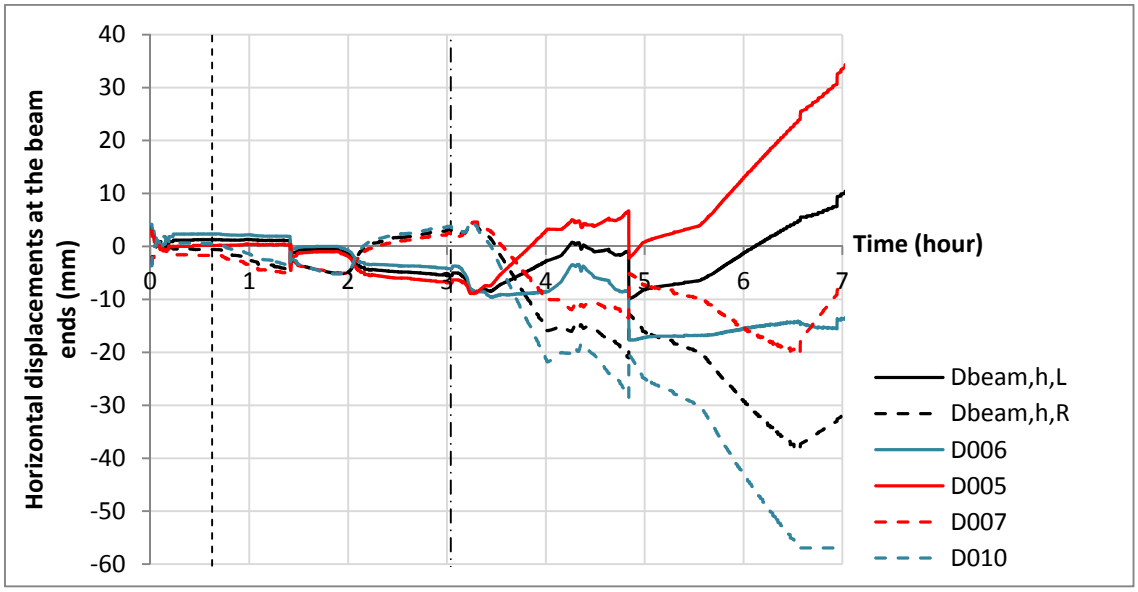

Figure 141: Horizontal displacements at the end of the beams

III.5 Results of test 4

The global behaviour of the joint during the test is described in the following section, then the step by step behaviour is detailed, for each loading step, and finally, additional data a presented.

III.5.1 Joint behaviour (entire test)

III.5.1.1 Temperature results

Figure 142 presents the temperatures evolution during the entire test 4 in the right and left beams (at 200 mm from the connection), in the column centre, in bolts from row 3 and in concrete. Around 1h, during step 2, the temperature increase rate was modified from the maximum rate to 400ºC/hour, which created a peak in temperatures curves. Finally, 500ºC was reached in the beam bottom flanges, whereas the temperatures increased faster in the beams webs because of the reduced thickness. Temperatures in beams top flanges were much lower because they were only heated by heat transfer from the web, which was reduced by the composite slab protection. However, a problem occurred in the right beam: the temperatures values were varying with quite high oscillations. It should probably be due to a deficient contact in a thermocouple of control (see §II.6.2). During step 3, the temperature was well kept constant in the beam bottom flanges, mainly in the left beam. Concrete temperatures did not rise above 200ºC. At the end of the test, maximum temperatures measured at the joint were: 371ºC in bolt heads, 389ºC in beam end-plates, 430ºC in column web and 372ºC in column flanges. The evolutions of all measured temperatures are detailed in §III.5.3.

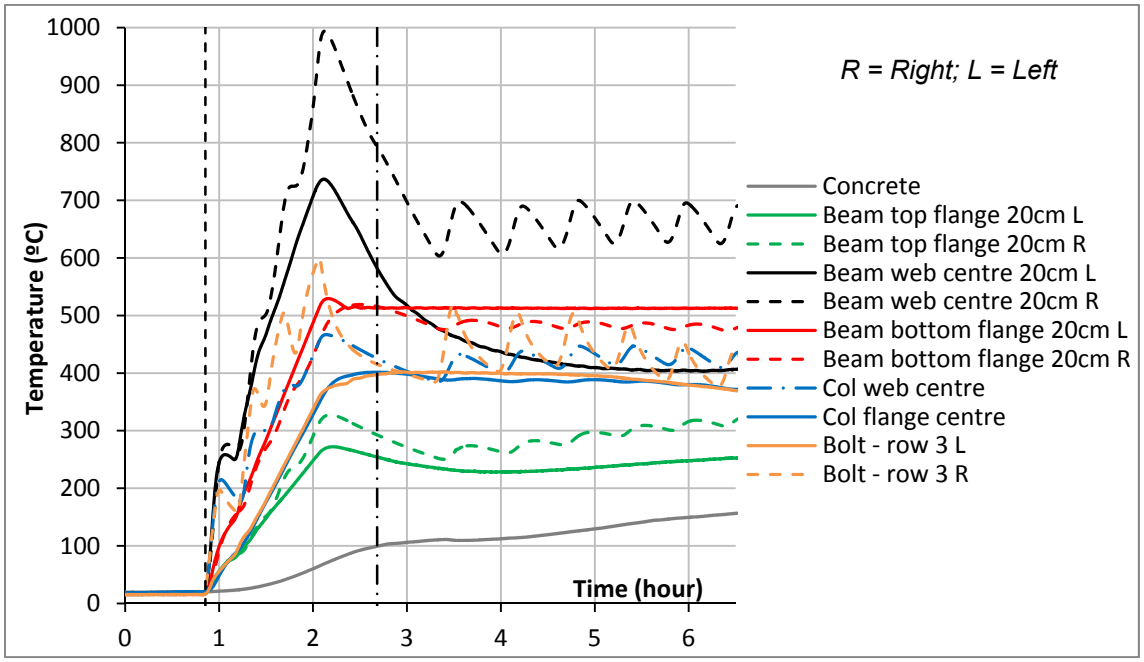

Figure 142: Evolution of the temperatures during test 4

III.5.1.2 Bending moments variation and failure modes

The evolution of the total reaction load *versus* the vertical displacement of the joint, and the bending moment *versus* the rotation are depicted in Figure 143 and Figure 144, whereas Figure 145 shows the evolution of the bending moment at the joint *versus* the beam axial load (measured at the restraint and projected in the beam direction, $F_{restr,ax}$).

The hogging bending moment was initially reached during step 1, followed by a variation of this moment during the increase of temperatures in step 2. This initial hogging bending moment reached -226 kNm on the left and -229 kNm on the right connections respectively. At the beginning of step 2, reaction loads increased due to the thermal expansion of the structure. After a while, these reaction loads decreased because of the steel properties degradation due to high temperatures: the minimum hogging bending moment reached -372 kNm on the left and -379 kNm on the right connections (which correspond to a vertical load at the column (F_{HJ}+F_3) equal to -275 kN). In step 3, the loss of the column was really progressive as the hydraulic jack at the column top imposed a constant displacement rate, and in order to a better characterization of the elastic stiffness of the joint, an “unloading-reloading” was performed before the concrete crushing in compression. The maximum total vertical reaction load (439 kN) was reached for a rotation of 20 mrad, a vertical displacement of 60 mm, and axial restraint compression loads equal to 1045 kN and 1019 kN on the left and right sides. The axial restraints were connected to the beams since the beginning of the test. During step 1, the reaction loads and displacements created by the application of the initial hogging bending moment were not sufficient to create axial forces to the beams. During steps 2 and 3, the beams ends were moving outwards and the restraints worked in compression. Concrete crushing in compression was the first failure observed, but this failure was really progressive and cannot be identified on the force-displacement /

moment-rotation curves; the concrete was crushed against the column flange (Figure 146) around 79 mm of vertical displacement (total reaction load of 430 kN, bending moments around 730 kNm, and rotations around 25 mrad); and around 148 mm of vertical displacement, the concrete from the composite slab was crushed on the entire slab width (total reaction load of 357 kN, bending moments around 750 kNm, and rotations around 50 mrad). Finally bending moments of 768 kNm and 746 kNm were reached on the left and right connections respectively, for which corresponded rotations respectively equal to 41 mrad and 42 mrad (or 123 mm of vertical displacement; a total vertical reaction load (F_L+F_R) equal to 387 kN; and axial restraints loads equal to 1080 kN and 1055 kN on the left and right sides respectively).

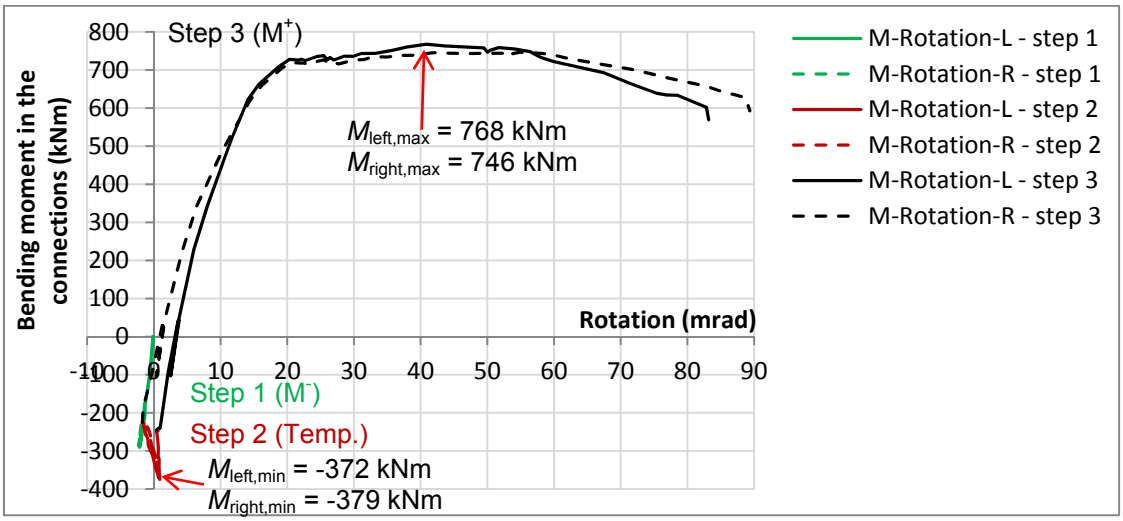

Figure 143: Bending moment vs rotation at the connection (the different gradient of colors define the different steps)

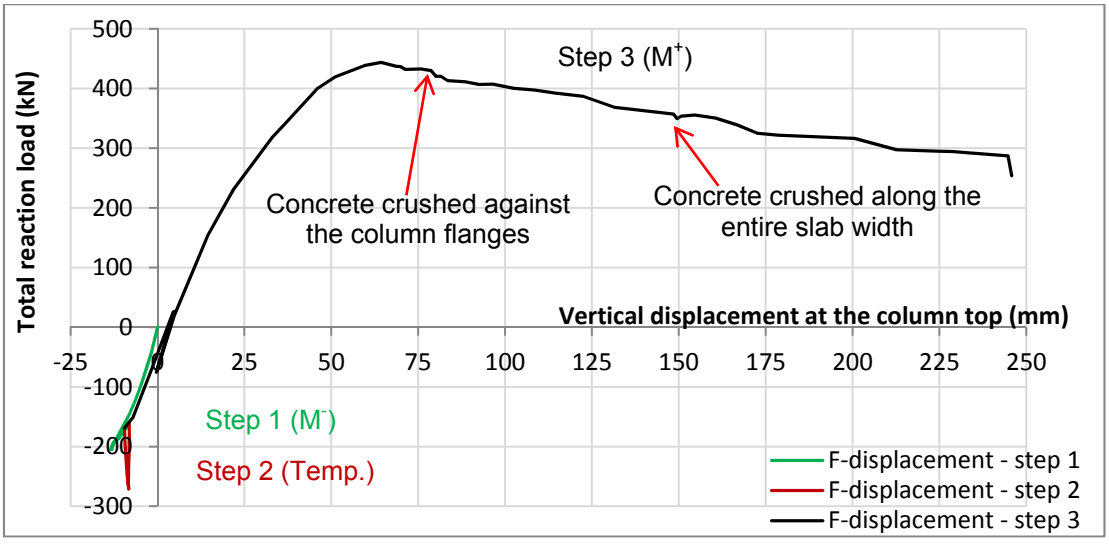

Figure 144: Total reaction load (F_L+ F_R) vs vertical displ. measured at the column top (D_{HJ})

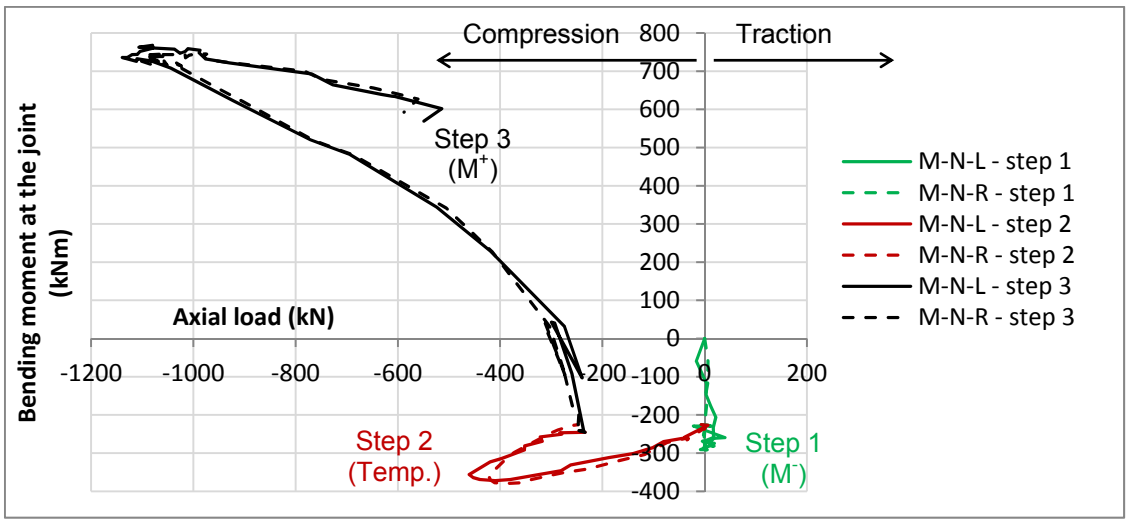

Figure 145: Bending moment vs axial forces at the connections ($F_{restr,ax}$)

Figure 146: Concrete crushed against the column flange

Figure 147 shows the rotations at the joint left and right sides versus time, as well as the column rotation. The column rotation was very small (2.4 mrad) thanks to the lateral restraints of the column (see Figure 7 in §II.2). The test was stopped at 83 mrad and 89 mrad of connections left and right rotations.

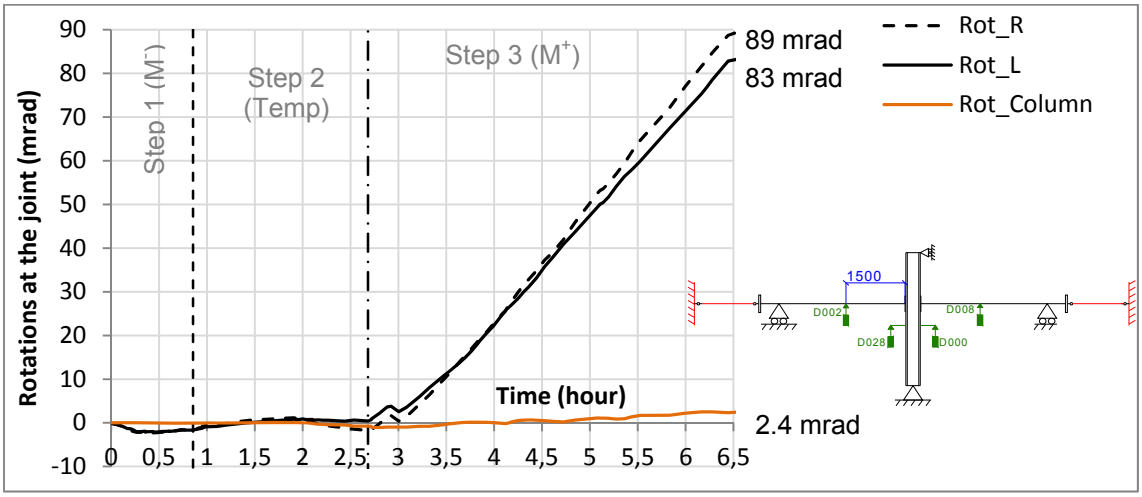

Figure 147: Rotations at the connections (Rot_Connection Left and Right) and column rotation

The test was stopped because the maximum vertical displacement was reached by the jack: the vertical displacement of the joint was 246 mm. During the cooling phase, the final deformation was maintained by the hydraulic jack, and

two bolts failed. The two failed bolts were located in the fourth row of the connection right (see Figure 148). The steel end-plates deformed in the bottom and centre part and showed a high ductility. The final deformation of the sub-frame is shown in Figure 149.

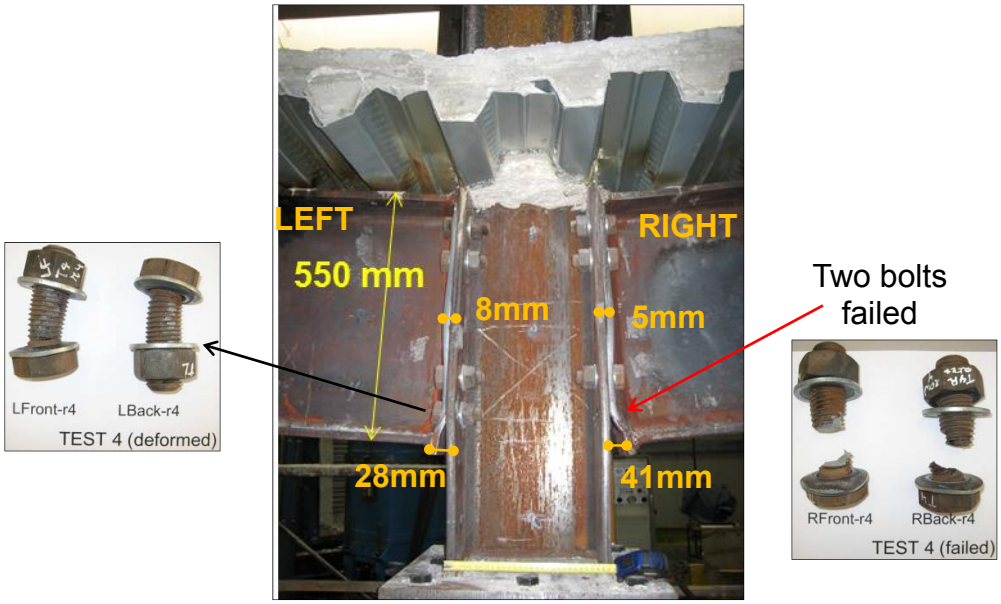

Figure 148: Deformations of the joint (view from the front side)

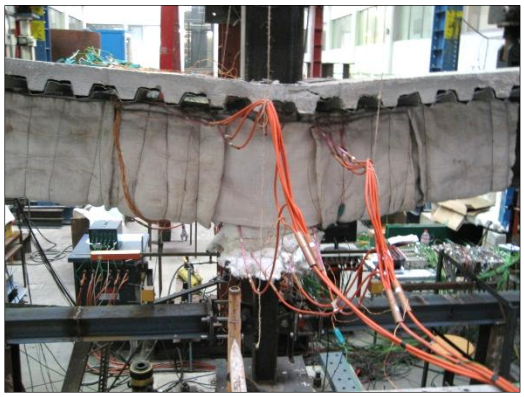

Figure 149: Final deformation of the sub-frame

Due to the high compression forces from the total restraint to the beam, combined to thermal expansions and sagging bending moment, local deformations happened: the two webs from beams left and right slightly locally buckled (Figure 150); the steel web of the column (level of rows 1 and 2) locally buckled (Figure 151a); the left side of the column deformed just behind the slab (Figure 151b); the right beam flanges locally buckled (Figure 152). Figure 151c shows the column flanges on the bottom part slightly deformed under tensile loads (under sagging bending moment).

a) b)

Figure 150: Local buckling of the beam webs: a) right beam, view from the back, b) left beam, view from the back

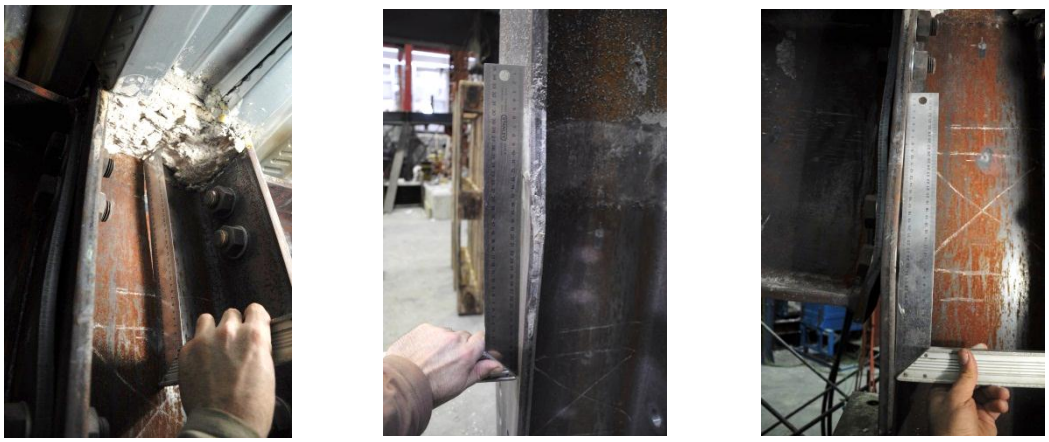

a) b) c)

Figure 151: a) Local buckling of the column web (view from the front side); b) local deformation of the column flange left side (at the level of the concrete slab), view from the back; c) local deformation of the column flange at the bottom part

Figure 152: Local buckling of the flanges from the right beam (view from the back)

III.5.2 Step by step behaviour: step 1 - Initial hogging bending moment

Figure 153 presents the evolution of the vertical displacements measured near the beam-to-column joint during the step 1. The initial hogging bending moment

was applied in three phases (see §II.5): i) the beams were restrained at the supports and the column was free at the base; ii) phase 1: the hydraulic jack increased the vertical load at the column top and pulled the column upwards; iii) phase 2: the column base support (single acting cylinder) was set up; iv) phase 3: the load at the column top was completely transferred to the sub-frame supports. During the phase 2 (set up of the column base support), the cylinder increased the load at the column base, and slightly modified the displacement of the column joint as well as the reaction load at the column top (see Figure 154).

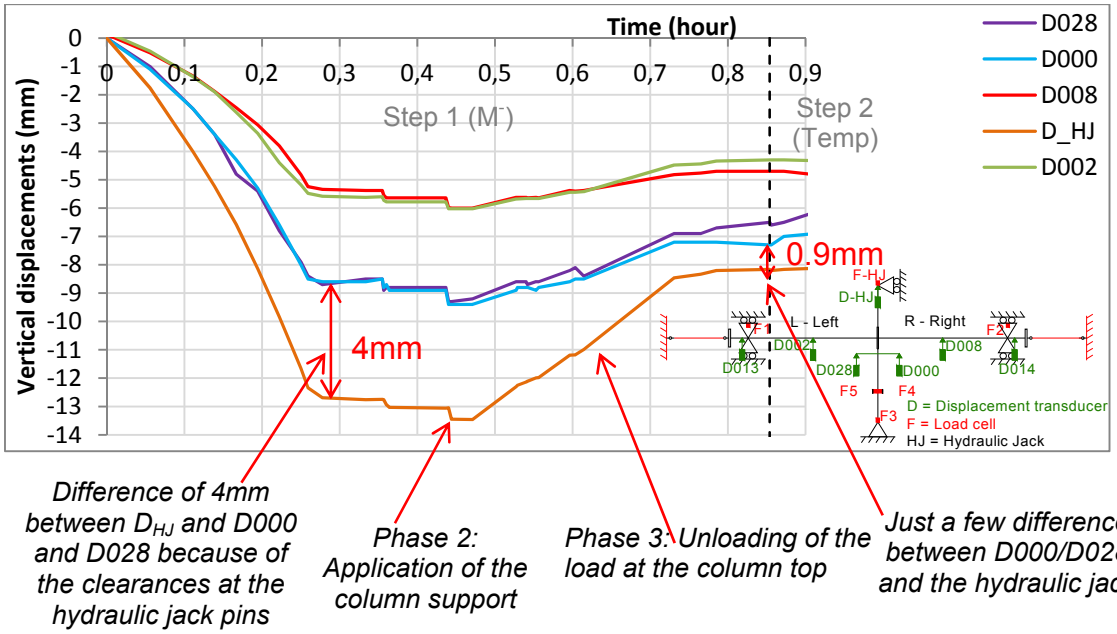

Figure 153: Vertical displacements near the beam-to-column joint during the application of the initial loads (hogging bending moment)

Figure 154 presents the comparison between the sum of the loads measured at the column ($F_{HJ}+F_3$) and the sum of the reaction loads measured at the beam supports (F_L+F_R). Before loading the joint, the end of each beam was vertically restrained and an initial load (-117 kN) was measured by the load cells F_1 and F_2.

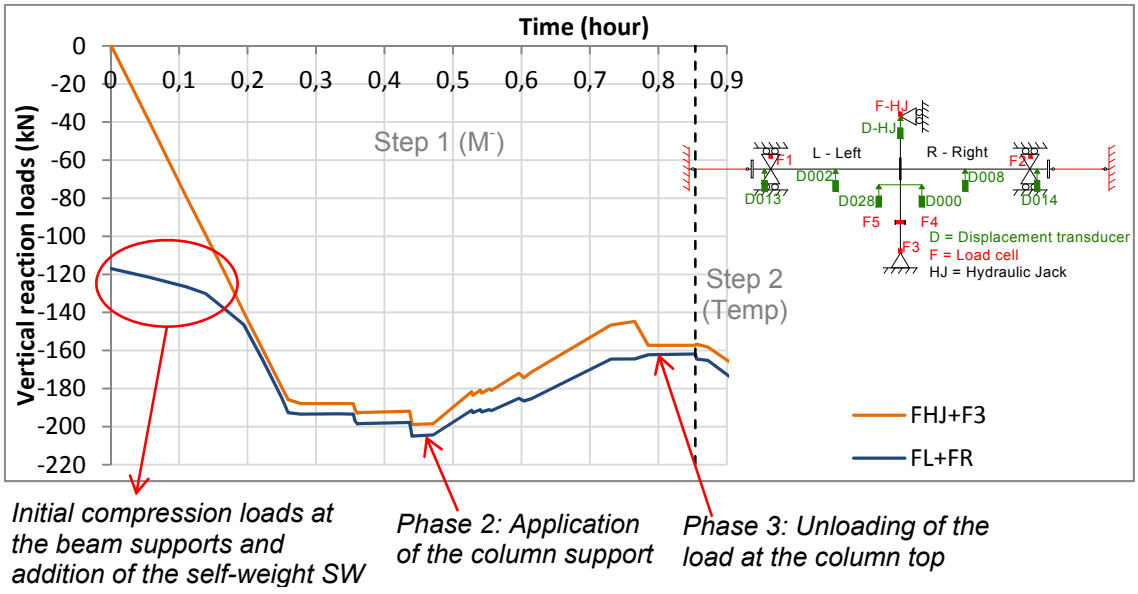

Initial compression loads at the beam supports and addition of the self-weight SW

Phase 2: Application of the column support

Phase 3: Unloading of the load at the column top

Figure 154: Load applied by the hydraulic jack compared to the sum of the reaction loads at the supports

III.5.3 Step by step behaviour: step 2 - Temperatures (500ºC)

The second loading step consisted to the slow increase (around 400ºC/hour) of the temperature in the heated zone, until reaching 500ºC in the beam bottom flanges (at a distance of around 20 cm from the joint). Increasing slowly allowed a better control of the sub-frame behaviour. The hydraulic jack at the column top was in force control; in order to allow free thermal expansion of the column top, a constant load of 0.1 Tf was imposed (see §II.6.1.1).

III.5.3.1 Evolution of the temperatures

Figure 155, Figure 156 and Figure 157 show the evolution of the temperatures in the beams at respectively 20 cm, 50 cm and 1 m from the end-plate. Note that a problem occurred in the right beam: the temperatures values are varying with quite high oscillations. The problem should probably be due to a deficient contact in a thermocouple of control (see §II.6.2).

Figure 158, Figure 159 and Figure 160 show the evolution of the temperatures at shank and at head of the bolts at each side of the joint, and at the end-plates surface.

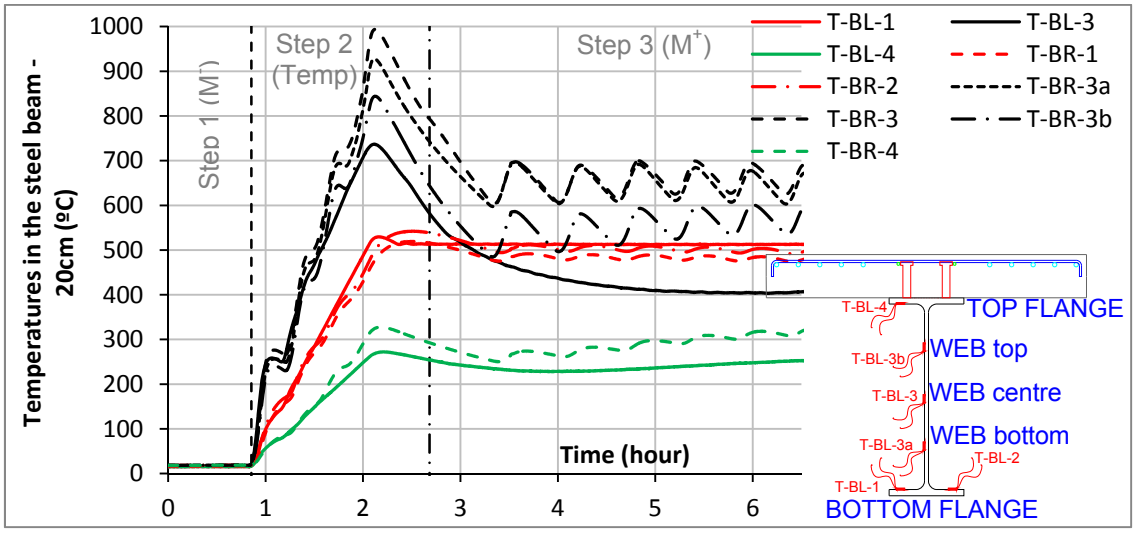

Figure 155: Evolution of the temperatures (T) in the beams at 20 cm from the connection during the test 4 (BR = beam right; BL = beam left)

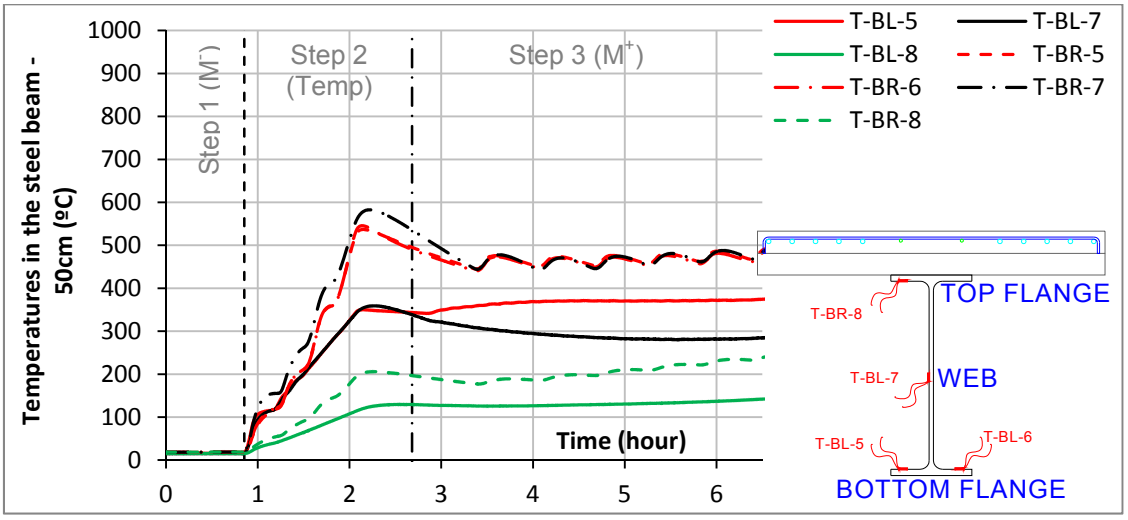

Figure 156: Evolution of the temperatures (T) in the beams at 50 cm from the connection during the test 4 (BR = beam right; BL = beam left)

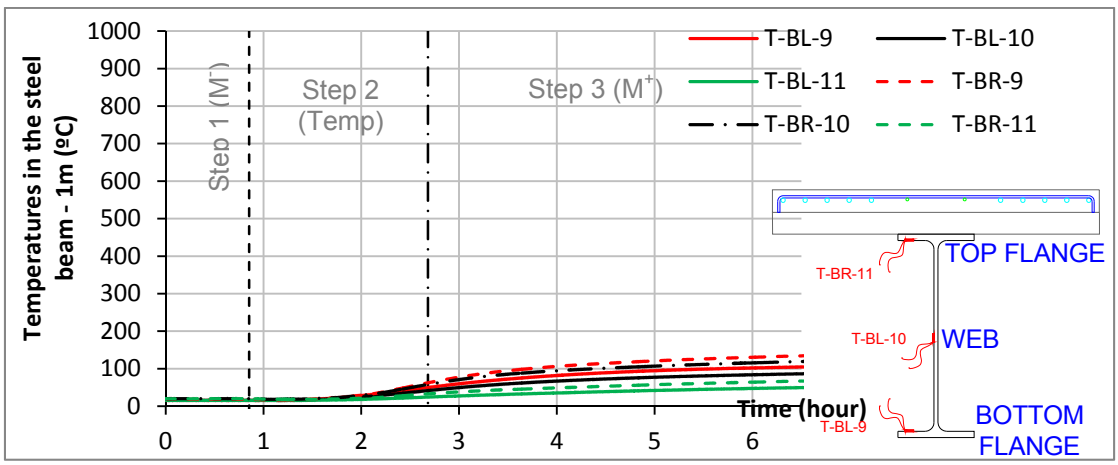

Figure 157: Evolution of the temperatures (T) in the beams at 100 cm from the connection during the test 4 (BR = beam right; BL = beam left)

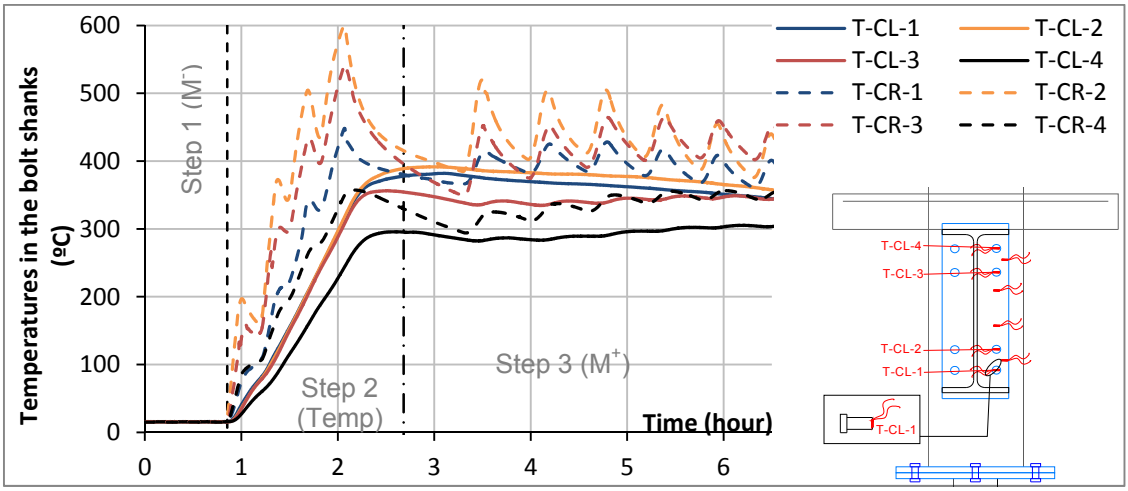

Figure 158: Evolution of the temperatures (T) in the shank of the bolt during the test 4 (CR = connection right; CL = connection left)

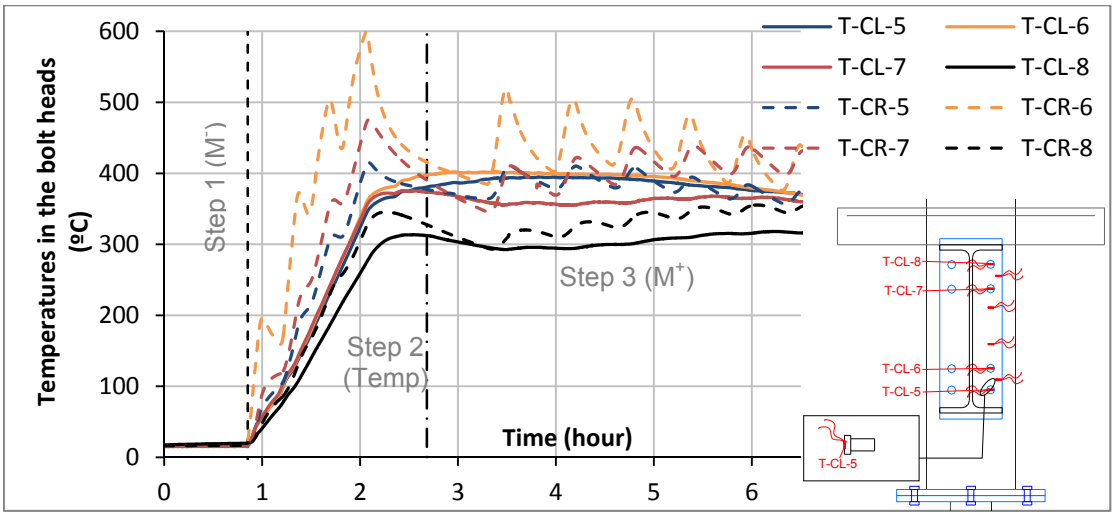

Figure 159: Evolution of the temperatures (T) in the head of the bolts during the test 4 (CR = connection right; CL = connection left)

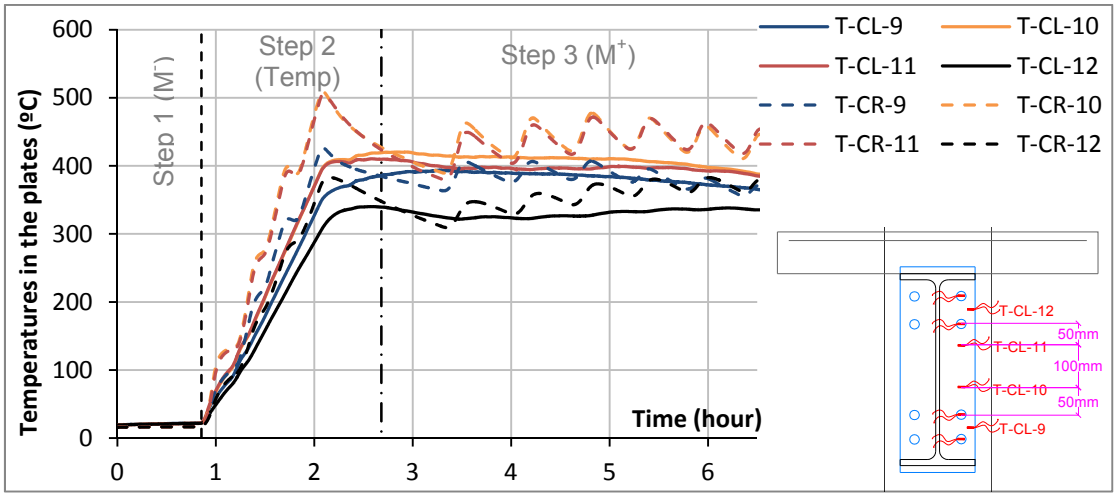

Figure 160: Evolution of the temperatures (T) in the end-plates during the test 4 (CR = connection right; CL = connection left)

The evolution of temperatures in the column is presented in Figure 161; temperatures at the column centre (T-Col-1 to 3) are higher than at the web ends (top – T-Col-7, or bottom – T-Col-4/5).

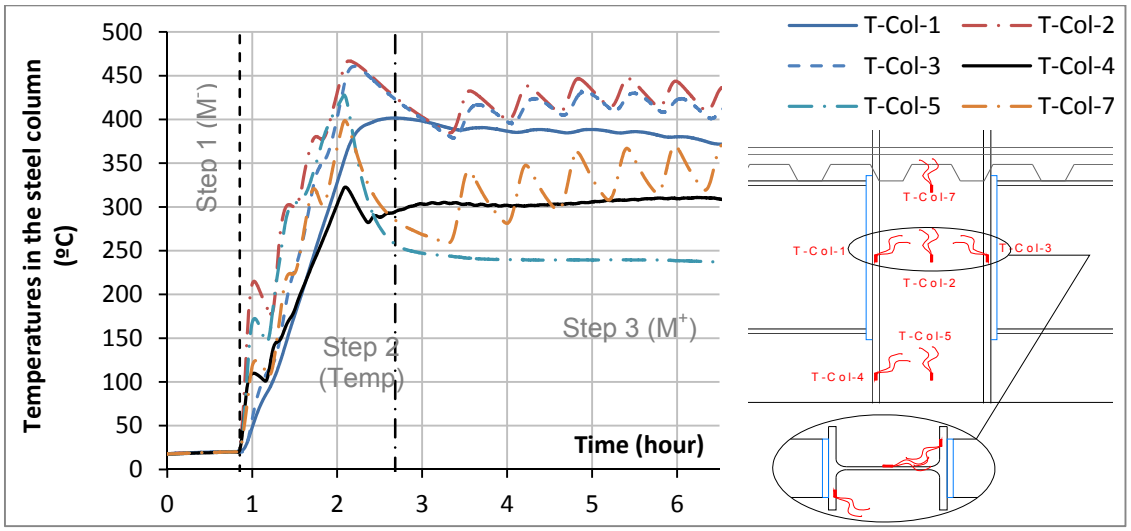

Figure 161: Evolution of the temperatures in the column during the test 4

The evolution of temperatures in the composite slab is depicted in Figure 162, and measured points are shown in Figure 34, section II.8.3 (p24).

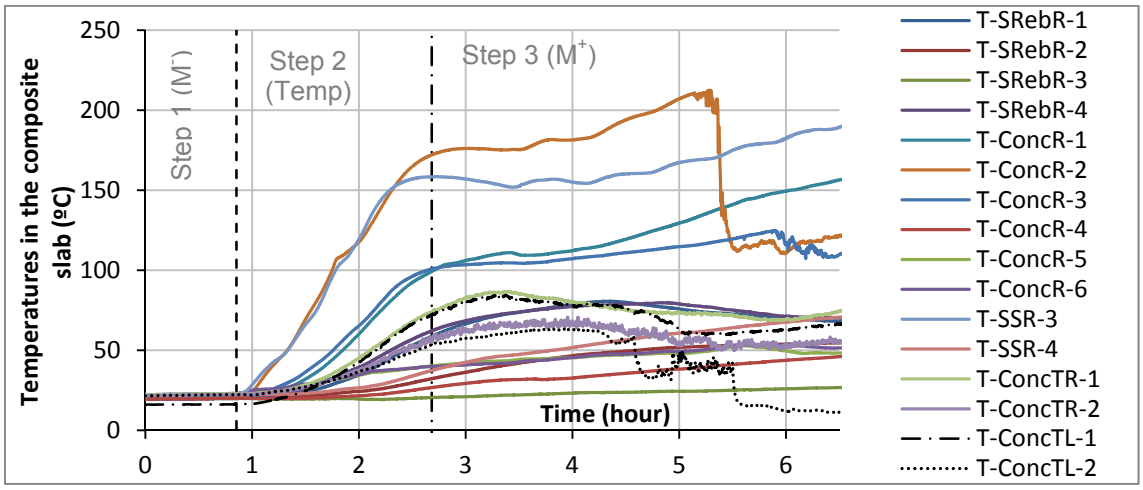

Figure 162: Evolution of the temperatures in the composite slab during the test 4

III.5.3.2 Evolution of the displacements and loads

In Figure 163 are compared the evolution of the reaction loads in both beams supports (F_L+F_R) with the reaction loads at the column (F3 + F_{HJ}). At the beginning of step 2, the reaction loads increased due to the thermal expansion in the heated zone. The reaction loads reached a maximum value (-271 kN). At this moment, the temperatures in the beams bottom flanges were equal to 433ºC on the left and 404ºC on the right beams (Figure 164). The following decrease of the loads should be due to the reduction of the steel mechanical properties.

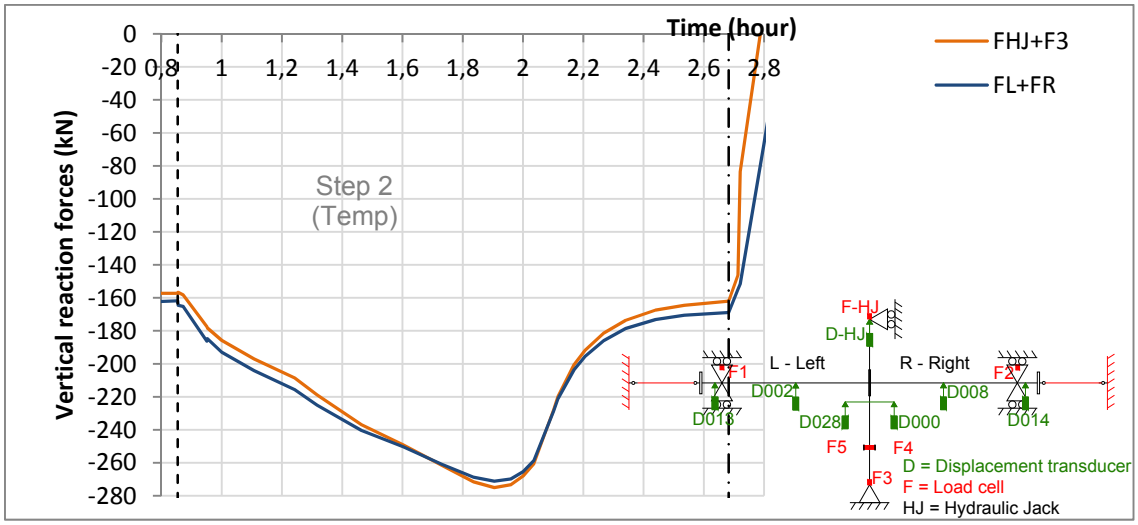

Figure 163: Comparison of the total load into the column (FHJ + F3) with the total reaction load at the beams supports (F1 + F2)

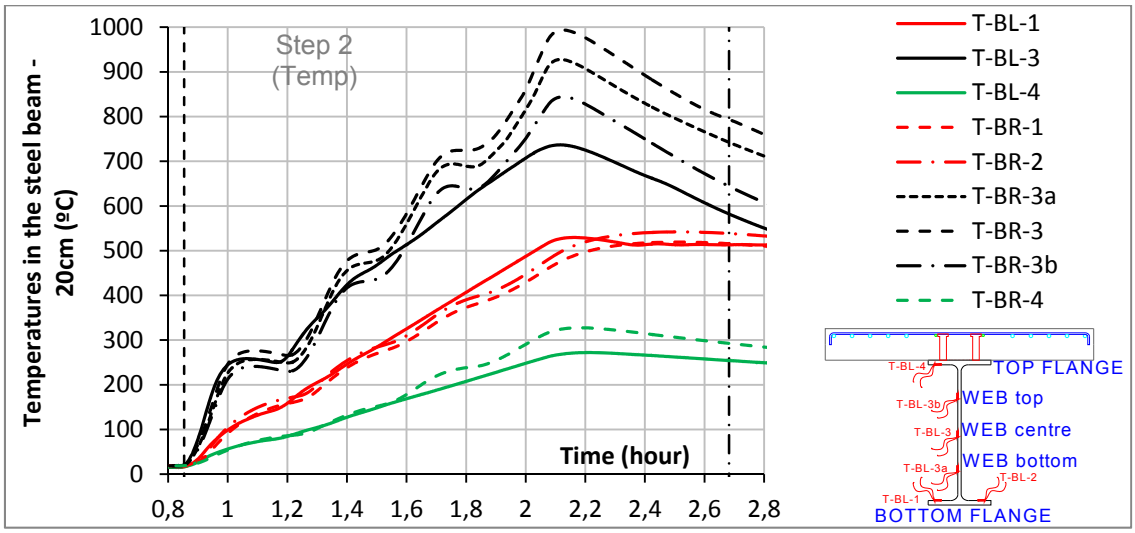

Figure 164: Evolution of the temperatures (T) in the beams at 20 cm from the connection during the step 2 (BR = beam right; BL = beam left)

Figure 165 shows the vertical displacements measured during step 2 below the joint (D000 and D028), at the beams mid-span (D002 and D008) and at the hydraulic jack located at the top of the column.

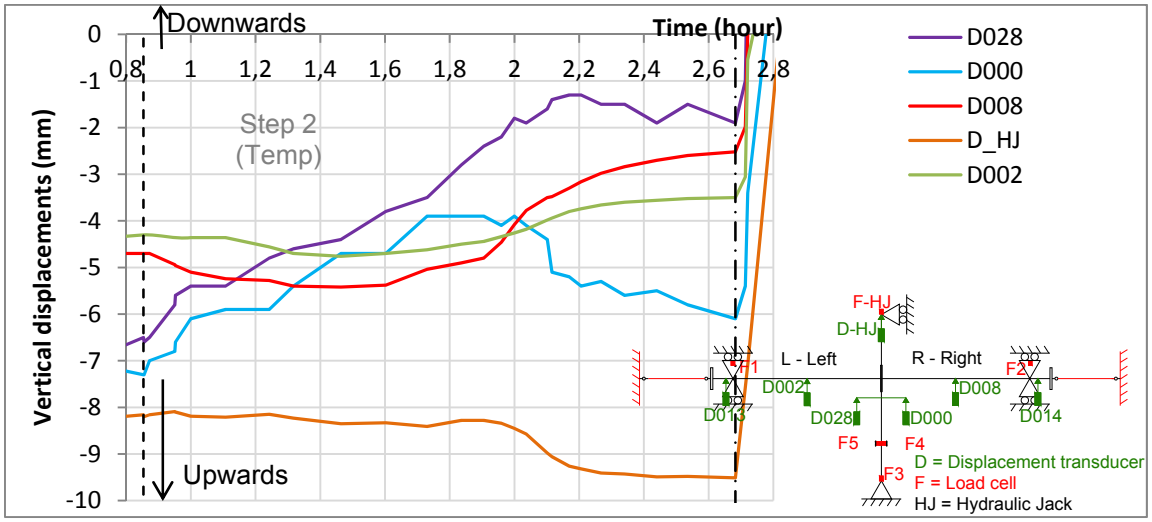

Figure 165: Vertical displacements near the beam-to-column joint during the increase of temperatures

At the beginning of step 2, the column section below the joint was moving downwards (transducers D000 and D028). The column was supported at the base by a cylinder, and in order to check if the cylinder kept its position constant during the increase of the temperatures, the vertical movement of the column base was measured by two wire transducers (D031 and D032, see Figure 166). During the heating, the pressure of the cylinder was regularly adapted in order to keep D031 and D032 as much as possible constant (Figure 167); however, D000 and D028 measured vertical displacements of the joint in the downwards direction. One reason could be that the steel bars where the wire transducers D000 and D028 were connected could be hot and perhaps slightly deformed in the downward direction (under self-weight).

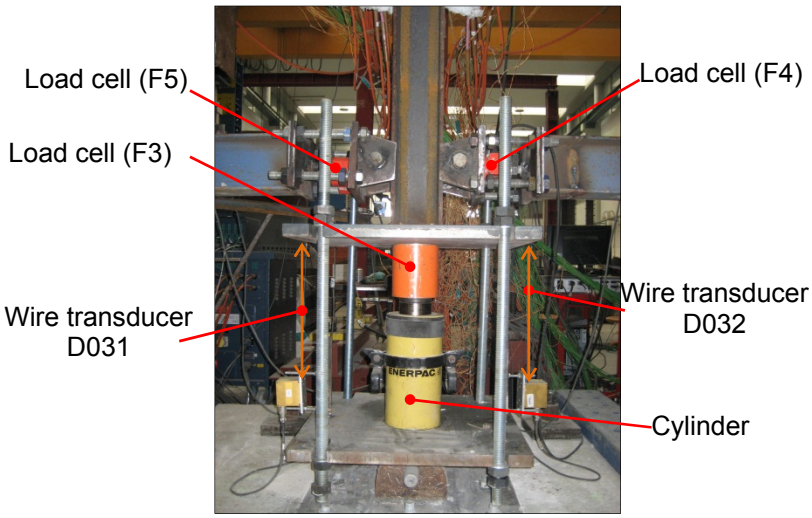

Figure 166: Wire transducers (D031 and D032) at the column base support (back view)

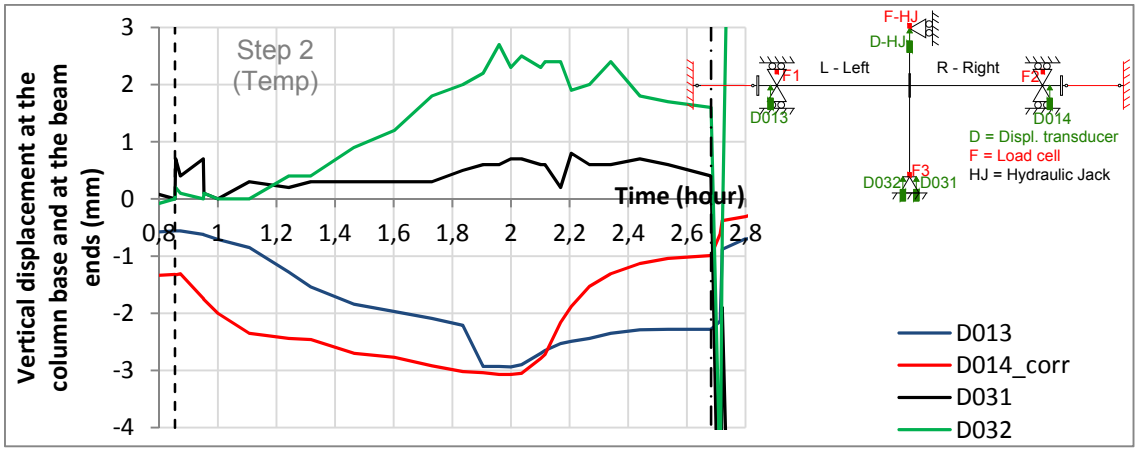

Figure 167: Vertical displacements measured near the beam supports (D013 and D014) and at the column base (D031 and D032) during the increase of temperatures

The thermal expansion of the column can be deduced from the vertical displacements measured at the column top (D_{HJ}) and at the joint (D000/D028). As shown in Figure 168, from the beginning to the end of the step 2, the column top (D_{HJ}) displaced upwards of 1.35 mm, and the joint displaced downwards of 2.9 mm (average value). Finally, the dilatation was estimated as the addition of both dilatations, i.e. 4.25 mm of dilatation.

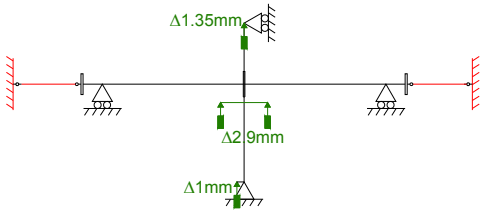

Figure 168: Total dilatation of the column during step 2

The evolution of the bending moment during the increase of temperatures is shown in Figure 169.

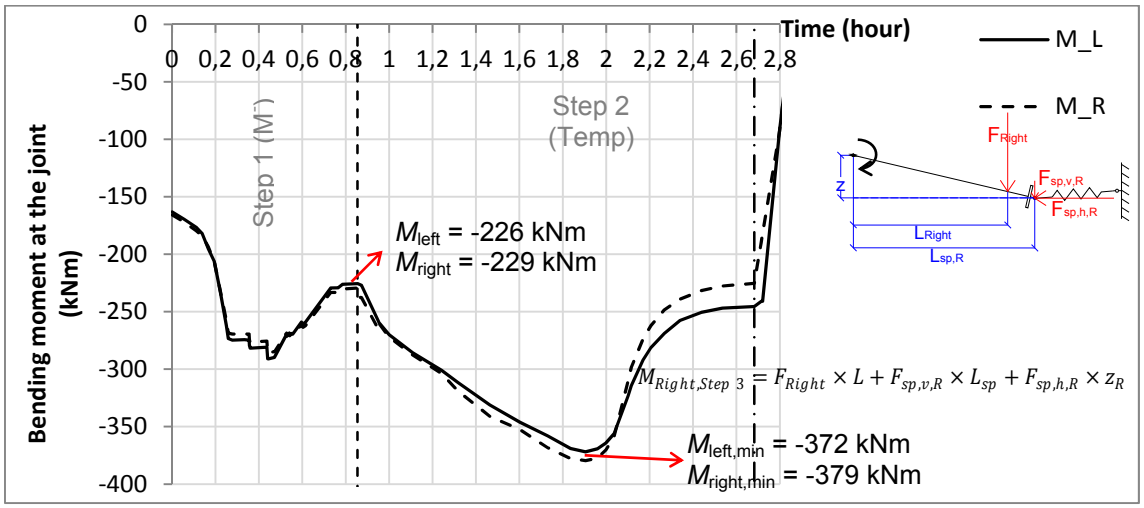

Figure 169: Evolution of the bending moment in the connections (Left and Right) during the steps 1 and 2

III.5.4 Step by step behaviour: step 3 - Loss of the column and sagging bending moment

The step 3 corresponded to the loss of the column and the increase of the sagging bending moment in the joint. Before the loss of the column, the hydraulic jack at the top of the column was changed to displacement control (velocity equal to 0.02 mm/sec); the cylinder at the base was progressively removed; and finally, the displacement at the top of the column was increased (increase of the joint sagging bending moment) up to the failure of the joint. Note that the structural system at the beams supports (see Figure 16 in section II.6.1.2) was not unloaded after the loss of the column: the beams supports continued to apply vertical loads, measured by F_1 and F_2.

Figure 170 shows the evolution of the vertical loads measured by the hydraulic jack ($F_{HJ}+F_3$) at the top of the column, by the load cells (F_1+F_2) at the top of the beams supports, and by the vertical components of the restraints loads ($F_{\_restr\_v\_R+L}$); the load applied at the column top was reduced by the two loads F_1 and F_2 measured at the beam supports: $F_{HJ}+F_3+F_1+F_2$, with F_1 and $F_2 < 0$. The evolution of the slab deformation and cracks is shown in Figure 171. The concrete crushed against the column flanges around 4h06min, and finally the entire slab width failed (5h). The concrete crushing against the column flanges correspond more or less to the maximum load F_{HJ}. The concrete also crushed at the ends of the composite slab: this failure happened under sagging bending moment, and should be due to the concrete compression struts created on the last row of the shear studs because the slab was stopped before the end of the beam.

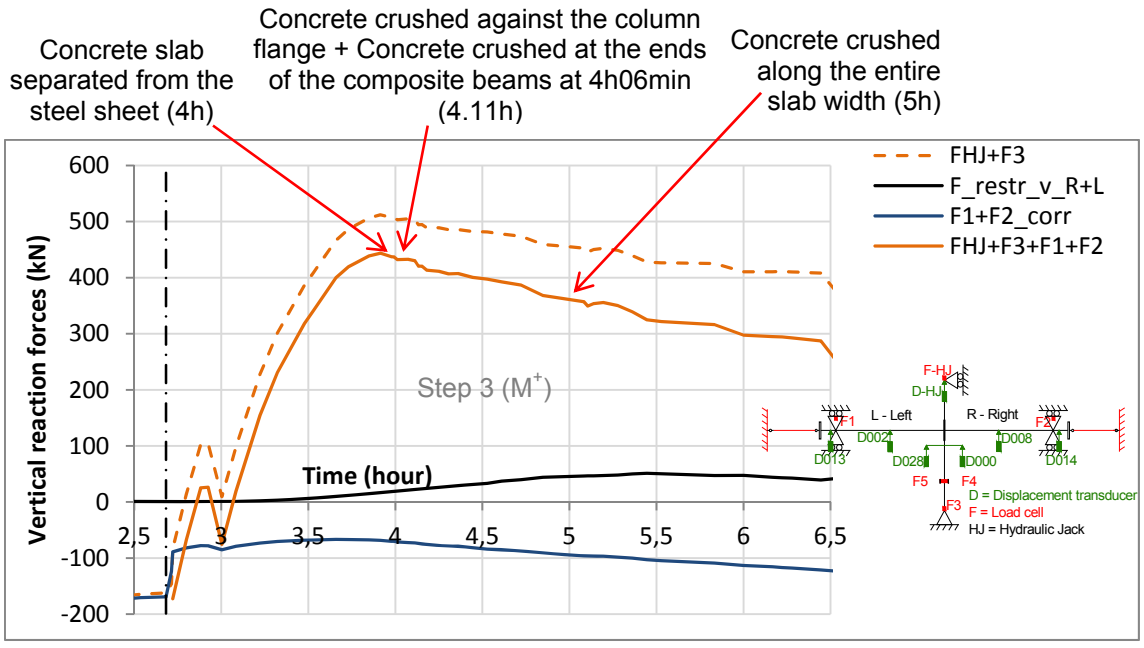

Figure 170: Evolution of the vertical loads during the step 3 (loss of the column and increase of the vertical load)

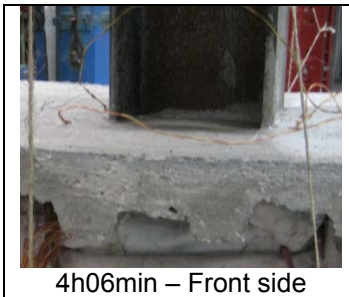
4h06min – Front side

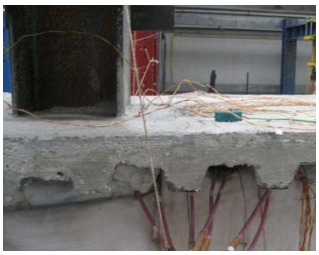
4h06min – Front side


4h06min – Right side


4h32min – Left/Front side


4h32min – Back side


4h36 – Left side


End of the test – Front side


End of the test – Left side

Figure 171: Evolution of the concrete crushing

Figure 172 shows the evolution of the vertical displacements measured i) by the hydraulic jack D_{HJ}; ii) by the wire transducers D000 and D028, and iii) by the displacement transducers at mid-span of the beams (D008 and D002). The maximum displacement measured by the hydraulic jack was 246 mm.

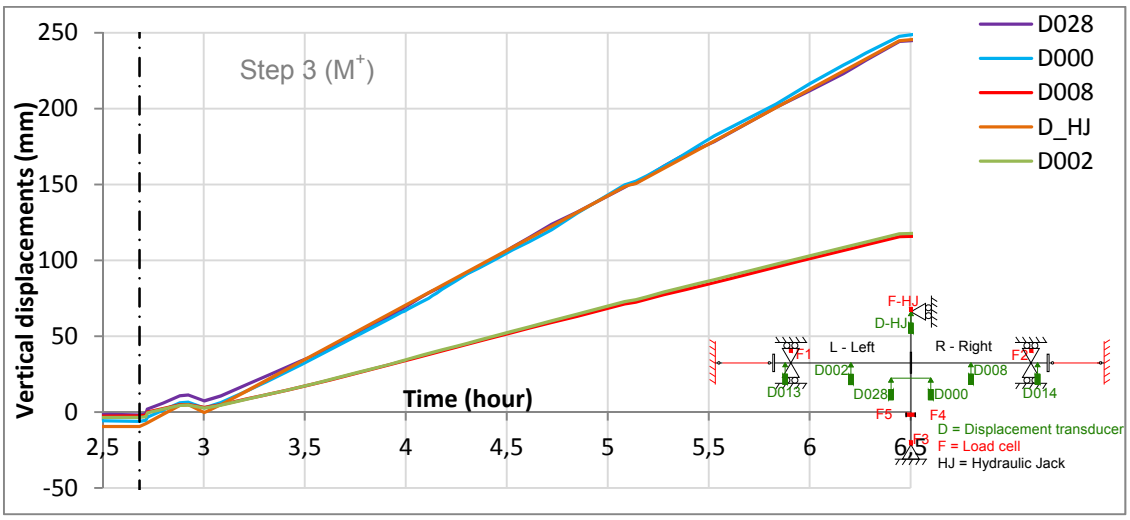

Figure 172: Vertical displacements near the beam-to-column joint during the entire test

Figure 173 presents the reaction loads measured during the test 4: at the hydraulic jack (F_{HJ}), at the column base (F_3), at the beams ends (F_1 and F_2), and finally at the axial restraints to the beams ($F_{restr,R\ and\ L}$) (see §III.1).

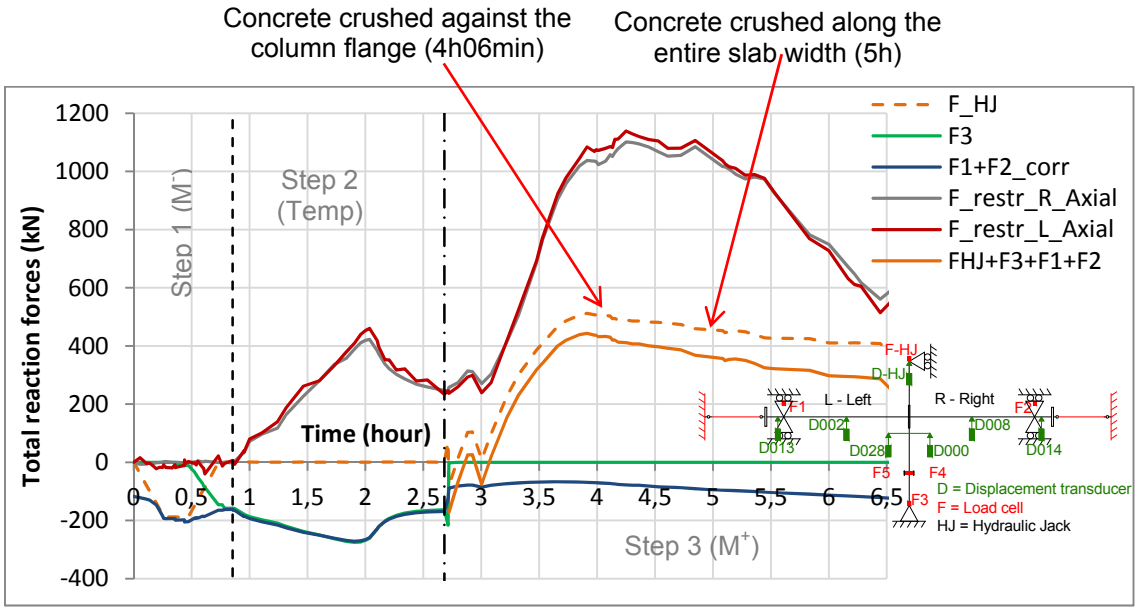

Figure 173: Evolution of the loads during the entire test

Figure 174 shows the evolution of the bending moment *versus* time at the connections during the entire test.

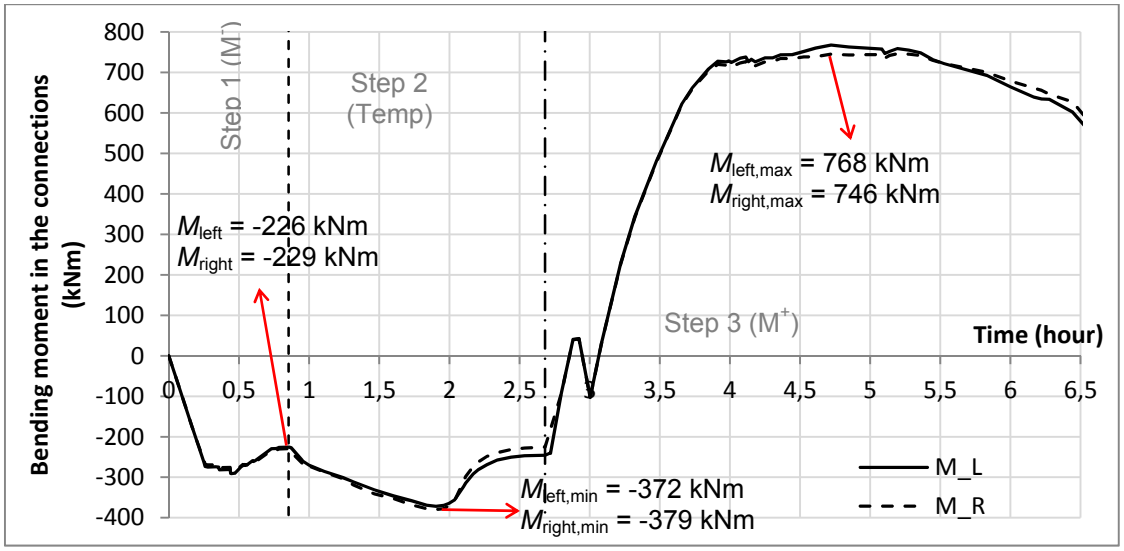

Figure 174: Bending moments at the connections left and right

Figure 175 and Figure 176 present the evolution of the total reaction load *versus* the joint rotation and the beam axial load respectively.

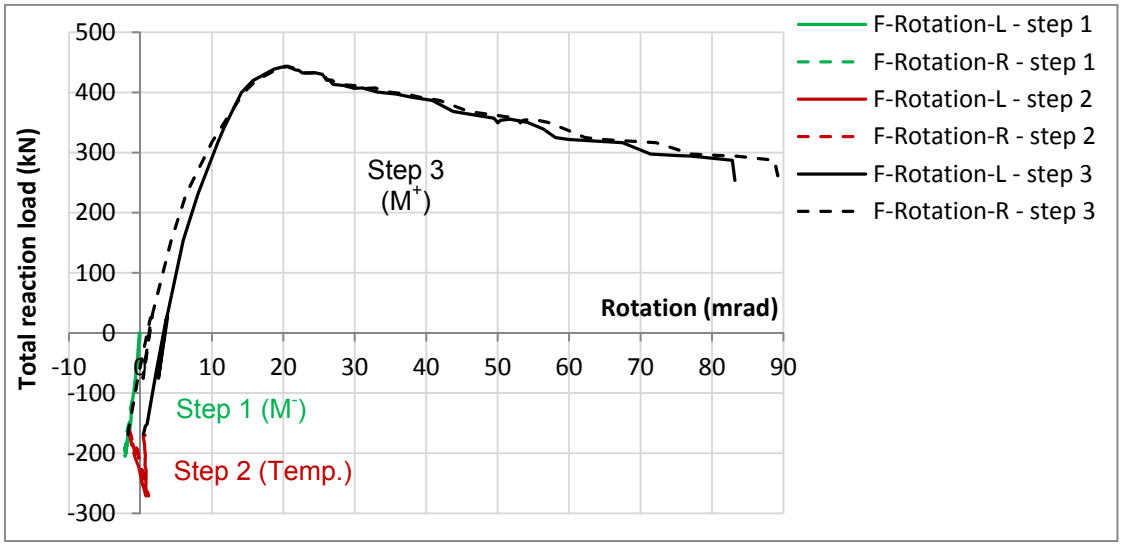

Figure 175: Total reaction load (F_L+ F_R) vs rotation at the joint

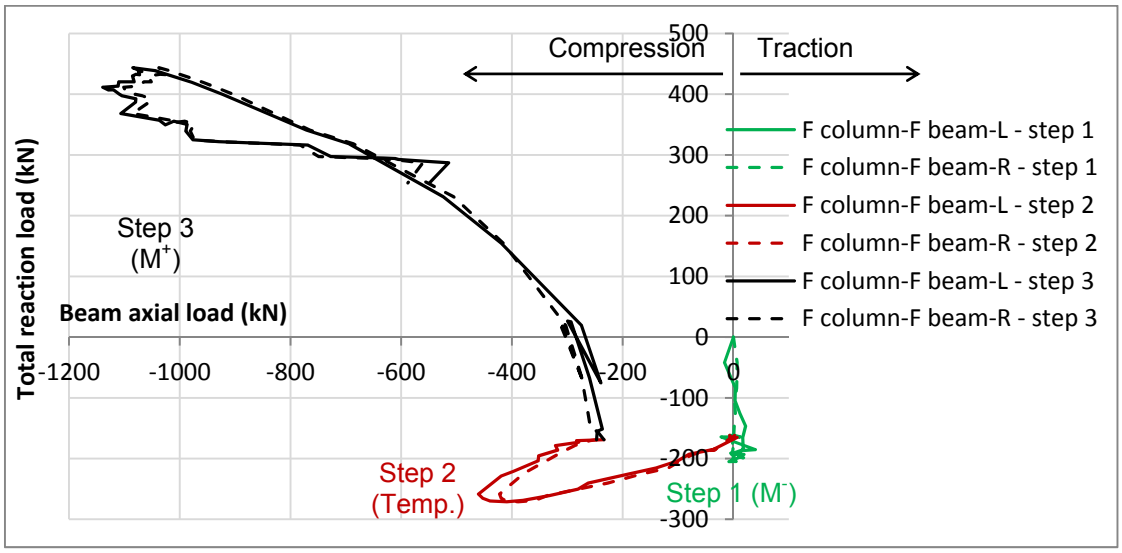

Figure 176: Total reaction load (F_L+ F_R) vs axial forces at the joint ($F_{restr,ax}$)

III.5.5 Additional data

The evolution of the vertical and horizontal components of the axial restraint loads, $F_{sp,v}$ and $F_{sp,h}$, are showed in Figure 177. The rotations of the axial restraints are shown in Figure 178, with maximum 38 mrad on the left and 35 mrad on the right.

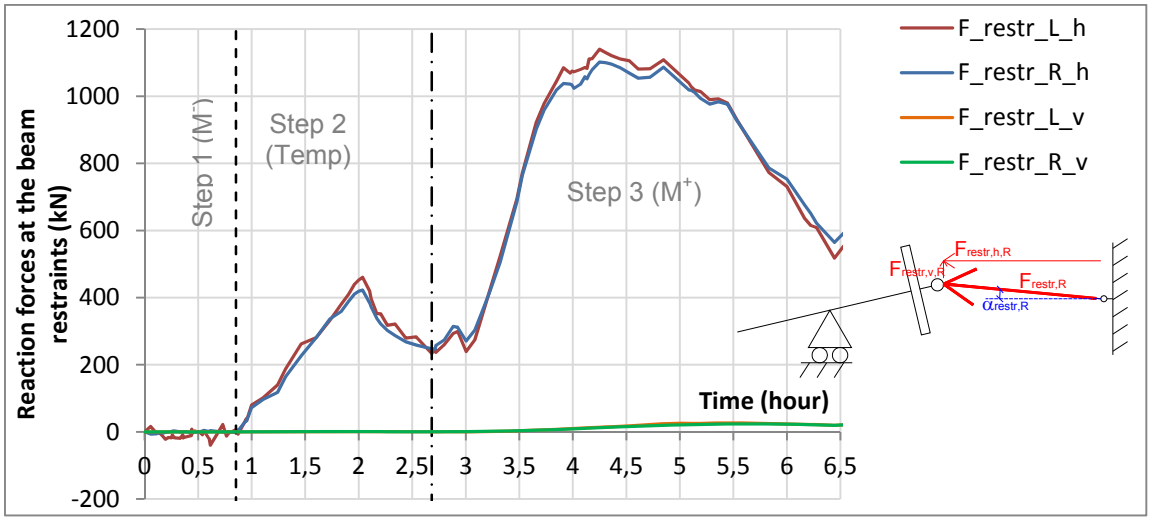

Figure 177: Projections of the restraints loads along the horizontal (h) and vertical (v) axis

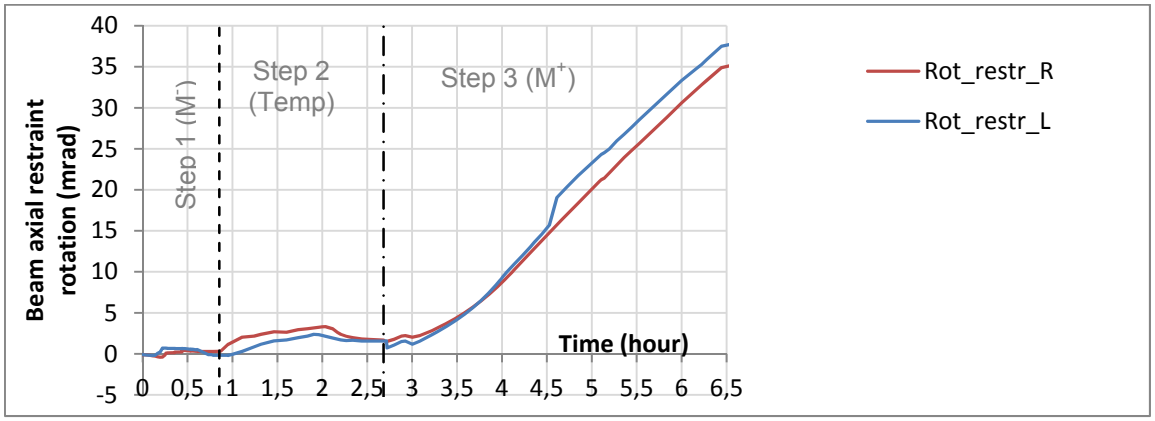

Figure 178: Axial restraints rotations (L = left; R = right)

The horizontal displacements measured at the beam ends are showed in Figure 179. The estimated horizontal displacements at the neutral axis of the steel beams $D_{beam,h,L\ and\ R}$ are represented by the black curves (see §III.1).

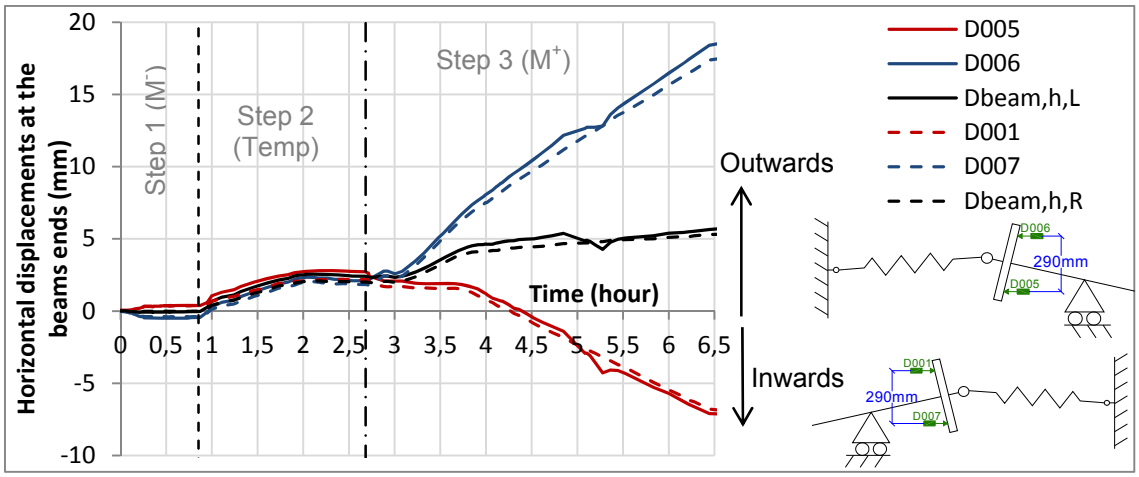

Figure 179: Horizontal displacements at the beams ends

Figure 180 presents the displacements of the beams out of the plan, measured by the two displacement transducers D025 and D026 at the beam ends, and by

the two transducers D003 and D009 on the beams webs, initially situated at 1500 mm from the end-plate.

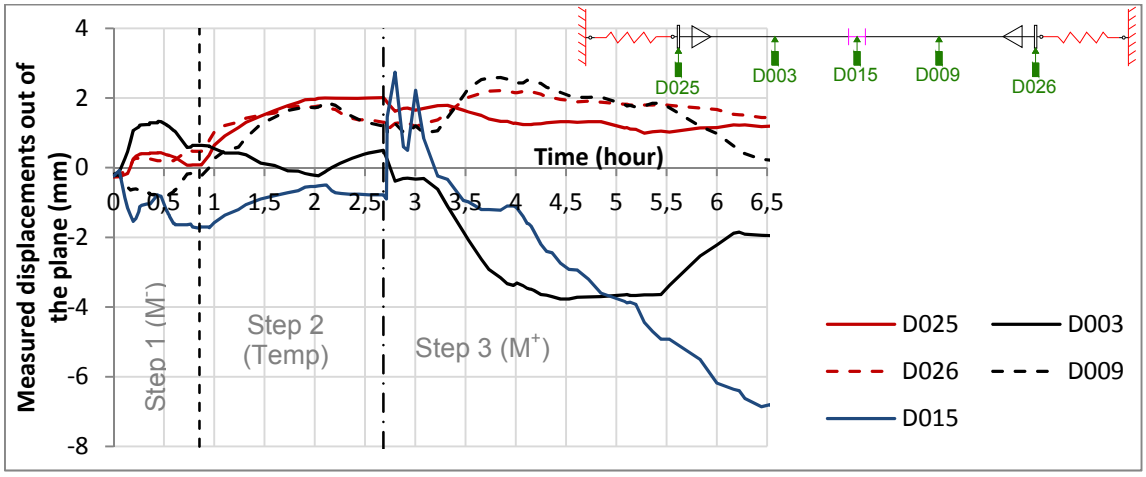

Figure 180: Evolution of the displacements measured out of the plan

Figure 181 presents the measured displacements of the auxiliary's structures (steel and concrete footings and strong beams connected to the strong walls).

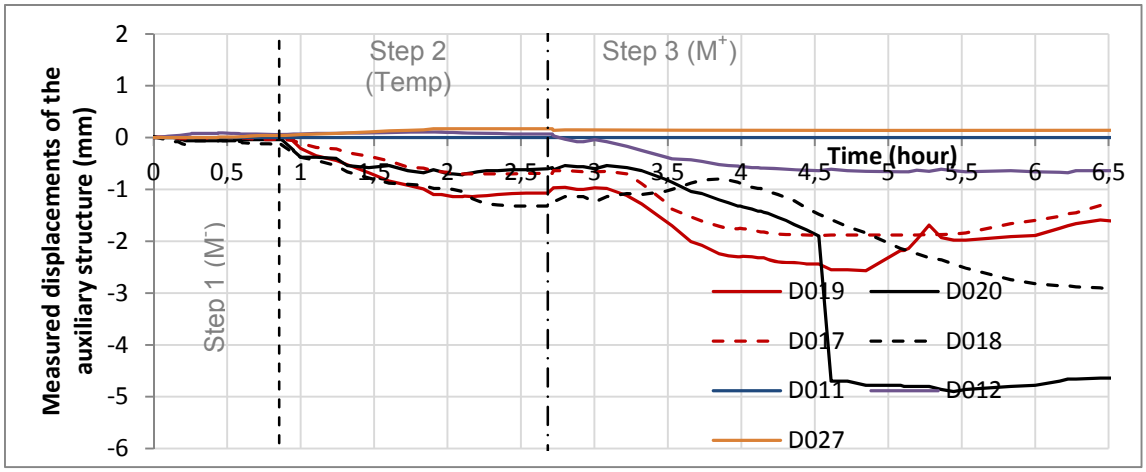

Figure 181: Measured displacements of the steel and concrete footings, and of the strong beams linked to the walls (see Figure 31 in §II.8.2 for the position of the displacement transducers)

III.6 Results of test 5

The global behaviour of the joint during the test is described in the following section, then the step by step behaviour is detailed, for each loading step, and finally, additional data a presented.

III.6.1 Joint behaviour (entire test)

III.6.1.1 Temperature results

Figure 182 presents the temperatures evolution during the entire test 5 in the right and left beams (at 200 mm from the connection), in the column centre and in bolts from row 4. One modification for this test was the position of the four FCP elements on bolts: instead of being located on the end-plate, they were

placed on the column flanges (see §II.6.2). The objective of this modification was to observe if the position of these elements would influence the local deformation of the end-plate centre; obviously, as presented after, the FCP elements position had no influence and the end-plate deformed in the same way. The temperature increase rate was 300ºC/hour in the beam bottom flanges. These bottom flanges reached 700ºC, whereas the temperature increased faster in the right beam web because of the reduced thickness; the left beam web did not increased so much because one FCP element located on the web burned and stopped working at the beginning. Temperatures in beams top flanges were much lower because they were only heated by heat transfer from web, which was reduced by the composite slab protection. During step 3, the temperature was well kept constant in the beam bottom flanges. Around 7h, the deformation of the sub-frame created openings at the thermal isolation which reduced the temperatures in the beams bottom flanges; the transformer machine increased electrical power sent to the FCP elements, which made increased some temperatures at beams webs, and column. Concrete temperatures did not rise above 200ºC, with maximum 100ºC measured at the top of the slab. At 7h, maximum temperatures measured at the joint were: 502ºC in bolts, 500ºC in beam end-plates, 533ºC in column web and 495ºC in column flanges. The evolutions of all measured temperatures are detailed in §III.6.3.

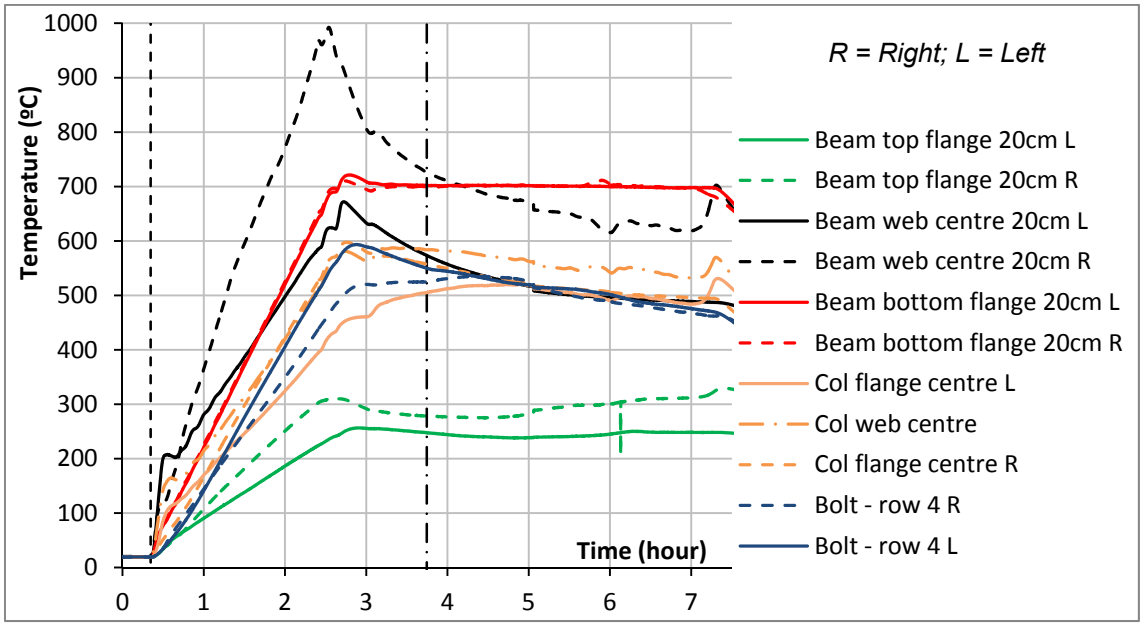

Figure 182: Evolution of the temperatures during test 5

III.6.1.2 Bending moments variation and failure modes

The evolution of the total reaction load versus the vertical displacement of the joint, and the bending moment versus the rotation are depicted in Figure 183 and Figure 184. Figure 185 shows the evolution of the bending moment at the joint versus the beam axial load (measured at the restraint and projected in the beam direction, $F_{restr,ax}$). The hogging bending moment was initially reached during step 1, followed by a variation of this moment during the increase of temperatures in step 2. This initial hogging bending moment reached -392 kNm

on the left and -393 kNm on the right connections. These values are higher than it should be (target bending moment: -236 kNm) and increased when the column base support was applied (see step by step behavior in §III.6.2). At the beginning of step 2, reaction loads increased due to the thermal expansion of the structure. After a while, these reaction loads decreased because of the steel properties degradation due to high temperatures: the minimum hogging bending moment reached -499 kNm on the left and -490 kNm on the right connections (which corresponds to a vertical load at the column equal to -376 kN). In step 3, the loss of the column was really progressive as the hydraulic jack at the column top imposed a constant displacement rate, and in order to a better characterization of the elastic stiffness of the joint, an “unloading-reloading” was performed around 3h56min, before the concrete crushing in compression. The maximum total vertical reaction load (435 kN) was reached for a rotation of 20 mrad, a vertical displacement of 61 mm, and axial restraint compression loads equal to 1528 kN and 1518 kN on the left and right sides. The axial restraints were connected to the beams since the beginning of the test. During step 1, the loads and displacements created by the application of the initial hogging bending moment were not sufficient to create axial forces to the beams. During steps 2 and 3, the beam ends were moving outwards and the restraints worked in compression. Concrete crushing in compression was the first failure observed, but this failure was really progressive; around 69 mm of vertical displacement, the concrete was crushed against the column flange (Figure 186a, b), around 108 mm of vertical displacement (rotation of 35 mrad on the left connection), half of the concrete slab was crushed on the front, and around 156 mm of vertical displacement, the concrete from the composite slab was crushed on the entire slab width (Figure 146c). During the concreting of test 5, a support situated near the column (back side) fell down, which created a higher thickness of the slab on this side (the slab thickness on the extreme front side was 60 mm, whereas the slab thickness on the extreme back side was 100 mm). Maxima sagging bending moments were reached: 827 kNm and 898 kNm on the left and right connections respectively, for which corresponded rotations respectively equal to 45 mrad and 50 mrad (or 138 mm of vertical displacement; a total vertical reaction load (FL+FR) equal to 325 kN; and axial restraints loads equal to 1640 kN and 1668 kN on the left and right sides respectively). The jack length capacity was increased after the concrete crushing against the column flanges.

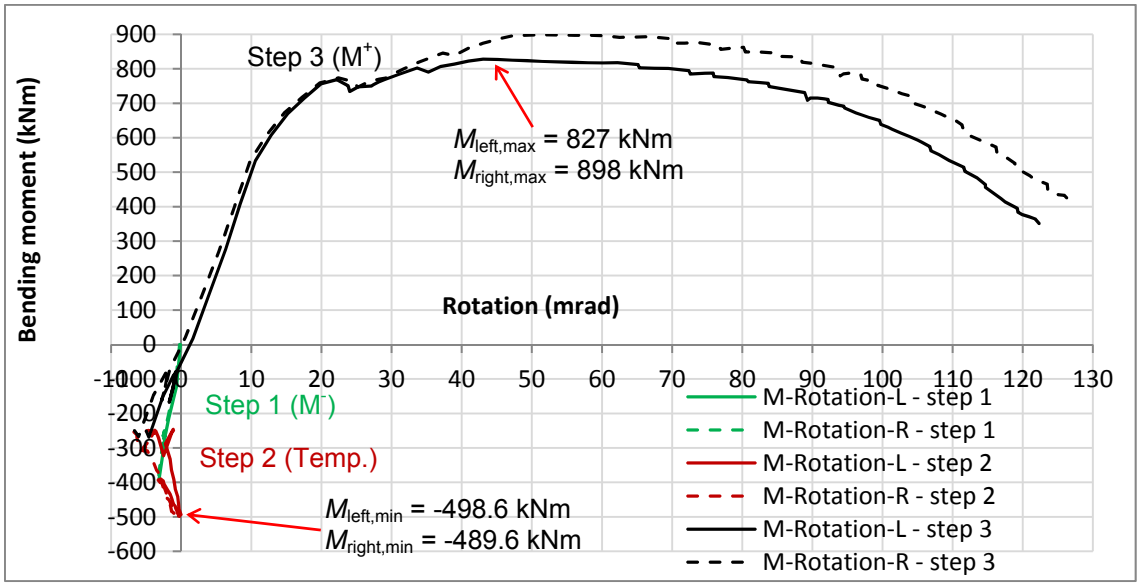

Figure 183: Bending moment vs rotation at the connection

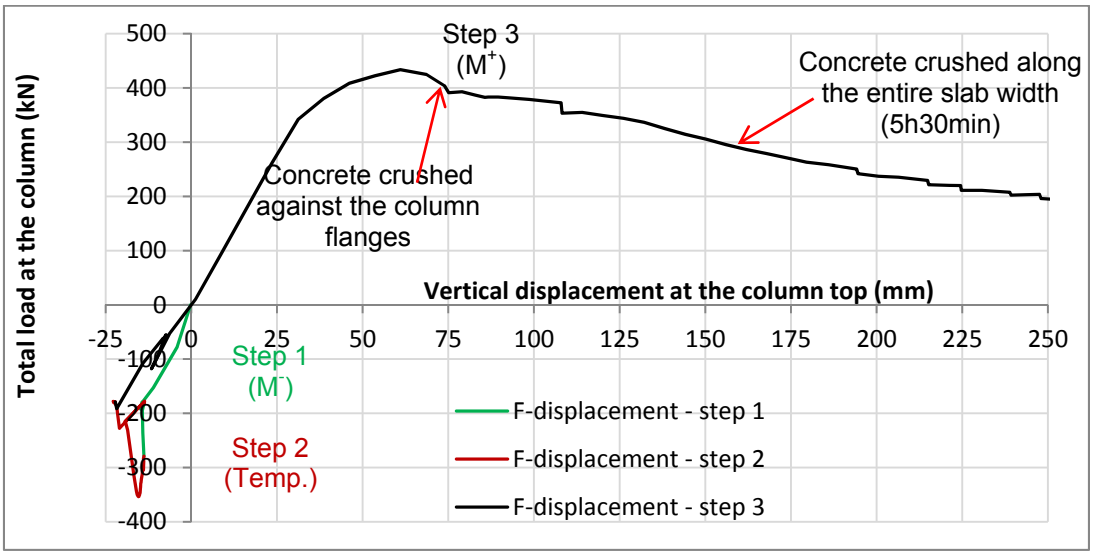

Figure 184: Total reaction load (F_L+ F_R) vs vertical displ. measured at the column top (D_{HJ})

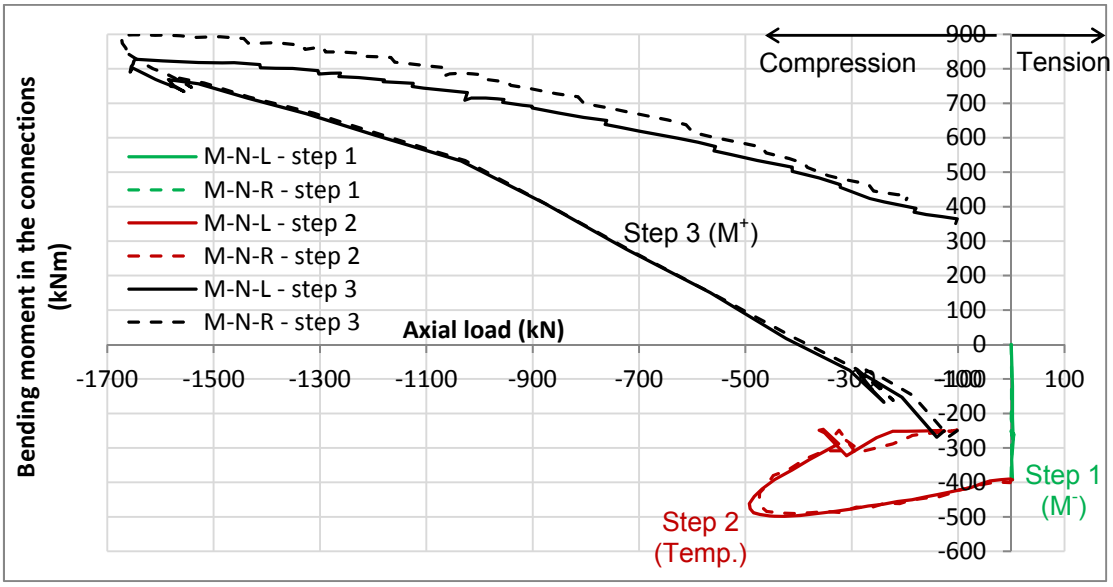

Figure 185: Joint bending moment vs axial forces at the joint ($F_{restr,ax}$)

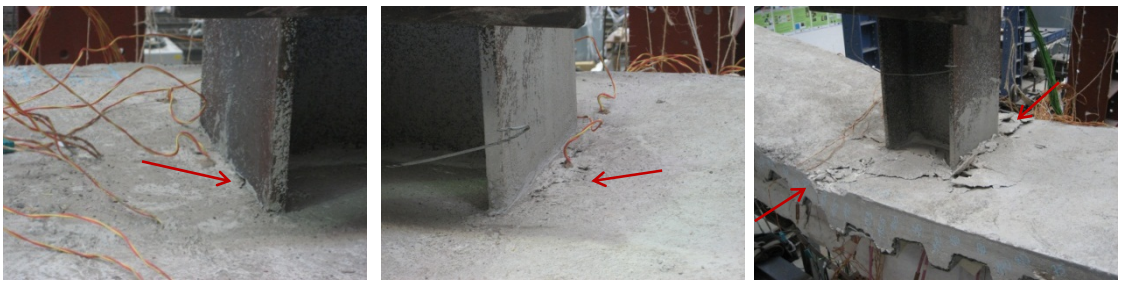

a) Right side b) Left side c)

Figure 186: Concrete crushed: a) and b) against the column flanges (4h42min); c) at the end of the test

The test was stopped because the maximum vertical displacement was reached by the jack: the vertical displacement of the joint was 337 mm. No bolts failed during this test; the steel end-plates deformed in the bottom and centre part and showed a high ductility (see Figure 187). The final deformation of the sub-frame is shown in Figure 188.

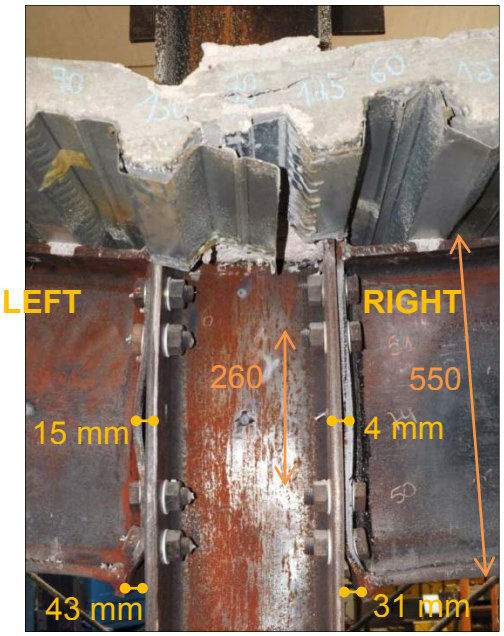

Figure 187: Deformations of the joint (view from the front side)

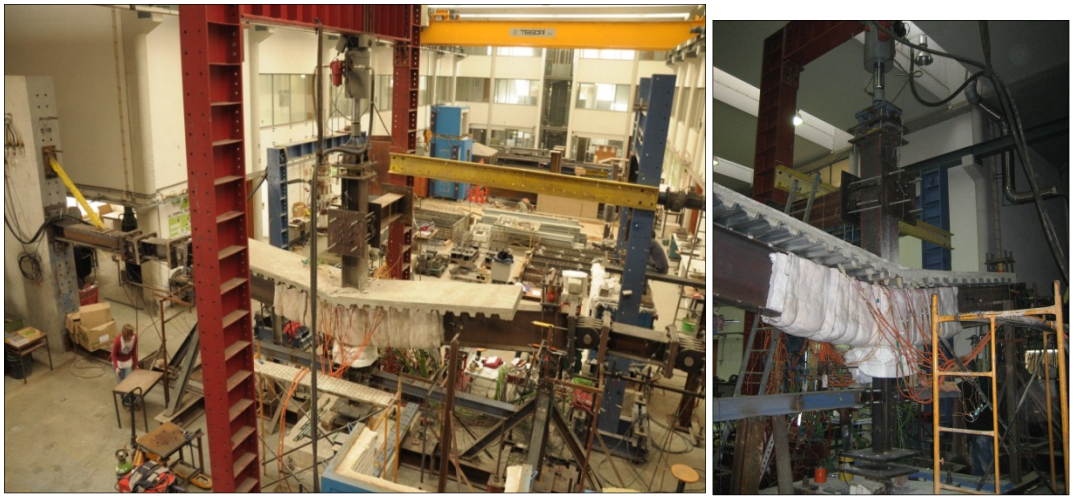

Figure 188: Final deformation of the sub-frame

Local buckling under compression loads of beams webs was not observed; however, due to the web thermal expansion under elevated temperatures, the beam bottom flange deformed (Figure 189a). Moreover, the right beam bottom flange straitened (Figure 189b). Due to the high compression forces (total restraint to the beam) combined to hogging and sagging bending moments, local bucklings happened: at the steel web of the column (level of rows 3 and 4) under hogging bending moment (Figure 190a); at the right beam top flange under sagging bending moment (Figure 190b).

a) b)

Figure 189: Local deformations of the beams: a) slight deformation out of the plane – left beam, b) shrinkage of the bottom flange – right beam

a) b)

Figure 190: Local buckling a) of the column web at the bottom part (view from the front side), b) of the top flange from the right beam (view from the back)

Figure 191 shows the rotations at the joint left and right sides versus time, as well as the column rotation. The column rotation was very small (6 mrad) thanks to the lateral restraints of the column (see Figure 7 in §II.2). The test was stopped at 122 mrad and 126 mrad of connection left and right rotations. The joint rotation calculation included any beam rotation or deformation: Figure 192 and Figure 189b show the eventual formation of a plastic hinge at the border between the heated zone and the cooler part of the right beam (more visible than for the left beam).

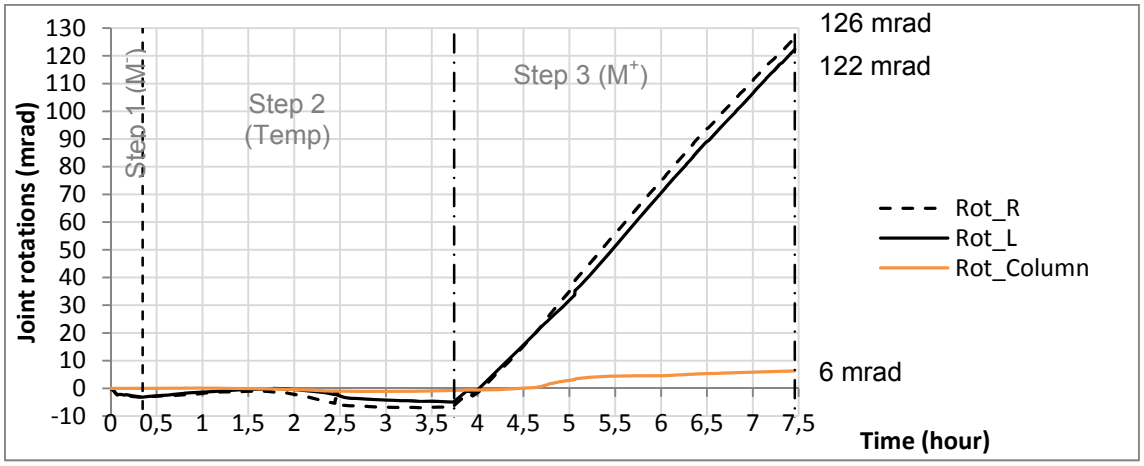

Figure 191: Rotations at the connections (Rot_Connection Left and Right) and column rotation

Figure 192: Beam rotation near the joint

III.6.2 Step by step behaviour: step 1 - Initial hogging bending moment

Figure 193 presents the evolution of the vertical displacements measured near the beam-to-column joint during the step 1. The initial hogging bending moment was applied in three phases: i) the beams were restrained at the supports and the column was free at the base; ii) phase 1: the hydraulic jack increased the vertical load at the column top and pulled the column upwards; iii) phase 2: the column base support (single acting cylinder) was set up; iv) phase 3: the load at the column top was completely transferred to the sub-frame supports.

Figure 194 presents the comparison between the sum of the loads measured at the column (F_{HJ}+F_3) and the sum of the reaction loads measured at the beam supports (F_L+F_R). Before loading the joint, the end of each beam was vertically restrained and an initial load (-125 kN) was measured by the load cells F_1 and F_2.

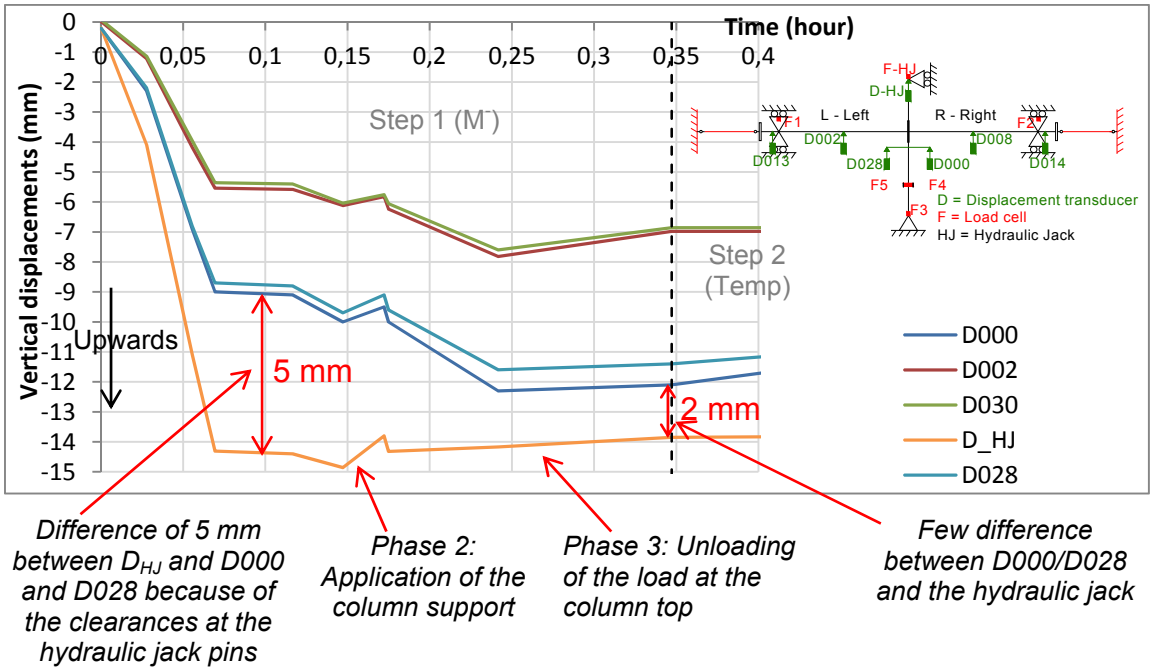

Figure 193: Vertical displacements near the beam-to-column joint during the application of the initial loads (hogging bending moment)

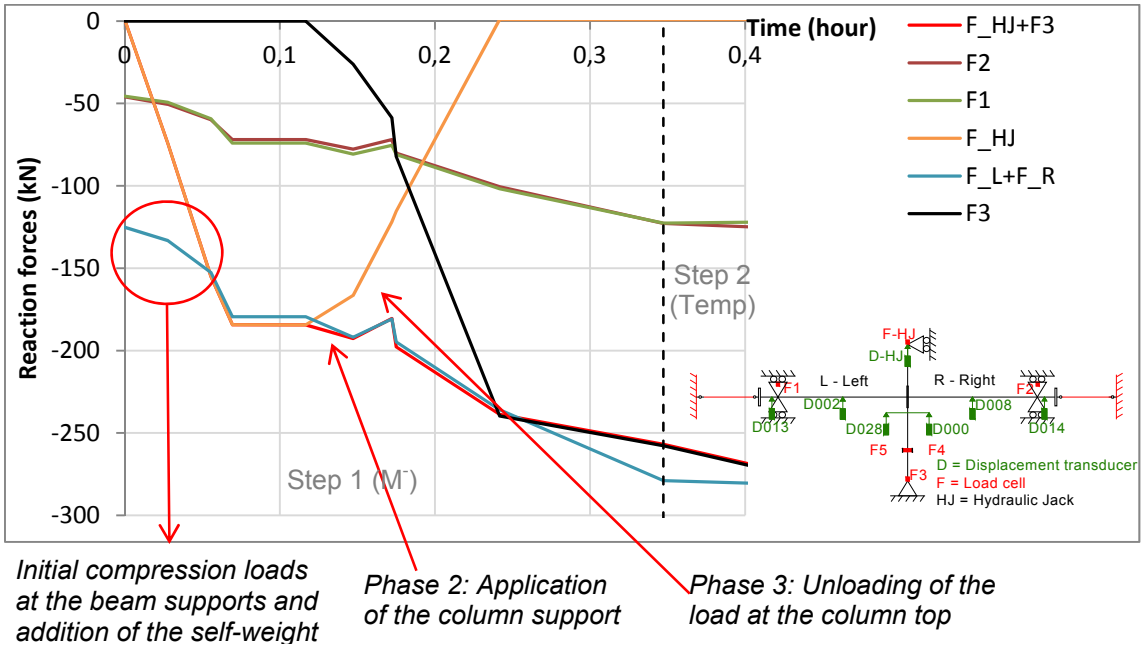

Figure 194: Comparison between the load applied by the hydraulic jack at the top of the column and the reaction loads at the beams supports

III.6.3 Step by step behaviour: step 2 - Temperatures (700ºC)

The second loading step consisted to the slow increase (around 300ºC/hour) of the temperature in the heated zone, until reaching 700ºC in the beam bottom flanges (at a distance of around 20 cm from the joint). Increasing slowly allowed a better control of the sub-frame behaviour. The hydraulic jack at the column top was in force control; in order to allow free thermal expansion of the column top, a constant load of 0.1 Tf was imposed (see §II.6.1.1).

III.6.3.1 Evolution of the temperatures

Figure 195, Figure 196 and Figure 197 show the evolution of the temperatures in the beams at respectively 20 cm, 50 cm and 1 m from the end-plate.

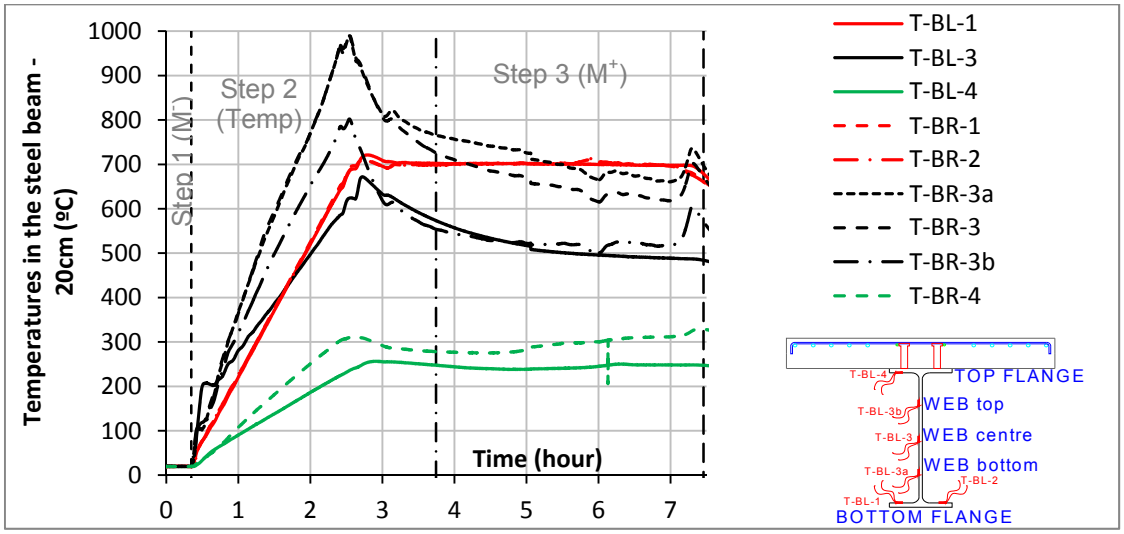

Figure 195: Evolution of the temperatures (T) in the beams at 20 cm from the connections during the test 5 (BR = beam right; BL = beam left)

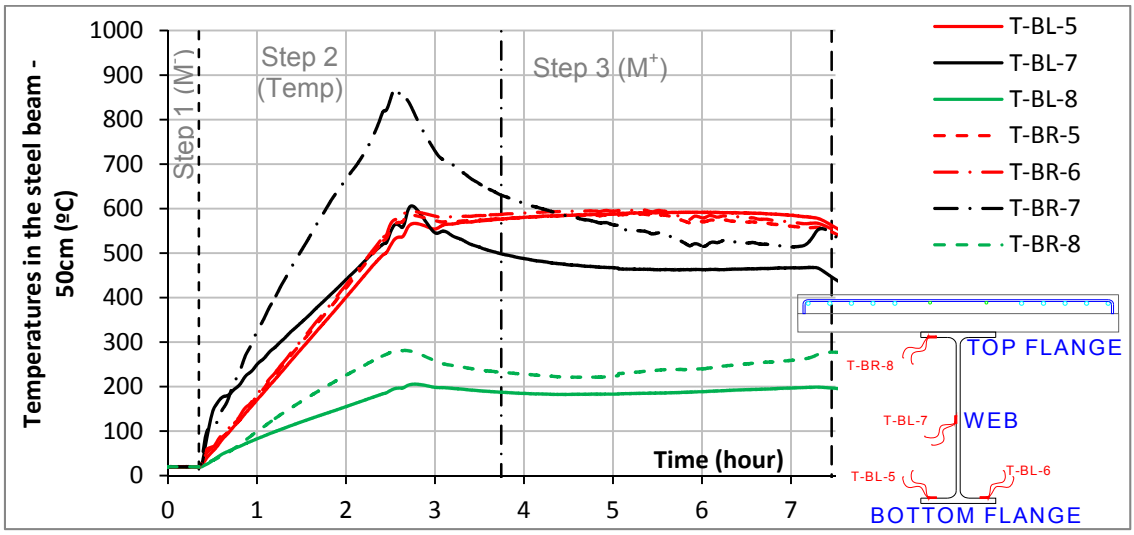

Figure 196: Evolution of the temperatures (T) in the beams at 50 cm from the connections during the test 5 (BR = beam right; BL = beam left)

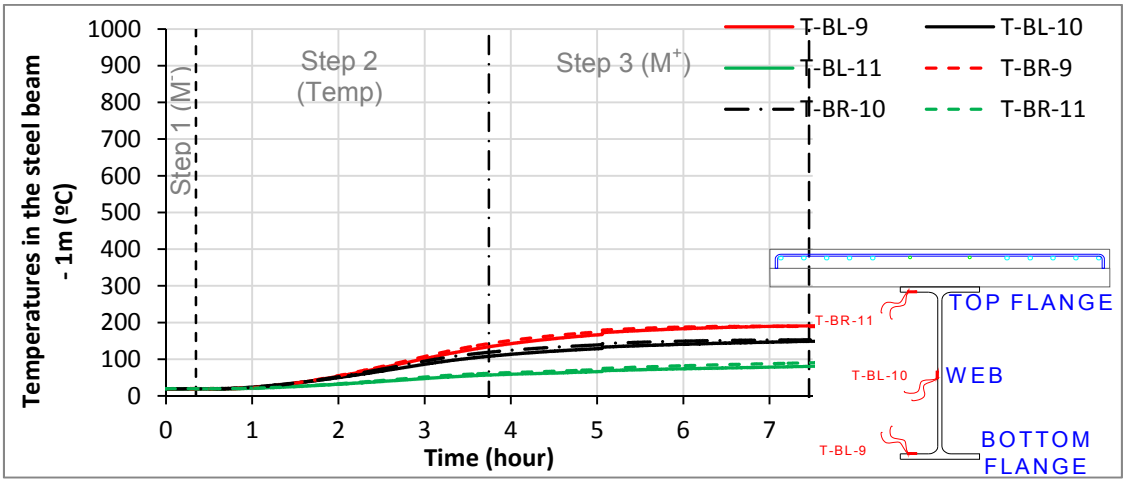

Figure 197: Evolution of the temperatures (T) in the beams at 100 cm from the connections during the test 5 (BR = beam right; BL = beam left)

Figure 198, Figure 199 and Figure 200 show the evolution of the temperatures at shank and at head of the bolts at each side of the joint, and at the end-plates surface.

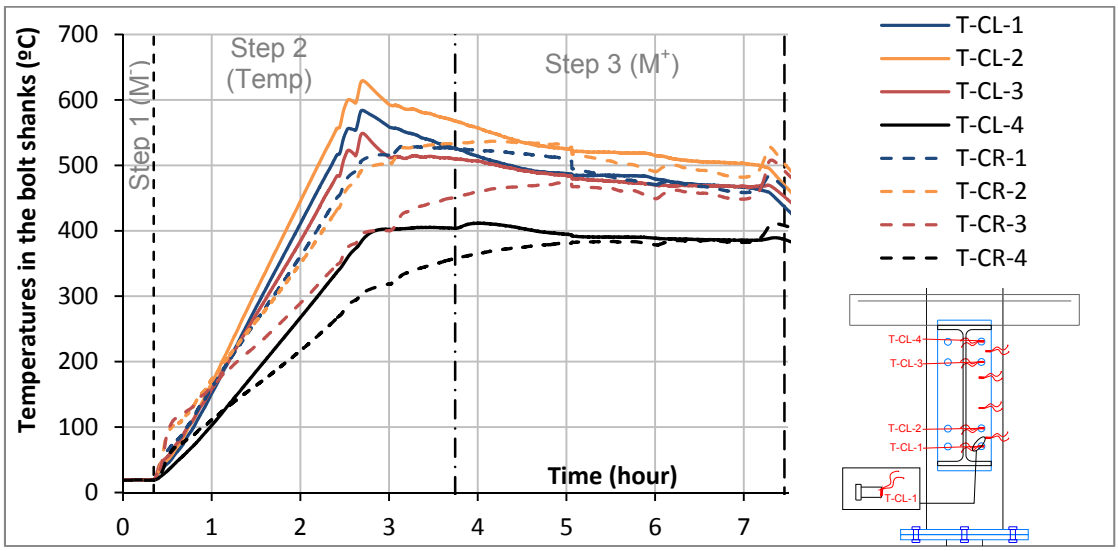

Figure 198: Evolution of the temperatures (T) in the shank of the bolt during the test 5 (CR = connection right; CL = connection left)

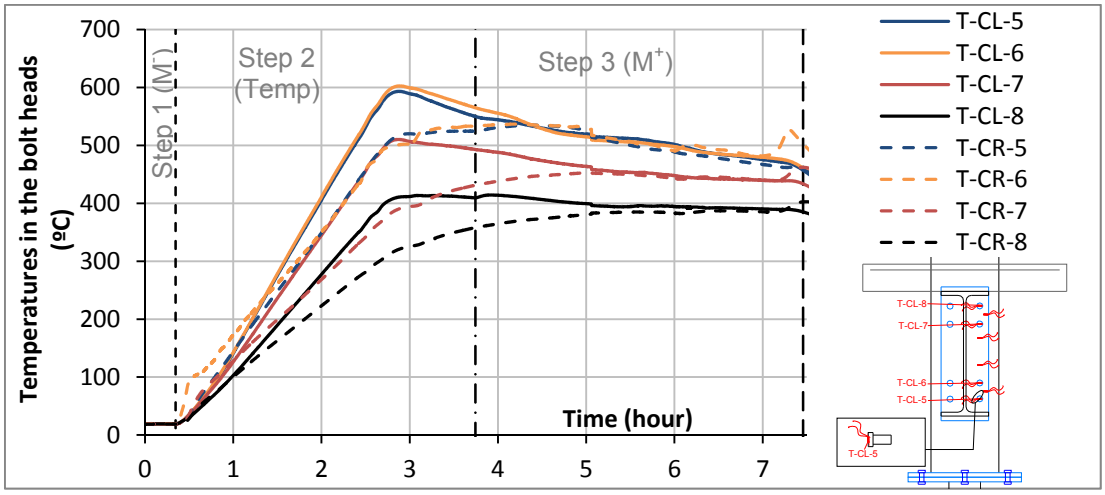

Figure 199: Evolution of the temperatures (T) in the head of the bolts during the test 5 (CR = connection right; CL = connection left)

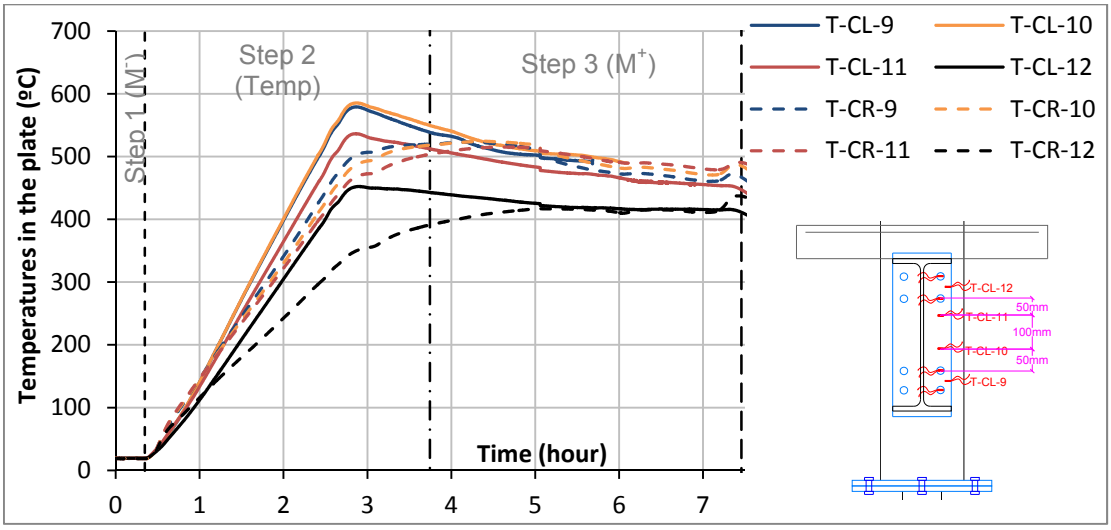

Figure 200: Evolution of the temperatures (T) in the end-plates during the test 5 (CR = connection right; CL = connection left)

The evolution of temperatures in the column is presented in Figure 201; temperatures at the column centre (T-Col-1 to 3) are higher than at the web ends (top – T-Col-7, or bottom – T-Col-5).

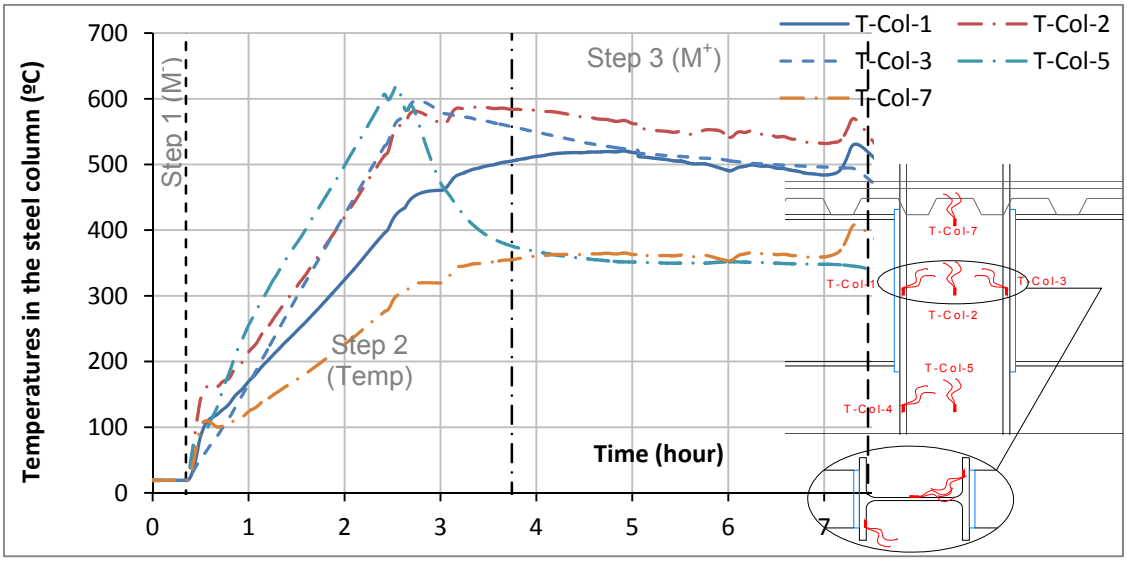

Figure 201: Evolution of the temperatures in the column during the test 5

The evolution of temperatures in the composite slab is depicted in Figure 202, and measured points are shown in Figure 34, section II.8.3 (p24).

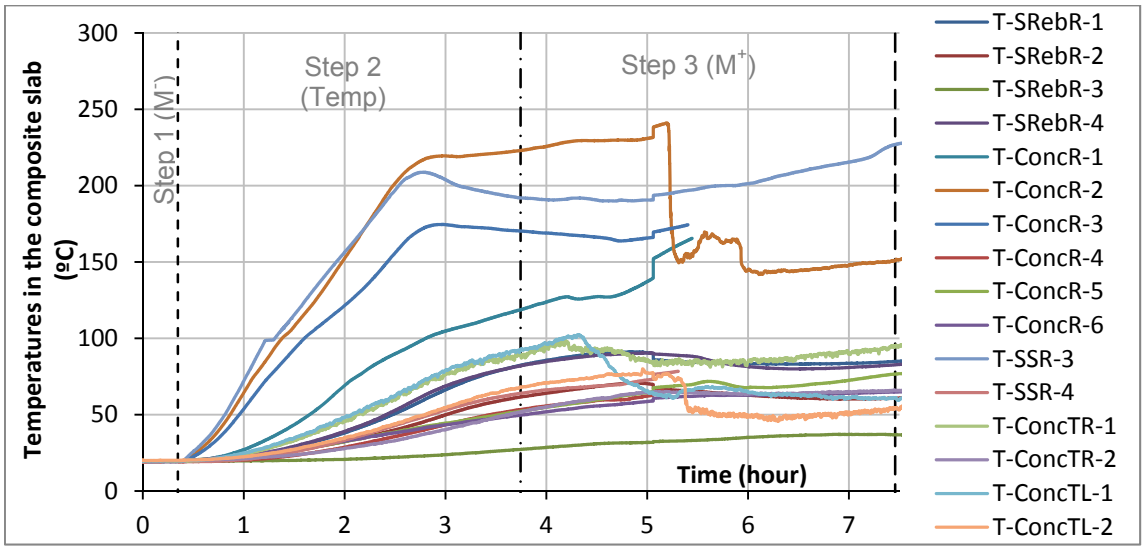

Figure 202: Evolution of the temperatures in the composite slab during the test 5

III.6.3.2 Evolution of the displacements and loads

In Figure 203 are compared the evolution of the reaction loads in both beams supports (F_L+F_R) with the reaction loads at the column (F3+F_{HJ}). At the beginning of step 2, the reaction loads increased due to the thermal expansion in the heated zone and reached a maximum value (-376 kN). At this moment, the temperatures in the beams bottom flanges were equal to 425ºC on the left and 429ºC on the right (Figure 204). The following decrease of the loads should be due to the reduction of the steel mechanical properties. The oil pressure was adapted in the cylinder at the column base during the step 2; once the reaction loads decreased, the oil pressure in the cylinder was reduced; however, instead of a slight reduction, the hydraulic pump removed too much oil pressure, which

is showed by the sudden decrease of the loads; then a certain level of oil pressure was increased again.

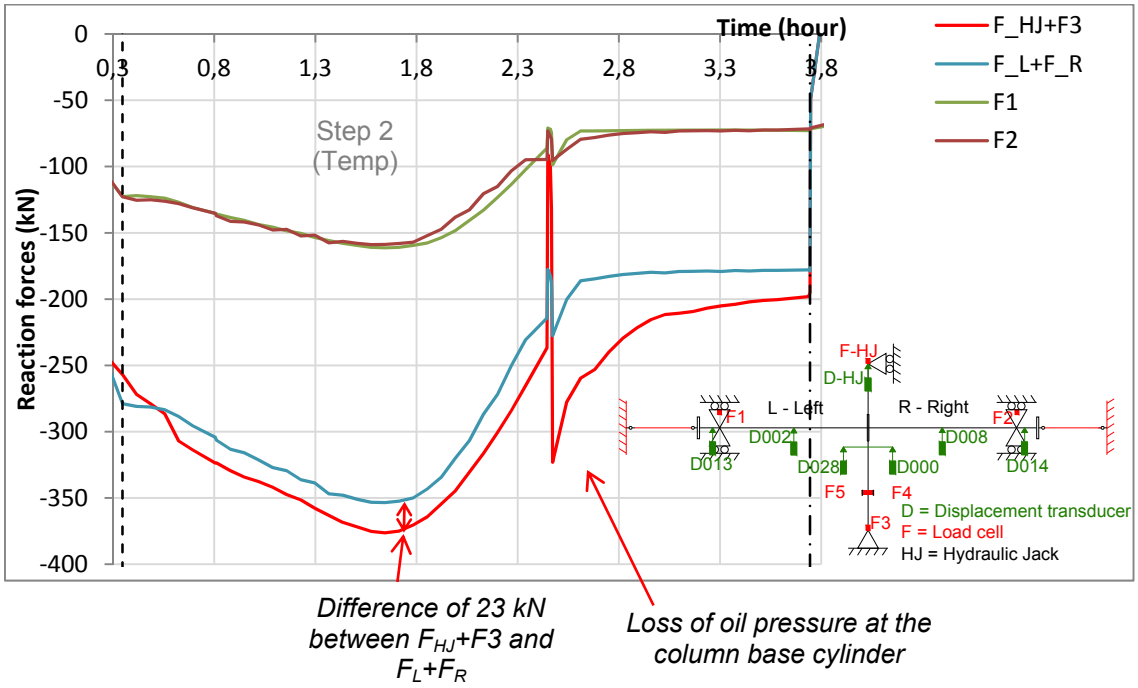

Figure 203: Comparison of the total load into the column (FHJ + F3) with the total reaction load at the beams supports (FL + FR)

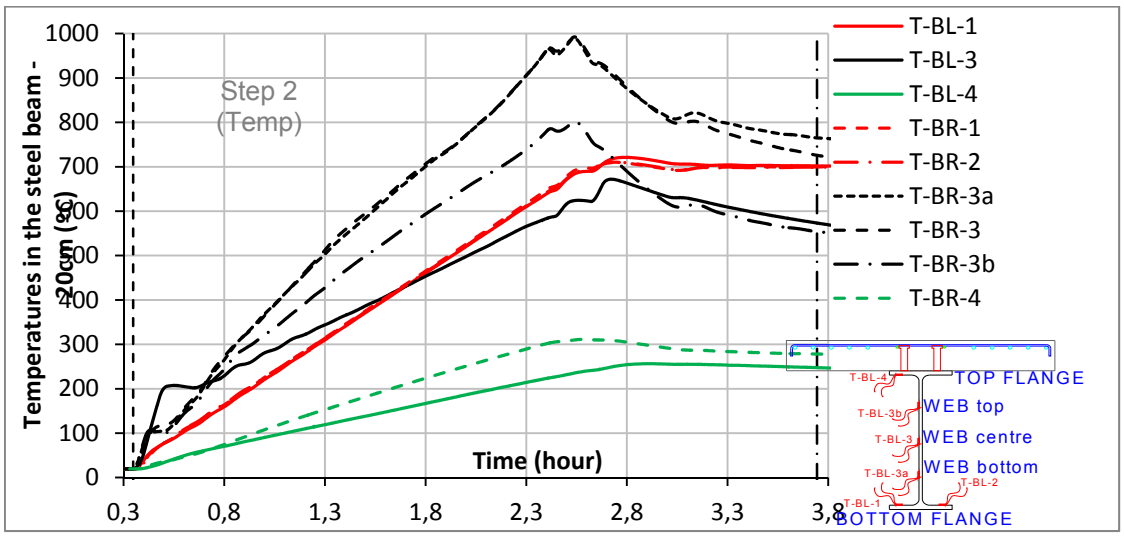

Figure 204: Evolution of the temperatures (T) in the beams at 20 cm from the connection during the test 5 (BR = beam right; BL = beam left)

Figure 205 shows the vertical displacements measured during step 2 below the joint (D000 and D028), at the beams mid-span (D002 and D008) and at the hydraulic jack located at the top of the column.

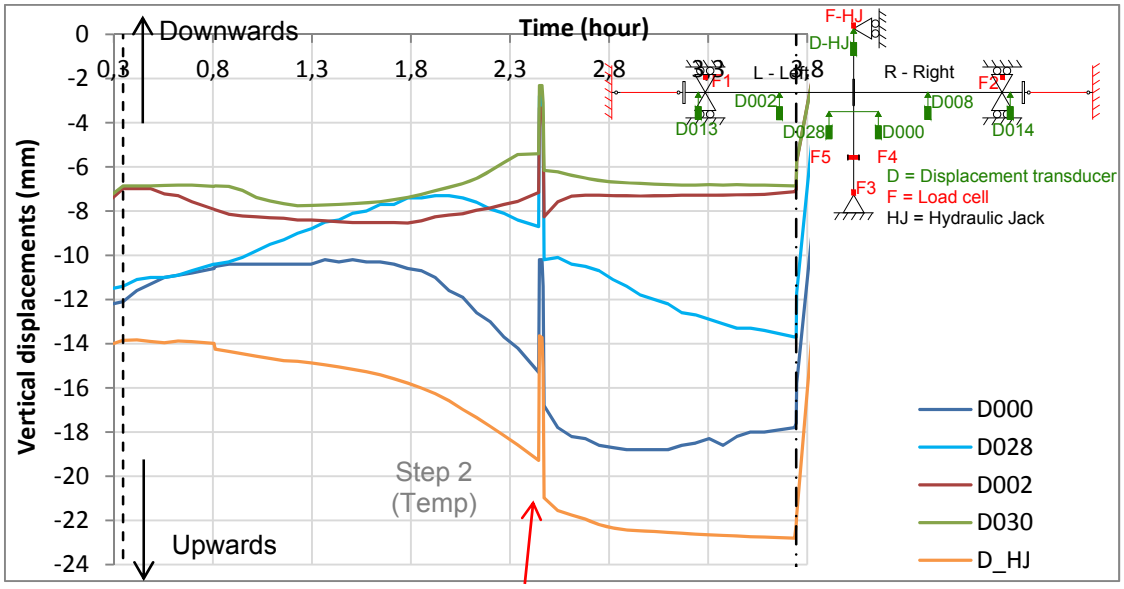

Loss of oil pressure at the column base cylinder

Figure 205: Vertical displacements near the joint during the increase of temperatures

At the beginning of step 2, the column section below the joint was moving downwards (transducers D000 and D028). The column was supported at the base by a cylinder, the vertical movement of the column base was measured by a wire transducer (D031, see Figure 206). During the heating, the pressure of the cylinder was regularly adapted in order to keep D031 as much as possible constant (Figure 207); however, D000 and D028 measured vertical displacements of the joint in the downwards direction. One reason could be that the steel bars where the wire transducers D000 and D028 were connected could be hot and perhaps slightly deformed in the downward direction under the self-weight.

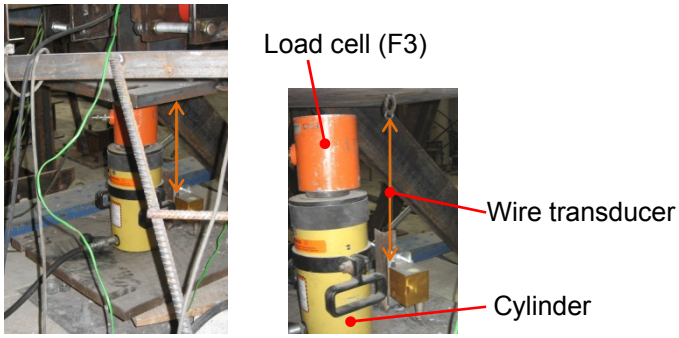

Figure 206: Wire transducer (D031) at the column base support

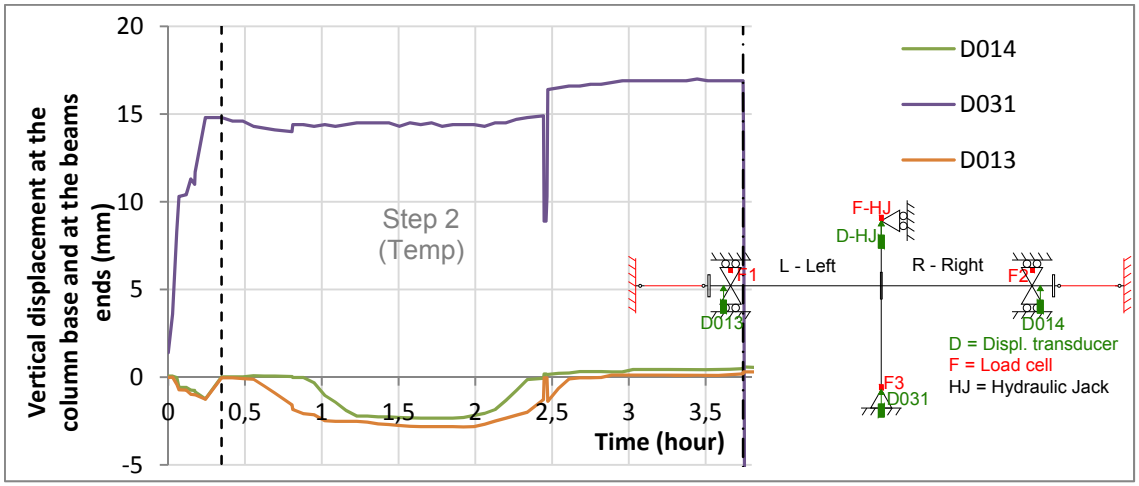

Figure 207: Vertical displacements measured near the beam supports (D013 and D014) and at the column base (D031) during the increase of temperatures

The thermal expansion of the column can be deduced from the vertical displacements measured at the column top (D_{HJ}) and at the joint (D000/D028). As shown in Figure 208, from the beginning to the end of the step 2, the column top (D_{HJ}) displaced upwards of 8.52 mm, and the joint displaced upwards of 4.25 mm (average value). Finally, the dilatation was estimated as the difference, i.e. 4.27 mm of dilatation.

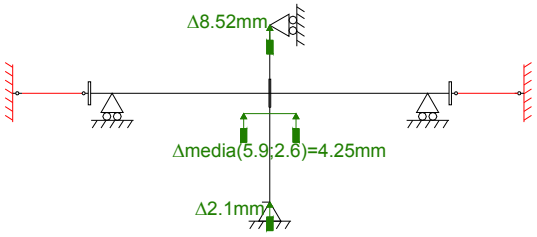

Figure 208: Total column dilatation during the step 2

The evolution of the bending moment during the increase of temperatures is shown in Figure 209.

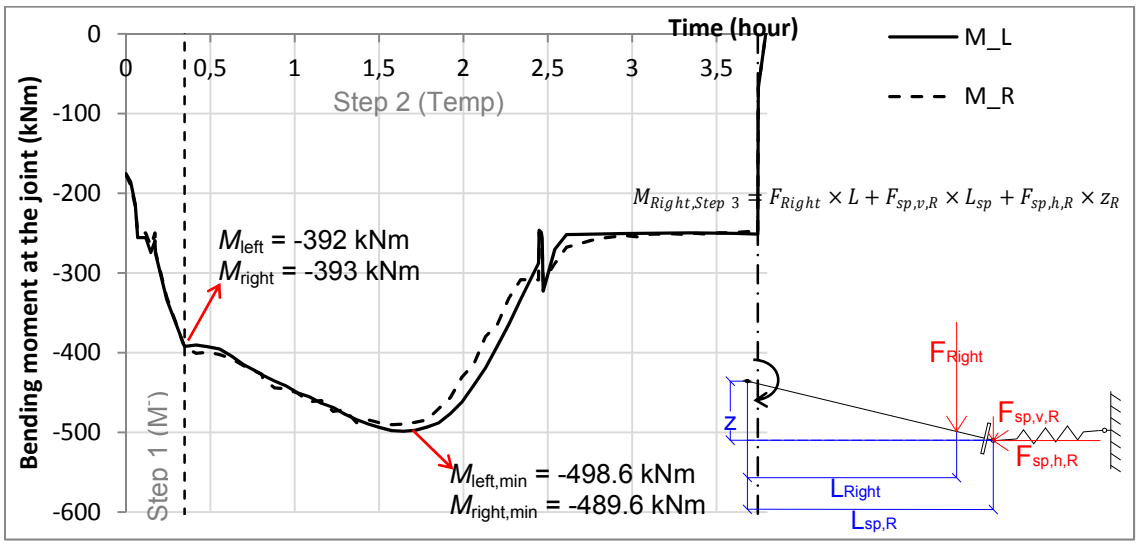

Figure 209: Evolution of the bending moment in the connections (Left and Right) during the steps 1 and 2

III.6.4 Step by step behaviour: step 3 - Loss of the column and increase of the sagging bending moment

The step 3 corresponded to the loss of the column and the increase of the sagging bending moment in the joint. Before the loss of the column, the hydraulic jack at the top of the column was changed to displacement control (velocity equal to 0.03 mm/sec); the cylinder at the base was progressively removed; and finally, the displacement at the top of the column was increased (increase of the joint sagging bending moment) up to the failure of the joint. Note that the structural system at the beams supports (see Figure 16 in section II.6.1.2) was unloaded, after the loss of the column, by loosening the nuts.

Figure 210 shows the evolution of the vertical loads measured by the hydraulic jack F_{HJ} at the top of the column, by the load cells F1+F2 at the top of the beams supports and by the vertical components of the axial loads. The evolution of the slab deformation and cracks is shown in Figure 211. First the concrete crushed against the column flanges around 4h42min, then half of the concrete slab was crushed at 5h04min (on the front), and finally the entire slab width failed (5h30min).

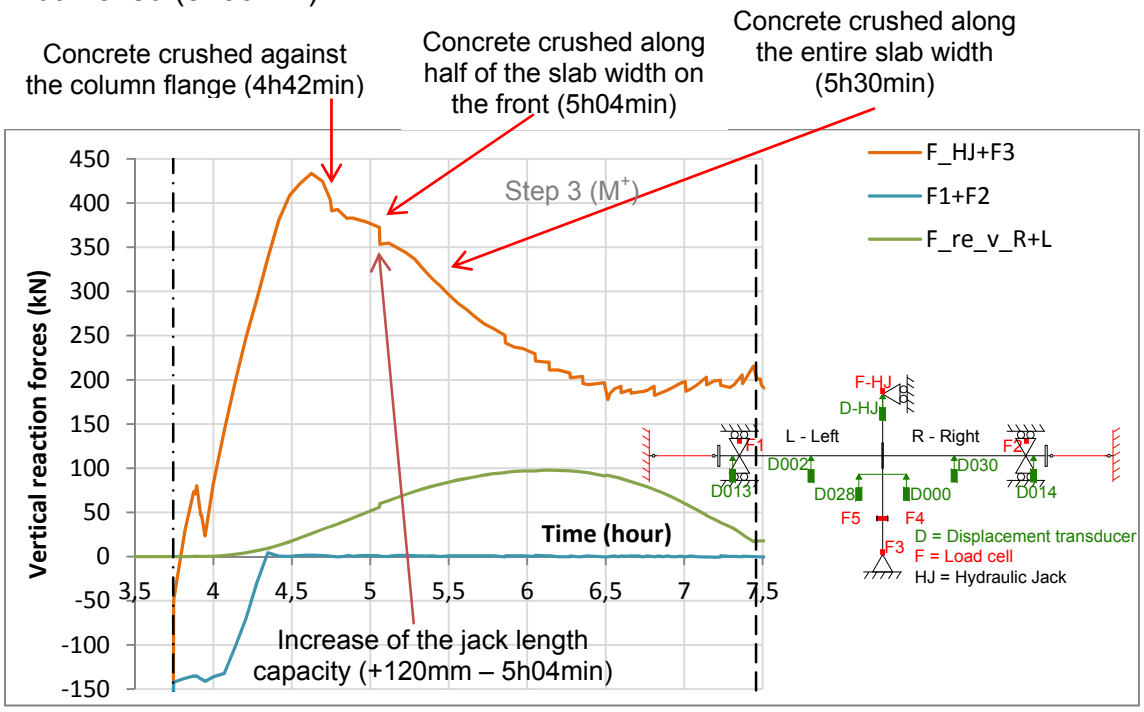

Figure 210: Evolution of the vertical loads during the step 3

Figure 211: Evolution of the concrete crushing

Figure 212 shows the evolution of the vertical displacements measured i) by the hydraulic jack D_{HJ}; ii) by the wire transducers D000 and D028, and iii) by the displacement transducers at mid-span of the beams (D008 and D002). The maximum displacement measured by the hydraulic jack was 337 mm.

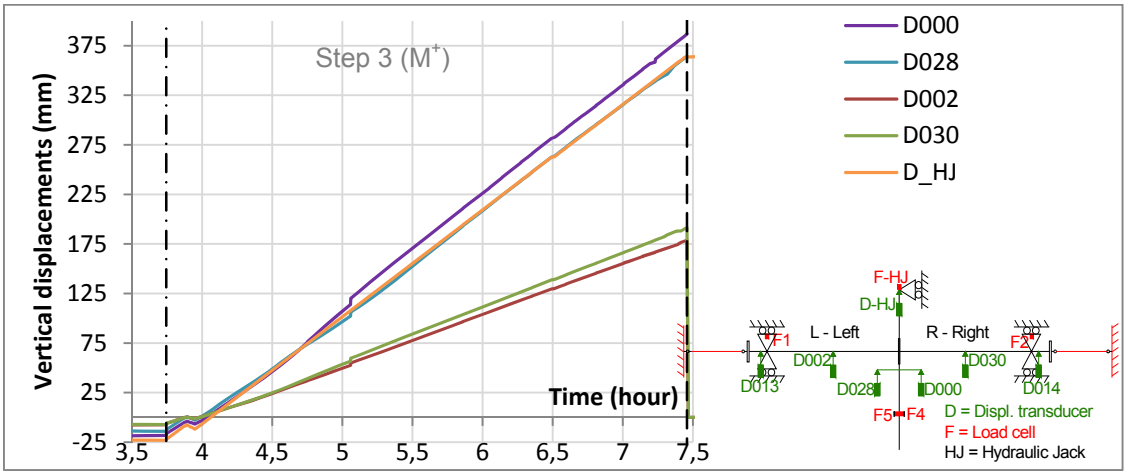

Figure 212: Vertical displacements near the beam-to-column joint during step 3

The hydraulic jack stroke was increased once during this test, around 5h05min (see §II.6.1.1, p13); no bolt failed. Figure 213 shows the deformed end-plates after disassembly the tested frame.

a) Beam right b) Beam left

Figure 213: Deformed end-plates after disassembly the tested frame

Figure 214 presents the reaction loads measured during the test 5: at the hydraulic jack (F_{HJ}), at the column base (F_3), at the beams ends (F_1 and F_2), and finally at the axial restraints to the beams ($F_{restr,R\ and\ L}$) (see §III.1).

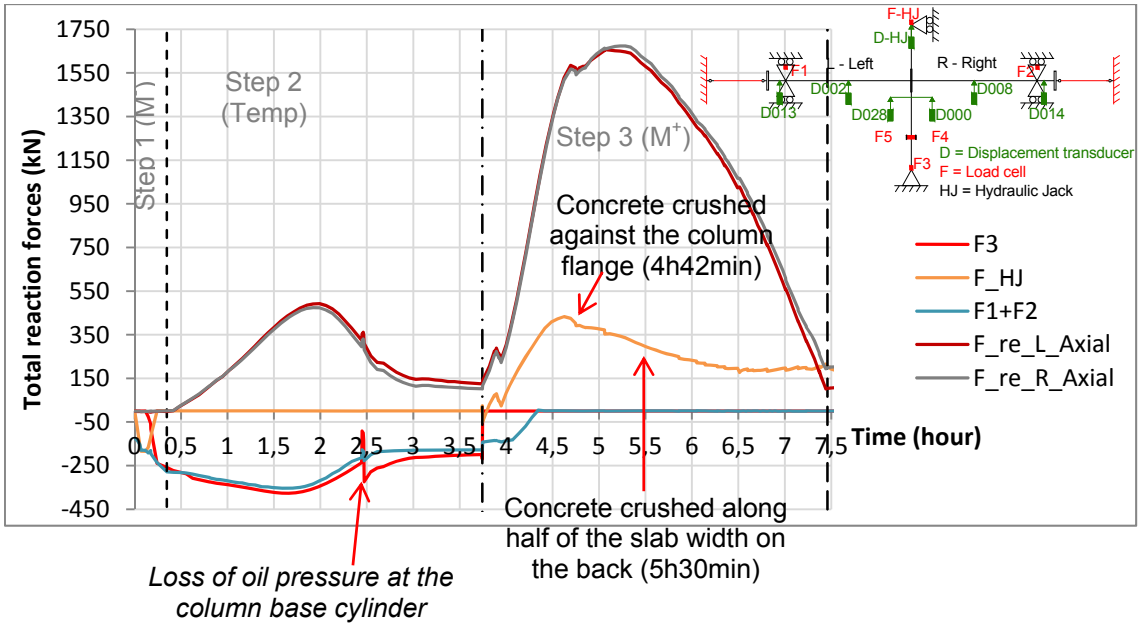

Figure 214: Evolution of the loads during the entire test 5

Figure 215 shows the evolution of the bending moment *versus* time at the connections during the entire test.

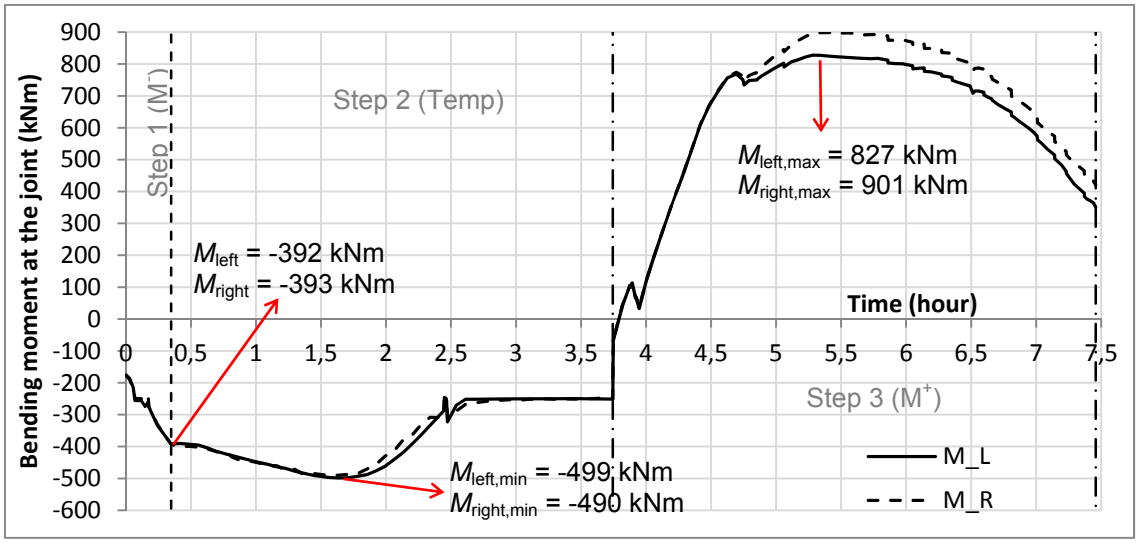

Figure 215: Bending moments at the connections left and right

Figure 175 and Figure 176 present the evolution of the total reaction load *versus* the joint rotation and the beam axial load respectively.

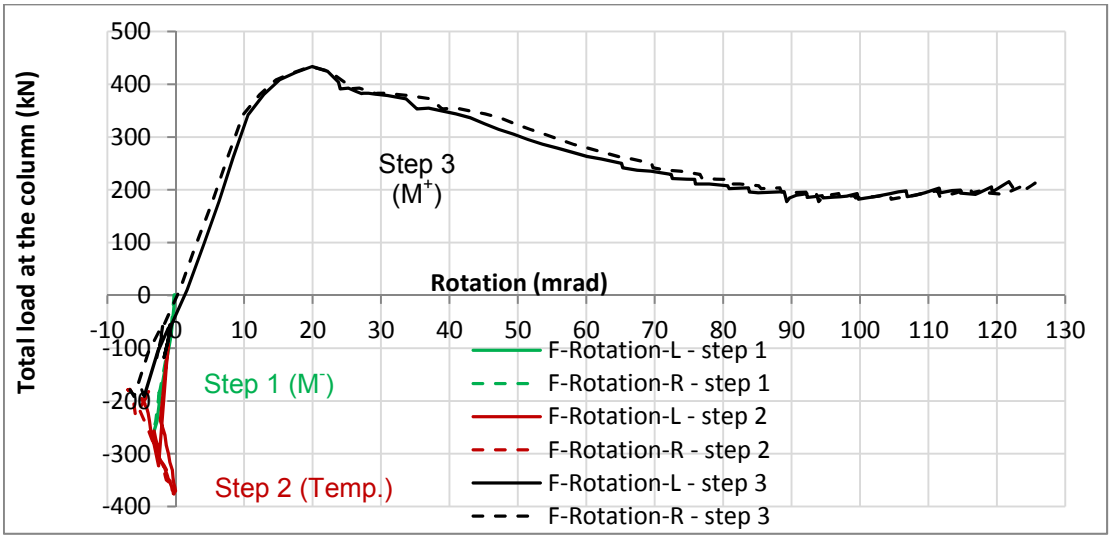

Figure 216: Total reaction load (F_L+ F_R) vs rotation at the joint

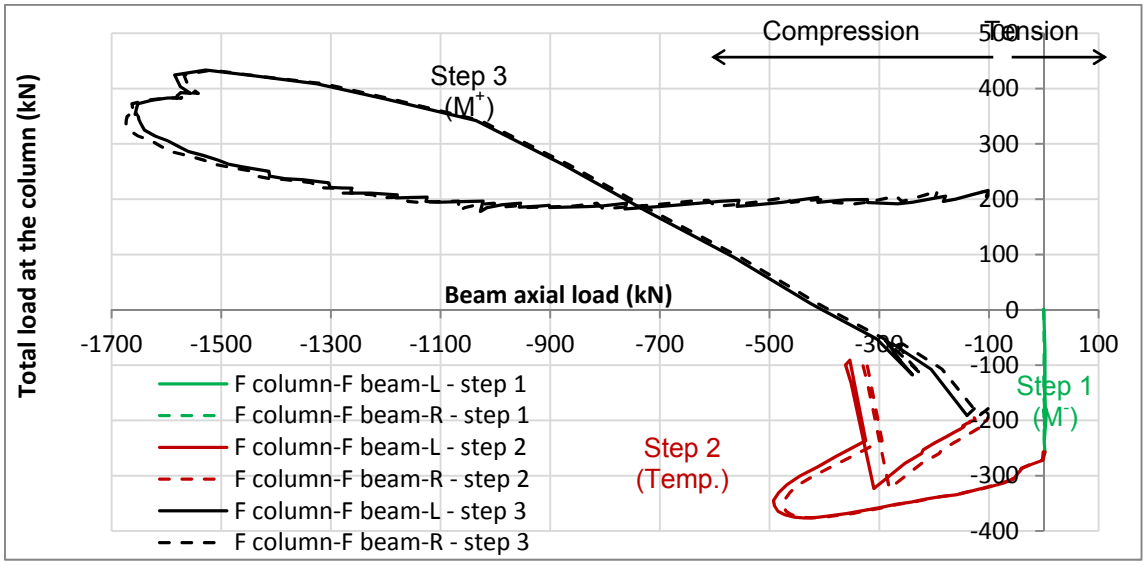

Figure 217: Total reaction load (F_L+ F_R) vs axial loads at the joint ($F_{restr,ax}$)

III.6.5 Additional data

The evolution of the vertical and horizontal components of the axial restraint loads, $F_{sp,v}$ and $F_{sp,h}$, are shown in Figure 218. The rotations of the beam axial restraints are shown in Figure 219.

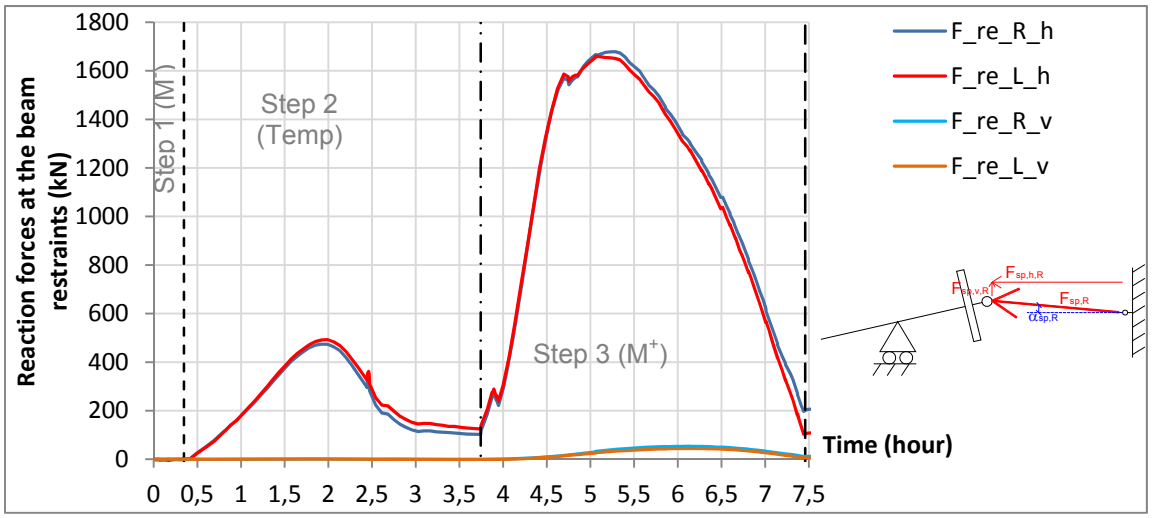

Figure 218: Projections of the axial restraints loads along the horizontal (h) and vertical (v) axis

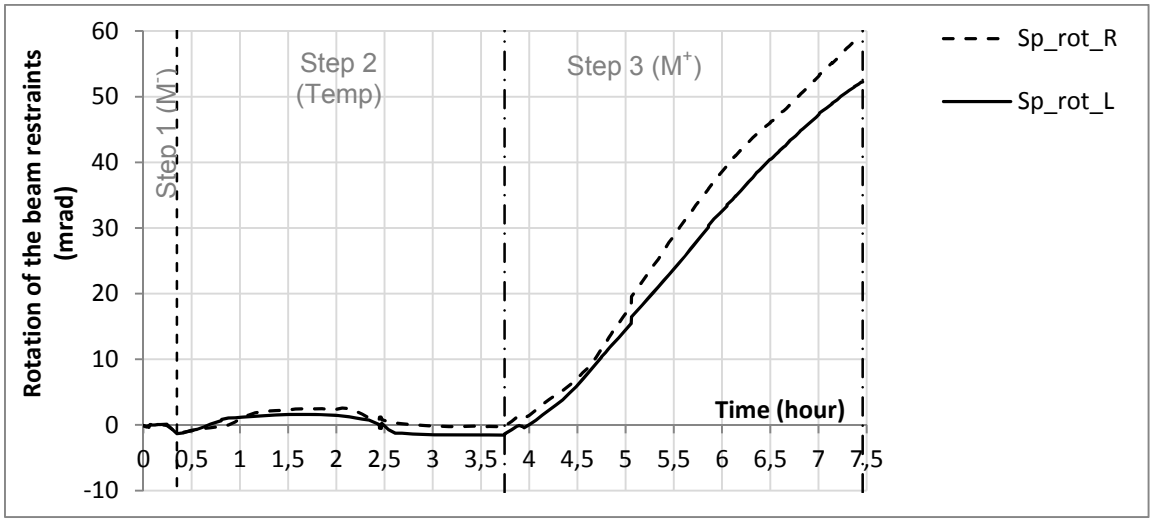

Figure 219: Axial restraints rotations (L = left; R = right)

The horizontal displacements measured at the beam ends are showed in Figure 220. The estimated horizontal displacements at the neutral axis of the steel beams $D_{beam,h,L\ and\ R}$ are represented by the black curves (see §III.1).

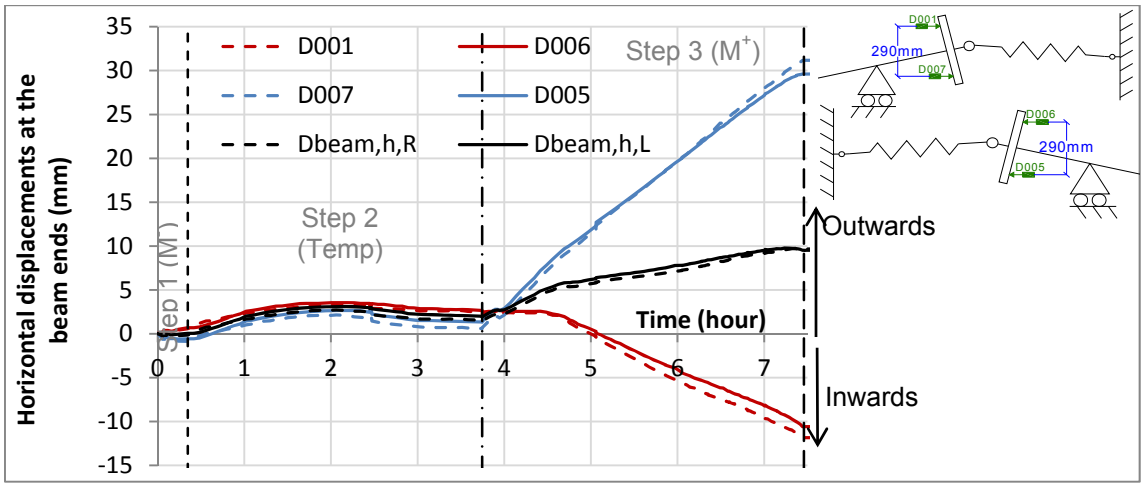

Figure 220: Horizontal displacements at the end of the beams

Figure 221 presents the displacements of the beams out of the plan, measured by the displacement transducer D015 at the bottom column, by the two displacement transducers D025 and D026 at the beam ends, and by the two transducers D003 and D009 on the beams webs, initially situated at 1500 mm from the end-plate.

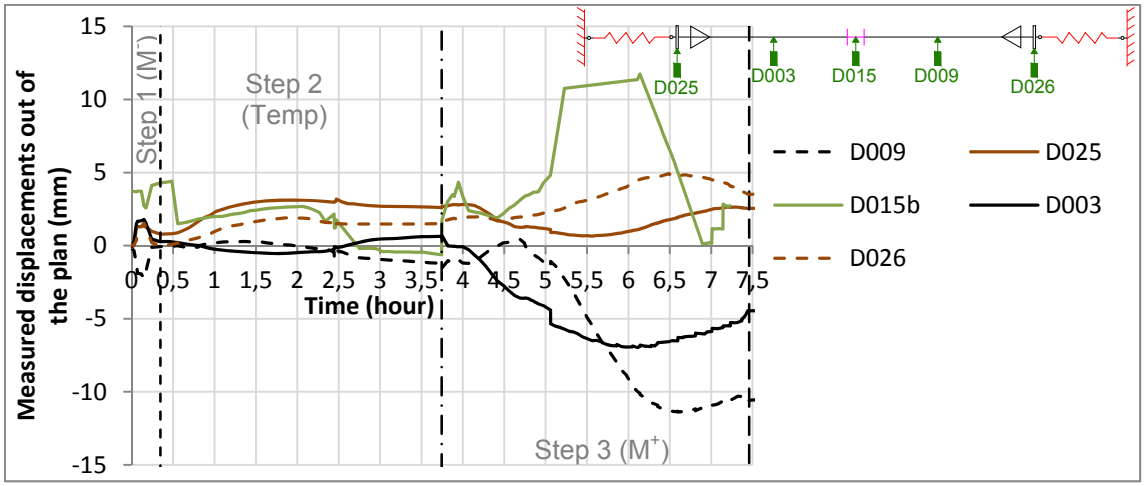

Figure 221: Evolution of the displacements measured out of the plan

Figure 222 presents the measured displacements of the auxiliary's structures (steel and concrete footings and strong beams connected to the strong walls).

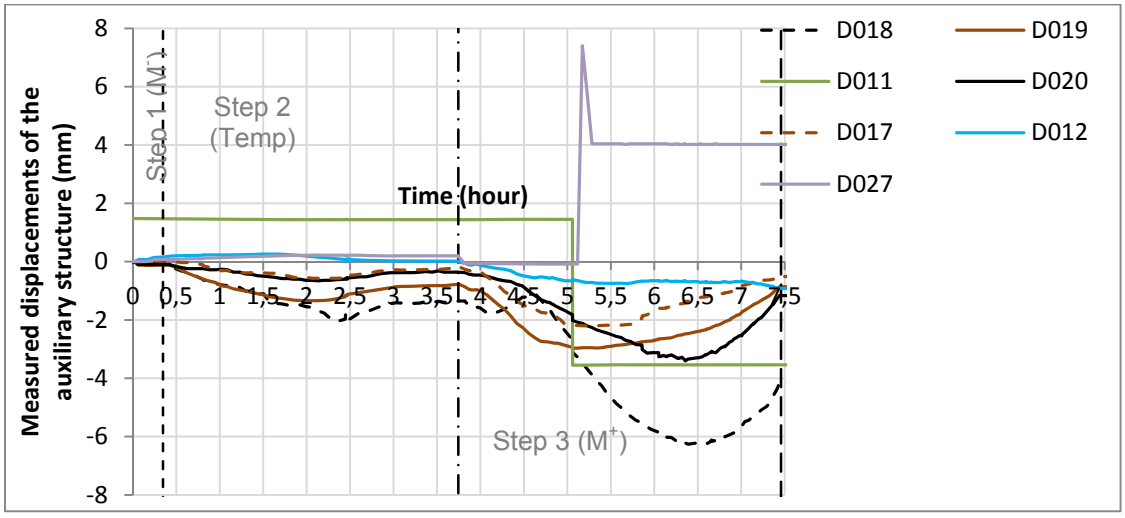

Figure 222: Measured displacements of the steel and concrete footings, and of the strong beams linked to the walls (see Figure 31 in §II.8.2 for the position of the displacement transducers)

III.7 Results of test 6

The global behaviour of the joint during the test is described in the following section, then the step by step behaviour is detailed, for each loading step, and finally, additional data a presented.

III.7.1 Joint behaviour (entire test)

III.7.1.1 Temperature results

Figure 223 presents the temperatures evolution during the entire test 6 in the right and left beams (at 200 mm from the connection), in the column centre, in the bolts from row 4 and in the concrete in contact to the column flange. In step 2, the temperature increase rate was 300°C/hour in the beam bottom flanges, and they reached 700°C, whereas the temperature increased faster in the beam

and column webs because of the reduced thickness. Temperatures in beams top flanges were much lower because they were only heated by heat transfer from web, which was reduced by the composite slab protection. During step 3, the temperature was well kept constant in the beam bottom flanges. From 6h, the deformation of the sub-frame created openings in the thermal isolation (mainly on the right side); the transformer machine increased the electrical power sent to the FCP elements to keep constant the temperature in the beams bottom flanges, which made increase some temperatures of the right beam web and top flange, and the column. Temperatures measured in concrete reached: around 300ºC in the part in contact with the column, and maximum 396ºC in the concrete rib in contact with the beam. At 10h30min, maxima temperatures measured at the joint were: 566ºC and 695ºC in left and right bolts, 582ºC and 705ºC in left and right end-plates, 798ºC in column web, and 571ºC and 653ºC in left and right column flanges. The evolutions of all measured temperatures are detailed in §III.7.3.

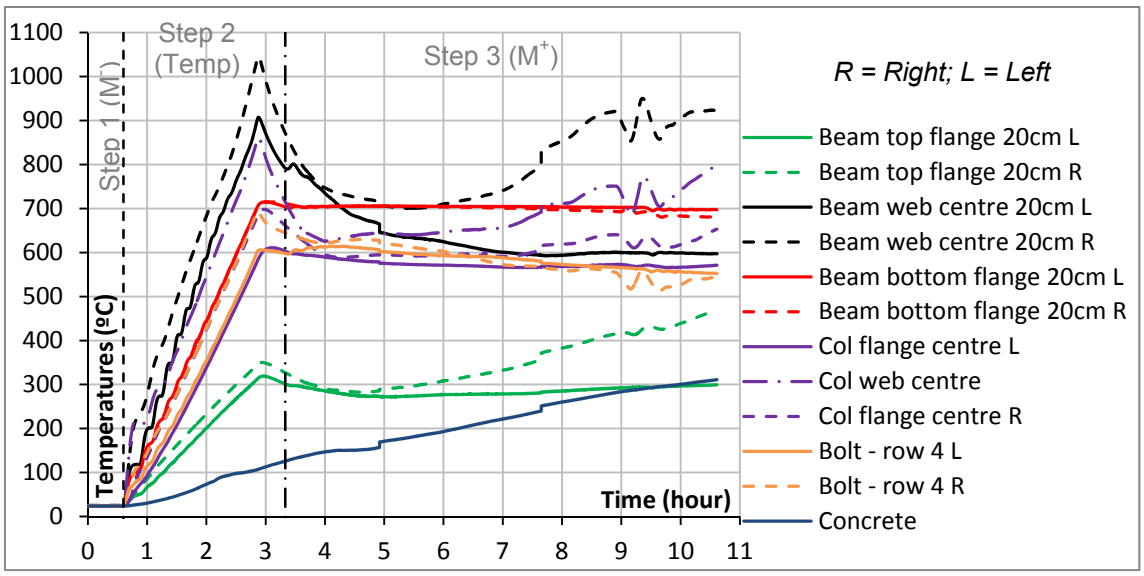

Figure 223: Evolution of the temperatures during test 6

III.7.1.2 Bending moments variation and failure modes

The joint behaviour for each loading step is presented in following figures (step 1 – Initial hogging bending moment; step 2 – Temperatures; and step 3 – Loss of the column and increase of the sagging bending moment). Figure 224 and Figure 225 show the evolution of the bending moment at the joint versus the joint rotation and the beam axial load $F_{restr,ax,R\ and\ L}$ from the axial restraints. The evolution of the total reaction load (F_L+F_R, defined in §III.1.2) versus the vertical displacement measured at the column top is presented in Figure 226. The hogging bending moment was initially reached during step 1, followed by a variation of this moment during the increase of temperatures in step 2. This initial hogging bending moment reached -228 kNm on the left and -234 kNm on the right connections. At the beginning of step 2, reaction loads increased due to the thermal expansion of the structure; the reaction loads reached a minimum value (F_L+F_R = -343.5 kN) and the minima hogging bending moments reached -489 kNm on the left and -479 kNm on the right connections; the corresponded axial loads were -68 kN and -58 kN (compression loads). At this moment, the

temperatures in the beams bottom flanges and in the beams webs were equal to, respectively, 450ºC and 600/650ºC. After that, these reaction loads decreased because of the steel properties degradation due to high temperatures.

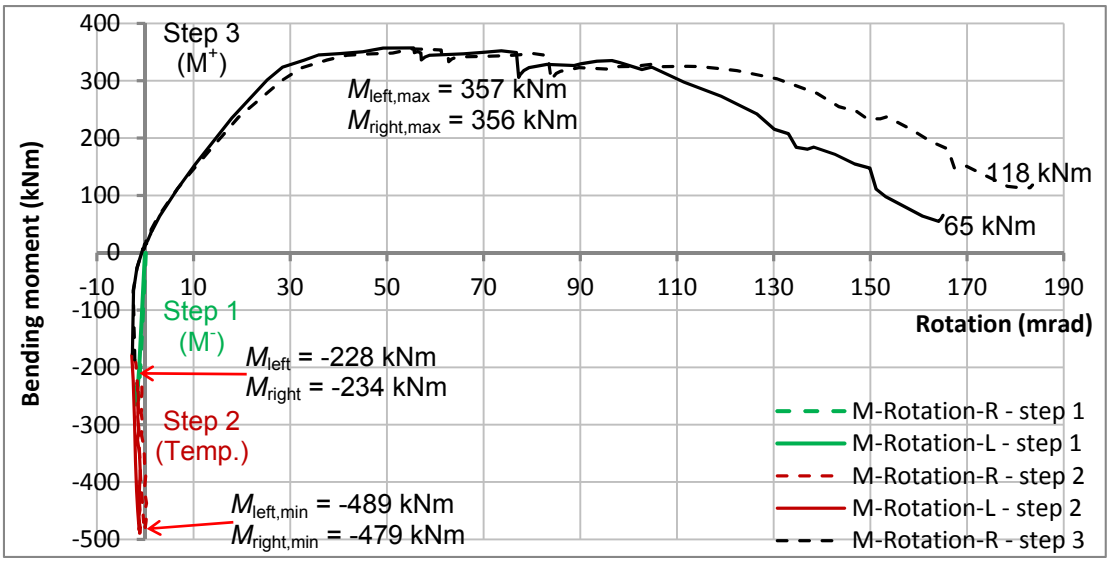

Figure 224: Bending moment vs rotation at the connection (the different gradient of colors define the different steps)

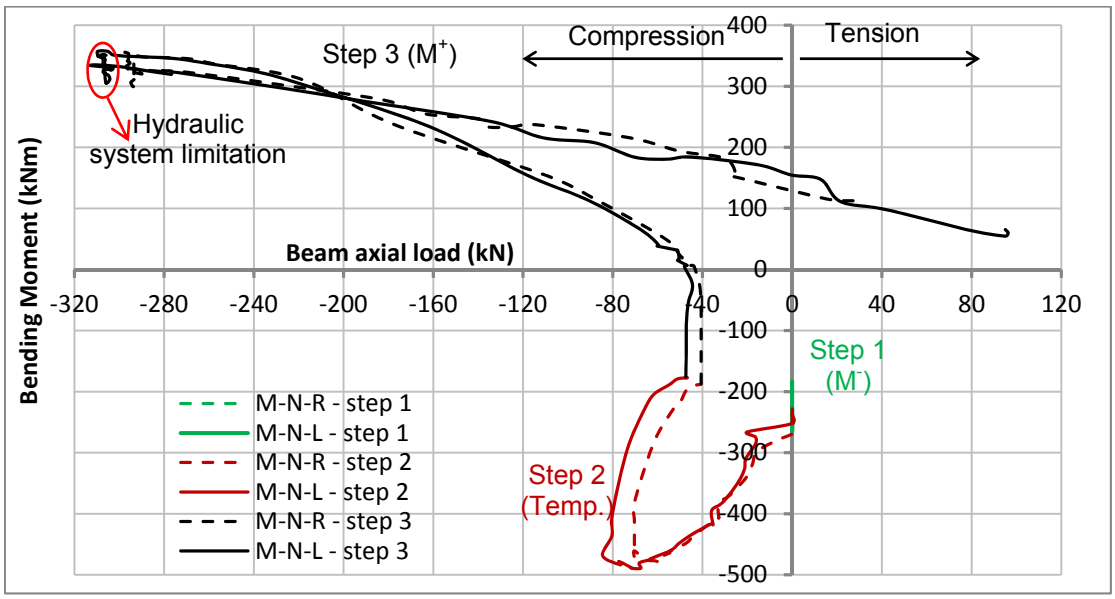

Figure 225: Joint bending moment vs axial forces at the joint ($F_{restr,ax}$)

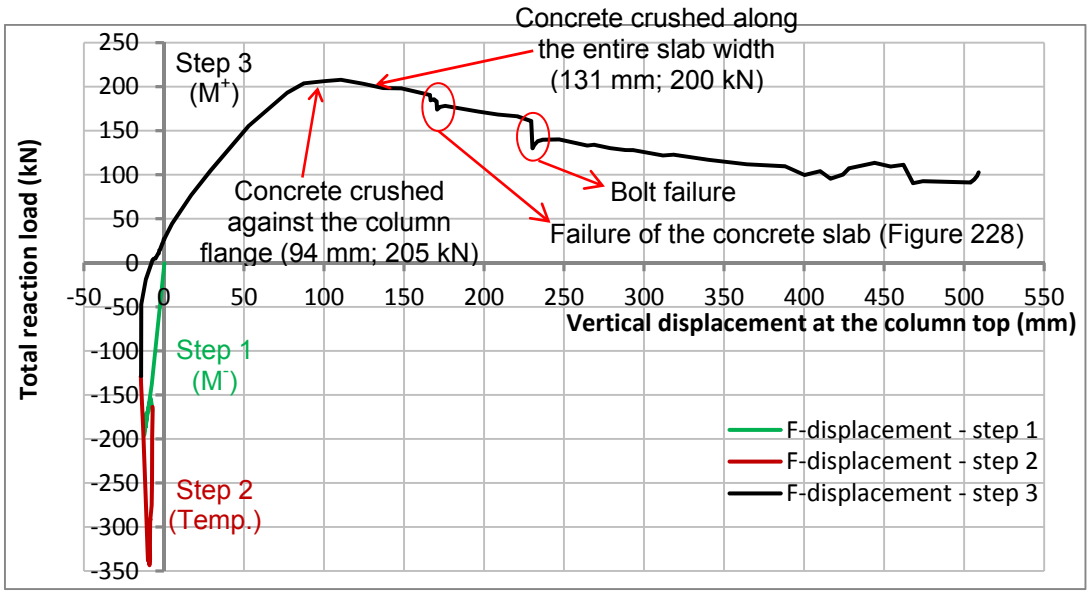

Figure 226: Total reaction load (F_L+ F_R) vs vertical displ. measured at the column top (D_{HJ})

In step 3, the loss of the column was really progressive as the hydraulic jack at the column top imposed a constant displacement rate. Concrete crushing in compression was the first failure observed under sagging bending moment, but this failure was really progressive; first concrete cracks were observed near the column flange (at 82 mm of vertical displacement and 198 kN of total reaction load), then the concrete crushed against the column flanges around 94 mm of vertical displacement and 205 kN of reaction load (Figure 227a), and finally the entire slab width failed (at 131 mm of vertical displacement, 200 kN of reaction load and rotations of 42 mrad on the left and 50 mrad on the right connections - Figure 227b). Figure 227c shows the concrete completely crushed at the end of the test.

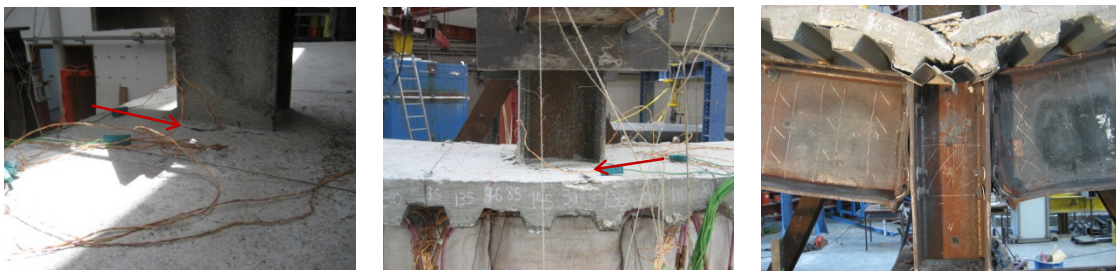

a) b) c)

Figure 227: Concrete crushed: a) against the column flanges; b) along the entire slab width; c) at the end of the test (front view)

The restraints were connected to the beams since the beginning of the test. During step 1, the loads and displacements created by the application of the initial hogging bending moment were not sufficient to create axial loads to the beams. During steps 2 and 3, the beam ends were moving outwards and the restraints worked in compression. The “unloading-reloading” that permits to a better characterization of the elastic stiffness of the joint was not performed at the beginning of step 3 because of the difficulties to manually control the restraints at the beams ends.

The maximum vertical reaction load F_{HJ} was 208 kN, and corresponded to axial restraints to beams of 274 kN and 267 kN on the left and right sides respectively, and to a vertical displacement of 111 mm (which corresponded more or less to the concrete crushing of the slab). From this maximum, the increase rate of the axial loads from the restraints began to decrease. The maximum axial load at the restraints was not reached because of the capacity limitations of the hydraulic pump material (max. 300 kN in compression – see §II.7.2.2): loads had to be kept constant during 2 hours, instead of increasing up to a maximum and then decreasing (as in tests 4 and 5). Finally, tension loads developed for the last 30 minutes of the test (see §II.7.2.3).

Maxima sagging bending moments of 357 kNm and 356 kNm were reached on the left and right connections respectively, for which corresponded 149 mm of vertical displacement and a total vertical reaction load (F_L+F_R) equal to 198 kN. At this maximum sagging bending moment, the joint rotations and the beam axial loads were equal to 49 mrad on the left and 55 mrad on the right, and 305 kN and 297 kN on the left and right sides respectively. The forces in the spring restraints left and right were different and the bending moments were affected.

The first decrease of the vertical load F_{HJ} (from 190.9 kN to 184.8 kN, for 166 mm of vertical displacement, and rotations of 56 mrad and 62 mrad on the left and right connections) indicated the failure of the concrete slab at the back side: Figure 228 shows two pictures taken before and after the concrete failure.

a) b)

Figure 228: Concrete crushing on the back side of the slab at vertical displacement equal to: a) 158 mm; b) 214 mm

The day after the test, the failure of three bolts was observed: two bolts at the bottom bolt row of the right connection and one bolt at the bottom bolt row of the left connection (Figure 229). One bolt failure (probably the first one) was registered and the load suddenly decreased from 161.3 kN to 130.3 kN at 230 mm of vertical displacement; around 600ºC was measured in the bolts from row 4; the rotations left and right were equal to 77 mrad and 84 mrad respectively. At this moment, the column rotation in the clockwise direction began to increase much faster, which leaded to conclude that the failed bolt was localised in the bottom row of the right connection (in order to facilitate the column rotation in the clockwise), probably on the back side (where a small dust cloud was observed near the joint). The two other bolts failures are not visible in the charts and were not observed during the test. The steel end-plates deformed in the bottom and centre part and showed a high ductility (Figure 229). The test was stopped because the maximum vertical range was reached and the column base touched the concrete footing (Figure 230): the vertical displacement of the joint was 509 mm. The jack length capacity was increased two times: after the

concrete crushing against the column flanges (at 101 mm of vertical displacement), and at 312 mm of vertical displacement. At the end of the test, the vertical position of the column top was maintained constant by the hydraulic jack during the cooling phase.

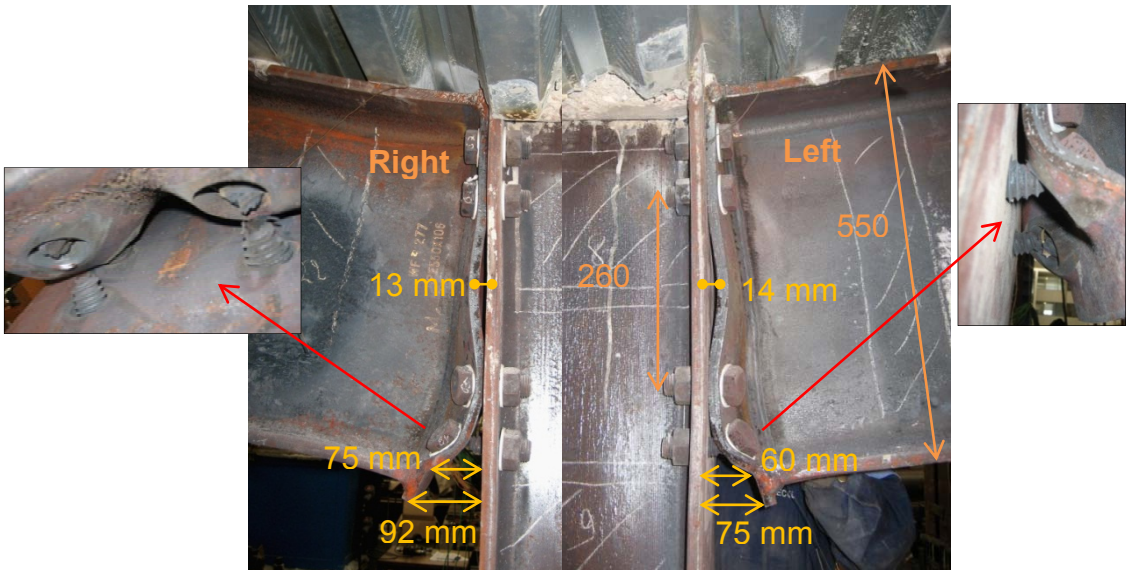

Figure 229: Deformations of the joint (view from the front side)

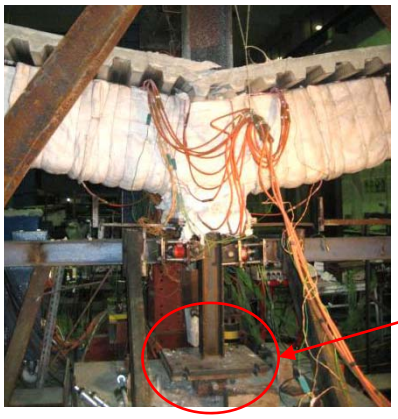

Figure 230: Final deformation of the sub-frame

Figure 231 shows the rotations at the joint left and right sides versus time, as well as the column rotation. The column rotation was very small (10 mrad) thanks to the lateral restraints of the column (see Figure 7 in §II.2). The test was stopped at 165 mrad and 184 mrad of connections left and right rotations. The joint rotation calculation includes any beam rotation or deformation: Figure 232 shows the eventual formation of a plastic hinge at the border between the heated zone and the cooler part of the right beam (more visible than for the left beam).

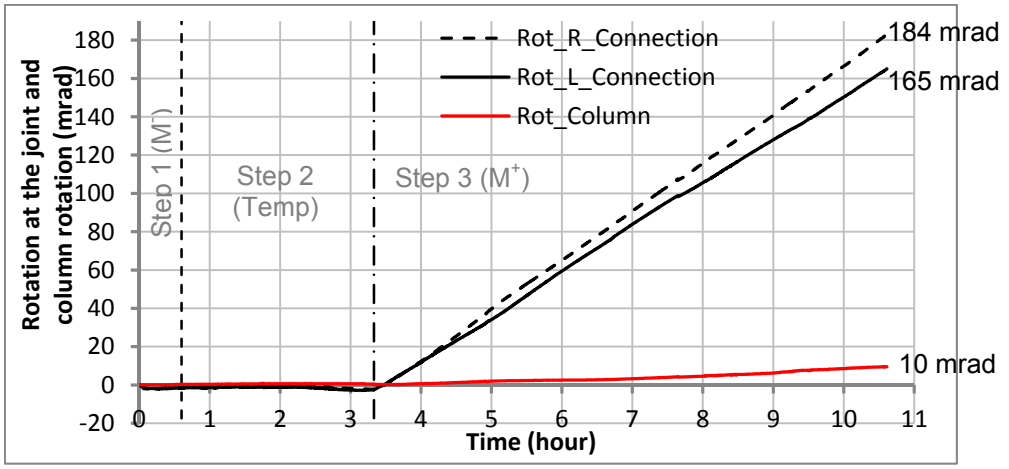

Figure 231: Rotations at the connections (Rot_Connection Left and Right) and column rotation

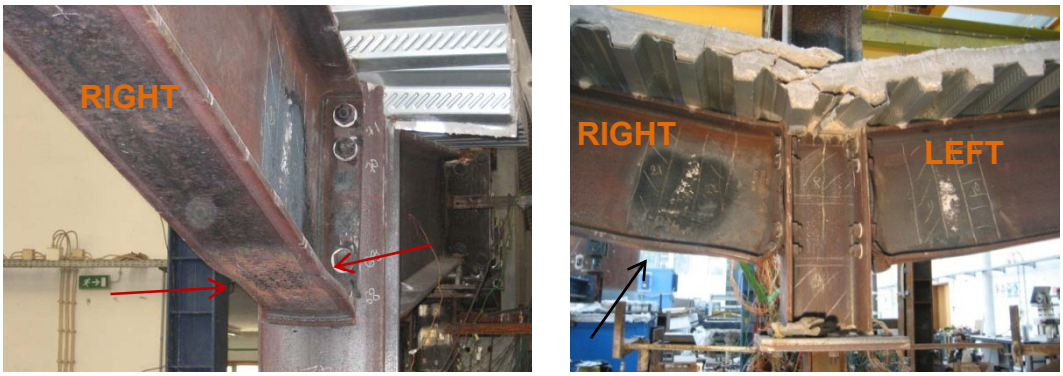

Figure 232: Beam rotation near the joint

Finally, Figure 233 shows the evolution of the loads in the spring restraints according to the average displacement measured at the geometrical centre of the steel beam section (see §II.7.2.2): the spring stiffness of 50 kN/mm was well respected up to the load of 200 kN, then the stiffness slightly decreased, and finally, at 300 kN, no more stiffness was applied during 2 hours; once the horizontal displacements at the beams ends began to go inward, the 50 kN/mm were applied again. At the end of the test, the rotation was higher on the right side than on the left side: respectively 184 mrad and 165 mrad. However, the right beam end reached less displacements at the restraints because of the higher deformation of the end-plate (see Figure 229); this is why the tensile loads were smaller at the right spring restraint (31 kN) than at the left one (98 kN). Consequently, the bending moment was higher at the right connections than at the left connection: respectively 118 kNm and 65 kNm.

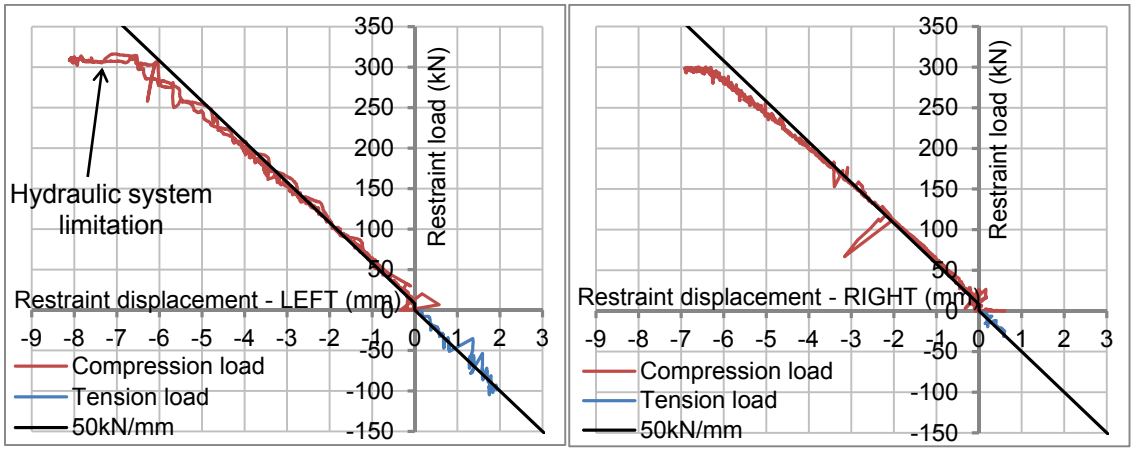

Figure 233: Displacement vs load at the two spring restraints

III.7.2 Step by step behaviour: step 1 - Initial hogging bending moment

The initial step reproduced the internal loads in the connection as in the real car park building (see §II.5.1, p11): hogging bending moment in the joint equal to $M_{fi,d} = \eta_{fi} M_{Ed} = 236.4\ kNm$. In the laboratory, the initial hogging bending moment was introduced to the sub-frame using the hydraulic jack at the top of the column (Figure 234): i) the beams were restrained at the supports and the column was free at the base; ii) phase 1: the hydraulic jack increased the vertical load at the column top and pulled the column upwards; iii) phase 2: the column base support (single acting cylinder) was set up; iv) phase 3: the load at the column top was completely transferred to the sub-frame supports.

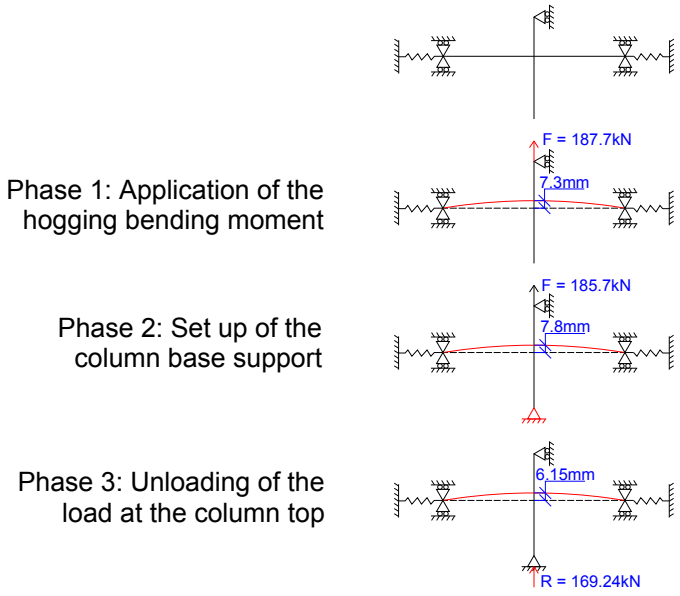

Figure 234: Initial hogging moment in the connection

Figure 235 presents the evolution of the vertical displacements measured near the beam-to-column joint during the step 1. During the phase 2 (set up of the column base support), the cylinder increased the load at the column base, and slightly modified the displacement of the column joint as well as the reaction load at the column top.

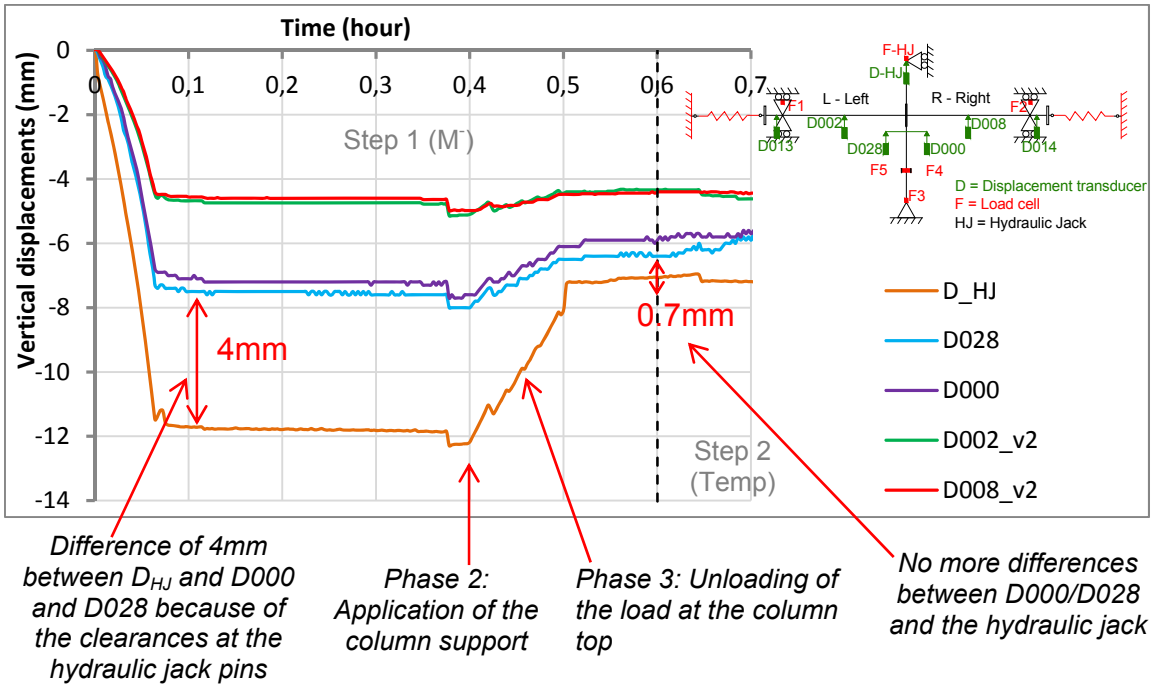

Figure 235: Vertical displacements near the beam-to-column joint during the application of the initial loads (hogging bending moment)

Figure 236 presents the comparison between the sum of the loads measured at the column ($F_{HJ}+F_3$) and the sum of the reaction loads measured at the beam supports (F_L+F_R). Before loading the joint, each beam end was vertically restrained and an initial load (-134.5 kN) was measured by the load cells F_1 and F_2. Table 9 presents the values of displacements and reaction loads at the end of the step 1.

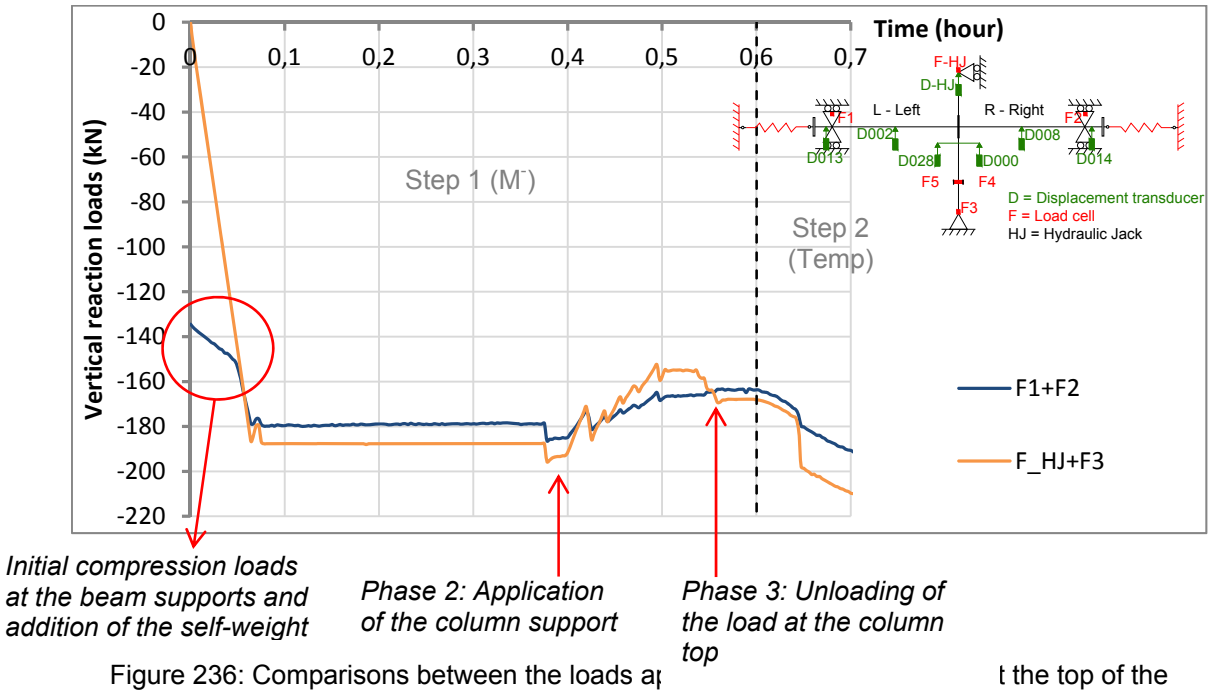

Figure 236: Comparisons between the loads ap t the top of the column and the reaction loads at the beams supports

Table 17: Displacements and Loads (step1)

	End of step 1 (after 36min)	
Step 1 - Initial hogging bending moment	Load (kN)	Displ. (mm)
Column base (F3 and D000)	-169.2	-5.9*
Beam mid-span Left (D002)	----	-4.3
Beam mid-span Right (D008)	----	-4.4
Beam support Left (F_{Left})	-80.7	----
Beam support Right (F_{Right})	-83.0	----
Spring left ($F_{sp,L}$)	0	----
Spring right ($F_{sp,R}$)	0	----
Hydraulic Jack (F_{HJ} and D_{HJ})	+1.0	-7.07
Hogging bending moments at the joint	M_{left} = -228 kNm M_{right} = -234 kNm	

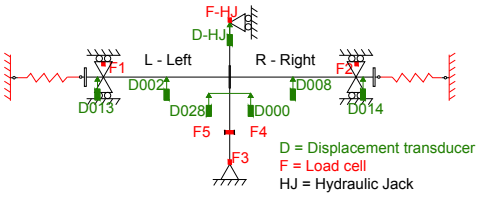

* Average value between by the wire transducers D000 and D028

At the end of the step 1, the hogging bending moment applied to the connection was around -228 kNm on the right side and -234 kNm on the left side, which corresponded to 51% and 52% of the actual bending moment (52.5% was the target value).

III.7.3 Step by step behaviour: step 2 - Temperatures (700ºC)

The second loading step consisted to the slow increase (around 300ºC/hour) of the temperature in the heated zone, until reaching 700ºC in the beam bottom flanges (at a distance of around 20 cm from the joint). Increasing slowly allowed a better control of the sub-frame behaviour. The hydraulic jack at the column top was in force control; in order to allow the thermal expansion of the column top as free, a constant load of 0.1 Tf was imposed; the behaviour of the structure should not be affected by this small load.

III.7.3.1 Evolution of the temperatures

Figure 237, Figure 238 and Figure 239 show the evolution of the temperatures in the beams at respectively 20 cm, 50 cm and 1 m from the end-plate. During the following step 3 (loss of the column and increase of the sagging bending moment), the temperature was well kept constant in the beam bottom flanges, but was increased or decreased in the webs. Indeed, the temperature control was made in the bottom flanges, and the temperature in the web depended of the power with which the electric current was sent to the FCP elements: as the web was thinner than the flanges, the temperatures evolved in different ways (increased or decreased faster). Temperatures in the beam left and in the beam right had slightly different evolutions during the step 3. This could be explained by the lack of thermal isolation: because the rock-wool is not extensible, openings were observed in the rock-wool interfaces due to the large deformations of the joint (Figure 240). With these openings, additional power was needed by the FCP elements to maintain constant the temperature in the beams bottom flanges.

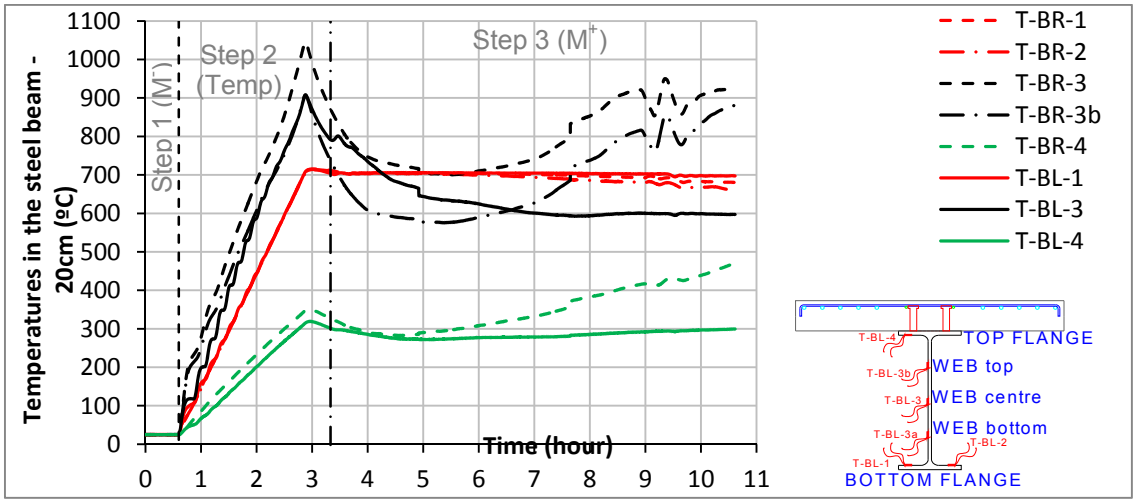

Figure 237: Evolution of the temperatures (T) in the beams at 20 cm from the connection during the test 6 (BR = beam right; BL = beam left)

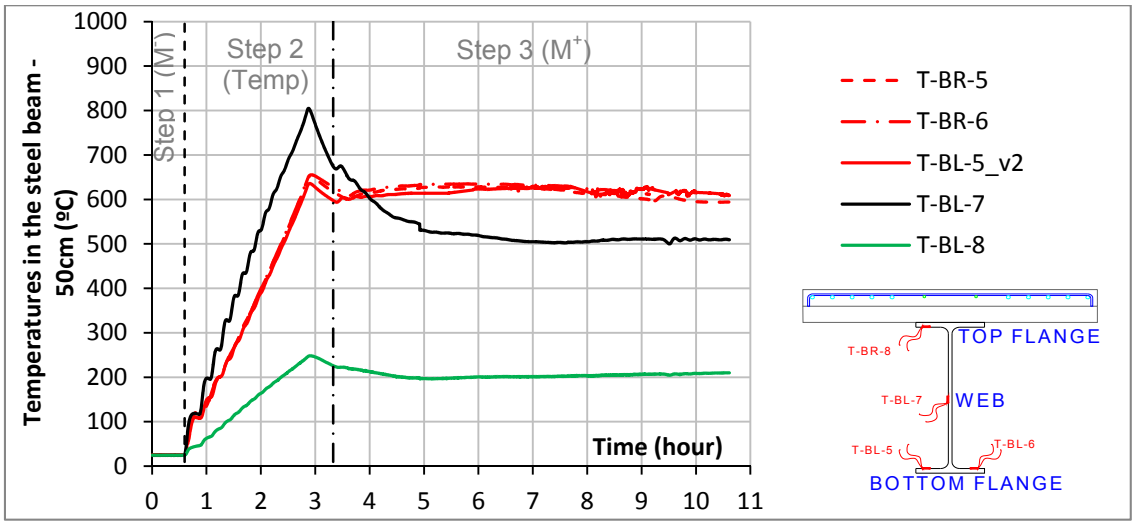

Figure 238: Evolution of the temperatures (T) in the beams at 50 cm from the connection during the test 6 (BR = beam right; BL = beam left)

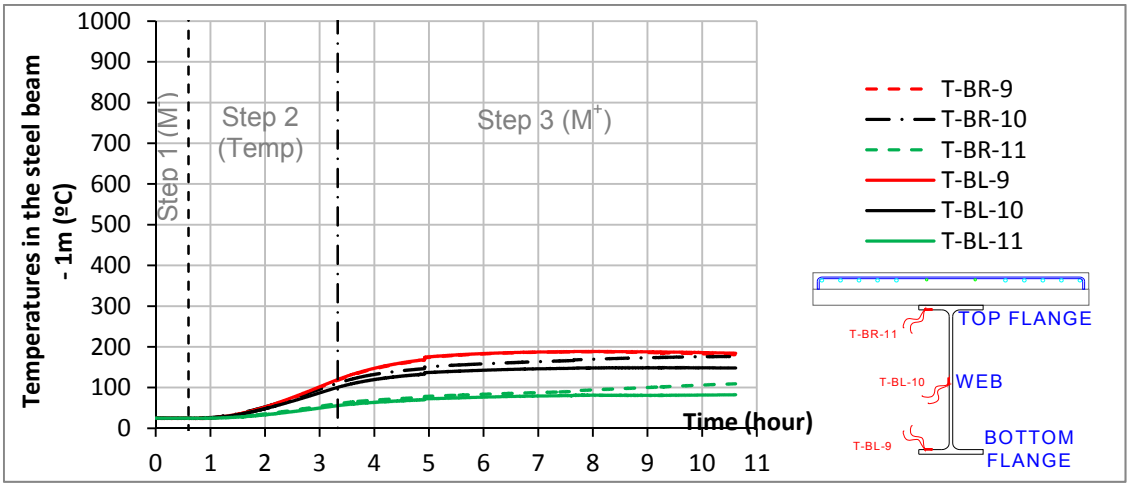

Figure 239: Evolution of the temperatures (T) in the beams at 100 cm from the connection during the test 6 (BR = beam right; BL = beam left)

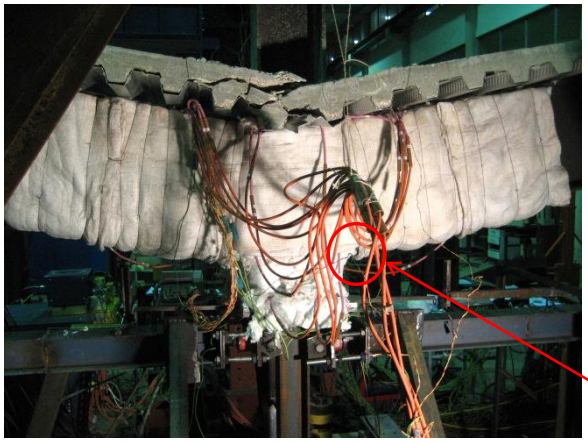

Figure 240: Openings in the thermal isolation at the beam bottom flange under high deformations

Figure 241, Figure 242 and Figure 243 show the evolution of the temperatures at head and at shank of the bolts at each side of the joint, and at the end-plates surface. For each row, the three measured temperatures (bolt head, bolt shank and end-plate) were similar (Table 19).

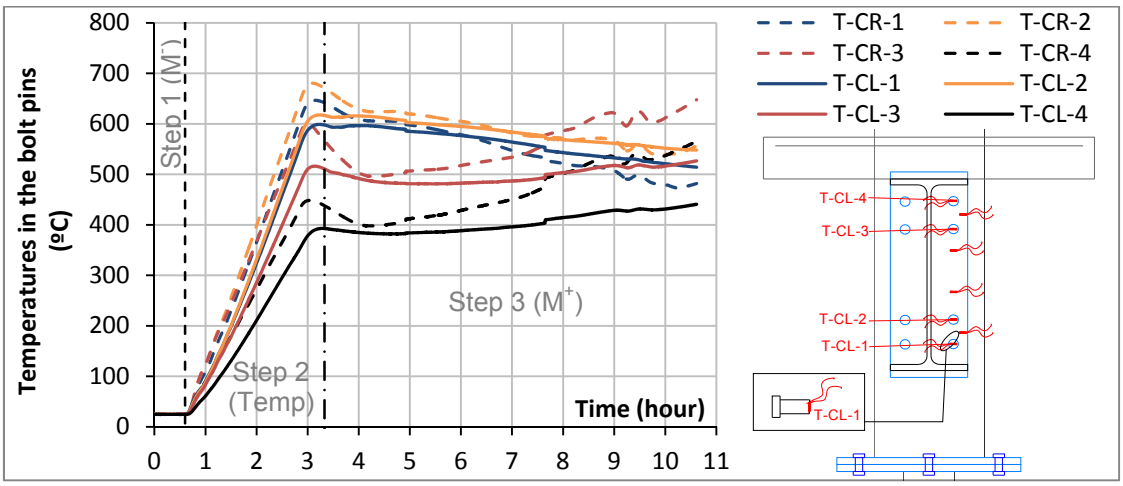

Figure 241: Evolution of the temperatures (T) in the shank of the bolt during the test 6 (CR = connection right; CL = connection left)

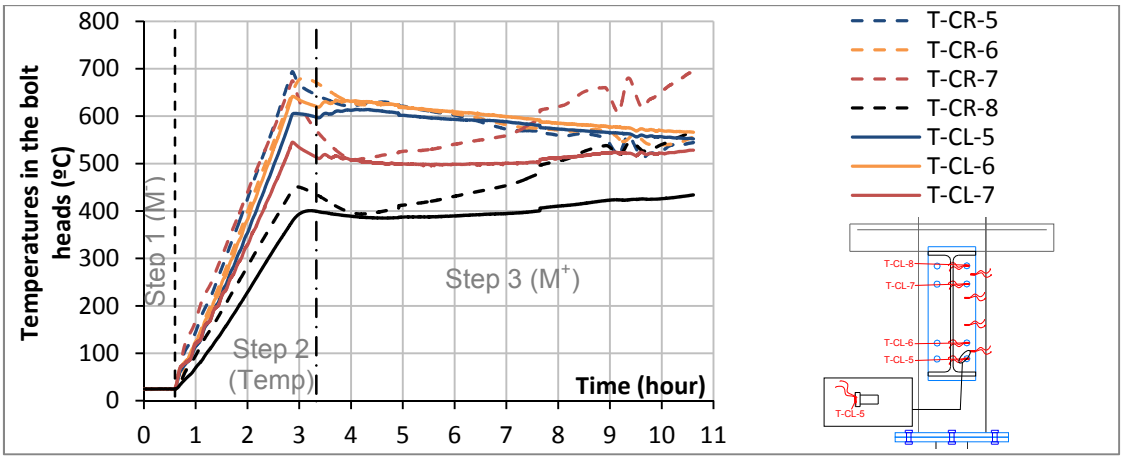

Figure 242: Evolution of the temperatures (T) in the head of the bolts during the test 6 (CR = connection right; CL = connection left)

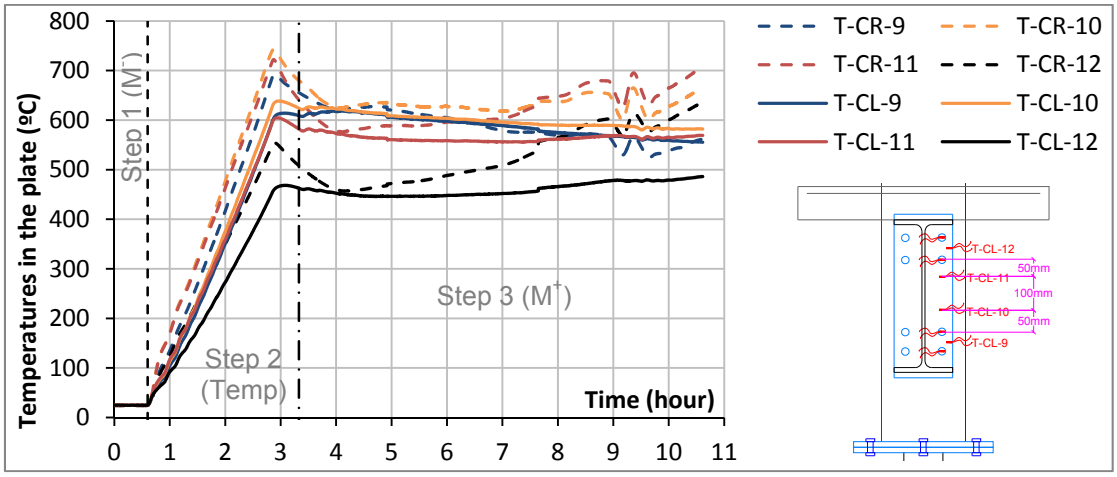

Figure 243: Evolution of the temperatures (T) in the end-plates during the test 6 (CR = connection right; CL = connection left)

The evolution of temperatures in the column is presented in Figure 244; temperatures at the column centre are higher than at the web ends (top or bottom). Column flanges reached around 600ºC, whereas the column web centre reached up to 800ºC at the end of the test.

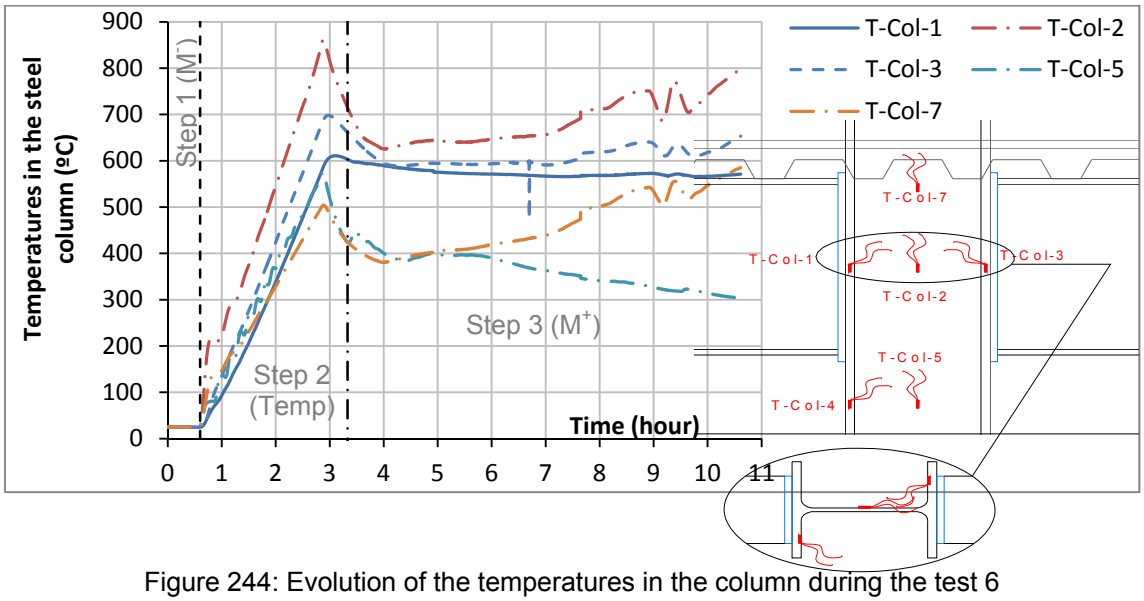

Figure 244: Evolution of the temperatures in the column during the test 6

The evolution of temperatures in the composite slab is depicted in Figure 245, and measured points are shown in Figure 34, section II.8.3 (p24). The maximum temperatures measured into the composite slab at the end of the test were equal to 396ºC in the concrete, 112ºC in the steel sheet and 182ºC in the steel rebar.

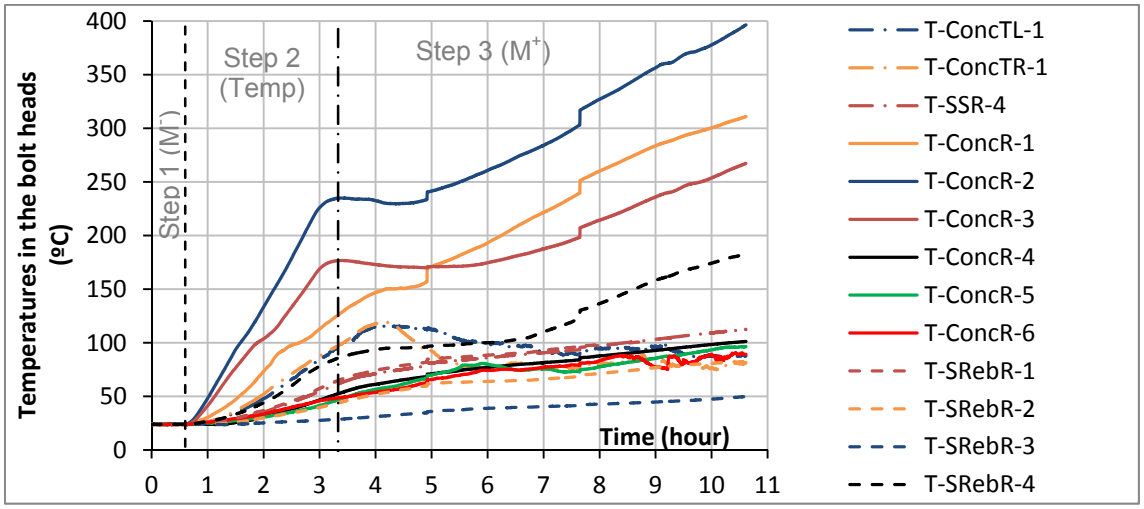

Figure 245: Evolution of the temperatures in the composite slab during the test 6

Table 18 and Table 19 detail the main temperatures measured in beams, columns and joint at three different moments of the test: at the end of the increase of the temperatures during the step 2 (stop of the increase), at the end of the step 2, and finally at the end of the test. The differences between left and right sides are calculated ("Diff. (%)"); the signal '-' means that the temperature in the left side was lower than the temperature in the right side.

Table 18: Main Temperatures measured in beams and column

	Stop of the increase of the temp. (2h52min)			End of step 2 (3h19min)			End of the test (10h36min)		
	Left	Right	Diff. (%)	Left	Right	Diff. (%)	Left	Right	Diff. (%)
T-B-1 (Bottom flange 20 cm)	708.5	707.6	0.1	703.7	711.5	-1.1	697.3	680.4	2.4
T-B-3 (Web 20 cm)	907.4	1045.7	-15.2	791.5	871.3	-10.1	597.2	922.5	-54.5
T-B-4 (Top flange 20 cm)	315.1	347.9	-10.4	301.3	326.6	-8.4	299.3	470.6	-57.2
T-B-5 (Bottom flange 50 cm)	635	650.8	-2.5	597.6	617.4	-3.3	608.9	594.3	2.4
T-B-7 (Web 50 cm)	804.8	---	---	674	---	---	509.3	---	---
T-B-8 (Top flange 50 cm)	247.7	---	---	225.7	---	---	209.9	---	---
T-B-9 (Bottom flange 1m)	95.4	93.7	1.8	119.6	117.8	1.5	184.3	180.8	1.9
T-B-10 (Web 1m)	82	90	-9.8	100.4	110.8	-10.4	148.1	176.4	-19.1
T-B-11 (Top flange 1m)	47.5	51.3	-8.0	55.6	60.4	-8.6	82.3	109.3	-32.8
T-Col-2 (Column web centre)	861.3		---	670.3		---	556.1		---
T-Col-1/3 (Column flange centre)	586.6	687.2	-17.1	641.7	566.5	11.7	481.8	647.8	-34.5

Table 19: Main Temperatures measured at the connection zones

	Stop of the temp. increase (2h52min)			End of step 2 (3h19min)			End of the test (10h36min)		
	Left	Right	Diff. (%)	Left	Right	Diff. (%)	Left	Right	Diff. (%)
T-C-4 (bolt pin row 1)	359	445.5	-24.1	392.8	392.1	0.2	440.8	564.9	-28.2
T-C-3 (bolt pin row 2)	488.5	599	-22.6	510.6	507.4	0.6	526.7	647.8	-23.0
T-C-2 (bolt pin row 3)	579.6	669	-15.4	616.7	615.1	0.3	548.1	556.1	-1.5
T-C-1 (bolt pin row 4)	563.3	631.2	-12.1	597.8	641.7	-7.3	514.1	481.8	6.3
T-C-8 (bolt head row 1)	380.6	450.7	-18.4	399.6	398	0.4	434	568.3	-30.9
T-C-7 (bolt head row 2)	544.8	651.7	-19.6	513.2	511	0.4	528.3	694.9	-31.5
T-C-6 (bolt head row 3)	641.7	728.3	-13.5	620.5	619.8	0.1	566.2	596	-5.3
T-C-5 (bolt head row 4)	605.2	677.4	-11.9	597.7	596.9	0.1	552.2	544.6	1.4
T-C-12 (End-plate)	459.6	550.8	-19.8	462.5	460.3	0.5	486.2	635.5	-30.7
T-C-11 (End-plate)	601.9	710	-18.0	582	578.1	0.7	569.2	705.5	-23.9
T-C-10 (End-plate)	634.2	733.7	-15.7	623.9	621.2	0.4	582	661.6	-13.7
T-C-9 (End-plate)	605.4	688.2	-13.7	609	607.4	0.3	555.4	562	-1.2

III.7.3.2 Evolution of the displacements and loads

In Figure 246 are compared the evolution of the reaction loads in both beams supports (F_L+F_R) with the reaction loads at the column (F3 + F_{HJ}). At the beginning of step 2, the reaction loads increased due to the thermal expansion in the heated zone. Around 2h03min, the reaction loads reached a maximum value (-343.5 kN). At this moment, the temperatures in the beams bottom flange and in the beams web were equal to, respectively, 450ºC and 600/650ºC (Figure 247). The following decrease of the loads should be due to the reduction of the steel mechanical properties.

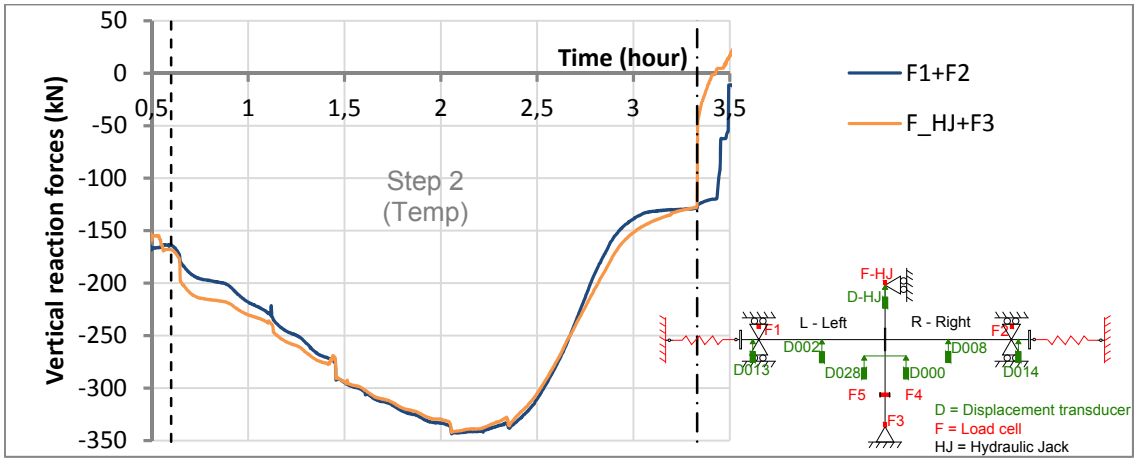

Figure 246: Comparison of the total load into the column (F_{HJ}+F_3) with the total reaction load at the beams supports (F_L+F_R)

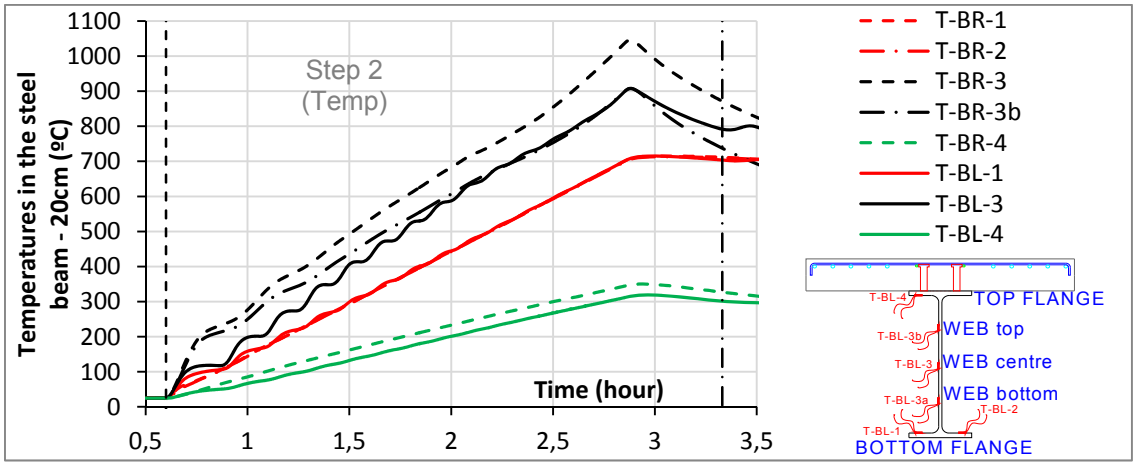

Figure 247: Evolution of the temperatures (T) at 20 cm from the connection during the step 2 (BR = beam right; BL = beam left)

Figure 248 shows the vertical displacements measured during step 2 below the joint (D000 and D028), at the beams mid-span (D002 and D008) and at the hydraulic jack located at the top of the column.

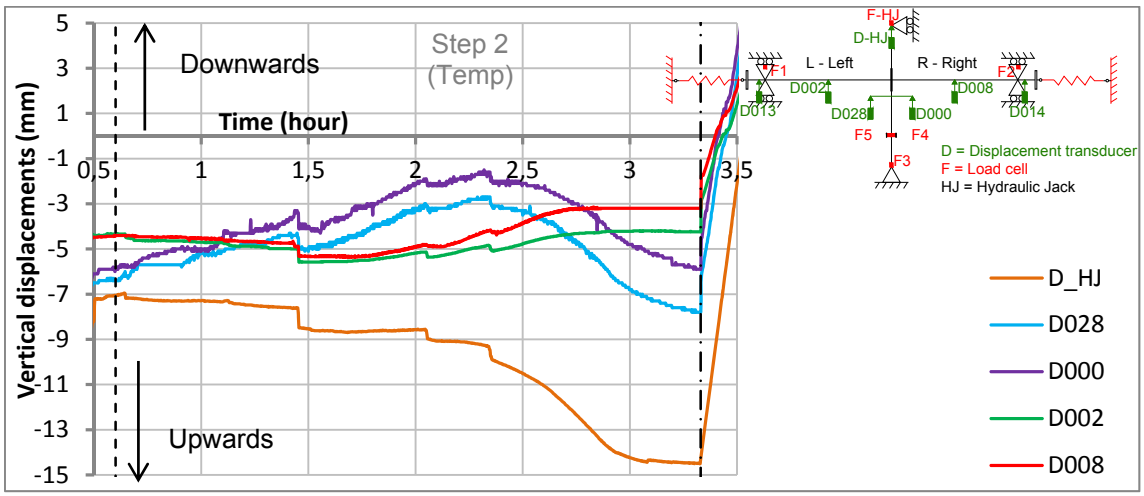

Figure 248: Vertical displacements near the beam-to-column joint during the increase of temperatures

At the beginning of step 2, the column section below the joint was moving downwards (transducers D000 and D028). The column was supported at the base by a cylinder, and in order to check if the cylinder kept its position constant during the increase of the temperatures, the vertical movement of the bottom column was measured by a wire transducer (D004, see Figure 249). During the heating, the pressure of the cylinder was regularly adapted in order to keep D004 constant (Figure 250); however, D000 and D028 measured vertical displacements of the joint in the downwards direction. One reason could be that the steel bars where the wire transducers were connected could be hot and perhaps slightly deformed in the downward direction under the self-weight. Finally, once the reaction loads reached their maximum and began to decrease, the column base was slightly displaced in the upwards direction (Figure 250).

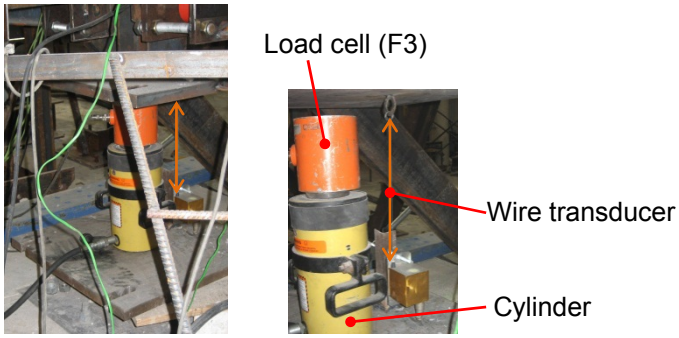

Figure 249: Wire transducer (D004) at the column base support

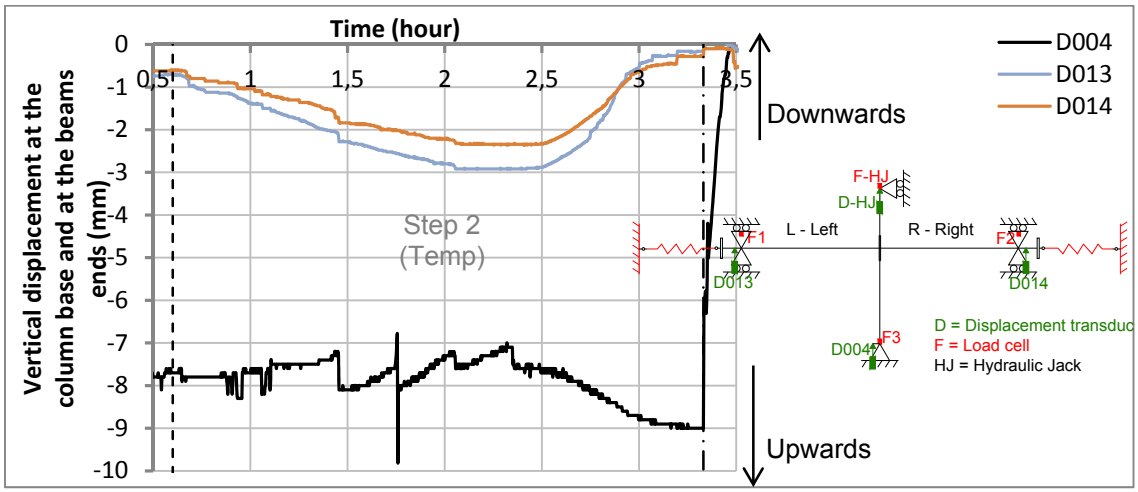

Figure 250: Vertical displacements measured near the beam supports (D013 and D014) and at the column base (D004) during the increase of temperatures

The measured displacements D013 and D014 (depicted in Figure 250) showed that the beams ends slightly separated themselves from their supports, with a maximum gap equal to 3 mm (during step 1). The beams were not anymore in contact with the supports and were just in contact with the load cell at the top (top support).

Around 2h18min, the vertical displacement at the column top (D_{HJ}) increases faster (upwards), from -9.2 mm to -14.2 mm. The thermal dilatation of the column can be deduced from the vertical displacements measured at the column top (D_{HJ}) and at the column base (D004). As shown in Figure 251, from the beginning to the end of the step 2, the column top (D_{HJ}) displaced upwards from -7.1 mm to -14.2 mm (i.e. 7.1 mm), and the column base displaced upwards from -7.7 mm to -9 mm (i.e. 1.3 mm). Finally, the dilatation was estimated as the difference between D004 and D_{HJ}, i.e. 5.8 mm of dilatation. This result was confirmed by a simple numerical model in Abaqus; this model only took into account the column; no effects due to the beam or concrete slab were modeled. The temperatures measured in the centre, top and bottom of the web and of the flanges were directly applied in the model. The thermal dilatation was equal to 6.8 mm, which showed that the measured dilatation (5.8 mm) is acceptable, regarding to the simplifications of the numerical model. Table 20 details the measured values at four moments of the step 2.

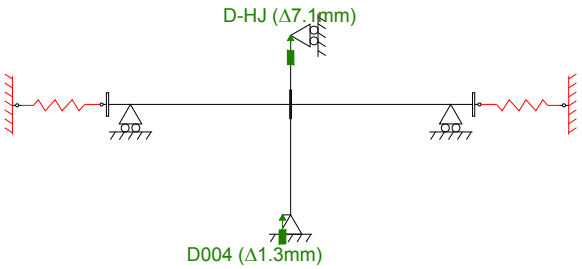

Figure 251: Total column displacements due to thermal expansion

Table 20: Main reaction loads and displacements during the step 2

		Begin of step 2 (36min)	Max load (2h33min)	Stop of the temp. increase (2h53min)	End of step 2 (3h20min)
TEMP (ºC)	Beam bottom flange LEFT - 20 cm	25.2	460.5	708.5	703.7
	Beam web LEFT - 20 cm	25.6	616.5	907.4	791.5
	Beam bottom flange RIGHT - 20 cm	25.3	460.3	707.6	711.5
	Beam web RIGHT - 20 cm	26	703.1	1045.7	871.3
Load (kN)	Reaction load Beam support Fleft	-80.7	-173.4	-78.5	-62.4
	Reaction load Beam support Fright	-83.0	-170.1	-82.5	-66.3
	Total reaction Load (FL+FR)	-163.7	-343.5	-161.0	-128.6
	Column base (F3)	-169.2	-343.2	-179.6	-128.5
	Column top (F-HJ)	1.0	1.0	0.9	3.8
	Total reaction column	-168.2	-342.2	-178.7	-124.7
	Axial load at the spring Fsp,L	0.0	67.5	64.5	47.4
	Axial load at the spring Fsp,R	0.0	58.2	53.4	40.6
Displ. (mm)	Beam mid-span LEFT (D002)	-4.3	-5.4	-4.2	-4.2
	Beam mid-span RIGHT (D008)	-4.4	-4.8	-3.2	-3.2
	Joint (average D000/D028)	-6.2	-6.0	-6.8	-7.4
	Column Top (D-HJ)	-7.1	-9.0	-13.6	-14.2

The loads and rotations at the spring restraints during the step 2 are presented in Figure 252 and Figure 253. The rotation was so small that the vertical component is equal 0 ($F_{sp,v} \approx 0$).

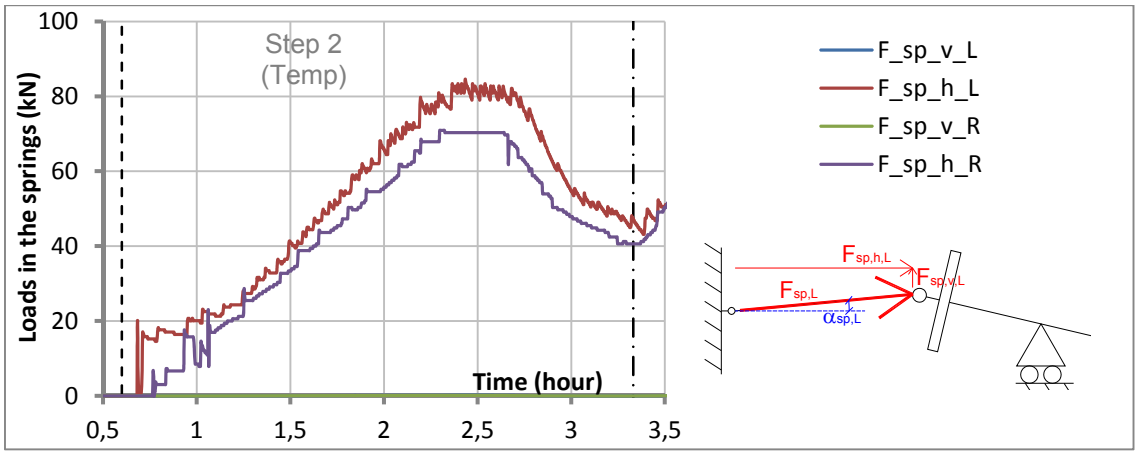

Figure 252: Horizontal (h) and vertical (v) projections of the spring loads during the step 2

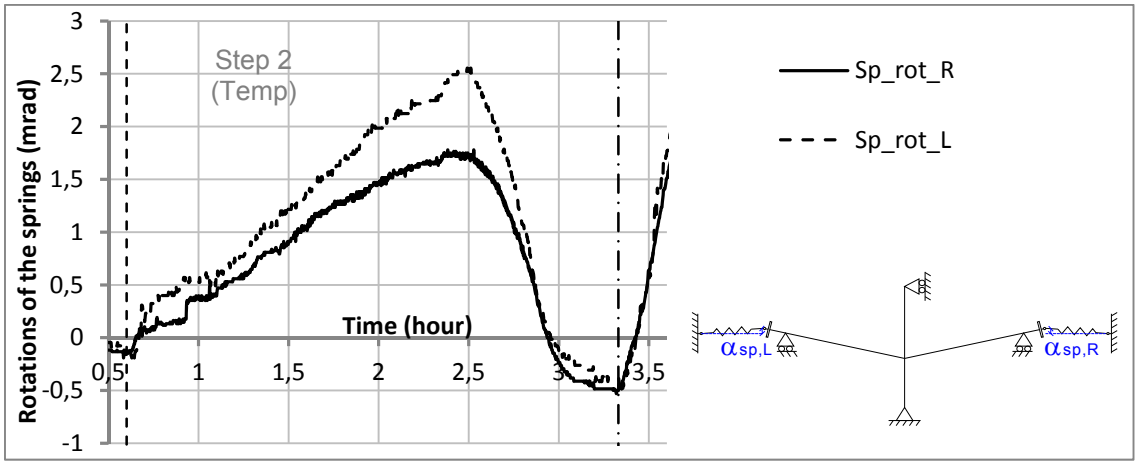

Figure 253: Spring rotations (L = Left; R = Right)

The evolution of the bending moment during the increase of temperatures is shown in Figure 254.

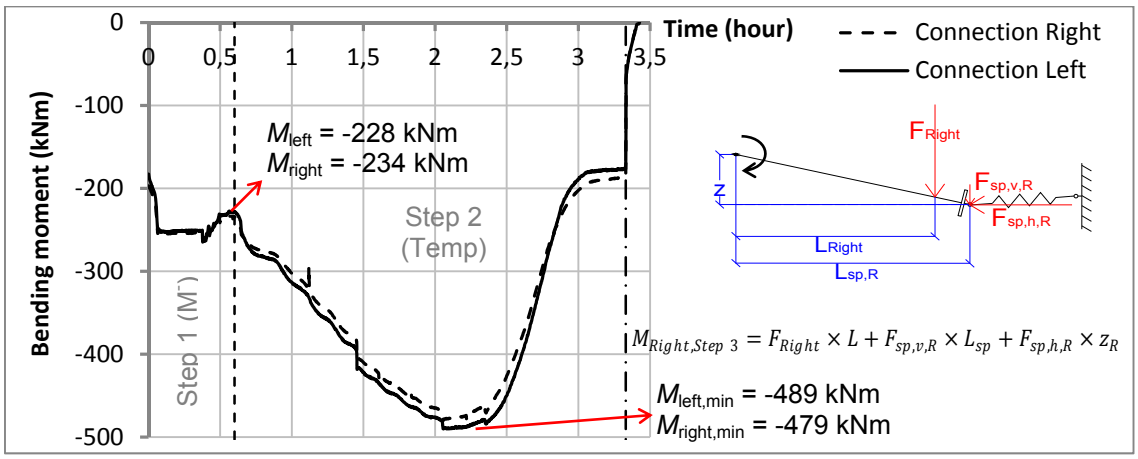

Figure 254: Evolution of the bending moment in the connections (Left and Right) during the steps 1 and 2

III.7.4 Step by step behaviour: step 3 - Loss of the column and sagging bending moment

The step 3 corresponded to the loss of the column and the increase of the sagging bending moment in the joint. Before the loss of the column, the hydraulic jack at the top of the column was changed to displacement control (velocity equal to 0.02 mm/sec); the cylinder at the base was progressively removed; and finally, the displacement at the top of the column was increased (increase of the joint sagging bending moment) up to the failure of the joint. Note that the structural system at the beams supports (see Figure 16 in section II.6.1.2) was unloaded, after the loss of the column, by loosening the nuts.

Figure 255 shows the evolution of the vertical loads measured by the hydraulic jack F_{HJ} at the top of the column, by the load cells F1+F2 at the top of the beams supports and by the vertical components of the spring restraints loads. The evolution of the slab deformation and cracks is shown in Figure 256. First concrete cracks were observed near the column flange at 4h41min (4.68h), then the concrete crushed against the column flanges around 4h50min, and

finally the entire slab width failed (5h21min – 5.35h). From that moment, the load at the column top, F_{HJ}, decreased; and the maximum load corresponded to the crushing of the concrete slab.

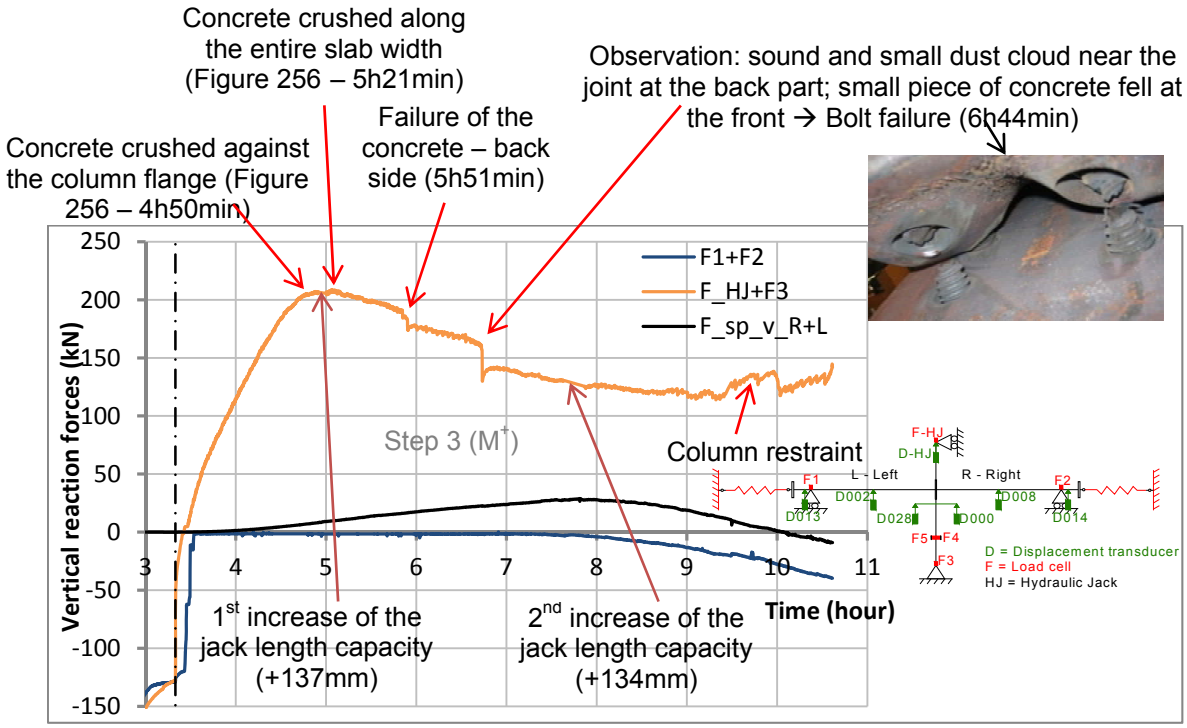

Figure 255: Evolution of the vertical loads during the step 3

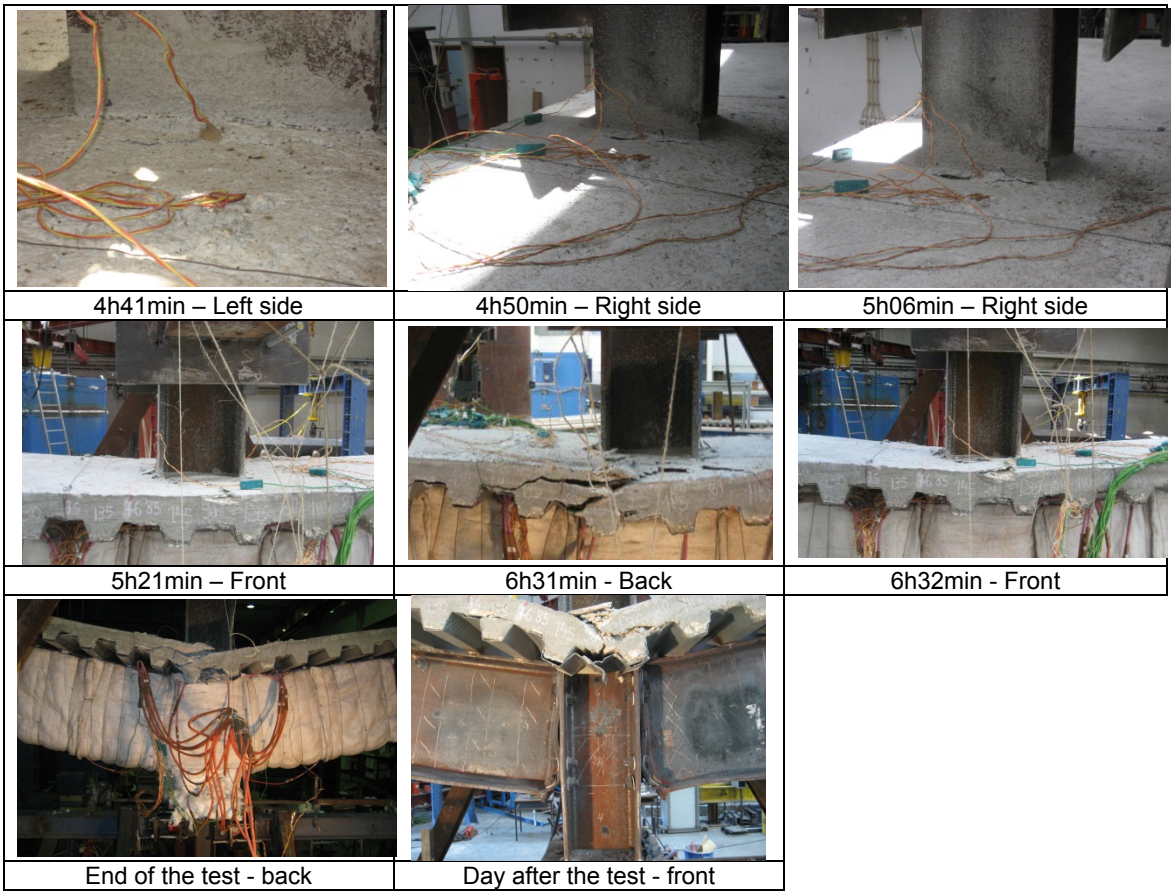

Figure 256: Evolution of the concrete crushing

The hydraulic jack stroke was increased two times during this test: first around 4h56min, then around 7h52min (see §II.6.1.1, p13).

In tests 1 and 2, it was observed that, once a bolt from a connection fails, the rotation of the column increases in the opposite direction. The column rotation is depicted in Figure 257; at 6h44min (1st bolt failure), the increase rate of the rotation (in the clockwise direction) was modified. It can be concluded that a bolt from the bottom row of the connection right failed. Figure 258 shows the bolt failure on the reaction load chart.

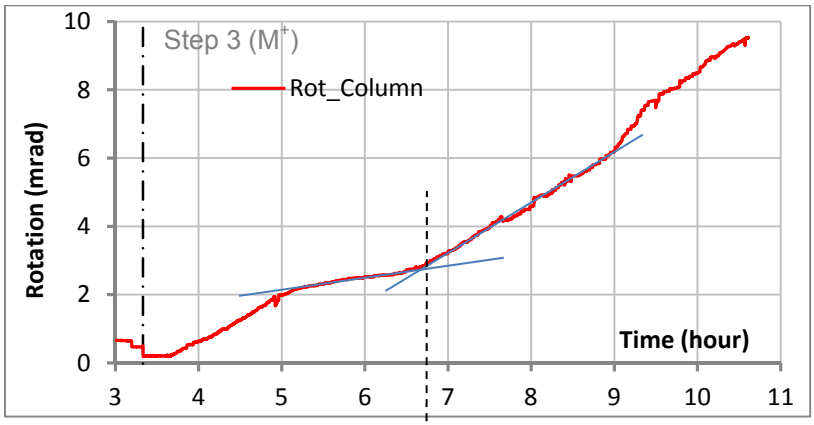

Figure 257: Column rotation and measured load at the column left restraint F5 (step 3)

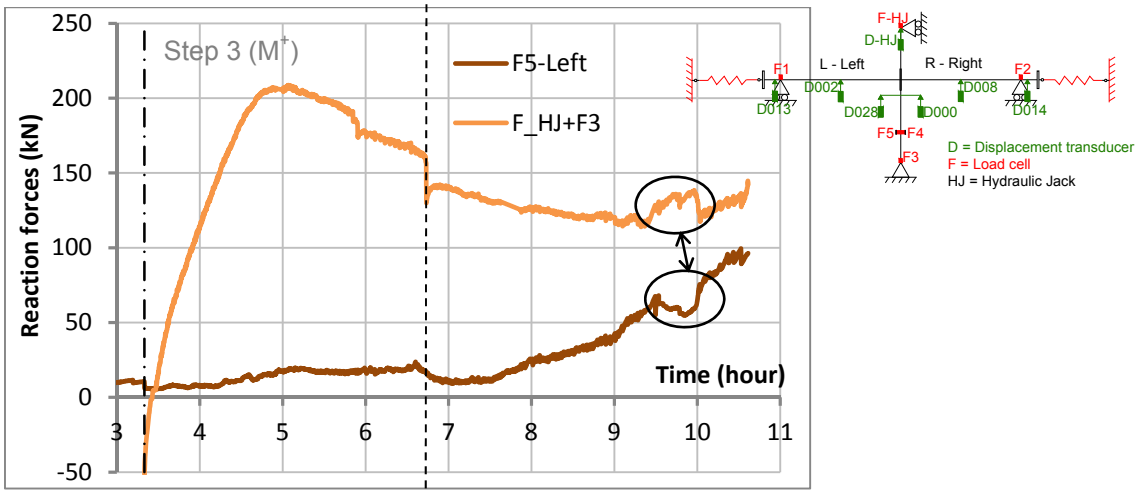

Figure 258: Evolution of the loads: at the column top (F_{HJ}) and at the column left restraint (F5)

Figure 258 also illustrates the evolution of the horizontal reaction load F5 measured at the bottom column restraint. Between 9 and 10 hours, the vertical load applied by the jack at the column top was increased locally: this increase of rigidity was due to the horizontal restraint, which was trapped by the column; the horizontal restraint displaced downwards with the column, up to escape at 10h, and come back to the horizontal position (the horizontal reaction load F5 is varying in the same time).

Figure 259 shows the evolution of the vertical displacements measured i) by the hydraulic jack D_{HJ}; ii) by the wire transducers D000 and D028, and iii) by the displacement transducers at mid-span of the beams (D008 and D002). The maximum displacement measured by the hydraulic jack was 509 mm. The wire transducers D000 and D028 stopped measuring at 8h and 8h24min

respectively, because they reached their maximum capacities; the dashed part of the curves represents the estimation of the displacements, which was a linear estimation based on the rate of displacement imposed by the hydraulic jack (0.02 mm/sec).

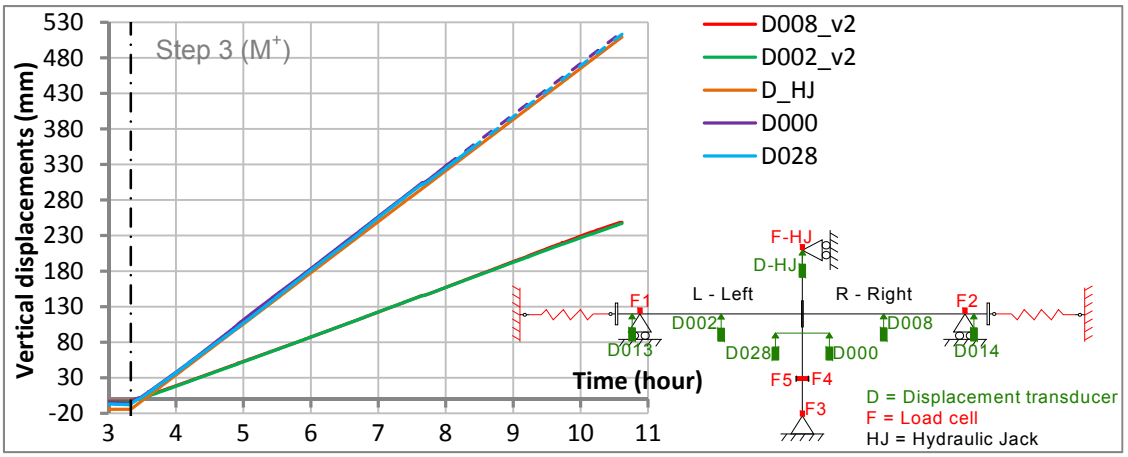

Figure 259: Vertical displacements near the beam-to-column joint during step 3

Figure 260 shows the deformed end-plates after disassembly the tested sub-frame. The end-plate (15 mm thick) bended between the bolt rows 2 and 3; note that the high 260 mm space was defined during the design of the joint (Demonceau, 2009), in order to consider two bolt rows resisting to the shear loads and the two other bolt rows resisting to bending.

a) Beam right b) Beam left

Figure 260: Deformed end-plates after disassembly the tested sub-frame

Figure 261 depicts the loads measured during the step 3: i) the measured loads at the beam supports, F1 and F2; ii) the reaction loads equals to $F_{HJ}/2$; and iii) the horizontal and vertical reaction loads from the spring restraints. In step 3, the load cells F1 and F2 did not measure anymore the real reaction loads because the structural system at the beams supports (see Figure 16 in section II.6.1.2) was unloaded after the loss of the column by loosening the nuts, and should be equal 0; but around 8 hours, once large displacements were observed, F1 and F2 slightly increased due to the high rotations of the beams ends, and the structural system at the beams supports was not unloaded anymore.

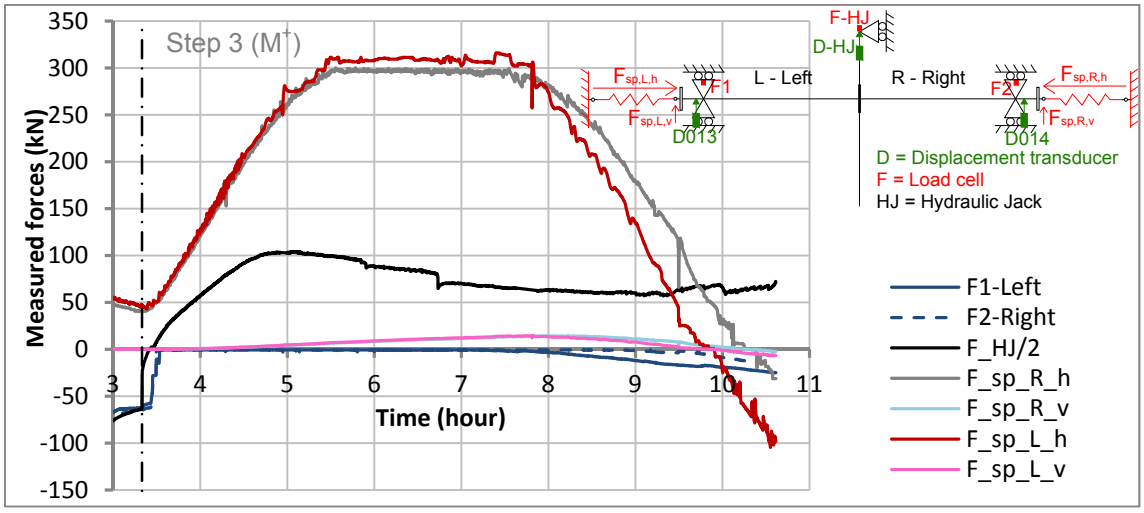

Figure 261: Measured loads at the beam ends (F_1 and F_2), at the column ($F_{HJ}/2$) and vertical and horizontal reactions at the springs

Figure 262 shows the evolution of the total reaction loads during the entire test, and Table 21 details the main measured loads and displacements during the step 3.

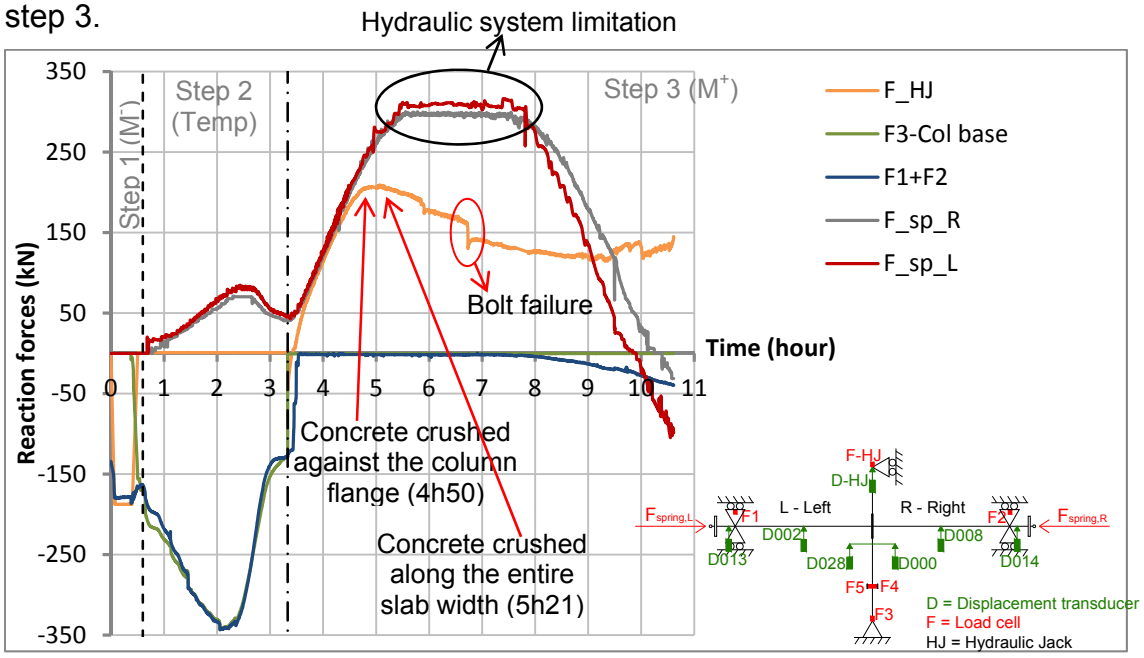

Figure 262: Evolution of the loads during the entire test

Table 21: Main reaction loads and displacements during the step 3

		begin of step 3, 3h20min	Max load 5h04min	1st bolt failure 5h51min	2nd bolt failure 6h44min	7h47min	end of the test 10h37min
TEMP (°C)	Beam bottom flange left 20cm	703.7	705.6	705	704.7	704	697.3
	Beam web left 20cm	791.5	641.3	628	605.1	593.2	597.2
	Beam bottom flange right 20cm	711.5	705.2	703.9	702	697.5	680.4
	Beam web right 20cm	871.3	704.8	705.8	731.2	842.3	922.5
Load (kN)	Reaction load beam support F_{left}	-62.4	-0.7	-0.7	-0.7	-2.1	-24.9
	Reaction load beam support F_{right}	-66.3	-0.9	-0.9	-0.9	-0.7	-14.6
	Total reaction Load (F1+F2)	-128.6	-1.6	-1.6	-1.6	-2.9	-39.5
	Column base (F3)	-128.5	-0.3	-0.3	-0.3	-0.3	-0.3
	Column top (F_{HJ})	3.8	209.0	190.9	130.3	127.4	139.0
	Total reaction column	-124.7	208.7	190.6	130.0	127.1	138.7
	$F_{sp,L}$	47.4	274.9	310.8	308.4	302.9	-99.4
	$F_{sp,R}$	40.6	268.0	297.1	295.9	288.6	-31.3
Displ. (mm)	Beam mid-span left (D002)	-4.2	54.7	81.6	113.1	149.6	246.7
	Beam mid-span right (D008)	-3.2	55.2	81.7	112.9	149.5	248.2
	Joint (average D000/D028)	-7.4	113.4	170.2	235.5	310.5	512.9
	Column Top (D_{HJ})	-14.2	110.3	166.3	230.3	306.2	508.3

Figure 263 shows the evolution of the bending moment *versus* time at the connections during the entire test.

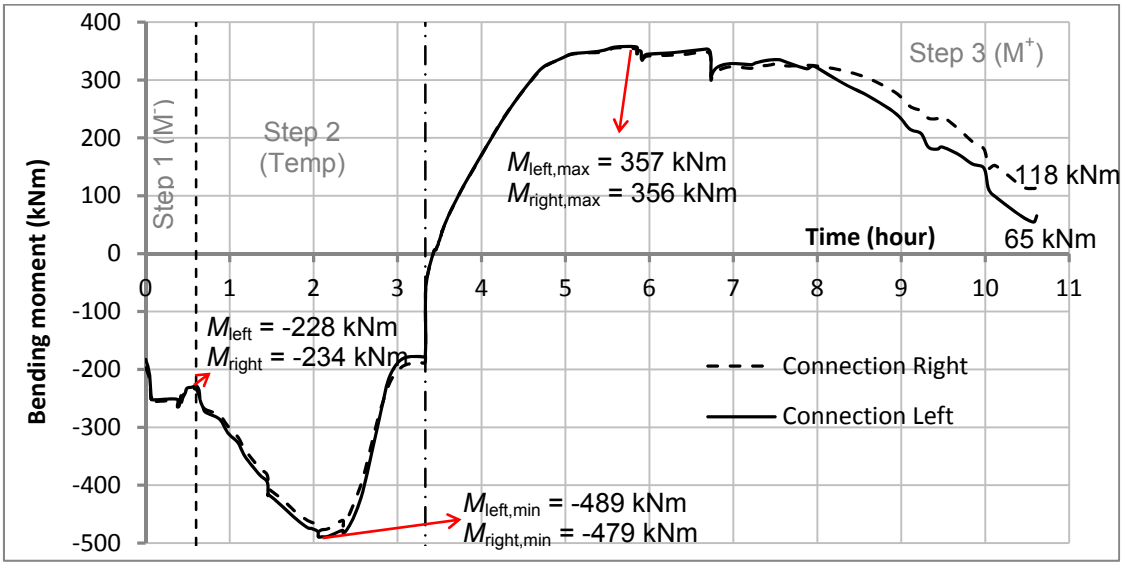

Figure 263: Bending moments at the connections left and right

Figure 264 and Figure 265 present the evolution of the total reaction load *versus* the joint rotation and the beam axial load respectively.

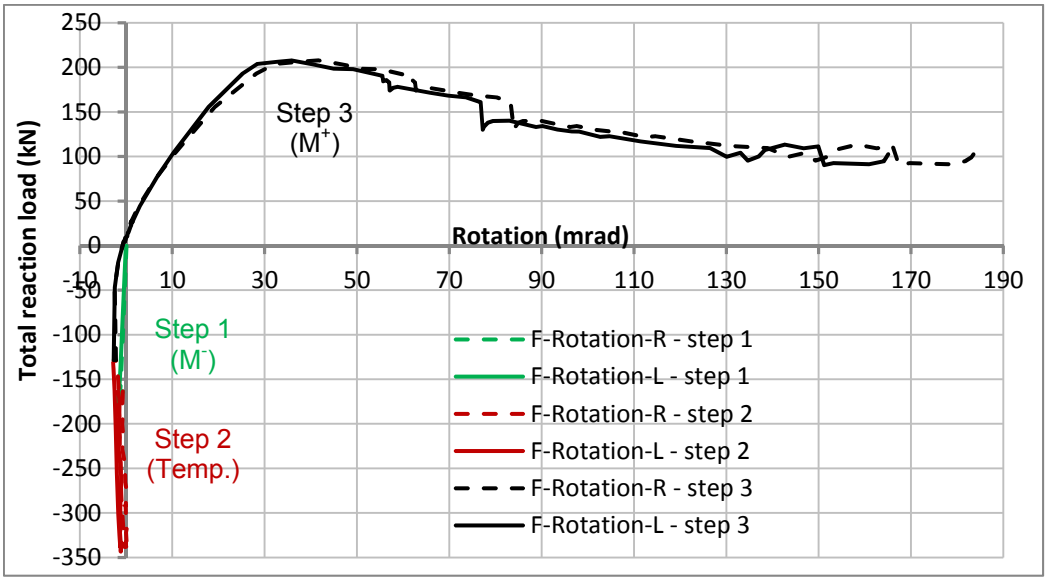

Figure 264: Total reaction load (F_L+ F_R) vs rotation at the connection

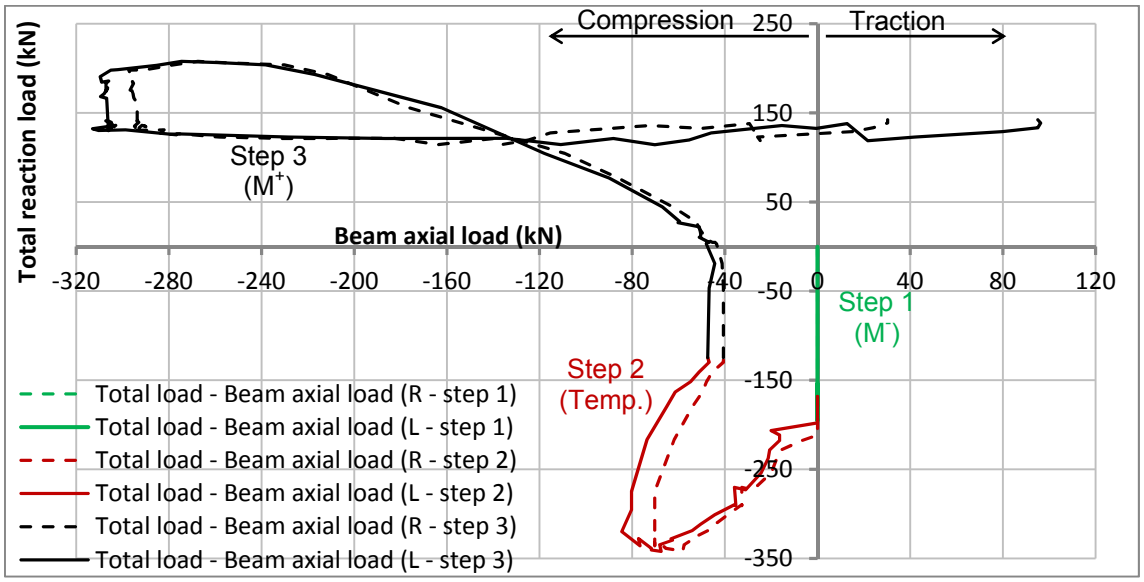

Figure 265: Total reaction load (F_L+ F_R) vs axial loads at the joint ($F_{restr,ax}$)

III.7.5 Additional data

The evolution of the vertical and horizontal components of the spring restraint loads, $F_{sp,v}$ and $F_{sp,h}$, are showed in Figure 266: the spring loads were nearby horizontal during the entire test (maximum value of the vertical component of the loads: +14.5 kN, around 8h). The rotations of the spring restraints are shown in Figure 267.

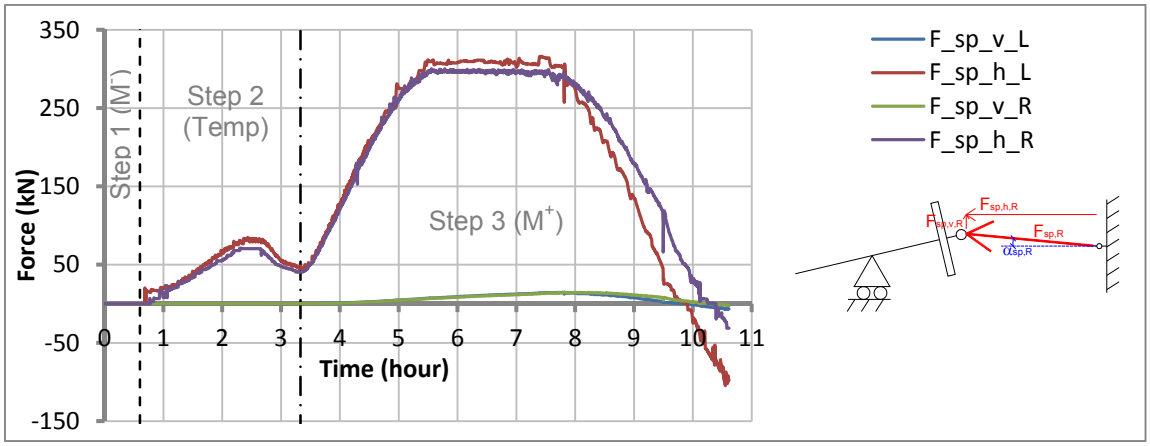

Figure 266: Projections of the spring restraint loads along the horizontal (h) and vertical (v) axis

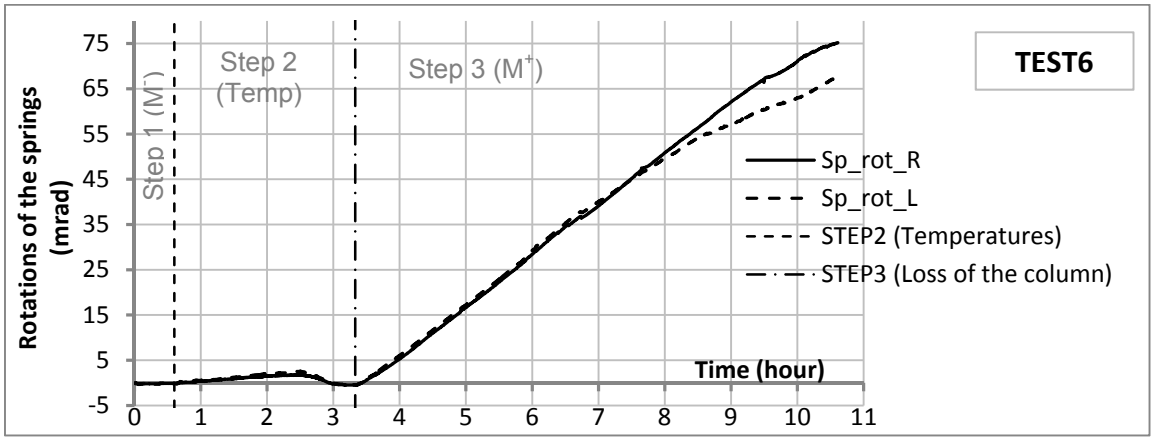

Figure 267: Spring rotations (L = left; R = right)

The horizontal displacements measured at the beam ends are showed in Figure 268. The estimated horizontal displacements at the neutral axis of the steel beams $D_{beam,h,L\ and\ R}$ are represented by the black curves (see §III.1).

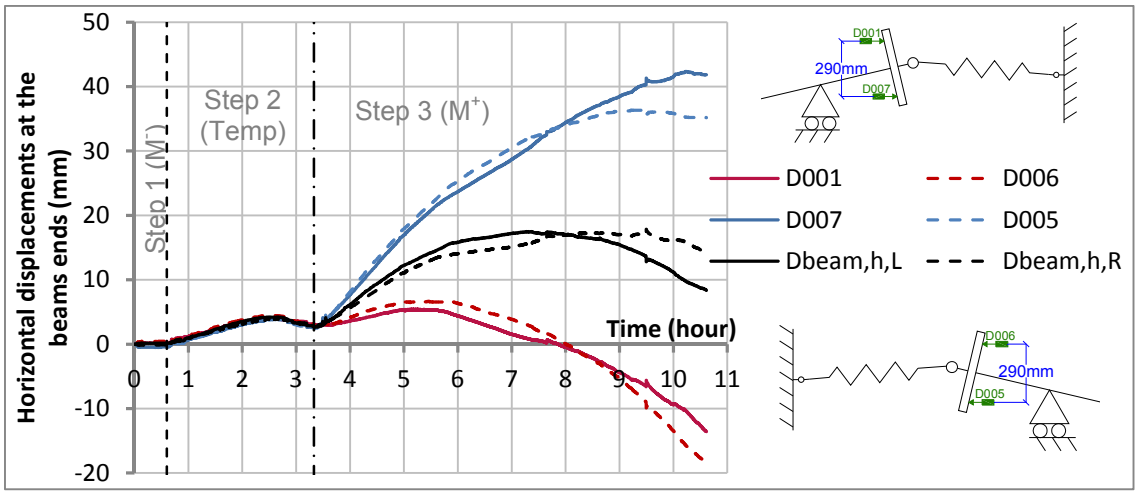

Figure 268: Horizontal displacements at the end of the left beam

Figure 269 presents the displacements of the beams out of the plan, measured by the two displacement transducers D025 and D026 at the beam ends, and by the two transducers D003 and D009 on the beams webs, initially situated at

1500 mm from the end-plate. The largest out of the plane displacement was measured on the column base (D015 = 23.5 mm).

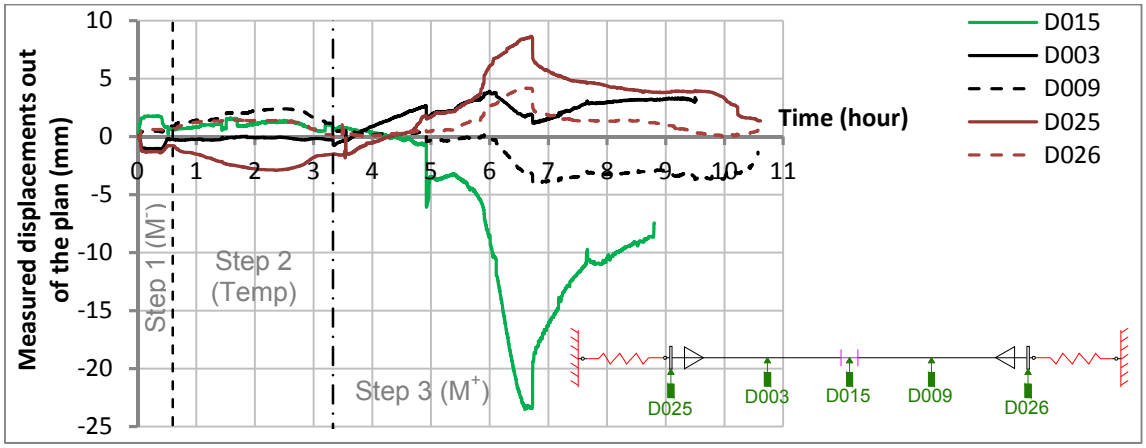

Figure 269: Evolution of the displacements measured out of the plan

Figure 270 presents the measured displacements of the auxiliary's structures (steel and concrete footings and strong beams connected to the strong walls).

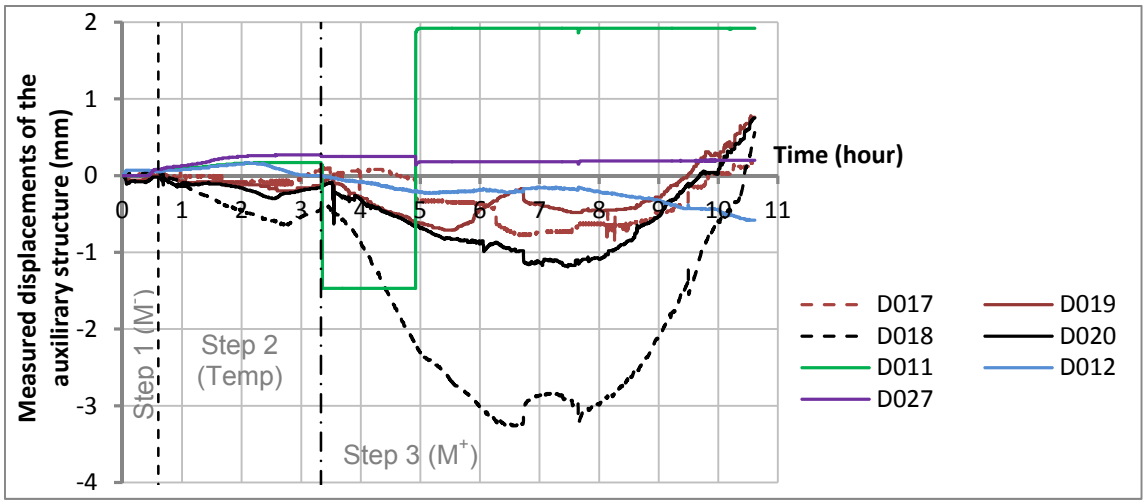

Figure 270: Measured displacements of the steel and concrete footings, and of the strong beams linked to the walls (see Figure 31 for the position of the displacement transducers)

Finally, Figure 271 shows the final deformation of the sub-frame.

Figure 271: Final deformation of the sub-frame the day after the test

III.8 Results of test 7 (Demonstration test)

The global behaviour of the joint during the test is described in the following section, then the step by step behaviour is detailed, for each loading step, and finally, additional data a presented.

III.8.1.1 Temperature results

The two dimension composite steel-concrete beam-to-column sub-frame was subjected to the loss of the column due to a localised fire (see §II.5.2). Figure 272 presents the temperatures evolution during the entire test 7 in the right (R) and left (L) beams (at 200 mm from the connection), in the column centre, in the bottom column HEB 140, in bolts from row 4, and in the concrete rib in contact with the steel beam near the joint. In step 3, the beams were heated up to 400ºC in the bottom flanges, and joint components and column reached lower temperatures; the bottom column reached its maximum resistance capacity under 578ºC (maximum 625ºC measured in the web centre) and failed (at 2h40min). The temperature increase rate was 200ºC/hour in the beam bottom flanges and around 300ºC/hour in the bottom column HEB 140. At the end of the step 3, the temperature distribution in the bottom column was not uniform: 754ºC at the top (at 394 mm from the centre), 815ºC at the centre and 634ºC at the bottom (323 mm from the centre); the average temperature was 733ºC. In step 4, the temperatures in the beam-to-column joint were increased, up to 800ºC in the beams bottom flanges (increase rate of 300ºC/hour), and finally, the entire sub-frame collapsed. Around 5h30min, temperatures in beam bottom flanges stopped increasing and were equal to 786ºC on the left and 787ºC on the right. At the end of the test (5h51min), maximum temperatures measured at the joint were: 686ºC and 669ºC in left and right bolts, 702ºC and 659ºC in left and right beam end-plates, 729ºC in column web and 633ºC and 608ºC in left and right column flanges. The maximum temperature measured in the shear studs near the joint was 179ºC, and the slab temperature reached 280ºC at the steel sheet and 110ºC in the concrete in contact with the column. The last sudden increase of temperatures corresponded to the increase of the hydraulic jack stroke (the test was stopped but the temperature continued increasing). The evolutions of all measured temperatures are detailed in §III.8.3.

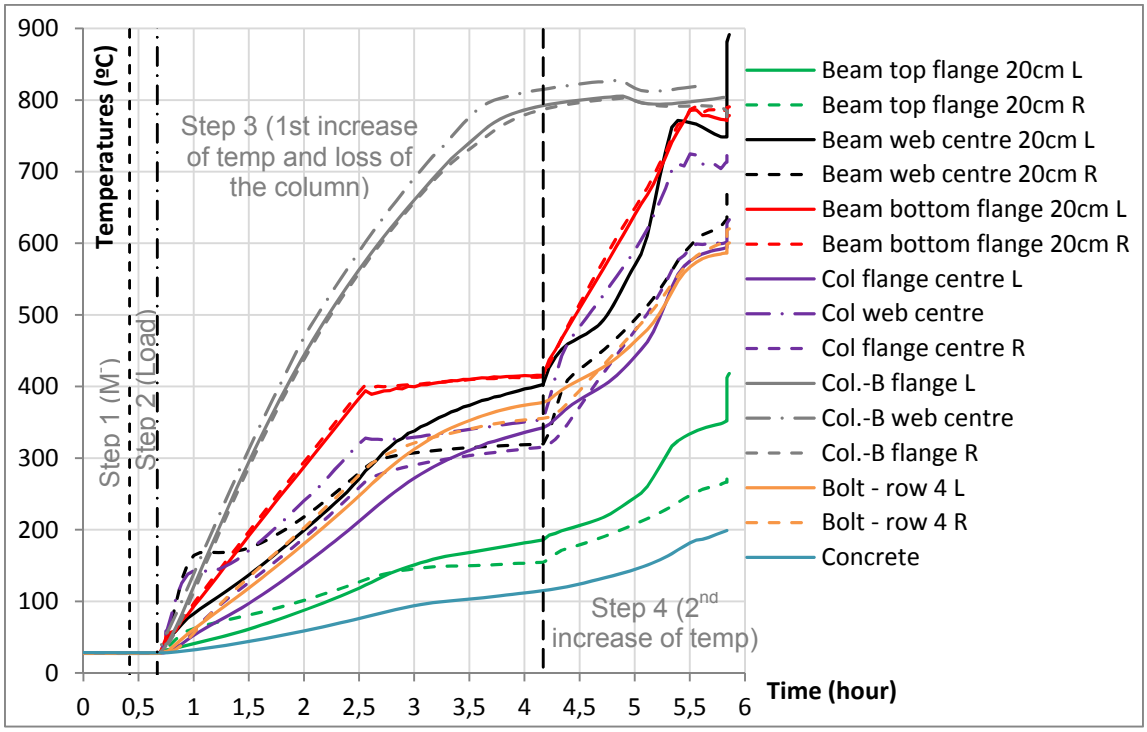

Figure 272: Evolution of the temperatures during test 7 (in beams at 200 mm from the connection, in column centre, in bottom column HEB 140 (Col.-B), in bolts from row 4 and in concrete rib in contact with the steel beam)

III.8.1.2 Bending moments variation and failure modes

Figure 273 and Figure 274 show the evolution of the bending moment at the joint *versus* the joint rotation, and the beam axial load $F_{restr,ax,R \text{ and } L}$. The evolution of the total reaction load (F_L+F_R, defined in §III.1.2) *versus* the vertical displacement measured at the column top is presented in Figure 275. The evolution of the vertical displacements *versus* time is shown in Figure 276. The hogging bending moment (-281 kNm) was initially reached during step 1 (F_{HJ}+F_3 = -200 kN). During step 2, the hydraulic jack increased the load at the column top up to reach +250 kN (see §II.5.2); however, due to the clearances at the column base (see §III.8.2), the total load at the column (F_{HJ} + F_3) reduced from -200 kN to -96 kN and consequently, the hogging bending moment was reduced to -134 kNm. In step 3, temperatures increased, as well as reaction loads under thermal expansion effects: they reached a maximum value of -359 kN (bending moments equals to -505 kNm), followed by a decrease due to the loss of resistance at the column base. The failure of the column was really progressive, and was defined as the moment at which the vertical reaction load came back to its initial value at the beginning of the step 3 (95.6 kN). At the end of the step 3, the total load was equal to +211 kN, and the column top dropped of +25 mm. The sagging bending moment increased up to 300 kNm, and the compression axial loads to the beams reached 61 kN on the left and 58.8 kN on the right. The axial restraints were connected to the beams since the beginning of the test. During steps 1 and 2, the loads and displacements created by the application of the initial hogging bending moment were not sufficient to create axial forces to the beams. During steps 3 and 4, the beam ends were moving outwards and the restraints worked in compression.

During step 4, the temperature in the joint increased under the constant load (+250 kN) applied at the top of the column and reached 770ºC in the beam bottom flange: the concrete slab began to crush against the column flange; the vertical displacement increased faster (Figure 276), and once the concrete slab was completely crushed, beam bottom flanges temperature reached 800ºC and the sub-frame completely failed. The test was stopped at a vertical displacement equal to 280 mm, at 150 mrad and 37 mrad of connection left and right rotations, the total vertical reaction load was 104 kN, and axial compression loads at the spring restraints were reduced from 266 kN to 222 kN after the concrete crushing. The sagging bending moment was slightly decreased from 290 kNm to 265 kNm on the left, and to 271 kNm on the right connections.

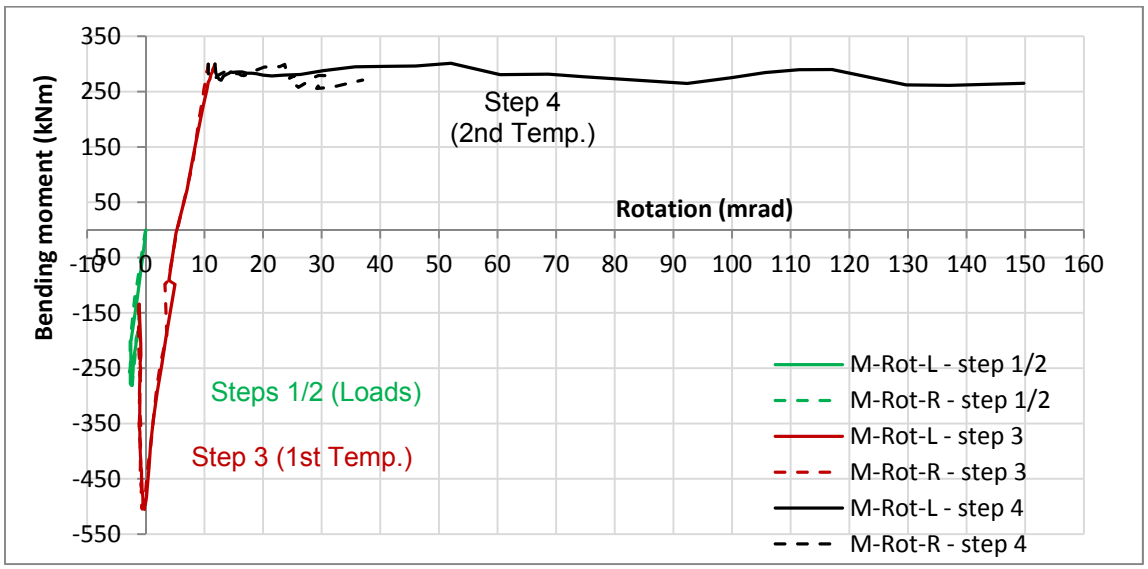

Figure 273: Bending moment vs rotation at the connection (the different gradient of colors define the different steps)

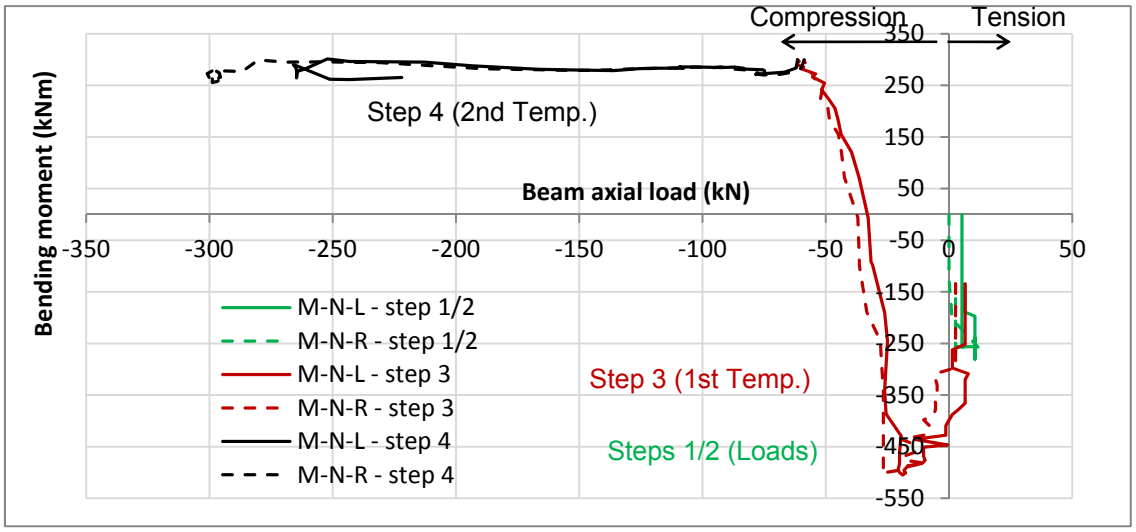

Figure 274: Joint bending moment vs axial loads at the joint ($F_{restr,ax}$)

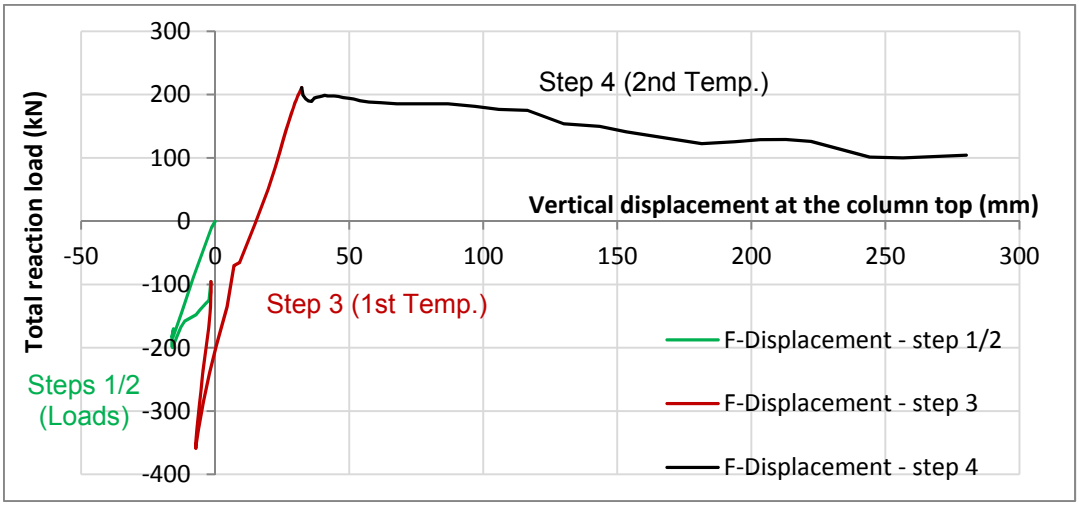

Figure 275: Total reaction load (F_L+ F_R) vs vertical displ. measured at the column top (D_{HJ})

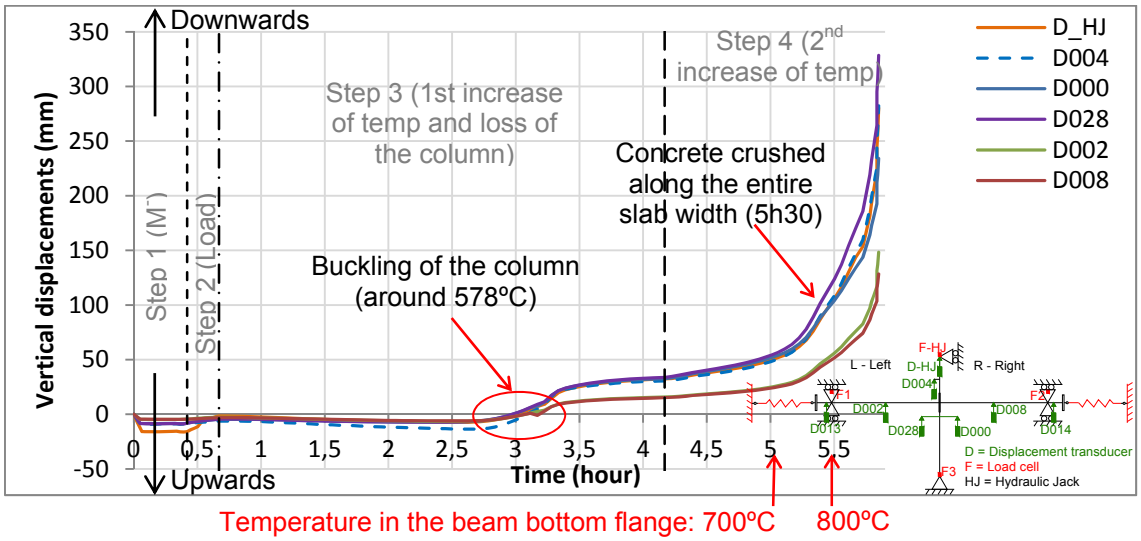

Figure 276: Evolution of the vertical displacements during the entire test 7

Concrete crushing in compression was the first failure observed under sagging bending moment; first concrete cracks were observed near the column flange (left side – 5h20min), and finally the entire slab width was cracked (5h30min) and failed. Figure 277 shows the concrete completely crushed at the end of the test.

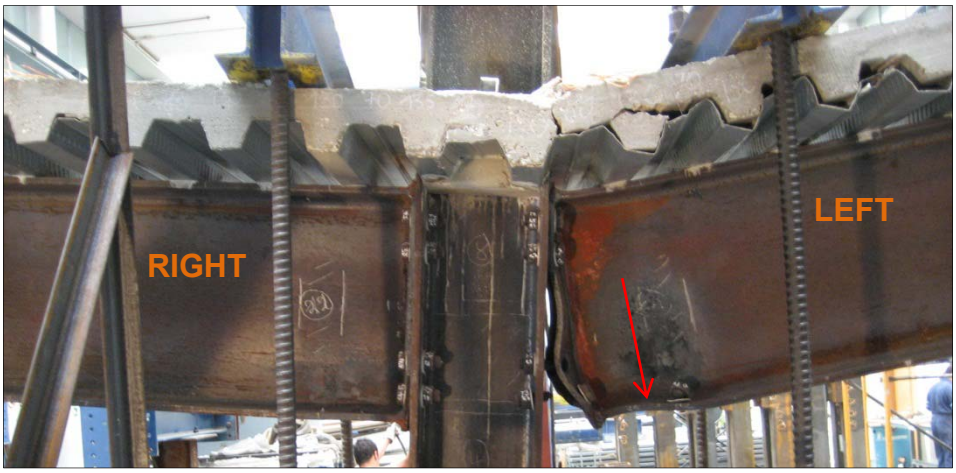

Figure 277: Concrete crushing at the back side of the slab (end of the test) and beam deformation

The maximum compression load in the beam right axial restraint was limited at 300 kN, by the capacity limitations of the hydraulic circuit material (see §II.7.2.2); and the maximum measured load was 266 kN on the left side. Once the sub-frame failed, the axial restraints to the beams decreased, but the test was stopped before reaching tensile loads for security reasons. The day after the test, the failure of three bolts from the left connection was observed: two bolts at the row 4 and one bolt at the row 3, but the failures were not observed on bending moment/rotation and load/displacement curves.

As the entire bottom column was heated, the column restraint at the base could not be used: the column rotated up to around 60 mrad in the opposite clockwise direction, and the joint deformation was not symmetrical (Figure 278). The steel end-plates deformed in the bottom and centre part, and due to high stresses/deformations, a crack at the base steel end-plate, just above the weld, was observed. The rotation was begun by the bottom column deformation; Figure 279 shows the final deformation of the sub-frame.

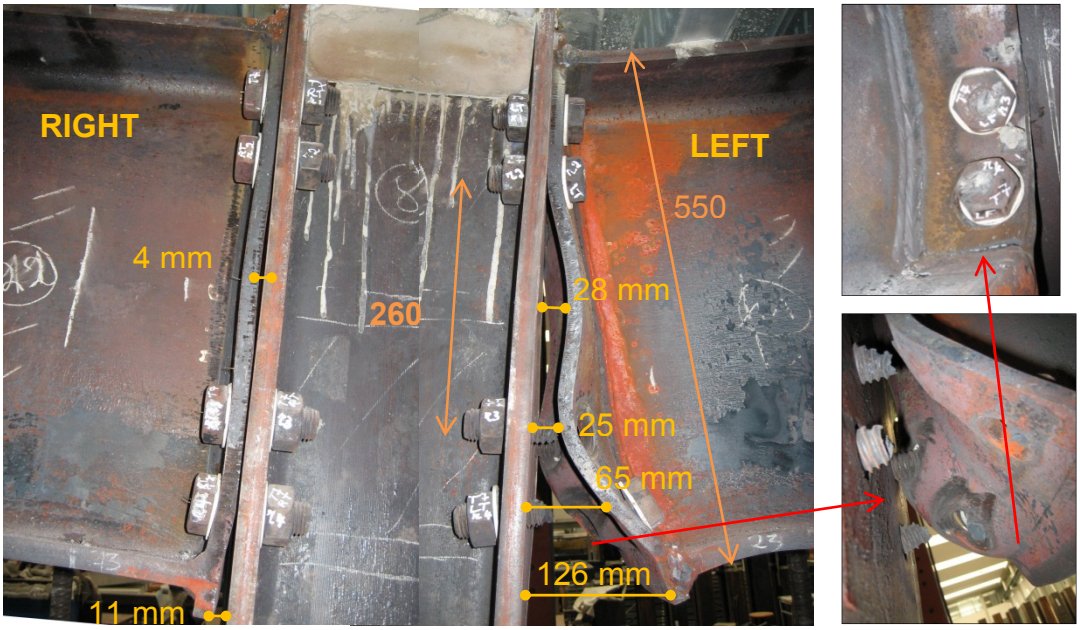

Figure 278: Deformations of the joint (view from the front side)

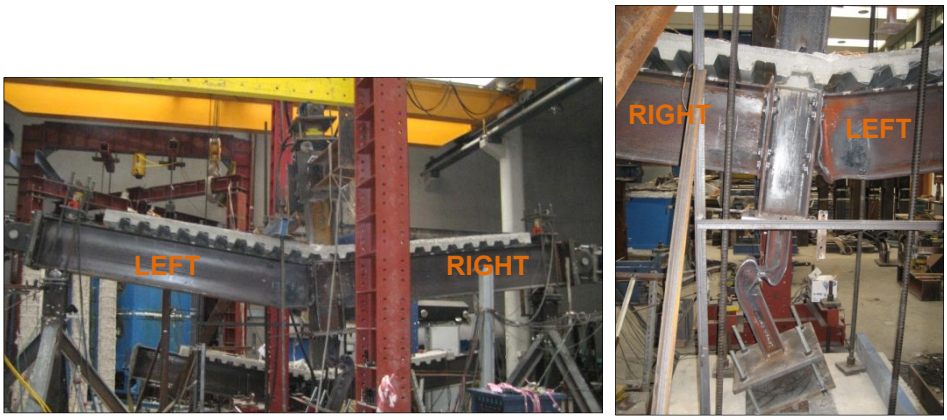

Figure 279: Final deformation of the sub-frame

Figure 280 shows the rotations at the joint left and right sides versus time, as well as the column rotation. The column rotation reached 63 mrad and the test was stopped at 150 mrad and 37 mrad of connection left and right rotations. The hydraulic jack stroke was increased once during this test (5h50min), and just a few moments after reloading the sub-frame, it collapsed and the test was stopped. The joint rotation calculation included any beam deformation, as shown in Figure 277 for the left beam.

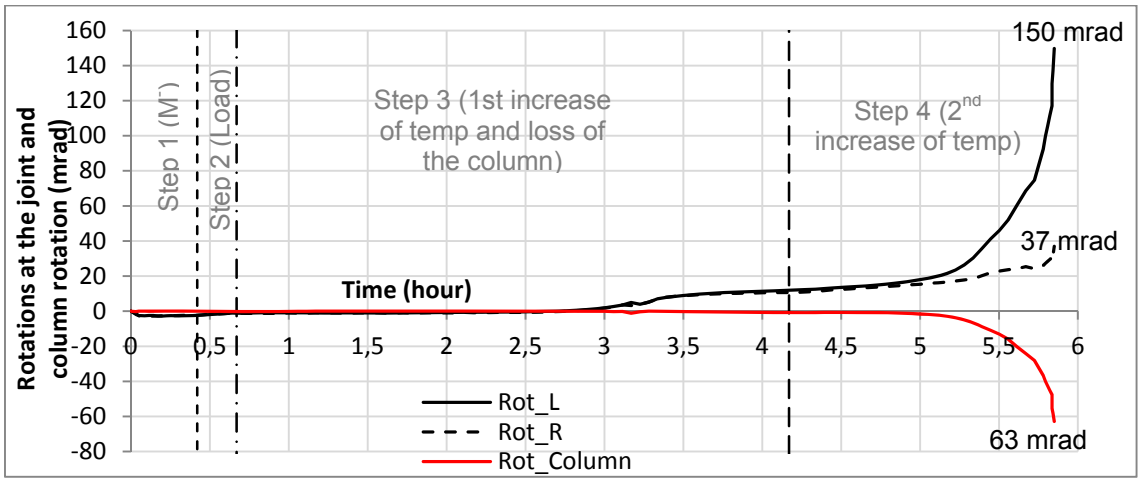

Figure 280: Rotations at the connections (Rot_Connection Left and Right) and column rotation

Finally, Figure 281 shows the evolution of the loads in the spring restraints according to the average displacement measured at the geometrical centre of the steel beam section (see §II.7.2.2): the spring stiffness of 50 kN/mm was mantained up to around 200 kN, then the stiffness slightly decreased.

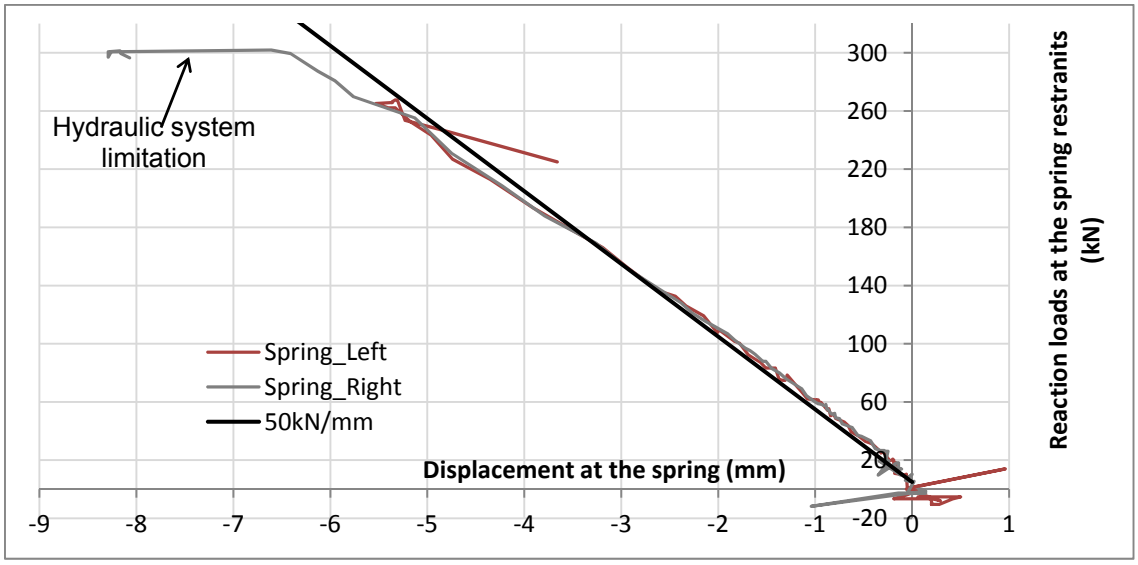

Figure 281: Displacement vs load at the two spring restraints

III.8.2 Step by step behaviour: steps 1 and 2 - Mechanical loadings

Figure 282 presents the evolution of the vertical displacements measured near the beam-to-column joint during the steps 1 and 2. The initial hogging bending moment was applied in three phases: i) the beams were restrained at the supports and the column was free at the base; ii) the hydraulic jack increased the vertical load at the column top and pulled the column upwards; iii) the column base support was set up; iv) the load at the column top was completely transferred to the sub-frame supports, and then increased up to reached +250 kN.

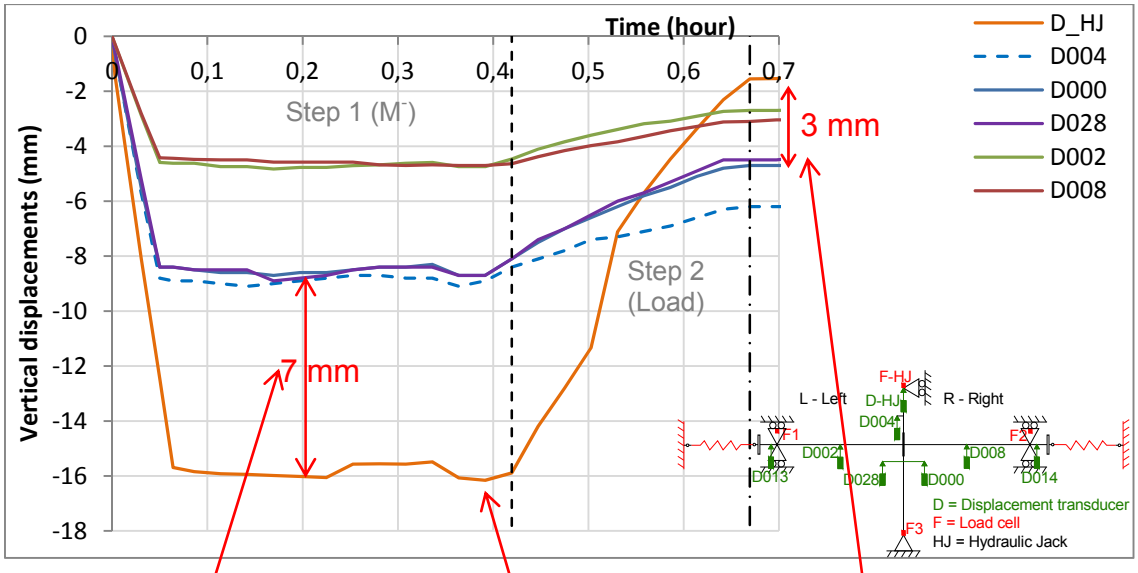

Difference of 7 mm between D_{HJ} and D000, D004 and D028 because of the clearances at the hydraulic jack pins

Application of the column support

Little difference between D000/D028 and the hydraulic jack

Figure 282: Vertical displacements near the beam-to-column joint during the application of the initial loads (hogging bending moment)

Figure 283 shows the measured reaction loads and the load applied at the top of the column by the hydraulic jack (F_{HJ}). Figure 284 shows the space at the column base support at the end of step 1, and the steel plate that was located to fill the gap. Nevertheless, clearances were not completely filled; at the end of the step 2, the total load at the column reduced from -200 kN to -100 kN (see red curve) due to the clearances at the column base support, and the hogging bending moment was reduced. The two load cells F1 and F2 did not measured the loss of load at the end of the step 2 (just as showed by the red curve – Fhj+F3), and they were not considered for the reaction loads (see §III.1.2.1)

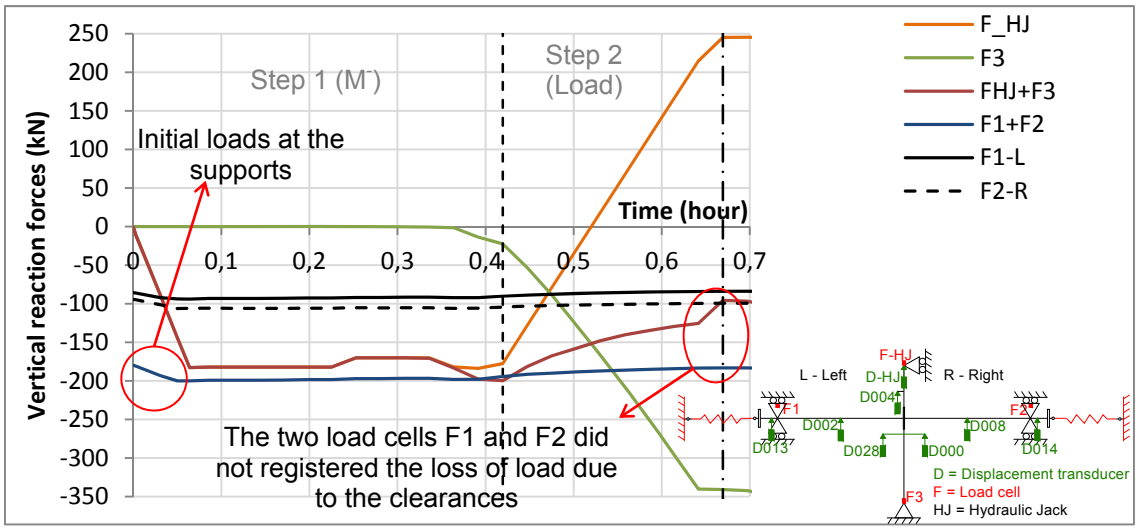

Figure 283: Comparison between the load applied by the hydraulic jack at the top of the column and the reaction loads at the beams supports

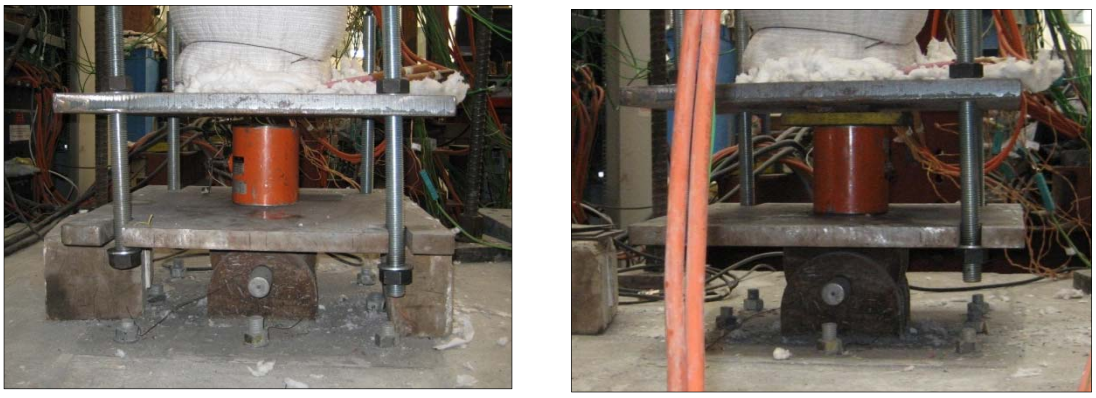

a) b)

Figure 284: Base support of the column with the load cell F3 and the clearances: a) at the end of the step 1 – Hogging bending moment; b) at the beginning of the step 2 – Loading at the column top

Figure 285 shows the evolution of the bending moment *versus* time at the connections during the steps 1 and 2.

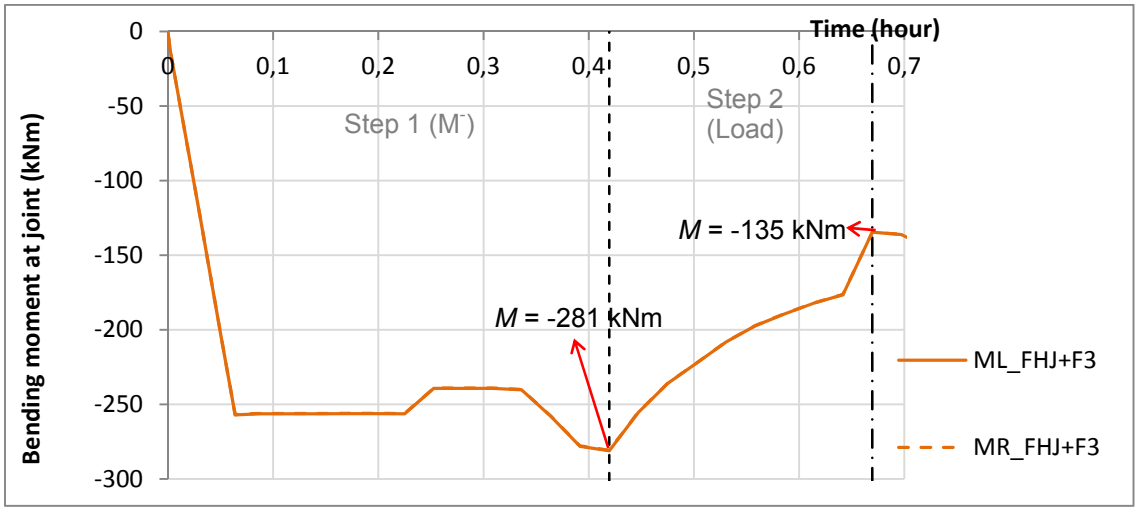

Figure 285: Evolution of the bending moment in the connections (Left and Right) during the steps 1 and 2

III.8.3 Step by step behaviour: steps 3 and 4 - Loss of the column and thermal loading

III.8.3.1 Evolution of the temperatures

Figure 286, Figure 287 and Figure 288 show the evolution of the temperatures in the beams at respectively 10 cm, 20 cm and 50 cm from the end-plate.

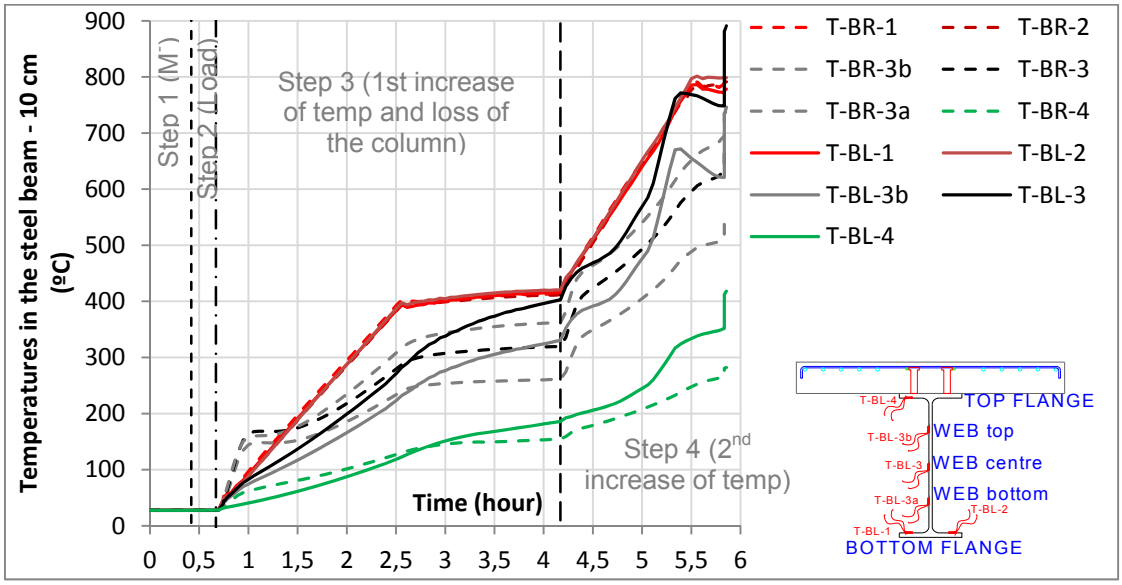

Figure 286: Evolution of the temperatures (T) in the beams at 10 cm from the connection during the test 7 (BR = beam right; BL = beam left)

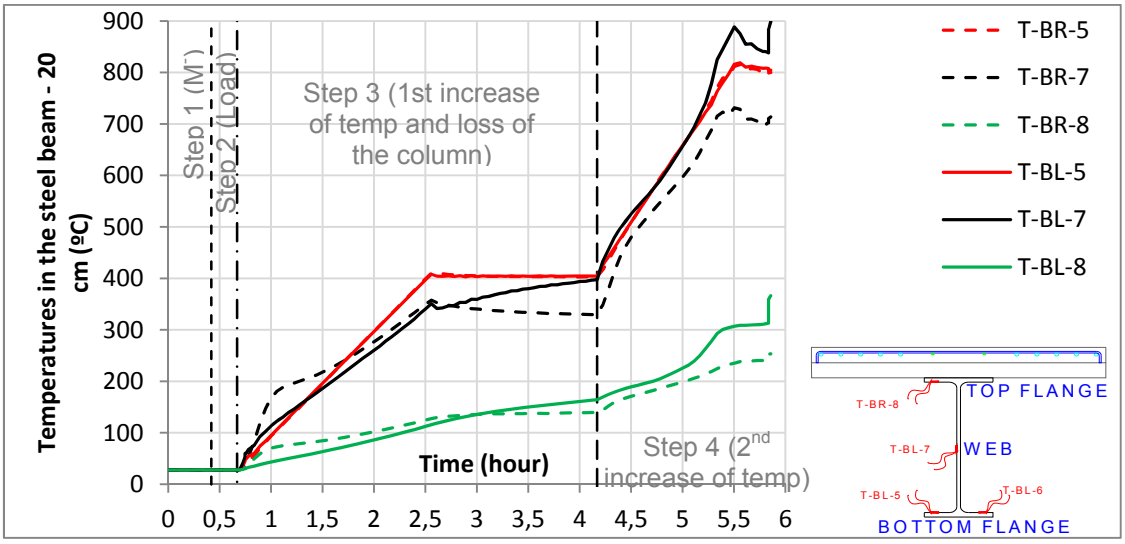

Figure 287: Evolution of the temperatures (T) in the beams at 20 cm from the connection during the test 7 (BR = beam right; BL = beam left)

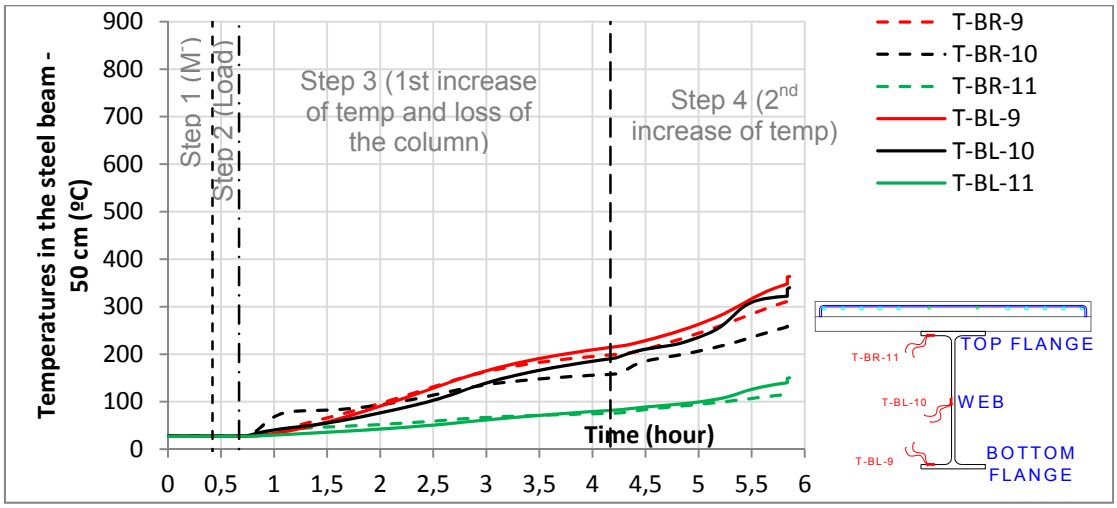

Figure 288: Evolution of the temperatures (T) in the beams at 50 cm from the connection during the test 7 (BR = beam right; BL = beam left)

Figure 289, Figure 290 and Figure 291 show the evolution of the temperatures at shank and at head of the bolts at each side of the joint, and at the end-plates surface.

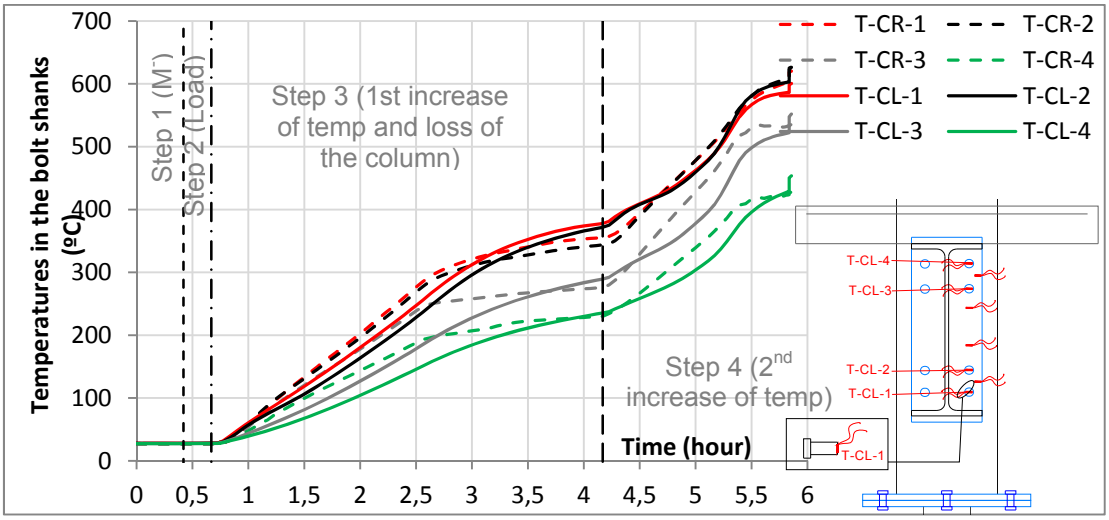

Figure 289: Evolution of the temperatures (T) in the shank of the bolt during the test 7 (CR = connection right; CL = connection left)

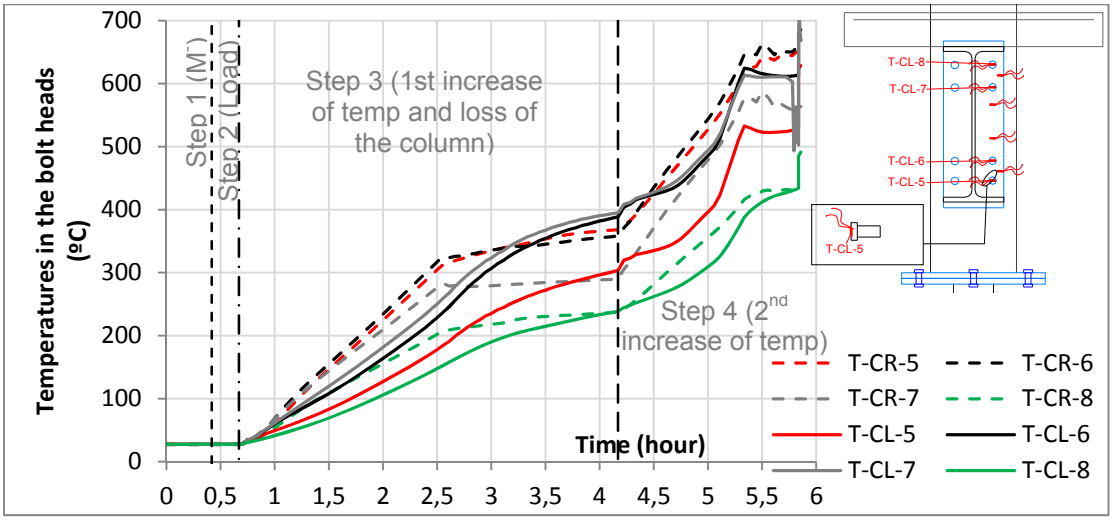

Figure 290: Evolution of the temperatures (T) in the head of the bolts during the test 7 (CR = connection right; CL = connection left)

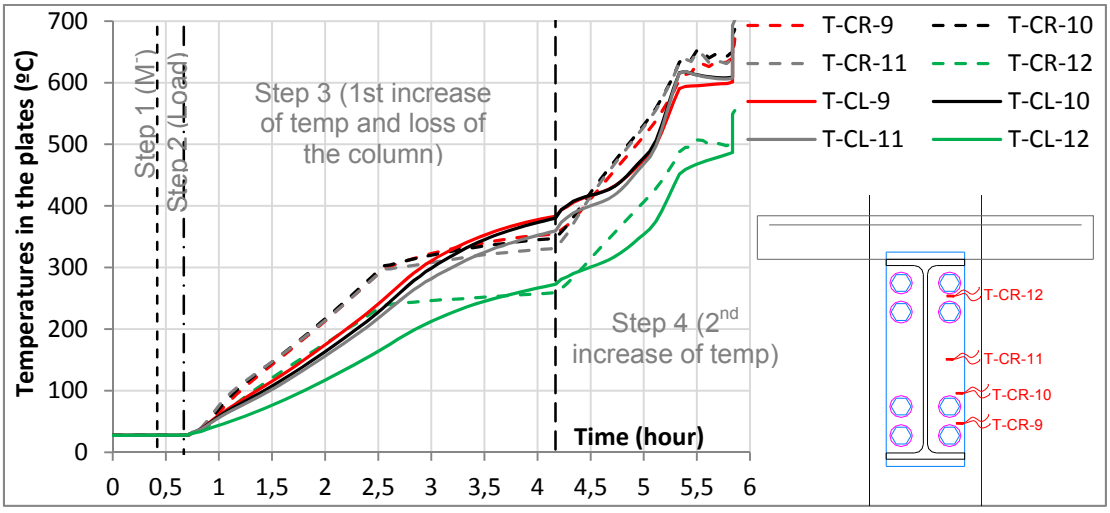

Figure 291: Evolution of the temperatures (T) in the end-plates during the test 7 (CR = connection right; CL = connection left)

The evolutions of temperatures in the main column and in the bottom column are presented in Figure 292 and Figure 293 respectively.

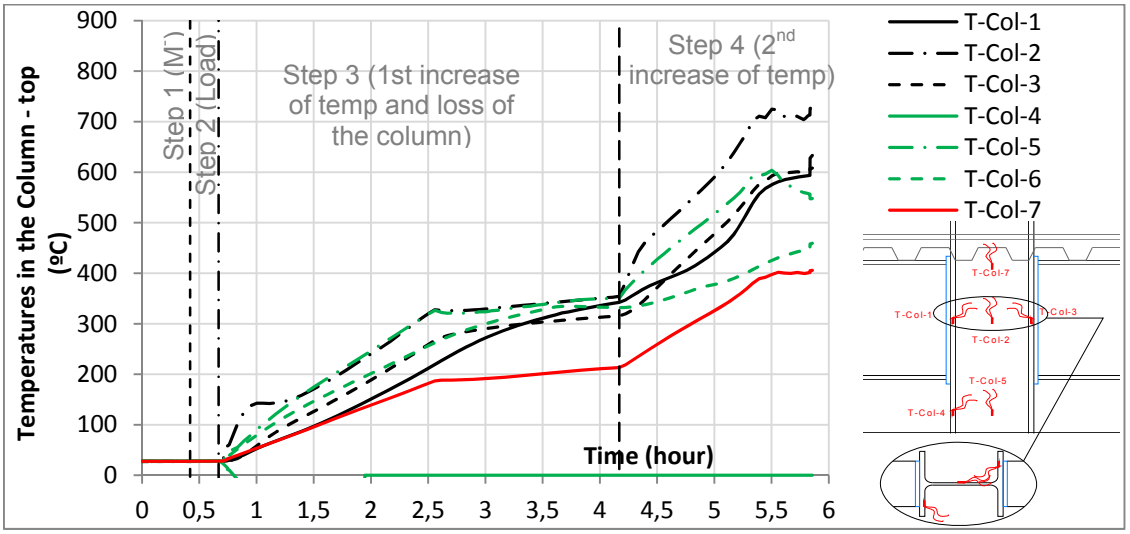

Figure 292: Evolution of the temperatures in the column (joint zone) during the test 7

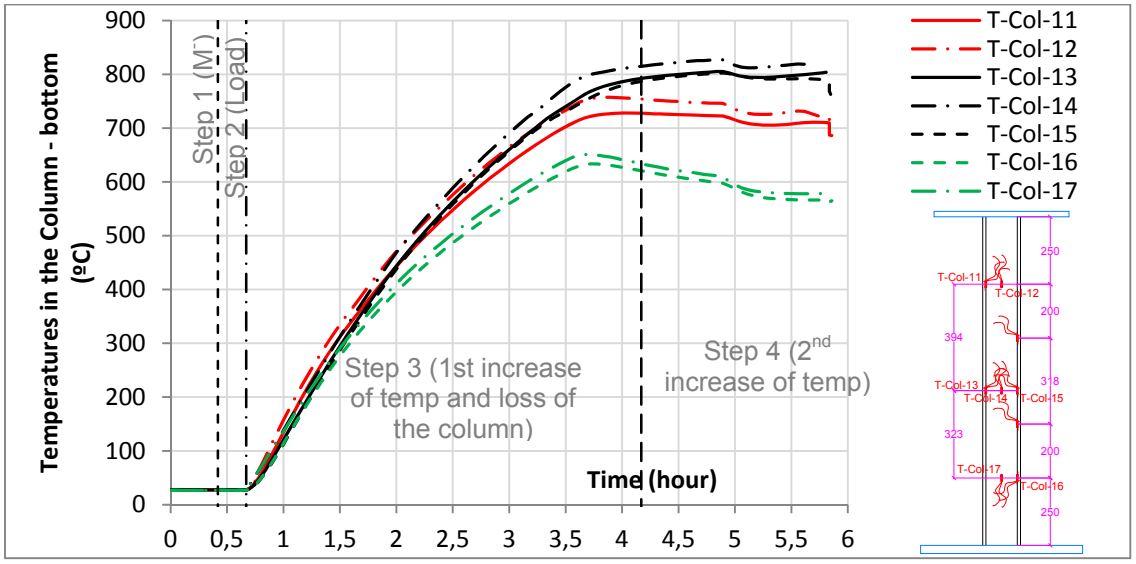

Figure 293: Evolution of the temperatures in the bottom column during the test 7

The evolution of temperatures in the composite slab is depicted in Figure 294, and measured points are shown in Figure 34, section II.8.3 (p24).

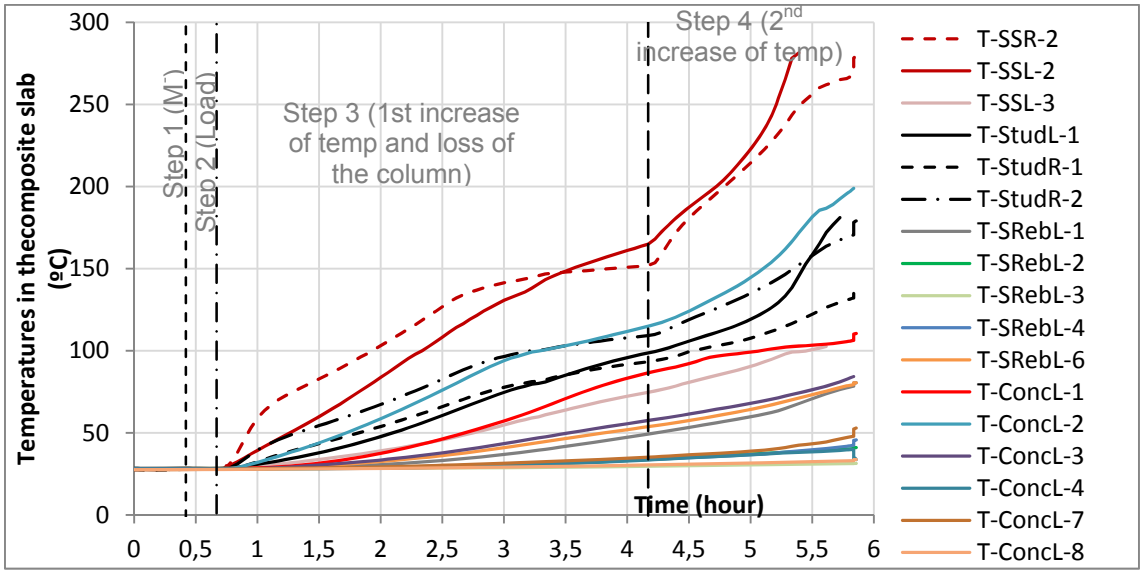

Figure 294: Evolution of the temperatures in the composite slab during the test 7

III.8.3.2 Evolution of the displacements and loads

In Figure 295, the evolution of the reaction loads in both beams supports (F_1+F_2) is compared with the reaction loads at the column (F_{HJ}+F3). The load at the jack was constant, equal to 250 kN. At the beginning of step 3, the reaction loads increased due to the thermal expansion in the heated zone: they reached a maximum value (-359 kN). The following decrease of the loads is due to the loss of the bottom column.

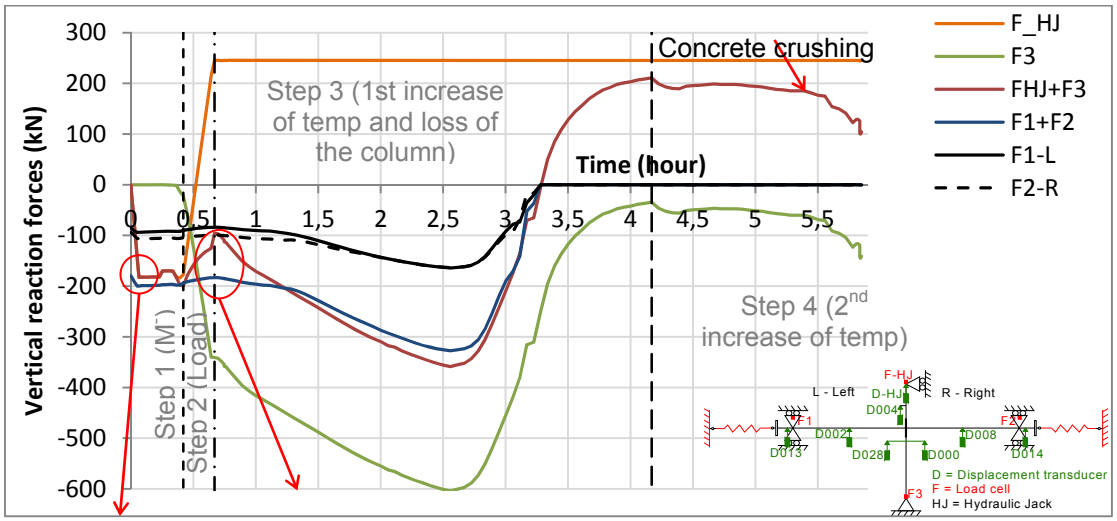

Figure 295: Comparison of the total load into the column (FHJ + F3) with the total reaction load at the beams supports (F1 + F2)

Figure 296 and Figure 297 show the vertical displacements measured during step 3 and step 4 respectively: below the joint (D000 and D028), at the beams mid-span (D002 and D008), at the hydraulic jack located at the top of the column, and at the column top (D004).

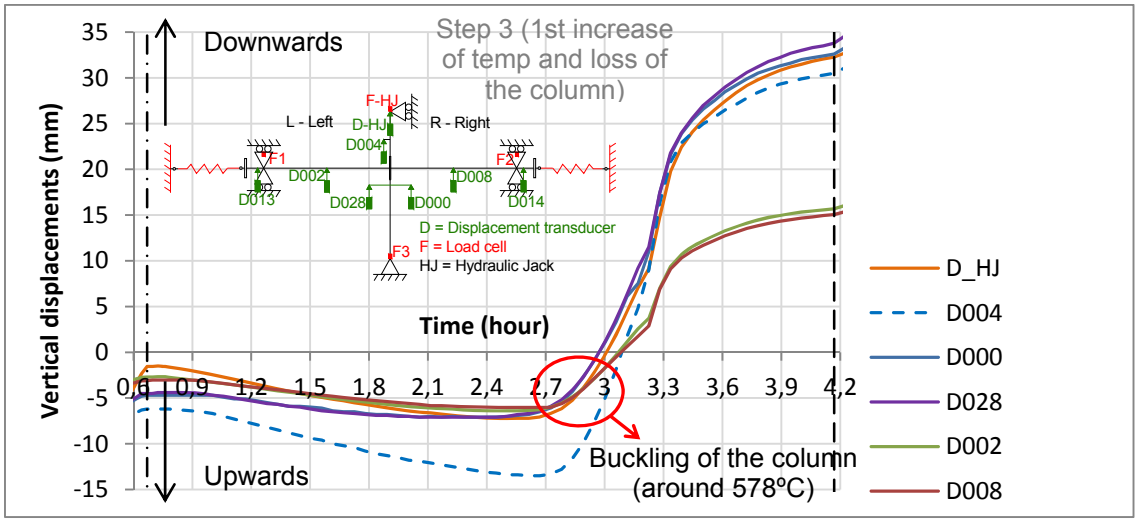

Figure 296: Vertical displacements near the beam-to-column joint during the increase of temperatures

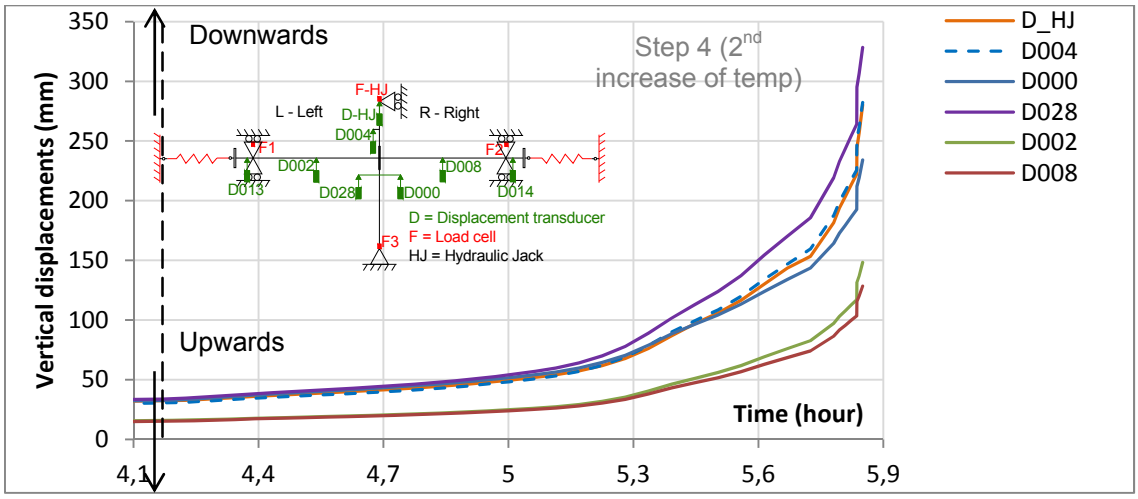

Figure 297: Vertical displacements near the beam-to-column joint during the increase of temperatures

Just a few moments after reloading the sub-frame (after the hydraulic jack stroke increase), the sub-frame collapsed and the test was stopped. Three bolts failed during the test, but the failures were not observed on the loading curves.

Figure 298 shows the evolution of the bending moment *versus* time at the connections during the entire test. The bending moments of the right and left connections are equal because they were calculated based on the vertical load at the column.

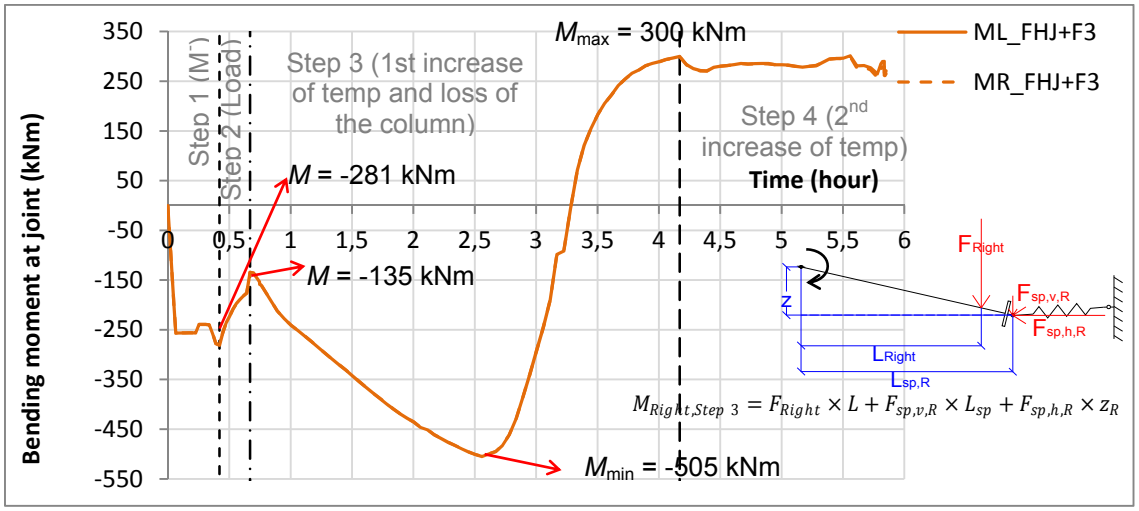

Figure 298: Evolution of the bending moment in the connections (Left and Right) during the test

For the two last tests (6 and 7), a pin at the top of the jack had to be added. During test 6, the column remained vertical and the column rotation could be estimated using the measured displacement D016, with the assumption that the jack remained vertical just like the column. During the test 7, the column and the jack rotated a lot. But due to a lack of instrumentation, the true rotation was not measured, and was estimated using the following expression:

$$\alpha_{column} = atan\left(\frac{D000-D028}{1500\ mm}\right) \times 1000\ [\text{mrad}] \qquad \text{(rotation > 0 in the clockwise)}$$

Of course, this value is not accurate because: i) the two displacements D000 and D028 were measured using wire transducers, which did not remain completely vertical due to the rotation of the column, and ii) the two bars welded to the column and at which the wire transducers were connected could slightly deform due to the effect of high temperatures.

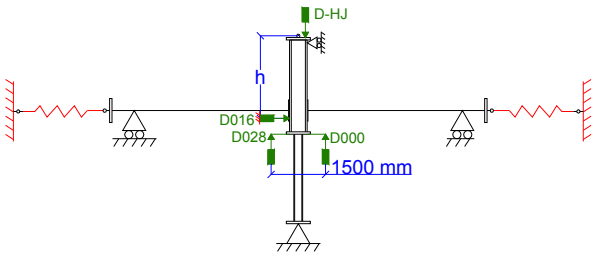

Figure 299: Measured displacements for the calculation of the column rotation

Figure 300 and Figure 301 present the evolution of the total reaction load vs the joint rotation and the beam axial load respectively.

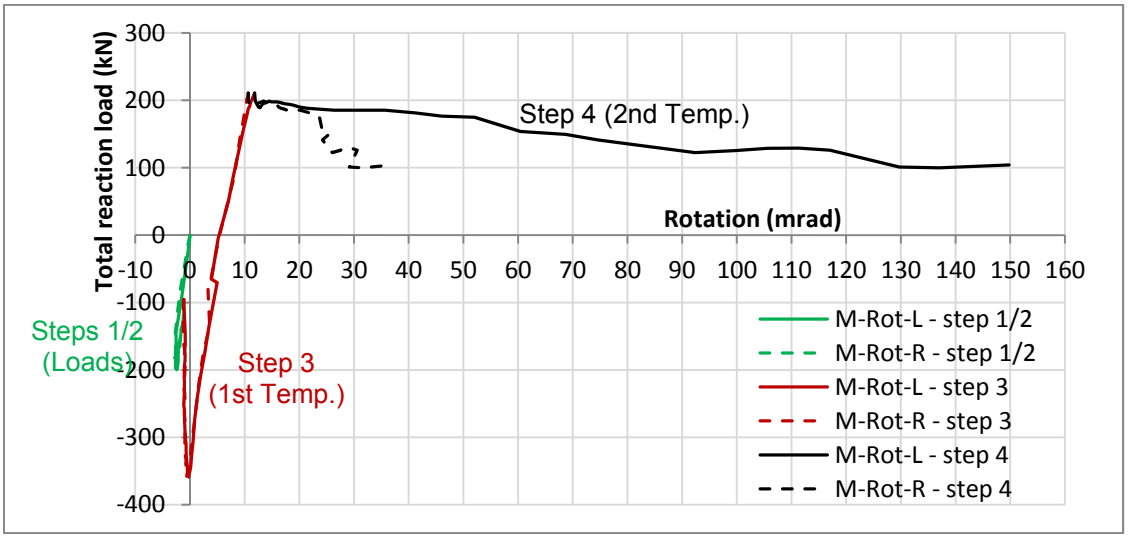

Figure 300: Total reaction load (F_L+ F_R) vs rotation at the connection

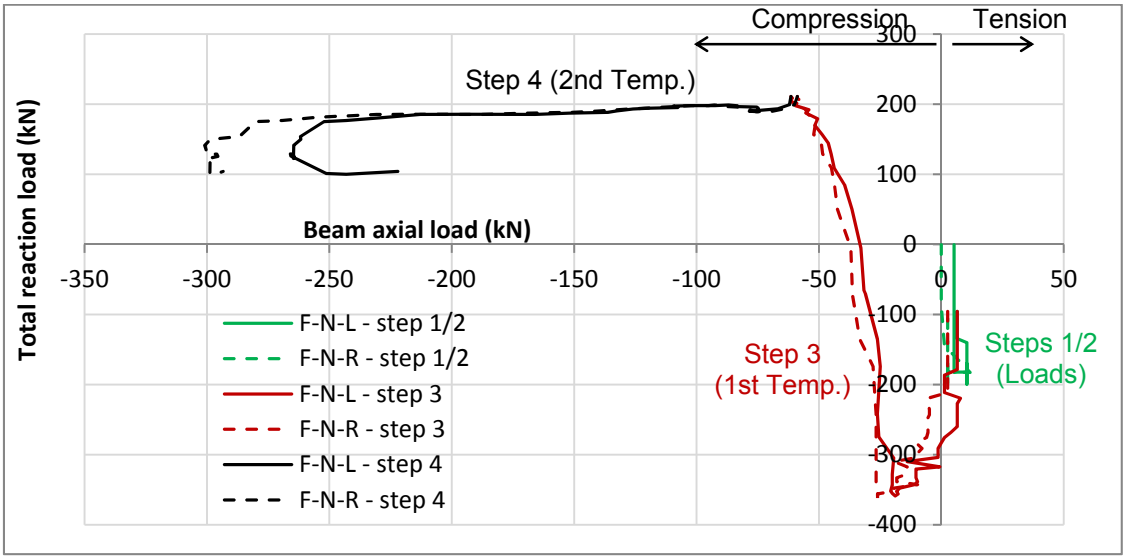

Figure 301: Total reaction load (F_L+ F_R) vs axial loads at the joint ($F_{restr,ax}$)

III.8.4 Additional data

The evolution of the vertical and horizontal components of the spring restraint loads, $F_{sp,v}$ and $F_{sp,h}$, are showed in Figure 302. The rotations of the springs are shown in Figure 303.

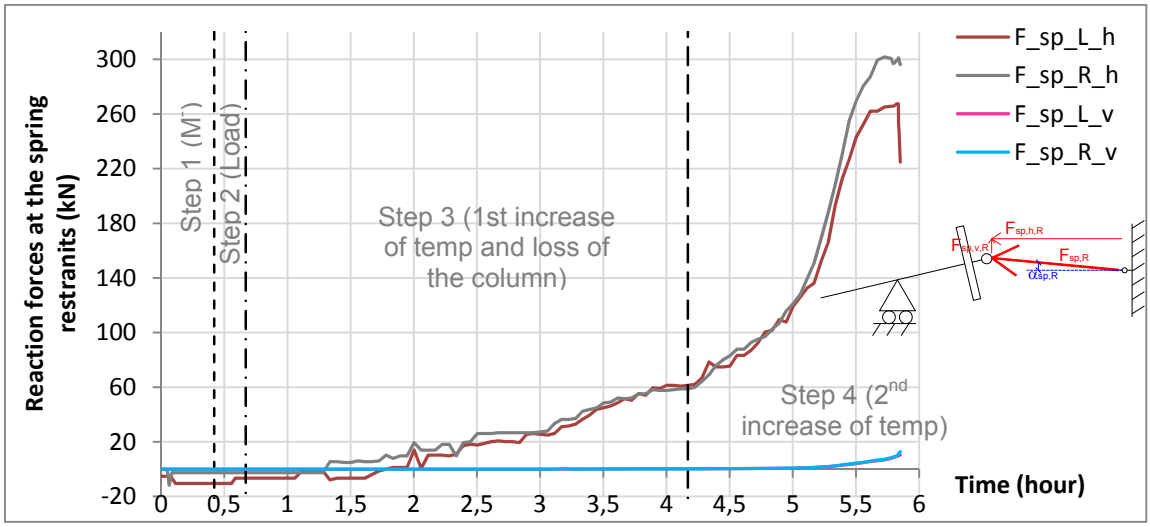

Figure 302: Projections of the spring loads along the horizontal (h) and vertical (v) axis

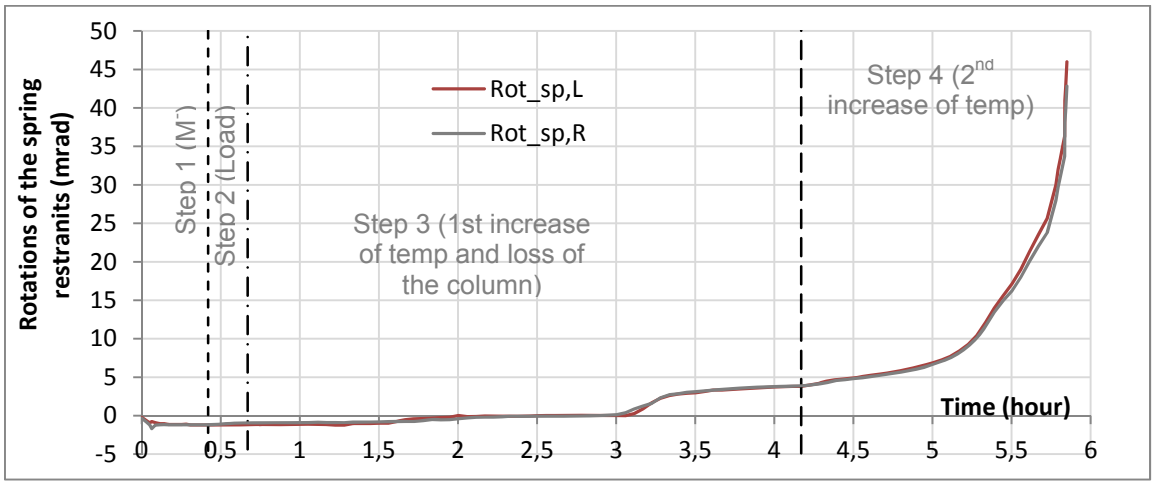

Figure 303. Spring rotations (L = left; R = right)

The horizontal displacements measured at the beam ends are showed in Figure 304. The estimated horizontal displacements at the neutral axis of the steel beams $D_{beam,h,L\ and\ R}$ are represented by the black curves (see §III.1).

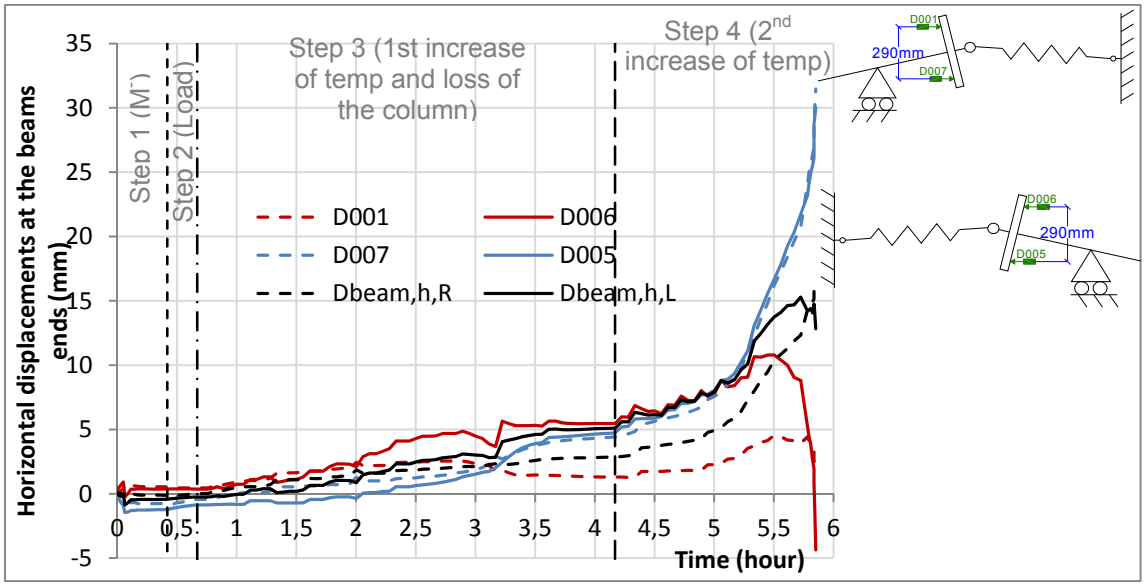

Figure 304: Horizontal displacements at the end of the left beam

Figure 305 presents the displacements of the beams out of the plan, measured by the displacement transducer D015 at the bottom column, by the two displacement transducers D025 and D026 at the beam ends, and by the two transducers D003 and D009 on the beams webs, initially situated at 1500 mm from the end-plate.

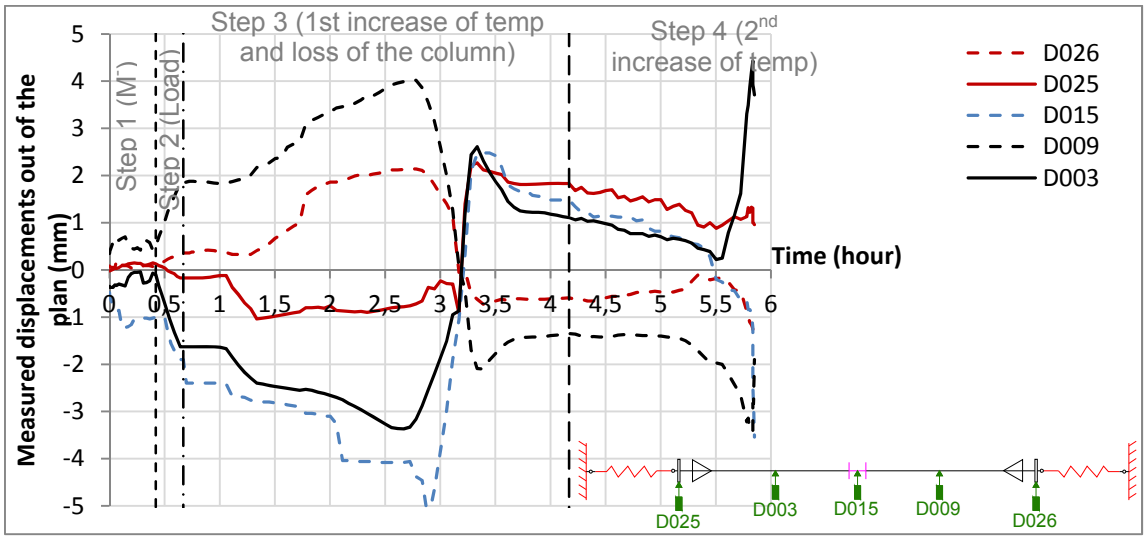

Figure 305: Evolution of the displacements measured out of the plan

Figure 306 presents the measured displacements of the auxiliary's structures (steel and concrete footings and strong beams connected to the strong walls).

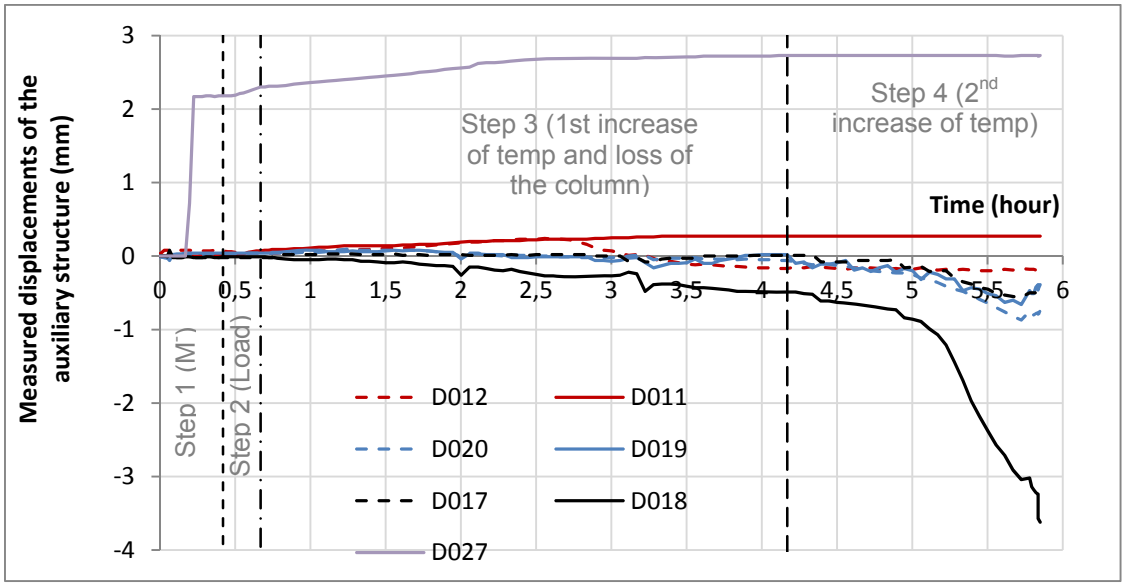

Figure 306: Measured displacements of the steel and concrete footings, and of the strong beams linked to the walls (see Figure 31 for the position of the displacement transducers)

IV Comparisons between the seven experimental tests

In order to simplify the comparisons between tests, only one connection from each joint is taken into account, which is either the connection where bolts failed, or, in case of no bolt failure, the connection the most deformed: left connection for tests 1, 2, 3, 5 and 7, and right connection for tests 4 and 6.

IV.1 Summary results of tests 1 to 6

Figure 307 shows the evolution of the connection bending moment *versus* the joint rotation, and Figure 308 shows the total vertical reaction load at the column *versus* the vertical displacement measured at the column top. The hogging bending moment was initially reached during step 1, followed by a variation of this moment during the increase of temperatures in step 2. As described in section II.5.1, this initial hogging bending moment should have reach -450 kNm at ambient temperature (test 1) and -236 kNm for the tests at elevated temperatures (tests 2 to 6). The target initial hogging bending moment was well reached in tests 1, 4 and 6, but some difficulties were faced in the laboratory, and this bending moment was higher of around 75% in tests 3 and 5, and lower of 14% in test 2. At the beginning of step 2, reaction loads increased due to the thermal expansion of the structure; the reaction loads reached a minimum value and the minima hogging bending moments reached around -500 kNm in tests 1, 3, 5 and 6, and around -357 kNm in tests 2 and 4. After that, these reaction loads decreased because of: i) the steel properties degradation due to high temperatures (higher than 600ºC in the webs of the steel beams) in tests 3, 4, 5, and 6; ii) the slight loss of the column support in test 2 due to oil losses in the bottom cylinder.

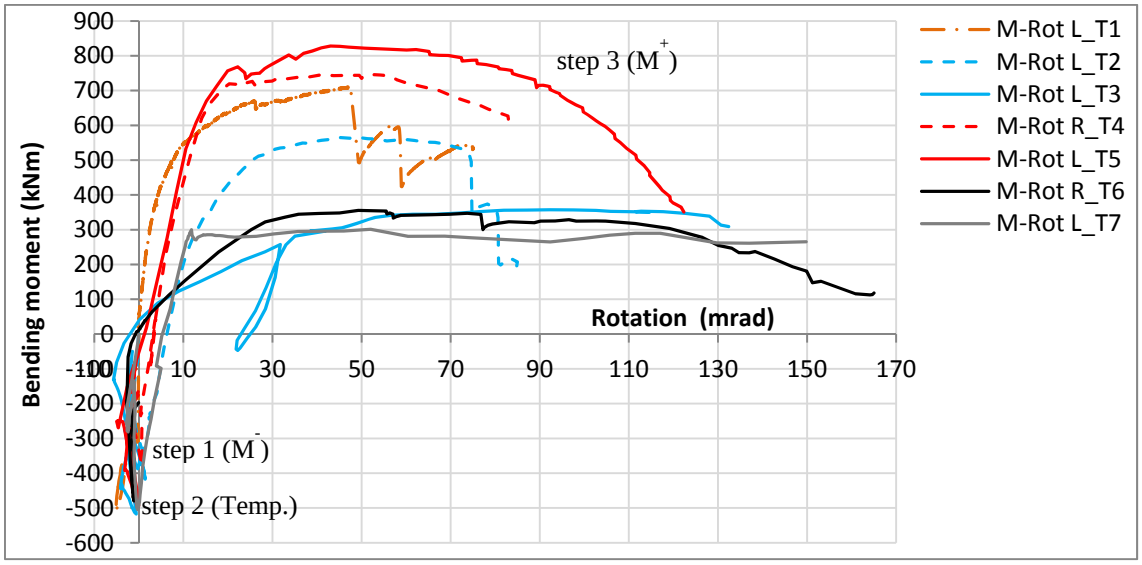

Figure 307: Joint bending moment vs rotation at the connection

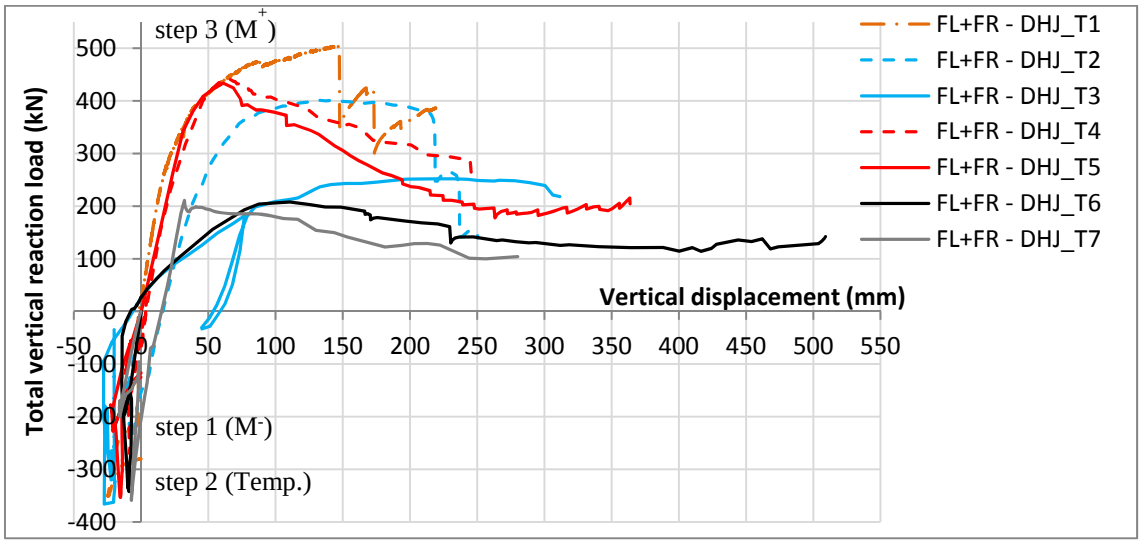

Figure 308: Total reaction load vs vertical displacement measured at the column top

Beams bottom flanges temperatures reached 500ºC in tests 2 and 4, and 700ºC in tests 3, 5 and 6: Figure 309 shows the temperatures measured during test 2. At about 40 min., during step 2, the temperature increase rate was modified from the maximum rate to 300ºC/hour, which created a peak in temperatures curves. Finally, 500ºC was reached in the beam bottom flanges, whereas the temperature increased faster in the web because of the reduced thickness. Temperatures in beams top flanges were much lower because they were only heated by heat transfer from web, which was reduced by the composite slab protection. During step 3, the temperature was well kept constant in the beam bottom flanges. Concrete temperatures did not rise above 200ºC.

The loss of the column was really progressive as the hydraulic jack at the column top imposed a constant displacement rate. Concrete crushing in compression was the first failure observed under sagging bending moment, but this failure was really progressive; first the concrete crushed against the column flanges (Figure 310a), and then the entire slab width failed (Figure 310b, c).

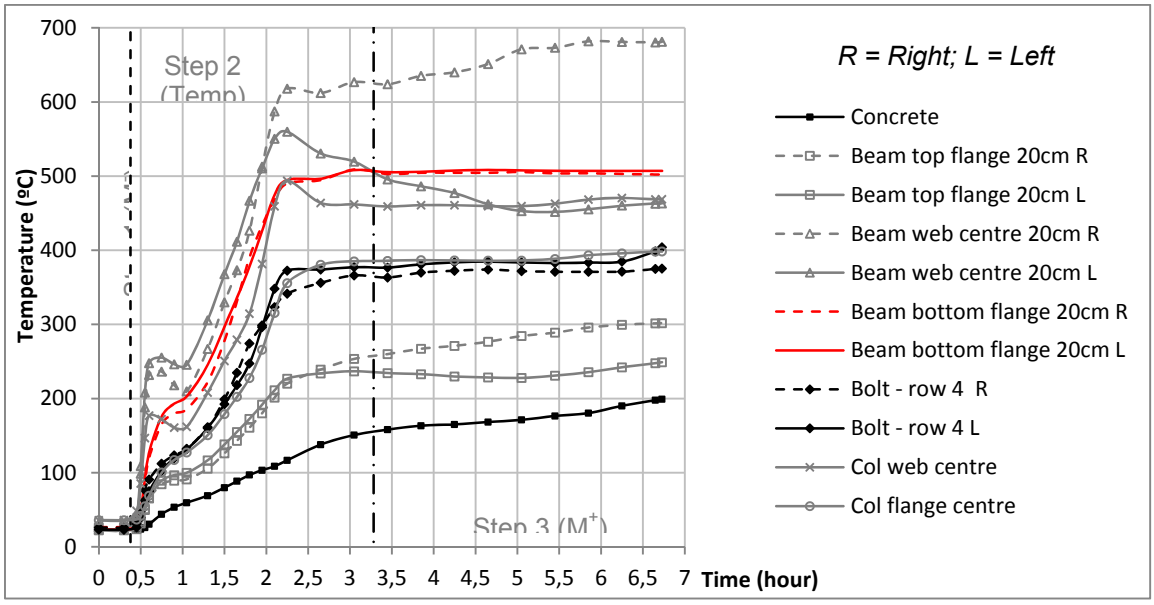

Figure 309: Evolution of the temperatures during test 2

a) b) c)

Figure 310: Concrete crushed: a) against the column flanges; b) along the entire slab width; c) at the end of the test (front view of test 6)

Bolts failures happened in tests 1, 2 and 6 (respectively under 47.5 mrad, 73.6 mrad and 83.3 mrad of connection rotation); the other tests were ended because the maximum vertical displacement of the hydraulic jack at the column top was reached. The failed bolts were identified in the bottom bolt rows, because of higher tensile forces under sagging bending moment. An "unloading-reloading" was performed at the beginning of the step 3 for tests 3, 4 and 5, and it allowed a better characterization of the elastic stiffness of the joint. In tests 1 and 6, this "unloading-reloading" was not performed because of the difficulties to manually control the spring restraints at the ends of the beams.

The evolution of the bending moment at the joint *versus* the beam axial load is presented in Figure 311 for tests 1, 4, 5, 6, and 7. In the following comparisons of the results, the test 1 is considered as performed without any restraint to the beam (see §II.7.2.3, p22). The restraints were connected to the beams since the beginning of the test. During step 1, the loads and displacements created by the application of the initial hogging bending moment were not enough to develop axial loads to the beams. During step 2 and at the beginning of step 3, the beam ends were moving outwards and the restraints worked in compression; then compression loads decreased during step 3, and tensile loads were reach at the end of the test 6.

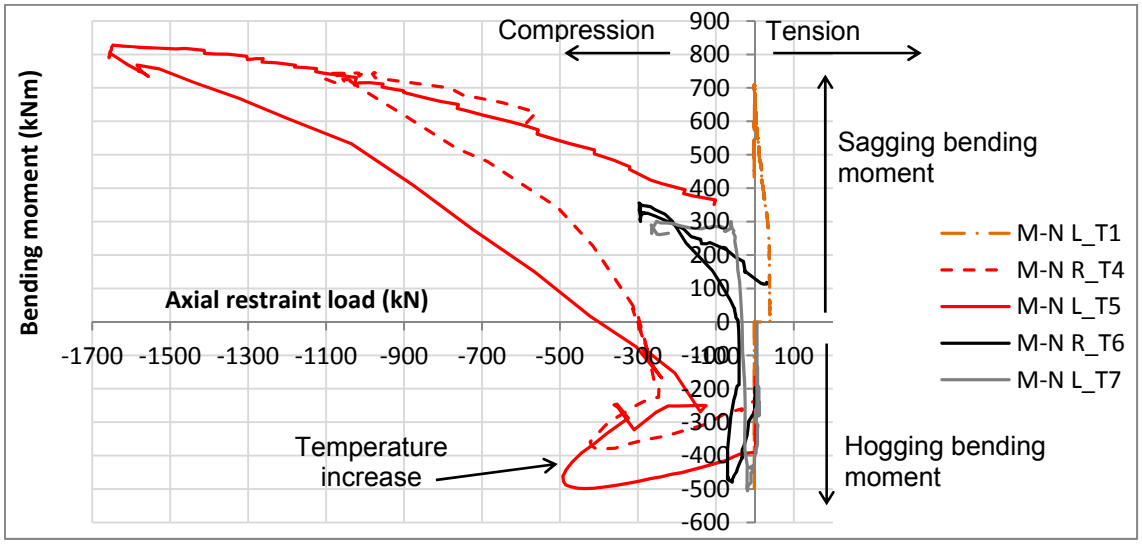

Figure 311: Joint bending moment vs axial loads at the joint

It was observed that the maximum axial compression load was reached: i) for a vertical displacement of the joint varying between 100 mm to 210 mm (Figure 312); ii) once the concrete from the slab was crushed in compression in tests 4 and 5. In test 6, the maximum axial compression load was not reached due to the limitation of the hydraulic system at 300 kN in compression (Figure 313), but it can be assumed that the maximum value would correspond to the 1st bolt failure.

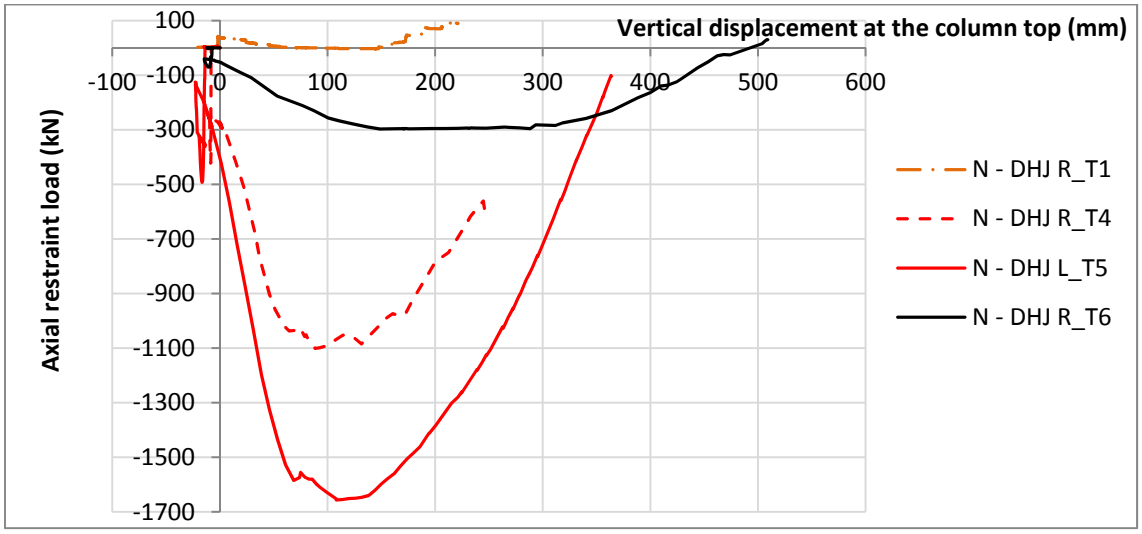

Figure 312: Vertical displacement measured at the column top vs axial loads

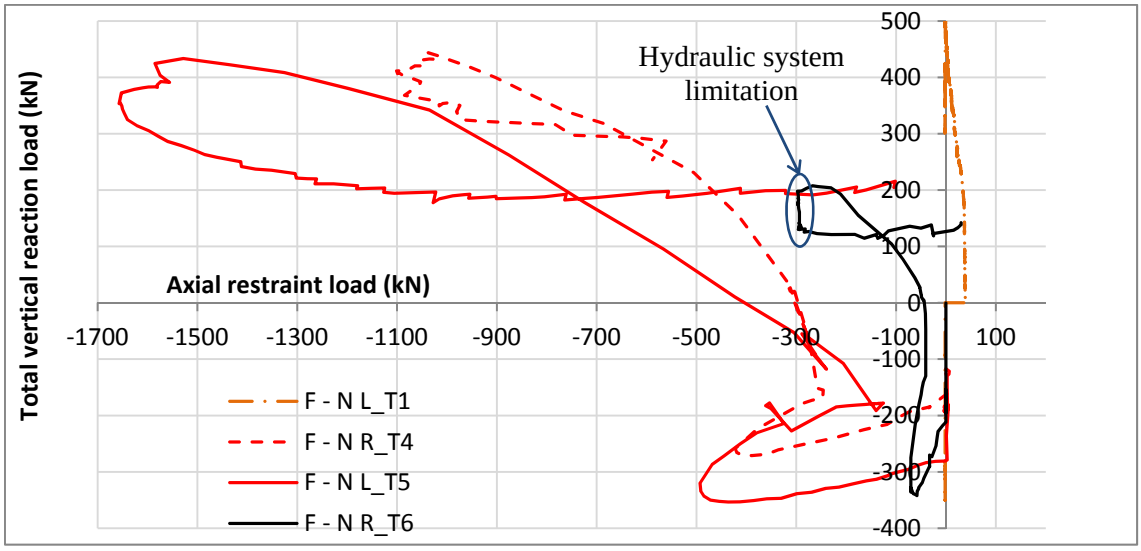

Figure 313: Total reaction load vs axial loads at the joint

Table 22 summarizes the main results of each test: the failure modes, the local deformations, the connection rotation at the end of the test and the symmetrical or unsymmetrical behaviour of the joint defined by the column rotation; in tests 3 and 7, the column rotated and the joint deformation was not symmetrical. The final deformation of the sub-frame of test 6 is showed in Figure 314.

Figure 314: Final deformation of the tested structure (test 6)

Table 22: Failure modes and local deformation of each test

Test	Temp (ºC)	Restraint (kN/mm)	Connection rotation* (mrad)	Col. rotation* (mrad)	Failure modes	Local deformations
T1	20	0 in comp., 50 in tension	74.9	-6	Concrete crushing in compression; failure of 2 bolts in tension (left side); crack at the end-plate bottom (left)	End-plate bottom and centre
T2	500	0	84.8	Not measured	Concrete crushing in compression; failure of 3 bolts in tension (left side)	End-plate bottom and centre
T3	700	0	132.4	-33	Concrete crushing in compression; failure of 2 bolts in tension (left side) during the cooling phase	End-plate bottom and centre; Column web (bottom part); Beam left bottom flange
T4	500	Total	89.4	2	Concrete crushing in compression; failure of 2 bolts in tension (right side) during the cooling phase	End-plate bottom and centre; Column web (top part); Beams webs; Column left flange deformed
T5	700	Total	122.3	6	Concrete crushing in compression	End-plate bottom and centre; Column web (bottom part); Top flange of the right beam; Plastic hinge at the right beam
T6	700	50	183.5	10	Concrete crushing in compression; failure of 3 bolts in tension (2 on the right - 1 on the left)	End-plate bottom and centre; Beams bottom flanges
T7**	400; 800	50	149.8	-63	Column failure; Concrete crushing in compression; failure of 3 bolts in tension (left side); crack at the end-plate bottom (left)	End-plate bottom and centre

* Rotations measured at the end of each test;

** Test 7 (demonstration test) is presented in §IV.2.

Finally, Figure 315 and Figure 316 show the final deformations respectively for tests 1 to 3 (without axial restraint to the beam), and tests 4 to 6 (with axial restraint to the beam). The steel end-plates deformed in the bottom and centre part in all tests, even at ambient temperature, and showed a high ductility. Due to high stresses/deformations, a crack at the base steel end-plate, just above the weld, was observed at the end of the test 1 at ambient temperature. Moreover, the localised deformation mode observed at the steel end-plate centre should happened because of the joint configuration: i) 4 bolt rows and quite a high space between the rows 2 and 3 (260 mm), ii) the end-plate (15 mm) was thinner than the column flange (19 mm), and iii) an initial

deformation noticed just after the bolts pre-loading (0.6 mm was measured for the reference test). Moreover, it seems that the beam web was pulling the end-plate due to the sagging bending moment (tensile loads at the bottom part), and the deformation of the end-plate was amplified where it was not linked by bolts to the column flange: in the bottom part and in the centre of the end-plate.

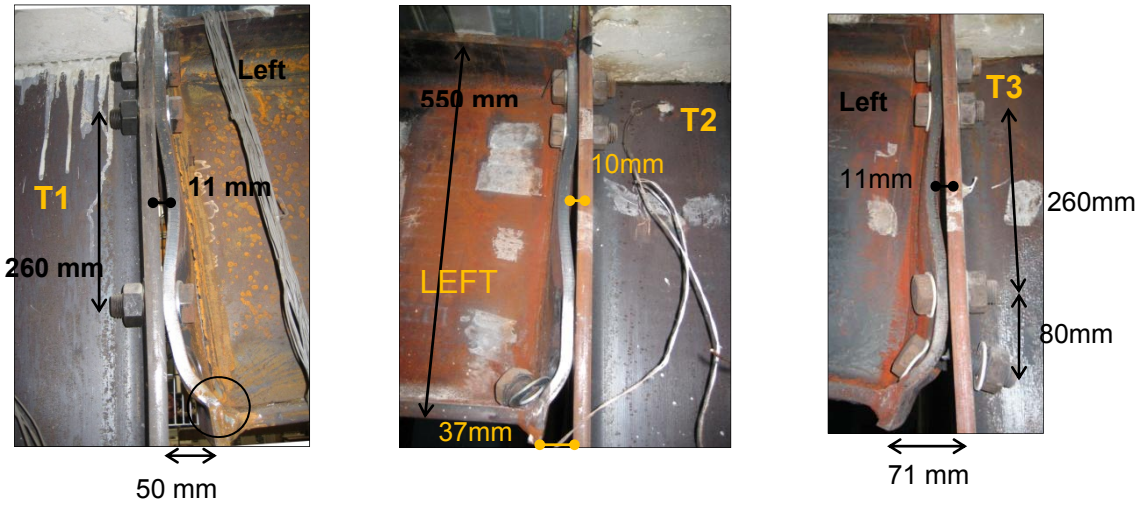

Figure 315: Deformations of the connections for tests 1, 2 and 3

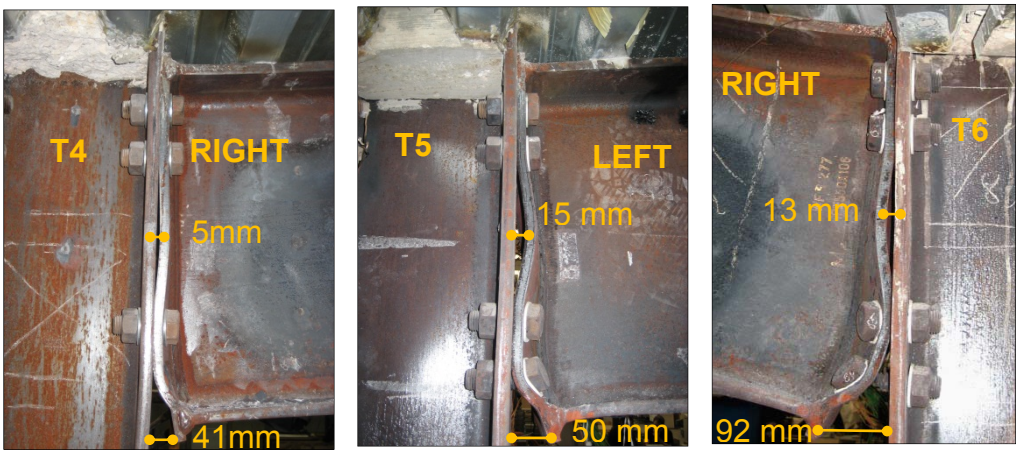

Figure 316: Deformations of the connections for tests 4, 5 and 6

Figure 317 presents the bolts failed in tests 1, 2 and 6. It could be noticed that the bolt failure in test 6 (at around 600ºC) was characterized by a smoother failure than in tests 1 or 2, for which temperatures (respectively 20ºC and around 400ºC) were not yet sufficient to decrease the steel properties.

Figure 317: Bolts failed in tests 1, 2 and 6

IV.2 Summary results of the demonstration test (test 7)

The objective of the demonstration test was to reveal the real behaviour of the sub-frame joint when subjected to a localised fire which leads to the loss of a column. Four main loading steps were defined by: step 1 – Initial hogging bending moment; step 2 – Mechanical loading (constant gravity load of 250 kN); step 3 – 1st increase of temperatures and column loss (400ºC in beams bottom flanges and 800ºC in the bottom column); and step 4 – 2nd increase of temperature and failure of the sub-frame. The bending moment/rotation, load/displacement and bending moment/axial loads curves were presented in Figure 307, Figure 308 and Figure 311, respectively. The hogging bending moment was initially reached during step 1 (-281 kNm). During step 2, the hydraulic jack increased the load at the column top up to reach +250 kN; however, due to clearances at the column base, the total load at the column reduced from -200 kN to -96 kN, and consequently the hogging bending moment was reduced to -134 kNm. In step 3, the beams were heated up to 400ºC in the bottom flanges, and joint components and column reached lower temperatures (Figure 318); the bottom column was heated up to 800ºC. First reaction loads increased under thermal expansion effects and reached a maximum value of -359 kN (bending moment equal to -505 kNm); then the bottom column reached its maximum resistance capacity under 578ºC and failed. The failure of the column was really progressive, and was defined as the moment at which the vertical reaction load came back to its initial value at the beginning of the step 3 (95.6 kN). At the end of the step 3, the total load was equal to +211 kN, and the column top dropped of 25 mm; Figure 319 presents the evolution of the vertical displacements *versus* time. The sagging bending moment increased up to 300 kNm, and the compression axial loads to the beams reached 61 kN.

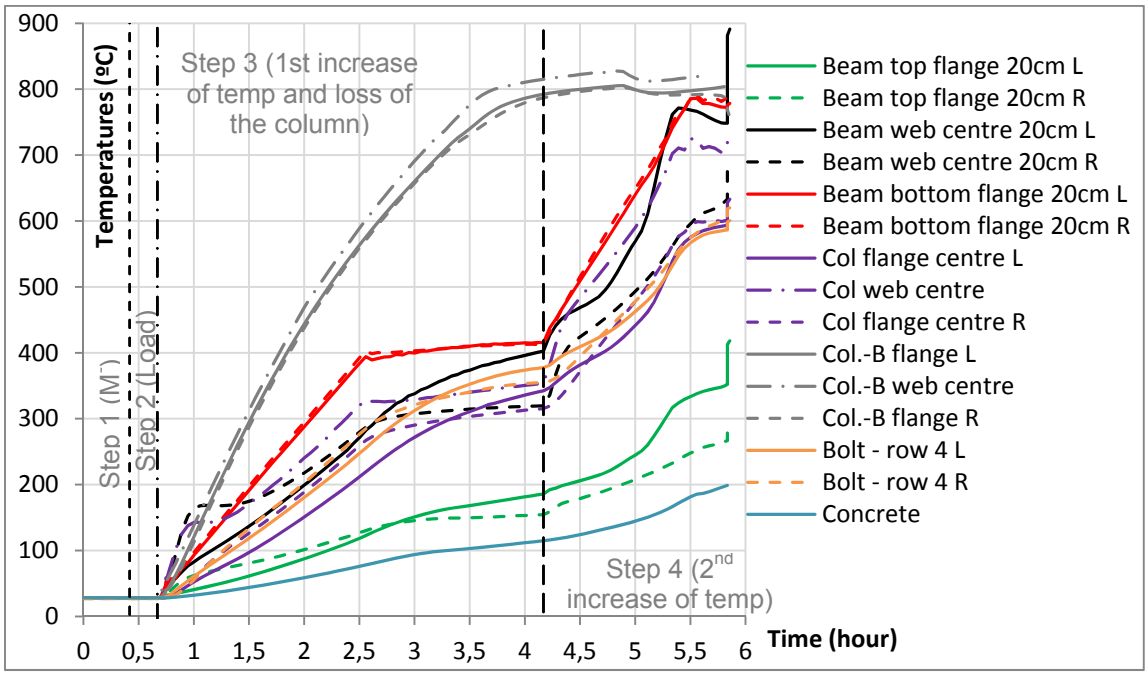

Figure 318: Evolution of the temperatures during test 7 (in beams at 200 mm from the connection, in column centre, in bottom column HEB 140 (Col.-B), in row 4 bolts and in concrete rib in contact with the steel beam)

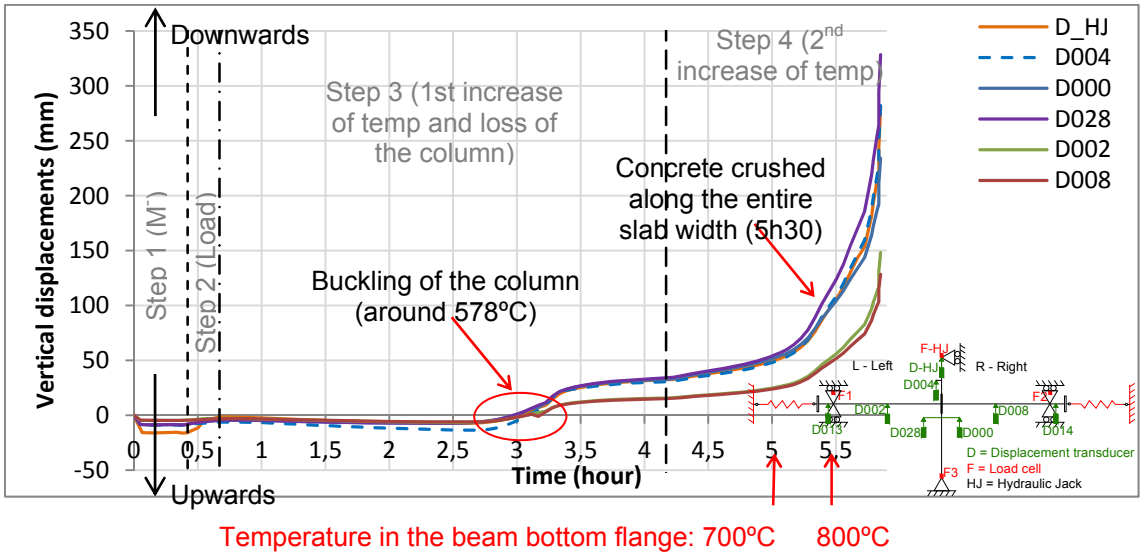

Figure 319: Evolution of the vertical displacements during the entire test 7

During step 4, the temperature in the joint increased under the constant load (+250 kN) applied at the top of the column and reached 770ºC in the beam bottom flange: the concrete slab began to crush against the column flange; the vertical displacement increased faster (Figure 276), and once the concrete slab was completely crushed, beam bottom flanges temperature reached 800ºC and the sub-frame completely failed. The test was stopped at a vertical displacement equal to 280 mm, at 150 mrad and 37 mrad of connection left and right rotations, the total vertical reaction load was 104 kN, and axial compression loads at the spring restraints were reduced from 266 kN to 222 kN after the concrete crushing. The sagging bending moment was slightly decreased from 290 kNm to 265 kNm. The day after the test, the failure of three bolts from the left connection was observed: two bolts at the row 4 and one bolt at the row 3 (Figure 320a), but the failures were not observed on bending moment/rotation and load/displacement curves. The steel end-plates deformed in the bottom and centre part, and due to high stresses/deformations, a crack at the base steel end-plate, just above the weld, was observed. Figure 320b shows the final deformation of the sub-frame.

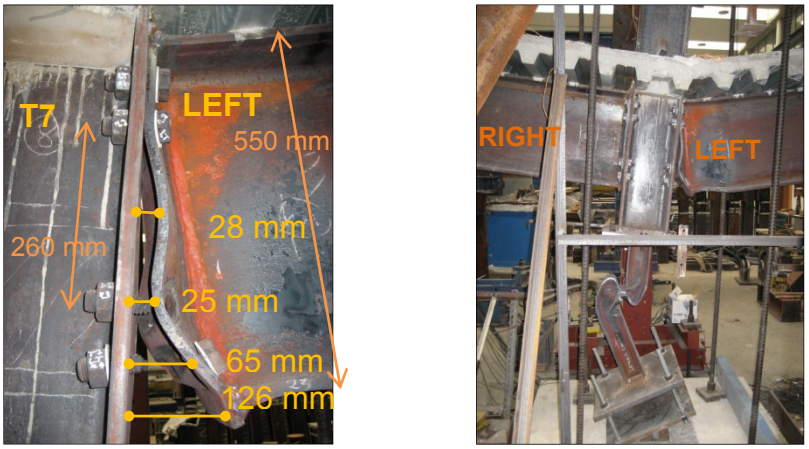

a) b)

Figure 320: a) Deformations of the left connection, and b) final deformation of the sub-frame (test 7)

IV.3 Effects of the temperature

In the tests performed without axial restraint to the beam (tests 1, 2 and 3), the maximum reaction load (F_{max}) and the corresponding maximum bending moment (M^{+}_{max}) decreased by 20% at 500ºC, and by 50% at 700ºC. Under these maxima loads, the connection rotation (θ_{M+max}) was more or less equal at 20ºC and 500ºC, but was increased by 97% at 700ºC (Table 23).

Table 23: Comparisons of the results: maximum sagging bending moment M^{+}_{max} (tests 1, 2, 3)

No axial restraint	**T1**	**T2**	**T3**	**Diff. T1-T2 (%)**	**Diff. T1-T3 (%)**	**Diff. T2-T3 (%)**
Temperature	20ºC	500ºC	700ºC			
M^{+}_{max} (kNm)	710.1	565.0	357.1	-20.4	-49.7	-36.8
Max. vert. load F_{max} (kN)	504.4	401.5	252.0	-20.4	-50.0	-37.2
Vert. displ. (mm)	145.6	143.6	220.3	-1.4	51.2	53.4
Rotation θ_{M+max} (mrad)	46.9	49.5	92.3	5.5	96.6	86.5

In test 1, just after the increase of the jack stroke (performed after the concrete crushing), loads continued to linearly increase, and leaded to a maximum sagging bending moment equal to 710 kNm, which is 21% higher than the theoretical value calculated in Haremza et al. (2012), section II (588 kNm).

Table 24 presents the initial stiffness of the load/displacement curves (Figure 308) estimated just after the column loss, or at the reloading curve in case that the "unloading-reloading" was performed. It can be observed that the initial stiffness of tests 3 and 6 (700ºC) were much lower than the other ones, but the reloading performed in test 3 showed a higher realistic stiffness (8 kN/mm); unfortunately, the "unloading-reloading" could not be performed in test 6, and the real stiffness is unknown. In comparison to the ambient temperature result (test 1), the effect of the temperature affects the initial stiffness and decreases it by 36% at 500ºC (test 2) and by 49% at 700ºC (test 3); the initial stiffness was also decreased by 21% between tests 2 (500ºC) and 3 (700ºC).

Table 24: Initial stiffness of the load/displacement curve after the column loss

TEST	**Temp. (ºC)**	**Restraint (kN/mm)**	**Initial stiffness (kN/mm)**	**Reloading stiffness (kN/mm)**
T1	20	0; 50	15.7	**---**
T2	500	0	10.1	**---**
T3	700	0	2.6	8.0
T4	500	Total	13.9	18.5
T5	700	Total	11.3	12.3
T6	700	50	2.9	**---**
T7	400; 800	50	10.9	**---**
		Average	11.2	

Table 25 presents the maxima rotations corresponding to the 1st bolt failure (tests 1, 2 and 6) or to the end of the test if no bolt failure was identified (tests 3, 4, 5, 7). In test 1, the first bolt failed for 49 mrad of rotation (503 kN); in test 2, the first bolt failed at 74 mrad of rotation (352 kN), and no bolts were failed at 132 mrad of rotation in test 3 (311 mm of vertical displacement). In comparison to test 1 at 20ºC, the rotation was then increased by 55% at to 500ºC (test 2), and by at least 179% at 700ºC (test 3). The rotation corresponding to the

maximum sagging bending moment θ_{M+max} was increased by 64% at the 1st bolt failure in test 2 and by 53% in test 6.

Table 25: Maxima connection rotation for each test, and the corresponding values of the vertical reaction load, axial load, sagging bending moment, and vertical displacement

TEST	Temp. (ºC)	Axial restraint (kN/mm)	Vertical reaction load (kN)	Vert. displ. (mm)	Axial load N (kN)	Bending moment (kNm)	Max. Rotation (mrad)	
T1	20	0; 50	502.5	147.5	-1.3	707.4	47.5	*1st bolt failure*
T2	500	0	375.1	215.5	0.0	527.9	73.6	*1st bolt failure*
T3	700	0	218.1	311.4	0.0	309.1	132.4	*end of the test*
T4	500	Total	253.8	245.8	-588.0	592.6	89.4	*end of the test*
T5	700	Total	204.5	363.8	-104.5	351.1	122.3	*end of the test*
T6	700	50	161.0	229.5	-293.6	343.9	83.3	*1st bolt failure*
T7	400; 800	50	104.1	280.2	-222.0	265.1	149.8	*end of the test (3 bolts failed)*

In tests 4 and 5, during the increase of the temperatures (step 2), the axial and vertical loads increased more in test 5 than in test 4 (Figure 311), due to the higher dilatations under 700ºC. During step 3, for a same axial compression load, the sagging bending moment in test 5 at 700ºC was lower than in test 4 (500ºC) because of the reduced steel properties. In test 5, under the maximum bending moment reached in test 4 (746 kNm), the axial load from the restraint was 58% higher. Table 26 shows that the maximum bending moment reached in test 5 was 11% higher than in test 4; at this point, the vertical reaction load was 5% lower in test 5, but the compression axial restraint was 66% higher; the rotation and vertical displacement were respectively 22% and 15% lower in test 5. Test 5, under higher steel temperatures, reached higher bending moment/axial restraint load than test 4 certainly because of the non-uniform concrete slab thickness in test 5. Indeed, during the concreting of test 5, a support situated near the column (back side) fell down, which created a higher thickness of the slab on this side (the slab thickness on the front side was 60 mm, whereas the slab thickness on the back side was 100 mm). As the concrete was only slightly heated, the concrete properties were not decreased by temperature, and the compression resistance of the joint was increased by the slab thickness, even under higher steel temperatures.

Table 26: Comparisons of the results: maximum sagging bending moment M_{+max} (tests 4 and 5)

Total axial restraint	T4	T5	Difference (%)
Temperature	500ºC	700ºC	
M^{+}_{max} (kNm)	746.4	828.0	10.9
Vert. load F_{max} (kN)	355.6	336.5	-5.4
Axial load N (kN)	-990.7	-1646.7	66.2
Vert. displ. (mm)	154.7	132.2	-14.5
Rotation θ_{M+max} (mrad)	54.9	43.0	-21.5

Tests 4 and 5 are also compared together in relation to the maximum vertical reaction load (Table 27). It can be observed that both reached the same vertical reaction load, under more or less the same vertical displacement and rotation, but with more 47% of compression load from axial restraints in test 5 (700ºC).

Table 27: Comparisons of the results: maximum vertical reaction load F_{max} (tests 4 and 5)

Total axial restraint	T4	T5	Difference (%)
Temperature	500ºC	700ºC	
M^+ (kNm)	719.6	756.6	5.1
Max vert. load F_{max} (kN)	443.6	433.6	-2.3
Axial load N (kN)	-1037.6	-1528.2	47.3
Vert. displ. (mm)	64.4	61.0	-5.2
Rotation θ_{Fmax} (mrad)	20.6	19.9	-3.3

IV.4 Effect of the axial restraints to the beams

Tests 2 and 4 were both performed under 500ºC in the beams bottom flanges, respectively without any axial restraint to the beam and with total axial restraint to the beam. In test 4, the maximum reaction load was 11% higher (Table 28), the vertical displacement under maximum reaction load was 55% lower, the bending moment was 27% higher and the rotation was 58% lower than in test 2.

Table 28: Comparisons of the results corresponding to the maximum vertical reaction load F_{max} (tests 2 and 4)

500ºC	T2	T4	Difference (%)
M^+ (kNm)	no	total	
Max vert. load F_{max} (kN)	565.0	719.6	27.4
Axial load N (kN)	401.5	443.6	10.5
Vert. displ. (mm)	0.0	-1037.6	---
Rotation θ_{Fmax} (mrad)	143.6	64.4	-55.2
M^+ (kNm)	49.5	20.6	-58.4

The maximum bending moment reached 565 kNm in test 2, whereas in test 4, the maximum bending moment was increased by 32%, for a rotation only 11% higher (Table 29).

In test 2, the first bolt failed at 74 mrad of joint rotation (216 mm of vertical displacement). Under the same rotation in test 4, the total reaction load was 17% lower, the bending moment was 32% higher and the axial compression load restraint was equal to 773 kN. So, due to the compression load from the axial restraint to the beam, the joint was able to resist to a higher sagging bending moment without any bolt failure. Indeed, the compression load from the axial restraint combined with sagging bending moment, moved the neutral axis of the connection downward, allowing the development of additional compression loads in the concrete slab, and reduction of the tensile loads in the bottom bolt rows. Once the concrete crushed against the column slab and along the entire slab width, tests 4 and 5 were still able to continue to deform without failure: between the maximum sagging bending moment and the end of the test, the rotation increased by 113% in test 4 and by 184% in test 5.

Table 29: Comparisons of the results: maximum sagging bending moment M^+_{max} (tests 2 and 4)

500ºC	T2	T4	Difference (%)
Restraint	no	total	
M^+_{max} (kNm)	565.0	746.4	32.1
Vert. load F_{max} (kN)	401.5	355.6	-11.4
Axial load N (kN)	0.0	-990.7	---
Vert. displ. (mm)	143.6	154.7	7.7
Rotation θ_{M+max} (mrad)	49.5	54.9	10.8

Between tests 3 and 6, the maximum bending moment (Table 30) was not affected by the axial restraint to the beam (difference of 0.5%); however, the corresponding rotation was 40% lower in test 6. Between tests 3 and 5, the maximum bending moment increased considerably (by 132%); the corresponding rotation was 53% lower in test 5. The same conclusions can be made for tests 5 and 6.

Table 30: Comparisons of the results: maximum sagging bending moment M^+_{max} (tests 3, 5, 6)

700ºC	T3	T6	T5	Diff. T3-T5 (%)	Diff. T3-T6 (%)	Diff. T5-T6 (%)
Restraint	no	50 kN/mm	total			
M^+_{max} (kNm)	357.1	355.5	828.0	131.8	-0.5	132.9
Vert. load F_{max} (kN)	252.0	198.0	336.5	33.5	-21.4	70.0
Axial load N (kN)	0	-297.3	-1646.7	---	---	453.8
Vert. displ. (mm)	220.3	148.7	132.2	-40.0	-32.5	-11.1
Rotation θ_{M+max} (mrad)	92.3	55.1	43.0	-53.4	-40.3	-22.0

The effect of the axial restraint affects the initial stiffness and increases it by 83% at 500ºC (from test 2 to test 4) and by 54% at 700ºC (from test 3 to test 5).

V Final comments

The main objective of the experimental tests was to observe the combined bending moment and axial loads in the heated composite steel-concrete joint after the loss of the column due to a localised fire. The effect of the localised fire (that led to the column loss) was simulated by the application of elevated temperatures in the composite joint zone. According to previous experimental works performed in real composite steel-concrete open car park buildings subjected to fire, a majority of the temperatures measured in the beam bottom flanges were lower than 500ºC; however temperatures of 700ºC were observed in recent tests performed in France (Jaspart et al., 2008), probably due to the manufacture evolution of cars, with more combustible plastic materials as well as higher petrol tank capacity. Based on these previous observations, five tests were heated up to 500ºC or 700ºC; one reference test (test 1) was carried out at ambient temperature, and finally a demonstration test (test 7) was performed, for which the frame was subjected to an increase of the temperature up to the failure of the column. The effect of the axial restraint to beam coming from the unaffected part of the building was also studied: tests 1, 2 and 3 - no axial restraint to the beam; tests 4 and 5 - total axial restraint to the beam; and tests 6 and 7 - realistic axial restraint to the beam. The two dimension sub-frame was extracted from an actual composite open car park building, keeping the real

cross-section dimensions of the beams (IPE 550, S355) and the columns (HEB 300, S460), and using bolts M30, cl 10.9 in the composite connection.

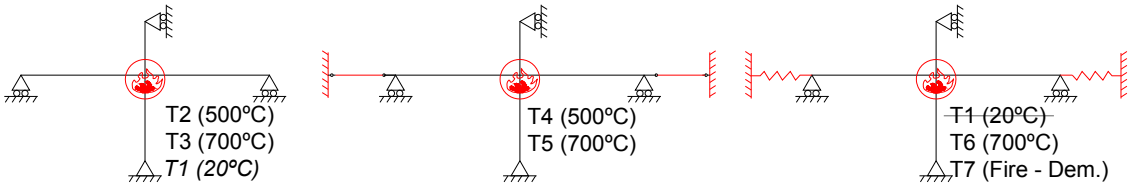

Figure 321: Seven experimental tests

In tests 1 to 6, a hogging bending moment was initially reached in the joint during the first loading step, followed by a variation of this moment during the increase of temperatures (step 2). In the third loading step, the column loss was simulated (very progressive), and the sagging bending moment increased under constant temperatures. The first failure observed in all the tests was the concrete crushing in compression; some bolts from the bottom bolt rows failed later in tension in tests 1, 2 and 6, under higher joint rotations. Finally, similar localised deformations at the centre and bottom parts of the end-plate were observed in all the tests. In the demonstration test 7, the bottom column (HEB 140, S355) failed under 578ºC and 359 kN of axial load; then steel temperatures in the joint increased to very high values (770ºC in the beam bottom flange) and the sub-frame resistance depended of the unheated composite slab resistance under sagging bending moment (which reached maximum of 200ºC). Finally, the concrete crushed in compression (under 180 kN of axial load), and the entire sub-frame failed a very few time later, because of the failure of three bolts in the bottom left row (around 600ºC in the bolts).

From tests performed without axial beam restraint, the joint rotation capacity, as well as the ductility, increased with the temperature, whereas the maximum reaction load, and the corresponding maximum sagging bending moment, decreased (by 20% at 500ºC and by 50% at 700ºC).

During the beam axial restraint tests, only compression loads were developed; the main reason for that was the position of the restraint: not at the gravity centre of the composite steel-concrete beam, but at the gravity centre of the steel beam. The advantage of the compression axial loads was the capacity of the joint to sustain a higher sagging bending moment without any problem of bolt failure: the compression load from the axial restraint combined with sagging bending moment, moved the neutral axis of the connection downward, allowing the development of additional compression loads in the concrete slab, and reducing tensile loads in the bottom bolt rows. The compression axial loads also increased the joint rotation capacity and the ductility of the joint.

Additionally, it was observed that the initial stiffness of the load/displacement curves decreased with the joint temperature and increased with the axial beam restraints.

REFERENCES

- Abaqus, 2007 - Abaqus Theory Manual & Users Manuals (2007), Version 6.7, Hibbitt, Karlsson and Sorensen, Inc. USA.
- *Demonceau, 2008* - Demonceau J.F. “Steel and composite building frames: sway response under conventional loading and development of membranar effects in beams further to an exceptional action”. Ph.D. Thesis, Faculty of applied sciences, University of Liege (BE), 2008.
- *Demonceau, 2009* - Demonceau, J.F. “ROBUSTFIRE Project - Design of the joints - notes”, Internal document, University of Liège, 2009.
- EN 1991-1-2:2002. “Eurocode 1: Actions on structures - Part 1-2: General actions - Actions on structures exposed to fire”. European committee for standardization, November 2002.
- *Gens, 2010* – Gens F. “ROBUSTFIRE Project - Pre-dimensionning of the reference’s car park”, Internal document, Greisch, 2010.
- Haremza et al. (2012). “Deliverable III: Development of simplified behavioural models”, Robustness of car parks against localised fire, Grant Agreement Number RFSR-CT-2008-00036.
- Jaspart et al. (2008). “Deliverable I: Definition of the problem and selection of the appropriate investigation ways”, Robustness of car parks against localised fire, Grant Agreement Number RFSR-CT-2008-00036.
- *NP EN 10002-1: 1996,* “Mettalic materials – Tensile testing – Part 1: Method of test at ambient temperature”, Instituto Português da Qualidade, 2006.
- *NP EN 10002-5: 1991,* “Mettalic materials – Tensile testing – Part 5: Method of testing at elevated temperature”, Instituto Português da Qualidade, 2001.
- *NP EN 206-1:2007*, “Concrete – Part 1: Specification, performance, production and conformity”, Norma Portuguesa, Instituto Português da Qualidade, Portugal, 2007.

ANNEX B – Column benchmark

Departamento de Engenharia Civil

Faculdade de Ciências e Tecnologia da Universidade de Coimbra

ROBUSTFIRE Project

Document 4 - Benchmark example 1: Column_v3(2)

From the University of Coimbra:

Cécile Haremza

Aldina Santiago

Luís Simões da Silva

From the University of Liege:

Hav Ly

Jean-Pierre Jaspart

Jean-François Demonceau

Jean-Marc Franssen

François Hanus

From the Imperial College of London:

Cheng Fang

Bassam Izzuddin

Ahmed Elghazouli

David Nethercot

March 2010

IR_2009-004

UC/DEC/ISISE/2009-004

RFS-PR-07039-Benchmark-column-v3(2)

TABLE OF CONTENTS

I Introduction

The increase of the market shares for steel and composite car parks in Europe is somewhat limited by the lack of information on how these structures behave under exceptional localised fire. The objective of the European RFCS ROBUSTFIRE project is to develop a general philosophy for the design of robust structures against exceptional events and to derive practical design guidelines for its application to car parks under localised fire. This project is divided into five basic tasks: i) Definition of the problem and selection of the appropriate investigation ways, ii) Study of the structural individual response of the affected structural elements, iii) Study of the structural response under selected fire scenario(s), iv) Derivation of design recommendations adapted to the industrial request for design efficiency as well as for easy fabrication, erection and control, and v) Application of the “event-independent” robustness requirements on a case study. The task ii) is actually on progress, and three approaches (experimental, numerical and theoretical) will be combined with the aim to derive behavioural models for elements. The experimental and numerical approaches will provide the required knowledge on the behavioural response of individual frame structural elements directly affected by a localised fire. The first results of the numerical part of the project are presented in this report by the benchmark study on a steel structure subjected to fire.

A lot of numerical tools are available to model a composite structure subjected to fire. Some of them are specialized programs dedicated to analyzing steel structural behaviour in fire. According to Wang (Wang, 2002), the programs being actively developed and used in major centres of steel structural fire research in Europe are ADAPTIC, initially developed at the Imperial College of London, UK (Izzuddin, 1991), FEAST, developed at the University of Manchester, UK (Liu, 1994; Liu, 1996), VULCAN developed at the University of Sheffield, UK, and SAFIR developed at the University of Liege, Belgium (Franssen et al., 2000). The three first ones were initially developed as analysis program of steel structures at ambient temperatures and were later extended to analyse the behaviour of steel or composite structures in fire. SAFIR has from the beginning been developed for structural analyses at high temperatures. His predecessor is the computer program CEFICOSS (Franssen, 1987). This program can be used for both thermal analysis and structural analysis at high temperatures, but these two analyses cannot be coupled. These specialized programs have generally been developed according to the needs of research works, such as simulating particular experimental tests. Consequently, these programs are not able to perform all the simulations or to simulate in detail local and global behaviours. It is then necessary to choose the right program in function of the numerical needs.

Commercial general finite element package, such as ABAQUS, has the ability to simulate complex structural behaviour under fire conditions even though it does not have special facilities to model structural behaviour in fire. All modes of structural behaviour involved in fire can be simulated thanks to a large library of finite elements which enables the creation of an efficient and detailed model, in which relevant material properties at high temperatures are included (Wang, 2002). Temperature distributions in structures under fire can be obtained by performing a heat transfer analysis. ABAQUS is able to simulate the detailed

behaviour of connections in fire and user defined subroutines enable modelling many of the special features of structural behaviour in fire.

This report presents a comparison between the finite element programs that will be used during the ROBUSTFIRE project by three partners: i) the specialized homemade finite element software dedicated to the analyses of structures subjected to fire, SAFIR, used by the University of Liege (Belgium), ii) the commercially available program ABAQUS used by the University of Coimbra (Portugal) and iii) the homemade finite element program ADAPTIC, used by the Imperial College of London (UK). The main objective is to validate the utilisation of the SAFIR, ABAQUS and ADAPTIC programs for steel structures subjected to fire. This benchmark example is based on the paper published by Franssen in 1995 about a natural fire test on a fully loaded, two dimensional, unprotected steel framework carried out in a purpose-built compartment in Cardington (Franssen et al., 1995). This paper is reproduced in full in annex. The influence of the model definition, axial restraint to beam, frame continuity, thermal expansion and non-uniform temperature is discussed, and the differences between the results of the three numerical software's SAFIR, ABAQUS and ADAPTIC are illustrated. The study cases are listed in Table 1. The experimental results as well as the numerical results presented by Franssen (Franssen et al., 1995) with the FE program CEFICOSS, the predecessor of SAFIR, are also showed.

Table 1. Overview of the considered study cases

	Parameter	***Study Cases***
1	Reference structure (§ V.1)	Modelling of a half structure with account of the symmetry (see Figure 4, § III.4.2)
2	Model definition (§V.2)	Complete Cardington structure modelling (see Figure 24, § V.2)
3	Axial restraint to beam (§ V.3)	a) Half structure without horizontal spring (see Figure 26(a), § V.3)
		b) Entire Cardington structure without horizontal springs (see Figure 26(b) - § V.3)
4	Frame continuity (§ V.4)	a) Beam analysed as a separate member (see Figure 31, §V.4.1)
		b) Column analysed as a separate member (see Figure 33, § V.4.2)
5	Thermal expansion (§ V.5)	Half structure without expansion coefficient (see Figure 4)
6	Non-uniform temperature (§ V.6)	Half structure with uniform temperature within the cross-sections (see Figure 4)

II Description of the benchmark study

The natural fire test reported by Franssen (Franssen et al., 1995) was carried out by British Steel in collaboration with the Fire Research Station. The fully loaded, two dimensional steel framework shown in Figure 1 was tested in fire in a purpose-built compartment of typical size of office accommodation (floor area of 50 m^2 and ceiling height of 3.9 m). Dimensions of this steel framework were specified for a building of two or three storey in height. The beam, 4550 mm long, with a universal beam section of 406 x 178 x 54, Grade 43A, was bolted to two columns of 3530 mm tall, with a universal column section of 203 x 203 x 52, Grade 43A. M20 grade 8.8 bolts were used to provide improved resistance to loss in strength at high temperatures. Columns were pin jointed at the base and extended above the beam.

Autoclaved aerated concrete blocks were built between the column flanges to protect the web from fire, but there were only considered to give thermal insulation (non-composite behaviour). A concrete slab, which has a cross-section of 1200 x 150 mm, was also only represented because of its influence on the temperature distribution in the beam (non-composite behaviour). Lateral and sway instabilities were prevented by a subsidiary framework specially designed for.

The loads, maintained constant throughout the fire test, were applied to the two columns by a hydraulic jack and load cell placed between the top bearing plate and the load reaction frame, and to the beam, at each four equal positions along the span.

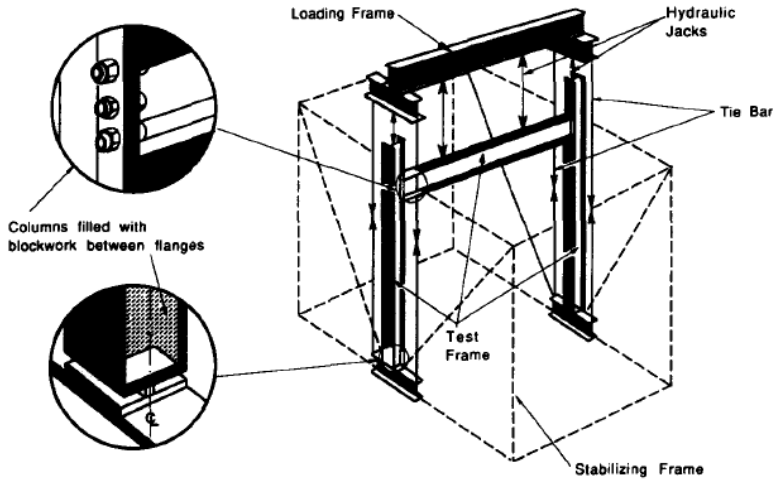

Figure 1. Schematic layout of the loaded frame used in the Cardington tests (Franssen et al., 1995)

Due to the combination of ventilation openings and the thermal loading (timber cribs), equivalent fire duration of 32.5 min was achieved in the test. The load was removed after 22 min when it could no longer be applied with safety. At this point the total deflection of the beam exceeded span/32. Plastic hinge approximately 600 mm from each end of the beam and some plastic distortion of the welded end plates at the top of the connection were formed. Maximum temperatures over 777℃ and 606℃ were observed in the beam and in the column, respectively, after 20 minutes.

III Numerical Model

III.1 Numerical tools

Several numerical analyses are detailed in this report, performed by the three different finite element programs used by three partners in the ROBUSTFIRE project: i) SAFIR (Franssen, 2005), used by the University of Liege; ii) ABAQUS (ABAQUS manual, 2007), used by the University of Coimbra; and iii) ADAPTIC (Izzudin, 1991), used by the Imperial College of London. The results are compared to the experimental results and to the numerical results obtained by the software CEFICOSS (Franssen, 1987) and presented in the paper of Franssen (Franssen et al, 1995).

III.1.1 Finite Element Program CEFICOSS

CEFICOSS (Computer Engineering of the Fire design of Composite and Steel Structures) is a special purpose finite element program developed in Liege, Belgium (Franssen, 1987), for analysing the behaviour of structures in fire. This program integrates thermal and structural analysis and is the predecessor to the SAFIR program.

The 2D finite difference program (thermal part of CEFICOSS) is first used for the calculation of temperatures in steel and composite steel-concrete building members exposed to fire. The heat flow from the environment to the section is assumed to be convective and radiative (Franssen et al., 1995). The structural part of the CEFICOSS program is then used to model the tested frame using beam finite elements.

III.1.2 Finite Element Program SAFIR

SAFIR is a special purpose computer program for the analysis of structures under ambient and elevated temperature conditions. The program, which is based on the Finite Element Method (FEM), can be used to study the behaviour of one, two and three-dimensional structures. The program (SAFIR) was developed at Liege University, Belgium, and is today viewed as the second generation of structural fire codes developed in Liege, the first generation being the computer program CEFICOSS.

As a finite element program, SAFIR accommodates various elements for different idealization, calculation procedures and various material models for incorporating stress-strain behaviour. The elements include the 2-D SOLID elements, 3-D SOLID elements, BEAM elements, SHELL elements and TRUSS elements. The stress-strain material laws are generally linear-elliptic for steel and non-linear for concrete.

With SAFIR, the analysis of a structure exposed to fire is made of several steps:

- The first step consists in predicting the temperature distribution inside the structural members subjected to the fire, referred to as the “thermal analysis”.
- Then, the so-called “torsional analysis” is necessary for 3-D BEAM elements, where warping effects may occur and for which the warping

function table and torsional stiffness of the cross-section are not available.

- The last step, called the “structural analysis”, is carried out to determine the response of the structure subjected to static and thermal actions.

III.1.3 Finite Element Program ABAQUS

ABAQUS is an American general commercial finite element package. It provides a complete and flexible solution for a large range of problems, including the analysis of structures subjected to fire. Two types of analyses are considered: i) the coupled thermal-stress analysis and ii) the static analysis. The coupled thermal-stress analysis (i) requires the use of elements with both temperature and displacement degrees of freedom, and in this study, beam elements are used, which only have displacement degrees of freedom and no temperature degree of freedom. So the static analysis (ii) is used with these beam elements. A heat transfer analysis is first realised to obtain the temperatures in beam and column cross-sections. The heat flow from the environment to the section is assumed to be convective and radiative. These first thermal results are then used in the static general analysis, where temperature gradients in the beam cross-section elements are applied as predefined temperatures (see §III.4.3).

III.1.4 Finite Element Program ADAPTIC

ADAPTIC is the homemade non-linear finite element program of the Imperial College of London (Izzuddin, 1991). The nonlinear analysis program ADAPTIC can explicitly take into account both geometric and material nonlinearity as well as the time variability of the response be used for analyzing structures of interest. To study the extreme effects such as fire and blast loading, a new method for integrated adaptive nonlinear analysis of steel frames was introduced. The main advantage of the proposed method over conventional nonlinear analysis is that both extreme loading events can be considered within the same analysis. The resulting integrated approach can therefore be used to study the behaviour of steel members and frames subject to scenarios of a blast followed by fire, enabling the influence of the explosion on the fire resistance to be evaluated.

III.2 Mechanical and Thermal Material Properties

III.2.1 Stress-Strain-Temperature Behaviour of Steel

The steel stress-strain relationship at high temperatures is introduced in each program according to the expressions given in the EN 1993-1-2:2005, and illustrated in Figure 2. At ambient temperature, the yield stress f_y considered by Franssen to simulate the experimental test is 408 MPa. This value was not experimentally measured, so five numerical simulations were carried out with CEFICOSS, using five different values: 255, 306, 357, 408 and 459 MPa (Franssen et al., 1995). The best numerical agreement with the test was reached using this yield stress equal to 408 MPa (Figure 18, Figure 19 Figure 20).

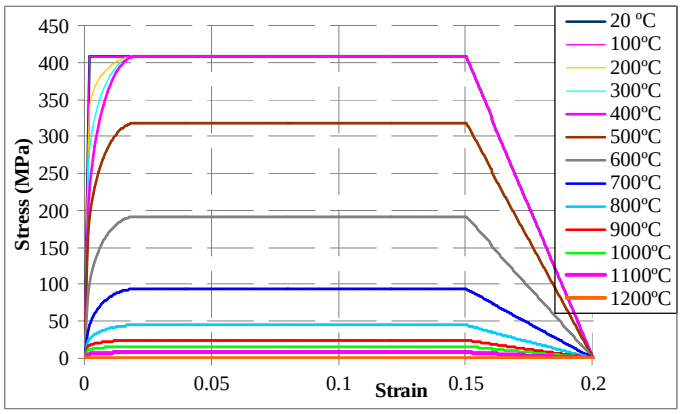

Figure 2. Nominal stress-strain relationship of steel at high temperatures

The elastic modulus considered is 210 GPa, which decreases at high temperatures according to the reduction factor $k_{E,\theta}$ (EN 1993-1-2:2005). The creep effect on the deformation of steel is included in the expressions of the EN 1993-1-2:2005. A Poisson ratio constant equal to 0.3 is used.

III.2.2 Thermal Properties of Steel

The thermal expansion coefficient used in SAFIR, ABAQUS and ADAPTIC is based on the value recommended in EN 1993-1-2:2005, which defines the steel thermal elongation Δl/l as a function of the temperature by the equations (2), (3) and (4).

$$\text{for } 20^{o}\text{C} \le \theta_a < 750^{o}\text{C}: \quad \Delta l/l = 1.2\times10^{-5}\theta_a + 0.4\times10^{-8}\theta_a^2 - 2.416\times10^{-4} \quad (2)$$

$$\text{for } 750^{o}\text{C} \le \theta_a \le 860^{o}\text{C}: \quad \Delta l/l = 1.1\times10^{-2} \quad (3)$$

$$\text{for } 860^{o}\text{C} < \theta_a \le 1200^{o}\text{C}: \quad \Delta l/l = 2\times10^{-5}\theta_a - 6.2\times10^{-3} \quad (4)$$

The conductivity and the specific heat of the steel at high temperatures are defined according to the expressions given by the EN 1993-1-2:2005. The convective heat transfer coefficient and the emissivity used by Franssen (Franssen et al., 1995) and given by the EN 1993-10:1990 are respectively equal to 25 W/m^{2}K and 0.5. However, for the column flange facing the wall of the fire compartment, the emissivity is taken equal to 0.3 to account for some degree of radiative shadowing (Franssen et al., 1995).

III.2.3 Concrete properties

In the thermal analysis, an elastic material law is assumed for the concrete as it is not taking part in the structural resistance but only plays an insulating role. The conductivity and the specific heat of the concrete slab are defined according to the EN 1992-1-2:2004, with a density equal to 2400 kg/m^3. The concrete blocks insulating the column have particular properties: a density equal to 677 kg/m^3, a constant specific heat of 1050 J/kgK, a thermal conductivity given by 0.20 + 0.0004θ_c W/mK and a moisture content of 25.7 kg/m^3 (Franssen et al., 1995). The concrete is not modelled in the mechanical analysis.

III.3 Thermal analysis

The heat-transfer problem analysed in CEFICOSS, SAFIR and ABAQUS involves conduction and boundary radiation. In these analyses, the stress/deformation state is not studied, only the temperature field is computed (ABAQUS Manual, 2007). With SAFIR, boundary conditions (i.e. temperatures or heat fluxes) are imposed and the temperature is computed at each point of integration of each finite element. The program ADAPTIC only deals with structural modelling, and the temperature distribution curves across the cross-section obtained from CEFICOSS will be directly adopted. The development of the average combustion gas temperature measured in the fire compartment is reproduced in Figure 3 (Franssen et al., 1995).

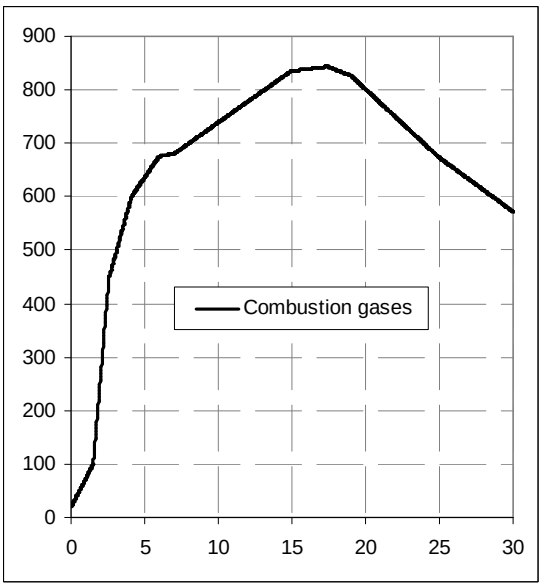

Figure 3. Temperature of the combustion gazes

III.4 Mechanical analysis

Nonlinearities arise from large-displacement effects and material nonlinearities, and are taken into account on the numerical models. Moreover, temperature dependent material properties and nonlinear temperature gradient over the cross-section are also considered. The energy associated to the shear deformation of the system is not considered.

III.4.1 Procedure adopted

In SAFIR, static or dynamic analyses can be performed for the mechanical analyses. Different loading sequences can also be defined. A step-by-step analysis is performed with the time as incremental factor. The temperature at each point of the structures is known at each considered time by extracting this information from the output files obtained for the different structural elements through the previously performed thermal analyses. The following information can be obtained for each iteration:

- Displacement at each node of the structure,

- Axial and shear forces and bending moments at the integration points in each finite element,
- Stains, stresses and tangent modulus at the integration points of each finite element.

In ABAQUS, the mechanical analysis of the structure is realised by a static stress procedure in which inertia effects are neglected. The method to solve the nonlinear equilibrium equations used by this static general analysis is the Newton's method. A series of increments are realised in order to obtain the solution. In each increment, equilibrium is obtained by iterations. The default automatic incrementation scheme is used and increment sizes are chosen by the program on the base of computational efficiency (ABAQUS Manual, 2007).

In ADAPTIC, dynamic analysis is adopted to predict both pre-buckling and post-buckling (if applicable) behaviours of this frame.

III.4.2 General modelling assumptions

Figure 4 presents the steel frame structure for which symmetry conditions are taken into account. In order to apply these symmetry conditions at mid-span of the beam, the axial displacement in the X-direction and the rotation around Z were restrained. At the bottom of the column, the displacements in the directions X and Y are restrained. As the concrete slab and the concrete blocks in the column only provide thermal boundary conditions for the temperature, they are not modelled in the structural analysis.

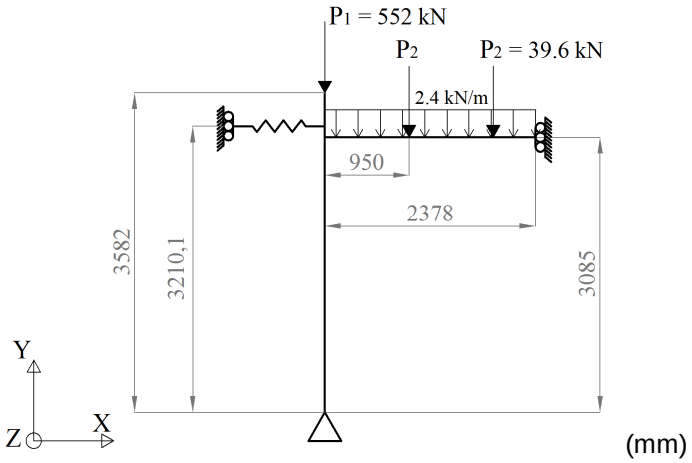

Figure 4. Reference frame (case 1)

According to Cooke and Latham (Cooke and Latham, 1987), during the experimental test, no relative rotation at the connection occurred and the temperature around the connection remained lower than elsewhere in the compartment during the fire. It is then allowed to suppose a rigid beam-to-column connection. In order to represent the restraint offered by the secondary steelwork, a bi-linear spring is modelled with nonlinear force-displacement behaviour, as illustrated in Figure 5. Franssen (Franssen et al., 1995) defined the following spring properties: an axial stiffness equal to 6700 kN/m and an axial plastic load equal to 86 kN.

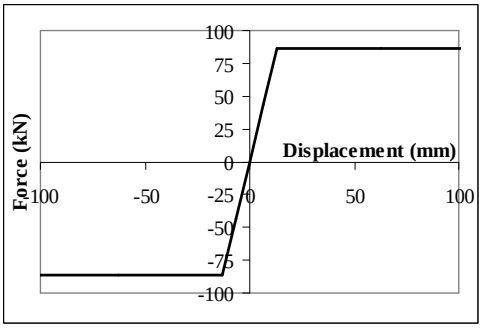

Figure 5. Behaviour of the spring

In SAFIR, 2D beam elements are used with two integration points. Within the cross-section, the concrete is not taken into account for the mechanical analysis; accordingly, integration points are only met within the steel profiles.

In ABAQUS, Two dimension beam elements type B21 are used to define the beam and the column, with three degrees of freedom per node (X, Y, θ_Z) - Timoshenko beams. These elements have five integration points in the beam element cross-section, as shown in Figure 6.

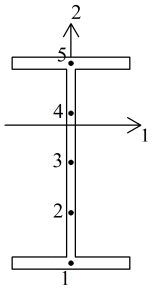

Figure 6. Default integration, cross-section of a beam used in ABAQUS

In ADAPTIC, cubic elasto-plastic 2D beam-column elements are adopted to simulate the beam and the column. Numerical integration is performed over two Gauss points. A number of monitoring areas are used at each Gauss section to monitor material direct stress and strains. This beam-column element is illustrated in the Figure 7.

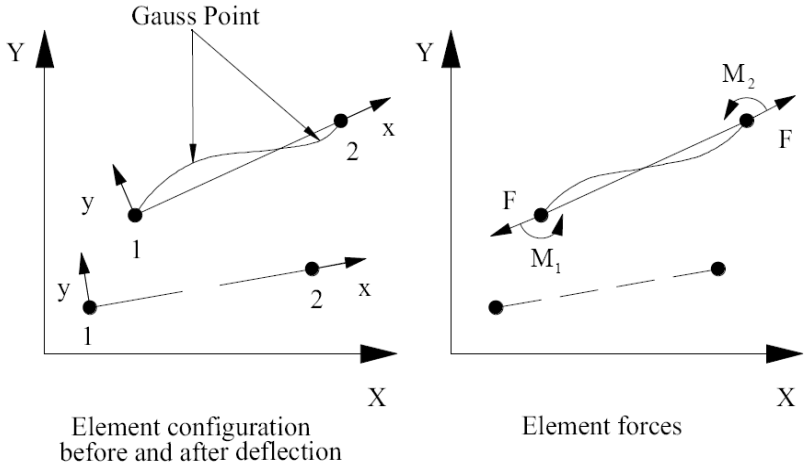

Figure 7. Configuration and forces in local system of the beam-column element used in ADAPTIC

III.4.3 Mechanical and Thermal Loading

III.4.3.1 Mechanical loading

The mechanical loads are applied at ambient temperature and maintained constant during the fire (see Figure 4 - §III.4.2). They correspond to:

- the self-weight,
- a vertical load on the column equal to 552 kN (P_1),
- two vertical load on the beam equal to 39.6 kN (P_2),
- a uniform loading of 2.4 kN/m distributed along the beam to represent the self-weight of the concrete slab.

III.4.3.2 Thermal gradient through the section

In SAFIR, there is one point of integration per steel finite element used for the thermal analysis and the calculated temperatures can be directly used by the structural part. For instance, 182 integration points are used for the steel beam cross-section.

In ABAQUS, thermal loading can only be specified at specific points through the section or by defining the value at the origin of the cross-section and specifying the gradients (ABAQUS Manual, 2007). Thermal loading is specified as a predefined field, as explained previously (see § III.1.3). The predefined temperature field affects temperature-dependent material properties: the elastic modulus, the stress-strain behaviour and the thermal expansion will change in function of the steel temperature. Column and beam have temperature variations across their section, as defined by the previous heat transfer analysis. In the static analysis, temperatures are specified at the three specific points through the section (ABAQUS Manual, 2007): i) centroid of the top flange; ii) centroid of the web and iii) centroid of the bottom flange. Only one amplitude curve defining the evolution of the temperature in function of the time can be introduced for each section type. The thermal gradients applied in the beam and column cross-sections are shown in Figure 8. The amplitude curve corresponds to the web temperatures for the beam and to the inner flange temperatures for the column.

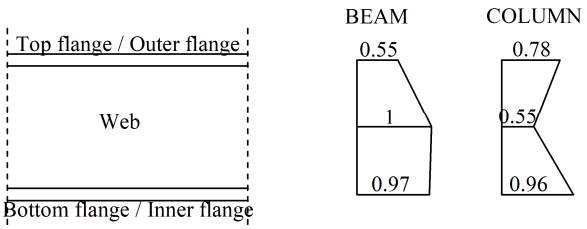

Figure 8. Thermal gradient within the beam and column cross-sections in ABAQUS

Since ADAPTIC only deals with structural modelling, the temperature distribution curves across the cross-section obtained from CEFICOSS are directly adopted. In modelling with ADAPTIC, up to three independent temperatures at three points can be considered over the cross-sections of the

steel beam, thus allowing the use of a quadratic temperature distribution across the cross-section (Figure 9).

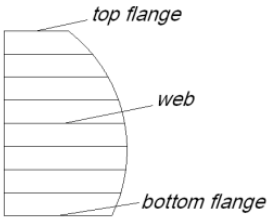

Figure 9. Temperature distribution in ADAPTIC across the cross-section

III.4.3.3 Temperature along the beam span

Because the measured temperatures of the combustion gases were slightly lower in the vicinity of the beam-to-column connection (Franssen et al., 1995), the beam has also a temperature variation along its length. In SAFIR, a reduction function of the temperatures along the longitudinal beam axis, f(x), with a sinusoidal shape (Figure 10), is taken into account (with a value of 0.90 θ_a at the beam/column interconnection and 1.00 θ_a at mid-span node of beam).

Figure 10. Coefficients of reduction of the temperatures along the beam used in SAFIR

In order to approximate this variation in ABAQUS, the half of the beam is divided into five parts where the temperature along each length part is constant (Figure 11).

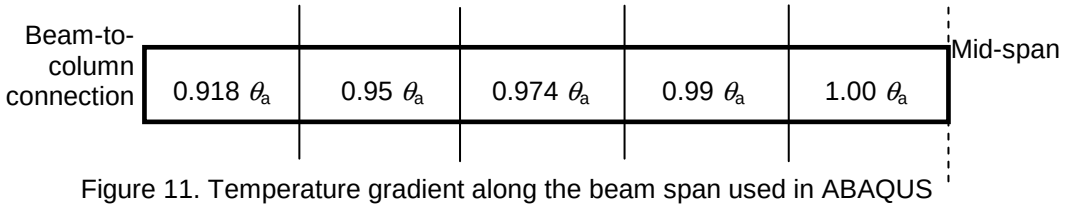

Figure 11. Temperature gradient along the beam span used in ABAQUS

In ADAPTIC, the temperature distribution along the length of the beam is illustrated in Figure 12.

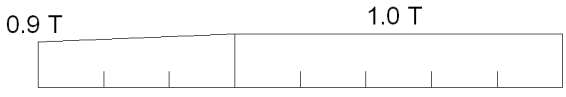

Figure 12. Temperature distribution in ADAPTIC along the length

IV Thermal results

IV.1.1 Finite elements and mesh discretization

The thermal analysis is performed to determine the distribution of temperatures in an element. For complex structures, the sub-structuring technique is used, i.e. the total structure is divided into several sub-structures and a thermal computation is performed successively for each so-defined sub-structures. In the present study, a thermal analysis is performed for each different type of structural elements met within the considered structure, i.e. the beam with the concrete slab and the column with the concrete between the flanges. The concrete slab and the concrete blocks are modelled as they provide thermal boundary conditions. In SAFIR, the thermal analyses are made using 2-D SOLID elements to determine the distribution of the temperature within the element cross-sections (Figure 13).

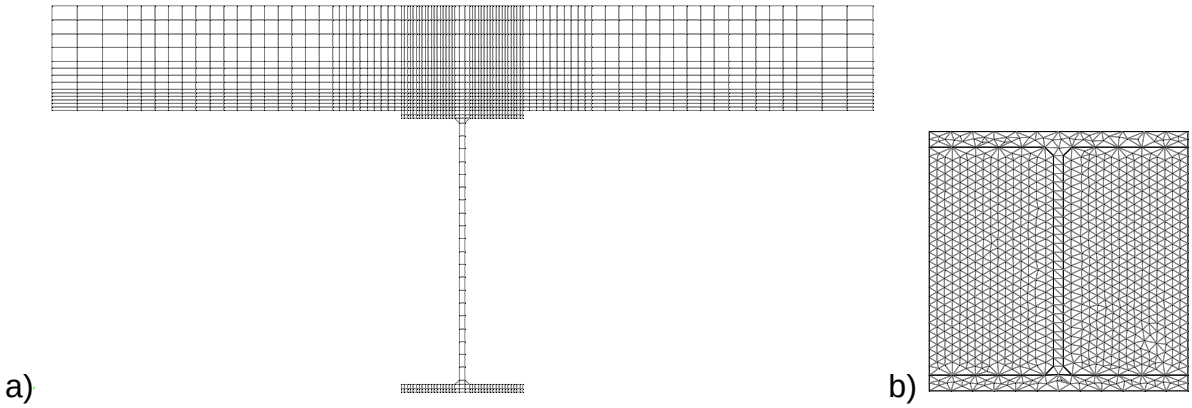

Figure 13. a) Beam and b) column cross-sections meshed in SAFIR

In ABAQUS, the two models (beam and column) are developed using 2D deformable element DC2D4, a 4-node linear heat transfer quadrilateral, and are simplified taken into account the symmetry of the section (Figure 14). The concrete slab and the concrete blocks are linked to the steel profiles by a tie constraint. The FE mesh is similar to the mesh used by Franssen (Franssen et al., 1995) in CEFICOSS program.

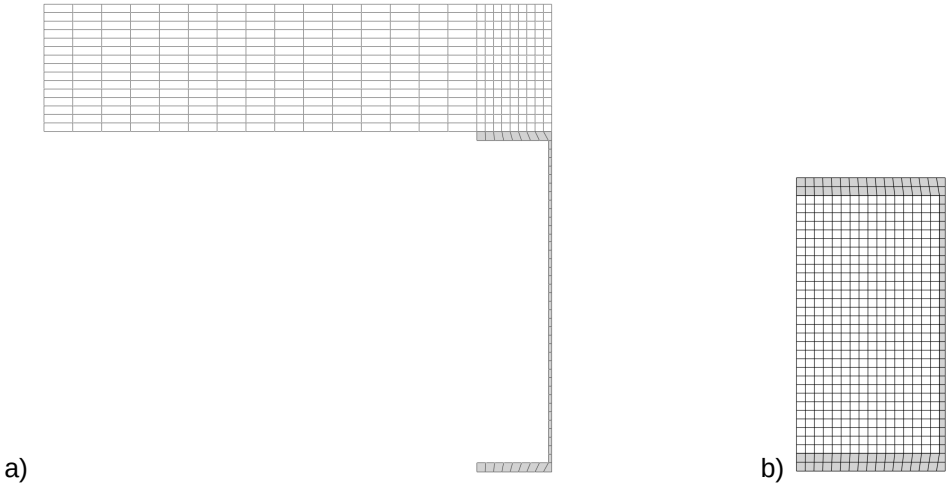

Figure 14. a) Beam and b) column cross-sections meshed in ABAQUS

IV.1.2 Steel temperatures

Figure 15 a) and b) show the evolution of the temperatures in the flanges and at mid-height of the web for the beam and column elements respectively, obtained from the experimental test and from the programs CEFICOSS, SAFIR and ABAQUS. The considered temperature for the air is reminded with the black curve. Numerical results obtained by SAFIR show a good agreement with the measured temperatures during the test, as well as with the temperatures computed through CEFICOSS and ABAQUS. The differences between temperatures calculated by CEFICOSS and by SAFIR are 1.30% for the beam and 5.80% for the column. The differences between temperatures calculated by CEFICOSS and by ABAQUS are 2.80% for the beam and 6.26% for the column.

a)

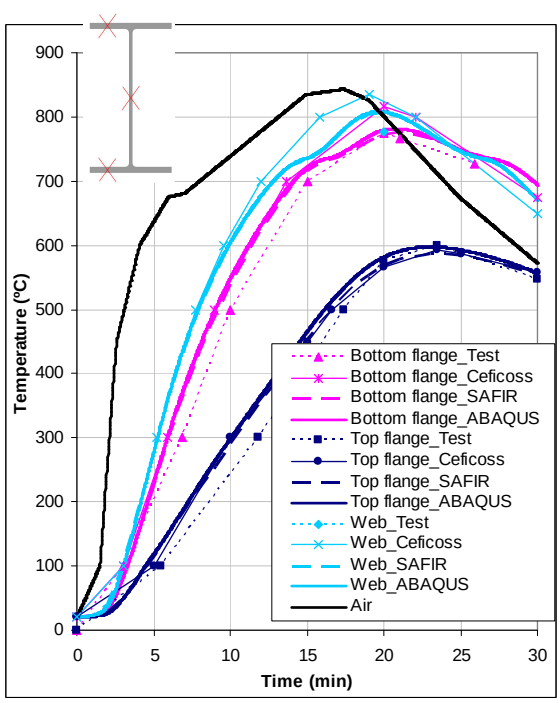

b)

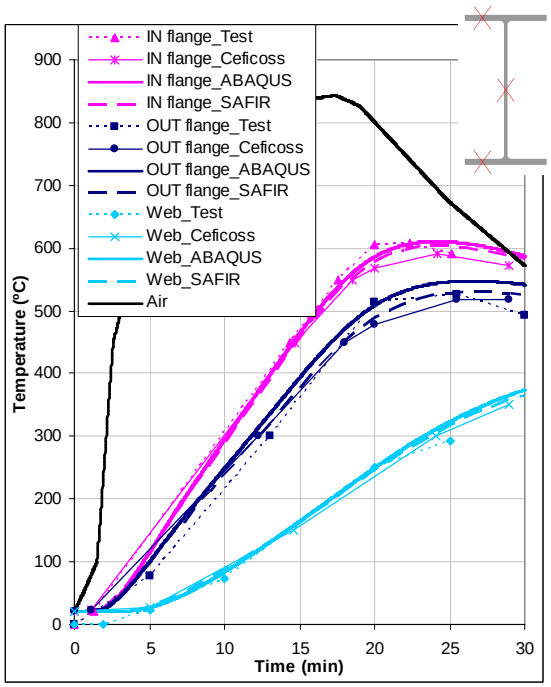

Figure 15. Temperatures a) in the beam and b) in the column

Based on the considerations presented in §III.4.3.2, Figure 16 compares the thermal loading applied in the mechanical analysis of ABAQUS (Applied) with the temperatures obtained from the heat transfer analyses (Result). Because the top flange of the beam shows the lower temperatures, good approximations were preferred to the bottom flange and to the web. The same consideration is made to the column.

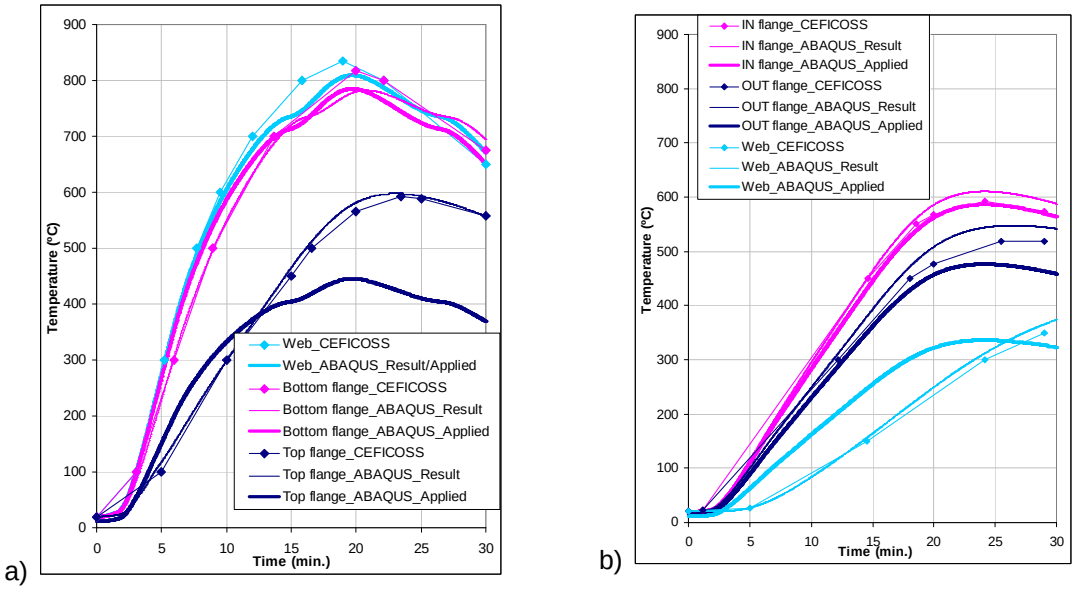

Figure 16. Applied thermal loading in ABAQUS: a) in the beam, b) in the column

V Mechanical Results

V.1 Reference case: behaviour and validation of the numerical model

Each model of the reference structure (Figure 4 - § III.4.2) is validated by comparing beam mid-span vertical displacement, beam axial load and column lateral displacement with the experimental and CEFICOSS results. A comparison of the results obtained by the three different programs SAFIR, ABAQUS and ADAPTIC is also showed. Figure 17 shows the frame deformation after 16 minutes computed with SAFIR, ABAQUS and ADAPTIC and compared to the lateral deformation of the column obtained during the experimental test.

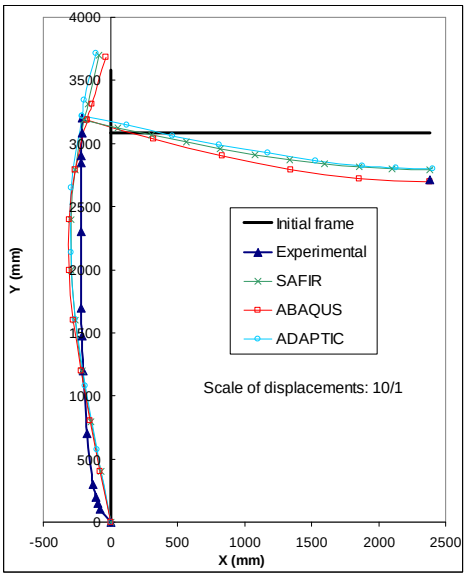

Figure 17. Deformation of the frame after 16 minutes (case 1)

One aspect which can explain the difference observed between the measured lateral displacements for the column and the computed ones is the presence of the concrete between the column flanges which is neglected for the mechanical analysis performed with the three programs.

V.1.1 Beam mid-span vertical displacement and beam axial load

Figure 18 compares the measured deflection using CEFICOSS and SAFIR for five different values of yield strength: 255, 306, 357, 408 and 459 MPa (Franssen et al., 1995), as the actual value for the steel used for the tested members was not available. Figure 19 and Figure 20 show the results of the same simulations using the five different values of yield strength with the programs ABAQUS and ADAPTIC respectively. A yield strength value equal to 408 MPa approximates with a good agreement for all the FE programs the actual behaviour of the structure observed during the experimental test. Accordingly, all the following numerical simulations are performed assuming this yield strength for the steel. Because on the experimental tests, displacement transducers were switched on only at the beginning of the fire, and numerical simulations include also the deflection due to the load applied before the fire, initial difference between numerical and experimental curves is observed.

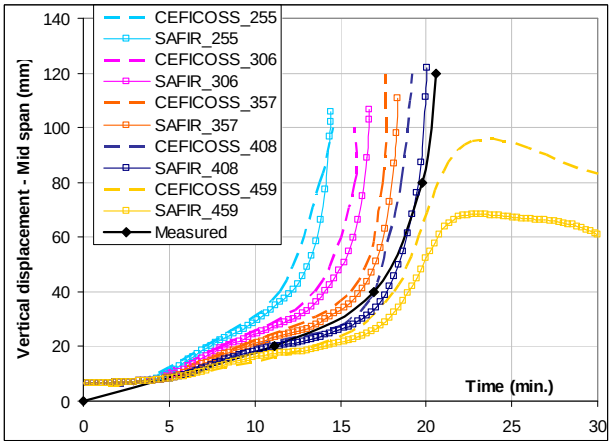

Figure 18. Numerical calibration of the yield stress (case 1) – CEFICOSS and SAFIR

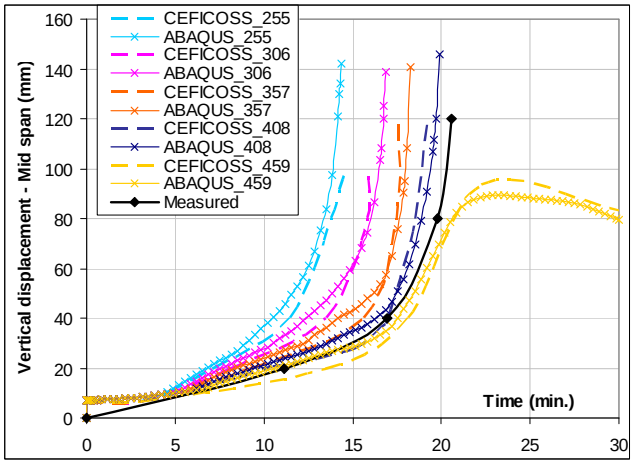

Figure 19. Numerical calibration of the yield stress (case 1) – CEFICOSS and ABAQUS

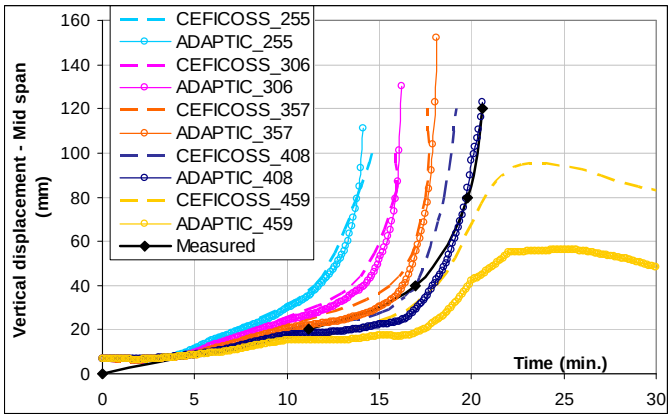

Figure 20. Numerical calibration of the yield stress (case 1) – CEFICOSS and ADAPTIC

With the yield strength of 459 MPa (yellow curves), the resistance of the frame is sufficient to reach the cooling phase of the fire. All the programs obtain a fire resistance time higher than 30 minutes, but with different maxima values of the beam vertical displacement varying from 48mm with ADAPTIC to 95mm with CEFICOSS.

The vertical displacement at mid-span and the calculated axial compression force in the beam are respectively represented in Figure 21 and Figure 22 for all the FE programs using the yield strength of 408 MPa. A very good agreement between SAFIR, ABAQUS and ADAPTIC is observed for the fire resistance time, equal to about 20 minutes as observed during the fire test (see Table 2 - § V.2). The beam vertical displacement calculated by ABAQUS increases slightly faster than with the other numerical programs (Figure 21), and the maximum value of the compression force in the beam calculated by ADAPTIC is the highest (Figure 22). These slight differences can be justified by slight different temperature gradients in the structural element cross-sections (see § IV.1.2), and a different way to take into account the gradient of temperature in the mechanical analysis (§ III.4.2).

Material properties used in CEFICOSS were taken from the EN 1993-10:1990, where a constant expansion coefficient α = 1.4 x 10^{-5} was recommended. An ABAQUS simulation was done using this constant coefficient expansion (blue curve of Figure 21) and obtained results closer to the experimental test and to the numerical programs.

Finally, it can be concluded that a good agreement between SAFIR, ABAQUS and ADAPTIC is observed, as well as for the resistance time than for the internal forces or the displacements calculations.

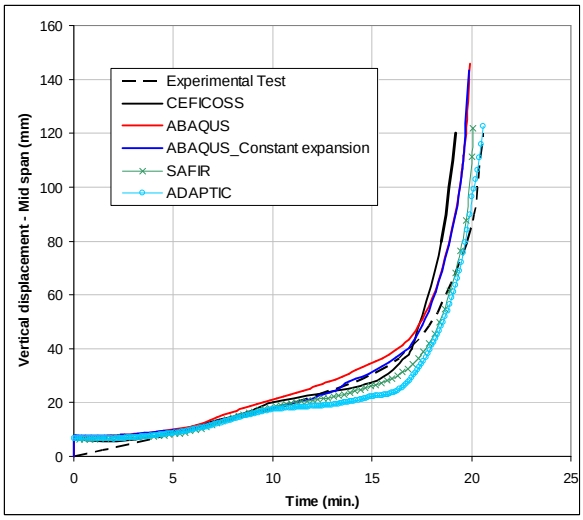

Figure 21. Case 1 - Vertical displacement of the beam in the fire test

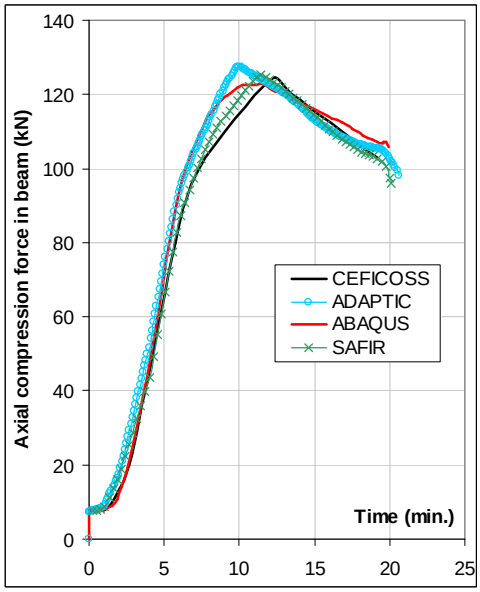

Figure 22. Case 1 - Calculated axial force in the beam

V.1.2 Column lateral displacement

The evolution of the lateral horizontal displacement at mid-height of column is shown in Figure 23. Due to the elongation of the beam, the column bows laterally up to the buckling at about 19-20 min, as observed at failure of the structure. The three numerical programs SAFIR, ABAQUS and ADAPTIC obtain quite close results.

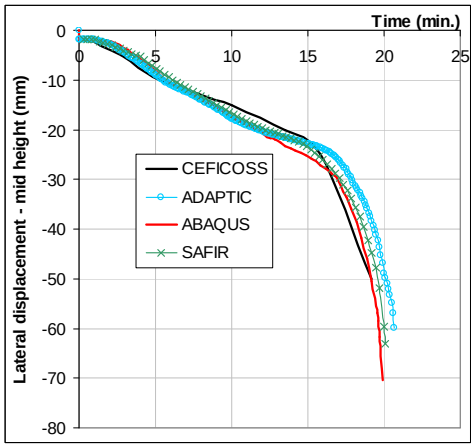

Figure 23. Calculated horizontal displacement at mid height of column (case 1)

V.2 Influence of the model definition

In order to verify that satisfactory results are obtained by simulating only one half of the frame (case 1 - Figure 4), the complete frame is modelled assuming the presence of two springs (case 2 - Figure 24). According to Franssen, an initial (sway) imperfection of 0.8 H_c/1000 is considered, where H_c is the column height (Franssen et al., 1995). The structural elements are the same than the ones met within the reference structure.

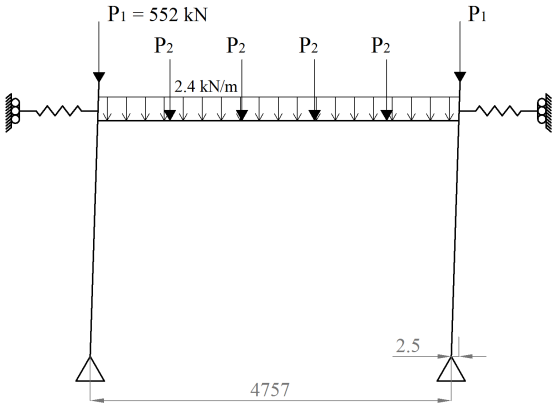

Figure 24. Complete frame (case 2)

Results of fire resistances are shown in Table 2 and a very good agreement is obtained between ABAQUS and ADAPTIC. A higher difference can be observed with SAFIR for the complete frame due to its difficulty in modelling the two springs working together.

Table 2. Fire resistance time (R_f) calculated by SAFIR, ABAQUS and ADAPTIC

	R_f SAFIR	**R_f ABAQUS**	**R_f ADAPTIC**
Case 1 (half of the frame)	20'04''	19'55''	20'36''
Case 2 (complete frame)	***17'55''***	***19'51''***	***20'05''***

It can also be observed in Figure 25 that simulating only half of the frame has almost the same structural behaviour of full model, which proves that satisfactory results are obtained by simulating only one half of the frame,

provided that restraint members are present. Again a very good agreement is showed between ABAQUS and ADAPTIC.

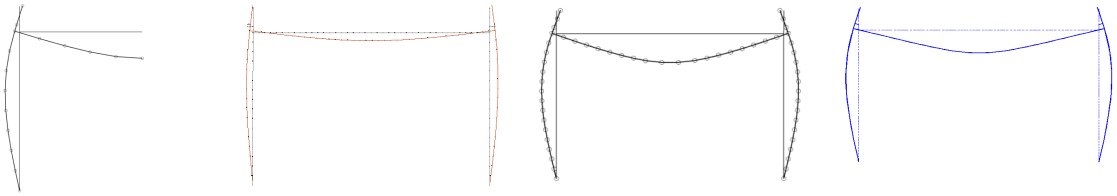

a) ABAQUS (19'55'') b) SAFIR (17'55'') c) ABAQUS (19'51'') d) ADAPTIC (20'05'')

Figure 25. Failure modes (scale 4/1) of the complete frame models in (b) SAFIR, (c) ABAQUS and (d) ADAPTIC compared to the reference case failure mode in (a) ABAQUS

V.3 Influence of the axial restraint to beam

The presence of the axial restraint at beam ends influences the elongation of the beam and the development of the axial loads in the latter. In this section, the influence of axial restraints to both complete and half model is considered by modelling them without the lateral springs at the beam extremities, as shown in Figure 26 a) and b).

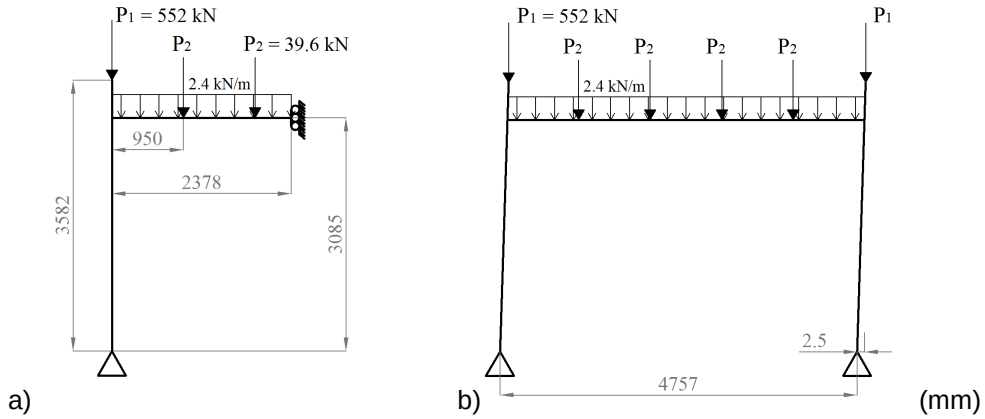

Figure 26. Cases 3a and 3b – No axial restraint

V.3.1 Case 3a – Half of the unrestrained frame

The beam axial compressive forces of both restrained (case 1) and unrestrained (case 3a) frames calculated by SAFIR, ABAQUS and ADAPTIC are shown in Figure 27. The existence of lateral restraints can cause considerable compression force compared with the cases without lateral restraints due to thermal expansion effects. It is also showed that the results from the three programs SAFIR, ABAQUS and ADAPTIC present a good correlation.

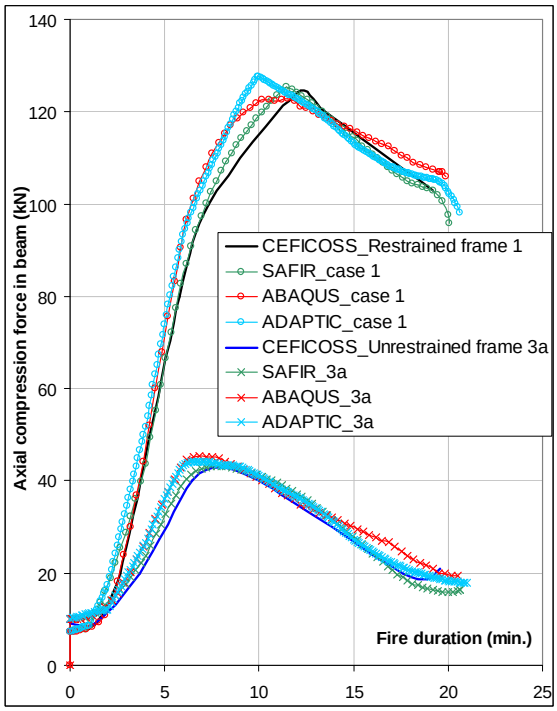

Figure 27. Calculated axial force in the beam

The peak values reached by the axial compression forces in the beam are equal to 125.40 kN and 43.23 kN with SAFIR, 122.92 kN and 45.43 kN with ABAQUS, and 127.60 kN and 44.20 kN with ADAPTIC when restraint is present and absent respectively, as shown in Table 3. At failure, the axial compression force in the beam is reduced from 95.97 kN to 16.43 kN with SAFIR, 105.83 kN to 19.38 kN with ABAQUS, and 98.1 kN to 17.80 kN with ADAPTIC, when lateral restraint is removed. However, it can be seen in Table 4 that the beam axial force does not significantly influence the fire resistance and the stability of the structure. Table 4 also shows that a good correlation is found between the fire resistance times calculated by the three programs SAFIR, ABAQUS and ADAPTIC.

Table 3. Axial compression forces (N) calculated by SAFIR, ABAQUS and ADAPTIC – All the values are given in kN.

		N SAFIR	**N ABAQUS**	**N ADAPTIC**
Peak value	Case 1 (restrained frame)	125.40	122.92	127.60
	Case 3a (unrestrained frame)	43.23	45.43	44.20
Failure value	Case 1 (restrained frame)	95.97	105.83	98.10
	Case 3a (unrestrained frame)	16.43	19.38	17.80

Table 4. Fire resistance time (R_f) calculated by SAFIR, ABAQUS and ADAPTIC

	R_f SAFIR	R_f ABAQUS	R_f ADAPTIC
Case 1 (restrained frame)	20’04’’	19’55’’	20’36’’
Case 3a (unrestrained frame)	***20’38’’***	***20’31’’***	***21’00’’***

V.3.2 Case 3b – Entire unrestrained frame

The failure mode of this complete frame without spring and with account of an initial imperfection (case 3b) is completely different from the one observed in the previous modelling (case 3a). Without spring and with the 0.8 H_c/1000 of initial imperfection (see § V.2), a non-symmetrical response of the frame can be developed as confirmed in Figure 28 by the shape of the structure deformation at failure. This leads to a significant reduction of the fire resistance, as shown in Table 5. The three programs obtain very close results.

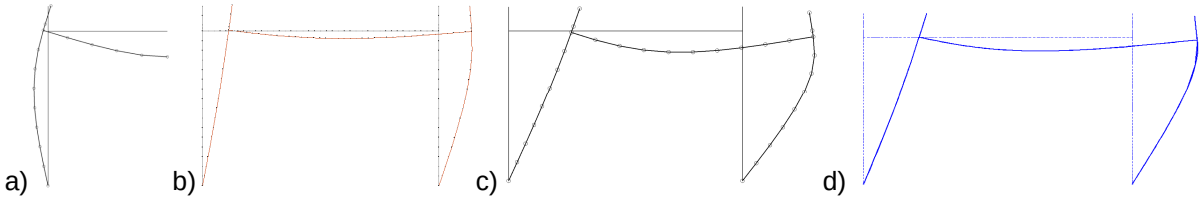

Figure 28. Calculated failure modes (scale 4/1) of the sway frame in (b) SAFIR, (c) ABAQUS and (d) ADAPTIC compared to the case 3a failure mode in (a) ABAQUS

Table 5. Fire resistance time (R_f) calculated by SAFIR, ABAQUS and ADAPTIC

	R_f SAFIR	R_f ABAQUS	R_f ADAPTIC
Case 1 (restrained frame)	20'04''	19'55''	20'36''
Case 3b (complete unrestrained frame)	***12'08''***	***12'17''***	***12'42''***

Figure 29 and Figure 30 present the horizontal and vertical displacements of the top of the column and the beam mid-span displacement calculated by the three programs. A similar behaviour is showed between ABAQUS (red curves) and ADAPTIC (blue curves), that reach higher displacements than SAFIR (green curves), but the fire resistance time computed by ABAQUS is closer to the fire resistance time obtained by SAFIR.

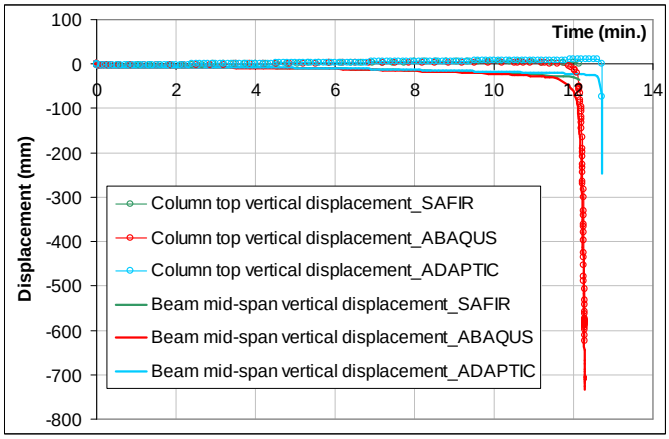

Figure 29. Column top vertical displacement and beam mid-span vertical displacement (case 3b) computed by SAFIR, ABAQUS and ADAPTIC

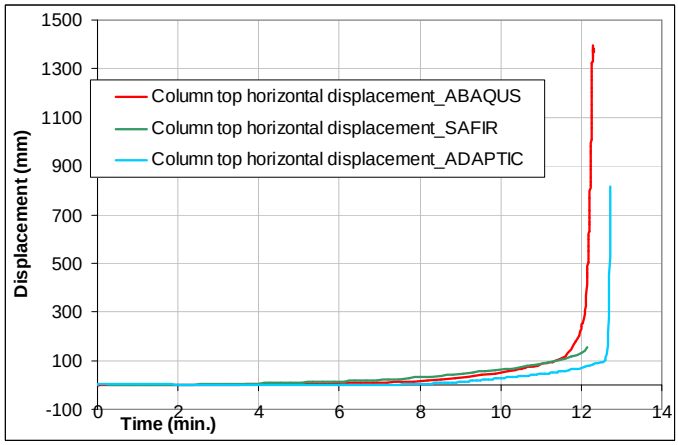

Figure 30. Column top horizontal displacement (case 3b) computed by SAFIR, ABAQUS and ADAPTIC

V.4 Influence of the frame continuity

It has long been recognized that the provision of continuity could increase the fire resistance of a structure and that a complete structure does not behave as the sum of its separate members. To illustrate and quantify this claim, the beam and column of the test frame have been analysed separately (cases 4a and 4b respectively).

V.4.1 Case 4a – Beam analysed separately

The beam is considered on its own. Figure 31 shows the bending moment and the horizontal force introduced by the column at ambient temperature and added to the load applied by the hydraulic jack during the test.

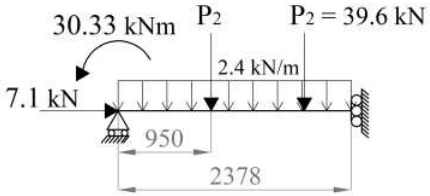

Figure 31. Beam as a separate member – Case 4a

Table 6 presents the fire resistance times and Figure 32 presents the evolution of the beam mid-span vertical displacement computed by the three programs for the beam as a separate member. These displacements are compared with the vertical displacement of the beam as part of the frame measured during the experimental test. It clearly shows that the fire resistance time reduces and the vertical displacement is higher in the absence of beneficial restraints from the column.

Table 6. Fire resistance time (R_f) calculated by SAFIR, ABAQUS and ADAPTIC

	R_f SAFIR	R_f ABAQUS	R_f ADAPTIC
Case 1a (restrained frame)	20’04’’	19’55’’	20’36’’
Case 4a (beam as a separate member)	***17’29’’***	***17’00’’***	***17’00’’***

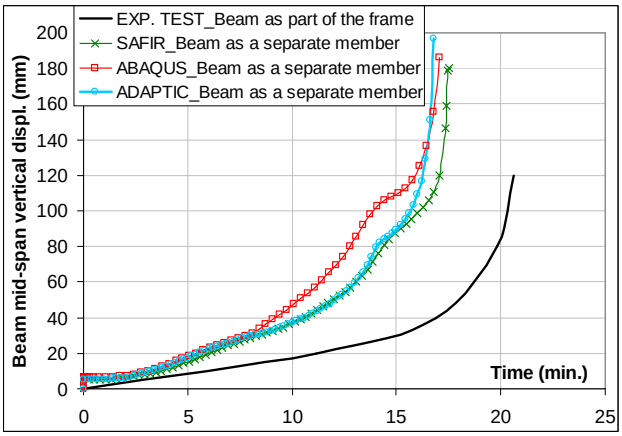

Figure 32. Beam mid-span displacement – Case 4a

V.4.2 Case 4b – Column analysed separately

The column is considered on its own, taking into account effects of the beam by applying a bending moment and a vertical force at the top of the column, as shown in Figure 33.

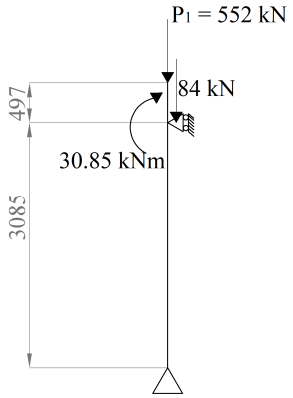

Figure 33. Column considered on its own – Case 4b

All the programs SAFIR, ABAQUS and ADAPTIC obtain fire resistances of at least 30 minutes. The column remains stable and no collapse is observed. The lateral displacement behaviour of the column as a separate member is presented in Figure 34 and compared to the behaviour of the column modelled as part of the frame (computed by CEFICOSS). It is showed that modelling the column on its own provides completely different results for the column behaviour, and it remains safe until the end of the analysis, against the failure at t = 20min. observed at the complete frame. The irregularity in the ABAQUS curve about 14-15 minutes is explained by the applied temperature gradient (see Figure 8 in the §III.4.3). Good correlations are obtained with the three programs for the column on its own as well as for the beam on its own.

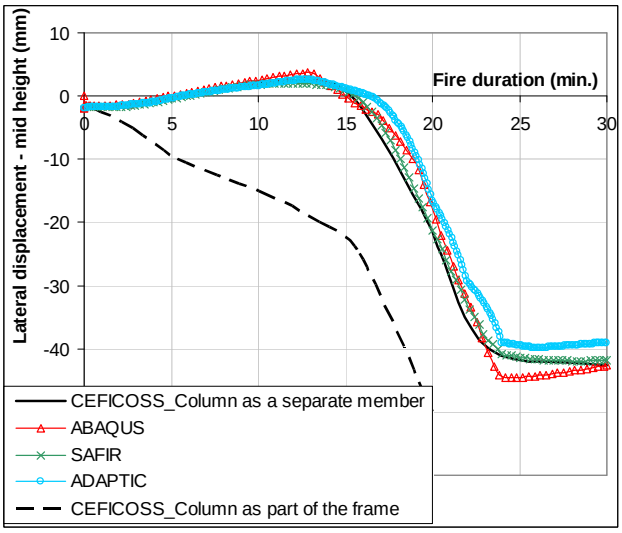

Figure 34. Calculated horizontal displacement at mid height of column

It can be noted that the ABAQUS result of this case 4b is influenced by mesh size, as shown in Figure 35, where four calculi are performed with four different average beam element length 0.4m (the average element length used in CEFICOSS), 0.2m, 0.1m and 0.01m.

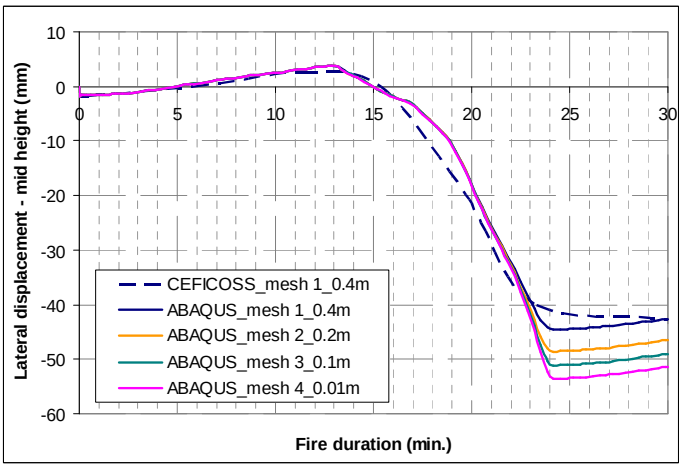

Figure 35. Calculated horizontal displacement at mid height of column (case 4b – separate member) – Influence of the mesh size

V.5 Influence of the thermal expansion

The total thermal expansion from a reference temperature is defined by the thermal expansion coefficients, which generate thermal strains. The influence of the thermal expansion on the fire resistance of the frame is tested by modelling the reference structure (Figure 4) without any thermal expansion coefficients (case 5). Franssen concluded that the expansion coefficients have a significant effect on the structure response (Franssen et al., 1995). Indeed, according to the results of SAFIR, ABAQUS and ADAPTIC, **without** expansion coefficients:

- The fire resistance increases from about 19-20 min. (case 1) up to the end of the analysis – 30 min. (case 5) and probably more because of the cooling of the steel as the fire decays (Franssen et al., 1995). However,

because no experimental temperatures were measured after 30 min., the numerical analyses were also limited to this time;

- The axial compression load in the beam increases much less;
- The lateral displacement of the column decreases because of the absence of the thermal expansion of the beam that was pushing the column outward.

The three programs ABAQUS, SAFIR and ADAPTIC presents good correlations. However, according to Franssen, when the fire is more severe, the expansion coefficient does not have such a significant effect (Franssen et al., 1995).

V.6 Influence of the non-uniform distribution of temperature

Within this paragraph, a uniform temperature for the cross-section of the beam and the column is calculated with a simplified method proposed in EN 1993-1-2: 2005. The emissivity of steel column is only 0.3 on the outer flange and 0.5 on the inner flange. According to Franssen (Franssen et al., 1995), an average emissivity equal to 0.4 can be used to calculate the uniform temperature. The column is assumed to be exposed to the fire only on its flanges because of the concrete blocks isolating the web. The section factor is then equal to $(2b_c+4t_{fc})/A_c = 69m^{-1}$; where b_c is the width of the column, t_{fc} is the thickness of the column flange and A_c is the area of the column cross-section. The top flange of the beam is protected by the concrete slab, so the beam section factor is equal to $(3b_b-2t_{wb}+2h_b)/A_b = 193m^{-1}$; where b_b is the width of the beam, t_{wb} is the thickness of the beam web, h_b is the height of the beam and A_b is the area of the beam cross-section.

Figure 36 illustrates the uniform temperatures computed by the actual EN 1993-1-2:2005 (EC3). These values are compared to the mean values of the temperatures calculated by the heat transfer analysis in CEFICOSS, SAFIR and ABAQUS. The maximum uniform temperature reached into the beam is 809ºC after 20 minutes whereas the maxima mean temperatures are 709℃ and 737ºC in SAFIR and ABAQUS respectively. In the column, a temperature of 500℃ is reached 3-4 minutes earlier with the uniform temperature assumption computed with Eurocode 3. The uniform temperatures at the end of the test are also 40ºC and 91ºC higher than mean temperatures for the column in SAFIR and ABAQUS respectively. Mean temperatures calculated by CEFICOSS, SAFIR and ABAQUS are lower than the uniform temperatures calculated with the simple model of EN 1993-1-2:2005 because the heat transfer from the steel to the concrete is not considered by the simplified calculation method.

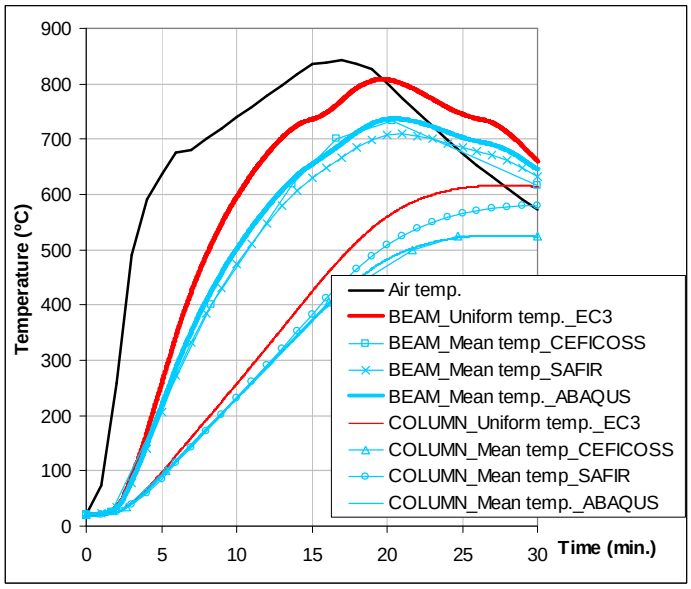

Figure 36. Calculated uniform and mean temperatures

Results and comparisons of the fire resistance obtained by the numerical tools SAFIR, ABAQUS and ADAPTIC using uniform temperatures (case 6) and temperature gradients in the cross-section (case 1) are presented in Table 7. The mechanical models in SAFIR, ABAQUS and ADAPTIC using the uniform temperature in the beam and column sections, calculated according EN 1993-1-2:2005, give a lower fire resistance time than with a thermal gradient (case 1). It can be explained by the fact that the mean temperatures computed through the programs are lower than the uniform temperatures computed with EN 1993-1-2:2005.

Table 7. Fire resistance time (R_f) calculated by SAFIR, ABAQUS and ADAPTIC

	R_f SAFIR	R_f ABAQUS	R_f ADAPTIC
Case 1 (gradient of temperature)	20'04''	19'51''	20'36''
Case 6 (uniform temperature)	***19'16''***	***19'00''***	***19'36''***

Then three temperature distributions are assumed and compared: i) Real tested non-uniform temperature distribution, which is used in all the above sections; ii) Uniform temperature distribution proposed in EN 1993-1-2: 2005; and iii) Mean temperature value of the non-uniform temperature distribution. The vertical displacement of beam mid-span and horizontal displacement of column mid-height for all the three cases are showed in Figure 37, Figure 38 and Figure 39 computed by, respectively, SAFIR, ABAQUS and ADAPTIC. However, the results from SAFIR with the mean temperatures into cross-sections were not available. It seems from ABAQUS (Figure 38) and ADAPTIC (Figure 39) that no collapse is observed for frames under the mean temperature distribution, which is due to the relatively lower calculated temperature and the absence of thermal bow. On the other hand, structural responses of the frame under calculated uniform temperature distributions (Eurocode) is similar to non-uniform temperature case, but the fire resistance time of uniform temperature case is slightly less than non-uniform one. So the uniform temperature calculated using EN 1993-1-2:2005 method leads to conservative results (premature failure)

while the mean temperature leads to unsafe results (no failure is observed until the end of the analysis).

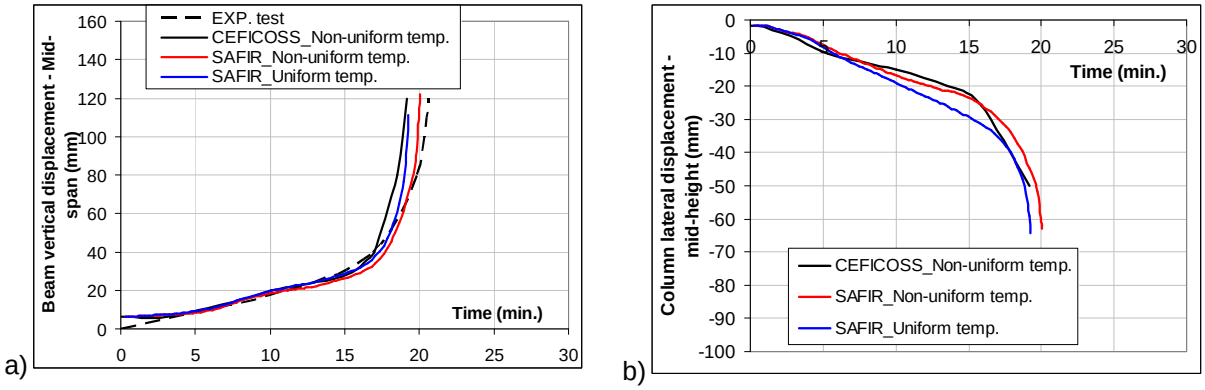

Figure 37. SAFIR results of the half of the frame calculated for different applications of the cross-section temperatures – a) Vertical displacement of the beam mid-span; b) Horizontal displacement at the column mid-height

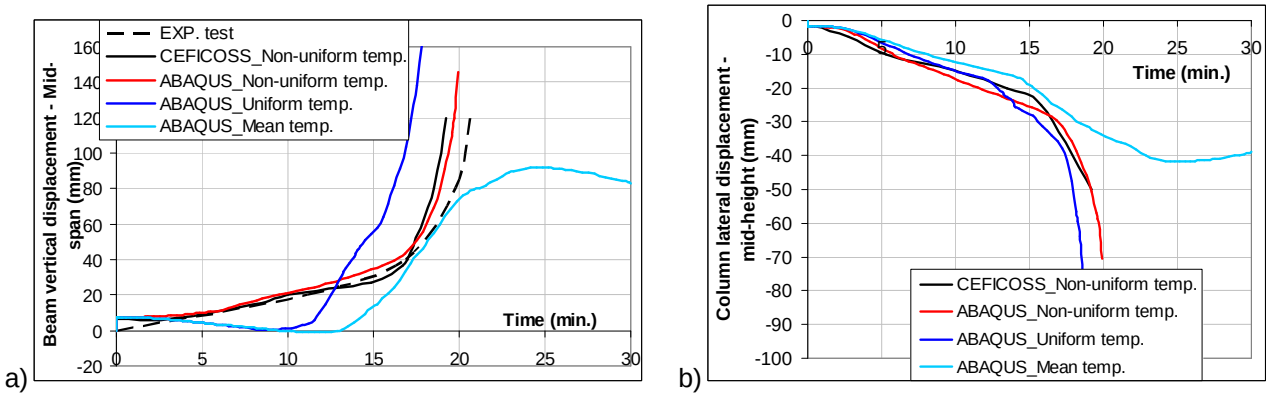

Figure 38. ABAQUS results of the half of the frame calculated for different applications of the cross-section temperatures – a) Vertical displacement of the beam mid-span; b) Horizontal displacement at the column mid-height

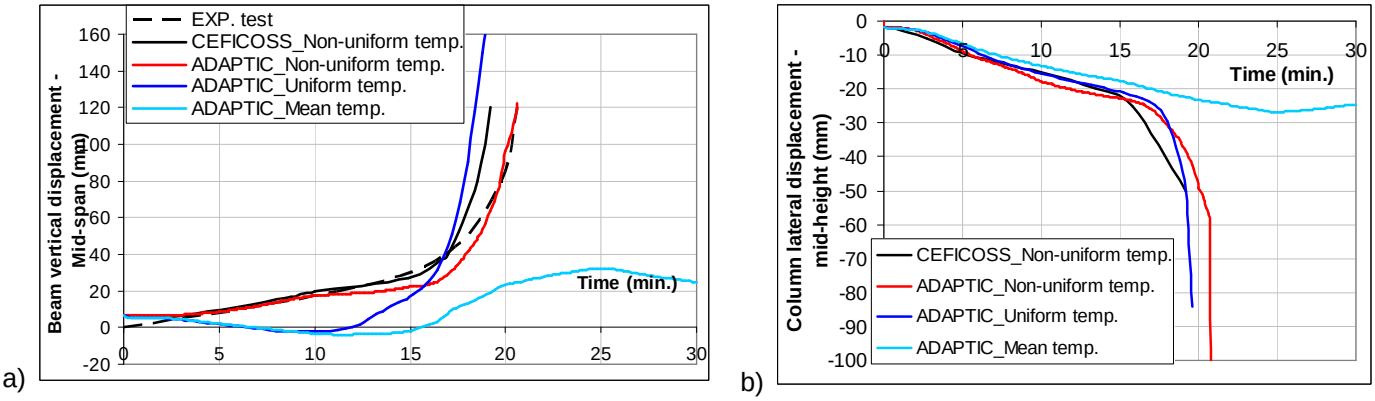

Figure 39. ADAPTIC results of the half of the frame calculated for different applications of the cross-section temperatures – a) Vertical displacement of the beam mid-span; b) Horizontal displacement at the column mid-height

VI Concluding remarks

This document presented a comparison between the finite element programs that will be used during the ROBUSTFIRE project by three partners: a specialized homemade program dedicated to the analyses of structures subjected to fire, SAFIR, a commercially available program ABAQUS and a homemade finite element program ADAPTIC. The main objective was to validate the utilization of the SAFIR, ABAQUS and ADAPTIC programs for steel structures subjected to fire. The results obtained were also compared to another FEM called CEFICOSS which is in fact the predecessor of SAFIR.

The simple 2D steel frame studied in this document was based on the paper of Franssen published in 1995 about a natural fire test on a fully loaded, two dimensional, unprotected steel framework carried out in a purpose-built compartment in Cardington (Franssen et al., 1995). The influence of the model definition, axial restraint to the beam, frame continuity, thermal expansion and non-uniform temperature were discussed.

SAFIR and ABAQUS performed well the heat transfer analysis to obtain temperature distributions in structures, while ADAPTIC was not able to realize such analysis and directly used the results obtained by the FE program CEFICOSS.

SAFIR, ABAQUS and ADAPTIC showed a good ability to simulate steel structural behaviour under fire conditions using beam elements.

Some of the differences between the different results could be explained by some reasons:

- The temperature gradients in cross-sections were approximated in ABAQUS as they only could be defined into three dependant points in the cross-section.
- The temperatures used by ADAPTIC were extracted from the paper of Franssen (Franssen et al., 1995), from the results of CEFICOSS, which could lead to slight inaccuracies.
- The difficulty to simulate the behaviour of springs with SAFIR (no dedicated finite element), in particular when investigating the behaviour of the complete structure.
- ABAQUS fire resistances were defined as the beginning of the strongly decrease of the beam axial compression-time curve. In reality, ABAQUS stops a few times after. So the precision of the fire resistance value depends of the increment sizes, but also of the appreciation of the person.
- The CEFICOSS and experimental results were only available via the paper of Franssen (Franssen et al., 1995) and all values were directly measured on this paper.
- CEFICOSS being the predecessor of SAFIR, with a version from 1995, some differences could be related to some changes of code that occurred in the last 14 years in terms of numerical techniques and abilities.

In conclusion, the numerical programs SAFIR, ABAQUS and ADAPTIC were validated for analysis of steel structures subjected to fire and modelled with beam elements. As part of the ROBUSTFIRE project, the next step will be to get preliminary results for the experimental tests preparation, and then to calibrate the FE models with the experimental tests results. Finally, parametric studies will be performed so as to investigate the influence of various parameters on the fire response of the structural elements.

REFERENCES

- ABAQUS Theory Manual & Users Manuals, Version 6.7, Hibbitt, Karlsson and Sorensen, Inc. USA, 2007.
- Cooke G.M.E., Latham D.J. “The inherent fire resistance of a loaded steel framework”. Steel Construction Today, 1, 49-58, 1987.
- EN 1992-1-2:2004. “Eurocode 2: Design of concrete structures – Part 1-2: General rules – Structural fire design”. European committee for standardization, December 2004.
- EN 1993-10:1990. “Eurocode 3: Design of Steel Structures, Part 10: Structural Fire Design”. Draft April 1990.
- EN 1993-1-2:2005. “Eurocode 3: Design of steel structures – Part 1-2: General rules – Structural fire design”. European committee for standardization, April 2005.
- Franssen J.M. “Etude du comportement au feu des structures mixtes acier béton”. PhD Thesis, University of Liège, 1987.
- Franssen J.M., Cooke G.M.E., Latham D.J. “Numerical Simulation of a Full Scale Fire Test on a Loaded Steel Framework”. Journal of Constructional Steel Research, 35, 377-408, 1995.
- Franssen J.M., Kodur V.K.R., and Mason J. “User Manual for SAFIR 2001, A computer program for analysis of structures submitted to the fire”. University of Liège, Belgium, 2000.
- Franssen J.-M. “SAFIR. A Thermal/Structural Program Modelling Structures under Fire”, Engineering Journal, A.I.S.C., Vol 42, No. 3, 143-158, 2005.
- Izzuddin, B.A. “Nonlinear Dynamic Analysis of Framed Structures”. PhD Thesis, Department of Civil Engineering, Imperial College, University of London, London, UK, 1991.
- Lim L., Buchanan A., Moss P., Franssen J.M. “Numerical modelling of two-way reinforced concrete slabs in fire”. Engineering Structures, 26, 1081-1091, 2004.
- Liu T.C.H. “Theoretical Modelling of Steel Bolted Connection under Fire Exposure”. Proceedings of International Conference of Computational Methods in Structural and Geotechnical Engineering Mechanics, Hong Kong, 1994.
- Liu T.C.H. “Finite element modelling of behaviour of steel beams and connections in fire”. Journal of Constructional Steel Research, 36(2), pp.181-199, 1996.
- Wang Y.C. “Steel and composite structures – Behaviour and design for fire safety”. Spon Press, 2002.

ANNEX – Franssen et al., 1995

ELSEVIER

J. Construct. Steel Research 35 (1995) 377–408
1995 Elsevier Science Limited
Printed in Malta.
0143-974X(95)00010-0
0143-974X/95/$9·50

Numerical Simulation of a Full Scale Fire Test on a Loaded Steel Framework

J. M. Franssen,[a] G. M. E. Cooke[b] & D. J. Latham[c]

[a]National Fund for Scientific Research, University of Liège, Belgium
[b]Fire Research Station, Building Research Establishment, Garston, Watford, UK
[c]Swinden Laboratories, British Steel Technical, Moorgate, Rotherham, UK

(Received 10 June 1993)

ABSTRACT

This paper presents the results of a number of numerical simulations of the behaviour in a real fire of a full-size, loaded, two-dimensional, mainly unprotected steel frame. Data from the fire test, reported in Steel Construction Today 1987, provides the benchmark. The application of one, two and three-dimensional heat flow models is discussed, and the basis of the structural model used is described. The influence of lateral restraint, frame continuity and thermal expansion is quantified using the computer model. In contrast the simple method in draft Eurocode 3 is used to calculate the frame stability assuming that the temperatures of the beam and columns are uniform across their sections, and good agreement with the test result is shown. It is suggested that a rigorous computer program, like that described in the paper, could be usefully employed to identify those types of structure which might be analysed safely by the simplified method.

1 INTRODUCTION

It has been known for many years that, in common with all other materials, a steel structure may suffer loss of load bearing capacity and even collapse when submitted to the action of a severe fire.

The problem of steel in fire is not so much the loss of strength and stiffness with increasing temperature (comparable with the behaviour of other building materials) as the fact that the temperature in steel tends to increase rapidly due to the action of the fire and the high thermal conductivity of steel. One way to solve, or rather to avoid, the problem is to protect steel structures

with insulating materials, thus delaying the temperature increase in the steel.

However, it is also known that a structure may reach higher temperatures while remaining stable provided that the load factor, i.e. the ratio between the actual load and the ultimate load at ambient temperature, is reduced.[1] Continuity (hyperstaticity) can therefore be a good solution in order to reduce the amount of insulating material used. At ambient temperatures, but even more at elevated temperatures, a continuous structure behaves better than the separate members and it is thus desirable to design as a complete structure.

Historically, the first fire safety design method relied entirely on full scale tests. Tests are expensive, time consuming and difficult to perform, especially on complete structures. Yet they may still be necessary to investigate new building systems or to validate theoretical models. British Steel plc (BS) and the Department of Environment (DoE) sponsored such a fire test which was performed in the Fire Research Station's Cardington Laboratory on a full size, fully loaded, two-dimensional steel frame[2] to generate data for use in the complementary development of analytical techniques to simulate the structural stability of steelwork in natural fire.

As elastic analysis leads to conservative results, theoretical design methods for steel structures exposed to fire mainly rely on the theory of plasticity, and this is widely used and accepted for simple structures such as continuous beams.

For other structures, where large displacements and the effect of restraint affect stability, the complexity of the problem makes it amenable to solution by numerical models which, based on acknowledged principles of the theory of structural mechanics, are able to consider, amongst other things, the visco-elasto-plastic behaviour of steel, the effects of thermal gradients, large displacements, restraint forces, and residual stresses. The first author has been active in the development of such a computer code at the University of Liège[3,4] and the other two authors are deeply involved in UK fire modelling work involving FRS, BS, Sheffield University,[5] City University,[6] and others. Much work on the subject has been undertaken elsewhere.[7–14]

Recent recommendations have been presented in Luxembourg within the Eurocode context[15,16] for the thermal and mechanical properties of steel at elevated temperatures for use in numerical models. The recommendations are under discussion and may be modified but they indicate what could be utilised in Europe for the foreseeable future.

The aim of this paper is to show how the recommendations can be applied in a numerical model of frame behaviour and how the results provided by the numerical model compare with the fire test results. Results are reported for sensitivity analyses which explored the effect of varying some important parameters, for example, yield stress of steel.

2 THE CARDINGTON FIRE TEST ON A LOADED STEEL FRAMEWORK

A natural fire test on a fully loaded, two dimensional steel framework was carried out by British Steel in collaboration with the Fire Research Station of the Department of the Environment and is described in detail elsewhere.[2] The experiment was carried out in a purpose-built compartment with a floor area of 50 m^2 and a ceiling height of 3·9 m, a size typical of office accommodation. The front elevation of the compartment is shown in Fig. 1. Ventilation was controlled by means of shutters placed within the long walls to obtain as symmetrical a heating exposure as possible. The fuel load comprised timber cribs which, together with the selection of ventilation openings, achieved an Equivalent Fire Duration of 32·5 min in the test. This was considered sufficient to ensure that the loaded beam reached its limiting temperature during the fire.

2.1 Test frame

The steel framework selected for testing under load was typical of that used in a building of two or three storeys in height. It comprised a

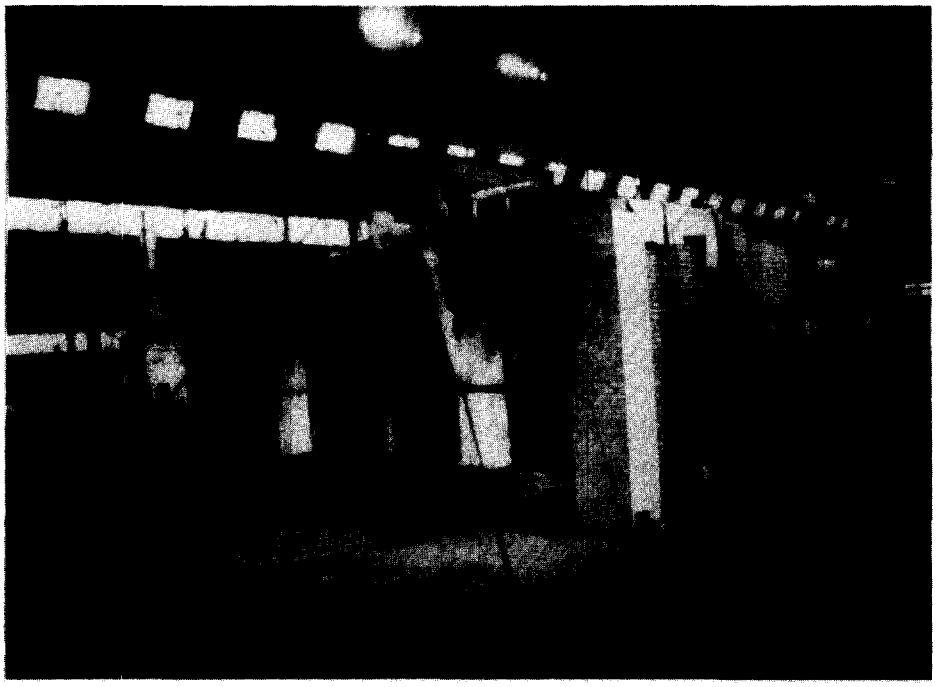

Fig. 1. Compartment with fire test in progress.

4550 mm length of 406 × 178 mm × 54 kg/m BS 4360:1979 Grade 43A universal beam section bolted to two 3530 mm lengths of 203 × 203 mm × 52 kg/m Grade 43A universal column section.

The test beam which spanned the compartment at ceiling height remained unprotected, but four 1200 × 5550 × 150 mm precast concrete slabs, which formed part of the compartment roof, were attached to the top flange by welded 12 mm diameter threaded bars. The slabs were separated by a gap of 25 mm to prevent composite action with the beam, and the gap was filled with ceramic fibre blanket. Each column, which extend above the beam, was pin jointed at the base. The webs were protected by autoclaved aerated concrete blocks with a density of 677 kg/m^3 (3·8% water content by weight) built between the flanges using an ordinary mortar mix. This system had been shown to be a relatively cheap method of raising the fire resistance of lighter freestanding columns to 30 min in the ISO 834 fire test. The beam/column connections utilised M20 Grade 8.8 bolts to provide improved resistance to loss in strength at high temperatures.

2.2 The loads

The complete assembly is shown schematically in Fig. 2. The test frame was centrally positioned inside the compartment, parallel to the short walls. It was surrounded by load reaction frames which gave a closed loading system so that only dead loads were transmitted to the floor. A

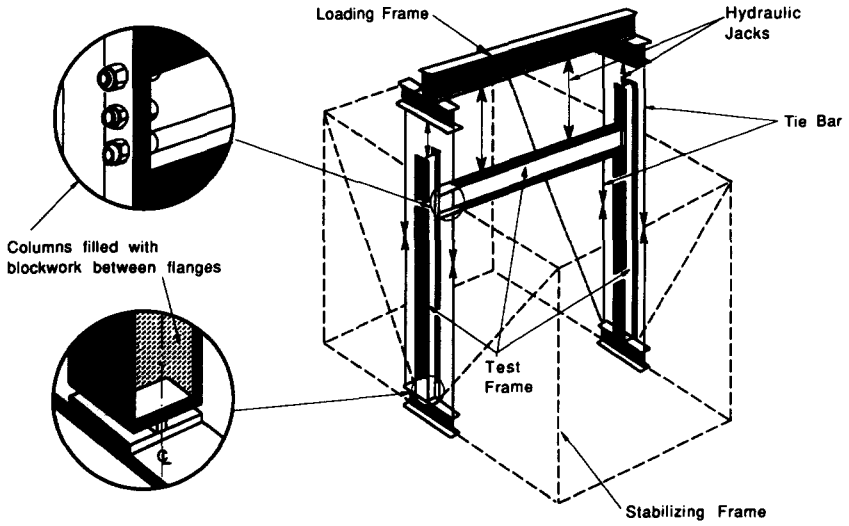

Fig. 2. Schematic layout of the loaded frame used in the Cardington tests.

subsidiary framework was designed to prevent lateral and sway instability in the test frame. A maximum axial compressive load of 552 kN was applied to each test column by an hydraulic ram and load cell placed between the top bearing plate and the load reaction frame. The test beam was loaded to 39·6 kN at each of four equal positions along the span. The loads were maintained constant throughout the fire test.

With the exception of the test frame, the remainder of the structure was fire protected.

2.3 Steel temperatures

During the fire, thermocouples fixed into the steel framework measured the changes in temperature in the flanges and the webs. The heating rate was fastest at the centre of the unprotected beam. Maximum temperatures of 775, 777 and 577°C were measured in this locality in the lower flange, centre of the web and upper flange, respectively, after 20 min. The corresponding temperatures in the lower flange and web close to the connections were 671 and 720°C, the web heating up more rapidly since it was thinner than the flange.

With regard to the blocked-in columns, the exposed flanges facing into the compartment heated up faster than the exposed flanges facing towards the walls mainly due to the difference in the radiation configuration factor. Thus for one column, a maximum temperature of 606°C was measured on the inward facing flange after 20 min, by which time the outward facing flange reached 514°C. Due to the protection provided by the blockwork, the centre of the web only attained a temperature of 251°C after 20 mins.

The load was removed from the structure after 22 min into the natural fire test. At this time the temperatures reached by the thread beneath the bolt heads were 397°C for the upper and 441°C for the lower bolt. The reduction in temperature along the thread, which extended into the blockwork, was approximately 100°C.

2.4 Deflection behaviour

The deflection of the structure was more complicated than the behaviour of isolated elements due to the effect of structural continuity and the non-uniform fire exposure which caused thermal bowing. The downward mid-span deflection of the beam increased with the rise in the steel temperature and the rate of deflection increased up to approximately 40 mm/min. The load was removed after 22 min when it could no longer be applied with safety. At this point the total deflection of the beam exceeded span/32.

At failure the beam exhibited considerable twisting as well as vertical deformation, together with tilting of the concrete slabs attached to the upper flange. Subsequent examination revealed the presence of a plastic hinge approximately 600 mm from each end of the beam and some plastic distortion of the welded end plates at the top of the connection.

The blocked-in columns expanded axially to reach a maximum extension of 20 mm after 15 min. The distance between the columns increased during the test due to the axial expansion of the beam and rotation of the ends of the beam due to thermal bowing. The average lateral displacements measured on the columns at different heights with time are shown in Fig. 3.

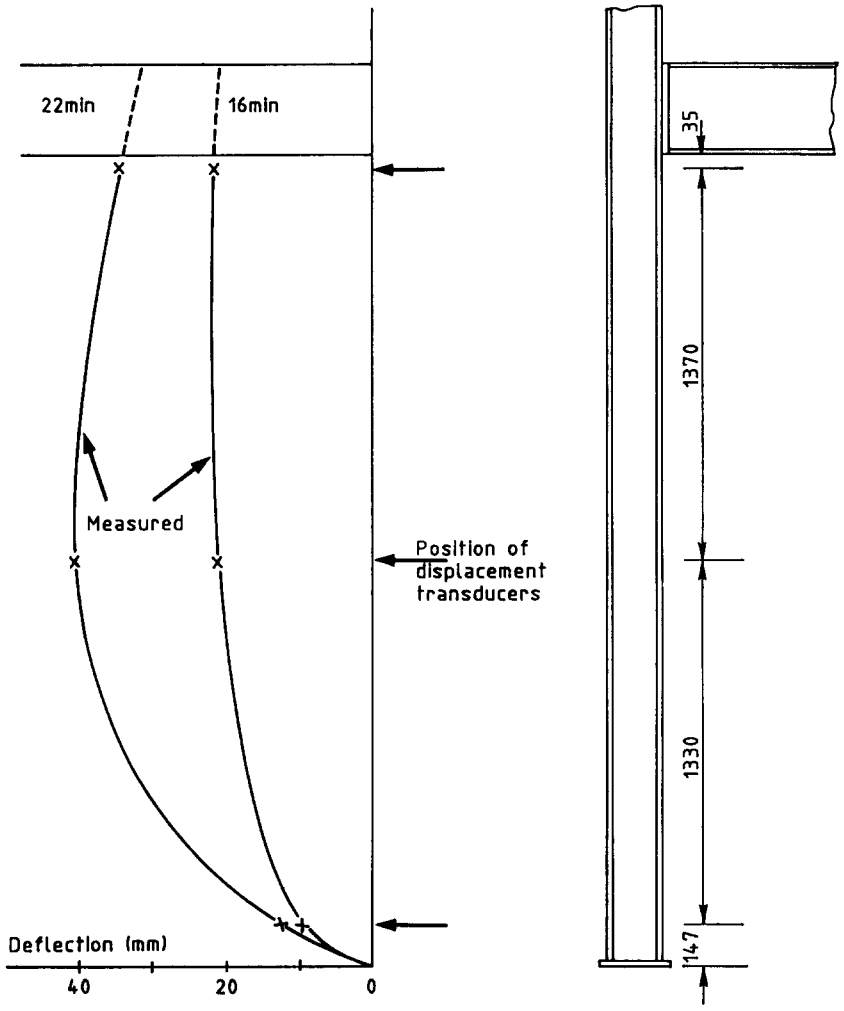

Fig. 3. Average lateral deflection of column in the fire test.

3 THE NUMERICAL MODEL

Before a calculation of load bearing capacity can be made it is necessary to know the temperature distribution in the structure. The temperature data may come from a fire test or be predicted from a knowledge of the fire environment. Except at the moment of complete collapse, the rates of deformation are low enough to neglect the heat that is caused by plastic straining. Hence the static state of the structure does not influence the temperatures of the structure. This generally accepted assumption allows the calculation of temperatures in the structure to be separated from the calculation of deformations, strains and stresses (structural calculation).

It should be noted that it is not at present possible to calculate the effect of excessive deformation of the supporting structure on the adhesion/cohesion of applied insulation material or the effect of cracks developing in concrete. Both effects could influence the temperatures attained by the structure.

Whatever method is used to calculate the temperatures within the structure, it is usual to regard the temperature of the environment (combustion gas) as the main parameter affecting the heat exchange between the environment (the fire or the furnace) and the structural member. Indeed, specifications for fire tests very often deal only with the evolution of combustion gas temperature in the furnace, without reference to the radiation from the furnace linings or burner flames which can markedly affect the heat transfer to the specimen as a test proceeds.

3.1 One-dimensional temperature distribution

An often-used approximation is the assumption of a uniform temperature distribution within the steel section, justified by the high thermal conductivity of steel. The section is then characterised at any point in time by one temperature (from which comes the concept of a critical or limiting temperature) and the equation describing this temperature increase is of the one-dimensional type. The section is characterised by its section factor (i.e. heat-exposed perimeter divided by cross-section area) and the heat flow equation can be adapted to consider the effect of an insulation protection.[17,18]

This method does not consider the temperature gradient that may arise over the depth of the cross-section. This can considerably influence the bowing of beams or the buckling of columns. Furthermore, if a steel beam is in direct contact with a concrete slab (as in the Cardington test) the heat transferred from the steel section to the concrete slab cannot be considered so that the uniform temperature calculated by the one-dimensional

approach differs from the average value of the two-dimensional temperature field.

This approximate method is therefore unsatisfactory if the deflection response is to be reliably modelled, but is commonly used together with the simple plastic design methods mentioned in the Introduction.

3.2 Two-dimensional temperature distribution

For slender structural members such as beams, columns or bars, a less restrictive assumption is that the temperature distribution does not vary along the length of the member. The main equations of the problem are two-dimensional with respect to the Cartesian coordinates y and z that are perpendicular to the longitudinal axis x.

Except for very simple cases, these equations must generally be solved numerically using finite element or finite difference techniques. In Liège, the first author has been using a two-dimensional finite difference program (thermal part of CEFICOSS see Refs 3 and 4), specifically written for the calculation of temperatures in composite steel-concrete building members exposed to fire. The cross section is discretized by a rectangular mesh, Fig. 4. The temperature and the type of material (steel, concrete or insulating material) are assumed to be uniform within each rectangle. The equation of heat transfer is transformed into a finite difference equation which can be written for every rectangle of the cross-section. The heat flow from the environment to the section is assumed to be convective and radiative.

The equations are integrated with respect to time by a totally explicit scheme which provides an equation in which all thermal properties are evaluated at the beginning of every time step. As the equation is written for each rectangle, there is no need to form and solve a large system of equations: for one time step it is only necessary to solve as many equations with one unknown as there are rectangles in the cross-section. The time step has to be chosen to ensure stability and convergence of the solution. The maximum allowable time step can be automatically computed[3] and, because of the temperature-dependent thermal properties of building materials, it usually increases as the member heats up. The limited size of most two-dimensional problems means that they can be easily solved with commonly-available desktop computers.

An advantage of the rectangular discretization is that the temperatures can be presented in a rectangular array which directly gives a good idea of the temperature distribution in the cross section, Table 1.

The main disadvantages of this code arise from its inability to deal with curved surfaces (as for circular columns or for the root radius of a hot

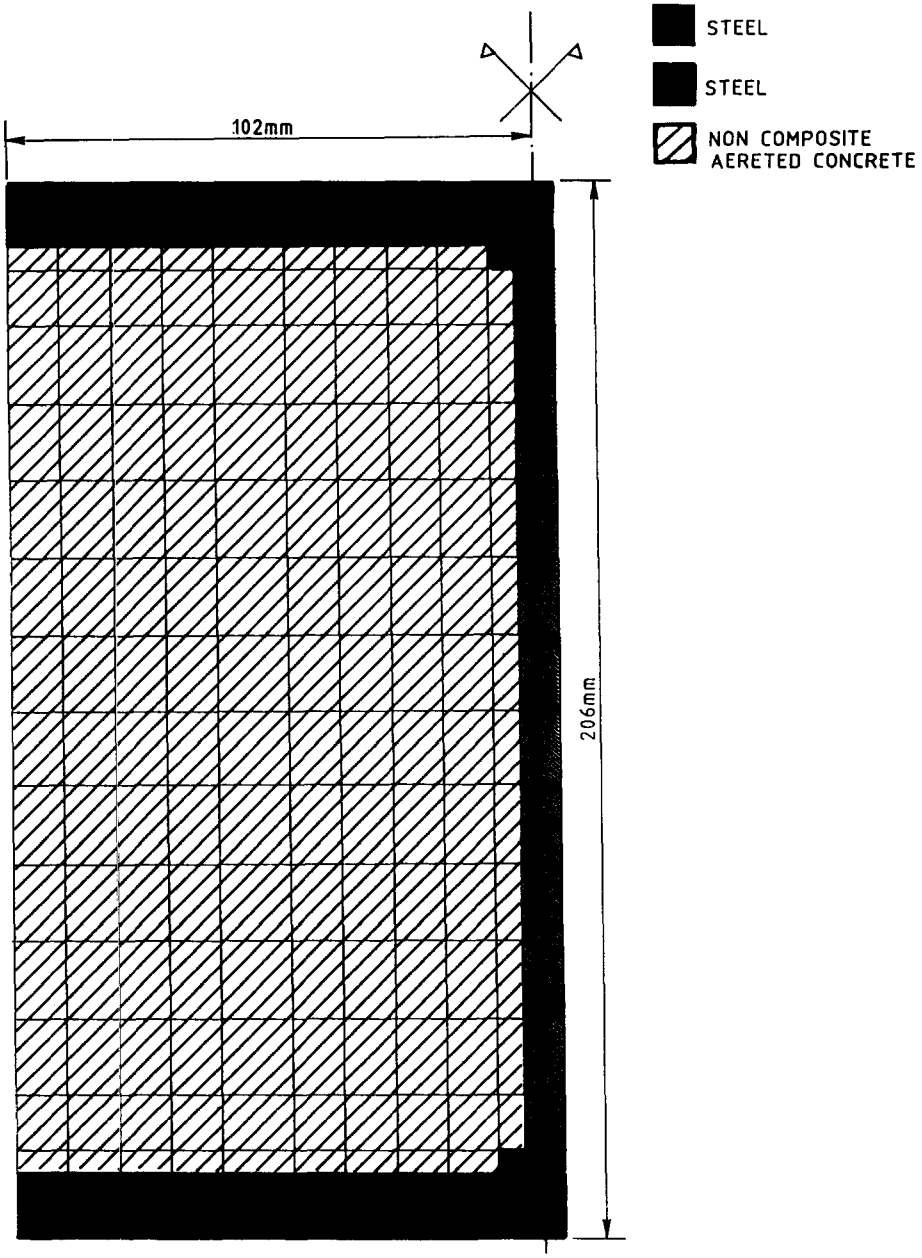

Fig. 4. Discretization of the column cross-section by $11 \times 16 = 176$ rectangles.

rolled steel profile) and with radiation between surfaces of internal voids (in hollow core concrete slabs or a steel profile insulated by a box casing). That is why a new thermal code based on the finite element technique has been written in Liège (THERMIN, see Ref. 19). However, as some

TABLE 1
Typical Presentation of Calculated Temperatures

Section type: 1 after 600 Seconds of Fire

The time step of the thermal calculation is 0·86 sec.

737·0	737·0	737·0	737·0	737·0	737·0	737·0	737·0	737·0	737·0	737·0	737·0
737·0	269·0	261·0	253·0	246·0	237·0	229·0	222·0	214·0	206·0	200·0	197·0
737·0	337·0	247·0	214·0	206·0	199·0	191·0	185·0	180·0	177·0	189·0	182·0
737·0	436·0	222·0	100·0	100·0	100·0	95·0	93·0	97·0	100·0	143·0	162·0
737·0	469·0	217·0	100·0	62·0	40·0	36·0	36·0	42·0	68·0	100·0	133·0
737·0	475·0	215·0	96·0	46·0	27·0	23·0	23·0	29·0	48·0	91·0	110·0
737·0	475·0	215·0	94·0	44·0	25·0	21·0	21·0	25·0	41·0	76·0	94·0
737·0	475·0	215·0	94·0	44·0	25·0	21·0	21·0	24·0	37·0	69·0	85·0
737·0	475·0	215·0	94·0	44·0	25·0	21·0	21·0	24·0	36·0	65·0	81·0
737·0	475·0	215·0	94·0	44·0	25·0	21·0	21·0.	24·0	36·0	67·0	83·0
737·0	475·0	215·0	94·0	44·0	25·0	21·0	21·0	25·0	39·0	73·0	91·0
737·0	475·0	215·0	94·0	44·0	25·0	21·0	22·0	26·0	44·0	86·0	105·0
737·0	475·0	216·0	97·0	47·0	27·0	24·0	24·0	31·0	55·0	100·0	126·0
737·0	472·0	221·0	100·0	68·0	47·0	42·0	42·0	50·0	85·0	106·0	156·0
737·0	451·0	241·0	100·0	100·0	100·0	100·0	100·0	100·0	100·0	170·0	194·0
737·0	380·0	295·0	259·0	250·0	242·0	233·0	226·0	219·0	214·0	230·0	221·0
737·0	330·0	320·0	310·0	301·0	291·0	281·0	272·0	263·0	253·0	244·0	240·0
737·0	737·0	737·0	737·0	737·0	737·0	737·0	737·0	737·0	737·0	737·0	737·0

modifications have still to be introduced to make the results of THERMIN utilizable by the structural part of CEFICOSS and because the thermal part of CEFICOSS has been used for the simulations presented in this paper, this new program THERMIN will not be described here.

3.3 Three-dimensional temperature distribution

Structural members may have temperature variations along their length as well as across their section due to differences in heat input and heat loss (axial heat sink effects). Three-dimensional temperature distribution can occur in, for example:

- continuous beams (or columns) with some spans (or storey heights) exposed to fire and others not;
- continuous beams with every span exposed to fire but supported on masonry walls which provide shielding and act as local heat sinks;
- connections between members of different type (different size and shape).

There are several programs specifically dedicated to the calculation of three-dimensional temperature fields in building members exposed to fire. One is FIRES-3D[20] mainly used for reinforced concrete. Important endeavours have also been made in Germany concerning composite steel-concrete structures.[12]

To model three-dimensional temperature distributions it is usually sufficient to extend the two-dimensional discretization of the cross-section along the third dimension prismatically so that the discretization of the cross-section is the same at every location on the longitudinal axis. Such three-dimensional temperature distributions can be directly used in the structural computer code avoiding tedious manual input of temperatures if beam (i.e. prismatic) finite elements are used.

There are however some problems for which beam finite elements are unsuitable, and brick finite elements should then be used. An example is a connection detail for a beam-to-column joint. The temperatures resulting from such a calculation can be used in the structural computer code if the latter is also based on the brick model. The amount of data to introduce, the time taken to sort the results and analyse them, as well as the time taken in computing, make such three-dimensional brick models suitable mainly for the analysis of local details, and not the analysis of complete structures.

In the structural part of the program CEFICOSS from Liège, the effect of the third dimension in the temperature distribution can be introduced to some extent by an approximate method. If $T_2(y, z, t)$ is the two-dimensional temperature distribution that has been calculated, it is possible to consider in the structural calculation that the temperature increase at a particular point, $\Delta T_3(x, y, z, t)$, is only a fraction of ΔT_2, such that:

$$\Delta T_3(x, y, z, t) = f(x)\Delta T_2(y, z, t)$$

or

$$T_3(x, y, z, t) - T_0 = f(x)\,(T_2(y, z, t) - T_0)$$

where:

t = time
T_0 = initial temperature
f = reduction function obtained from experimental data or a more specific thermal analysis.

This approximate method makes it possible to get some qualitative information about the influence of the third dimension. It has also been

used here when considering the temperature increase in the beam of the Cardington test.

3.4 Basis of structural model

Though finer discretization could be necessary to investigate local problems such as local buckling phenomena, the beam element discretization seems to be suitable for the analysis of complete steel frames.

The structural part of the CEFICOSS program developed in Liège[3] is based on a plane beam finite element. The element has two nodes with three degrees of freedom. It is accepted that it would probably be better to use an element with three nodes and seven degrees of freedom if highly unsymmetrical (with respect to the depth of the section) plastic zones are expected.[21] Shear energy is not considered and the expression of Jennings[22] is used for the axial strain.

The cross-section is discretized using the rectangular mesh used for the thermal calculation so that the calculated temperatures can be directly used by the structural part of the program. All variables (type of material, temperature, strain, stress, tangent modulus, plastic strain...) change from one rectangle to another. The same advantage of a clear presentation of the results derives from the rectangular discretization, Table 2.

The effect of large displacements are taken into account by an updated Lagrangian description. The developments are classical if not for the fact of the numerical integration on the rectangles of the cross-section to compute the tangent stiffness matrix and the internal forces (fibre model). The longitudinal integration is by the Gauss method, using two points of integration.

It is possible to use the non-linear stress–strain relationships and thermal strains of materials recommended in Parts 10 of Eurocode 3[15] or Eurocode 4[16] which means that creep strain is implicitly introduced in the stress-related strain.

The program proceeds step by step. The load is first applied in several increments at ambient temperature. Stresses, strains and displacements are then calculated at a number of time steps during the fire up to failure.

4 MODELLING THE CARDINGTON FIRE TEST

In the first simulation, no initial imperfection of the frame geometry was introduced and, for reasons of symmetry, the longitudinal discretization and node numbering is as shown in Fig. 5. The restraint offered by the secondary steelwork may be regarded as a spring at node 11. The

TABLE 2
Typical Presentation of Calculated Stresses

After 600·0 Seconds of fire

Stresses in element: 8, point of integration: 2

3·10	5·12	7·15	9·10	11·34	13·58	15·54	17·61	19·83	21·62	22·46
0·00	0·00	0·00	0·00	0·00	0·00	0·00	0·00	0·00	20·35	22·19
0·00	0·00	0·00	0·00	0·00	0·00	0·00	0·00	0·00	0·00	24·12
0·00	0·00	0·00	0·00	0·00	0·00	0·00	0·00	0·00	0·00	25·51
0·00	0·00	0·00	0·00	0·00	0·00	0·00	0·00	0·00	0·00	24·13
0·00	0·00	0·00	0·00	0·00	0·00	0·00	0·00	0·00	0·00	20·34
0·00	0·00	0·00	0·00	0·00	0·00	0·00	0·00	0·00	0·00	14·56
0·00	0·00	0·00	0·00	0·00	0·00	0·00	0·00	0·00	0·00	7·22
0·00	0·00	0·00	0·00	0·00	0·00	0·00	0·00	0·00	0·00	−1·62
0·00	0·00	0·00	0·00	0·00	0·00	0·00	0·00	0·00	0·00	−12·01
0·00	0·00	0·00	0·00	0·00	0·00	0·00	0·00	0·00	0·00	−23·98
0·00	0·00	0·00	0·00	0·00	0·00	0·00	0·00	0·00	0·00	−37·18
0·00	0·00	0·00	0·00	0·00	0·00	0·00	0·00	0·00	0·00	−37·59
0·00	0·00	0·00	0·00	0·00	0·00	0·00	0·00	0·00	0·00	−36·41
0·00	0·00	0·00	0·00	0·00	0·00	0·00	0·00	0·00	−35·54	−35·77
−33·97	−34·09	−34·21	−34·34	−34·50	−34·67	−34·83	−35·01	−35·23	−35·41	−35·50

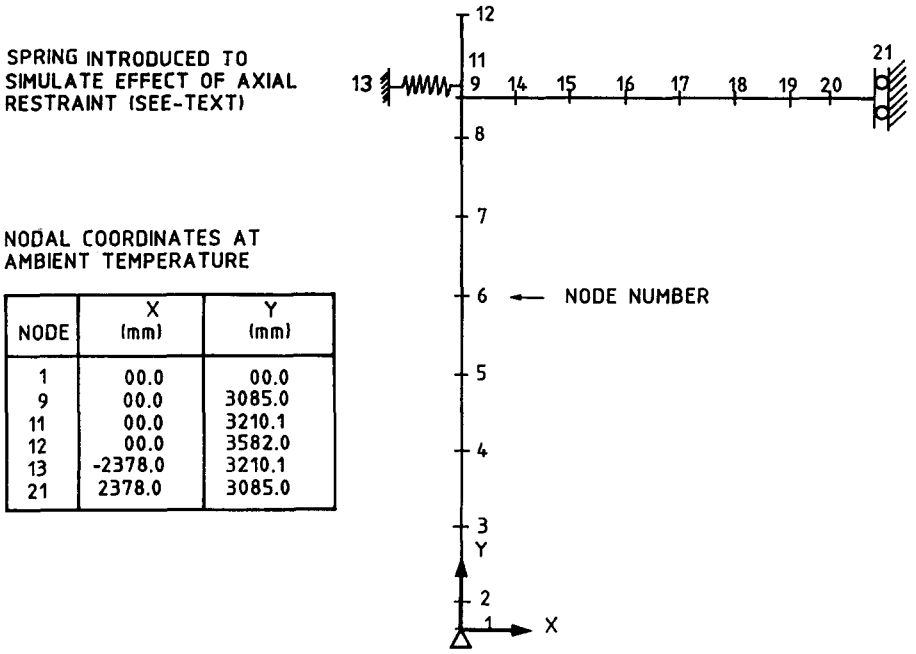

Fig. 5. Longitudinal discretization of frame.

calculated values of the axial stiffness (67 kN/cm) and the axial plastic load (86 kN) represents the bending stiffness and resistance of the supporting framework which remained at room temperature due to the presence of thermal insulation. The influence of lateral restraint and the assumption of symmetry are discussed later.

Although residual stresses are known to have a significant influence on the fire behaviour of concentrically loaded steel columns,[23] they are ignored in the analysis because of the over-riding effects of thermal bowing and the presence of bending moments in the columns. The columns are pin-jointed at the base while the beam is rigidly fixed to the columns. Full rigidity was assumed in the fire condition because the connection detail was at a lower temperature than the rest of the structure due to a lower section factor and the loss of heat into the concrete filled column through this connection. This was justified from an examination of the beam-to-column connection after the fire.

The cross-section of the column is discretized as shown earlier in Fig. 4. All the thermal and mechanical properties of steel are assumed to vary according to Part 10 of Eurocode 4,[16] from which a relative emissivity of 0·5 is recommended; however, for the column flange facing the wall of the fire compartment it was considered appropriate to reduce the value arbitrarily to 0·3 to account for some degree of radiative shadowing. A

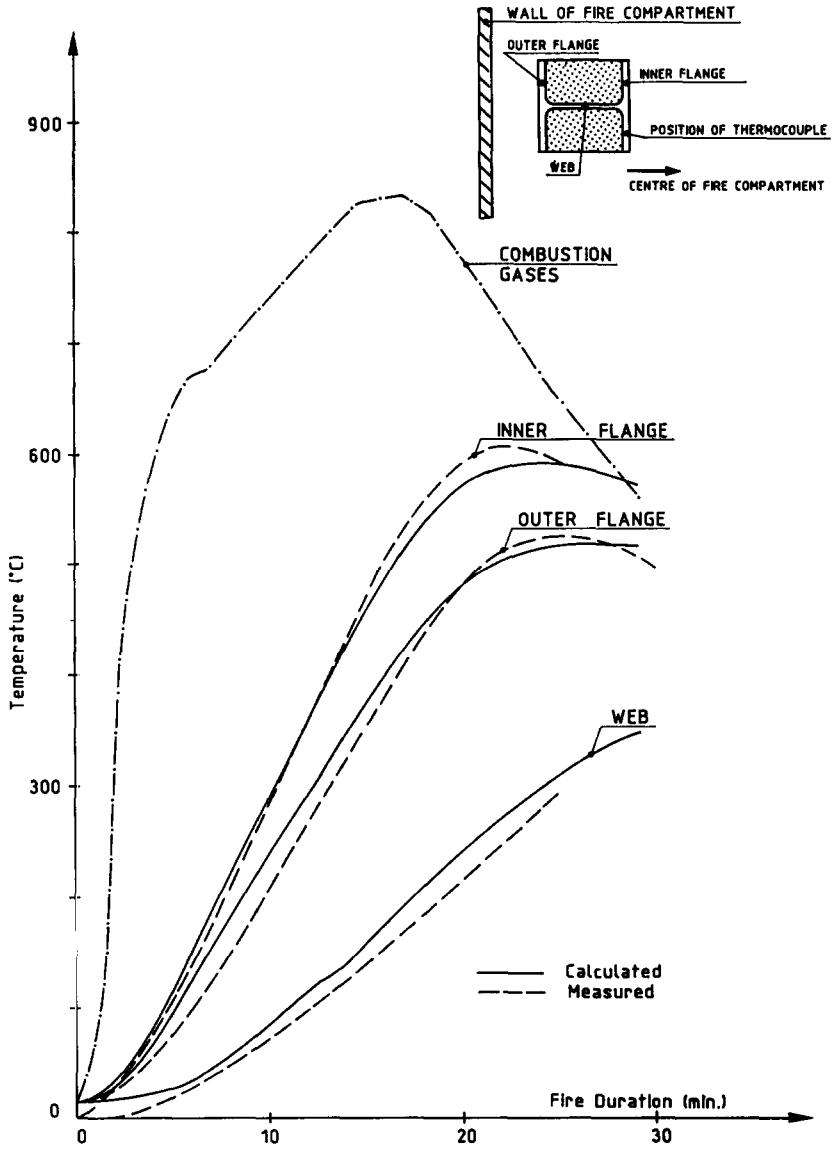

Fig. 6. Temperature in the column.

convective heat transfer coefficient of 25 W/m^2K was used as in the Eurocode. The lightweight (aerated) concrete blocks used to fill the column flange voids are considered to give only thermal insulation (they do not carry any load) and their thermal properties are assumed to be:

density	= 677 (kg/m^3)
specific heat	= 1050 (J/kgK)

thermal conductivity = 0·20 + 0·0004 * T (W/mK)
moisture content = 25·7 (kg/m^3).

Figure 6 shows the development of the average combustion gas temperature measured in the fire compartment and the development of calculated temperatures in the flanges and the middle of the web of the column. The computed temperatures agree well with the measured temperatures.

The discretization of the cross-section of the beam is shown in Fig. 7. The concrete cover slab is represented because of its influence on the temperature distribution in the beam. The concrete was given zero

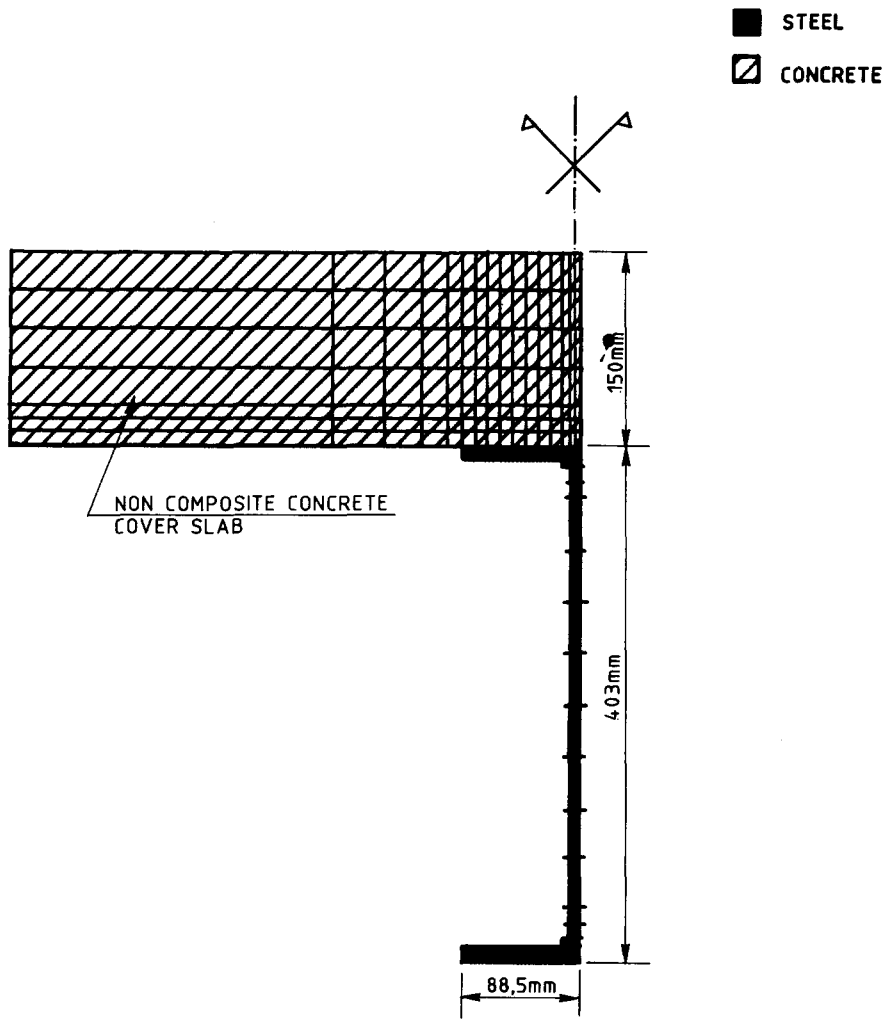

Fig. 7. Discretization of the beam cross-section and concrete cover slab by 141 rectangles.

strength because the slab makes no structural contribution due to its segmented form.

Figure 8 shows the development of the calculated temperatures in the steel beam compared with the measured data. The agreement is good, confirming that the transient temperature distribution in the profile can be accurately calculated by numerical methods using the recommendations of the Eurocodes for the thermal properties of materials.

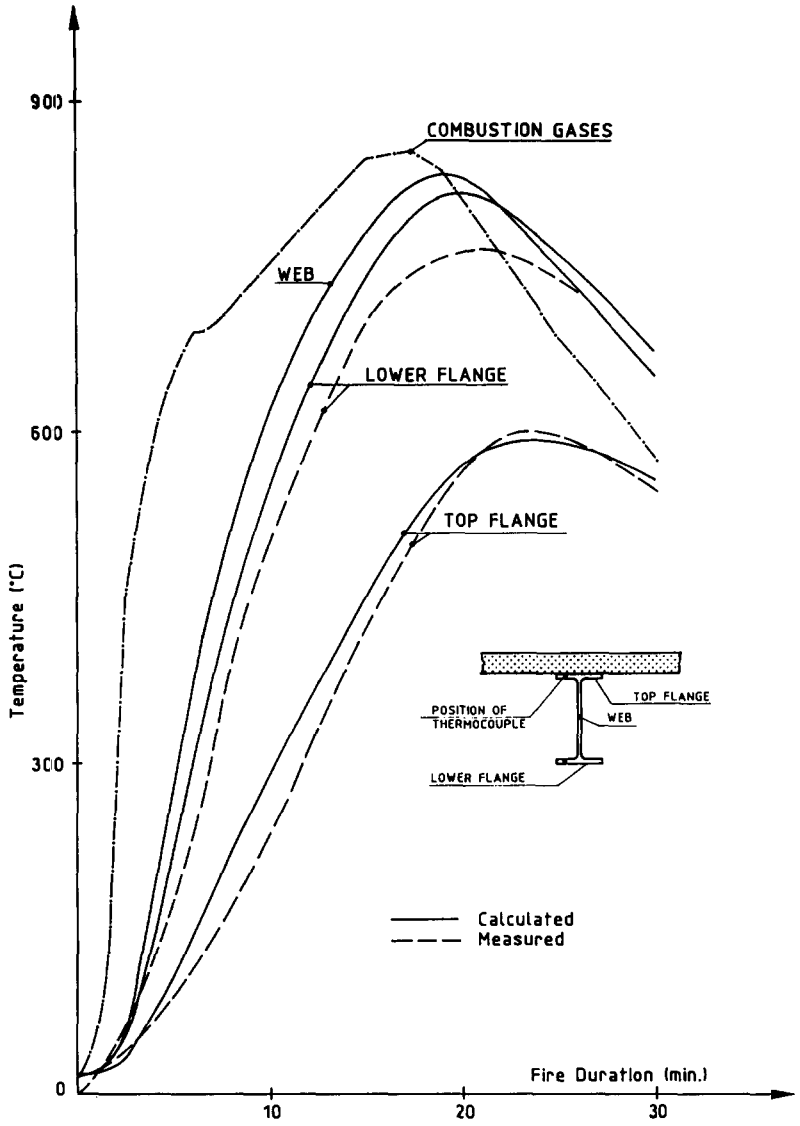

Fig. 8. Temperatures in the beam.

To represent the fact that the measured temperatures of the combustion gases were slightly lower in the vicinity of the beam-to-column connection, the increase of temperature in the beam has been multiplied by a reduction function ($f(x)$ given in 3.3) based on experimental results which has a sinusoidal shape along the beam axis with values of 0·90 at the beam/column interconnection and 1·00 at node 21, Fig. 5.

The vertical load on the columns, the two concentrated loads on the beam and the dead weight of the beam, columns and precast concrete slabs are all assumed to act on the frame.

The beam and column sections were made from BS 4360 Grade 43A steel. A hardness test confirmed that the steel satisfied the nominal tensile strength requirements in force at that time, i.e. 430-510 N/mm^2. As no tests on the actual yield strength of steel were made at the time of the test, five numerical simulations have been carried out using five different values of yield strength: 255 (the minimum requirement), 306, 357, 408 and 459 N/mm^2. Figure 9 shows the mid-span vertical deflection of the beam for the five yield strength simulations defined together with the changes in measured deflection during the fire test. Note that the calculated values of deflection include the deflection due to the load applied before the fire, whereas the measured deflection is the increase in deflection during the fire.

The curves confirm that the fire resistance of a structure is increased as the load factor is decreased (the higher the yield strength the lower the load factor). In the particular case of a so called 'natural fire curve' having a cooling down phase, it is possible that the structure remains stable during and after the fire, albeit with residual deflections, provided that the load factor is small enough. Because of the lack of knowledge of the actual yield strength of the steel used, it is not possible to be certain of the ability of the program accurately to predict the fire resistance of the frame. Nevertheless, the shapes of the calculated and measured deflection curves are very similar which suggests that the numerical model can predict the failure mode. It is observed that the fit between the measured and calculated deflection curves is best when using a yield strength of 408 N/mm^2. Although this value is higher than the statistical maximum normally associated with structural steel sections rolled to the Grade 43A specification, it has been used in the sensitivity analyses reported in this paper.

Various case studies ranging from Ia to VIb are illustrated in the Appendix. The calculated fire resistance time for the reference case, Case Ia, is 19 minutes and 12 seconds.

Figure 10 shows the calculated deflections of the frame at the very moment before collapse. The correlation between the calculation deflec-

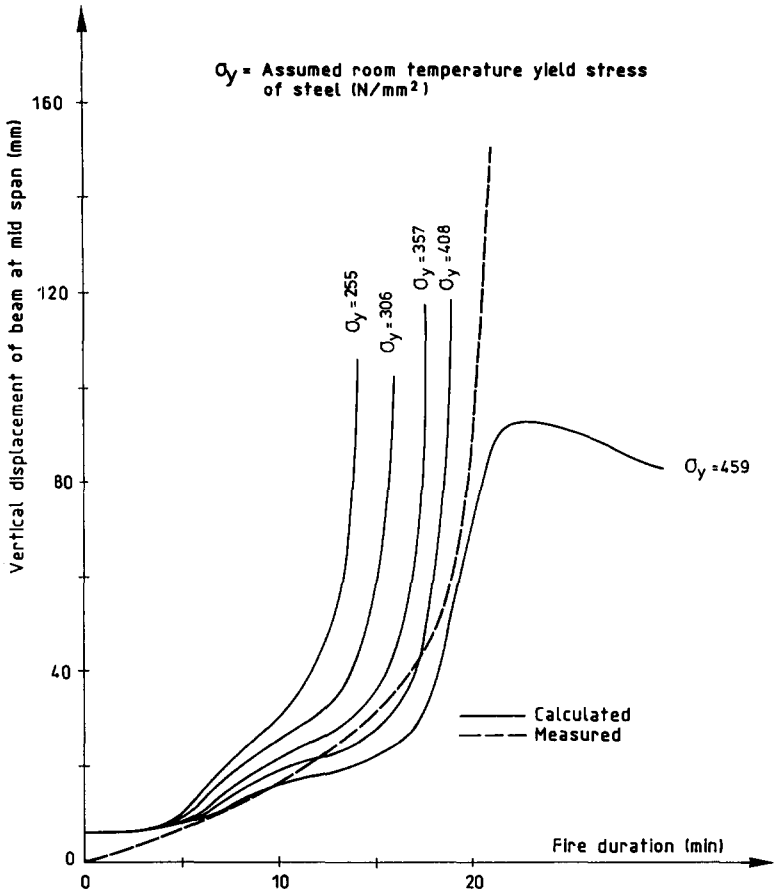

Fig. 9. Vertical displacement of the beam in the fire test.

tions of the column and the measured deflections in Fig. 3 is good. The failure mode is neither solely due to gross flexure of the beam nor buckling in the columns, but seems to concern both phenomena. The situation is complicated by internally induced bending moments caused by temperature gradients across the column and the beam section, Figs 6 and 8.

It has been verified that if the complete frame (rather than half the frame) is modelled assuming the presence of two springs and an initial lateral imperfection (sway) of 0·8H/1000 (where H = height of column), the failure mode is exactly the same and the calculated fire resistance is only very slightly increased from 19 minutes and 12 seconds (Case Ia) to 19 minutes and 22 seconds (Case Ib). This proves that satisfactory results are obtained by simulating only one half of the frame, provided that restraint members are present.

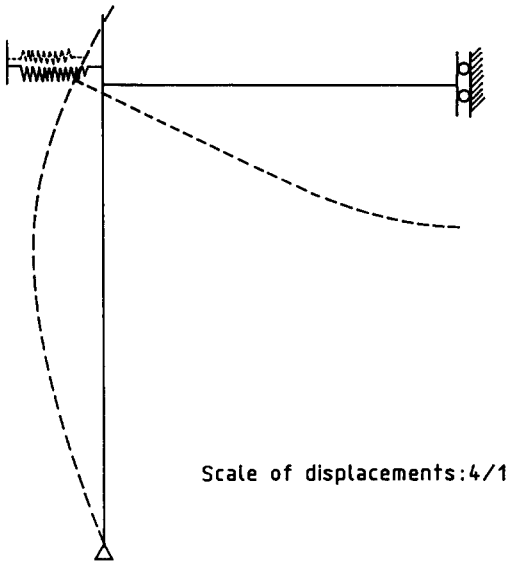

Fig. 10. Calculated failure mode of the restrained frame.

The photographs of the frame after the fire test indicated that no relative rotation at the connection occurred. The temperature in the vicinity of the connections remained lower than elsewhere in the compartment during the fire. This fact together with the additional mass of the connections compared with the members justified treating the connections as fully rigid in fire.

4.1 Influence of axial restraint to beam

Because of the bending stiffness of the columns and mainly because of the axial restraints, the beam cannot expand freely along its axis when it heats up. Thus an axial compressive force develops in the beam during the fire and this could influence the stability of the frame.

For the first sensitivity analysis, the fire behaviour of the frame has been simulated assuming that axial restraint does not exist. Symmetry about mid-span of the beam is assumed (Case IIa). Figure 11 shows that the axial compression force in the beam reaches peak values of 124 kN and 43 kN when restraint is present and absent respectively. At the moment of collapse, the axial compression force in the beam is reduced from 103 kN to 21 kN when lateral restraint is removed. Nevertheless, the failure mode remains the same and the fire resistance is only increased by 2%—from 19 minutes and 12 seconds with restraint (Case Ia) to 19 minutes and 35 seconds without restraint (Case IIa).

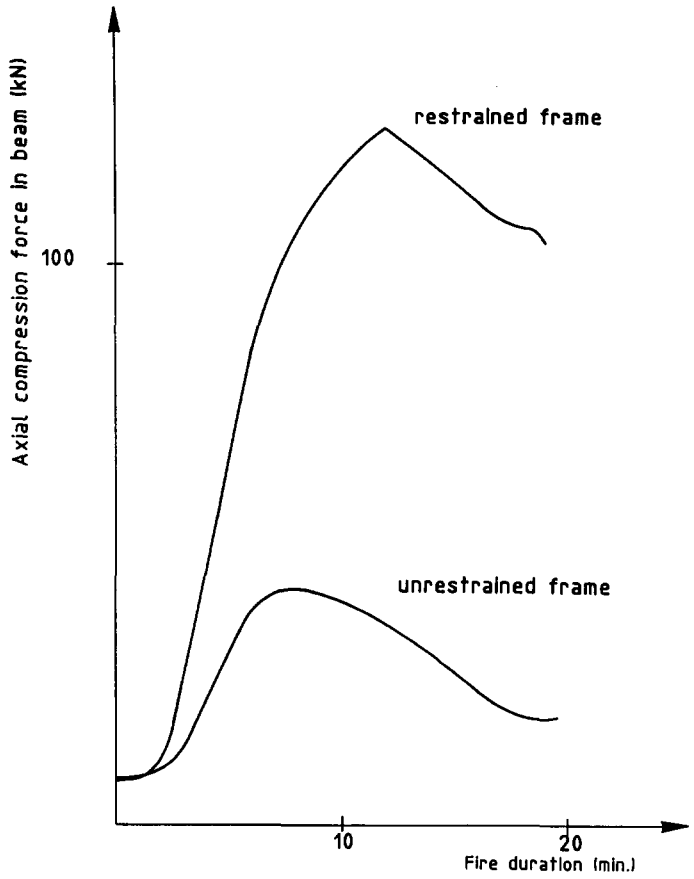

Fig. 11. Calculated axial force in the beam.

The complete frame with an initial lateral imperfection (out of plumb by 2·5 mm) has also been simulated without lateral restraint (Case IIb). This time, the failure mode of the frame is completely different if lateral restraint is removed (compare Figs 10 and 12). The structure sways with little vertical mid-span deflection of the beam which, at this moment, still possesses a high measure of stiffness. The fire resistance is reduced by 29%—from 19 minutes and 22 seconds for the restrained frame (Case Ib) to 13 minutes and 45 seconds for the same frame unrestrained (Case IIb).

4.2 Influence of frame continuity

It has been said that the provision of continuity could increase the fire resistance of a structure and that a complete structure does not behave as

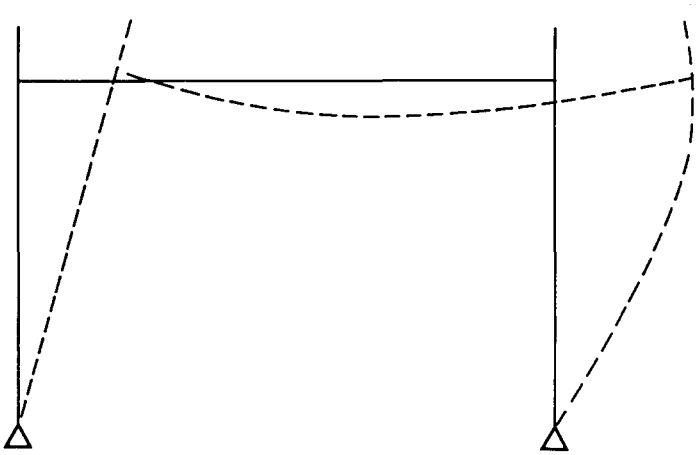

Fig. 12. Calculated failure mode of the sway frame.

the sum of its separate members. To illustrate and quantify this claim, the column and beam of the test frame have been analysed separately.

In addition to the load applied by the hydraulic jack, the column is subjected to the vertical force and bending moment introduced by the beam, Fig. 13. The values of the loads come from the analysis of the frame

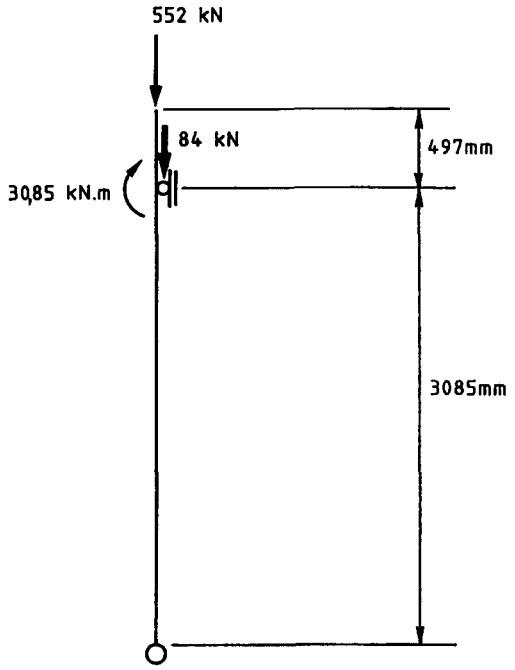

Fig. 13. The column as a separate member.

at ambient temperature and they remain constant in the analysis of the column as a separate member. The beam/column connection is not allowed to displace horizontally but is free to move vertically and rotate (Case IIIb).

Figure 14 shows the horizontal displacement at mid height of the column when acting as a separate member. At the beginning of the simulation, the column bows outwards because of the bending moment introduced by the beam. The development of the thermal gradient between the flanges, acting on a section that is still mainly elastic, then bows the column inwards. Later, when the flanges yield, the effect of the bending moment combines with the effect of the thermal gradient and the bowing is

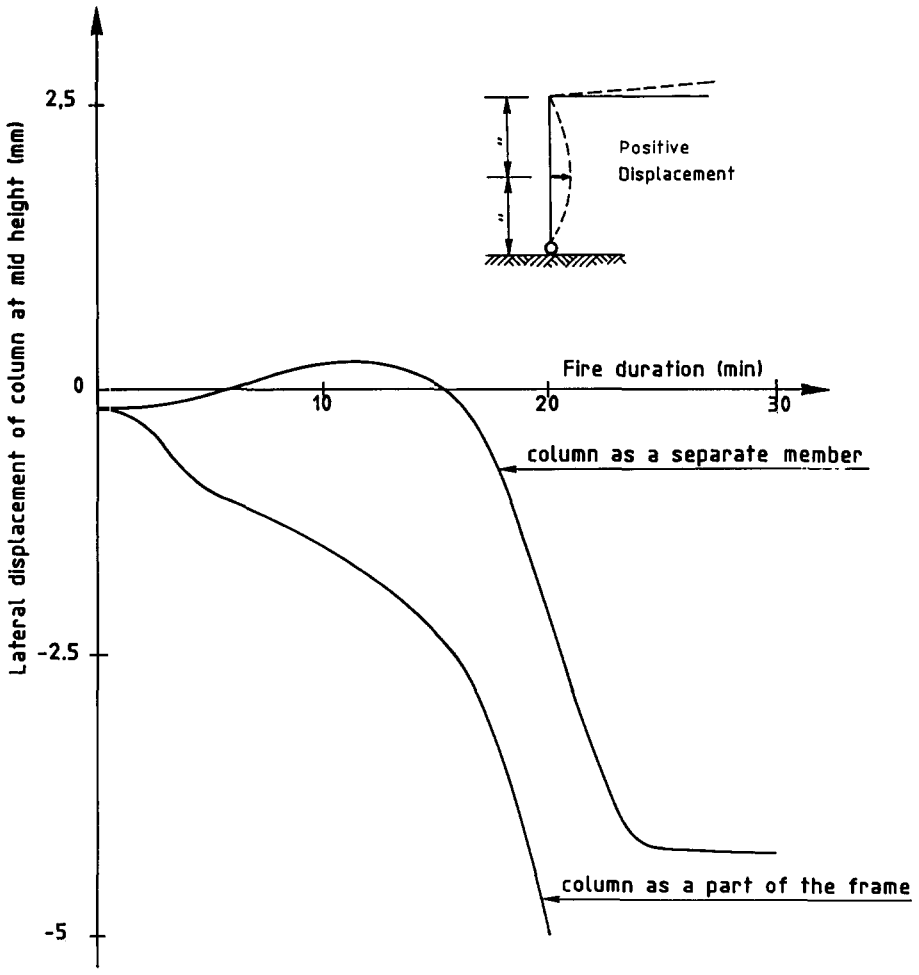

Fig. 14. Calculated horizontal displacement at mid height of column.

again to the outside. After approximately 25 minutes the section begins to cool down and, because the mechanical properties of structural steel are unaffected after cooling from 600°C,[24] the column remains stable and no collapse is observed.

The horizontal displacement at mid height of the column when acting as part of the frame is also shown in Fig. 14. The effect of the thermal gradient across the section of the beam and the elongation of the beam causes outward bowing of the column throughout the fire duration resulting in buckling after 19 minutes and 12 seconds (Case Ia).

The loads acting when the beam is considered on its own are shown in Fig. 15. In addition to the loads applied by the hydraulic jacks, the beam is subjected at its ends to the axial load and bending moment representing the frame effect at ambient temperature. The beam is free of externally applied axial restraint (Case IIIa). In the later stage of the fire the absence of beneficial restraint from the columns (which still have a large amount of stiffness) results in a reduction of fire resistance (15 minutes and 30 seconds) and larger displacements than for the complete frame.

In this particular case, the calculated fire resistance of the frame is increased by 24% when, instead of the sum of separate members, it is considered as a whole structure. This highlights the need for theoretical or numerical tools which enable the benefits of composite action to be quantified and reflected in more economic design.

4.3 Influence of thermal expansion

The numerical program CEFICOSS takes account of non-uniform temperature distributions in the cross-section and, to some extent, along the

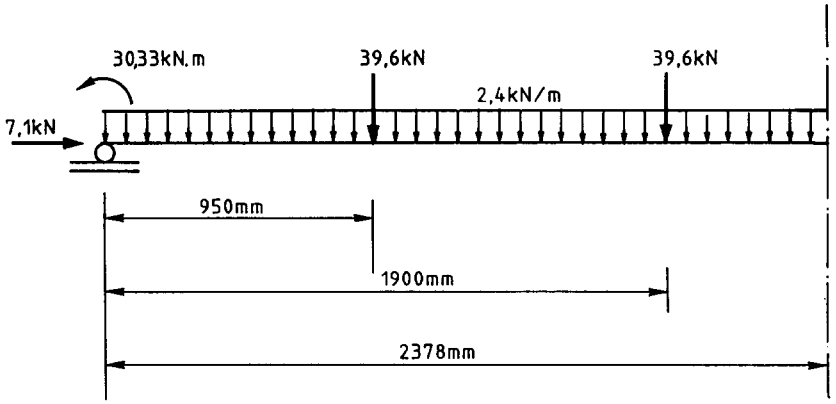

Fig. 15. The beam as a separate member.

length of the member, the influence of thermal strains, second order effects, non linear stress-strain relationships, and effects of large displacements, etc. This is integrated in a time history analysis, which means that the state of the structure is determined minute after minute up to the moment when no state of equilibrium can be found or, if desired, when a prescribed deflection is reached. This rigorous approach involves significant theoretical and numerical effort to write and validate the program, not to mention the degree of experience required by the user when simulating non-linear problems before confidence can be placed in the results obtained. The need for such complex analysis is debatable. Perhaps an ultimate state plastic design of the structure, considering the temperature dependent properties of steel, would be sufficient for most situations?

In an attempt to answer part of this question, the influence of thermal expansion has been investigated. The Cardington frame has been simulated assuming that steel does not expand when heated, a hypothetical condition (Case IVa). The time history simulation illustrates two main differences in frame behaviour.

First the axial force in the beam increases much less when thermal expansion is zero. From a value of 7 kN at ambient temperature, it reaches a peak value of 21 kN after 17 minutes instead of a maximum value of 124 kN for normal steel. However, axial force has been shown to have little effect on the stability of the frame. The bending moments developed in the frame are also smaller because the thermal gradients in the sections cause no thermal bowing. The positive bending moment in the beam at mid-span reduces as the stiffness and ultimate capacity reduce at that point. This reduction leads to an equivalent increase in the negative bending moment at the ends of the beam. The changes are caused by the progressive formation of a plastic hinge in the central part of the beam and not the thermal strains, and are less severe than the variations observed in the frame with normal steel.

Secondly, the absence of thermal expansion of the beam delays the lateral displacement of the beam-to-column connection, and the absence of thermal bowing (which was caused by the thermal gradients in the sections) delays the outward bowing of the column.

As a consequence, the simulation shows that the frame made of a hypothetical 'non-expanding' steel does not collapse but remains stable up to 30 minutes and probably well beyond this time because of cooling of the steel as the fire decays. The frame made of normal steel however, had a fire resistance of 19 minutes and 12 seconds (Case Ia). Such an important difference is mainly due to the decay of the fire and, as a consequence, the decrease in temperature of the steel sections. A detailed analysis of the results of Case IVa shows that the frame is very near to collapse when,

after 21 minutes, the lower flange of the beam begins to cool down. A simulation of the same frame exposed to fire with increasing severity (the ISO 834 temperature-time curve for example) would lead to less spectacular differences between expanding and non-expanding steel.

4.4 Influence of non-uniform temperature

Part 10 of Eurocode 3[15] recommends a simplified method which assumes that the temperature of steel is uniform throughout the cross-section of the member. The uniform temperature has been calculated for the column and beam using the one-dimensional equation given in.[15]

For the column, the thermal conductivity and specific heat of the lightweight concrete blocks have been assumed to be zero. This allows the steel profile to be considered as thermally uninsulated but exposed to the action of the fire only on its flanges. The section factor (massivity) of the profile (heat-exposed perimeter/cross section area) is then equal to $(2B+4T)/A = 69\ m^{-1}$. To allow for the fact that the emissivity of steel is 0·30 on the outer flange and 0·50 on the inner, the simplified calculation has been made with an emissivity of 0·40. The simplified method in the Eurocode is not intended to cover the configuration for a partially insulated section and it is therefore not surprising that the uniform temperature calculated in this way is quite different to the real temperature.

For the beam, the simplified method is said, in Ref. 15, to be directly relevant. The massivity of the section, assuming that the top surface of the upper flange is not exposed to fire, is $193\ m^{-1}$. However, the heat sink effect of the cover slab is neglected so that the calculated uniform temperature is higher than in reality.

Figure 16 presents, for the column and beam, the uniform temperature calculated by the Eurocode simplified method and the mean temperature (mean value of the non-uniform temperature distribution calculated by the two-dimensional approach). In the column, a temperature of 500°C is reached 5 minutes earlier for the uniform temperature. This uniform temperature is also 125°C higher than the mean temperature at the end of the test. These differences may be due to the fact that the way the column section is insulated is not one of the traditional types foreseen for the simplified method. Of more concern is the difference between the uniform and mean temperatures in the beam since the simplified method is supposed to be valid for this type of unprotected section. The uniform temperature is higher than the average temperature by 102°C at 15 minutes. 817°C is the maximum value of the uniform temperature, reached after 20 minutes, whereas the maximum value of the mean temperature is 735°C.

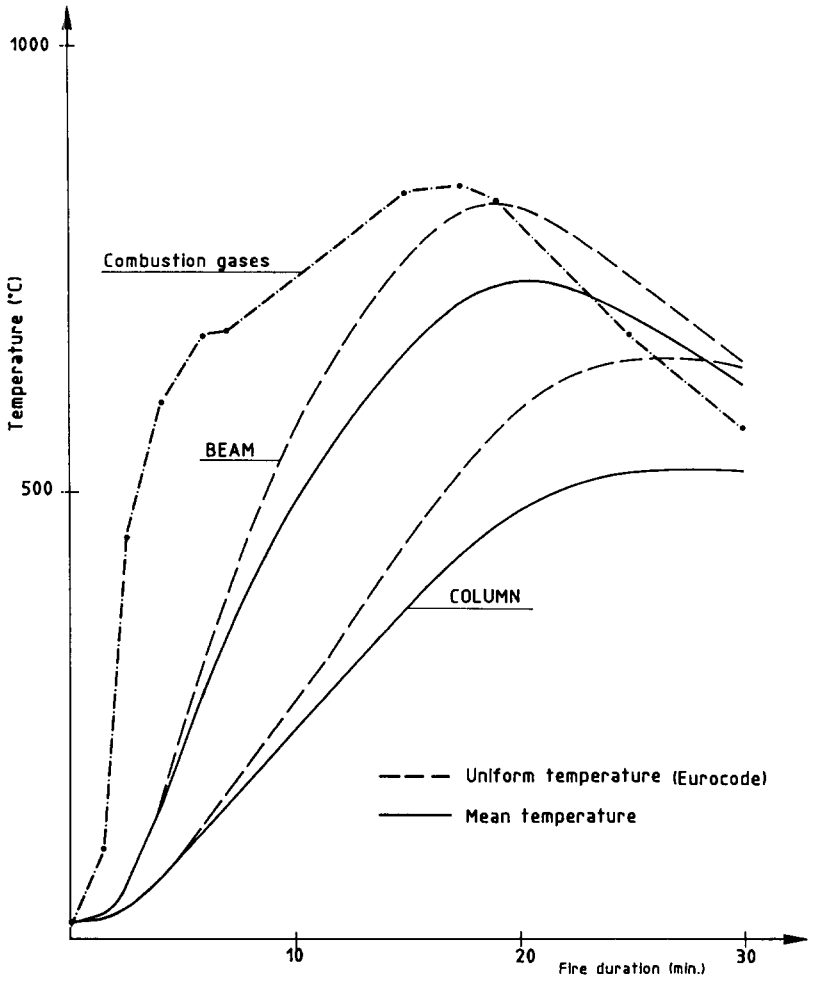

Fig. 16. Calculated uniform and mean temperatures.

Nevertheless, the unfavourable fact that the uniform temperature is higher than the mean temperature is partly compensated by the fact that the bowing caused by thermal gradients is not considered. The fire resistance calculated by the structural part of CEFICOSS on the basis of a simplified uniform temperature (Case Va) is 18 minutes and 15 seconds which is only one minute less than the reference Case Ia.

5 SIMPLIFIED PLASTIC DESIGN OF THE FRAME

The simple method described in Part 10 of Eurocode 3[15] is used here to assess the fire resistance of the members of the Cardington frame. The

uniform temperatures reported in the previous paragraph are used. A yield strength of 408 N/mm^2 is used, as in the earlier simulations.

In the simplified method, the critical temperature of the elements is directly related to $k \times n$

where k = adaptation factor
n = load factor

For the beam, (Case VIa), the adaptation factor is 0·70 (because the beam is heated on three sides) multiplied by 0·85 (because the beam is hyperstatic, i.e. rotationally restrained, if the columns are assumed to remain stable for longer than the beam)

i.e., $k = 0{\cdot}595$.

The load factor is equal to the ratio between the isostatic (free) bending moment in the beam divided by twice the plastic moment of the section (plastic hinges are assumed to develop in the central part of the beam and at the supports).

$$n = \frac{M_{\text{centre}} - M_{\text{support}}}{2M_p}$$

$$= \frac{114{,}600{,}000}{2 \times 408 \times 7{,}048{,}000}$$

$$= 0{\cdot}134$$

so that $k \times n = 0{\cdot}595 \times 0{\cdot}134 = 0{\cdot}08$.

This ratio is reached when the steel has a critical temperature of 860°C. The uniform calculated temperature of the beam never reaches this value during the test and the fire resistance of the beam assessed by the simplified method is therefore greater than 30 minutes.

For the column, (Case VIb), the adaptation factor is 1·20 assuming the column is subjected to an axial force and a bending moment.

The load factor can be calculated assuming the following:

- buckling length in the plane of the frame = 0·80 × 3085 = 2468 mm according to Annex E of Part 1 of Eurocode 3[25]
- out of plane buckling length = 0·50 × 3582 = 1791 mm if out of plane rotation is prevented at the support and at the level of the hydraulic jack.

It can be shown that the minimum reduction factor is for in-plane buckling (curve c) and is equal to 0·903. According to 5.5.2 of Ref. 25,

$$n = \frac{636{,}000}{0{\cdot}903 \times 408 \times 6640} + \frac{1{\cdot}01 \times 30{,}850{,}000}{408 \times 568{,}100} = 0{\cdot}394$$

and $k \times n = 1{\cdot}20 \times 0{\cdot}394 = 0{\cdot}473$.

This ratio is reached when the steel has a critical temperature of 500°C. In the column, this temperature is reached after 20 minutes and 30 seconds, i.e. only 7% more than the value provided by the numerical method.

6 CONCLUSIONS

(a) The numerical model, based on acknowledged principles of the theory of structures and utilising the recommendations for material properties given in Part 10 of the Structural Eurocodes, proved able to simulate with reasonable agreement the thermal and the structural behaviour of a full size steel frame tested in a fire compartment in the Fire Research Station's Large Laboratory at Cardington in 1987. The behaviour of the frame was correctly predicted up to failure, except for local buckling of the beam that occurred at the moment of failure which cannot be modelled using the beam finite element.

(b) The computer model has been used to highlight the influence of several physical parameters on the behaviour of the test frame:
   - The value of yield strength at ambient temperature (which determines the load factor) has an important influence on the fire resistance of the structure.
   - The increase of axial force in the beam due to the external restraint resulting from thermal expansion is significant, but it has a very limited influence on the fire resistance.
   - A variation of the lateral in-plane restraint (provided to the frame to ensure a symmetrical failure mode) has a major effect on the fire resistance of the structure.
   - The behaviour of the column and beam considered as separate members (i.e. no composite action) during the fire is totally different from the behaviour of the frame as a whole. The fire resistance of the weakest member (the beam) is considerably less than the fire resistance of the complete frame.
   - The influence of the thermal expansion of steel cannot be neglected in the frame simulation because it proves to have a significant effect.

(c) The simple (Eurocode) method applied to the frame members to calculate the temperature in the sections as well as the structural behaviour provides a fire resistance time that is reasonably close to that of the frame when simulated by the general method using the more rigorous numerical model. Less safe results are provided by the simple method when applied to structures where there is no heat sink effect. The present work also suggests that the simple method should not be applied to sway frames.
(d) A good application of general (rigorous) computer programs similar to the one described here could be to identify which types of structure can be analysed by the simplified method and which types require the use of the general method.

ACKNOWLEDGEMENT

The paper is contributed by courtesy of the Director of Building Research Establishment and the Director of Research and Development, British Steel, Plc. Crown Copyright 1995—Building Research Establishment.

REFERENCES

1. Arnault, P. *et al.*, Résistance au feu des systèmes hyperstatiques en acier. CTICM, doc *CECM 3-74/6 F*, 1974.
2. Cooke, G. M. E. & Latham, D. J., The inherent fire resistance of a loaded steel framework. *Steel Construction Today*, **1** (1987) 49–58.
3. Franssen, J. M., Etude du comportement au feu des structures mixtes acierbéton. Thèse de doctorat. Univ. de Liège, publications de la FSA, No 111, 1987.
4. Schleich, J. B. REFAO-CAFIR. Computer Assisted Analysis of the Fire Resistance of Steel and Composite Concrete – Steel Structures. CEC, Final Report *EUR 10828 EN*, 1987.
5. Burgess, I. W. *et al.*, A secant stiffness approach to the fire analysis of steel beams. *J. Construct. Steel Research.*, **11** (1988) 105–20.
6. Jeyarupalingam, N. & Virdi, K. S, Steel beams and columns exposed to fire hazard. In *Structural Design for Hazardous Loads—the role of physical testing*, (eds Clarke, J. L. *et al.*) E & F N Spon, London, 1992.
7. Forsen, N. E., *Steelfire—Finite Element Program for Non linear Analysis of Steel Frames Exposed to Fire. Users Manual.* Multiconsult A/S, Oslo, 1983.
8. Schaumann, P. Zur Berechnung Stählerner Bauteile und Rahmentragwerke unter Brandbeanspruchung. Technisch-wissenschaftliche Mitteilungen Nr. 84–4, Institut für Konstructiven Ingenieurbau, Ruhr-Universität Bochum, Dissertation, 1984.

9. Peterson, A., Finite Element Analysis of Structures at High Temperatures, with Special Application to Plane Steel Beams and Frames. Lund Inst. of Technology, Division of Struct. Mec., Report *TVSM-1001*, 1984.
10. Baba, S. & Nagura, H., Effect of material properties on the deformation of steel frame in fire. In *Proc. JSCE. Struct, Engng/Earthquake Engng.*, **2**, 1985.
11. Van Foeken, R. J. & Snijder, H. H., Steel column and frame stability analysis using finite element techniques. *Heron*, **30** (1985).
12. Jungbluth, O. & Gradwohl, W., Berechnen und Bemessen von Verbundprofil-staben bei Raumtemperatur und unter Brandeinwirkung. Ernst & Sohn, Verlag fur Architektur und technische Wissenschaften, Heft 382, 1987.
13. Valente, J., Simulacoa do comportamento das estruturas metalicas sujetitas a altas temperatures. Dissertacao. Instituto Superior Technico da Universidade Technica de Lisboa, 1988.
14. Furumura, F., A study on in-plane elasto-plastic creep behaviour of steel beam-columns at elevated temperatures. Report of the Research Laboratory of Engineering Materials, Tokyo Institute of Technology, Number 13, 1988.
15. Eurocode No 3. Design of Steel Structures, Part 10: Structural Fire Design. Draft April 1990.
16. Eurocode No 4. Design of Composite Structures. Part 10: Structural Fire Design. Draft April 1990.
17. European Recommendations for the Fire Safety of Steel Structures. *ECCS-TC3*, Elsevier, 1983.
18. Association of Structural Fire Protection Contractors and Manufacturers Ltd (ASFPCM), Fire protection for structural steel in buildings (2nd edition), 1988.
19. Luycks, P., Elaboration d'un programme éléments-finis pour le calcul de la distribution de température dans les éléments de constuction soumis à l'incendie. Univ. of Liège, FSA, Travail de fin détudes, 1991.
20. Bresler, R. *et al.*, FIRES-T3, A computer program for the fire response of structures—thermal. Report No *UCB FRG 77-15*. University of California, Berkeley, 1977.
21. Boeraeve, P., Contribution à l'analyse statique non linéaire des structures mixtes planes formées de poutres, avec prise en compte des effets différés et des phases de construction. Thèse de doctorat, Univ. de Liège, Départment MSM, 1991.
22. Jennings, A., Frame analysis including change of geometry. *J. Struct. Engng.*, ASCE, **94** (1967).
23. Franssen, J. M., Modélisation et influence des contraintes résiduelles dans les profils métalliques soumis à l'incendie. *Construction Métallique*, CTICM No 3, 1989.
24. Kirby, B. R. *et al.*, *The reinstatement of fire damaged steel and iron framed structures*. BSC, Swinden Laboratories, 1986.
25. Eurocode No 3 Design of Steel Structures. Part 1. General Rules and Rules for Buildings. Draft December 1988.

APPENDIX: LOAD CASES EXAMINED BY CALCULATION

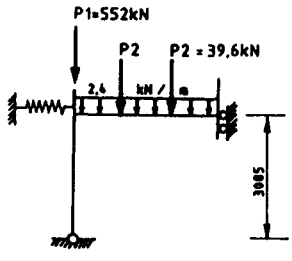

CASE I a ; Rf=19min.12sec. (CEFICOSS)
CASE IIIa ; > 30min. If no thermal expansion (=CEFICOSS)
CASE Va : Rf=18min.15sec. If uniform temperature (= CEFICOSS)

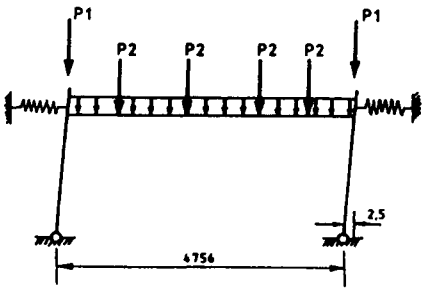

CASE I b ; 19min.22sec. (CEFICOSS)

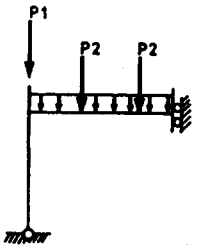

CASE IIa ; 19min.35sec. (CEFICOSS)

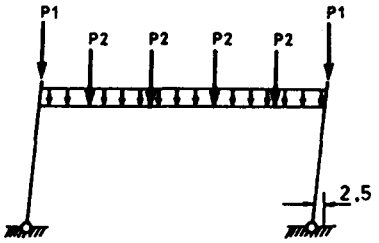

CASE IIb; 13min.45sec. (CEFICOSS)

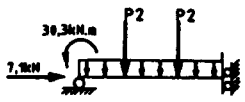

CASE III a ; 15min.30sec. (CEFICOSS)

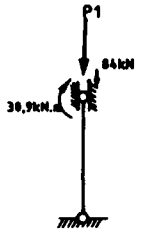

CASE III b ; > 30min. (CEFICOSS)

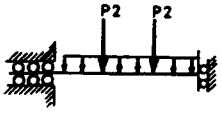

CASE VIa ; > 30min. (simple method)

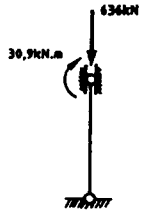

CASE VIb ; 20min.30sec. (simple method)

ANNEX C – Behaviour study of a steel column subject to a localised fire

Departamento de Engenharia Civil
Faculdade de Ciências e Tecnologia da Universidade de Coimbra

ROBUSTFIRE Project

Document 7: Behaviour study of columns subject to fire

Cécile Haremza
Aldina Santiago
Luís Simões da Silva

February 2012

TABLE OF CONTENTS

I Introduction

This document presents a behaviour study of a steel column subject to elevated temperatures. The purpose of this study is to show that: i) the column completely loses any residual resistance after heated by a localised fire; ii) consequently, in the ROBUSTFIRE project studies, the column loss is assumed by the total removal of the column. The real open steel-concrete car park building designed for the project is detailed in Gens (2010), and is showed in Figure 1. The studied steel column is located on the fourth floor and is 3 m height, with HEB 300 steel cross-section, class S460.

The design value of the axial force in the column for the fire situation $N_{Ed,fi,20^oC}$ (2713 kN) was calculated in a 2D model in Abaqus (2011), considering the loads at the service limit state (SLS) defined during the design of the car park structure (Gens, 2010).

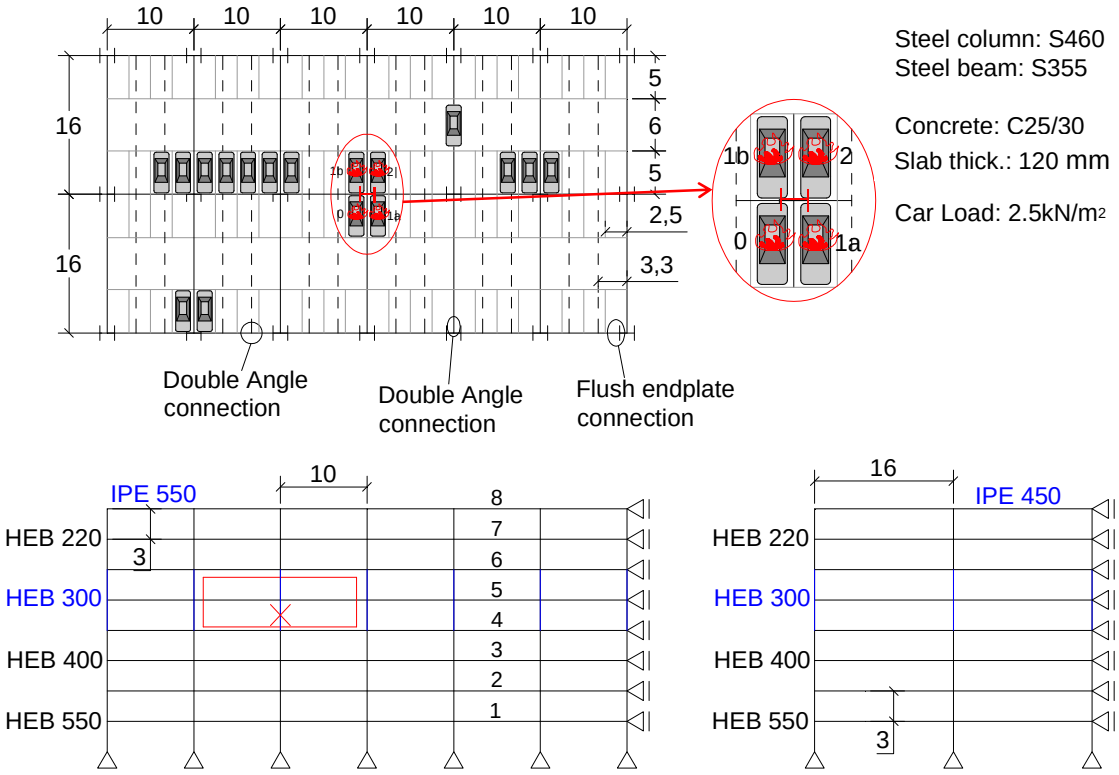

Figure 1: Steel composite open car park structure and the extracted sub-frame to be tested

Two alternative studies are developed in this document: i) the column behaviour analysed under constant temperatures, using the Euler method (Eurocode 3 part 1.2) is compared with the behaviour obtained by a finite element model, and ii) the column behaviour is analysed under localised fire, and the critical temperature of the column is defined using the method described in Franssen (2000). The FE models of the column are developed using the commercial general finite element package Abaqus (2011).

II Description of the finite element model

II.1 Mechanical properties

The steel stress-strain relationship at ambient and elevated temperatures is defined according to Eurocode 3 part 1.2 (Figure 2). The thickness of HEB 300 profile is higher than 16 mm, and the yield strength at ambient temperature is reduced from 460 MPa to 440 MPa (EN 10113-3:1993).

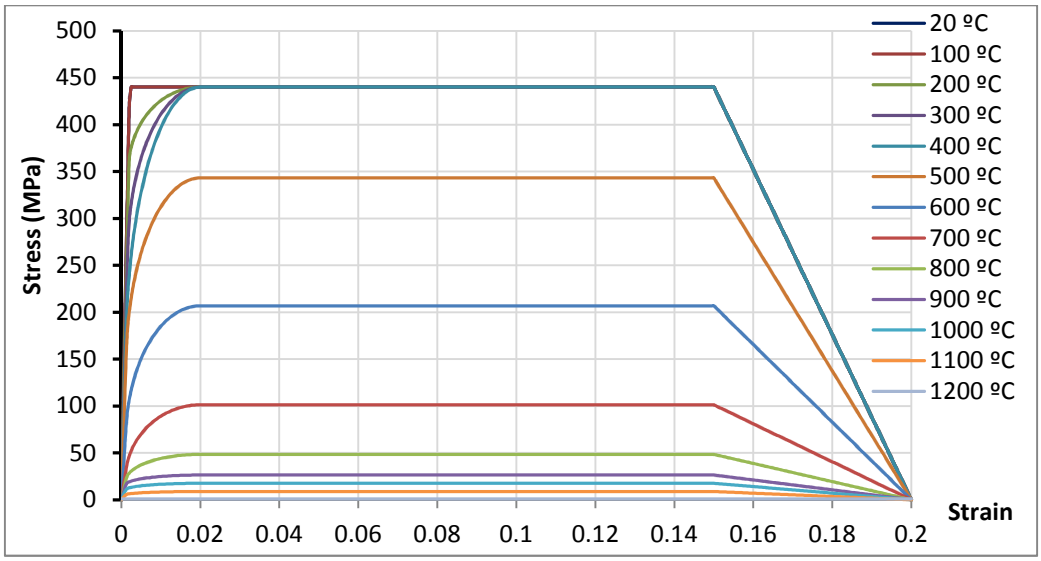

Figure 2: Nominal stress-strain relationship of steel at ambient and elevated temperatures

The nominal stress-strain values $(\sigma_{\mathrm{nom}}, \varepsilon_{\mathrm{nom}})$ from Figure 2 are converted to the true stress-strain measures $(\sigma_{\mathrm{tru}}, \varepsilon_{\mathrm{tru}})$ calculated by the equation (1) (Malvern, 1969):

$$\sigma_{tru} = \sigma_{nom}(1 + \varepsilon_{nom}) \quad \text{and} \quad \varepsilon_{tru} = \ln(1 + \varepsilon_{nom}) \tag{1}$$

The elastic modulus considered is 210 000 MPa, which decreases at elevated temperatures according to the reduction factor $k_{E,\theta}$ defined in Eurocode 3 part 1.2. A Poisson ratio equal to 0.3 and thermal expansion coefficient equal to $1.4\ 10^{-5}$ /ºC are used. These steel properties are kept constant for all temperatures.

II.2 General modelling assumptions

The HEB 300 steel column of 3 m height is modelled using general B31 beam elements. The buckling around the minor axis is considered, and an initial imperfection e_0 of h/1000 = 3 mm is applied with initial sinusoidal shape (see Figure 3a). Rotations at the column top and the column base are restrained, as well as horizontal displacements. Vertical displacements are restrained at the column base and free or restrained at the column top (Figure 3).

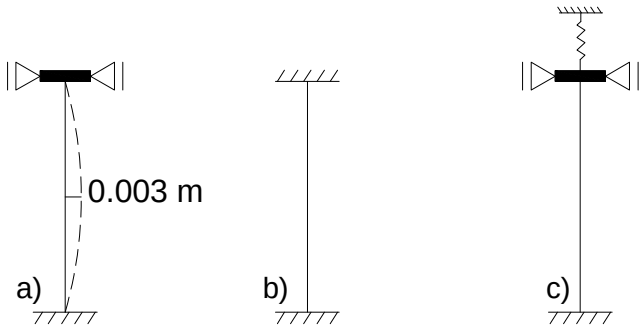

Figure 3: Numerical models of the column

III Steel column HEB 300 under constant temperatures

In this section, the column behaviour is studied under constant temperatures, with change of the axial load. First, theoretical values of the design buckling resistance of the compression member at different temperature are calculated according to Eurocode 3 part 1.1 at ambient temperature, and part 1.2 at elevated temperature. Then FE models of the column under ambient and elevated temperatures are developed to observe the column behaviour up to the complete failure.

III.1 Theoretical buckling resistance

At ambient temperature, the plastic resistance of the column HEB 300 of 3 m height is only slightly reduced by the effect of buckling. Indeed the non-dimensional slenderness $\bar{\lambda}$ calculated according to Eurocode 3 part 1.1 is very low (0.29). Table 1 presents the evolution of the slenderness and the maximum load capacity for the HEB 300 steel column at ambient and elevated temperatures according to Eurocode 3 part 1.1 and 1.2: the buckling of the column influences the maximum load capacity. Table 1 shows that, after 600ºC, the resistance of the column is not anymore sufficient to support the design axial force in the column for the fire situation $N_{Ed,fi,20^oC}$ (2713 kN), and the column fails.

Table 1: Buckling resistance of the HEB 300 steel column

Temperature	Column height	Buckling length	Slenderness	Critical force	Plastic resistance	Max. load capacity
ºC	mm	mm	λ	kN	kN	kN
20 (EC3-1.1)	3000	1500	**0.29**	78879	6560	6430
20 (EC3-1.2)	3000	1500	**0.29**	78879	6560	5716
100	3000	1500	**0.29**	78879	6560	5716
200	3000	1500	**0.30**	70991	6560	5670
300	3000	1500	**0.32**	63103	6560	5616
400	3000	1500	**0.34**	55215	6560	5550
500	**3000**	**1500**	**0.33**	**47328**	**5117**	**4366**
600	***3000***	***1500***	***0.36***	***24453***	***3083***	***2594***
700	***3000***	***1500***	***0.38***	***10254***	***1509***	***1250***
800	*3000*	*1500*	***0.32***	*7099*	*722*	*619*
900	*3000*	*1500*	***0.27***	*5324*	*394*	*346*

III.2 Numerical results

Figure 4 presents the axial load versus the vertical displacement at the column top once the HEB 300 steel column is subjected to an increasing of axial load (Figure 3a), at 20ºC, 500ºC, 600ºC and 700ºC. The buckling was not so obvious as previously showed according to Eurocode 3, and the maximum load capacity corresponds to the plastic yielding of cross-sections: three plastic hinges are developed at the column top, the column base and at the column mid-height. The failure criterion is established by assuming that cracking occurs when the ultimate strain ε_u is reached (0.2 % as defined in Eurocode 3 part 1.2). Figure 5 presents the axial load versus the horizontal displacement at the column mid-height.

The maximum load capacity of the column at ambient temperature (6193 kN) is reduced of: i) 32% at 500ºC (4217 kN); ii) 59% at 600ºC (2541 kN); and iii) 80% at 700ºC (1245 kN). Slight differences with Eurocode 3 loads are noted. Anyway, at 600ºC, the maximum load capacity is not sufficient to support $N_{Ed,fi,20ºC}$ (2713 kN).

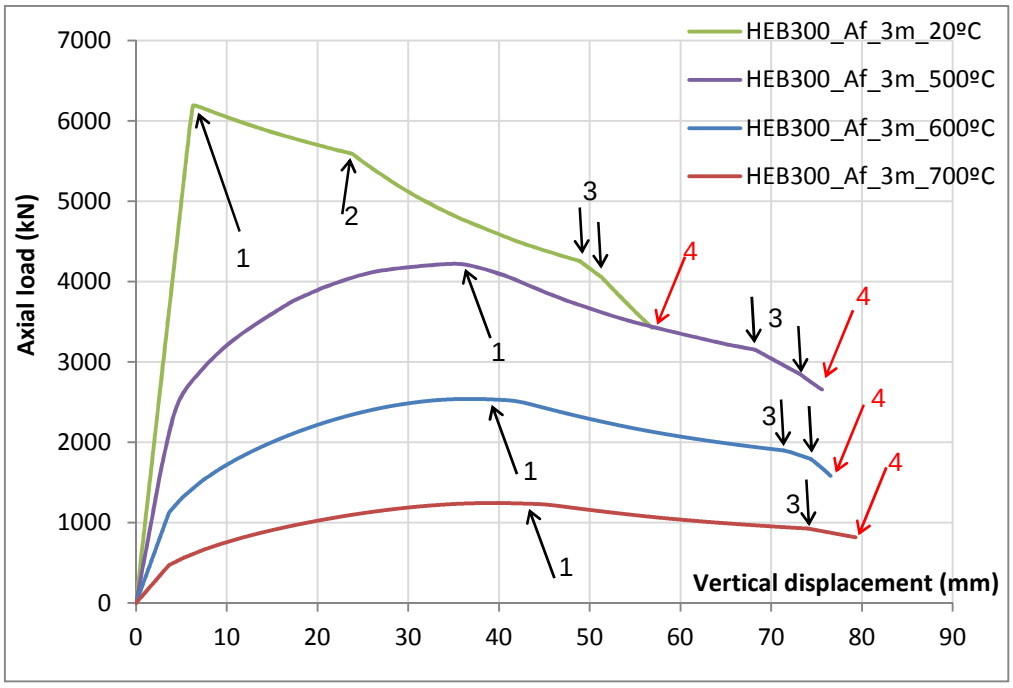

1- Stress in the extreme compression fibre reaches the yield strength at the column top, base and mid-height cross-sections;

2- Stress in the extreme tensile fibre reaches the yield strength at the column top, base and mid-height cross-sections. This yielding does not appear clearly for columns under elevated temperatures;

3- Failure of the section (the ultimate stress is gradually reached in the extreme fibres)

4- The maximum strain (0.2 %) is reached

Figure 4: Axial load *vs* vertical displacement at the HEB 300 steel column top at 20ºC, 500ºC, 600ºC and 700ºC

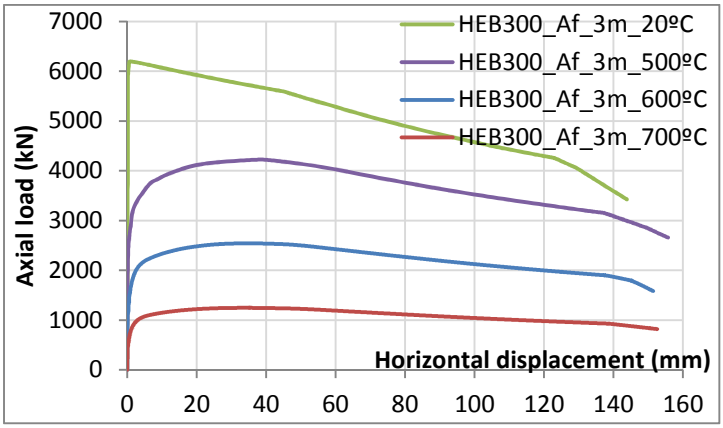

Figure 5: Axial load *vs* horizontal displacement at the HEB 300 steel column mid-height at 20ºC, 500ºC, 600ºC and 700ºC

Note that, all steel profiles of 3 m height used in the considered open car park building (from cross-sections HEB 220 to HEB 550) are strong columns for which yielding of cross-sections should be more evident than buckling, even at elevated temperature.

IV Steel column HEB 300 under localised fire

The studied fire scenario is the most unfavourable scenario for the column and involves four class3-cars burning around the column (see Figure 1): the fire starts in car 0, then propagates to cars 1a and 1b, and finally to car 2. The fire propagation time from a car to another is 12 min. (Fraud et al., 2004). The rate of heat release of each car is presented in Figure 6.

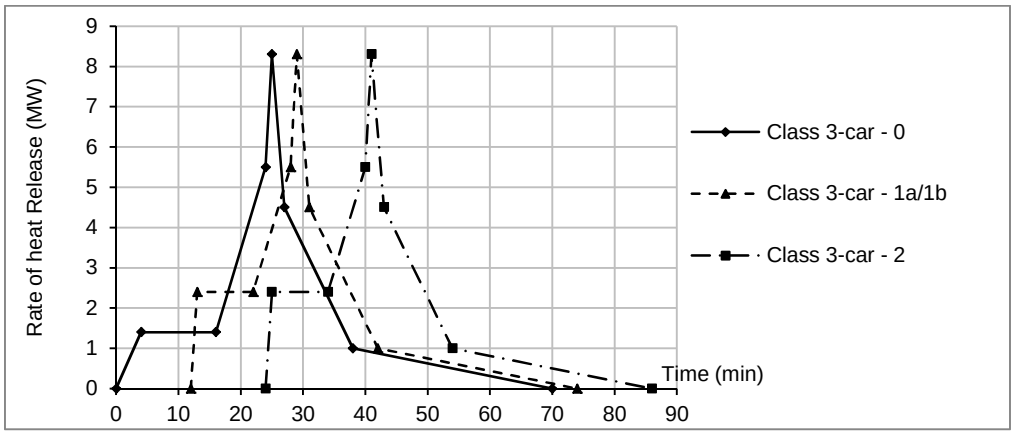

Figure 6: Rate of heat release of four burning class3-cars

To calculate the temperatures of beams subject to localised fire, Eurocode 1 part 1.2, Annex C, recommends the Hasemi method (in case the flames are impacting the ceiling) or the Heskestad method (in case the flames are not impacting the ceiling). For each burning car, the rate of heat release *Q* has to be defined (according to Figure 6), as well as the parameters *D, r* and *H* (see Figure 7):

D (m): diameter of the fire (for a vehicle with an area equal to 12 m^2, *D* = 3.9 m (Schleich et al., 1999))

r (m): horizontal distance between the vertical axis of the fire and the point along the ceiling where the thermal flux is calculated;

H (m): vertical distance between the fire source and the ceiling.

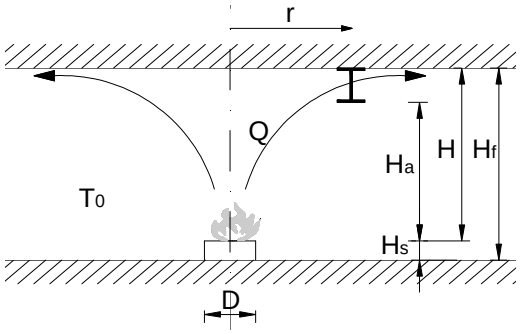

Figure 7: Parameters used to model a vehicle in fire with flames impacting the ceiling

According to Fraud et al. (2004), the temperature in the column subjected to fire all around can be estimated using the Hasemi method, where *H* is defined as the vertical distance from the fire source to the column section where the temperature is calculated. Using this method, the temperature at the column base near the fire source is always higher than the temperature at the column top. This could be the case if, for example, the petrol tank of the car would break and the petrol would accumulate at the column base, creating a significant source of heat. But in an open car park building, the effects of the wind would also influence the temperature distribution along the column. Nowadays, no accurately (and simple) method is defined to calculate the real column temperature in case of a localised fire. In this document, the software ELEFIR-EN (2010) is used to calculate the column temperatures, which apply the Hasemi method. Figure 8 shows the temperatures calculated at 4 points along the column height. The average temperature is also represented.

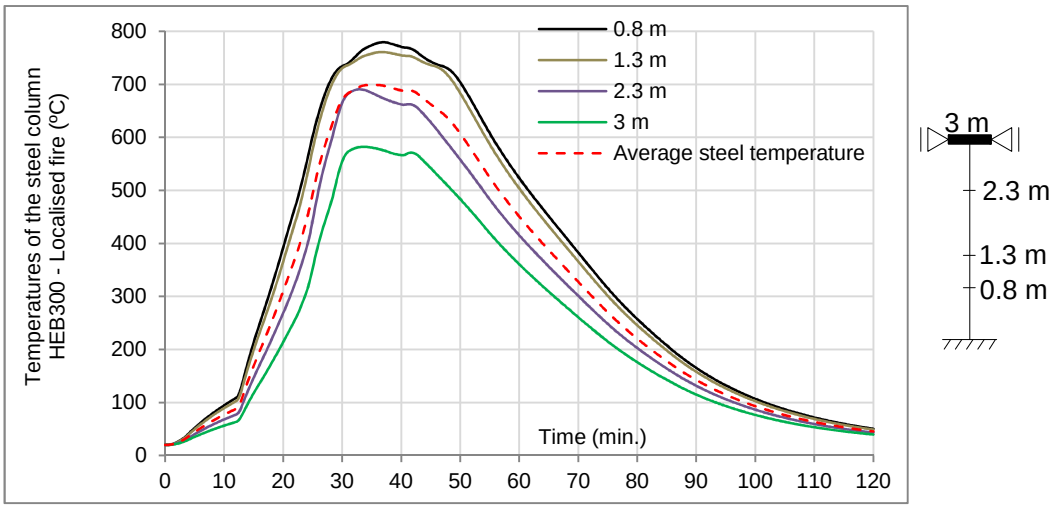

Figure 8: Temperatures along the steel HEB 300 column height calculated using the Hasemi method

The column is axially restrained by the surrounding structure during the localised fire, but it is difficult to evaluate the degree of restraint. According to Franssen (2000), the temperature of the heated column leading to its failure can be estimated by modelling the heated column as totally restrained (Figure 3b)).

The evolution of the axial load with the increase of temperature (due to the dilatation) is observed and once the heated column supports fewer loads than the initial load it supported before the fire, the column failure occurs. This statement is checked and the steel column HEB 300 is modelled with a spring at the top (Figure 3c)) in order to represent the effect of restraints (the spring stiffness is varying from 0 to the infinite). Two loading steps are defined: step 1 – a compression load is applied at the column top; step 2 – the average fire temperature (Figure 8) is applied along the entire column height. The applied load (step 1) depends of the spring restraint and is defined in order to always have in the column the design value of the axial force for the fire situation $N_{Ed,fi,20ºC}$ (2713 kN).

Figure 9a) presents the evolution of the ratio of the axial load on the initial load versus the average temperature in the column, and Figure 9b) shows the evolution of the axial load ratio versus time. For the column totally restrained (infinite restraint), and during the heating phase, the axial load reaches the maximum value (5685 kN) around 15 min, then decreases and reaches the design value of the axial force for the fire situation $N_{Ed,fi,20ºC}$ (2713 kN). This point is considered to be the failure of the column and it happens at 578ºC (26.9 min). After this instant, the heated column is not able anymore to support the loading and fails.

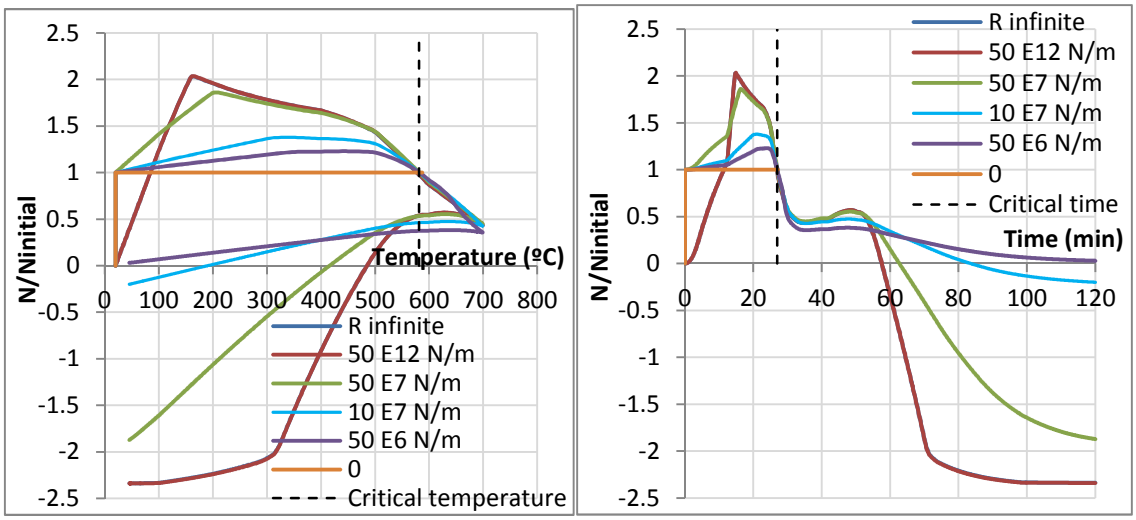

Figure 9: a) Evolution of the axial force *vs* increase and decrease of the average temperature in the column; b) Evolution of the axial force *vs* time

Table 2 presents the critical time and temperature of the steel column under localised fire, with different spring stiffness's for the axial restraint. Note that, the axial restraint does not affect so much the critical values, and the average temperature value is equal to 581ºC after 27 min of fire.

Table 2: Critical time and temperature of HEB 300 steel profile according to the spring stiffness

Spring stiffness	Time (min)	Temperature (ºC)	*N* (kN)
0	27.2	587	2713
50 E6 N/m	27.0	582	2713
10 E7 N/m	27.0	582	2713
50 E7 N/m	27.0	582	2713
50 E12 N/m	26.9	578	2713
Infinite	26.9	578	2713
Average values	**27.0**	**581**	**2713**

V Conclusion

This document presented a behaviour study of a steel column subject to a localised fire. The purpose of this study was to show that the column completely loses any resistance once the localised fire develops around it, so that for the ROBUSTFIRE project studies, the column loss can be assumed by the total removal of the column. The studied steel column is 3 m height, HEB 300 steel cross-section, class S460. Two alternative studies were developed: i) the column behaviour was analysed under constant temperatures, using the Eurocode 3 and a numerical model; and ii) the column behaviour was analysed under localised fire, using the method described in Franssen (2000).

According to Eurocode 3, the buckling of the column slightly influences the maximum load capacity. However, the numerical model showed that at ambient and elevated temperatures, the column fails by yielding of the cross-section and three plastic hinges are formed at the top, bottom and centre of the column. A mechanism is created, and the column sustains the loads until the complete failure of the hinges. It was also showed that the maximum load capacity of the column at ambient temperature (6193 kN) is reduced up to 80% at 700ºC (1245 kN). Moreover, under constant temperature equal to 600ºC, the column load capacity is reduced of 59% according to the FE model (2541 kN), and 60% according to Eurocode 3 (2594 kN), and the column is not able anymore to support the column axial force design value for the fire situation $N_{Ed,fi,20ºC}$ (2713 kN).

The column was also analyzed under varying temperatures, defined by a fire scenario including 4 class3-cars. Steel temperatures were estimated using the Hasemi method, and the average temperature was applied to the column. It was observed, as in Franssen (2000), that the restraint from the unaffected part of the building has no effect on the column critical temperature. The column was not able anymore to sustain to $N_{Ed,fi,20ºC}$ (2713 kN) from 578ºC (after 26.9 min. of fire).

REFERENCES

Abaqus Analysis User's manual, v6.11, Dassault Systems Simulia Corp., Providence, USA, 2011.

EN 1991-1-2:2002 – “Eurocode 1: Actions on structures – Part 1-2: General actions – Actions on structures exposed to fire”, European committee for standardization, November 2002, 59p.

EN 1993-1-1:2005 – “Eurocode 3: Design of steel structures – Part 1-1: General rules and rules for buildings”, European committee for standardization, May 2005.

EN 1993-1-2:2005 – “Eurocode 3: Design of steel structures – Part 1-2: General rules – Structural fire design”, European committee for standardization, April 2005.

EN 10113-3:1993, Hot rolled products in weldable fine grain structural steels - Delivery conditions for thermomechanical rolled steels, 1993.

Franssen, J.-M., “Failure temperature of a system comprising a restrained column submitted to fire”, Fire Safety Journal, 34, 2000, p191-207.

Fraud, C., Zhao B., Joyeux D., Kruppa J. – “Guide pour la vérification du comportement au feu de parcs de stationnement largement ventilés en superstructure métallique”, CTICM, INSI – 03/233d – BZ/PB, 2004, 75p.

Gens, F. “Pre-dimensionning of the reference’s car park”. Internal document, Greisch, ROBUSTFIRE Project, February 2010.

Malvern, L.E. “Introduction to the mecanics of a continuous medium”, Englewood Cliffs, NJ: Prentice-Hall, 1969.

Schleich et al., “Development of Design Rules for Steel Structures Subjected to Natural Fires in Closed Car Parks”, European Commission, C.E.C. Research 7210-SA/518. Final Report EUR 18867 EN, 1999, 154p.

Simões da Silva L., Santiago A., Haremza C. “ROBUSTFIRE Project, Document 1 – Car Parks – v1(11)”. Internal report, University of Coimbra, 2009.

Vila Real, P., Franssen, J. M. – Elefir-EN V1.2.3, Software for fire design of steel structural members according the Eurocode 3, 2010.

ANNEX D – Composite beam benchmark

ROBUSTFIRE REPORT

Benchmark Study of Composite Beams

Imperial College London

Cheng fang

Bassam Izzuddin

Ahmed Elghazouli

David Nethercot

University of Coimbra

Cécile Haremza

Aldina Santiago

Luís Simões da Silva

Table of contents

I Introduction

The aim of this report is to present benchmark studies on the response of steel/concrete composite beams under ambient or elevated temperature scenarios. The benchmark composite beams are selected based on the paper published by Huang et al. (1999), who selected two test programmes, one for the ambient condition and one for the fire condition. For the ambient temperature cases, two simply-supported composite beam tests, specifically tests A3 and A5 conducted by Chapman and Balakrishnan (1964), are considered. For the elevated temperature conditions, two fire tests, specifically tests 15 and 16 on simply-supported composite beams conducted by Wainman and Kirby (1988), are referred to. The benchmark study is conducted using two FEM tools: ADAPTIC (Izzuddin, 1991) and ABAQUS (2011). Since from previous numerical predictions done by Huang et al. (1999), it has been shown that the behaviour of the composite beams with partial and full interactions are similar, thus for simplicity this report only considers the composite beams with full concrete slab-steel interaction.

II Composite beams at ambient temperature

II.1 Test description

Two simply-supported beams were considered under increasing central point loads until failure. Details of the tests, including the material properties and the shear stud arrangement, are listed in Table1, and the illustrations of the test specimens are shown in Figure 1, where $f_{y,b}$ is the yield strength of the steel beam, f_c is the compressive strength of concrete, and $f_{y,r}$ is the yield strength of reinforcing steel. d and f_u are respectively the diameter and the specified ultimate shear strength of the shear stud, which are however not considered in this study due to the assumption of full shear interaction.

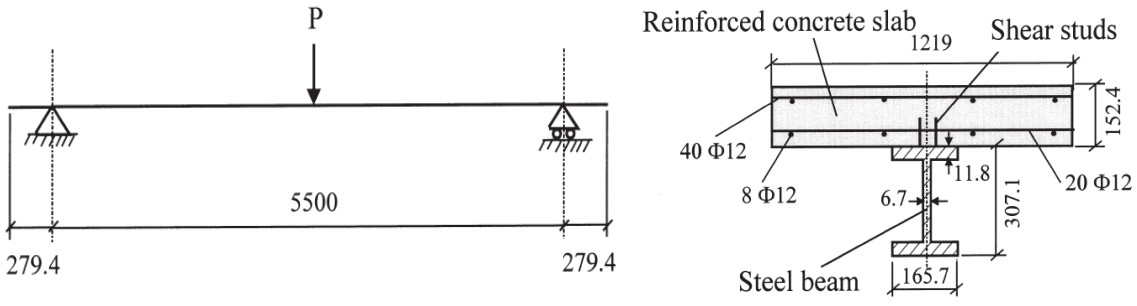

Fig 1 dimensions of tested composite beams, Huang et al. (1999)

Table 1 material properties and stud members for specimens A3 and A5 Huang et al. (1999)

Code	$f_{y,b}$ (MPa)	f_c (MPa)	$f_{y,r}$ (MPa)	No. of studs	d (mm)	f_u (MPa)
A3	302	27	600	68	19	600
A5	290	43	600	44	19	600

II.2 Modelling approach

Beam-column elements are employed for modelling the steel beam and the concrete flange. The steel beams and the concrete flanges are connected by rigid links which represent a full interaction between steel and concrete. The illustration of the ADAPTIC model is given in Figure 2.

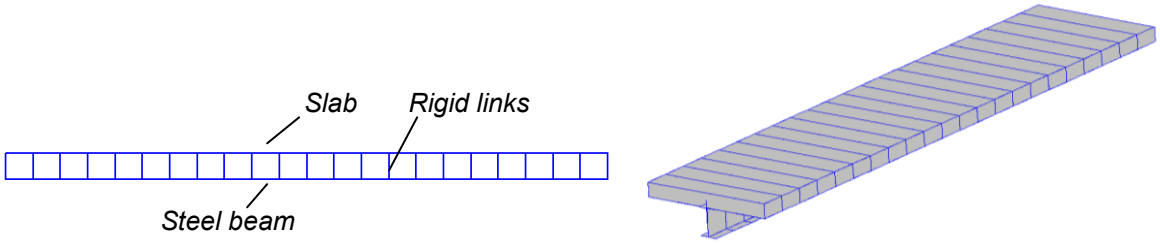

Fig 2 composite beam model in ADAPTIC

The properties of steel and concrete are defined according to EN 1993-1-1:2005 and EN 1992-1-1:2004 respectively. For both the steel beam and reinforcement, a bilinear elasto-plastic model with kinematic strain hardening is adopted. The initial modulus of elasticity E_s is 210000MPa and the elastic strain ε_s is 0.0014. With respect to the tensile concrete material properties, a linear initial response is employed, while for the compressive response of the concrete, two stress-strain relationships are considered, quadratic and linear, where for the quadratic response the initial tangent compressive modulus is taken equal to the tensile modulus. The strain-stress relationships for both steel and concrete are illustrated in Figure 3, where 'qua' represents a quadratic compressive response of concrete and 'lin' represents a linear compressive response of concrete. The details for concrete properties are listed in Table 2, where f_c is the compressive strength of the concrete, ε_c is the compressive strain in the concrete at the peak stress f_c, f_t is the value of axial tensile strength of concrete, ε_{t1} is the tensile strain in the concrete at the peak stress f_t, and ε_{t2} is the ultimate tensile strain in the concrete.

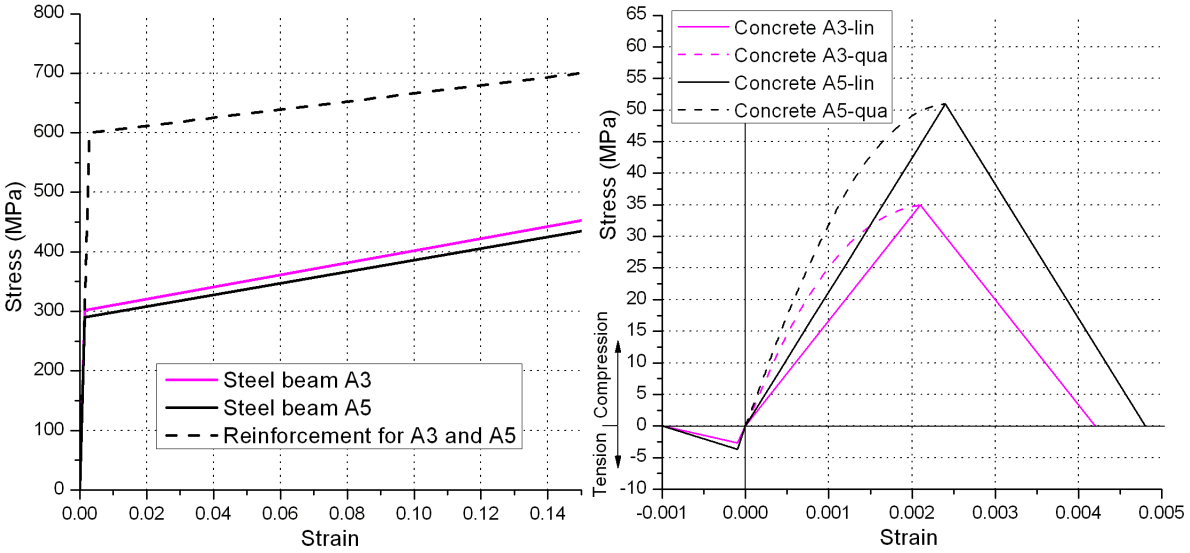

Fig 3 material stress-strain behaviour

Table 2 Concrete properties in ADAPTIC for specimens A3 and A5

Name	f_c (MPa)	ε_c	f_t (MPa)	ε_{t1}	ε_{t2}
A3	35	0.0021	2.7	0.0001	0.001
A5	51	0.0024	3.7	0.0001	0.001

II.3 Numerical results

The beam mid-span deflection versus central point load responses for specimens A3 and A5 are presented. These results are compared with VULCAN results and the test outcomes, as shown in Figures 4 and 5. Good correlations are observed between numerical and experimental results up to relatively large deflections, thus validating the accuracy of ADAPTIC and ABAQUS in predicting the behaviour of composite beams.

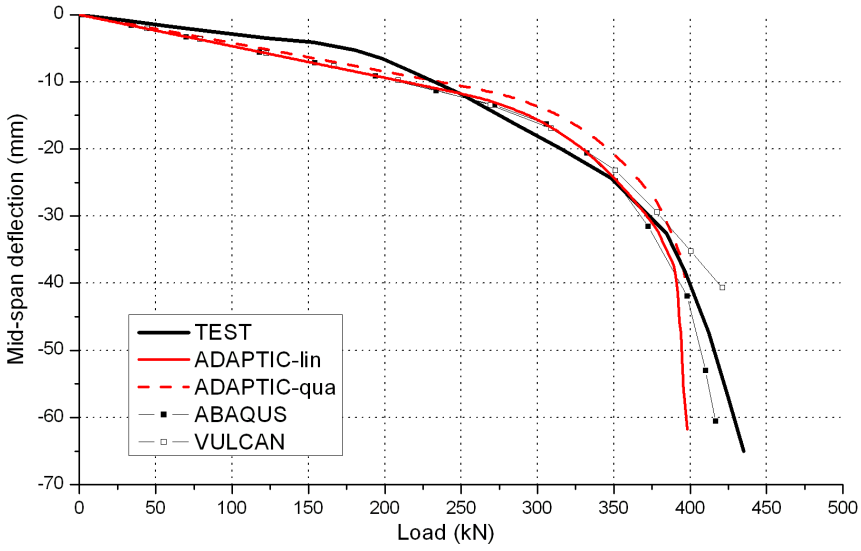

Fig 4 comparison of load-deflection relationships for beam A3 with full concrete-steel interaction

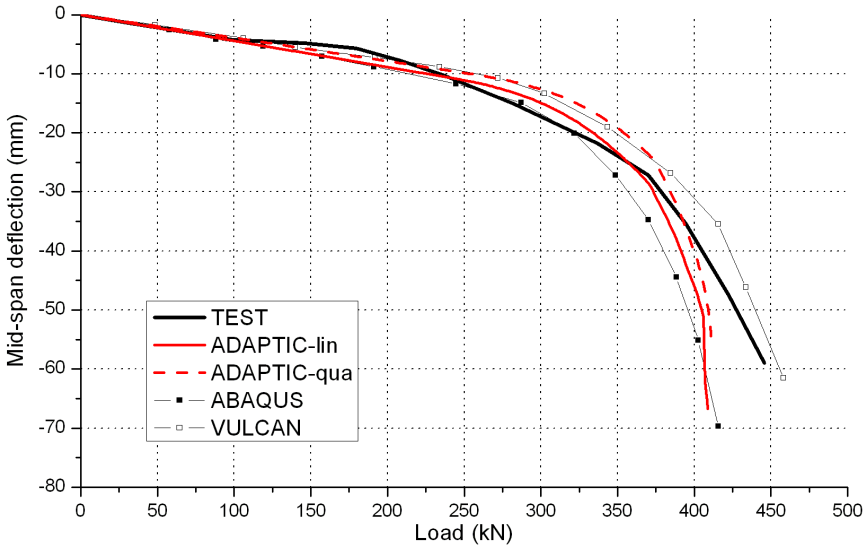

Fig 5 comparison of load-deflection relationships for beam A5 with full concrete-steel interaction

III Composite beams in fire

III.1 Test description

Two of the fire tests conducted by Wainman and Kirby (1988) are chosen for this benchmark study, specifically tests 15 and 16. The aim of the tests was to investigate the fire behaviour of simply-supported composite beams subject to the standard fire ISO834. Four point loads were applied along the length of the beam, and two levels of load ratio were considered: 0.294 and 0.564, corresponding to a point load of 32.47kN and 62.36kN respectively. UB 254×146×43 was adopted for the steel beam and 130mm thick reinforced slab was connected to the steel beam with 32 shear studs all along the length. The details of the test specimens are illustrated in Figure 6. Full interaction between concrete and steel are assumed.

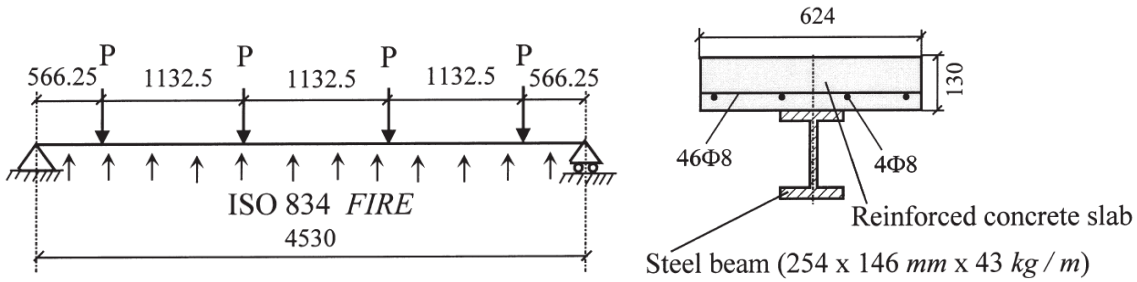

Fig 6 dimensions of tested composite beams in fire, Huang et al. (1999)

III.2 Modelling approach

The mechanical modelling approach for the composite beams in fire is similar to the modelling technique employed in the aforementioned analysis investigating the behaviour of composite beams at ambient temperature. Since ADAPTIC only deals with structural modelling, the temperature distribution curves across the cross-section

obtained from ABAQUS thermal analysis (Haremza et al. 2009) is directly adopted, as given by Figure 7. In ADAPTIC, up to three independent temperatures at three points can be considered over the cross-sections of the steel beam and the concrete slab, thus allowing the use of a quadratic temperature distribution. No temperature variation is considered along the length of the composite beam.

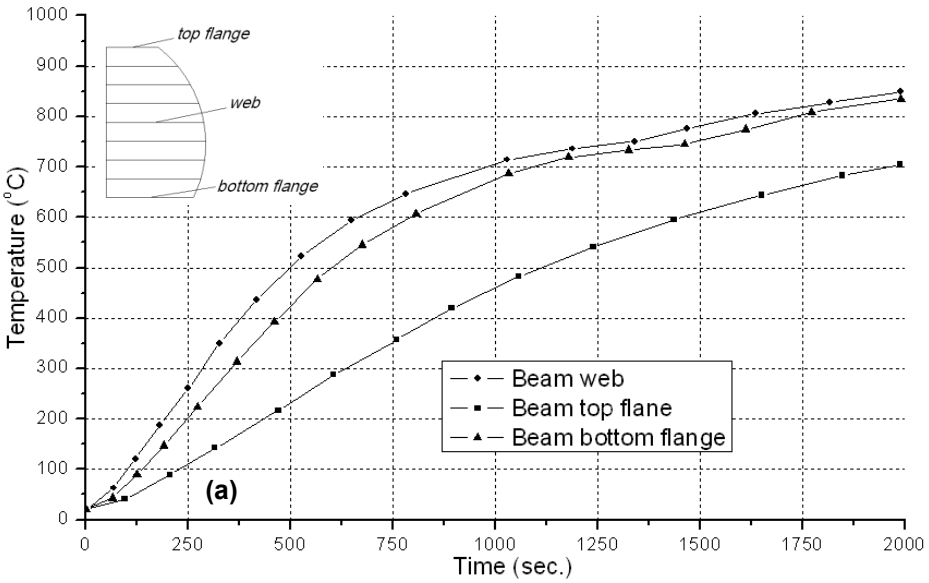

Fig 7(a) temperature distributions across the cross-section: steel beam (cont'd…)

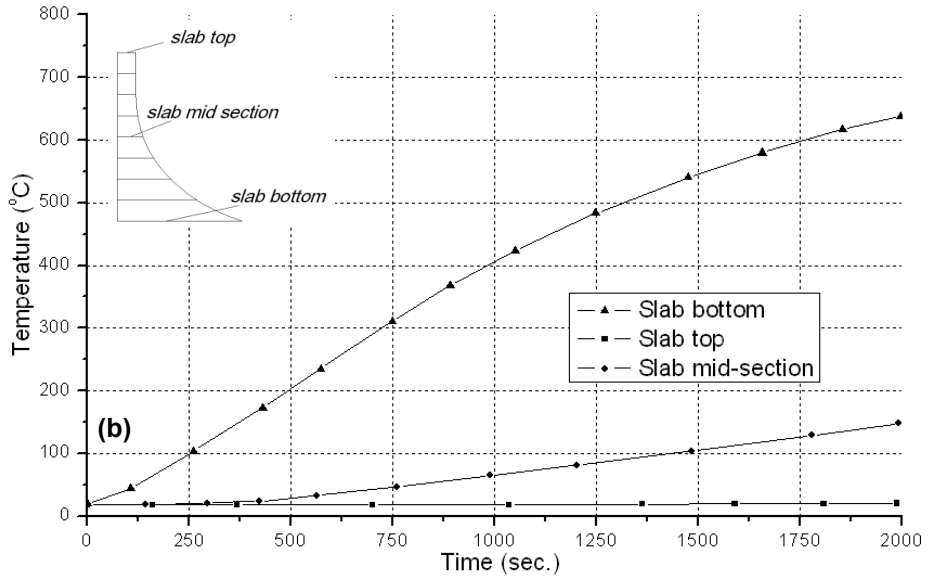

Fig 7(b) temperature distributions across the cross-section: concrete slab

The ambient temperature properties of steel and concrete are defined according to EN 1993-1-1:2005 and EN 1992-1-1:2004 respectively. The graphical representations of the ambient material behaviour laws are illustrated in Figure 8 and the details of ambient material properties used in ADAPTIC for the steel beam, the

reinforcement, and the concrete are listed in Tables 3 and 4. For steel/reinforcement, f_y is the yield strength, E_s is the modulus of elasticity, ε_y is the elastic strain and ε_u is the ultimate strain; for concrete, f_{c1} is the compressive strength, ε_{c1} is the compressive strain in the concrete at the peak stress, ε_{c2} is the ultimate compressive strain, f_{t1} is the cracking strength, ε_{t1} is the tensile strain in the concrete at the peak cracking stress, and ε_{t2} is the ultimate tensile strain.

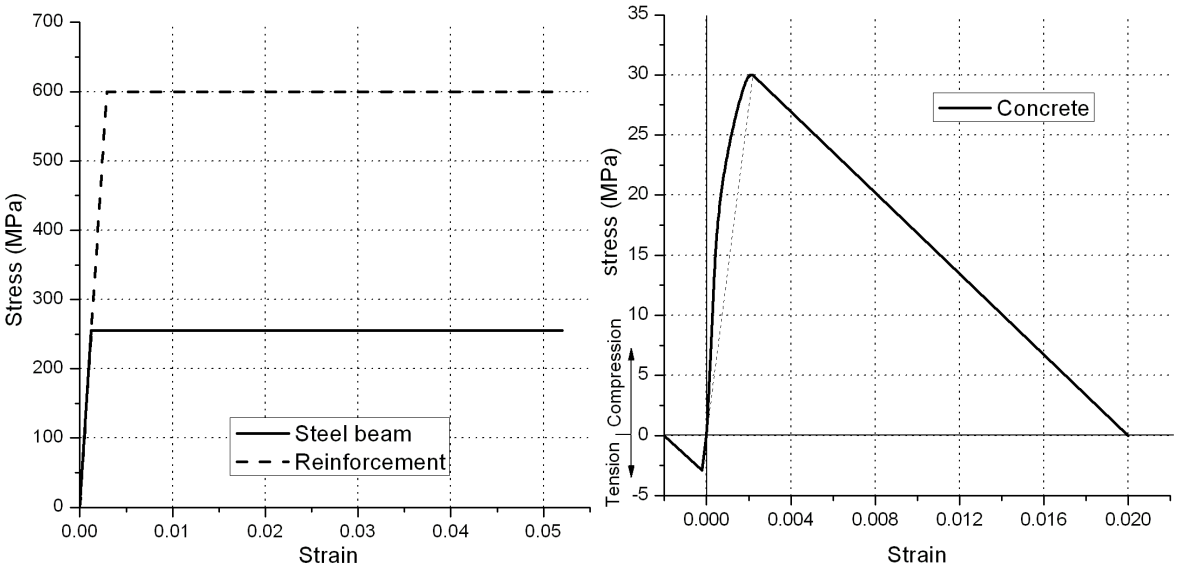

Fig 8 Ambient material stress-strain relationships

Table 3 Ambient steel/reinforcement properties for Tests 15 and 16

material	f_y (MPa)	E_s (Mpa)	ε_y	ε_u
steel beam	255	210000	0.0012	0.2
reinforcement	600	210000	0.0029	0.2

Table 4 Ambient concrete properties for Tests 15 and 16

material	f_{c1} (MPa)	ε_{c1}	ε_{c2}	F_{t1} (MPa)	ε_{t1}	ε_{t2}
concrete	30	0.0025	0.02	2.9	0.00025	0.002

With respect to elevated temperature conditions, the material degradations are based on the recommendations specified in EN 1994-1-2:2005 and EN 1992-1-2:2004. The key temperature-dependent material properties of steel and concrete used in the ADAPTIC models are listed in Tables 5 and 6, which are in terms of ratios of their respective values at elevated temperatures over ambient conditions. Piecewise linear interpolation is used for temperatures between the values indicated in these two tables. Constant thermal expansion coefficients of $1.4\times10^{-5}/^{o}C$ and $1.8\times10^{-5}/^{o}C$ are assumed for steel and concrete respectively.

Table 5 Variation of steel properties with temperature

Temperature (°C)	0-100	500	600	700	1200
Elastic modulus (E_t/E_0)	1.0	0.6	0.31	0.13	0.0
Temperature (°C)	0-400	500	700	800	1200
Yield strength (f_t/f_0)	1.0	0.78	0.47	0.11	0.0
Temperature (°C)	0-100	400	500	700	1200
Proportional limit (p_t/p_0)	1.0	0.42	0.36	0.075	0.0

Table 6 Variation of concrete properties with temperature

Temperature (°C)	200	800	1000
Compressive strength (f_{ct}/f_{c0})	0.95	0.15	0.04
Temperature (°C)	300	400	600
Peak compressive strain ($\varepsilon_{c1t}/\varepsilon_{c10}$)	2.8	4.0	10
Temperature (°C)	300	800	1000
Ultimate compressive strain ($\varepsilon_{c2t}/\varepsilon_{c20}$)	1.35	1.9	10
Temperature (°C)	100	300	600
Tensile strength (f_{tt}/f_{t0})	1.0	0.6	0.0
Temperature (°C)	300	400	600
Peak tensile strain ($\varepsilon_{t1t}/\varepsilon_{t10}$)	2.8	4.0	10
Temperature (°C)	300	600	600
Ultimate tensile strain ($\varepsilon_{t2t}/\varepsilon_{t20}$)	1.35	10	10

III.3 Numerical results

The deflection-temperature curves of ADAPTIC, ABAQUS, VULCAN as well as the test results are given in Figures 9 and 10 for tests 15 and 16 respectively. The results show a good correlation. The numerical predictions derived from three numerical tools are perfectly matched at small deflections (0-50mm). At later stages, small discrepancies are found; this is possibly due to some inaccuracies in predicting material properties (ambient and elevated temperature) and temperature distributions.

The numerical predictions have some obvious discrepancies compared with the test results especially for test 16. In addition to the above explanations, this discrepancy here is also attributed to the difficulty in producing prefect simple support conditions in a furnace at high temperatures (Huang et al. 1999).

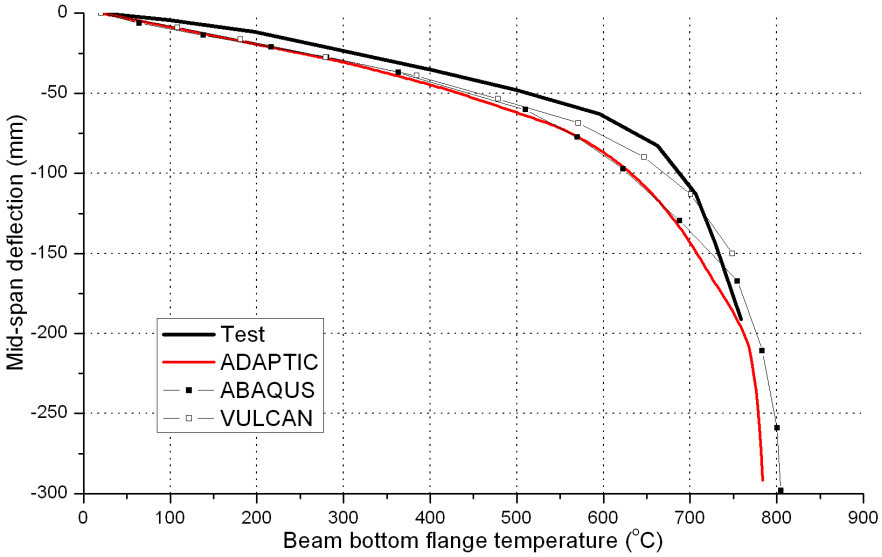

Fig 9 comparison of temperature-deflection relationship for test 15 with full concrete-steel interaction

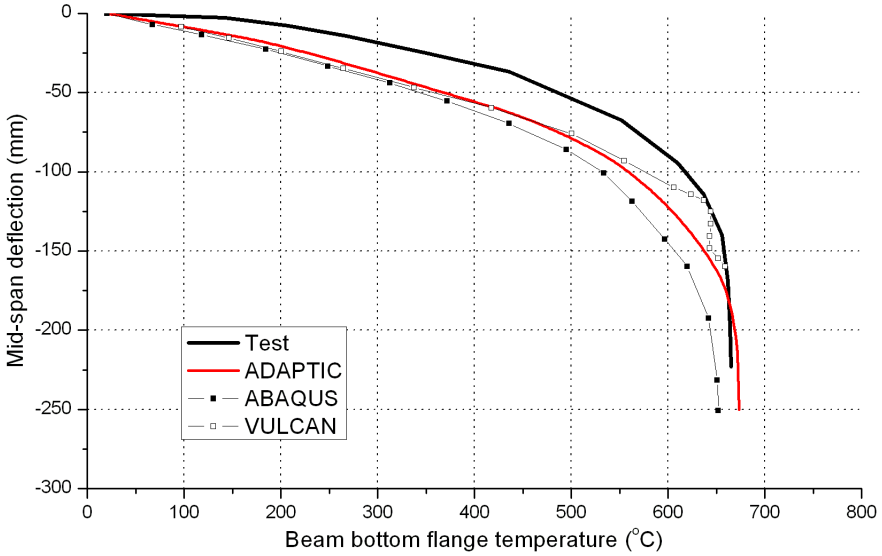

Fig 10 comparison of temperature-deflection relationship for test 16 with full concrete-steel interaction

IV Discussion

The results show the reliability of ADAPTIC and ABAQUS in predicting the response of composite structure at both ambient and elevated temperature conditions. It is also shown that the ADAPTIC 1D beam-column element has sufficient accuracy in simulating the behaviour of concrete slab flanges compared with the 2D shell element used in ABAQUS. Of course, for a detailed model of a floor system including membrane effects shell elements would still be required for modelling the floor slab. Some of the difference between ADAPTIC results and other results are discussed below:

1) The material properties used in ADAPTIC are slightly different from other models. For example, in the ADAPTIC concrete model considering elevated temperature responses, tensile strength is ignored.

2) The temperatures specified in the ADAPTIC models are based on heat transfer analysis of ABAQUS, and these may be different from real temperature distributions and VULCAN heat transfer results. Parabolic temperature distributions are assumed in the ADAPTIC model, which may also be associated with some inaccuracy. In addition, even the ABAQUS models do not exactly follow the obtained temperature distributions during the heating procedure because only one predefined fields of temperature is used throughout the analysis. Furthermore, a uniform temperature along the length of the beam cannot be ensured in real tests.

3) Only full interaction between the concrete slab and the steel beam is considered in the above analyses, which is only an approximation of the real interaction.

4) Perfect simple supports cannot be guaranteed in the real tests, especially at high temperature.

V References

Abaqus (2011). Analysis User's manual, v6.11, Dassault Systems Simulia Corp., Providence, USA.

ADAPTIC user manual, Version 1.3b, Izzuddin, 2009, March.

Chapman J.C., Balakrishnan S. "Experiments on composite beams". The Structural Engineering, 42(11), 369–83, 1964.

Huang Z., Burgess I.W., Plank R.J. "The influence of shear connectors on the behaviour of composite steel-framed buildings in fire". Journal of Constructional Steel Research, 51, 219-237, 1999.

EN 1992-1-1:2004. "Eurocode 4: Design of concrete structures - Part 1-1: General rules and rules for buildings". European committee for standardization, December 2004.

EN 1992-1-2:2004. "Eurocode 2: Design of concrete structures – Part 1-2: General rules – Structural fire design". European committee for standardization, December 2004.

EN 1993-1-1:2005. "Eurocode 3: Design of steel structures - Part 1-1: General rules and rules for buildings". European committee for standardization, May 2005.

EN 1993-1-2:2005. "Eurocode 3: Design of steel structures – Part 1-2: General rules – Structural fire design". European committee for standardization, April 2005.

EN 1994-1-1:2004. "Eurocode 4: Design of composite steel and concrete structures – Part 1-1: General rules and rules for buildings". European committee for standardization, December 2004.

EN 1994-1-2:2005. “Eurocode 4: Design of composite steel and concrete structures – Part 1-2: General rules – Structural fire design”. European committee for standardization, 2005.

Haremza et al.（2009） Internal_report_5_BEx2_CObeam_v1(5)B

Izzuddin, B.A. (1991) Nonlinear Dynamic Analysis of Framed Structures. PhD Thesis. Department of Civil Engineering, Imperial College, University of London, London, UK.

Izzuddin, B.A., Song, L., Elnashai, A.S., and Dowling, P.J. (2000) An Integrated Adaptive Environment for Fire and Explosion Analysis of Steel Frames – Part II: Verification and Application. Journal of Constructional Steel Research, 53(1), 87-111.

Izzuddin, B.A., and Elghazouli, A.Y. (2004) Failure of Lightly Reinforced Concrete Members under Fire. Part I: Analytical Modeling. Journal of Structural Engineering, ASCE, 130(1), 3-17.

Izzuddin, B.A. (2005) A Simplified Model for Axially Restrained Beams Subject to Extreme Loading. International Journal of Steel Structures, 5, 421-429.

Izzuddin, B.A., Vlassis, A.G., Elghazouli, A.Y., and Nethercot, D.A. (2007) Progressive Collapse of Multi-Storey Buildings due to Sudden Column Loss – Part I: Simplified Assessment Framework. Under review.

Wainman D.E., Kirby B.R. “Compendium of UK standard fire test data, unprotected structural steel — 1”. Ref. No. RS/RSC/S10328/1/87/B. Rotherham (UK): Swinden Laboratories, British Steel Corporation, 1988.

ANNEX E – Joint benchmark

Imperial College London

ROBUSTFIRE REPORT

Component modelling of sagging composite joints under fire

Authors:

Cheng fang

Bassam Izzuddin

Ahmed Elghazouli

David Nethercot

Table of contents

I Introduction

This report is aimed at validating the reliability of the proposed component model in predicting the response of joints under elevated temperature conditions. Results from the ROBUSTFIRE joint tests are used for comparison. The component joint model is established in ADAPTIC (Izzuddin, 1991) employing spring and rigid link elements.

II Modelling assumptions

Under elevated temperature conditions, joints can exhibit significant degradation in strength and stiffness, hence it is required that the component-based spring models are capable of identifying the fire response of the considered joints. Based on the results from three sets of bare-steel joint tests, Al-Jabri (1999) presented the observed strength and stiffness reduction factors of these joints, as shown in Figure 1. It was found that the reduction trends of stiffness and strength obtained in the three tests correlate well with the strength reduction factor recommended by EN1993-1-2 (2005) for carbon steel at strain levels of the proportional limit and 1.0%, respectively. In line with this finding, Ramli-sulong *et al.* (2007) proposed new strength and stiffness reduction factors for the material of joints under fire, and employed these for the new joint models developed in ADAPTIC. In this study, the component strength and stiffness reductions factors proposed by Ramli-sulong *et al.* (2007) are slightly modified, as shown in Figure 1 and Table 1, so as to achieve a closer comparison with the test results (Al-Jabri, 1999).

Table 1 Strength and stiffness reduction factors for joint steel

Temperature (^{o}C)	Strength SRF	Stiffness SRF
20°C	1.000	1.000
100°C	1.000	1.000
200°C	0.971	0.807
300°C	0.941	0.613
400°C	0.912	0.420
500°C	0.721	0.280
600°C	0.360	0.100
700°C	0.160	0.035
800°C	0.110	0.020
900°C	0.060	0.010
1000°C	0.040	0.005
1100°C	0.020	0.0025
1200°C	0.000	0.000

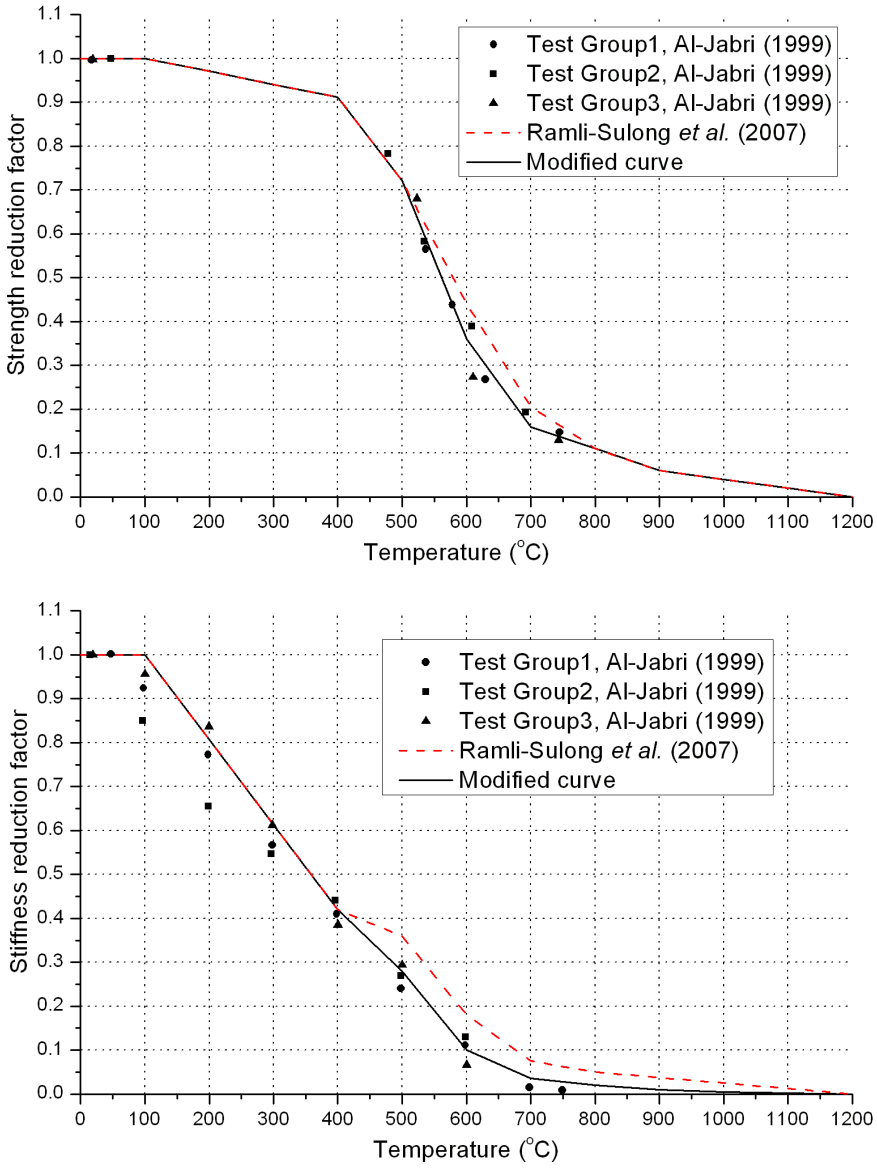

Fig. 1 Degradation of steel properties of joints with temperature

Monotonic load-deformation responses of joint components can be usually represented by bi-linear, tri-linear or nonlinear curves. Ambient behaviour of the components within the elastic range has already been well clarified in the component-based method recommended in EN1993-1-8 (2005), whereas rather limited test data is available for the post-limit response of components. The post-limit stiffness is typically obtained through multiplying the elastic stiffness with a strain hardening coefficient. Atamiaz Sibai and Frey (1988) suggested a value ranging from 1.9% to 2.4% for strain hardening coefficient of steel material property of joints at ambient temperature. Ren and Crisinel (1995) adopted a value of 6% for double web-cleat joints. In this study, various post-limit responses of components (e.g. bi-linear and tri-linear responses) are considered, and the influence of different post-limit strain hardening coefficients on joint response is discussed. Due to lack of available data for the strain hardening coefficients of components under elevated

temperatures, the same values as used under ambient conditions are employed for the current study.

III Joint fire test

Under a typical localised fire scenario where the fire occurs near a column, the joint directly exposed to fire can be subjected a significant sagging bending moment subsequent to column buckling. In order to evaluate the ductility supply of the fire affected joint after the loss of the column, a test programme (as shown in Figure 2) was proposed as part of the European RFCS ROBUSTFIRE project, where emphasis is given to the design of car parks exhibiting sufficient robustness against localised fire. The test specimens are designed according to a standard open car park structure specially designed for the ROBUSTFIRE project (Gens, 2010), and this building was deemed to be a typical European car park structure. The tested frame was comprised of two unprotected 3m length composite beams with IPE550 steel cross-sections, grade S355, and one unprotected HEB300 cross-section steel column, grade S460. The steel beams are fully connected to the 130 mm thickness composite slab through fully rigid shear studs. Flush end-plates are employed with eight M30 grade 10.9 steel bolts. The geometric properties of the tested frame are given in Figure 3.

Fig. 2 Joint test programme in ROBUSTFIRE project (Haremza *et al.* 2011)

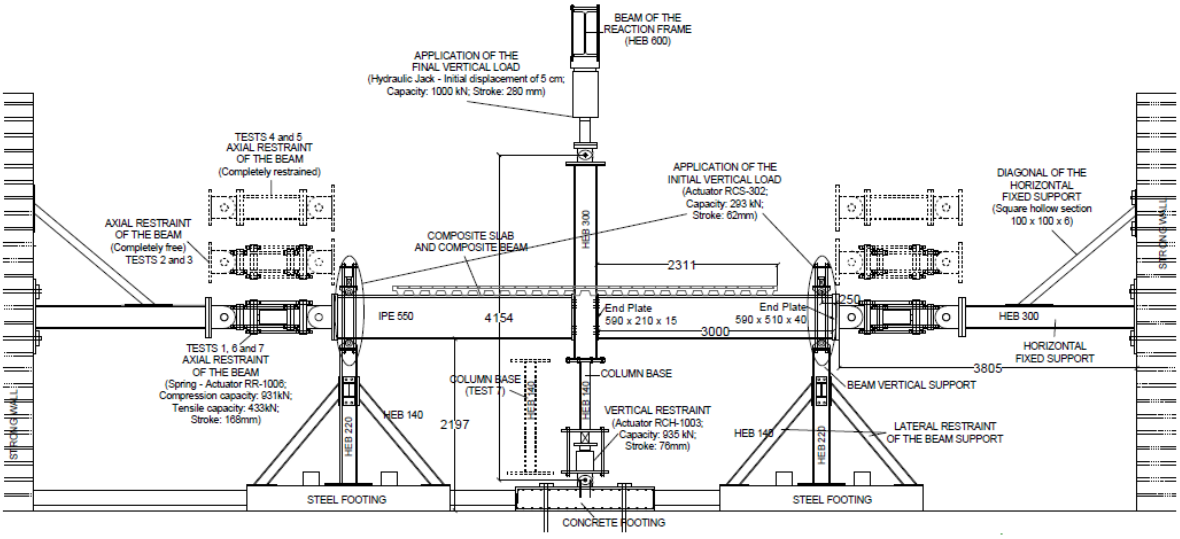

Fig. 3 Geometric properties of tested frame (Haremza *et al.* 2011)

Three tests (tests 2, 3, and 6) are selected to compare with the component-based joint models employed in this report. The joint was first heated to a stabilised peak temperature, then the column base was gradually relaxed and subsequently an increasing downward vertical point load was applied at the top of the HEB 300 column. No axial restraint is applied at the beam ends throughout the entire test for tests 2 and 3, and linear axial restraint with the stiffness of 50kN/mm is applied at the beam ends for test 6. The maximum temperatures in the bottom flange of the steel beam were 500°C and 700°C for tests 2 and 3/6 respectively, and the temperature was kept unchanged during the loading procedure. However, the temperature distribution was not uniform in the entire joint area, and different maximum temperatures were found at other parts of the joint, as given in Table 2. Therefore, for the component-based joint model considered in this study, various temperatures are applied to different joint components.

Table 2 Temperature distribution of tested joint

Positions	Test 2	Test 3	Test 6
Column flange	400°C	483°C	570°C
Column web	470°C	565°C	710°C
End-plate	430°C	529°C	575°C
Beam web	470°C	620°C	600°C
Beam flange	500°C	700°C	700°C
Bolt	390°C	505°C	550°C
Concrete	180°C	216°C	260°C

IV Component joint modelling

The component-based model for simulation developed in ADAPTIC is illustrated in Figure 4. For the four inner bolt-row spring series, the axial property in tension is contributed from four components, namely, column web in tension (cwt), column flange in bending (cfb), bolt in tension (bt), and end-plate in bending (epb). The effective width of the T-stub is selected as the bolt-row is considered as in a group. The compressive characteristic for all the five spring series are based on the resistance of column web in compression (cwc). For the up and bottom outer spring series representing contacting positions between the beam flanges and the column flange, the resistance of beam flange/web in compression (bfwc) is considered. The effect of column web in shear (cws) is ignored due to the symmetry of the tested frame.

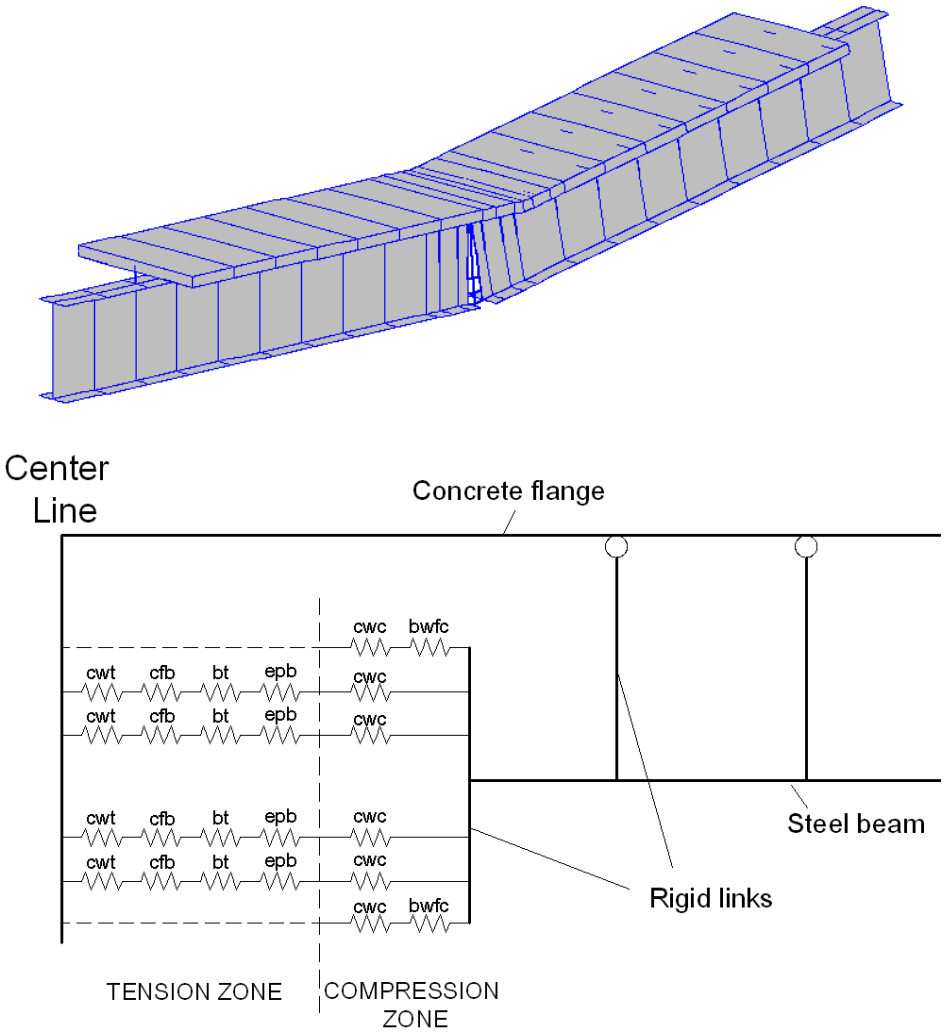

Fig. 4 Frame model with joint components in ADAPTIC

Three types of post-limit responses for each ductile component in the steel connection are considered, namely, no strain hardening (μ=0), bilinear response (μ=3%), and bilinear response (μ=5%). The concrete slab is simulated via beam-column elements neglecting the ribs and the steel deck. Rigid links are employed to connect the steel beam and the concrete to consider a fully rigid shear interaction. The material properties for the flange and the web of steel beams are E = 205kN/mm^2, f_y = 395.7N/mm^2, f_u = 516.7N/mm^2, and E = 205kN/mm^2, f_y = 432.3N/mm^2, f_u = 538.7N/mm^2 respectively. For the endplates the material properties are E = 205kN/mm^2, f_y = 395.7N/mm^2, and f_u = 516.7N/mm^2. The properties for the S3460 column flange and web are E = 205kN/mm^2, f_y = 515.7N/mm^2, f_u = 599N/mm^2, and E = 205kN/mm^2, f_y = 503.7N/mm^2, f_u = 571.3N/mm^2 respectively. The compressive strength for concrete f_c = 33N/mm^2. The temperatures listed in Table 2 are used in different joint components.

The bending moment vs. rotation relationships predicted from the component-based spring models are illustrated in Figures 5 to 7 for the tests 2, 3, and 6, respectively. Failure of joint in the component-based model is associated with the tensile failure of the lowest bolt-row, where the elongation exceeds the allowed value of 25mm which is determined as one of the joint failure criteria for this study. Good correlation is observed in relation to test 2, but for tests 3 and 6 the initial stiffness is overestimated. The bending capacities are well predicted for all the three tests. In addition, the ductility supplies / maximum rotations of the joints in both tests are underestimated by the component-based model. This is due to the predefined limitation of the 25mm maximum bolt-row elongation, which can be over conservative at elevated temperature.

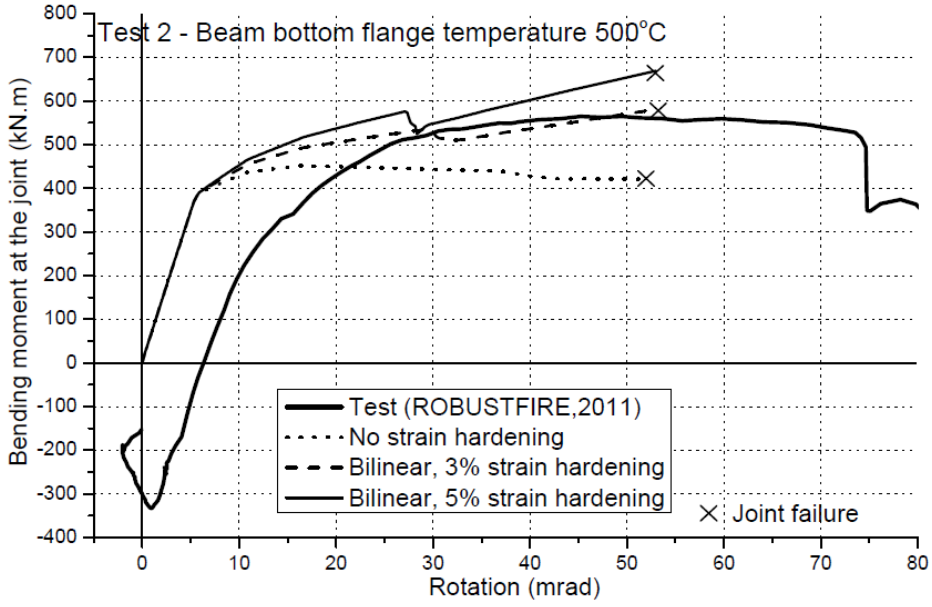

Fig. 5 moment-rotation relationship of joint in test 2

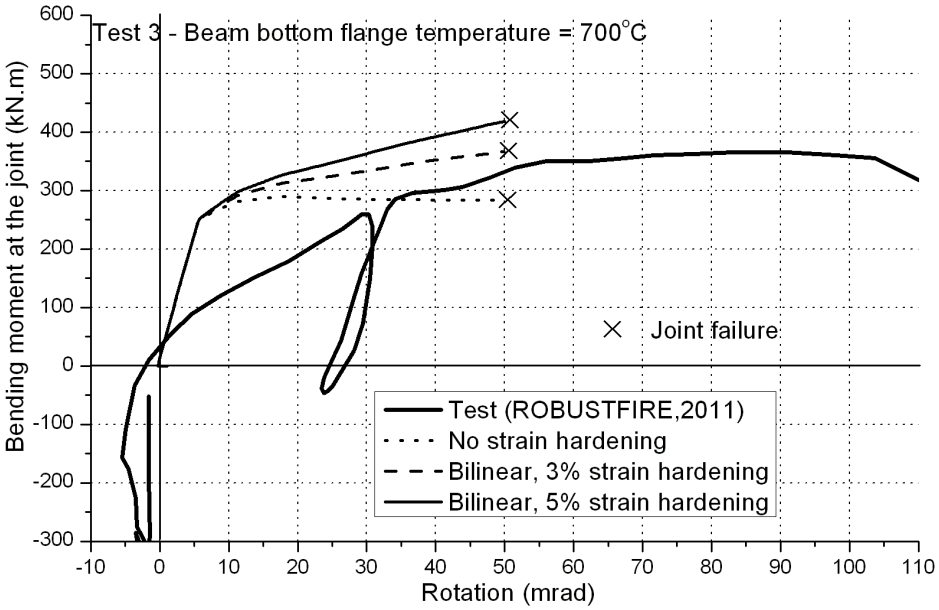

Fig. 6 moment-rotation relationship of joint in test 3

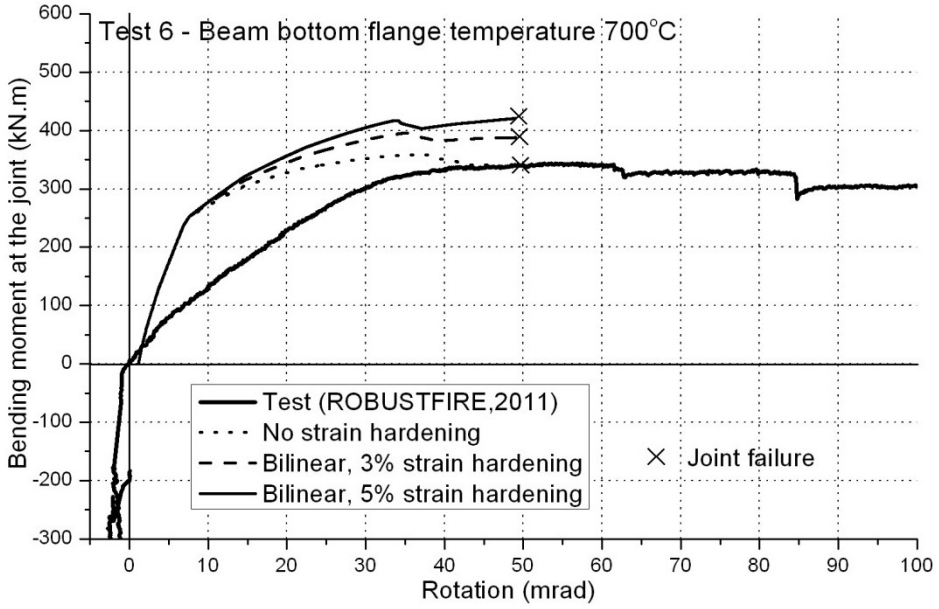

Fig. 7 moment-rotation relationship of joint in test 6

V References

Atamiaz Sibai W, Frey F. Numerical simulation of the behaviour up to collapse of two welded unstiffened one-side flange connections. In: Bjorhovde R et al., editors. Connections in steel structures: behaviour, strength and design. London: Elsevier Applied Science; 1988. p. 85–92.

Ren P, Crisinel M. Prediction method for moment–rotation behaviour of composite beam to steel column connection. In: Bjorhovde R et al., editors. Connections in steel structures III: behaviour, strength and design (Proc. of 3rd international workshop). 1995. p. 33–46.

Ramberg W, Osgood WR. Description of stress–strain curves by 3 parameters. Technical Report 902, National Advisory Committee for Aeronautics; 1943.

Cécile Haremza, Aldina Santiago, and Luís Simões da Silva. Experimental behaviour of heated composite joints subject to variable bending moments. EUROSTEEL, 2011, Budapest, Hungary.

Gens, F, “ROBUSTFIRE Project - Pre-dimensionning of the reference’s car park”, Internal document, Greisch, 2010.

ANNEX F – Joint thermal finite element model

Université de Liège

University of Liège
Faculty of Applied Sciences
Department of Architecture, Geology, Environnement & Constructions

ArGEnCo

March 20th, 2012

ROBUSTFIRE

JOINT THERMAL FINITE ELEMENT MODEL

Deliverable II

Authors:
Ludivine Comeliau
Jean-François Demonceau
Clara Huvelle
Jean-Pierre Jaspart
Long Van Hoang

Table of contents

I. Introduction

This section presents a thermal finite element model of a composite beam-to-column joint submitted to the standard temperature-time curve (iso fire). The studied joint links two IPE550 beams to a HEB300 column. It is the same as the one designed for the connections of the primary beams to the columns in the reference car park structure designed and investigated in the present project (the resistance of this joint is studied in DELIVERABLE III, section II), except that a 12cm thick solid concrete slab is considered here instead of a composite slab.

The temperature analysis was performed with the finite element software SAFIR (Refs. [1] and [2]). In the following, the model is first described before the evolution of the temperature distribution is presented.

II. Description of the numerical model

The developed model uses 3D elements with 8 nodes. For reasons of symmetry, only 1/4 of the column was modelled, with the associated parts of beam and joint. The bolts and slab reinforcement have not been represented in the model (Figure 1).

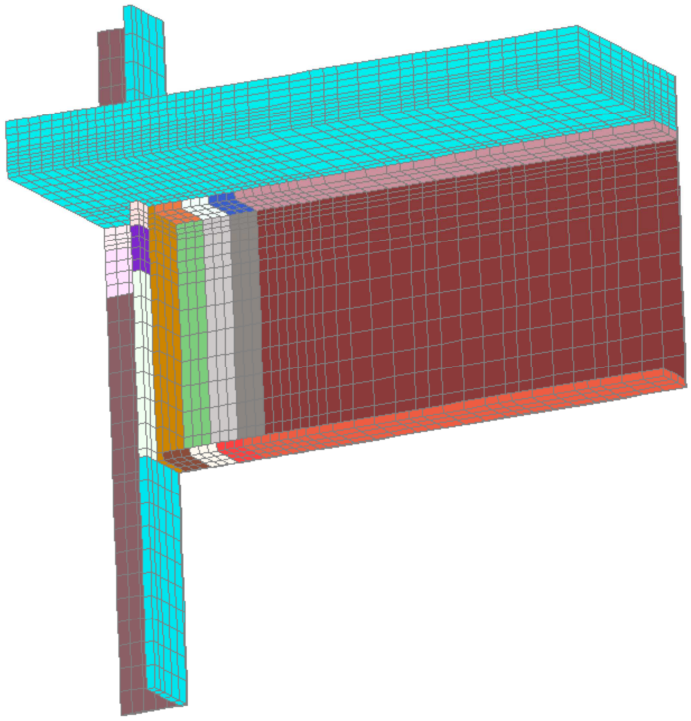

Figure 1. Joint model

The limit conditions are defined as shown in Figure 2: nominal iso fire curve on the frontiers below the slab and ambient conditions above the floor (upper face of the slab included, though not visible in the figure).

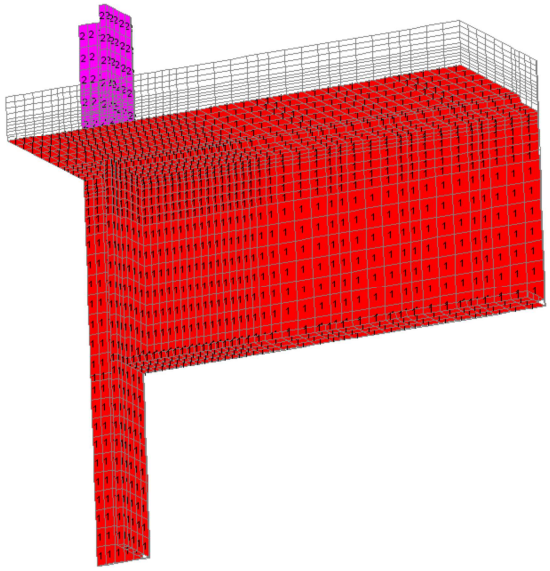

Figure 2. Frontier conditions: (1-red) iso fire, (2-pink) 20°C

Steel and concrete properties are in accordance with Eurocode 3 and 2 respectively. The convection coefficient on hot surfaces is taken equal to 25 W/m²K and the convection coefficient on cold surfaces is taken equal to 4 W/m²K. The relative emissivity of concrete surfaces is taken equal to 0,7. This parameter should also be taken equal to 0,7 for carbon steel according to Eurocode 3. However, in order to take account of the position and shadow effects in the numerical simulation, the relative emissivity of steel surfaces is multiplied by a reduction factor k_ε (≤ 1) based on the configuration factors related to the different zones as explained below (the different volumes defined with proper k_ε values are represented in different colours in Figure 1).

III. Computation of the configuration and reduction factors

According to Annex G of the EN1991-1-2, the configuration factor ϕ measures the fraction of the total heat leaving a given radiating surface that arrives at a given receiving surface. Its value depends on the size of the radiating surface, on the distance from the radiating surface to the receiving surface and on their relative orientation. In particular, this annex gives formulae to derive the configuration factor for a receiving surface parallel to the radiating surface (formula (G.2)) and for a receiving surface perpendicular to the radiating surface (formula (G.3)).

In the present case, and as far as the beam is concerned, a value of the configuration factor can be computed for any point of the end-plate, the beam web and the internal face of the beam top and bottom flanges, considering these surfaces as receiving ones and the vertical fictitious surface between the beam flanges as the radiating one (Figure 3).

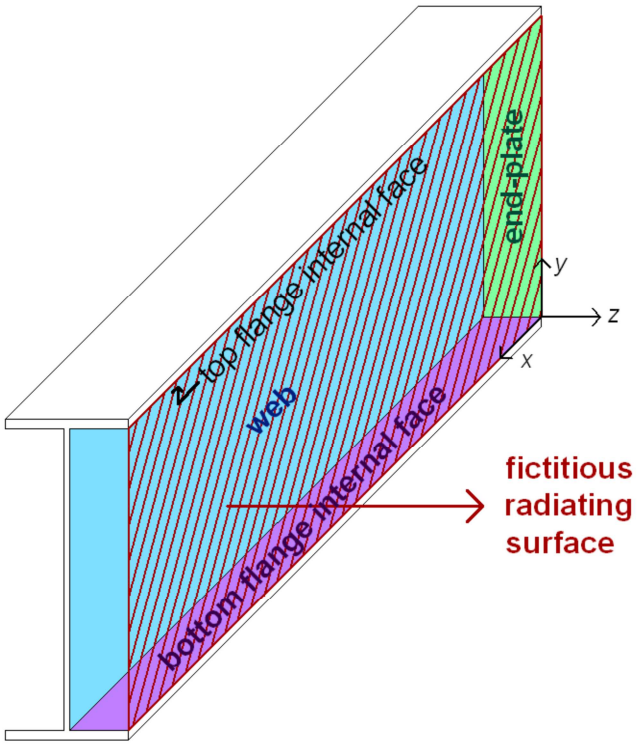

Figure 3. Radiating surface for the computation of the configuration factors

For example, Figure 4 shows the variation of the configuration factor at mid-height of the beam web (y=0,5.h_i=257,8mm, see definition of y-axis in Figure 3) as a function of the distance from the end-plate (see x-axis in Figure 3). On this figure, the vertical lines represent the limits of the four web zones for which different values of the reduction factor k_ε have been defined in the model (see II and Figure 1), based on the value of the corresponding configuration factors ϕ as detailed in the following. Figure 5 shows the variation of ϕ along the web height for a given value of x=92,5mm (middle of web zone 2). The red line gives the average value along the web height, which was considered as the configuration factor for the surface of web zone 2.

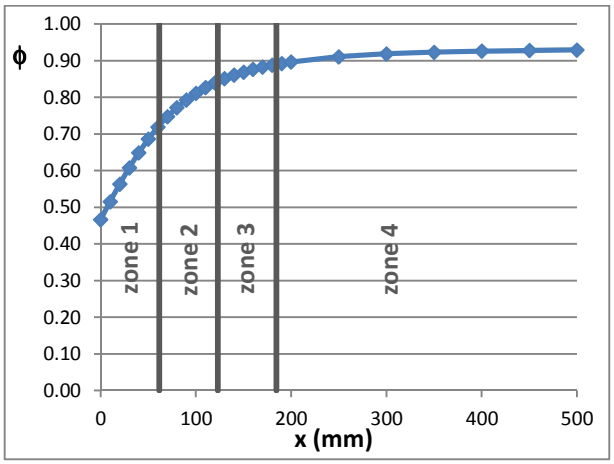

Figure 4. Configuration factor at mid-height of the web

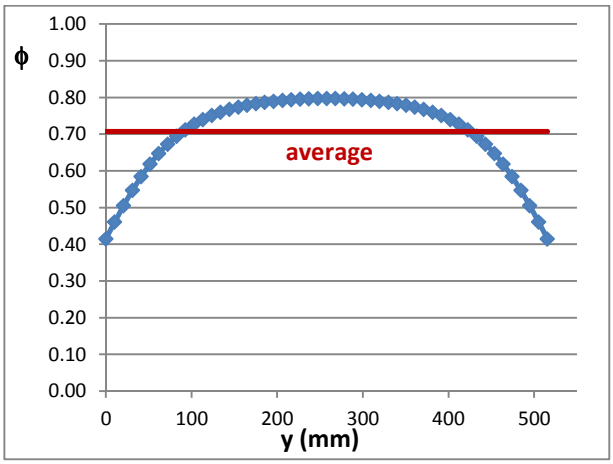

Figure 5. Configuration factor of the web at x=92,5mm

Similarly, an average value of the configuration factor could be established for the end-plate surface, for different zones of the web surface and for different zones of the beam top and bottom flanges internal face. Based on these configuration factors, the reduction factors k_ε defined in section II are evaluated as explained below.

For the beam web, the reduction factor k_ε is equal to the configuration factor ϕ. Indeed, both faces of the web are similarly heated by the fire. It is not the case for the other elements. Indeed, the different faces

of the beam flanges are not heated in the same way. For example, the lower and side faces of the beam bottom flange are directly subjected to the fire (ϕ=1) while a configuration factor smaller than 1 has to be considered for the upper face to account for shadow and position effects. So an average value had to be defined, as there is only one layer of elements forming the beam flange in the model. Such an average value, which is k_ε, had also to be defined for the top flange (upper face not directly heated) and for the end-plate. The used formulae are the following (the parameters h_i, c, b, t_f and h are defined in Figure 6 and t_p is the end-plate thickness):

- For the beam web: $k_\varepsilon=\phi$;
- For the beam bottom flange: $k_\varepsilon=(\phi_{f,in}.c+1.b/2+1.t_f)/(c+b/2+t_f)$, where $\phi_{f,in}$ is the configuration factor associated to the flange internal face;
- For the beam top flange: $k_\varepsilon=(\phi_{f,in}.c+1.t_f)/(c+t_f)$, where $\phi_{f,in}$ is the configuration factor associated to the flange internal face;
- For the end-plate: $k_\varepsilon=(\phi_{ep,in}.c.h_i+1.b/2.t_p+1.h.t_p)/(c.h_i+b/2.t_p+h.t_p)$, where $\phi_{ep,in}$ is the configuration factor associated to the face of the end-plate between the beam flanges.

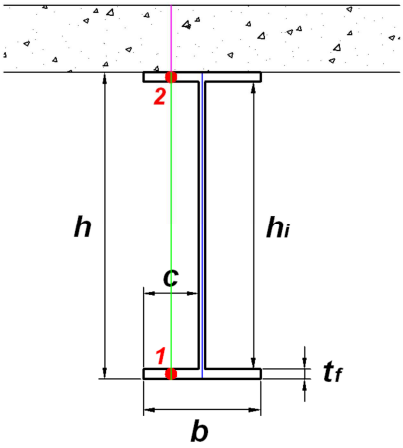

Figure 6. Beam cross-section

The same procedure has been applied for the column.

IV. Temperature distribution

Figure 7 shows the temperature distribution in the joint after 10, 20, 30, 40, 50, 60, 90 and 120 minutes.

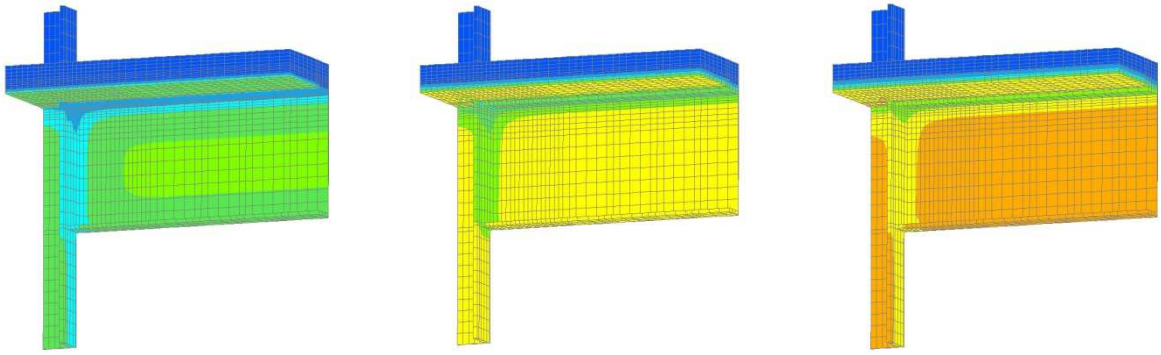

10 minutes *20 minutes* *30 minutes*

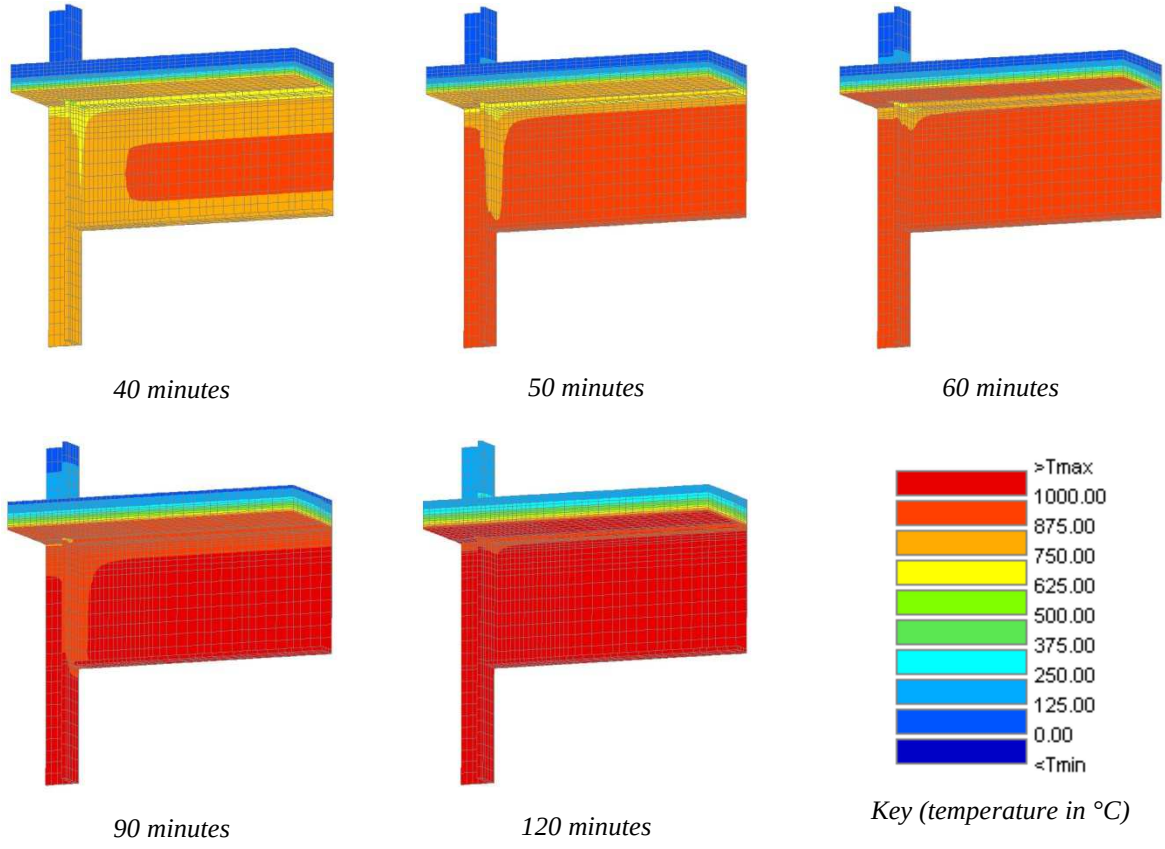

Figure 7. Temperature distribution after 10, 20, 30, 40, 50, 60, 90 and 120 minutes

Figure 8 gives the temperature of the beam bottom and top flanges in the connection section versus time (see points 1 and 2 in Figure 6 respectively) and compares this evolution with the temperature of the gases corresponding to the standard iso fire curve.

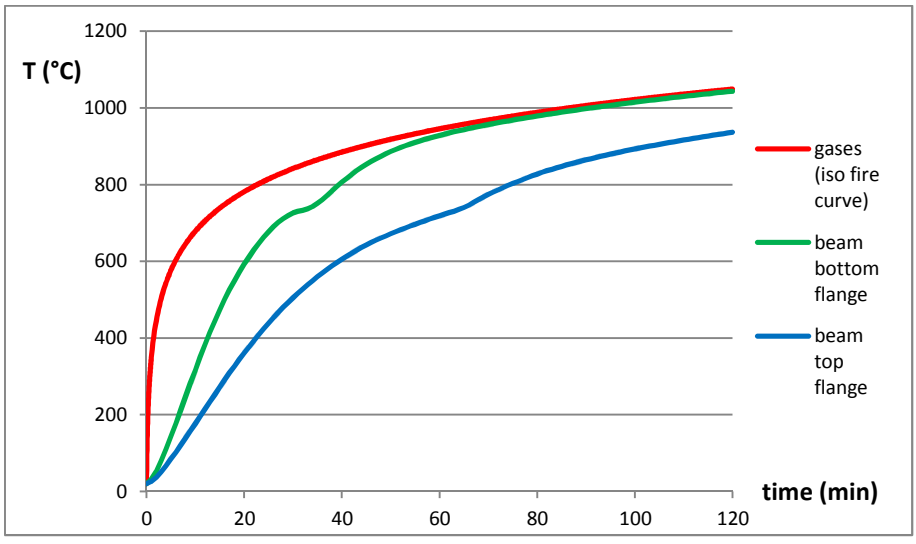

Figure 8. Temperature in the beam flanges versus time

Figure 9 shows the temperature profiles along the end-plate and beam web (see green and blue line in Figure 6 respectively), after 10, 20, 30, 60 and 120 minutes. The vertical coordinate *y* is equal to 0mm at the level of the beam bottom flange lower face and to 550mm at the level of the beam top flange upper face.

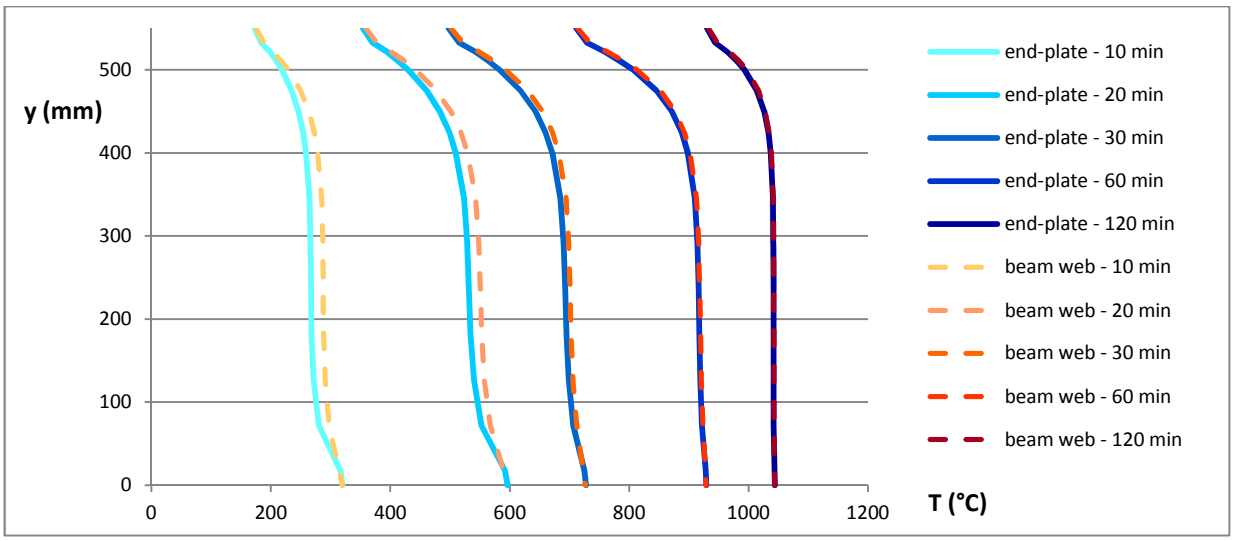

Figure 9. Temperature profiles in end-plate and beam web

Figure 10 shows the temperature profile in the concrete slab at a distance of 10cm from the column flange, along the pink line represented in Figure 6, after 10, 20, 30, 60 and 120 minutes. The vertical coordinate *y* is equal to 550mm at the level of the beam top flange upper face (slab lower face) and to 670mm at the level of the concrete slab top face.

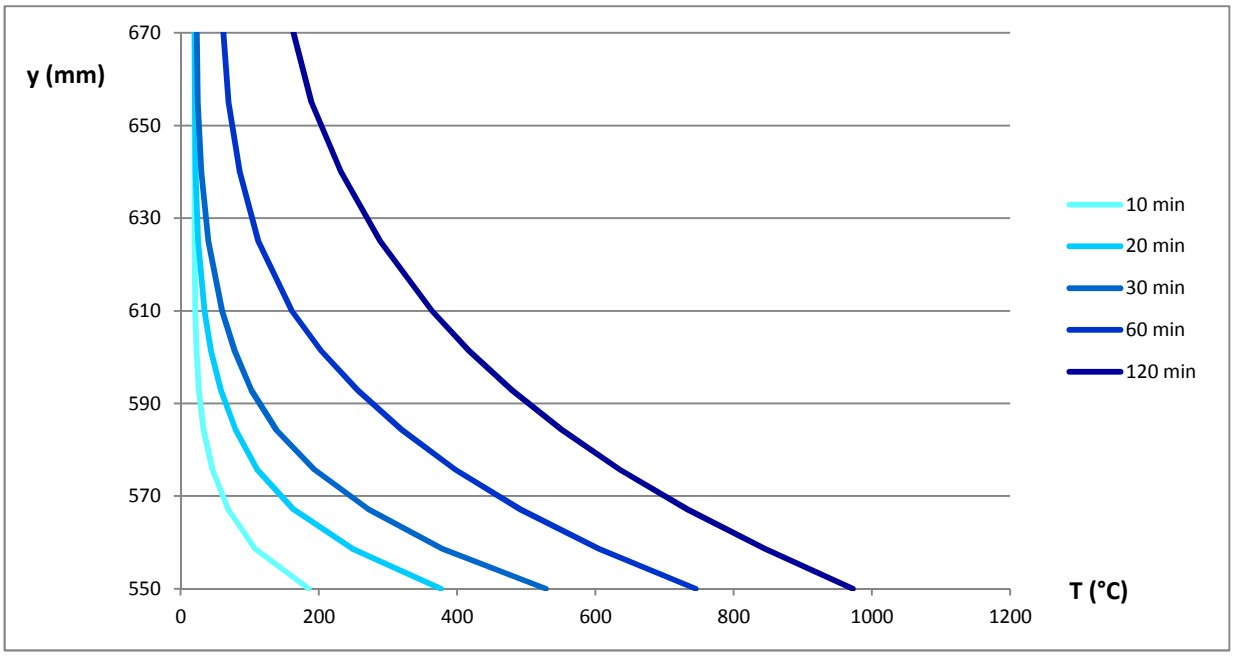

Figure 10. Temperature profiles in concrete slab

V. Conclusion

In this section, the evolution of the temperature distribution within a composite beam-to-column joint subjected to the standard fire curve has been investigated through a thermal finite element analysis, performed with the software SAFIR. Such simulations could be carried out for other limit conditions corresponding to particular fire scenarios or for other joint configurations. The temperature of the different joint components at any moment during the fire can be deduced from these analyses, which is necessary to evaluate the joint resistance. Indeed, the material resistances decrease with the increase in temperature.

In DELIVERABLE III section II, an analytical model for the prediction of joint resistance at elevated temperature is introduced. It is also applied to the joint considered here above, based on the described

thermal finite element simulation. The M-N resistance curves established considering the temperature distributions after 10, 20, 30 and 60 minutes are presented.

VI. References

[1] J.M. Franssen. « User's manual for SAFIR 2007a – A computer program for analysis of structures subjected to fire ». University of Liège, Belgium, January 2008.

[2] J.M. Franssen. « SAFIR – A Thermal/Structural Program Modelling Structures under Fire ». *Engineering Journal*, A.I.S.C., 42(3), 143-158. 2005.